

DTIC FILE COPY

25851.2-MS-CF

①

AD-A209 678

DTIC  
ELECTE  
JUN 29 1989  
S D<sub>as</sub> D

89 6 15 021

**DISTRIBUTION STATEMENT A**  
Approved for public release  
Distribution Unlimited

UNCLASSIFIED

SECURITY CLASSIFICATION OF THIS PAGE (When Data Entered)

REPORT DOCUMENTATION PAGE		READ INSTRUCTIONS BEFORE COMPLETING FORM
1. REPORT NUMBER ARO 25851.2-MS-CF	2. GOVT ACCESSION NO. N/A	3. RECIPIENT'S CATALOG NUMBER N/A
4. TITLE (and Subtitle) Superplasticity and Superplastic Forming		5. TYPE OF REPORT & PERIOD COVERED Book
		6. PERFORMING ORG. REPORT NUMBER N/A
7. AUTHOR(s) C. H. Hamilton and N. E. Paton		8. CONTRACT OR GRANT NUMBER(s) DAAL03-88-G-0032
9. PERFORMING ORGANIZATION NAME AND ADDRESS Washington State Univ Pullman, WA		10. PROGRAM ELEMENT, PROJECT, TASK AREA & WORK UNIT NUMBERS N/A
11. CONTROLLING OFFICE NAME AND ADDRESS U. S. Army Research Office P. O. Box 12211 Research Triangle Park, NC 27709		12. REPORT DATE 1988
		13. NUMBER OF PAGES 706
14. MONITORING AGENCY NAME & ADDRESS (if different from Controlling Office)		15. SECURITY CLASS. (of this report) Unclassified
		15a. DECLASSIFICATION/DOWNGRADING SCHEDULE
16. DISTRIBUTION STATEMENT (of this Report) Submitted for announcement only.		
17. DISTRIBUTION STATEMENT (of the abstract entered in Block 20, if different from Report)		
18. SUPPLEMENTARY NOTES The view, opinions, and/or findings contained in this report are those of the author(s) and should not be construed as an official Department of the Army position, policy, or decision, unless so designated by other documentation.		
19. KEY WORDS (Continue on reverse side if necessary and identify by block number)		
20. ABSTRACT (Continue on reverse side if necessary and identify by block number)		

DD FORM 1 JAN 73 1473 EDITION OF 1 NOV 65 IS OBSOLETE

UNCLASSIFIED

SECURITY CLASSIFICATION OF THIS PAGE (When Data Entered)

# Superplasticity and Superplastic Forming

Proceedings of an International Conference on Superplasticity and Superplastic Forming, sponsored by The Shaping and Forming and The Titanium Committees of TMS, held in Blaine, Washington, August 1-4, 1988.

*Edited by*

**C. Howard Hamilton**  
*Washington State University*  
Pullman, Washington

and

**Neil E. Paton**  
*Rockwell International*  
Canoga Park, California

A Publication of

**TMS**  
Minerals • Metals • Materials



Accession For	
NTIS CRAD	N
DTIC TAG	<input type="checkbox"/>
Unannounced	<input type="checkbox"/>
Justified	
By	140.00
Distrib	
Availability	
Dist	A-1 21

A Publication of The Minerals, Metals & Materials Society  
 420 Commonwealth Drive  
 Warrendale, Pennsylvania 15086  
 (412) 778-9024

The Minerals, Metals & Materials Society is not responsible for statements or opinions and absolved of liability due to misuse of information contained in this publication.

Printed in the United States of America  
 Library of Congress Catalog Number 88-62444  
 ISBN Number 0-87339-089-X

Authorization to photocopy items for internal or personal use, or the internal or personal use of specific clients, is granted by The Minerals, Metals & Materials Society for users registered with the Copyright Clearance Center (CCC) Transactional Reporting Service, provided that the base fee of \$3.00 per copy is paid directly to Copyright Clearance Center, 27 Congress Street, Salem, Massachusetts 01970. For those organizations that have been granted a photocopy license by Copyright Clearance Center, a separate system of payment has been arranged.

**TMS**  
 Minerals • Metals • Materials

© 1988



## Preface

This book contains the proceedings of the International Conference on Superplasticity and Superplastic Forming, which was held in Blaine, Washington, USA, August 1-4, 1988.

Over the past 15 to 20 years, superplasticity has progressed from a laboratory curiosity to become utilized on a world-wide basis through superplastic forming processes in the manufacture of parts for many types of applications, ranging from aerospace to architectural. Recent work has demonstrated that superplasticity can be observed in many types of material systems, including ceramics, metal-matrix composites, and intermetallic compounds, as well as in alloys. The science and technology of superplasticity and superplastic forming are both intriguing and challenging, and the potential benefits to be gained through continuing research and development have caused this to be an area of vital interest.

Subsequent to the first international conference held in San Diego, California in 1982, several focused conferences and seminars have been held. At a recent conference held in Grenoble, France, in 1985, an ad hoc committee was convened to assess the need and coordinate scheduling for future conferences. It was decided at that meeting that there was significant progress and interest in superplasticity and related forming processes, and that an international conference should be held about 1988. It was further suggested by the committee that the conference should include papers on the full spectrum of superplasticity from fundamental mechanisms to the forming and applications, in order to provide all those interested in superplasticity the opportunity to develop greater appreciation of the potential benefits as well as limitations of aspects related to, but outside, their field of specific interest. This conference was organized with consideration of these suggestions.

These proceedings contain the manuscripts of presentations made at this conference. The proceedings are organized in seven sections: Fundamentals; Microstructural Dynamics; Rheology and Cavitation; Fundamentals of Forming; Alloy Design; SPF Methods and Diffusion Bonding; Design Concepts and Future Directions.

The conference organizers were Drs. Neil Paton, Rockwell International Corp., and C.H. Hamilton, Washington State University, who were supported by an International Organizing Committee consisting of the following:

Dr. B. Baudalet, Institute National Polytechnique de Grenoble, France.  
Dr. Hai Jintao, Beijing Research Institute of Mechanical and Electrical Technology, Peoples Republic of China.  
Dr. O.A. Kaibyshev, Academy of Sciences, USSR.  
Dr. M. Kobayashi, Technological University of Nagaoka, Japan.  
Dr. R. Raj, Cornell University, USA.  
Dr. N. Ridley, University of Manchester/UMIST, England.  
Dr. D.S. Wilkinson, McMaster University, Canada.  
Dr. P.J. Winkler, MBB, West Germany.

The Session Chairmen participating in the conference were Peter Partridge, Royal Aircraft Establishment; Oleg Sherby, Stanford University; Peter Winkler, MBB, West Germany; Norman Ridley, University of Manchester/UMIST; Amit Ghosh, University of Michigan; Neil Paton, Rockwell International; and C.H. Hamilton, Washington State University.

The administration, correspondence, and registration was under the responsibility of Ms. Nancy Mack, Conferences and Institutes, Washington State University, and with the support of Ms. Mary Carloye and Ms. Kreta Johnson. The authors are indebted to Washington State University for hosting the conference, and to The Shaping and Forming Committee and the Titanium Committee of TMS for sponsoring the conference. Financial support was provided by:

The Aluminum Company of America  
The Boeing Company  
College of Engineering & Architecture, Washington State Univ.  
Research Group of Superplasticity in Japan  
Rockwell International  
U.S. Air Force Office of Scientific Research  
U.S. Army Research Office-Durham  
U.S. Office of Naval Research  
Washington Technology Center

The editors are also indebted to Mr. Bob Tucker, Mr. Binyan Ren and Mr. Brad Benson, graduate students at Washington State University, for their help with audio-visual aids during the presentations, and to Ms. Jan Palmer for helping with many of the conference on-site needs.

A special note of gratitude is extended to all participants and to the authors without whom the conference and this proceedings would not have been possible.

**C. Howard Hamilton**  
Washington State University  
Pullman, Washington

**Neil E. Paton**  
Rockwell International  
Canoga Park, California

December, 1988

## Table of Contents

Preface .....	v
---------------	---

### Fundamentals

Current Problems of the Material Science of Superplasticity .....	3
<i>O.A. Kaibyshev</i>	
Metallographical Research on Superplasticity.....	17
<i>Shigenori Hori and Norio Furushiro</i>	
Direct Observations and Micromechanical Testing of Superplastic Alloys .....	21
<i>M.J. Mayo and W.D. Nix</i>	
Investigation of Region I in Rapidly Solidified Powder Aluminum Alloys.....	27
<i>G.S. Murty and M.J. Koczak</i>	
The Mechanism of Superanelasticity and its Implications.....	33
<i>R.I. Todd and P.M. Hazzledine</i>	
The Role of Grain Boundary Dislocations During Superplastic Deformation of an Aluminum Alloy.....	39
<i>Shanyou Zhou, Liqin Wang and Chin Liu</i>	
The Physical Model of Superplasticity Based on the Notion of Nonequilibrium Grain Boundaries .....	45
<i>R.Z. Valiev</i>	
Superplastic Behavior of Zn-20Al-2Cu at Room Temperature and Deformation Mechanisms .....	51
<i>G.T. Villaseñor and J. Negrete</i>	
Some Recent Advances in the Development of Fine-Grained Superplastic Aluminum Alloys, Ceramics, and Laminated Composites.....	57
<i>J. Wadsworth, T.G. Nieh and O.D. Sherby</i>	
A Deformation Mechanism for Superplastic Deformation of Age Strengthening Cu Alloy .....	63
<i>Jin Tao, Zhao Min and Chen Puquan</i>	
A Complex Mechanism for Superplastic Deformation of Magnesium Alloys.....	67
<i>Zhao Min and Chen Puquan</i>	
Mechanisms of Superplastic Flow in Inconel 718.....	73
<i>M.W. Mahoney and R. Crooks</i>	

for PV1 Contents

Microstructural Dynamics

Microstructural Instability During Superplastic Flow.....	81
<i>D.S. Wilkinson</i>	
Dynamic Recrystallization and Superplasticity of a Magnesium Alloy.....	91
<i>N.G. Zaripov and R.O. Kaibyshev</i>	
Grain Refinement by Torsion and Superplasticity in High Strength Al-Alloy.....	97
<i>Jin Quanlin, Bai Bingzhe, Lai Weihua, Guo Xusheng and Zhang Hong</i>	
The Transformation of Ti Alloy Laminar Microstructure into a Microduplex One.....	103
<i>G.A. Salishchev and R.Y. Lutfullin</i>	
The Role of Matrix Dislocations in the Superplastic Deformation.....	109
<i>P. Lukac</i>	
Superplastic Deformation Induced Grain Growth in Microduplex and Second Phase Dispersed Alloys.....	115
<i>Eiichi Sato, Kazuhiko Kuribayashi and Ryo Horiuchi</i>	
The Microstructural Characteristics of an Al-Li-Cu-Mg-Zr Alloy During the Initial Stage of Superplastic Deformation.....	121
<i>B. Ren and C.H. Hamilton</i>	
Details of the Alpha Grain Boundaries in Annealed and Superplastically Deformed Ti-6Al-4V Alloy.....	129
<i>L.R. Zhao, S.Q. Zhang and M.G. Yan</i>	

Rheology and Cavitation

Plastic Stability and Strain to Fracture During Superplastic Deformation.....	135
<i>B. Baudalet and M. Suery</i>	
The Role of Cavitation in the Failure of Superplastic Alloys.....	149
<i>A.H. Chokshi and A.K. Mukherjee</i>	
High Rate Superplastic Behavior of Mechanical Alloyed Aluminum IN90211.....	161
<i>T.R. Bieler, T.G. Nieh, J. Wadsworth and A.K. Mukherjee</i>	
Effect of Accelerated/Decelerated Strain Rate on Sheet Formability of $\sigma = K \dot{\epsilon}^m \epsilon^n$ Materials.....	167
<i>H. Ohsawa</i>	

An Investigation of the Characteristics of Cavitation in Superplastic Materials .....	173
<i>Yan Ma and T.G. Langdon</i>	
Rheological Criteria for Rational Use of Superplasticity in Metal Working by Pressure .....	179
<i>O.M. Smirnov</i>	
Effect of Strain Rate Dependence of $m$ on Ductility in Superplastic Materials .....	185
<i>Takuji Okabe, Tomei Hatayama and Hideo Takei</i>	
Evolution of Cavitation During Superplastic Deformation .....	191
<i>J.J. Blandin and M. Suéry</i>	
An Experimental Investigation of Hole Growth and Interlinkage in the Superplastic Zn-22% Al Eutectoid Alloy .....	197
<i>Norio Furushiro and T.G. Langdon</i>	
Cavitation Behavior and Dislocation Structure of Commercial Manganese-Brass During Superplastic Deformation .....	203
<i>Zhao You-Chang and Li Xiu-Qing</i>	
Deformation of Ti-6Al-4V Bar and Extrusion Under Superplastic Forming Conditions .....	209
<i>D.V. Dunford and P.G. Partridge</i>	
Effect of Superplastic Deformation on the Surface Roughness of Sheet .....	215
<i>P.G. Partridge and D.V. Dunford</i>	
Superplasticity and Cavitation of the 2091 Al-Cu-Li-Mg Alloy .....	221
<i>J.J. Blandin, J.Y. Lacroix and M. Suéry</i>	
The Influence of Specimen Profile and Notch Geometry on Superplasticity in Zn-22% Al .....	227
<i>P. Shariat and T.G. Langdon</i>	
The Relationship Between Strain-Rate Sensitivity Index and Strain in Superplasticity .....	233
<i>Chen Hechun and Yang Zhenheng</i>	
Factors Affecting Superplastic Stability in an Al-Li-Cu-Zr Alloy .....	239
<i>B. Ash and C.H. Hamilton</i>	
Effect of Grain Size on Region Transition Behavior in Superplastic Deformation .....	245
<i>Jianzhong Ciu, Qinling Wu and Longxiang Ma</i>	
Influence of Uni- and Bi-Axial Straining on Cavitation in a Superplastic Aluminum Alloy .....	251
<i>A. Varloteaux, J.J. Blandin and M. Suéry</i>	
Effects of Second Phase Particles on the Cavity of Superplasticity .....	257
<i>J.F. Ycng, Peng Xu and H. Wang</i>	

Superplasticity in Ti-10V-2Fe-3Al Alloy .....	263
<i>Pan Ya qin, Liu Weimin and Song Zuozhou</i>	

### Fundamentals of Forming

Novel Processing Methods for Superplastic Alloys .....	271
<i>Masaru Kobayashi</i>	
Membrane Element Analysis of Axisymmetric and Non-Axisymmetric Superplastic Metal Forming Processes .....	283
<i>N. Chandra and B. Roy</i>	
Finite Element Modelling of the Superplastic Forming of Thin Sheet .....	291
<i>J. Bonet, R.D. Wood and O.C. Zienkiewicz</i>	
Incorporation of Sliding Friction into a Closed-Form Model of Plane Strain Superplastic Forming .....	297
<i>J.M. Story</i>	
Bulge-Forming of Domes; A Comparison of Theoretical Prediction and Experiment .....	303
<i>Z.X. Guo, J. Pilling and N. Ridley</i>	
A Study on Superplastic Alloy Sheet Bulging Under the Microcomputer Control .....	369
<i>Tao Shuxue and Ma Longxiang</i>	
Superplastic Forming of Ti-Alloy Vessel .....	315
<i>Chen Bingkin and Hai Jintao</i>	
Theoretical and Experimental Studies on the Pressure Thermoforming of Hemispheres of Alloy Ti-6Al-4V .....	321
<i>D. Viswanathan, S. Venkataswamy and K.A. Padmanabhan</i>	
New Advance of Superplastic Forming Process for Commercial Structural Alloys .....	327
<i>Wang Cheng and Luo Ying-She</i>	
Superplastic Formability to Distinguish the Metallic Thin Wall Component by Criteria and Criterion-Model .....	333
<i>Wang Chunrong, Song Hailong, Qu Li and Chao Shuzhi</i>	
An Experimental Study of Yield Criterion Using Superplastic Thin-Walled Tubes Subjected Tension- Torsional Combined Loads .....	339
<i>Z.R. Wang, Xu Yanwu, Guo Dianjian and Yin Changkui</i>	
Mechanical Analysis About Deformation Laws of Superplastic Extrusion Through Cone-Shaped Dies .....	345
<i>Song Yu-quan, Zhang Zhen-jun and Lian Shu-jun</i>	

## Alloy Design

Alloy Design of Superplastic Nickel-Base and Titanium-Base Alloys.....	353
<i>Michio Yamazaki</i>	
Development of Superplastic Behaviour in Various Commercial Materials .....	365
<i>N. Ridley and C. Hammond</i>	
Superplastic Optimisation for Diffusion Bonding Applications in Al-Li Alloys .....	377
<i>R.A. Ricks and P.J. Winkler</i>	
The Development of LFC-X1 Alloy .....	383
<i>Zhou Tiecheng, Zhang Zhimin and Zhang Yanhui</i>	
Microstructural Refinement Via Continuous Recrystallization in a Superplastic Aluminum Alloy .....	389
<i>R. Crooks, S.J. Hales and T.R. McNelley</i>	
Superplasticity of Rapidly Solidified 7475-0.7 wt% Zr Alloys .....	395
<i>K. Matsuki, M. Tokizawa and G. Staniak</i>	
Optimization of Heterogeneity as General Principle of Controlling Alloys Structure for Superplastic Forming .....	401
<i>I.I. Novikov and V.K. Portnoy</i>	
Superplastic Properties of the Cold Formable Titanium Alloy SP35.....	407
<i>S. Yamazaki, T. Oka, Y. Mae and M. Kobayashi</i>	
Grain Refinement and Superplasticity in a Hard Nickel-Base Alloy.....	413
<i>I. Kuboki, Y. Motohashi and M. Imabayashi</i>	
Superplastic Low Manganese Zinc-Manganese Alloys .....	419
<i>N. Dyulgerov, A. Istatkov, N. Mitev and I. Spirov</i>	
Properties of a Microduplex Stainless Steel Superplastically Deformed .....	429
<i>K. Osada</i>	
The Study of Reducing Superplastic Temperature in Titanium Alloys.....	435
<i>Huang Liping</i>	
An Approach to the Superplasticity of Aluminium Brass (HAL 66-3-2) .....	441
<i>Su Shenggui, Shen Huanxiang and Song Shengzhe</i>	
Thermomechanical Processing and Superplasticity in a Commercial Copper-Base Alloy.....	447
<i>K. Higashi and N. Ridley</i>	

The Effects of Superplastic Deformation on the Microstructure and Hardening Characteristics of High Strength 8091 Aluminum-Lithium Alloy .....	453
<i>R.D. Tucker and C.H. Hamilton</i>	
Improvement in the Superplasticity of Ti-6Al-4V Alloy by Hydrogenation.....	459
<i>L.R. Zhao, S.Q. Zhang and M.G. Yan</i>	
A Study on Superplasticity of Commercial 2024Al Alloy.....	465
<i>Hailing Huang, Qinglin Wu and Jin Hua</i>	
<b>SPF Methods and Diffusion Bonding</b>	
Diffusion Bonding in Superplastic Materials.....	475
<i>J. Pilling</i>	
Diffusion Bonding and Superplastic Forming, Two Complementary Manufacturing Techniques.....	491
<i>P.-J. Winkler</i>	
Application of Superplastic UHC Steel for Isothermal Forging of Machine Component.....	507
<i>J. Wittenauer, P. Schepp and B. Walser</i>	
A Dynamic Model for Diffusion Bonding of Metals .....	513
<i>Huang Yan and Ma Longxiang</i>	
Effects of Transformation Superplasticity on the Early, Deformation Process of the Solid State Bonding in Pure Iron.....	517
<i>Yasunori Saotome and Nobuhiro Iguchi</i>	
Diffusion Bonding and Superplastic Forming of 7475 Aluminum Alloy.....	523
<i>J. Kennedy</i>	
Mechanical Properties of Titanium and Aluminium Alloys After Superplastic Deformation .....	529
<i>D.S. McDermid and P.G. Partridge</i>	
The Application of Superplastic Forming for Making Plastic Injection Mould—Cavity Design and Superplastic Pressing .....	541
<i>Zhang Dixiang</i>	
Combined Extrusion of Superplastic Al-Zn System Alloys .....	545
<i>M. Hirohashi and H. Asanuma</i>	
Superplastic Behaviour of Die Steel 4Cr3Mo3W2V and Application .....	551
<i>Yang Yongchun</i>	



Bonding of Aluminium-Lithium Base Alloys Using Roll Clad Zinc Interlayers.....	557
<i>R.A. Ricks, J. Ball, H. Stoklossa, P.J. Winkler and R. Grimes</i>	
Transformation Superplasticity Solid-State Bonding in Steels.....	563
<i>Wang Yanwen, Feng Zezhou and Sun Shangchen</i>	
<b>Design and Concepts and Future Directions</b> , Book 1	
Development of Superplastic Forming Technology in China.....	571
<i>Hai Jintao, Dai Jilin, Chen Sanshan, Z.R. Wang and Zhang Kaifeng</i>	
Mechanisms of Superplastic Deformation in Ceramics.....	583
<i>R. Raj</i>	
Forming Non-Superplastic Materials with Superplastic Membranes.....	595
<i>D.M. Ward</i>	
S.P.F.-D.B. Applications for Military Aircraft.....	601
<i>B. Rolland</i>	
Fabrication of Fiber Reinforced Metal Using Superplastic Metal Powder as Matrix.....	613
<i>H. Nishimura, S. Wakayama, H. Yamamoto and S. Yamagishi</i>	
Superplasticity of ZrO <sub>2</sub> Toughened Ceramics.....	619
<i>Fumihiko Wakai</i>	
Extrusion of tet-ZrO <sub>2</sub> at Elevated Temperatures.....	625
<i>B. Kellett, P. Carry and A. Mocellin</i>	
Superplastic Deformation of Y-TZP Zirconia.....	631
<i>T. Hermansson, K.P.D. Lagerlöf and G.L. Dunlop</i>	
Post-SPF Fatigue Properties in Ti-6Al-4V Alloy.....	637
<i>Y. Mutoh, M. Kobayashi, Y. Mae and K. Toyofuku</i>	
The Manufacture of SPF Military Aircraft Doors in Aluminium Alloy.....	643
<i>G.W. Hughes, S.H. Johnston and B. Ginty</i>	
SPF/DB on the Way to the Production Stage for Ti and Al Applications Within Military and Civil Projects.....	649
<i>H.E. Friedrich, R. Furlan and M. Kullick</i>	
Production of Ti6Al4V-Components for a New Turbo-Fan-Engine.....	665
<i>R. Furlan, P.-J. Winkler, D. Hagg and L. Reisinger</i>	

Study on SPF and SPF/DB of the Bulk-Head Structure with Non-Symmetric Shape.....	679
<i>Li You-qin and Zhang Si-ling</i>	
DE/SPF Cooler Outlet Duct for Aircraft Application .....	685
<i>W. Beck</i>	
Subject Index.....	699
Author Index .....	705

# **FUNDAMENTALS**

CURRENT PROBLEMS  
OF THE MATERIAL SCIENCE OF SUPERPLASTICITY

O. A. Kaibyshev

Institute of the Metal Superplasticity Problems  
USSR Academy of Sciences, Ufa 450001 USSR

Abstract

The current material science problems of superplasticity are reviewed with particular reference to the regularities of fine grain microstructure formation in commercial alloys and the possibility of intermetals and ceramics conversion to the superplastic state. During the hot straining under certain temperature-rate conditions the formation of a fine grain microstructure in metals, intermetals, and ceramics is followed by their transition to the superplastic flow. The phenomenological and structural changes during the superplastic flow of the said materials are identical, which indicates the universal character of deformation mechanisms operating under these conditions. For the superplasticity effect to be displayed, the enlargement of the ordinary high angle boundary regions in a polycrystal is of crucial significance.

Superplasticity and Superplastic Forming  
Edited by C.H. Hamilton and N.E. Paton  
The Minerals, Metals & Materials Society, 1988

## Introduction

The main significance of the investigation of the nature of superplastic (SP) flow is that it has resulted in the determination of operative deformation mechanisms, the quantitative evaluation of their contribution to the overall deformation, and the confirmation of the universal character of the phenomenon, i.e. the ability of any commercial alloy to display SP (1-5).

The application of superplastic treatment to various materials has become possible due to the solution of a number of material science problems:

- the development of the ultrafine microstructure producing methods applicable to commercial alloys;
- the determination of the effect of SP treatment on the performance of alloys.

Besides, SP treatment has proved to be both an efficient way of product shaping and a method of obtaining homogeneous microstructure, providing a remarkable complex of physical and mechanical properties of an alloy (4).

The possibility of conversion of materials, traditionally considered to be strain resistant, to the SP state is another problem to be solved.

Some data obtained during the study of ultrafine grain microstructure formation regularities in commercial alloys are presented in this paper. The possibility of intermetals and ceramics conversion to the SP state is also considered.

## Materials and Experimental Details

The regularities of the ultrafine grain microstructure formation have been studied on magnesium and titanium alloys. The MA14 magnesium alloy was selected as a typical representative of the matrix microstructure alloys: it is practically single-phase, though there is a number of additional phases, stimulating the stabilization of microstructure. The VT9 titanium alloy with a laminar microstructure represents the two-phase alloy.

The composition and initial treatment of the studied alloys were as follows: for MA14 - 6 wt% Zn, 0.65 wt% Zr, balance Mg. An ingot with the grain size of about 150  $\mu\text{m}$ , annealed at 390°C for 6 hours in order to increase its technological plasticity, was used as a blank. For VT9 - 6.6 wt% Al, 3.5 wt% Mo, 1.7 wt% Zr, balance Ti. The alloy casting was forged and annealed in the single-phase  $\beta$ -region at 1040°C. Such treatment produced a coarse grain laminar microstructure.

The SP flow of the low plasticity materials was studied on the titanium intermetals and magnetic alloy systems of Fe-Cr-Co and Mn-Al-C.

TiAl: 36 wt% Al, balance Ti. The alloy blanks sized 90x120, obtained by the compaction of granules dusted in vacuum, were 80% compression strained at 1000°C with the rate of  $10^{-3}\text{s}^{-1}$ . Then they were held at 925°C for 24 hours (state A). Part of material was annealed at 1050°C for 24 hours (state B). The forgings were

cooled together with the furnace. Alongside with the basic  $\gamma$ -phase (TiAl - superlattice  $L_{10}$ ) the alloy contained about 3 vol.% of  $\alpha_2$ -phase (Ti<sub>3</sub>Al - DO<sub>19</sub>).

X30K23: 30.5 wt% Cr, 23 wt% Co, 0.4 wt% Ti, 0.4 wt% Si, balance Fe. After forging in the temperature interval of 1000-1200°C and quenching to a single-phase  $\alpha$ -solid solution, the alloy was rolled at room temperature with the 70% straining and annealed at 950°C for 15 min. Such treatment produces a fine grain microduplex structure with a mean grain size of about 2  $\mu$ m, composed of the following phases: 35%  $\gamma$ -f.c.c. and 65%  $\delta$ -superlattice  $L_{10}$ .

Mn<sub>70</sub>Al<sub>29.5</sub>Co<sub>0.5</sub>: a fine grain state was obtained by means of 70% compression straining at the rate of 3.1 mm/min at 700°C after preliminary homogenization at 1150°C for 2 hours. The mean grain size in  $\tau$ -phase (superlattice  $L_{10}$ ) was about 1  $\mu$ m.

Ceramic materials were represented by the ceramic compound YBa<sub>2</sub>Cu<sub>3</sub>O<sub>7- $\delta$</sub> , which is a promising material for the high-temperature superconductivity research. The blanks were produced according to the technique described in (8). The testing of materials in a broad temperature and rate interval has been conducted on the INSTRON plant. The microstructure was studied using the optical microscopy, high-temperature metallography, transmission and scanning electron microscopy.

## Results

### The microstructure refining during hot straining

Dynamic recrystallization is the process providing for the most efficient refining of the microstructure of commercial alloys (4). A systematic study of microstructural changes due to hot straining has been accomplished on the MA14 matrix structure commercial alloy (9). The MA14 alloy stress-strain curves in the straining temperature interval of 200-500°C are shown in Fig.1. It is evident that after the rapid increase of flow stress at the initial stage the alloy deformation at 250-450°C is accompanied by a slight hardening. During the deformation at 450°C repeated jumps are detected on the  $\sigma=f(\epsilon)$  curve. But when the temperature of deformation is above 450°C no  $\sigma$  oscillation of the stress-strain curve is observed.

The investigation of the prestrained alloy indicates that the flow stress at the 25% straining is in a linear relation to the rates ( $m < 0.25$ ), and after the 40% straining has been reached the alloy starts to display the SP flow features ( $m = 0.38$ ).

The metallographic analysis of the as-50% upset specimens has revealed the dynamic recrystallization developing in the alloy at 250-500°C. New grains are formed non-uniformly, mainly in the boundary regions of original grains. The recrystallization is not complete even at 500°C. The study of the microstructure evolution at 450°C, with the flow stress changing abruptly, is the most stimulating.

Pronounced changes in the alloy microstructure can be observed even when the deformation is quite small. Grain boundaries become twisted and migrations of their local regions take place.

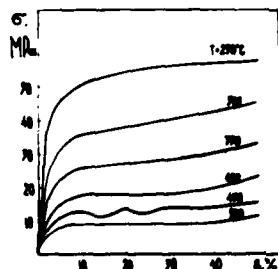


Fig.1 The MA14 alloy stress-strain curves  
( $\dot{\epsilon} = 4.3 \cdot 10^{-3} s^{-1}$ )

New grains whose orientation determined in polarized light is close to that of the original grains (Fig.2a), appear in the vicinity of triple points. The growth of straining results in the formation of the chains of fine grains round the original ones. The higher is the strain the larger is the number of recrystallized fine grains (Fig.2b). However, this process will eventually die out, for even after the 75% straining the recrystallization never spreads over the whole volume of material.



Fig.2 The as-strained MA14 alloy  
microstructure ( $t=450^{\circ}C$ ,  $\dot{\epsilon} = 4.3 \cdot 10^{-3} s^{-1}$ ):  
a)  $\epsilon = 15\%$ ; b)  $\epsilon = 50\%$ .

The alloy surface study during the plastic flow has revealed the multiple slip going on in the boundary regions. The nonbasic slip (wavy slip-lines) takes place alongside with the basic one. At the initial stage of deformation the multiple slip results in the formation of cell boundaries in the boundary region, and with further increase of deformation they are transformed into high angle boundaries.

The formation of fine grains in the boundary region makes possible the development of grain boundary sliding (GBS) along

them. The higher is the hot straining the more significant is the role of this deformation mechanism. Meanwhile a sharp decrease in the localization of stresses near the boundaries is observed, which impedes the operation of nonbasic slip systems and, consequently stops the formation of new grains. This accounts for the fact that the alloy microstructure refining is incomplete even when the straining is very high.

Let's consider the laminar microstructure transformation during the Ti-alloy hot straining. To establish the role played by deformation, the VT9 alloy was annealed in the ( $\alpha$ + $\beta$ )-region at 950°C for 50 hours and also strained at the same temperature (i.e. at the optimum temperature of SP flow). Annealing causes a significant coarsening of microstructure while preserving the laminar morphology of  $\alpha$ -phase and the matrix type of original microstructure. Moreover, the annealing of the globular  $\alpha$ -phase alloy makes the  $\alpha$ -phase grains change into the laminar-like ones due to the straightening of the interface boundaries.

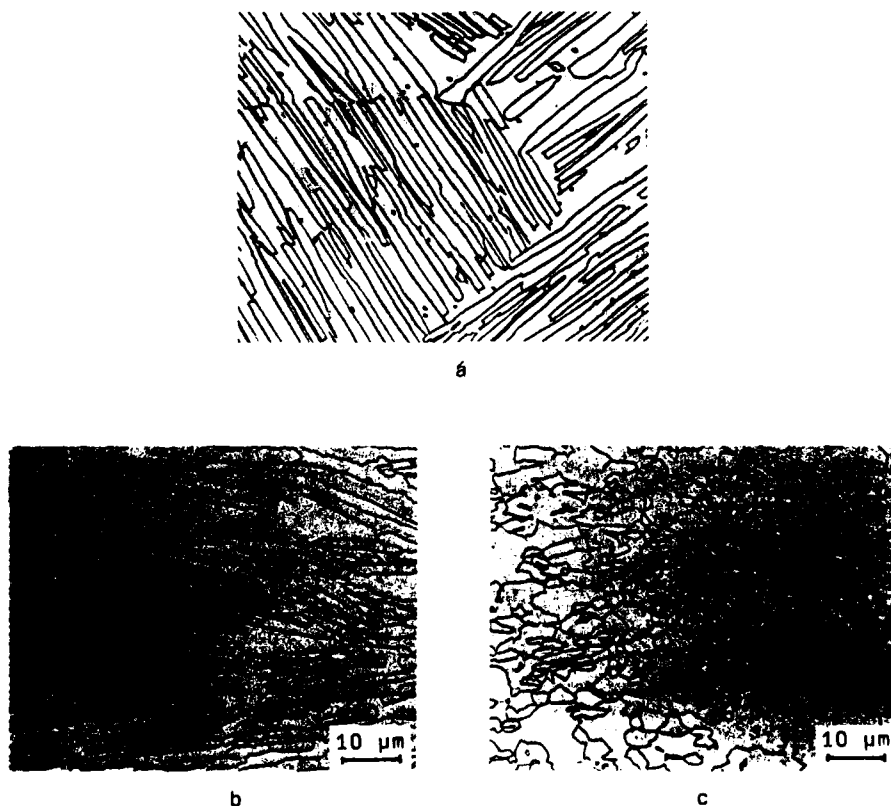


Fig.3 The as-hot-strained VT9 alloy microstructure ( $t=950^{\circ}\text{C}$ ,  $\dot{\epsilon}=5.5 \cdot 10^{-4} \text{s}^{-1}$ ): a)  $\epsilon=0\%$ ; b)  $\epsilon=30\%$ ; c)  $\epsilon=70\%$ .



Only when the hot straining is conducted in the modes corresponding to the SP flow, the transformation of the matrix type laminar microstructure into a microduplex one takes place (Fig.3). The structure investigations have revealed the peculiarities of this phenomenon. The initial stage of deformation ( $\epsilon=10\%$ ) is characterized by the dislocation slip which results in the formation of metallographic and sharp crystallographic texture (Fig.4). Besides, at the initial stage of deformation the interface boundary sliding takes place. The  $\alpha$ -laminae turn in the direction of the plastic flow.

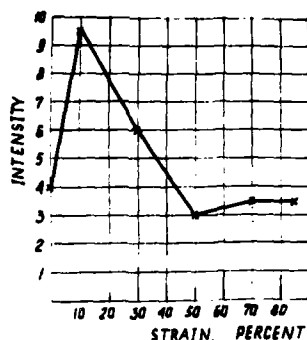


Fig.4 The change of the texture maximum intensity of the  $\alpha$ -phase (1011) plane during the VT9 alloy hot straining ( $t=950^\circ\text{C}$ ,  $\dot{\epsilon}=5.5 \cdot 10^{-3}\text{s}^{-1}$ ).

It is important to emphasize the following structural feature: during hot straining the  $\alpha$ -phase reduces quicker than when being annealed. Thus the alloy held at  $950^\circ\text{C}$  for an hour contains 52 vol.% of  $\alpha$ -phase, while in the as-hot-strained one ( $\dot{\epsilon}=5.5 \cdot 10^{-3}\text{s}^{-1}$ ,  $\epsilon=85\%$ , for less than three minutes) the  $\alpha$ -phase constitutes only 41 vol.%.

Deformation is accompanied by the accumulation of dislocations in  $\alpha$ -laminae. Their entering an interface boundary makes its energy and misorientation increase. The interface boundary becomes twisted (Fig.3b), mobile and high-angle. The active development of grain boundary sliding (GBS) along high angle interface boundaries results in the decrease of crystallographic texture (Fig.4). At the same time, due to the dynamic recovery the phase dislocation structure changes. Cross subboundaries are formed, their misorientation increasing from 1 to  $10-15^\circ\text{C}$ .

The active division of  $\alpha$ -laminae (Fig.5) and the turning and shearing of individual fragments due to the GBS development are observed. The microduplex microstructure having been formed at the final stage, the SP flow is observed in the alloy.

#### The superplasticity of intermetals

The first alloy to be considered is X30K23, consisting of the 65 vol.% intermetallic  $\delta$ -phase and 35 vol.% metallic  $\gamma$ -phase.



Fig.5 The  $\alpha$ -phase laminae division during the hot straining of VT9 alloy ( $t=950^{\circ}\text{C}$ ,  $\dot{\epsilon}=5.5 \cdot 10^{-4}\text{s}^{-1}$ ,  $\epsilon=50\%$ ).

Fig. 6 shows that at  $850-1000^{\circ}\text{C}$  in the strain rate interval of  $10^{-4} - 10^{-3}\text{s}^{-1}$  this alloy displays SP features. This is proved by the low flow stress values, high relative extension to rupture and  $m$  factor values in the said rate interval.

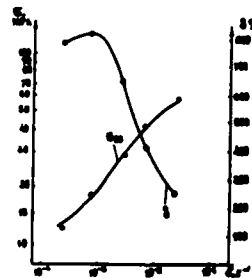


Fig.6 The strain rate effect on plasticity and flow stress of the fine grain microstructure X30K23 alloy:  $\delta$  - relative extension to rupture,  $\sigma_{50}$  - flow stress under the 50% straining.

Thus, in spite of the intermetallic phase, the SP flow of this material is analogous to that of the usual metallic alloys with microduplex microstructure.

The same conclusion is drawn from the mechanical properties analysis of the  $\text{Mn}_{70}\text{Al}_{29.5}\text{Co}_{0.5}$  alloy consisting of the intermetallic  $\tau$ -phase. At  $700^{\circ}\text{C}$  and the strain rate of  $10^{-3}\text{s}^{-1}$  the alloy displays an increased strain rate sensitivity:  $m=0.42$ . The  $\sigma=f(\dot{\epsilon})$  curve is characterized by the absence of deformation hardening and low flow stresses. At the same time the SP deformation of intermetals has its specific features which distinguish them from metallic materials and are determined by the peculiarities of

their grain boundary structure. A good example of this is provided by the TiAl intermetallic alloy.

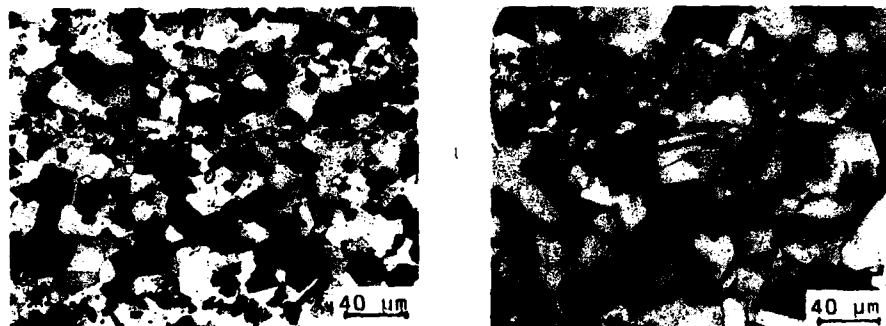


Fig.7 The TiAl alloy microstructure:  
a) state A; b) state B.

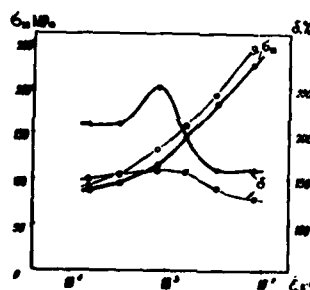


Fig.8 The strain rate effect on the TiAl alloy plasticity and flow stress:  $\delta$  - relative extension to rupture;  $\sigma_{50}$  - flow stress under the 50% straining;  $\bullet$  - state A;  $\circ$  - state B.

The study of the alloy mechanical properties in states A and B which are close in their grain sizes (8 and 9.5  $\mu\text{m}$  respectively), but contain different amount of twin boundaries (A - 5%; B - 35%), indicates the following (Fig. 7,8). In a certain strain rate interval an increased rate sensitivity is observed in state A as against state B. Thus in the rate interval of  $(0.83 \pm 1.6) \cdot 10^{-3} \text{ s}^{-1}$  the state A flow stress sensitivity factor ( $m$ ) varies from 0.33 to 0.43. The largest relative extensions to rupture ( $\delta = 200-250\%$ ) correspond to the interval of high  $m$  values. In state B  $m$  is constant throughout the considered rate interval and equals to 0.26, while relative extension to rupture depends on the strain rate only slightly ( $\delta = 130 \pm 160$ ).

Thus, in state A the TiAl alloy displays SP features, while in state B these features are less pronounced. Fig. 9 shows the  $\sigma=f(\epsilon)$  curves obtained during the extension of the alloy specimens in states A and B in the optimum strain rate interval. It is evident that in the state A alloy the steady flow stage is preceded by a prolonged hardening stage. Such a curve is typical of the low strain rates too. In state B the flow stress peak, characteristic of the dynamic recrystallization process is registered at the initial stage of deformation. With further straining the flow stress decreases monotonously and approaches the same level as that of state A. Such a curve is also observed at high strain rates. From the study of GB absorption properties conducted during the foil annealing in situ in the column of the electron microscope the following data have been obtained. The relaxation temperature ( $t_{rTLD}$ ), i.e. the disappearance of the electron microscope contrast due to TLD, of the twin boundaries has not been determined exactly, but it was found to be above 650°C. The other boundaries have  $t_{rTLD}$  in the interval of 400-550°C.

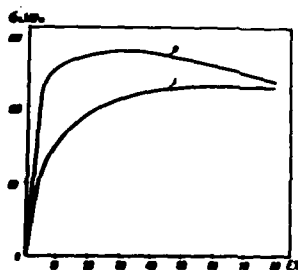


Fig.9 The TiAl alloy stress-strain curves of states A (1) and B (2) ( $t=1025^{\circ}\text{C}$ ,  $\dot{\epsilon}=0.83 \cdot 10^{-3}\text{s}^{-1}$ ).

#### The Superplasticity of Ceramics

Mechanical testing of ceramics based on the  $\text{YBa}_2\text{Cu}_3\text{O}_{7-\delta}$  compound has proved that at a temperature below 650°C ( $0.75 T_{pl}$ ) the failure of ceramics occurs in the elastic region. When the temperature is above 650°C the ceramic compound displays a pronounced plasticity which grows with the rise of temperature. The typical  $\sigma=f(\epsilon)$  curves obtained at different testing temperatures are shown in Fig. 10. The  $\sigma_s$  flow stress decreases with the rise of temperature and the form of the curves changes. At 700 and 800°C, even at the initial stage of deformation,  $\sigma_s$  displays a series of abrupt falls, which is attributed to the formation of vertical cracks in the lateral surface of specimens (see curves 1 and 2). At 900°C or more the  $\sigma=f(\epsilon)$  curves become monotonous. At these temperatures the steady flow stage is preceded by the  $\sigma_s$  peak (curves 3 and 4). In the course of deformation at 900, 930 and 950°C the specimen lateral surface cracking also occurs, but the cracks form an angle of 45° with the compression axis and

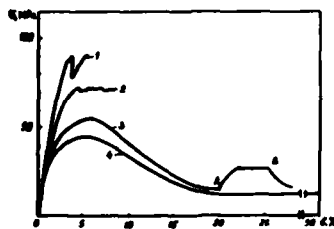


Fig.10 The stress-strain curves, typical of ceramics based on the  $\text{YBa}_2\text{Cu}_3\text{O}_{7-x}$  superconducting compound, at different temperatures of deformation: 1)  $700^\circ\text{C}$ ; 2)  $800^\circ\text{C}$ ; 3)  $900^\circ\text{C}$ ; 4)  $930^\circ\text{C}$ . In the AB interval the strain rate is  $2 \cdot 10^{-4} \text{s}^{-1}$ .

appear at relatively high strains ( $\epsilon \geq 25-30\%$ ). At the same time the specimens preserve their ability to resist straining.

The main feature of SP deformation, i.e. a high strain rate sensitivity ( $m$ ), can be determined at the steady flow stage when the strain rate is changed from  $10^{-4} \text{s}^{-1}$  to  $2 \cdot 10^{-4} \text{s}^{-1}$  ( $m > 0.3$ ), which is accompanied by the  $\sigma_s$  growth from 15 to 28 MPa (Fig.10, curve 3). Besides, the  $\sigma_s$  value at the hardening stage is considerably lower.

Structural investigations have indicated that pores and residuals of unreacted components can be metallographically discovered in the original state alongside with the  $\text{YBa}_2\text{Cu}_3\text{O}_7$  matrix phase (Fig.11a). Their volume fractions, specific for each specimen, vary between 4-7 and 20-40 vol.% respectively. The matrix phase microstructure is essentially laminar. Many laminae have flat patches inside, resembling twin boundaries in metals. The microstructure described is also preserved after the quenching from the temperature of deformation.

During the deformation at 900, 930, and  $950^\circ\text{C}$  the microstructure refining is observed (Fig.11b). The deformation surface analysis at the said temperatures shows that at the initial stage of deformation ( $\epsilon = 8\%$ ) cross boundaries are formed in some laminae. With further deformation ( $\epsilon = 20-25\%$ ) an equiaxial fine grain microstructure is produced in the matrix phase.

The decrease of stress after the  $\sigma_s$  peak, is probably caused by the microstructure refining. Like in metals, the said process in the materials in question can be termed dynamic recrystallization during the hot straining of ceramics has also been stated in (6) where the  $\text{MgO} \cdot 2\text{Al}_2\text{O}_3$  spinel was the case.

Further deformation is accompanied by an active grain bound-

ary sliding (GBS) (Fig. 11b). The sliding accommodation seems to be facilitated by the existence of pores in the original material. A high strain rate sensitivity indicated by the strain rate switch-over experiment and the development of GBS testify to the SP deformation going on in the ceramics under study.

At a higher straining degree the pores were found to be migrating from the center of specimen to its periphery. After the 50% straining has been reached, the central part of a specimen is practically devoid of pores. The coalescence of pores in the peripheral area results in the formation of cracks at the 25-30% straining.

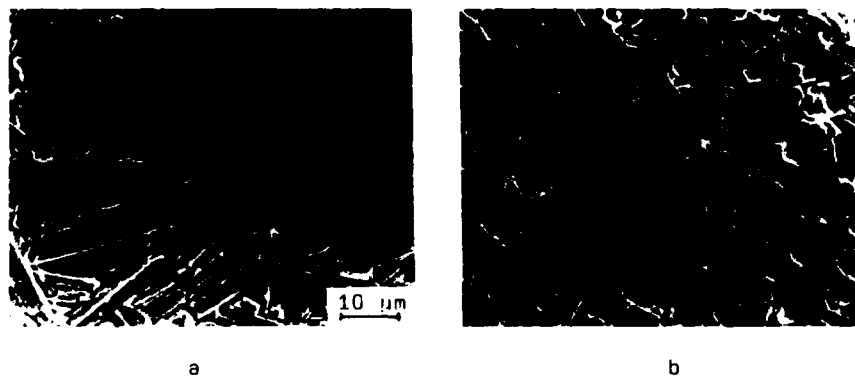


Fig.11 The microstructure of ceramics: a) in the original state (the metallographic specimen is chemically etched); b) as-strained at  $t=900^{\circ}\text{C}$  and  $\epsilon=20\%$  (the deformation surface).

#### Discussion

The main condition for the superplasticity to be displayed in metals and alloys is their having a fine grain microstructure (1-3). However, data presented in this paper and elsewhere (4, 7, 9-12) prove that even originally coarse grain materials can be converted to the SP state immediately during the hot straining. In this case the superplastic flow is usually preceded by dynamic recrystallization whose mechanism greatly depend on the nature of material. For example, the magnesium alloy dynamic recrystallization may be represented by a well known model which includes the migration of some isolated regions of originally high angle grain boundaries, the formation of a developed subgrain structure in boundary regions, a gradual conversion of low angle boundaries to high angle ones (13). It should be emphasized that such a mechanism can operate only if a multiple slip, enhanced in this case by the local elastic stresses, is developing during the deformation in the vicinity of original boundaries. When the distance from the boundaries increases, the said stresses become smaller than  $\tau_{cr}$  for the nonbasic slip systems, hence no subgrains are produced.

Another microstructure refining mechanism operates during the deformation of the VT9 titanium alloy. As it has been already mentioned, due to the existence of semicoherent low-energy interface boundaries the alloy laminar microstructure is rather stable even if subjected to a prolonged annealing. However, in the course of SP hot straining the said microstructure is transformed into a duplex one, which is the result of the conversion of interface boundaries from semicoherent to high angle ones, acceleration of the  $\alpha \rightarrow \beta$  phase change, division of the  $\alpha$ -laminae, and development of GBS (10). A still more complicated mechanism of dynamic recrystallization operating during the material conversion to the SP state has been observed in the TiAl intermetallic alloy where the process of hot straining was accompanied by an active mechanical twinning (11).

The investigation of ceramic materials has shown that dynamic recrystallization and superplasticity consistently develop in them during the hot straining. Thus, in spite of the difference in the actual mechanisms, determined by the nature of crystalline materials, SP flow is usually preceded by dynamic recrystallization.

Another important problem is to find out how the grain boundary structure effects SP flow. The experimental data show a significant influence of original structure on the mechanical properties of the TiAl intermetallic alloy under SP. States A and B are close in their grain sizes and have the same amount, form and arrangement of the  $\alpha$ -phase particles, but their mechanical properties are quite different. This difference in the alloy properties in states A and B seems to be conditioned mainly by the grain boundary structure, in particular by the difference in the number of grain boundaries.

Due to the high mobility of GBS's and according to the grain boundary dislocation kinetics model, the GBS rate is higher in random boundaries than in twin ones (4, 5). At the steady flow stage the GBD density in random boundaries tends to a stationary value, while in twin boundaries the GBS accumulation takes place. That is why a greater number of twin boundaries in state B as against that in state A hinders the development of GBS in the TiAl intermetallic alloy. As a result, the state B alloy has lower values of strain rate sensitivity ( $m$ ) and relative extension to rupture ( $\phi$ ) than those in state A.

Basing on the data obtained we can now assume that for the effect of superplasticity to be displayed it is important that regions occupied in a polycrystal by ordinary grain boundaries with their specific structure should increase. The investigation of the GB absorption properties in TiAl confirms this conclusion. The low absorption capacity of twin boundaries in comparison with that of random ones disturbs the kinetic agreement between the dislocation nucleation and absorption processes which is indispensable for the SP flow development.

Thus, the formation of a fine grain microstructure in metals, intermetals, and ceramics eventually causes the SP flow of these materials under certain temperature-rate conditions, the phenomenological features and structural changes during the SP flow being identical. These facts can be regarded as an indication of the universal character of deformation mechanisms operat-

ing in these materials under the SP flow conditions, no matter how different these materials are in their nature.

#### References

1. O. A. Kaibyshev, Plasticity and Superplasticity of Metals (Moscow: Metallurgia Publ., 1975), 280 p. (in Russian).
2. J. W. Edington, K. N. Melton, and C. P. Cutler, "Superplasticity," Progr. Mater. Sci., 24(1976), 61-158.
3. I. I. Novikov and V. K. Portnoy, Superplasticity of Ultrafine Grain Alloys (Moscow, Metallurgia Publ., 1981), 167 p. (in Russian).
4. O. A. Kaibyshev, Superplasticity of Commercial Alloys (Moscow, Metallurgia Publ., 1984), 163 p. (in Russian).
5. O. A. Kaibyshev and R. Z. Valiev, Grain Boundaries and the Properties of Metals (Moscow, Metallurgia Publ., 1987), 213 p. (in Russian).
6. P. C. Panda and R. Raj, "Superplastic Deformation in Fine-Grained MgO-2Al<sub>2</sub>O<sub>3</sub> Spinel," J. Amer. Ceram. Soc., 68(10)(1985), 522-529.
7. O. A. Kaibyshev, "Current Problems of Superplasticity," Czech. J. Phys., (1988)(in press).
8. Ya. N. Blinovskov et al., "Superconducting Properties of the RBa<sub>2</sub>Cu<sub>3</sub>O<sub>7+y</sub> Compounds," Fizika Metallov i Metallovedenie (FMM), 64(2)(1987), 338-342 (in Russian).
9. N. G. Zaripov, A. R. Vagapov, and R. O. Kaibyshev, "Dynamic Recrystallization of a Magnesium Alloy," FMM, 63(4)(1987), 774-781 (in Russian).
10. O. A. Kaibyshev, R. Ya. Lutfullin, and G. A. Salishchev, "Microstructural Changes during the Laminar Microstructure VT9 Titanium Alloy Heat Treatment and Hot Straining," FMM, 59(3)(1985), 578-583 (in Russian).
11. O. A. Kaibyshev et al., "The Influence of Hot Straining on the Ti-36 wt.% Al Cast Alloy Structure," FMM, 64(5)(1987), 1005-1010 (in Russian).
12. O. A. Kaibyshev, R. M. Imaev, and M. F. Imaev, "Superplasticity of the Ceramic YBa<sub>2</sub>Cu<sub>3</sub>O<sub>7-δ</sub> Compound," Doklady Akademii Nauk SSSR, (1988)(in press)(in Russian).
13. S. S. Gorelik, Recrystallization of Metals and Alloys (Moscow, Metallurgia Publ., 1987), 568 p. (in Russian).



## METALLOGRAPHICAL RESEARCH ON SUPERPLASTICITY

Shigenori Hori and Norio Furushiro

Department of Materials Science and Engineering,  
Faculty of Engineering, Osaka University,  
2-1 Yamadaoka, Suita, Osaka 565, Japan

### Absaract

Metallographical research on superplasticity has been carried out to clarify the role of the grain boundary sliding (GBS) in the deformation. The contribution of GBS to the total strain  $\xi$  was measured first under various conditions of  $m$  ( $\sigma = K\dot{\epsilon}^m$ ,  $\sigma$ :flow stress,  $\dot{\epsilon}$ :strain rate,  $K$ :constant). It has been revealed that the contribution  $\xi$  increased remarkably with an increase of  $m$ . Then, ratio of number of grain boundaries where GBS was detected, to the total number of grain boundaries observed was examined under these conditions. It increased with an increase in the  $m$  value up to about 0.5. At larger values than about 0.5, the ratio was unity. These imply that GBS acts a significant role in the superplastic deformation. The criterion for the superplasticity will be also discussed briefly.

Superplasticity and Superplastic Forming  
Edited by C.H. Hamilton and N.E. Paton  
The Minerals, Metals & Materials Society, 1988

### Introduction

It has been expressed for a long time that the amount of the elongation in superplastic deformation is mainly due to the grain boundary sliding (GBS) process (1,2). However, the contribution of GBS to the total strain  $\xi$  has not been made clear as a function of  $m$  ( $\sigma = K\dot{\epsilon}^m$ ,  $\sigma$ : flow stress,  $\dot{\epsilon}$ : strain rate,  $K$ : constant). Further, it is still unknown whether the GBS takes place at all grain boundaries or not under various conditions of  $m$ . These should be clarified to understand and to establish the deformation mechanism of superplasticity.

Therefore, the objective of the present paper includes the metallographical examination of the dependence on  $m$  for both  $\xi$  and the ratio of number of grain boundaries where GBS was detected, to the total number of grain boundaries observed. It is another object to discuss briefly the criterion for the superplasticity from points of view of the  $m$  value.

### Experimental

Alloys of Al-33wt% Cu and Sn-37.88% Pb were melted and cast under vacuum, respectively. Each composition is close to the eutectic one. The ingot of the Al-Cu alloy was extruded at about 773K into rods of 10mm in diameter, machined to the tensile specimen of gauge length 15mm and diameter 4mm, and then annealed at 808K for 14.4ks. Specimens had fine and uniform structures of equiaxed grains of 5 $\mu$ m.

The ingot of the Sn-Pb alloy was forged and rolled at room temperature, and then annealed at 438K for 3.6ks and quenched into water. It was rolled again at room temperature with 90% reduction in thickness resulting in a sheet of 1mm thickness. Finally, specimens were stored for 2 weeks at room temperature. These had also uniform structures of equiaxed grains sized 6 $\mu$ m.

The contribution of strain due to GBS to the total strain was measured on specimen which was scratched and deformed as described previously (3). The measurements were carried out on photographs taken with an optical microscope.

### Results and Discussion

Figure 1 shows an almost linear relationship between  $m$  and  $\xi$  for both alloys. This reveals that the contribution of GBS is more for the deformation having higher  $m$  value. The behavior of GBS has been examined also for prestrained specimens during the further straining of about 0.3. The prestrain was less than 1.8, followed by polishing and scratching before the final straining of 0.3. Results suggested that GBS contributed similarly to the deformation in any prestrained specimens (4). Therefore, with regard to the mechanism resulting the high elongation, the GBS is considered to play a significant role at any time during superplastic deformation at least up to several hundred percent in elongation.

During evaluation of  $\xi$ , it was realized that GBS did not take place at all boundaries, especially under conditions of low  $m$  value. Therefore, the number of grain boundaries where GBS was detected was examined for specimens of the  $\xi$  experiment and its ratio to the total number of grain boundaries observed was evaluated next. The result shown in Fig. 2 reveals that the ratio increases with an increase in  $m$  and that GBS takes place at all boundaries under  $m \geq 0.5$ .

As a criterion for superplasticity,  $m \geq 0.3$  is adopted often (5,6). This may be introduced from their finding that, for  $m$  greater than about 0.2 to 0.3 (roughly the upper limit for "normal" hot materials), necking resistance increases rapidly with rising  $m$ . "Superplasticity" is characterized by the large elongation and the high strain rate sensitivity of flow stress. It has been shown (3,7) that both of the characteristics

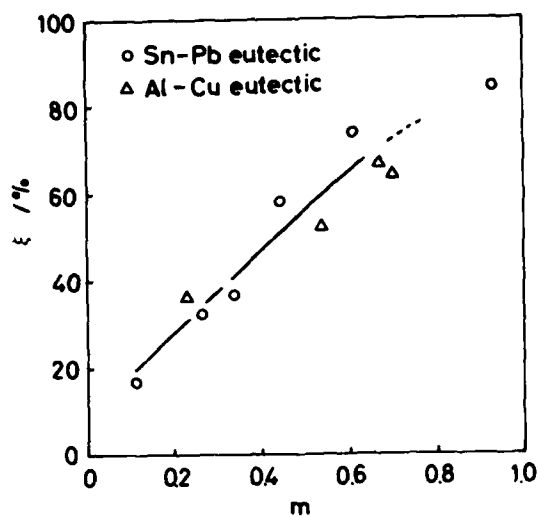


Figure 1 - Relationship between  $m$  and  $\xi$  for the the Al-Cu and the Sn-Pb eutectic alloys deformed up to  $\epsilon=0.3$  under various conditions.

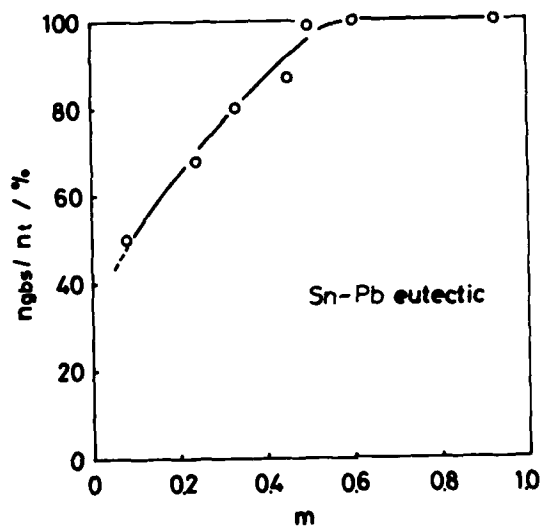


Figure 2 - Relationship between  $m$  and the ratio of number of grain boundaries where GBS was detected  $n_{gbs}$  to the total number of grain boundaries observed  $n_t$  for the Sn-Pb eutectic alloy deformed up to  $\epsilon=0.3$  under various conditions.

resulted from the GBS of the significant process in superplastic deformation. Any criterion should be concerned with the fundamental of the mechanism for a phenomenon considered. Therefore, the criterion for superplasticity is considered to be based on GBS. It is very possible that the condition of  $m \geq 0.5$  recognized reasonably as the criterion for the Sn-Pb eutectic because GBS takes place at all boundaries, as shown in Fig. 2. More experimental support for the criterion may be needed before it can be recognized as the generalized one.

#### Conclusions

Metallographical research on superplasticity was carried out to clarify the role of the grain boundary sliding (GBS) in the deformation. The contribution of GBS in the deformation increased remarkably with an increase in  $m$ . Ratio of number of grain boundaries where GBS was detected, to the total number of observed grain boundaries was estimated and found to increase with an increase in the  $m$  value up to about 0.5. At larger values than about 0.5, the ratio was unity. These imply that GBS acts a significant role in the superplastic deformation. The condition of  $m > 0.5$  has been considered to be a possible criterion for the superplasticity.

#### Acknowledgement

The authors wish to thank Mr. M. Kohno for his experimental collaboration.

#### References

1. P. Shariat, R. B. Vastava and T. G. Langdon, "An Evaluation of Inter-crystalline and Interphase Boundary Sliding in Two-phase Superplastic Alloys," Acta Metall., **30** (1982), 285-296.
2. K. Matsuki *et al*, "Quantitative Metallographic Study on Superplastic Deformation in Zn-Cu-Mn Alloy," Metal Sci., **17** (1983), 503-510.
3. N. Furushiro and S. Hori, "The Role of Grain Boundary Sliding in Superplasticity," Suppl. Trans. Jap. Inst. Metals, The Jap. Inst. Metals, Sendai (1987), 937-941.
4. N. Furushiro, N. Matsuura and S. Hori, unpublished works in Osaka University.
5. W. A. Backofen, I. R. Turner and D. H. Avery, "Superplasticity in an Aluminum-Zinc Alloy," ASM Trans. Quart., **57** (1964), 980-990.
6. D. H. Avery and W. A. Backofen, "A Structural Basis for Superplasticity," ASM Trans. Quart., **58** (1965), 551-562.
7. N. Furushiro and S. Hori, "Direct Determination of the Strain Rate Sensitivity of Flow Stresses Based on Grain Boundary Sliding in a Sn-Pb Eutectic during Superplastic and Non-superplastic Deformation," Scri. Metall., **13** (1979), 653-656.

DIRECT OBSERVATIONS AND MICROMECHANICAL TESTING  
OF SUPERPLASTIC ALLOYS

M.J. Mayo\* and W.D. Nix

Department of Materials Science and Engineering  
Stanford University, Stanford, CA 94305

\*currently at Sandia National Laboratories, Div. 1845  
Albuquerque, New Mexico 87185

Abstract

Recent studies of superplasticity in indentation and torsion are reviewed.<sup>1-3</sup> Indentation results show that grain boundaries are vital to the enhanced strain rate sensitivity of the superplastic alloy studied (Sn-38wt%Pb), but both studies indicate that grain boundary sliding is not responsible for this enhancement and may, in fact, be an artifact of surface conditions. Torsion studies further suggest that a core-mantle model for superplasticity may be more appropriate, for the striking change in grain shape during torsional straining can best be explained by two deformation mechanisms operating simultaneously within each grain. This core-mantle approach can also account for the stress-strain rate relationship exhibited by Sn-38wt%Pb during deformation.

Superplasticity and Superplastic Forming  
Edited by C.H. Hamilton and N.E. Paton  
The Minerals, Metals & Materials Society, 1988

### Introduction

The exact mechanism responsible for superplasticity has long been debated, but one of the predominant beliefs is that deformation does not take place by the extensive straining of individual grains, as in slip creep, but by the simple rearrangement of (essentially) non-deforming grains to conform to the macroscopic shape change of the sample. The details of local accommodation between adjacent, translating grains have yet to be convincingly explained, but the rearrangement process as a whole, often termed grain boundary sliding (GBS), is attractive for two major reasons. First, a mechanism that relies on the existence of grain boundaries explains the universally observed requirement of small grain size (many grain boundaries) for structural superplasticity. Secondly, the GBS mechanism agrees with numerous observations of relative grain motion during superplastic deformation in tension (e.g., refs. 4-6).

Recent experiments of superplastic deformation in indentation and torsion<sup>1-3</sup> have confirmed the need for grain boundaries to achieve superplasticity, but they have placed the significance of GBS in some doubt. This paper reviews the findings of these studies and demonstrates that superplasticity can be described effectively in terms of a core-mantle model instead of a grain rearrangement mechanism.

### Grain Boundary Enhancement of Strain Rate Sensitivity

The primary feature of superplastic materials is their extensive ductility in the superplastic regime of moderate stresses, strain rates, and temperatures. This ductility can in turn be attributed to an anomalously high strain rate sensitivity ( $m$ ) in the regime of interest, typically  $m \geq 0.5$ , which inhibits the material's tendency to neck and hence forestalls premature failure. If a grain boundary-dependent mechanism is responsible for superplasticity, then the presence of grain boundaries must account for this high strain rate sensitivity.

To test this relationship directly, a technique was developed for accurately measuring strain rate sensitivities on a sub-micron scale using the Nanoindenter.<sup>1,2</sup> Then, by varying the grain size with respect to the indentation size, it was possible to obtain strain rate sensitivities for the interiors of individual grains (behavior of the lattice only) as well as for multiple grains (lattice + grain boundaries, i.e., polycrystalline behavior) in Pb, Sn and superplastic Sn-38wt%Pb.<sup>1,2</sup> The data clearly show that the presence of grain boundaries increases the strain rate sensitivity of the material. For example, when 6  $\mu\text{m}$  wide indentations were placed in the centers of 600  $\mu\text{m}$  grains, the strain rate sensitivity of pure Sn was measured at  $m=0.088$ . However, when the grain size of the sample was reduced to 4  $\mu\text{m}$  so that grain boundaries participated in the deformation, the measured strain rate sensitivity increased to  $m=0.159$ . A similar enhancement was demonstrated by small-grained (1.3  $\mu\text{m}$ ) Sn-38wt%Pb, whose strain rate sensitivity was superplastically high at  $m=0.5$ . This value was far greater than would have been predicted from the lattice-only behavior of its constituent phases ( $m=0.125$  for Pb and  $m=0.117$  for Sn). In further tests, Sn-38wt%Pb of a slightly larger grain size (3.5  $\mu\text{m}$ ) showed that an intermediate number of grain boundaries present resulted in an intermediate strain rate sensitivity,  $m=0.385$ . In fact, for all cases tested, the presence of grain boundaries correlated highly with increased strain rate sensitivity.

### Grain Boundary Sliding

Despite proving that grain boundaries contribute significantly to the high  $m$  values characteristic of superplasticity, the indentation tests<sup>1,2</sup> also provided evidence that grain boundary sliding was not the cause of this enhanced strain rate sensitivity. Figure 1 shows the variation in indenter descent rate which is observed when indenting superplastic Sn-38wt%Pb. The sudden increase in descent rate is attributed to GBS, for the depth at which it occurs corresponds reasonably well with the appearance of dark outlines of grain shape near the indentation. Scanning electron microscopy revealed these to be grains which had slid along their boundaries so as to tilt downward toward the indentation. The relevant feature of Figure 1, however, is not that GBS is seen to occur, but that it seems to stop almost as rapidly as it starts: after its initial plunge, the indenter comes to a virtual halt as if the grains, once having slid and tilted, had now become stuck on each other. If, indeed, the sudden decrease in indenter descent rate marks the cessation of the GBS mechanism, then it is

significant to note that the superplastic values of  $m$  for the Sn-38wt%Pb sample were calculated from data taken well after the sliding event. Thus GBS may have ceased, but not superplasticity.

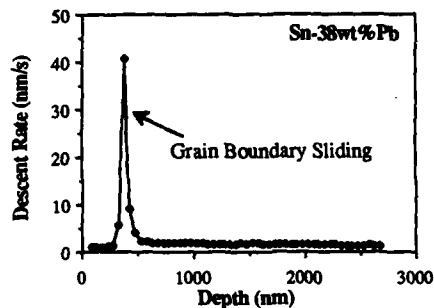


Figure 1 - Sudden variation in indenter descent rate during indentation of Sn-38wt%Pb.

difference between the two deformation modes, though, is that in torsion, grains are constrained in the surface plane, for the gage section does not increase in area during testing. Unlike tension, room does not become available on a continual basis for the surface grains to slide past each other if they wish to do so. Thus in-plane sliding is prohibited in torsion, and it is only in the radial direction that GBS can occur. Even then, as in indentation, GBS in this direction halts when the grains have tilted sufficiently to become "stuck". Nevertheless, in torsion as in indentation, the high  $m$  values characteristic of superplastic deformation are maintained even after GBS on the sample surface is observed to cease. The authors speculate that GBS is simply a surface artifact, for its cessation does not appear to affect the deformation behavior of the sample as a whole. Furthermore, the torsion and indentation observations indicate that GBS occurs only under conditions in which a certain degree of spatial freedom is available to the grains, and this requirement is met primarily at the sample surface, and then most easily in tensile deformation.

#### Core-Mantle Deformation

If GBS cannot be considered responsible for the high strain rate sensitivities associated with superplasticity, then another mechanism is required. One candidate for this other mechanism is suggested by observations of grain morphology conducted on the superplastically deformed Sn-38wt%Pb torsion samples.<sup>1,3</sup> After GBS was exhausted on the sample surface, the grains took on an inverted hourglass shape composed of a relatively undeformed grain core and highly deformed "ligaments" extending from the grain boundary region in the direction of maximum elongation (Figures 2 and 3).

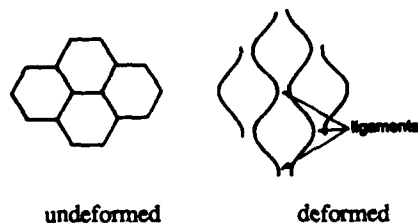


Figure 2 - Schematic illustration of the grain shape evolution observed in torsionally deformed Sn-38wt%Pb.



Figure 3 - Sn-38wt%Pb microstructure after torsional deformation to 1.18 true strain. Line indicates axial direction; arrows, the sense of shear.

Ligaments were easy to recognize, not only from their unusual aspect ratio, but also from their organic, "gooey" appearance. Evidence of ligaments persisted beneath the sample surface, as heavily re-polished samples attested, so it is unlikely that the unusual grain morphology was a surface artifact. The fact that, within any given grain, the near-boundary, or mantle, region seemed to be deforming much more rapidly than the grain core suggested that two power law behaviors--two mechanisms--were controlling deformation in the two different regions.

Additional torsion experiments<sup>1,3</sup> indicated that at low stresses and strain rates (Regime I), mantle processes dominated, for a larger proportion of the grain volume was devoted to ligament formation. At high stresses and strain rates (Regime III), ligament formation was suppressed, and the grains elongated uniformly, in a rigid manner visually reminiscent of the deformation of grain cores in Regime II. Thus a model of superplasticity began to emerge in which core processes dominated deformation in Regime III, mantle processes dominated in Regime I, and both processes operated in Regime II, the superplastic regime. Regime II thus seemed to be a transition between the other two regimes.

#### A Core-Mantle Model

A full core-mantle model accounting for the observed grain shape changes, as well as the stress-strain rate relationship, exhibited by Sn-38wt%Pb in all three regimes has been developed.<sup>1</sup> The main features of the model are as follows. The increased rate of deformation in the grain mantles is attributed to grain boundary-enhanced dislocation climb, a suitably fast process with a strain rate sensitivity of  $m=0.25$ . This is considered to be the mechanism responsible for Regime I behavior and is consistent with Sn-38wt%Pb data in that regime. On the other hand, the core behavior dominant in Regime III is ascribed to "normal" slip processes, that is, the slip processes that would normally occur in the lattices of the given phases were no grain boundaries present. For Sn-38wt%Pb, the behavior of the alloy was estimated from creep experiments performed on large-grained (few grain boundary effects) pure Sn, the dominant phase in alloy deformation. This method correctly predicted the strain rate sensitivity of Regime III to be  $m=0.125$ . The argument that lattice processes alone control Regime III behavior is supported by the fact that Sn-38wt%Pb alloys of many grain sizes all converge to the same power law behavior in Regime III.<sup>7</sup>

In Regime II the balance between core and mantle processes within a grain is determined by the fraction of dislocations able to travel freely to the grain boundary (and participate in grain boundary enhanced dislocation climb) vs. the fraction which become embroiled in interdislocation reactions and never escape the grain core. Since the probability of interdislocation reaction is proportional to the number of dislocations already in the grain, the fraction,  $f$ , of dislocations which do not interact and hence pass freely to the grain boundary is simply  $f=1/N$ . This term has an inherent stress dependence of  $f \propto \sigma^{-2}$ . Finally, the transitional behavior of Regime II is modelled as an isostress average of core and mantle behaviors; the strain rate is therefore given by

$$\dot{\epsilon}_{II, \text{superplastic}} = f \dot{\epsilon}_{I, \text{mantle}} + (1-f) \dot{\epsilon}_{III, \text{core}}. \quad (1)$$

The result of this averaging process is an impressive prediction of Sn-38wt%Pb deformation behavior in the superplastic regime, with the typical, high strain rate sensitivity of  $m=0.5$ . The one flaw in the model, as it currently stands, is that it does not predict the grain size dependence of stress in Regime I. This dependence must be estimated before an accurate prediction of Regime II behavior can be made.

#### Core-Mantle Behavior in Tension

If a core-mantle process is indeed responsible for superplastic deformation, then the question arises as to why such deformation, as characterized by ligament formation, is so ubiquitous in the torsional observations but has remained largely unnoticed in tension. The reasons for this are several. First, it is simply more difficult to observe superplastic morphologies in tension than in torsion. As Figure 4 illustrates, shear occurs through the thickness of a tensile sample as well as along the sample face. This shear continually causes heavily deformed grains from the specimen interior to emerge onto the surface plane, where they obscure observation. In torsion, by contrast, all deformation which affects the surface plane is confined to that plane (no radial strains), and a



cleaner, more easily observed microstructure is produced. Indeed, the authors have recreated classic observations of superplastic deformation in tension<sup>1,3</sup> and noted that ligaments are visible on the surface of tensile samples but that they are obscured by the confusing sea of heavily deformed, recently-emerged grains in which they lay.

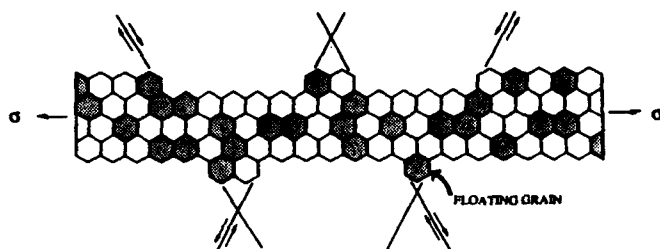


Figure 4 - Sheet tensile specimen viewed in cross-section; the upper and lower edges correspond to the faces of the sample. "Floating" grains can be produced by the combined action of shear on alternate planes.

The existence of ligaments in tension was also revealed upon gallium-fracturing a sample previously deformed 1,324% in tension.<sup>1,3</sup> In this instance, the ligaments were not as preferentially oriented, nor as long in any particular direction, as those observed in torsion or on the tensile sample surface. This was to be expected, however, because of the three-dimensional nature of straining within the tensile sample interior.

Thus ligaments do exist in tension, but they are more difficult to observe. Another reason for the historical lack of ligament observations in tension may be that, in large strain studies, attention was centered instead on "floating grains". Figure 4 shows how shear on alternate planes through the specimen thickness can combine so as to push a surface grain to the extreme surface. As its name implies, this "floating grain" is now free to drift along the sample surface without being constrained by, or participating in, bulk deformation processes. Since these floating grains retain their pristine shape, they would tend to be chosen more often as exemplars in large strain studies in which most grains are too deformed to be recognizable. Floating grain artifacts do not exist in torsion, where through-thickness shear has been eliminated.

In small strain tensile studies the problems associated with advanced through thickness shear are minimized, but ligaments in these studies would also be easy to ignore because they simply are not developed enough to be noticed by the observer. Also, small strain studies have historically focussed on grain boundary sliding, which the current studies suggest may be a surface artifact.

#### References

1. M. J. Mayo, "A Study of Superplasticity in Indentation and Torsion" (Ph.D. dissertation, Stanford University, 1988).
2. M. J. Mayo and W. D. Nix, "A Micro-Indentation Study of Superplasticity in Pb, Sn, and Sn-38wt%Pb," to be published in *Acta Met.*
3. M. J. Mayo and W. D. Nix, "Direct Observation of Superplastic Flow Mechanisms in Torsion," submitted to *Acta Met.*
4. G. Rai and N. J. Grant, "Observations of Grain Boundary Sliding During Superplastic Deformation," *Met. Trans.* 14A (1983) 1451-1458.
5. R. B. Vastava, T. G. Langdon, "An Investigation of Inter-crystalline and Interphase Boundary Sliding in the Superplastic Pb-62%Sn Eutectic," *Acta Met.* 27 (1979) 251-257.
6. A. E. Geçkinli, "On the Rate Controlling Mechanism Operative During Superplastic Flow" (Ph.D. dissertation, Stanford University, 1973).
7. D. Grivas, K. L. Murty, and J. W. Morris, Jr., "Deformation of Pb-Sn Eutectic Alloys at Relatively High Strain Rates," *Acta Met.* 27 (1979) 731-737.

**INVESTIGATION OF REGION I IN RAPIDLY SOLIDIFIED  
POWDER ALUMINUM ALLOYS**

G. S. Murty\* and M. J. Koczak\*\*

\*Department of Metallurgical Engineering  
Indian Institute of Technology  
Kanpur - 208016, India

\*\*Department of Materials Engineering  
Drexel University, Philadelphia, PA 19104, U.S.A.

Abstract

Despite numerous studies of superplastic behavior in several alloys, the origin of region I of low rate sensitivity remains uncertain. In this study the characteristics of region I were investigated in Al - Ti and Al-Zn-Mg-Cu-Mn alloys processed by the rapid solidification / powder metallurgy route. Different grain sizes in a narrow range were obtained through coarsening treatments following the powder processing of the alloys. While the microstructures were characterized by transmission electron microscopy, their superplastic behavior was assessed by the strain rate change test. Region I of low rate sensitivity is observed to be dominant in these ultrafine grained alloys. A drop in flow stress as the grain size increases and an anomalously high activation energy for flow are observed in this region. Since these observations are consistent with the concept of a threshold stress for superplastic flow, the threshold stress is estimated making use of an extrapolation procedure. The origin of the grain size and temperature dependent threshold stress is suggested to be the inhibition of grain boundary migration by fine particles during grain boundary sliding in superplastic flow.

Superplasticity and Superplastic Forming  
Edited by C.H. Hamilton and N.E. Paton  
The Minerals, Metals & Materials Society, 1988

### Introduction

The stress - strain rate plots of a typical superplastic material are divided into three regions; the intermediate region II of maximum strain rate sensitivity is the superplastic region. The loss in rate sensitivity in regions I and III limits the strain rate range in which superplastic forming is possible. An understanding of the factors responsible for these regions of low rate sensitivity is essential in exploiting the superplastic forming characteristics. While the region III behavior is a consequence of the dominance of dislocation creep, region I remains unexplained despite numerous studies. The suggested interpretations of region I are (i) a threshold stress for superplastic flow (1), (ii) a distinct flow mechanism (2,3) and (iii) concurrent grain growth (4) during deformation. The concurrent grain growth effect cannot account for the observation of region I when the strain rate change test is conducted on a single test specimen in the increasing sequence of crosshead speeds (5). Moreover, concurrent grain growth can be minimized by testing under stable microstructural condition. In this regard, Al alloys processed by the rapid solidification / powder metallurgy route are of special interest. Making use of such powder processed Al-Ti and Al-Zn-Mg-Cu-Mn alloys, wherein an ultrafine grain size is stabilized by fine dispersoids, the characteristics of region I were investigated in this study.

### Experimental details

Two alloys (an Al - 4 wt% Ti alloy and a 7075 Al alloy modified with the addition of Mn) processed by the rapid solidification / powder metallurgy route were investigated. Their composition, processing and microstructural details are available elsewhere (6,7). Different grain sizes were obtained by coarsening the microstructures of the initially powder processed alloys. Making use of cylindrical compression specimens of 6mm diameter and 9mm height, strain rate change tests were performed on an Instron machine at elevated temperatures. The grain size was assessed by transmission electron microscopy.

### Results and Discussion

A typical microstructure of these alloys with an ultrafine grain size which is stabilized by dispersoids, is illustrated in Fig.1. The elevated temperature response indicated a transition from region I to superplastic region II. A typical stress ( $\sigma$ ) - strain rate ( $\dot{\epsilon}$ ) plot and the corresponding strain rate sensitivity index ( $m = d \log \sigma / d \log \dot{\epsilon}$ )

$d \log \dot{\epsilon}$ ) versus  $\dot{\epsilon}$  plot are shown in Fig.2. From grain size measurements before and after the strain rate change tests, the deformation induced coarsening was noted to be negligible in these alloys. The steady state stress - strain rate data of region I were analyzed by the relation

$$\dot{\epsilon} = K \left( \sigma^{-1/m} / d^p \right) \exp \left( - Q / RT \right) \quad (1)$$

where K is a constant, d the grain size, p the grain size exponent, Q the activation energy, R the gas constant and T the absolute temperature. The activation energy for flow thus obtained is in the range of 350 - 795 KJ/mol, which is anomalously high relative to the self-diffusion activation energy for Al. On comparing the stress - strain rate plots for various grain sizes, there is a cross-over in the grain size dependence of flow stress between regions I and II, as illustrated in Fig.3. The above features of region I favor its interpretation in terms of a threshold stress ( $\sigma_0$ ) for superplastic flow rather than a distinct flow mechanism. Replacing the applied stress by an effective stress ( $\sigma_e = \sigma - \sigma_0$ ) and assuming the typical value of m as 0.5 for superplastic region, the threshold stress was assessed by an extrapolation procedure as shown in Fig.4. The temperature and grain size dependence of the threshold stress thus obtained was assessed by an empirical relation

$$\sigma_0 = (K_1 / d^p) \exp \left( Q / RT \right) \quad (2)$$

where K is a constant. The Q value thus obtained is in the range of 30 - 80 KJ / mol, which is similar to that for grain boundary diffusion in Al. A grain size exponent of unity is in close agreement with the observations.

Since extensive grain boundary sliding (GBS) occurs during superplastic flow, the threshold stress may arise from the inability of the grain boundaries to act as perfect sinks and sources for point defects or the inhibition of GBS by the dispersoids at the grain boundaries. The interaction between the grain boundary dislocations and dispersoids is the basic source of threshold stress as per the above considerations. The temperature and grain size dependence cannot, however, be predicted on this basis. Alternatively, the origin of the threshold stress may arise from the restricted mobility of the grain boundaries during grain boundary sliding. It is often experimentally observed that grain boundary migration accompanies sliding. The results of computer simulation of sliding confirm that GBS and boundary migration are coupled processes on an atomic scale (8). The Zener pinning of the boundaries by second phase particles can then result in a threshold stress, which varies inversely with the grain size. Since the boundary migration is a thermally activated



Fig.1.  
Electron micrograph  
representing the  
microstructure of Mn  
modified 7075-Al  
alloy coarsened for  
100 hours at 525°C  
after powder  
processing.

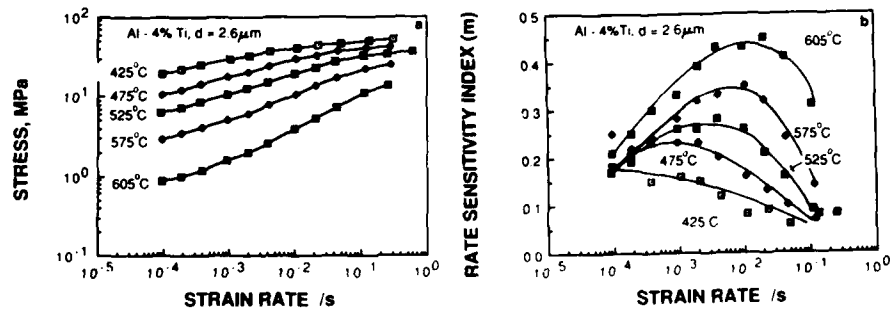


Fig.2.(a) Stress-strain  
rate and (b) Rate  
sensitivity index-strain  
rate plots (Al-4 wt.% Ti,  
 $d=2.6 \mu m$ )

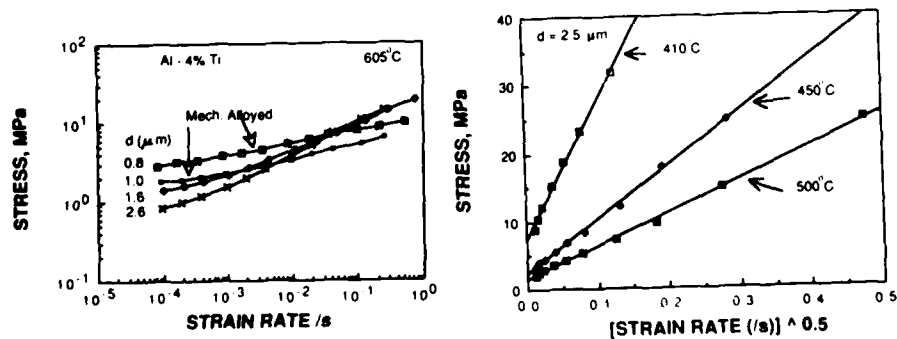


Fig.3. The effect of grain  
size on stress-strain rate  
behavior in Al-4 wt.%Ti  
alloy.

Fig.4. Plot showing the  
extrapolation procedure to  
estimate threshold stress  
for the Mn modified 7075 Al  
alloy.

process, the threshold stress arising from this is also expected to be temperature dependent. However, the problem of quantitative prediction of threshold stress on this basis remains to be considered.

### Conclusions

1. The flow stress in region I of low strain rate sensitivity is observed to decrease as the grain size increases.
2. The activation energy for flow in region I is anomalously high.
3. A grain size and temperature dependent threshold stress as assessed by an extrapolation procedure accounts for the above characteristics of region I. The threshold stress is interpreted in terms of the inhibition of boundary migration by particles during grain boundary sliding.

### References

1. "Superplasticity" Ductility(Metals Park,OH: American Society for Metals, 1968) 279-310.
2. F.A. Mohamed and T.G. Langdon, "Creep at low stress levels in the superplastic Zn-22 % Al eutectoid" Acta Metall., 23(1975) 117-124.
3. F.A. Mohamed and T.G. Langdon, "Creep behaviour in the superplastic Pb-62% Sn eutectic" Phil. Mag.,32 (1975) 697-709.
4. G.Rai and N.J.Grant, "On the measurements of superplasticity in an Al-Cu alloy" Metall. Trans. A,6 (1975) 385-390.
5. R.S. Mishra and G.S. Murty, "Effect of concurrent grain growth on the stress-strain rate curve of superplastic materials" J. Mater. Sci. Letters, (In press).
6. G.S.Murty and M.J.Koczak, "Superplastic behavior of an Al-4 wt.% Ti alloy processed by the powder metallurgy route" Mater. Sci. Eng.,100 (1988) 37-43.
7. G.S. Murty and M.J. Koczak, "Investigation of region I of a superplastic Al-Zn-Mg-Cu-Mn alloy",Mater. Sci. Engg.,96 (1987) 117-124.
8. J.W.Christian, P.Haasen and T.B.Massalski, eds.,Progress in Materials Science Chalmers Anniversary volume (Oxford, U.K. Pergamon Press, 1981), 49 G.H. Bishop Jr., et al.

## THE MECHANISM OF SUPERANELASTICITY AND ITS IMPLICATIONS

R. I. Todd and P. M. Hazzledine

Department of Metallurgy and Science of Materials,  
Oxford University,  
Parks Road, Oxford, OX1 3PH, U.K.

### Abstract

The very large anelastic strains observed after superplastic deformation have previously been explained by a model in which deformation-induced voids sinter once the load is removed. Recent experiments, however, have shown that large anelastic strains can also be recovered when cavitation is not present, implying that there is a second mechanism which occurs at constant volume. This mechanism is believed to be a form of Coble creep driven by the reduction in grain boundary energy as elongated grains resume their equiaxed shapes. Although previously discarded on the grounds that the resulting strain rates would be too slow and of the wrong form unless an unreasonably large spread of grain sizes were present [1], it is shown here that these deficiencies in the theory need not apply if the shape changes of the grains are those necessary to accomplish grain neighbour switching. In this paper the predicted time for anelastic straining to saturate and the influence of grain size, temperature, stress and prior loading time on this quantity are tested against experiments on fine grained Zn-Al eutectoid alloy. These particular predictions were chosen because they are almost independent of unknown details such as the exact geometry of the switching event and the distribution of grains at different stages of this operation. The agreement found between theory and practice indicates that superanelasticity is a universal feature of superplastic alloys, being intimately connected with the grain neighbour switching which must occur during flow, and is therefore not confined to cavitating conditions. Study of superanelasticity provides a potentially powerful method of studying the "unknown details" of grain switching mentioned above. Its proportionality to stress, for example, indicates that the number of grains involved in switching is also proportional to the stress, or that the distribution of grains at different stages of the process changes significantly with stress. Anelasticity could also reduce the tolerance of components produced using superplastic forming if they are annealed for long periods afterwards. The same mechanism may explain the anelasticity observed in as-cast solder, which has recently been shown to have a potentially strong effect on the fatigue lives of soldered joints.

*Superplasticity and Superplastic Forming*  
Edited by C.H. Hamilton and N.E. Paton  
The Minerals, Metals & Materials Society, 1988

### Introduction

Schneibel and Hazzledine [1] and Vale [2] showed that several superplastic alloys exhibit very large anelastic contractions (>100 times the elastic strain) upon removal of a tensile load, and interpreted it in terms of the sintering of deformation induced cavities. Ridley, Livesey and Mukherjee [3] observed the same effect by measuring the variation in density of superplastic alloys after deformation. The anelastic strain,  $\epsilon_{an}$ , depends on stress,  $\sigma$ , loading time,  $t$  and grain size,  $L$ , according to the approximate relation:

$$\epsilon_{an} \propto \frac{\sigma t^n}{L} \quad \text{where } 1/4 < n < 1/2 \quad (1)$$

Some superplastic alloys, however, show anelasticity under conditions where cavitation does not occur [4,5]. Recent experiments in this department [6] have proved that both superplastic and anelastic deformation can occur at constant volume, indicating that a second anelastic mechanism operates.

### An Alternative Mechanism

The fact that grains remain approximately equiaxed and retain their identity during deformation implies that grains must change their neighbours. At constant volume this in turn demands a transient increase in grain boundary area. The change in interfacial energy could drive a partially completed switching event to completion or back to its starting position by Coble creep and grain boundary migration if the stress is removed, causing an anelastic strain. Relaxation from the "critical position", at which a non-equilibrium number of grain boundaries meet, would be extremely rapid in the early stages as the diffusing atoms would be removed from a grain face of very small area. The Lee model [7] for grain switching (fig.1) is useful for illustrating this idea as it is relatively simple to analyse and definitely predicts a net anelastic strain from a large number of switching events because all the strain takes place before the critical position is reached. An approximate analysis for an infinite array of hexagonal prisms of height  $L_0$  relaxing back towards position (a) from a starting point between (a) and (c) gives an expression:

$$t = \frac{kTL_0^4}{32D_b\delta\Omega\Gamma} \left[ \frac{2}{3} \ln \left( \frac{L_i^2 - L_0^2}{L^2 - L_0^2} \right) - 3 \ln \left( \frac{L_i}{L} \right) + \frac{L_i^2 - L^2}{6L_0^2} \right] \quad (2)$$

for the time taken for the grains to contract from an initial length  $L_i$ , to  $L$ , as defined on the figure,  $L_0$  being the equilibrium length of the grains,  $\Gamma$  the grain boundary energy, and  $D_b$ ,  $t$ ,  $\delta$ ,  $\Omega$ ,  $k$  and  $T$  having their usual meanings. Plots of  $\ln \Delta L$  versus  $\ln t$  for various values of  $L_i$ , where  $\Delta L$  is the change in grain length from that at  $t=0$ , are shown in fig.2, using physical values for zinc [2,10] with a grain size of  $1\mu\text{m}$  at  $150^\circ\text{C}$ . As the

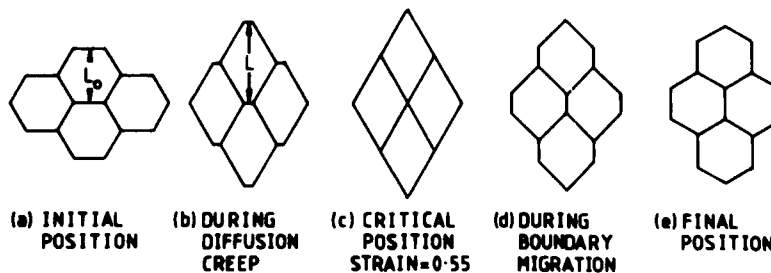


Fig.1: The Lee Grain Neighbour Switching Mechanism.



curves show, starting points near the critical position ( $L_i = L_0/3$ ) give curves with a steadily reducing gradient of 0.5-0.25, as observed by Schneibel and Vale. The maximum contraction possible from this mechanism is 0.55, which is about two orders of magnitude greater than contractions obtained in practice; this is not a problem, as for one thing, only a small fraction of the grains would be expected to be involved in switching at any one time.

Although the shape of the curves is encouraging, it is not a very good test of the theory because the precise form of measured contractions varies with experimental conditions, and the predicted contraction must depend on the real topological details of the grain switching mechanism and the distribution of grains at different stages of the process, of which nothing is known.

Fortunately, measurement of the time required for the contraction effectively to cease provides a simple but substantial test of the theory, as this removes these unknowns from consideration. At saturation  $L$  is very close to  $L_0$ , so the geometrical term in brackets in eq.2 becomes dominated by a term in  $\ln(L^2 - L_0^2)$ , and the initial position of the grains is unimportant as fig.2 shows. The distribution of grains in different positions does not, therefore, affect the saturation time, which is proportional to  $T$  and  $L_0^4$ , inversely proportional to  $D_0$  and independent of stress and loading time. Furthermore, this result holds whatever the exact geometry of the switching mechanism, so the second unknown is also dispatched.

Testing the validity of the suggested mechanism for anelasticity by this method also has considerable experimental benefits in that the onset of steady state flow and distortion of the results by bending of the specimen are unimportant to the measurement of the saturation time, so the substantial scatter in the results of previous experiments should be improved upon.

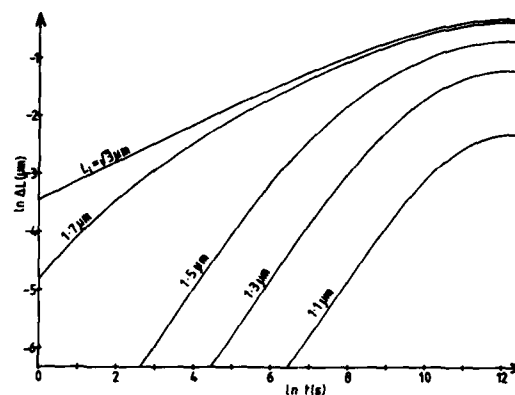


Fig.2: Predicted Plots of  $\ln \Delta L$  versus  $\ln t$  for various initial positions. Constants for Zn, 150°C,  $L=1\mu\text{m}$ .

### Experimental

Tensile specimens were punched from commercially produced nominally eutectoid Zn-Al sheet. The actual composition of the alloy was found to be 76.6±0.5wt% Zn, 0.1% Si, 0.05%Fe, bal.Al. The specimens were annealed under argon at 363°C for 18 hours and then quenched into an ice/water mixture. Different grain sizes were obtained by annealing for various times at temperatures between 180 and 230°C; very fine grain sizes were used to give reasonably small projected saturation times at moderate temperatures and to minimize the risk of void formation [4]. Specimens were strained at constant load in a creep rig suspended in an electrically heated bath of silicone fluid. Loading stresses of between 0.84 and 3.74 MPa were imposed on the specimens for times between 30 and 1000 minutes, at temperatures of 150 and 180°C. Two specimens were used for each set of conditions, one of which was allowed to contract until the anelasticity had clearly saturated and the other of which was removed from the oil bath immediately after unloading and cooled to -20°C. Polished sections of all specimens were prepared and the

mean linear phase intercepts (MLPI) were estimated from scanning electron micrographs taken in backscattered mode.

### Results

Plots of  $\ln \epsilon_{an}$  against  $\ln t$  were constructed for each of the relaxing specimens, from which the saturation time was estimated.

Comparison of the MLPI's of specimens which had and had not been allowed to relax revealed that grain growth had occurred during relaxation in all cases. This was accounted for by using grain growth data for this alloy [8] to estimate the average value of MLPI<sup>4</sup> during the contraction period.

All the results were plotted as  $\ln t_s$  against  $0.25 \ln \langle \text{MLPI}^4 \rangle$  as shown in fig.3. Each point is associated with pessimistic error bars. The lines of best fit (solid) have gradients of 3.73 at 150°C and 4.47 at 180°C. Best fit lines with the predicted gradient of 4 are shown dashed, and can be seen to lie well within the error bars for all the points. No systematic variation in proximity to the lines of best fit is observable with loading time or stress, as the theory predicts. An activation energy of  $58 \pm 13 \text{ kJ/mol}$  can be calculated from eq.2, which is close to the value for grain boundary diffusion in zinc of  $61 \text{ kJ/mol}$ .

Assuming MLPI is approximately equal to the mean linear grain intercept and converting this to a spatial grain diameter by multiplying by 1.74 [9] gives an upper limit to the grain size. Using data for zinc taken from Vale [2] and a grain boundary energy for zinc of  $0.34 \text{ J/m}^2$  [10], the absolute values of the theory's predicted saturation times are within a factor of 1.5 in excess of the experimental best fit lines of gradient 4. This quality of agreement is probably somewhat fortuitous when the errors in the parameters used for the calculations are considered, but does at least demonstrate that the theory predicts values of sensible magnitude.

### Discussion

All the predictions of the theory have been borne out by experiment to a degree well within experimental error. It would be very difficult to explain this combination of results by any other known mechanism; the sintering void theory in particular, is incapable of explaining the insensitivity of the saturation time to loading time and stress.

If this mechanism is accepted, the study of anelasticity can be used to gain insight into the mechanism of superplastic flow. For instance, the fact that the magnitude of the anelastic strain (but not its saturation time) depends strongly on the loading stress shows that details of the deformation process must change significantly with stress; one possibility that would explain the observed stress dependence is that the number of grains involved in switching is proportional to the applied stress, but more complex possibilities also exist, such as a change in the relative number of grains at different stages of switching. Such changes may occur with different grain sizes or

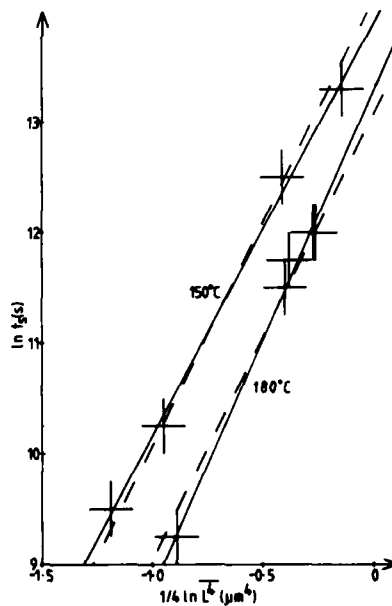


Fig.3: Log-Log Plot of Saturation Time vs. Effective MLPI. Solid Line=Best Fit, Dashed=Best Fit Gradient 4.

temperatures as well, but insufficient results are available at the present time to make meaningful conclusions in this respect.

This work also has more direct potential applications. One of the advantages of superplastic forming is its high tolerance, owing to the small elastic strains produced by the low forming stresses; if a prolonged period of annealing follows forming this advantage may be lost as anelastic recovery takes place.

Recent work on the fatigue of solder joints, such as occurs in electronic packages, has concluded that anelasticity may have a strong influence on joint life at different cycle frequencies [11]. Independent work [12] has shown that anelastic strains of more than 10 times the elastic strain can be produced in as-cast Sn-Pb solder, and that the kinetics of the contraction are similar to those observed in superplastic specimens. This mechanism, albeit on a more limited scale could, therefore, also provide an explanation for this observation.

#### Acknowledgement

RIT would like to thank the SERC for financial support.

#### References

- [1] J.H.Schneibel and P.M.Hazzledine, "Superanelasticity in Superplastic Sn-Pb Alloys," Acta Met., 30 (1982) 1223-1230.
- [2] S.H.Vale, "Anelasticity in Fine Grained Materials," Acta Met., 32 (1984) 693-706.
- [3] N.Ridley, D.W.Livesey and A.K.Mukherjee, "Effect of Cavitation on Post-Deformation Tensile Properties of a Superplastic Copper-Base Alloy," Met. Trans. A, 15A (1984) 1443-1450.
- [4] D.W.Livesey and N.Ridley, "Effect of Grain Size on Cavitation in Superplastic Zn-Al Eutectoid," J.Mat.Sci., 17 (1982) 2257-2266.
- [5] C.W.Humphries and N.Ridley, "Effect of Relatively Hard Particles on Cavitation of Microduplex Pb-Sn Eutectic During Superplastic Flow," J.Mat.Sci., 12 (1977) 851-853.
- [6] S.A.Wolton, Thesis, Oxford University, 1987.
- [7] D.Lee, "Structural Changes During Superplastic Deformation," Met.Trans., 1 (1970) 309-311.
- [8] A.O.Sepulveda and R.S.Mishra, "An Analysis of Grain-Growth Data in Duplex Materials on Static Annealing and During Superplastic Deformation," J.Mat.Sci., 22 (1987) 2153-2157.
- [9] A.W.Thompson, "Calculation of True Volume Grain Diameter," Metallography, 5 (1972) 366-369.
- [10] M.C.Inman and H.R.Tipler, "Interfacial Energy and Composition in Metals and Alloys," Metall. Reviews, 8 (1963) 105-166.
- [11] R.C.Weinbel et al., "Creep Fatigue Interaction in Eutectic Lead-Tin Solder Alloy," J.Mat.Sci., 22 (1987) 3901-3906.
- [12] A.P.Moore, R.I.Todd and R.W.Elston, "Solder Modelling for SMT" (Paper Presented at CHMT-IEEE VLSI Packaging Workshop, Paris, 17-18 November 1986).

THE ROLE OF GRAIN BOUNDARY DISLOCATIONS  
DURING SUPERPLASTIC DEFORMATION OF AN ALUMINUM ALLOY

Shanyou Zhou, Liqin Wang, and Chin Liu

Department of Materials Science and Engineering,  
Shanghai Jiao Tong University, Shanghai 200030,  
The People's Republic of China

Abstract

In order to determine the role of grain boundary dislocations (GBDs) during superplastic deformation, the GBD structures in a fine grained superduralumin alloy have been investigated by means of transmission electron microscopy before and after superplastic deformation. The results show that during superplastic deformation, extrinsic GBDs were created through the interactions between lattice dislocations and grain boundaries. The strong interactions between GBDs and intergranular precipitates and between GBDs and grain boundary triple junctions led to the formation of GBD pile-ups. GBDs could move along grain boundaries by the glide-climb process. The glide component of the motion led to grain boundary sliding (GBS), while the climb component of the motion led to a diffusive flux and related diffusional creep, which could accommodate the grain boundary sliding strain. The reason that deformation in Region II occurred mainly by GBS while those occurred in Region I and III are not, is also discussed.

Superplasticity and Superplastic Forming  
Edited by C.H. Hamilton and N.E. Paton  
The Minerals, Metals & Materials Society, 1988

### Introduction

GBS plays a vital role in superplastic deformation [1]. For the conditions of peak superplastic behaviour, GBS contributes up to 80% of the total strain [2]. Some models concerning the mechanism of superplastic deformation based on GBDs moving along grain boundaries which leads to grain boundary sliding have been proposed [3][4]. However, very few structural evidences of the motion of GBDs during superplastic deformation have been provided. Recently, we have chosen LC4 super duralumin as the testing material in which insoluble fine disperse particles are present and can act as internal pinning points for dislocations. The evidence for GBDs movement has been successfully observed under the transmission electron microscope, and the role of GBDs during superplastic deformation have been clarified.

### Experimental Details

Tensile specimens with a gauge length of 15 mm were cut along the rolling direction from a LC4 super duralumin alloy sheet of 1.5 mm thickness with an average grain diameter of 6.8  $\mu\text{m}$ . Its chemical composition is given in Table I. The tensile tests were performed in air at  $505 \pm 3^\circ\text{C}$ . Specimens for optical and transmission electron microscope examinations were prepared from the deformed tensile specimens within the gauge length by standard techniques. The H700H type of TEM with an operating voltage of 200 KV were used.

Table I. The Chemical Composition of the Test Material

Elements	Zn	Mg	Cu	Mn	Cr	Fe	Si	Al
wt. %	5.7	2.7	1.57	0.33	0.11	0.39	0.19	Balance

### Results and Discussion

The  $\log \dot{\epsilon}$  -  $\log \epsilon$  plot for the material tested at  $505^\circ\text{C}$  is shown in Fig.1. The  $n$  values of the curve in Region I and Region III are  $\leq 0.3$ , whereas that in Region II (the superplastic region) is about 0.5. The strain rates of Region II are in the range from  $1.5 \times 10^{-4} \text{s}^{-1}$  to  $2.5 \times 10^{-3} \text{s}^{-1}$ .

A high temperature micrograph of a polished but un-etched specimen deformed superplastically at  $500^\circ\text{C}$  to 25% strain is shown in Fig.2. We can see that the grain boundaries can be revealed by the superplastic deformation, as the result of GBS and grain rotation of the material. Metallographic observation has shown that superplastic deformation can lead to the formation of precipitate-denuded zones adjacent to the grain boundaries (Fig.3). These precipitate-denuded zones were formed by diffusional creep. By means of quantitative metallography, we found that the contribution from diffusional creep to the total superplastic strain was 15%.

The structure of the specimen before deformation is typical of recrystallized materials, in which there are no dislocations within grains, and grain boundaries have no peculiarities and look like sets of thickness extinction contours (Fig.4). After superplastic deformation, there are some dislocations distributed within grain [Fig.6 (a)], and GBD pile-ups widely distributed are observed along grain boundaries [Fig.6 (a) and (b)]. Fig.6 (a) also shows that the GBDs are connected with the lattice dislocations, this implies that the observed GBDs are the extrinsic GBDs created by the interactions between lattice dislocations and the grain boundaries. The GBD

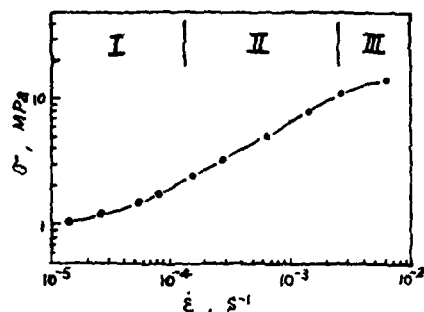


Fig.1 The  $\log\sigma$ - $\log\dot{\epsilon}$  plot for the experimental material tested at 505°C



Fig.2 High temperature micrograph of a polished but un-etched specimen deformed superplastically at 500°C. Tensile axis horizontal.  $\dot{\epsilon}=6.66 \times 10^{-4} \text{ s}^{-1}$ ,  $\epsilon=25\%$



(a)  $\epsilon=80\%$



(b)  $\epsilon=400\%$

Fig.3 The precipitate-denuded zones observed after superplastic deformation.  $T=505^\circ\text{C}$ ,  $\dot{\epsilon}=6.66 \times 10^{-4} \text{ s}^{-1}$ . Tensile axis horizontal



Fig.4 TEM micrograph of the experimental material before deformation



Fig.5 TEM photograph of the experimental material after 50% tensile strain in Region I at 505°C.  $\dot{\epsilon}=1.11 \times 10^{-4} \text{ s}^{-1}$

pile-ups are formed due to the interactions between GBDs and intergranular precipitates or grain boundary triple junctions and the obstructing action of intergranular precipitates or grain boundary triple junctions to the motion of GBDs along grain boundaries. Under the obstructing action, the GBDs must bypass the intergranular precipitates either through Orowan mechanism of glide/climb over the particle/matrix interface. In our research, no evidence for the formation of Orowan loops was observed, it is thus implied that the bypass must occur through glide/climb over the particle/matrix interface. Grain boundary triple junctions are other major obstacles to the motion of GBDs, and can be described as follows: when a GBD passed through a triple junction, a dislocation reaction is generally required. It includes decomposition or combination for forming new GBDs which are compatible with the structure of one or both of the other two boundaries. Since the dislocation reaction may be energetically unfavorable and the first formed new dislocations may exert a back stress on the triple junction, thus further dislocation reactions may be restricted and the passage of the GBDs through a triple junction can be hindered.

From the configuration and distribution characteristic of dislocations in the GBD pile-ups shown in Fig.6 (b), we can see that dislocations in the GBD pile-up are in a state of moving along the grain boundary during superplastic deformation. Because the Burgers vectors of the GBDs are generally at some angle to the local grain boundary plane, the motion of GBDs along grain boundary must occur through a glide/climb process. The glide component of the motion will lead to GBS, and the climb component of the motion will lead to a diffusive flux and induce diffusional creep, which will be able to accommodate the GBS strain. For alloys containing fine dispersed particles on a solid solution matrix, diffusional creep will lead to the formation of precipitate-denuded zones adjacent to grain boundaries. These precipitate-denuded zones can be used as a structural evidence for diffusional creep

We have also found that, strain rate has great influence on the GBD structure of the deformed specimen. For instance, when the strain and deformation temperature were 50% and 505°C respectively, with an initial strain rate of  $6.66 \times 10^{-4} \text{s}^{-1}$  (Region II), the mean spacing of dislocations in GBD pile-ups was about 0.1-0.2  $\mu\text{m}$  [Fig.6 (b)]. Whereas when an initial strain rate of  $1.11 \times 10^{-4} \text{s}^{-1}$  (Region I) was adopted, the dislocation density was very low, many grains and grain boundaries were dislocation-free (Fig.5). On the contrary, when an initial strain rate of  $1.18 \times 10^{-2} \text{s}^{-1}$  (Region III) was adopted, both intragranular and the GBD densities were high, there were dislocation tangles within grains [Fig.7 (a)], and the GBDs were in an intersected state [Fig.7 (b)].



Fig.6 TEM photographs of the experimental material after superplastic deformation in Region II at 505°C,  $\dot{\epsilon}=6.66 \times 10^{-4} \text{s}^{-1}$  (a)  $\epsilon=20\%$  (b)  $\epsilon=50\%$

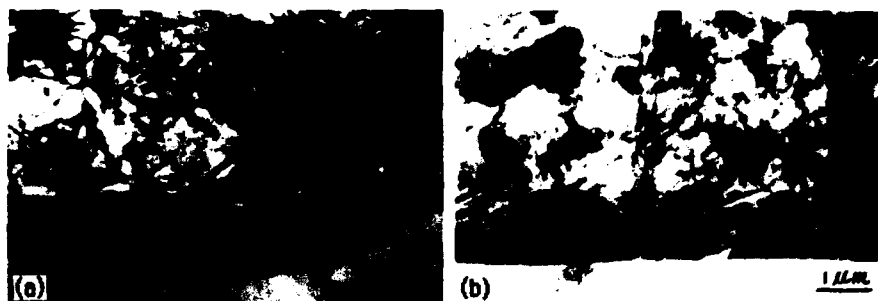


Fig.7 TEM photographs of the experimental material after 50% tensile strain in Region III at 505°C.  $\dot{\epsilon}=1.18 \times 10^{-2} \text{s}^{-1}$

According to the results mentioned above, we can consider superplastic deformation as a process of GBDs moving along grain boundaries. These GBDs are created mainly by interactions between lattice dislocations and the grain boundaries. Moving of GBDs along grain boundaries is a glide/climb process; it not only leads to GBS which is the major strain-providing mechanism during superplastic deformation, but also leads to a diffusive flux and induces diffusional creep which can accommodate the GBS strain. The strain rate of superplastic deformation is determined by the velocity of the GBDs along grain boundaries and is controlled by the climb process through self diffusion of atoms. When tensile deformation is performed within Region I, since the flow stress is too low to create enough extrinsic GBDs, deformation proceeds mainly by diffusional creep rather than GBS. When tensile deformation is performed within Region III, since the flow stress is too high, intragranular slip must occur on multiple slip systems and leads to dislocation intersection. As a result of this, dislocation tangles will form within grains, and the dislocations within GBD pile-ups will be in an intersected state. Under this condition, GBS for the deformation is difficult and the deformation proceeds mainly by dislocation creep rather than GBS. Only when the deformation is performed within Region II, the flow stress is appropriate. That is to say, sufficient extrinsic GBDs can be created by interactions between lattice dislocations and the grain boundaries. Since the flow stress is low, the slip within grains can occur only on one slip system. Under this condition, dislocations both within grains and within grain boundaries are not intersected. Therefore GBDs can move along grain boundary rather successfully and induce extensive GBS, so that a steady superplastic deformation process without apparent strain hardening can be obtained in the material.

#### Acknowledgement

This work was supported in part by the Committee of Chinese National Science Foundation under Grant No. 5860297.

#### References

1. D.M.R.Taplin, G.L.Dunlop and T.G.Langdon, *Aun. Rev. Mater. Sci.*, 9 (1979) 151.
2. K.Matsuki and M.Yamada, *J.Jap. Inst. Met.*, 37 (1973) 448.
3. A.K.Mukherjee, in "Grain Boundaries in Engineering Materials," J.L.Walter et al ed., Claitor Publishing, Baton Rouge, LA, 1975, P.93.
4. R.C.Gifkins, *Metall. Trans.*, 7A (1976) 1225.
5. B.Burton, in "Diffusional Creep of Polycrystalline Materials," Trans. Tech. Publications, 1977, P.71.



THE PHYSICAL MODEL OF SUPERPLASTICITY BASED  
ON THE NOTION OF NONEQUILIBRIUM GRAIN BOUNDARIES

R. Z. Valiev

Institute of the Metal Superplasticity Problems,  
USSR Academy of Sciences, Ufa, USSR

Abstract

Cooperative mechanisms of deformation, such as grain boundary sliding, intragranular dislocation motion, and diffusion creep, operating simultaneously under superplasticity (SP), enable the application of the notion of nonequilibrium grain boundaries to the description of the SP effect. A physical interpretation and quantitative evaluation of the SP materials mechanical properties characteristic features has been given. The suggested SP model is especially important for the development of the SP materials properties control methods, and for the realization of the so called "low temperature" SP effect.

Superplasticity and Superplastic Forming  
Edited by C.H. Hamilton and N.E. Paton  
The Minerals, Metals & Materials Society, 1988

### Introduction

It is universally acknowledged that such grain boundary (GB) processes as sliding, migration, diffusion, and GB's operating as sources and sinks of lattice dislocations play a decisive role in the display of SP. The nonequilibrium state of GB's due to mobile grain boundary dislocations (GBD) is of special significance here [1,2]. Such nonequilibrium GB's are formed during the dissociation of lattice dislocations in GB's and/or generated immediately in GB's. A sharp acceleration of kinetic processes, i.e. sliding and diffusion, occurring in nonequilibrium boundaries is important for the realization of SP. A new model of structural superplasticity based on these ideas has been suggested.

### The SP Model

The new model is essentially a development of a well-known hardening-and-recovery conception applied to the description of the SP behaviour, based on the knowledge of the actual GB processes. From the point of view of this conception SP can be displayed in case the hardening is insignificant while the rate of recovery is rather high. The former condition can be met if the polycrystal grain boundary sliding (GBS) is accompanied by a slight accommodation. The latter condition is determined by an active dynamic recovery developing in GB. At the microlevel these processes can be represented by the scheme shown in Fig.1.

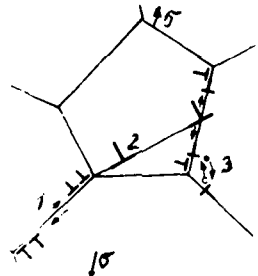


Figure 1 - Scheme of main deformation processes developing during SP deformation.  
1: grain boundary dislocations; 2: lattice dislocations; 3: local diffusion flow;  
 $\sigma$ : applied stress.

The start of deformation here is connected with the generation and motion of GBD's whose pile-ups in triple points initiate the generation of lattice dislocations. Passing through the grain interior dislocations are again caught and absorbed by the boundaries, which results in the enhancement of GBS and diffusion.

A system of equations describing the microscopic behaviour [4] can be obtained using the hardening-and-recovery conception. In particular the traditional plot of  $\dot{\epsilon} = f(\sigma)$  is presented in the following way:

$$\dot{\epsilon} = \frac{A}{KT} \left( \frac{\sigma - \sigma_0}{G} \right)^2 \left( \frac{b}{d} \right)^2 D_0 e^{-Q/KT} \quad (1)$$

and for the SP flow stress at the given strain rate it is:

$$\sigma_T \approx \sigma_i + d \sqrt{\frac{1.25 \cdot KTG \cdot \dot{\epsilon}}{DQ}} \quad (2)$$

where  $A = \frac{QG}{1.25 \cdot b^2}$ ;  $d$  - grain size;  $Q$  - grain boundary diffusion activation energy;  $\sigma_i$  - the GBD source operating stress, equal in this case to the lattice dislocation generation stress.

The suggested model renders a possibility to describe a number of SP effects which had no satisfactory description before. Among them are the considerable non-linear elasticity, the flow stress drop after a short time deformation at higher rates, the active grain growth, etc./4/. This model has proved to be of special importance for the development of SP materials properties control methods.

#### Properties Control Methods

The conception of the decisive role of GB processes in the display of SP, which is being developed, emphasizes the significance of GB state, i.e. nonequilibrium, type of boundaries, impurities. This statement agrees well with the data available/5,6/. Thus, in /5/ it has been shown for the first time that in the Al-alloy the domination of boundaries, close to special ones, results in the increase of the flow stress by more than 30% as against the same alloy with random boundaries dominating in its structure, grain size being the same in both cases. For the Ni-superalloy the demand that GB processes should contribute to the display of SP is realized in the fact that these alloys can be converted to the SP state under the condition that, alongside with the obtaining of fine grains, the coherent  $\gamma$ - $\gamma'$  interface boundaries should be transformed into the random  $\gamma$ - $\gamma'$  high angle interface ones (Fig.2).

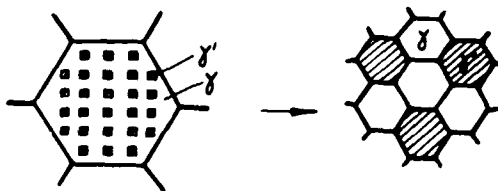


Figure 2 - Diagram illustrating the way Ni-superalloy structure is changing when converted to the SP state.

The suggested physical model has recently enabled the prediction and discovery of the "low temperature" SP effect /7/. Taking into account its importance for application we should like

to give a detailed consideration of this phenomenon

### "Low Temperature" Superplasticity

According to the model conceptions, the process which controls the SP flow is grain boundary diffusion. That is why the decrease of the SP temperature can be obtained by means of a considerable reduction of grain size. The fact is that the existence of submicron grains limits the mass transfer; besides, in materials of this kind GB's are highly nonequilibrium in their structure, which results in the sharp acceleration of grain boundary diffusion [2/].

This statement has received an experimental confirmation in the course of the Al-4%Cu-0.5%Zr alloy deformation, the grain size being about 0.3  $\mu\text{m}$ . The mechanical properties and structural changes of the same alloy with the grain size of about 8  $\mu\text{m}$  have been profoundly studied in [5/]. When strained at 500°C and at the rate of  $10^{-4} \cdot 10^{-3} \text{s}^{-1}$  this alloy displays typical SP features (see the Table).

Table. Al-4%Cu-0.5%Zr Alloy SP Deformation Conditions and Parameters

Grain size	T°C	SP Modes		SP Parameters	
		$\dot{\epsilon} = \text{s}^{-1}$	$\sigma, \text{MPa}$	$m = \frac{d \cdot \lg \sigma}{d \cdot \lg \dot{\epsilon}}$	$\delta, \%$
8	500	$3 \cdot 10^{-4}$	13	0.50	800
0.3	220	$\sim 10^{-4}$	27	0.48	>250

In the initial stage preceding the SP deformation the alloy structure contains equiaxial grains with the mean linear size of about 0.3  $\mu\text{m}$  and practically no dislocations. This structure is rather stable; no grain growth is observed during annealing at 220°C for 2 hours. It starts only at the temperatures above 250°C.

Mechanical testing has indicated that at temperatures below 220°C strain rates were too low to be registered experimentally ( $\dot{\epsilon} < 10^{-6} \text{s}^{-1}$ ). In order to provide strain rates, close to those usually observed under SP, the following mode of deformation was selected: T=220°C,  $\sigma=27 \text{MPa}$ . Data concerning the mechanical properties parameters measured under the said conditions are presented in the Table. Unfortunately we have failed to measure the maximum value of the specimen relative extension to rupture because of the limited extension travel. Data presented in the Table indicate that the submicron grain alloy displays typical SP behaviour, its properties at 220°C being close to the SP properties of the 8  $\mu\text{m}$  grain size alloy at 500°C.

The electron-microscopic studies have indicated that structural changes during the submicron grain alloy straining are those

typical of the SP materials; as-strained grains remain equiaxial, the structure is devoid of dislocations, a slight grain growth is observed too. Thus, after the 100% extension the alloy grain size was 0.5  $\mu\text{m}$ .

Thus, due to the submicron grain structure formation the alloy under study displayed typical SP behaviour. Up to now the SP effect has never been observed in Al-alloys at temperatures below 450°C /6/. That is why the SP effect displayed at 220°C may be termed a "low temperature" superplasticity. The generality of phenomenology and structural changes during both the submicron alloy SP deformation and "ordinary" SP deformation may imply the existence of common mechanisms providing for the SP flow in both cases and the possibility of their description in the framework of the suggested model. However, it is the problem of diffusion role and development in the relatively low temperature interval that is most stimulating.

Proceeding from equation (1) and using the data of the Table, the ratio of diffusion factors under both "ordinary" and "low temperature" deformation can be evaluated. This ratio is found to be  $10^3$ . The decrease of GB diffusion factor which is expected when temperature drops from 500°C to 200°C can easily be calculated too. Taking into account the exponential dependence on temperature (D), the following ratio is obtained:  $D_{500^\circ\text{C}}/D_{220^\circ\text{C}} = 5 \cdot 10^4$ .

Thus, during the submicron grain alloy deformation we are dealing with a pronounced acceleration of GB diffusion in the low temperature interval when the diffusion factor is by 1.5 order higher (with reference to that of the "ordinary" SP deformation). It is probably this abnormal increase of diffusion in the submicron grain structure alloy that enables the display of low temperature SP. Diffusion may also be caused by a considerable nonequilibrium of grain boundary structure in the submicron grain materials due to the high density of GBD's. As has been stated above, the submicron grain structure was in fact obtained in the alloy by means of fixing the initial stage of recrystallization, but in this case GB's are in a highly nonequilibrium state. Besides, a sharp acceleration of kinetic processes is observed in the latter. This point of view agrees well with the conception of nonequilibrium GB structure and properties /2/, but needs further justification for submicron materials.

#### References

1. M. W. Grabski, "Mechanical Properties of Internal Interfaces," J. de Physique, 46(C-4)(1985), 537-580.
2. R. Z. Valiev, V. Yu. Gertsman, and O. A. Kaibyshev, "Grain Boundary Structure and Properties under External Influences," Physica Status Solidi (a), 97(11)(1986), 11-56.
3. R. Z. Valiev et al., "The Nature of Grain Boundary Sliding and the Superplastic flow," Physica Status Solidi (a), 78(2)(1983), 439-448.

4. O. A. Kaibyshev, R. Z. Valiev, and A. K. Emaletdinov, "Deformation Mechanisms and the Theory of Structural Superplasticity of Metals," Physica Status Solidi (a), 90(1985), 197-206.
5. R. Z. Valiev et al., "Grain Boundary Structure and Superplasticity of Al-alloys," Fizika Metallov i Metallovedenie, 62(1) (1986), 180-186 (in Russian).
6. O. A. Kaibyshev, Superplasticity of Commercial Alloys (Moscow: Metallurgia, 1984), 264 p. (in Russian).
7. R. Z. Valiev et al., "Low Temperature Superplasticity of Metallic Materials," Doklady Akademii Nauk SSSR (in press) (in Russian).

SUPERPLASTIC BEHAVIOR OF Zn-20Al-2Cu AT ROOM TEMPERATURE

AND DEFORMATION MECHANISMS

G. Torres Villaseñor<sup>1</sup> and J. Negrete<sup>2</sup>

<sup>1</sup>Instituto de Investigaciones en Materiales  
Universidad Nacional Autónoma de México  
Apdo. Postal 70-360, 04510 México, D. F.

<sup>2</sup>Instituto de Metalurgia  
Universidad Autónoma de San Luis Potosí,  
San Luis Potosí, S. L. P. México

Abstract

The eutectoid Zn-Al alloy modified with 2% Cu, shows superplastic behavior when tested in tension at room temperature at constant strain rate of  $10^{-3}$ /sec. The maximum deformation reached was 200% with an "m" value of 0.34. Scanning electron microscope "in situ" observations of the deformation, shows that some big grains of zinc are chopped during the deformation, and some new material emerge to the surface to fill the gap. Some slip bands were observed in a few zinc grains, making  $45^\circ$  with the tension axis. Transmission electron microscopy of deformed specimens, led us to conclude that some hard aluminum grains break zinc or aluminum grains during the deformation. In this way an aluminum grain can surpass another grain during the deformation. Some evidence of this mechanism is presented.

Superplasticity and Superplastic Forming  
Edited by C.H. Hamilton and N.E. Paton  
The Minerals, Metals & Materials Society, 1988

## Introduction

One of the basic problems in superplastic deformation is to explain the process by which very large macroscopic strains, are produced in the specimen with almost no microscopic changes in the shape of the grains. At first sight, the Ashby-Verrall (1) grain switching mechanism has been attractive for explanation of this basic problem, although in its details it has been subject to criticism (2). The theory is a two dimensional model and as Gifkins (3) has pointed out, the grain switching process must be modified to account for the increase in surface area with strain. The model proposed by Gifkins is a 3-dimensional model which matches the observation that new surface is created during extension of the specimen but grain size remains unchanged. A new group of adjacent sliding grains, would open up a fissure on the free surface, as the deformation continues a new grain emerges at the surface to fill the gap. Grain boundary migration occurs at the same time as emergence in order to restore grain boundary dihedral angles; this result in the rounding of the emergent grain and curvature of all other grain boundaries, the process is regenerative to higher elongations. This process has been examined critically (4) and there is a lack of experimental observations.

In the present work the deformation of a fine grained alloy Zn-20 wt% Al-2 wt% Cu, was observed "in situ" by SEM at room temperature. The microstructure of the deformed specimens was studied by TEM.

## Microstructure and Mechanical Properties of the Alloy

Tensile specimens were cut from sheets of the Zn-20Al-2Cu alloy. The specimens were annealed for one hour at 533°K to give an average grain diameter of 2  $\mu$ m and then tested at room temperature on an Instron 1125 testing machine having a constant rate of cross-head displacement.

The experimental results are shown in Fig. 1a. The addition of 2 to 2.5%Cu to the eutectoid Zn-Al alloy increases its ductility at room temperature. The curve flow stress as a function of the strain rate, exhibits the characteristic sigmoidal shape of the superplastic material with a slope  $m = 0,34$  in the region II. The curve percentage elongation at fracture, as a function of strain rate indicate that the elongation to failure increases from 20% at high strain rates to a maximum of 180% in the middle region, and then decreases again for lower strain rates. The data therefore demonstrate very clearly that this material shows a superplastic behavior at room temperature. There is an optimum range of strain rate for maximum ductility in the way it has been found for the eutectoid Zn-Al at higher temperatures.

In all cases, during the deformation the stress-strain curves shows an oscillatory behavior. Fig. 1b.

## "In Situ" Deformation

Tensile specimens with the appropriate dimensions (16 mm long, 2 mm wide, 0,5 mm thick) to fit in the tensile stage of a JEOL T-20 SEM, were cut and annealed as described before. Pictures were taken as deformation took place at a strain rate of  $10^{-3}$ /sec. It was observed following some scratches on the surface that grain sliding is a main mechanism of deformation at room temperature of this alloy. The shape of the grains did not change even at high deformations (140%). At the beginning of the deformation some slip lines were observed making near 45° with the tensile axis, when deformation reaches 10% some fissures are observed inside of a conglomerate of zinc grains and they become apparent when deformation reaches 21%, Fig. 2b. These fissures do not propagate by the specimen to produce fracture. As the deformation progress, they get wider without increasing its length by the migration of



the two parts of the fractured grain in opposite directions parallel to the tensile axis. After 80% deformation Fig. 2c, several small grains of less than 2 microns coming from the bottom of the crack start to fill up the region in between the two parts of the grain. Higher deformations (up to 140%) exposes a bigger portion of the boundary facet and more grains are observed to move to the surface Fig. 2d. In addition to these grains that emerge, the lateral contraction of the specimen pushes some grains from the rim of the fissure, contributing to restore the surface. A similar behavior was observed in the cracks produced in a Fe-Al phase present in a few places of the specimen Fig. 3. It is noteworthy the fact that the cracks originated in this brittle phase do not affect the fracture behavior of this material. The same mechanism is expected to work in fissures originated by the separation of smaller grains, although it was not clearly observed. In order to study the emergence of the grains under a more controllable conditions, some small cracks were induced on the surface of a set of specimens using a razor blade. In all cases, the artificial cracks were ignored by the material and in some occasions the rupture of the specimen was initiated at the place, indicating that a fissure on the surface is not enough for the emergence of new grains.

#### Transmission Electron Microscopy Observations

Specimens for TEM were prepared from the deformed specimens and observed in a JEOL-200B electron microscope. In all the observed specimens the grains were equiaxed and almost free of dislocations Fig. 4. The number of subgrain boundaries is higher in the deformed specimen than in the non-deformed one. The way in which this subgrain boundaries were produced can be explained from Fig. 5a. In this figure an aluminum grain hits a zinc grain. The stress concentration at the contact point, induces a subgrain boundary in the target grain, in other cases Fig. 5b the target grain is fractured. Using this type of mechanism a hard grain can surpass an obstacle during the superplastic deformation, the stress concentration can produce either, grain fracture or activation of a slip plane. In both cases grain refinement is produced. This mechanism is very likely to occur in this two phase alloy where one phase is very weak (Zn-rich phase) and the other is a precipitation hardened alloy (Al-rich phase). The precipitates that strength the aluminum has been observed by high resolution transmission electron microscopy (5).

#### Discussion and Conclusions

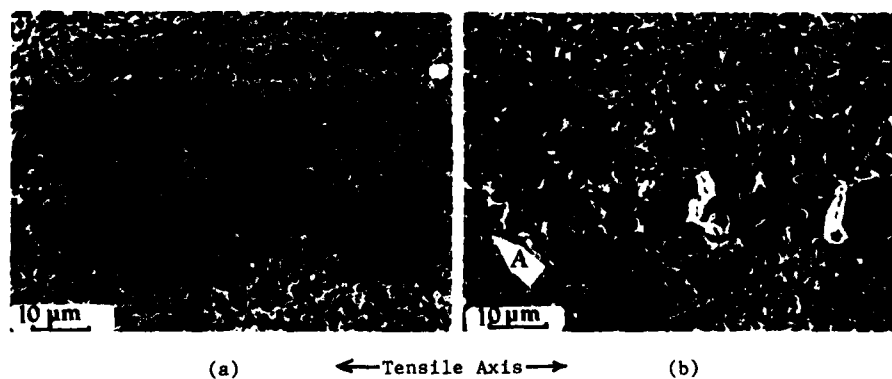
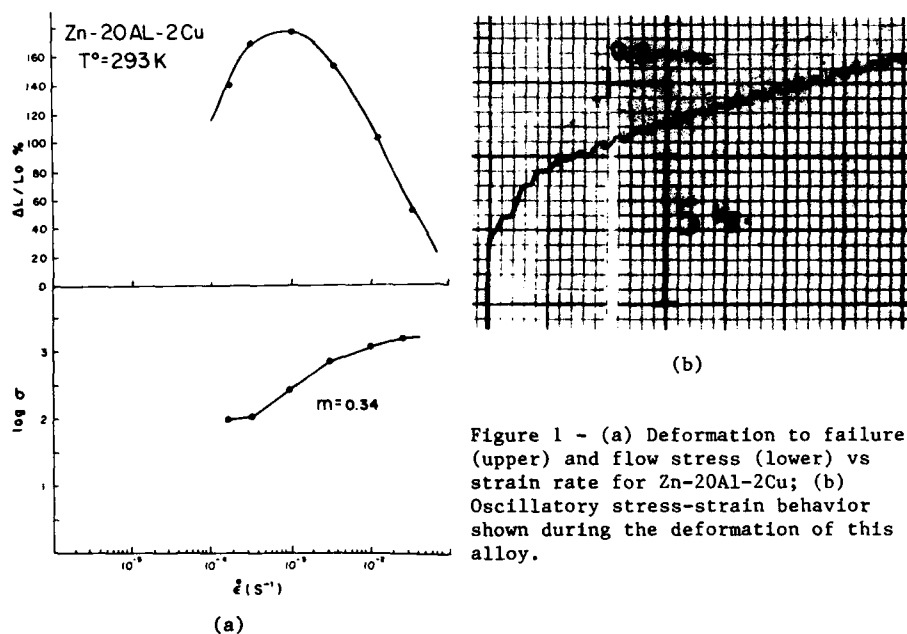
Copper additions of some 2 to 2.5% to the eutectoid Zn-Al increases its ductility at room temperature. The observed deformation mechanism and its stress vs strain rate and strain vs strain rate behavior, indicates that the alloy behaves superplastically at room temperature. "In situ" observations of the deformation show that a mechanism similar to that proposed by Gifkins for superplastic deformation takes place in this alloy. The initiation of the proposed fissure can be located at regions where the grains move apart by grain boundary sliding or cracks originated inside brittle phases produced by impurities such as Fe or Si.

In the studied alloy, the material that fills the fissure between grains is not a single grain, as was originally proposed by Gifkins, but a conglomerate of fine grains that moves to the surface. These grains are smaller than the original grain size observed before deformation. Fig. 2d shows that all the surface of the specimen after deformation is composed of grains that are finer than the initial ones. A mechanism that could explain this "grain refinement" inside the specimen is the grain cutting produced when a hard grain is stopped by a weaker grain. The stress concentration produced on the weak grain can fracture it or induces slip. At any case the hard grain will surpass the obstacle producing grain refinement.

It is possible that the observed oscillatory stress-strain behavior, be originated by a simultaneous cutting of soft grains by a set of hard grains distributed in the specimen.

#### References

1. M. F. Ashby and R. A. Verrall, *Acta Metall.*, 21 (1973) p. 1926.
2. A. H. Chokshi, T. G. Langdon, "Superplasticity", Conference Internationale, Grenoble, France, B. Baudalet Editor 1985, p. 2.1
3. R. C. Gifkins, *J. Mat. Sci.*, 13 (1978) p. 1926.
4. T. G. Langdon, *Metals Forum*, 4 (1981) p. 14.
5. G. Torres-Villaseñor, G. Van Tendeloo (In press) *Physica Status Solidi*.



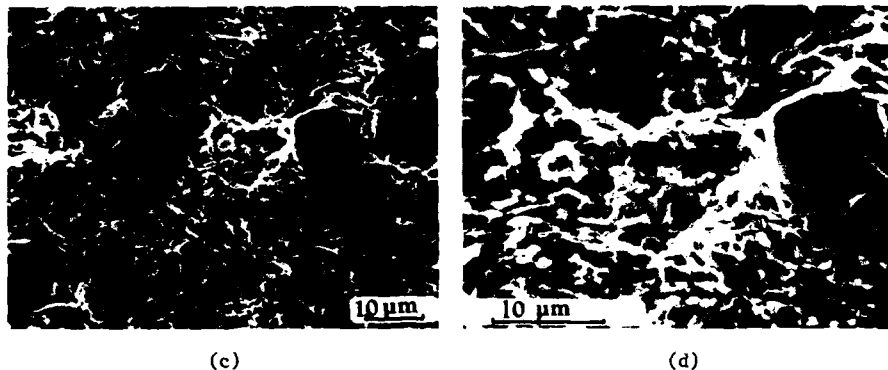


Figure 2 - "In situ" observation of the deformation stages. a) Initial structure. b)  $\epsilon = 0.21$ . The grain separation is apparent. Some slip lines are observed at "A". c)  $\epsilon = 0.80$ . Several small grains emerge to fill the gap between grains. d)  $\epsilon = 1.40$ . The surface is almost restored.

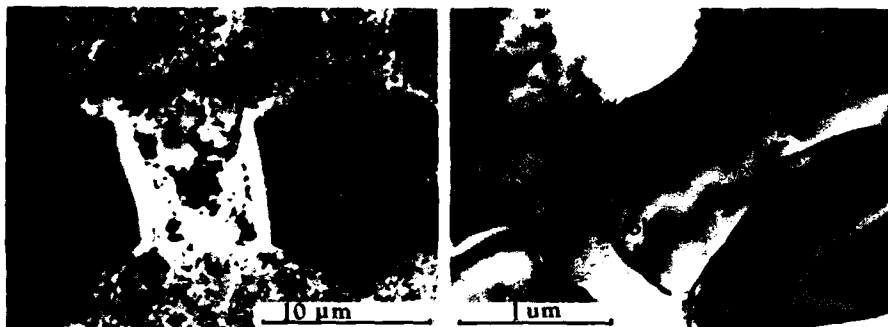


Figure 3 - Fe-Al phase produced by impurities. Deformation induces a crack in this brittle phase and new grains emerge to restore the surface in the same way shown in figure 2.

Figure 4 - After 140% deformation the grains remain equiaxed. Several subgrain boundaries (s.b.) are produced by the deformation. (TEM)

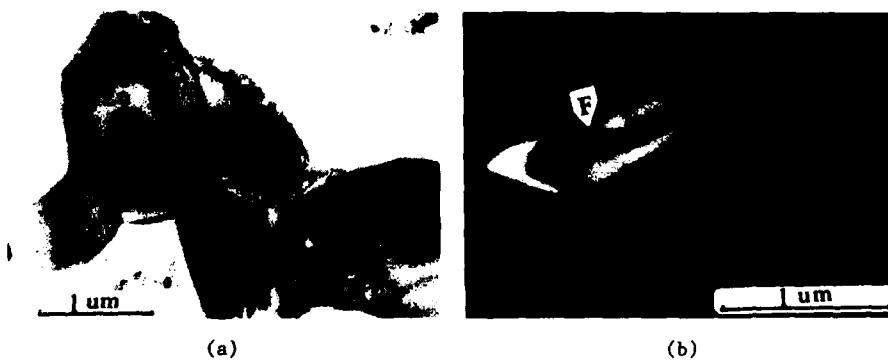


Figure 5 - a) An aluminum grain induces a subgrain boundary on a zinc grain. b) Fracture (F) induced on an aluminum grain (dark field). Any of these mechanism permits a grain surpass another grain during superplastic deformation. (TEM)

SOME RECENT ADVANCES IN THE DEVELOPMENT OF  
FINE-GRAINED SUPERPLASTIC ALUMINUM ALLOYS, CERAMICS,  
AND LAMINATED COMPOSITES

J. Wadsworth\*, T.G. Nieh\*, and Oleg D. Sherby\*\*

\*Lockheed Missiles & Space Company, Inc.,  
Research and Development Division  
O/93-10, B/204, 3251 Hanover Street  
Palo Alto CA 94304

\*\*Department of Materials Science and Engineering,  
Stanford University  
Stanford CA 94305

ABSTRACT

Over the last several years, superplasticity has been developed in fine microstructures in a range of aluminum alloys including aluminum-lithium alloys, mechanically alloyed aluminum, silicon carbide whisker-reinforced aluminum alloys, and aluminum-magnesium alloys. In some cases, the phenomenon is observed at extremely high strain rates by comparison with most superplastic alloys. In other areas of interest, true ceramic materials have been shown to be superplastic in tension tests and superplasticity has been developed in laminated composites.

Superplasticity and Superplastic Forming  
Edited by C.H. Hamilton and N.E. Paton  
The Minerals, Metals & Materials Society, 1988

## Introduction

Superplasticity is the capability of certain polycrystalline materials to undergo extensive tensile plastic deformation, often without the formation of a neck, prior to failure. In certain metal alloy systems, tensile elongations of thousands of percent have been documented as described in recent reviews (1,2). Most superplastic alloys, however, exhibit optimum tensile elongations of about 300 to 1000% but this is sufficient to make complex shapes. High values of the strain rate sensitivity exponent,  $m$ , are also required in order for uniform thinning to accompany high tensile elongations. The principal alloy systems which have been exploited commercially for superplastic forming are those based on nickel, titanium, and aluminum. Interest in superplasticity and superplastic forming is on the increase. Since the 1982 International Conference on Superplastic Materials in San Diego (3), at least six other international symposia have been held (2). Advances have been made in fine structure superplasticity in a number of alloy systems. A significant amount of this work has centered on aluminum-based alloys; very recently, superplasticity has also been demonstrated in ceramics and in laminated composites.

## Superplastic Aluminum-Based Alloys

There is considerable current research and development activity in Al-Li based alloys, Al-Mg alloys, SiC/Al alloys and mechanically alloyed (MA) Al alloys. Development of superplasticity in the Al-Li alloy system has principally been of interest in the aerospace industry because lithium simultaneously and significantly increases both the elastic modulus ( $E$ ) and decreases the density ( $\rho$ ) of Al. Superplasticity studies in Al-Li alloys at the Lockheed Palo Alto Research Laboratory have centered on work on both model systems and commercially-oriented compositions. In the latter case, alloys based on Al-3Cu-2Li-1Mg-0.2Zr have been produced by both ingot metallurgy (IM) and rapidly solidified powder metallurgy (PM) processing. Optimum superplasticity of 1000% was found at 500°C at strain rates of about  $5 \times 10^{-3} \text{ s}^{-1}$ . These optimum superplastic properties are more attractive than those in the Al 7475 alloy in which the optimum rate is only  $2 \times 10^{-4} \text{ s}^{-1}$ . This difference in strain rate between these alloy groups is attributed to the fine grain sizes in the Al-Li alloys (2-4 microns) by comparison with those in the Al-7475 alloy (15 microns). Lockheed has recently collaborated with Reynolds Metals and Superform USA (5) to produce a complex shape by superplastic forming a specially-processed 2090 alloy (Al-2.6%Cu-2.4%Li-0.18%Zr). This component is shown in Fig. 1.

Considerable effort has also been devoted to superplasticity studies in Al-Mg base alloys. Watanabe, Ohori, and Takeuchi have modified an existing Al-Mg alloy (AA 5083) by the addition of Cu; the grain size of a 0.6%Cu alloy was less than  $10 \mu\text{m}$  and an elongation of 700% was obtained at a strain rate of  $2.8 \times 10^{-3} \text{ s}^{-1}$  at 550°C. Salama and McNelley (7) have been studying the properties of an Al-10Mg alloy containing small additions of either Zr (0.2%) or Mn (0.5%). These authors show that superplasticity can be achieved at relatively low temperatures (300°C) in contrast to the high temperatures required in other superplastic Al alloy systems (typically 475 to 550°C). Finally, superplasticity in PM Al-5Mg-1.5Cr has been studied by Shin, et. al. (8). After consolidation by hot compaction, followed by thermal-mechanical processing, a fine-grained ( $d = 2 \mu\text{m}$ ) condition was developed. The Al-Mg-Cr material exhibited superplastic elongations (>1000%) at high strain rates ( $2 \times 10^{-2} \text{ s}^{-1}$ ) at 550°C.

A drawback of superplastic forming of commercial alloys is the relatively slow strain rates ( $\sim 10^{-4} \text{s}^{-1}$ ) at which optimal superplasticity is often found. In general, this strain rate is closely related to grain size. It was recently discovered (9) that a composite of Al-2124 containing 20 vol% of SiC whiskers behaves in a superplastic-like manner (up to 300% elongation) at the high strain rate of  $3 \times 10^{-1} \text{s}^{-1}$ . This strain rate is orders of magnitude faster than that for most of the aluminum alloys described above. A similar phenomenon was recently observed in ultrafine-grained, MA Al 9021 (4.2%Cu-1.0%Mg-1.1%C-0.8%O) alloy (10). In this latter case, maximum elongations of 500% were found at high strain rates of up to  $2.5 \text{s}^{-1}$  and tests have been performed up to  $340 \text{s}^{-1}$ . Work to identify the precise, operative, deformation mechanisms in these alloys is continuing. The observation is believed to be consistent with the extremely fine (submicron) grain size in these complex composites and alloys. This high strain rate phenomenon has previously been observed in a study of the mechanically alloyed (MA) nickel based superalloys, MA 754 and IN 6000 (11). An overview of the superplastic behavior of the alloys described in this section is given in Fig. 2 in which elongation-to-failure is plotted as a function of strain rate. The grain sizes for each of the alloy groups is indicated on the figure.

#### Superplastic Ceramics

The mechanism of superplasticity is not fully understood. Despite this, grain boundary sliding is often experimentally observed, and the major structural prerequisite for grain boundary sliding is a stable, very fine ( $< 10 \mu\text{m}$ ), grain size; this requirement for stability usually necessitates the presence of a finely-dispersed second phase. In addition, the grains need to be equiaxed and the grain boundaries are required to be mobile, high-angled, and to resist tensile separation (1). An interesting observation is that ceramics fulfill many of these structural prerequisites. In nearly all cases, however, despite exhibiting high values of strain rate sensitivity ( $m$  is often equal to 1), fine-grained ceramics usually show very limited tensile ductility.

In the past few years, a number of reports have appeared in the literature of apparent observations of superplasticity in ceramic systems (see Ref. 2). Critical evaluation (1) of these observations has led to the conclusion that until very recently no categorical evidence has been produced for true superplasticity in ceramics (i.e., large tensile elongations). We believe that the first true demonstration of superplasticity in a fine-grained polycrystalline ceramic has recently been demonstrated by Wakai, Sakaguchi and Matsuno (12) using tension tests at  $1450^\circ\text{C}$  on a yttria stabilized tetragonal (microduplex) zirconia polycrystal (Y-TZP). A maximum value of elongation to failure of 200% was found. The grain size of the material was extremely fine ( $d \approx 0.3 \mu\text{m}$ ). Current work at the Lockheed Research and Development Division has reproduced and improved upon the work on Y-TZP (13). An example from this work illustrating an elongation of 350% in Y-TZP is shown in Fig. 3.

#### Superplastic Laminated Composites

It is possible to make non-superplastic mild steel behave in a superplastic-like manner at intermediate temperatures by lamination to superplastic ultrahigh carbon steel (14). Strain-rate sensitivity exponents over 0.30 and elongations to fracture of over 400% have been obtained. The strain rate-stress results show good agreement with constitutive equations for creep based on an isostrain deformation model.

This model was also used to predict the conditions of strain rate, temperature, and percentage of non-superplastic component required to achieve nearly ideal superplasticity in a ferritic stainless steel clad to an ultrahigh carbon steel. Daehn, Kum, and Sherby (15) have shown that the predicted conditions are achieved for a UHC steel clad with a ferritic stainless steel (12% by volume). This combination of components and test conditions leads to the unexpected result that coarse-grained stainless steels can be made superplastic (>800% elongation at 825°C and at  $\dot{\epsilon} = 10^{-3} \text{ s}^{-1}$ ).

#### Acknowledgements

Part of this study was supported by the Lockheed Independent Research and Development Program and by the Office of Naval Research (N00014-82-K-0314).

#### References

1. O.D. Sherby and J. Wadsworth, "Development and Characterization of Fine-Grain Superplastic Materials," in Deformation, Processing and Structure, G. Krauss, ed., (Metals Park, OH: American Society for Metals, 1984), 355-389.
2. O.D. Sherby and J. Wadsworth, "New Superplastic Materials," Proceedings of AIME Symposium, Phoenix, AZ, January, 1988.
3. N.E. Paton and C.H. Hamilton, eds., Superplastic Forming of Structural Alloys, (Warrendale, PA: Metallurgical Society of AIME, 1982).
4. J. Wadsworth, T.G. Nieh, and A.K. Mukherjee, "Superplastic Aluminum Alloys - A Review," Aluminum Alloys: Their Physical and Mechanical Properties, E.A. Starke, Jr., and T.H. Sanders, Jr., eds., (London, United Kingdom: Chameleon Press Ltd., 1986), 1239-55.
5. C.A. Henshall, J. Wadsworth, M.J. Reynolds, and A.J. Barnes, "Design and Manufacture of a Superplastic-Formed Aluminum-Lithium Component," Materials and Design, VIII (6), (1987), 324-330.
6. H. Watanabe, K. Ohori, and Y. Takeuchi, "Superplastic Behavior of Al-Mg-Cr Alloys," Trans. Iron and Steel Institute of Japan, 27, (1987), 730-733.
7. A. Salama, "Analysis of Grain Refinement and Superplasticity in Aluminum-Magnesium Alloys," (Ph.D. Dissertation, U.S. Naval Postgraduate School, Monterey, CA, 1987).
8. D. Shin, D.A. Selby, J. Belzunce, J. Roberts, and O.D. Sherby, "Tensile Creep and Superplastic Behavior of a Fine-Grained Al-5%Mg-1.2%Cr Alloy," (ONR Technical Report/Program N00014-82-K-0314, Stanford University, 1987).
9. T.G. Nieh, C.A. Henshall, and J. Wadsworth, "Superplasticity at High Strain Rates in a SiC Whisker Reinforced Al Alloy," Scripta Metall., 18, (1984), 1405-10.
10. T.R. Bieler, T.G. Nieh, J. Wadsworth, and O.D. Sherby, "Superplastic-Like Behavior at High Strain Rates in Mechanically Alloyed Aluminum," Scripta Metall., 22, (1988), 81-86.

11. J.K. Gregory, J.C. Gibeling, and W.D. Nix, "High Temperature Deformation of Ultra-Fine-Grained Oxide Dispersion Strengthened Alloys," Metall. Trans., 16A, (1985), 777-787.
12. F. Wakai, S. Sakaguchi, and Y. Matsuno, "Superplasticity of Yttria Stabilized Tetragonal Zirconia Polycrystals," Advanced Ceramic Materials, 1 (3), (1986), pp. 259-263.
13. J. Wadsworth and T.G. Nieh, Work in Progress, Lockheed R&DD, Palo Alto, CA, March, 1988.
14. B.C. Snyder, J. Wadsworth, and O.D. Sherby, "Superplasticity in Ferrous Laminated Composites," Acta Metall., 32, (1984), 919-932.
15. G. Daehn, D.W. Kum, and O.D. Sherby, "Superplasticity of a Stainless Steel Clad Ultrahigh Carbon Steel," Metall. Trans., 17A, (1986), 2295-98.

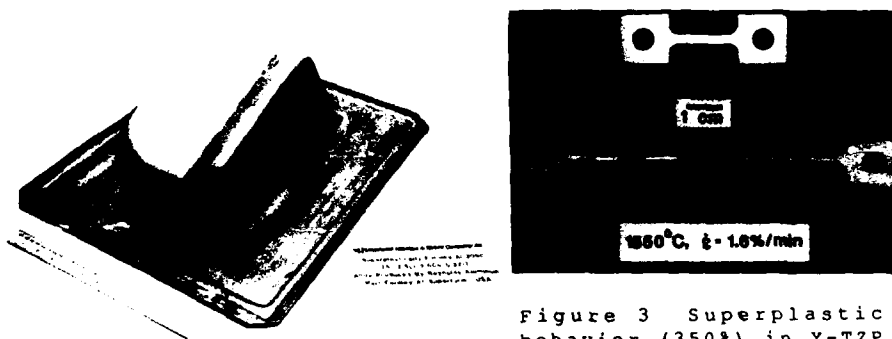


Figure 3 Superplastic behavior (350%) in Y-TZP ceramic.

Figure 1 Superplastically formed Al-Li (Al2090) alloy component.

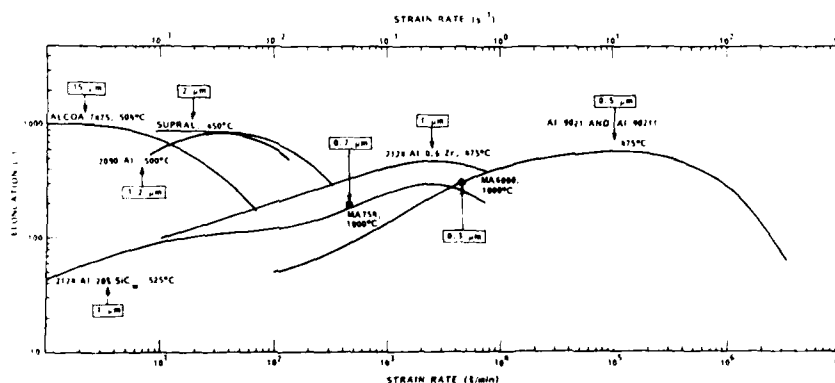


Figure 2 Overview of superplastic behavior as a function of strain rate.



## A DEFORMATION MECHANISM FOR SUPERPLASTIC

### DEFORMATION OF AGE STRENGTHENING CU ALLOY

Jin Tao Zhao Min and Chen Puquan

Department of Metal and Technology,  
Harbin Institute of Technology,  
Harbin, P.R.China.

#### Abstract

This paper is shown that the superplastic deformation of Cu-1.93e-0.2Ni alloy is caused by simultaneous operation of three cooperation mechanism (GBS, DS, DC). Dislocation slip is play the role in both accomodation mechanism and the process bring about the GBS development. Diffusion creep also makes contribution to accomodation process of GBS. The greatest contribution to total strain is made by GBS under condition of optimum superplasticity. The second phase particle is an effective source of lattice dislocation emitted into grain by particle and grain boundary dislocation movement. There also exists correlation between the intragranular particle and lattice dislocation. On the basis of present experimental results, a modle of superplastic flow mechanism is proposed to describe the deformation process of Cu-1.93e-0.2Ni alloy.

Superplasticity and Superplastic Forming  
Edited by C.H. Hamilton and N.E. Paton  
The Minerals, Metals & Materials Society, 1988

## Introduction

As yet, the majority of studies on mechanism of superplastic deformation have been made in quasi-single phase alloys (1, 2) or duplex phase alloys (3,4). For age strengthening alloys, large volume fraction second phase particles existed in the alloys, which result in superplasticity decreased by voids formation in early stage of deformation and made study on mechanism complicate. Recently, some reports indicated that high strength alloys, e.g., 7475 aluminum alloy (5), can manifest large elongation by controlling and utilizing second phase particles in pretreatment. The flow behavior of this kind of alloy is similar with other superplastic alloys. The purpose of present paper is to investigate the superplastic flow mechanism of an age strengthening alloy and the reasons of manifesting large elongation. The effects of second phase particles in deformation were examined as well.

## Experimental Procedures

For the reason that superplasticity of received state material was rather poor, the maximum elongation was only 265%, three kinds of pretreatment process were employed to improve superplasticity of the material. They are (a) quenching (740°C) + aging (320°C, 2.5hr), (b) quenching (780°C) + cold rolling ( $\epsilon=55\%$ ), (c) quenching (780°C) + cold rolling ( $\epsilon=55\%$ ) + ageing (320°C, 2.5hr). The material treated by the third kind of pretreatment manifests the maximum elongation, 1300%, at 550°C with  $1.67 \times 10^{-3} \text{ s}^{-1}$  and selected to investigate mechanism of superplastic deformation.

Specimens were cut from the plate of material along rolling direction and machined to final size. The gauge dimension of specimen was  $16 \times 16 \times 2 \text{ mm}$ .

Tensile deformation tests in vacuum were carried out on a Gleeble-1500 test machine. Optical microscope, SEM and TEM were used to observe and analyze the deformed microstructures. Texture measurement and dislocation density determination were conducted by x-ray diffractometer.

## Results and Discussion

Texture measurement. Pole figures for the specimens were determined by x-ray diffractometer. The major texture component of received state specimen was (110)(223). The (111) pole figures for specimens deformed to 50% at strain rate of region I, II and III show that the components of texture were similar with the major texture component of received state specimen, but the relative intensities of three regions were different. The relative intensities in all three regions decreased after deformation, especially in region I. In region II, DRX and rotating changed initial preferred orientation in the material, diffusion process also made a contribution to the change. In the region III, dislocation slip played the major role in deformation, so the relative intensity of texture was higher. No new texture was formed in all three regions during deformation.

Dislocation density estimation. Dislocation density was estimated by measuring real width of diffracted ray and calculating from equation (1). The values calculated were given in Table 1. These values show that the dislocation density in re-

gion I was lowest, in region III was the highest and in region II was middle.

$$P = KB^2/Fb^2 \quad (1)$$

Table 1, The dislocatin density in materials after deformatig to 50% at 550°C with strain rate of region I,II,III.

Region	$\epsilon(s^{-1})$	$B(^{\circ})$	$b_0/B\%$	$\beta(\text{radian})$	$\rho(\text{cm}^{-2})$
I	$8.33 \times 10$	0.300	0.830	$8.744 \times 10$	$1.53 \times 10^{10}$
II	$1.67 \times 10$	0.353	0.705	$1.798 \times 10$	$6.47 \times 10^{10}$
III	$3.33 \times 10$	0.408	0.610	$2.320 \times 10$	$1.48 \times 10^{11}$

$b_0$ -tool width;  $\beta_0$ -compound width of ray;  $\beta$ -real width of ray.

Dislocation structure. The dislocation structure of specimens which were tensioned to different strain rate of region II

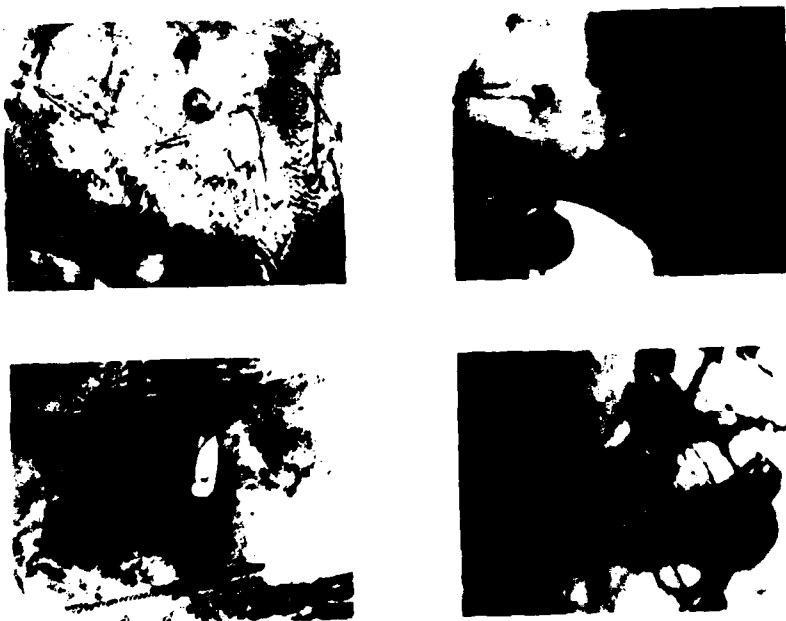


Fig.1. The dislocation structure of the specimens deformed to different strain at 550°C with rate  $1.67 \times 10^{-3} s$  (a) $\epsilon=18\%$ ; (b) $\epsilon=50\%$ ; (c) $\epsilon=90\%$ ; (d) $\epsilon=180\%$ .

was show in Fig.1. Grain boundary dislocations and lattice dislocation which were emitted from triple points and particles at grain boundary can be observed. The emitting into grains of dislocation was to relax the stress concentration that was resulted from blocking and pilling up of grain boundary dislocation. Stress concentration also happened at particles within

grains, especially at tip of particles, so dislocation were emitted from the particles to relax the stress concentration. Particles both at grain boundary and within grains are dislocation sources and were correlative with other dislocation, i.e., the dislocation tangled and help up around the particles with grains when they were blocked by the particles. As grain boundary dislocation motion was blocked by some obstacles, e.g., triple points, particles at grain boundary or step of grain boundary, lattice dislocation were emitted into grains to relax stress concentration.

A mechanism model. In terms of above results, a mechanism model was proposed to describe the process of GBS with accommodation of dislocation motion. The scheme of the model was shown in Fig.2. In the figure:

- 1-grain boundary dislocation pile up at particle;
- 2-dislocation emitted by particle at grain boundary;
- 3-resolving of lattice dislocation at opposite grain boundary;
- 4-triple point become a grain boundary dislocation source and dislocation pile up at grain boundary particle;
- 5-grain boundary particles became grain boundary dislocation source;
- 6-lattice dislocation emitted by triple point;
- 7-particle within grains became a dislocation source and emitted dislocation.

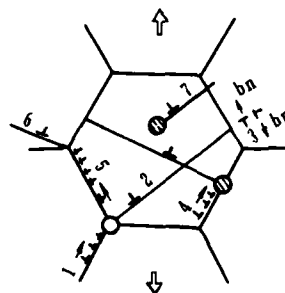


Fig.2 The scheme of the superplastic deformation mechanism model in Cu-1.93e-0.2Ni alloy.

#### References

1. A.Arieli and A.K.Mukherjee, Mat.Sci.Eng., 10 (1980),45.
2. A.E.Geckinli, Met.Sci., 17 (1983),12.
3. M.Suery and B.Baudelet, "Superplastic Forming of Structural Alloys", AIME, (1982), 105.
4. C.Hammond, "Superplastic Forming of Structural Alloy", AIME, (1982), 131.
5. P.Shaiat, R.B.Vastava and T.G.Langdon, Acta.Metall. 30 (1982) 285.
6. P.J.Chen and M.Zhao, Acta Metall.(China), 23 (4)(1987), 313.

## A COMPLEX MECHANISM FOR SUPERPLASTIC DEFORMATION OF MAGNESIUM ALLOYS

Zhao Min and Chen Puquan  
Department of Metals and Technology  
Harbin Institute of Technology, P.R.China

### Abstract

The mechanism of superplastic deformation are being developed and perfected. Research workers have put forwarded many models. This paper is to further probe the superplastic deformation mechanism for two selected alloys, coarse and superfine grain, by means of advanced techniques. The result shows that features of superplastic deformation differ from plastic deformation and diffusion creep. The mechanism of diffusion creep coordinating grain boundary sliding tallies with the model suggested by Ashby and the mechanism of dislocation slip coordinating grain boundary sliding tallies with the model suggested by Gifkins. According to the facts that DC and DS occur together in mantle, authors consider that the process of superplastic deformation is composed of macro grain rearrangement and micro coordinating of DC and DS. The beneath grains may progressively emerge in the site on which the cavities along the transverse grain boundaries appeared during superplastic deformation. Thus, the number of grains along the tensile axis may be increased continuously. Finally, this paper advanced a complex model in which three models suggested respectively by Ashby, Gifkins, Geckinli are combined. This model can explain satisfactorily the appearances during superplastic deformation.

Superplasticity and Superplastic Forming  
Edited by C.H. Hamilton and N.E. Paton  
The Minerals, Metals & Materials Society, 1988

## Introduction

Up to now, the mechanism on superplastic deformation may be divided into two types: one is the model that diffusion creep coordinates grainboundary sliding (1,2), another is the model that dislocation slip coordinates grain boundary sliding (3-8). The aim of this paper is to probe and verify (a) GBS, DC, DS exist simultaneously during superplastic deformation, (b) the relations between GBS, DC and DS, (C) the reason why large elongation can be obtained under the condition of superplastic deformation.

## Materials and Experimental Procedure

Mg-4.3Al-0.4Mn-1.0Zn and Mg-5.3Zn-0.5Zr alloys were selected as the test materials. Their grain sizes are 16.7  $\mu$ m and 3.8  $\mu$ m respectively. The two alloys were elongated using Shimadzu test machine. The micro structures after deformation were analyzed with the help of a transmission electron microscope. The microstructure changes during tensile process were also observed with a high temperature optical microscope. Meanwhile, the densities of dislocation were measured with a X-ray diffractometer.

## Experimental Results

1. The changes of mean grain diameter ( $\bar{d}$ ) and the grain diameter ratio of longitudinal to transversal ( $d_l/d_t$ ). In the suitable superplastic deformation conditions, the  $\bar{d}$  and  $d_l/d_t$  of two alloys were measured. The results are listed in table 1.

Table 1.  $\bar{d}$  and  $d_l/d_t$  of two alloys

item	original	aging/2h	20%	50%	100%	rupture
$\frac{d_l}{d_t}$ I	---	---	1.21	1.27	1.29	1.36
$\frac{d_l}{d_t}$ II	---	---	1.22	1.22	1.23	1.38
$\bar{d}$ I	16.67	14.12	14.58	15.00	18.80	25.70
$\bar{d}$ II	3.81	2.57	6.14	6.51	6.62	7.35

I- Mg-4.3Al-0.4Mn-1.0Zn alloy deformed at 375°C,  $\dot{\epsilon} = 8.33 \times 10^{-4} \text{ s}^{-1}$   
 II- Mg-5.3Zn-0.5Zr alloy deformed at 300°C,  $\dot{\epsilon} = 1.67 \times 10^{-3} \text{ s}^{-1}$

2. The observation of microstructure on the surfaces of specimen deformed. We found that the grain boundaries which emerge during superplastic deformation result from the uneven areas. With the strain rate increasing, the uneven areas change from transversal grainboundaries to around grainboundaries. Finally, they spread to grains. See the pictures of Fig.1 (a),(b).

close packed structure is not introduced in much literatures. So this paper adrops the relative density of dislocation to express the changes . See the formula (3).

$$p = A \beta^2 \quad (2)$$

$$\Delta p / p_0 = (\beta^2 - \beta_0^2) / \beta_0^2 \quad (3)$$

where the  $p_0$  is defined the density of dislocation before deformation. The results calulated with formula (3) are listed in table 3.

Table 2, Relative concentrations of atom in Mg-4.3Al-0.4Mn-1.0Zn alloy deformed to 50% .

element	Sx	intracryst.		transversal GB		longitudinal GB	
		I <sub>x</sub>	II	I <sub>x</sub>	II	I <sub>x</sub>	II
Mn	0.245	1.0	1.0	0.8	0.8	1.5	1.6
Zn	0.200	2.0	2.5	1.5	1.9	2.2	2.9
Mg	0.150	47.0	79.5	50.0	84.4	46.0	81.1
Al	0.075	5.0	16.9	4.0	13.5	4.0	14.0

Table 3, The variation of relative density of dislocation

deformation		$\frac{\beta}{\beta_0}$		$\frac{\beta^2}{\beta_0^2}$		$\frac{\Delta p}{p_0}$	
		a	b	a	b	a	b
300 c/15min	0%		9.8		96.04		0.00
375 c/15min	0%	10.2		104.04		0.00	
3.33x10 s	50%	10.8	10.1	116.64	102.01	0.12	0.06
8.33x10 s	50%	11.0		121.00		0.16	
1.67x10 s	50%		10.3		106.1		0.10
1.67x10 s	50%	12.0	11.5	144.00	132.3	0.38	0.38

a Mg-4.3Al-0.4Mn-1.0Zn alloy  
b Mg-5.3Zn-0.5Zr alloy

#### Analysis and Discussion

The role of DC during superplastic deformation. Authors consider that the diffusion creep at low strain rate occurs as Nabarro-Herring model , ie, takes place over a long distance. At the suitable strain rate, the diffusion creep takes place a short distance. In deformation process, DC can play the role as follow : (1) it can be helpful in retaining continuity between grains in combination with GBS; (2) it can relieve the stress concentration produced by GBS; (3) it makes GBS take place continuously.

The role of GBS during superplastic deformation. The boundaries between grains, that are uneven areas, are general weak bands in the strength. So

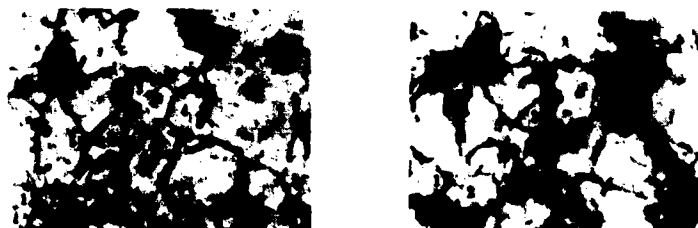


(a)

(b)

Fig.1, Two stage replica of (a) Mg-4.3Al-0.4Mn-1.0Zn alloy deformed to 50% at 375°C with  $\dot{\epsilon} = 8.33 \times 10^{-4} \text{ s}^{-1}$ , (b) Mg-5.3Zn-0.5Zr alloy deformed to 50% at 300°C with  $\dot{\epsilon} = 1.67 \times 10^{-3} \text{ s}^{-1}$ .

3. The dynamic observation of microstructure. The result shows that the transversal grain boundaries extend and the new grains emerge onto specimen surface from transversal grain boundaries with the elongation increasing. See the pictures of Fig.2.



(a)

(b)

Fig.2, The microstructures of Mg-4.3Al-0.4Mn-1.0Zn alloy deformed at 375°C with  $\dot{\epsilon} = 8.33 \times 10^{-4} \text{ s}^{-1}$ , (a) to 7%, (b) to 30%.

4. The experiment of microanalysis with Auger Scanning Microscope. According to the curves obtained from Auger scanning microscope, the Ix of each element was measured and put in formula (1).

$$Cx = Ix / SxDx / Ii / SiDi \quad (1)$$

The relative concentration (Cx) of atom can be gotten. The results are listed in the table 2.

5. The results from the X-ray diffractometer. The density of dislocation ( $\rho$ ) can be estimated with the formula (2), if the width of X-ray diffraction peak ( $\beta$ ) has been known. The A in formula (2) is a experimental coefficient. But it is unfortunate that the A value of metal with hexagonal



cavities are easily formed in this bands. For this reason, authors point out that the seats where the internal grains emerge preferentially onto specimen surfaces are the grain boundaries in which cavities are formed easily. Therefore the number of grain along the direction of the tensile axis are increasing continuously in the deformation process. So the large extensibility of specimen are obtained.

The role of DS during superplastic deformation. According to the relative densities of dislocation and the observation of transmission electron micrograph, it is demonstrated that the DS is almost concentrated in or near grain boundary. The role of DS is to relieve the stress concentration produced by GBS and make GBS take place progressively.

A complex mechanism. As above results and analysis, a complex deformation mechanism containing GBS, DC, DS has been suggested in this paper, in which GBS is taken as a dominant role. Meanwhile, GBS obtains DC, DS coordinating. Fig.3 is a sketchmap of the complex deformation mechanism.

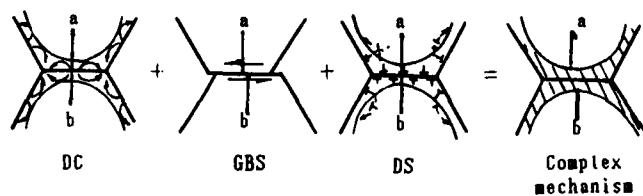


Fig.3, The sketchmap of complex deformation mechanism.

#### References

1. M.F.Ashby and R.P.Verall, *Acta Met.*, 121(1973),149.
2. A.Ball and M.M.Hutchison, *Met.Sci.J.*, 3(1969),1.
3. Chen Puquan and Zhao Min, *Heat Treat.of Met.(China)*, 9(1984),23.
4. Chen Puquan and Zhao Min, *Met.Sci.and Tech. (China)*, 4(1985),1.
5. Chen Puquan and Zhao Min, "Proceeding of the 7th International Conference on the Strength of Metals and Alloys" (Canada),(1985)
6. R.C.Gifkins, *Met. Trans.*, 7(8)(1976),1225.
7. A.K.Mukherjee, *Met.Sci.Eng.*, 8(1971),83.
8. J.R.Springar and W.D.Nix, *Acta Met.*, 27(1979),171.

## MECHANISMS OF SUPERPLASTIC FLOW IN INCONEL 718

Murray W. Mahoney and Roy Crooks

Rockwell International Science Center  
1049 Camino dos Rios  
Thousand Oaks, California 91360

### Abstract

Experimental data have shown that specially processed fine grain Inconel 718 can exhibit superplastic properties. However, evaluation of these results indicated that Inconel 718 did not respond in a manner characteristic of classical superplastic alloys. The strain rate sensitivity decreased rapidly with increasing strain while the grain size was observed to first increase, then refine, then again increase in size. Results presented in this manuscript illustrate that during superplastic flow of Inconel 718, dynamic recrystallization occurs. This grain morphology change has implications with regard to the controlling mechanisms for high temperature *superplastic flow* in Inconel 718.

*Superplasticity and Superplastic Forming*  
Edited by C.H. Hamilton and N.E. Paton  
The Minerals, Metals & Materials Society, 1988

### Introduction

There has been considerable controversy over the mechanisms of superplastic deformation and accordingly over the past 20 years theories have been proposed that attempt to describe superplastic metal flow in terms of either single or several deformation mechanisms. The experimental evidence now indicates that several processes can occur during superplastic deformation including grain boundary sliding, dislocation motion, diffusional processes and dynamic recrystallization.

In a previous publication (1), superplasticity was reported in a specially processed fine grain Inconel 718. Because of the limited experimental information available, the mechanisms controlling superplastic flow in this alloy were not well understood. Additional results on microstructural changes that occurred during superplastic forming in this fine grain Inconel 718 are now available and contribute to a better understanding of metal flow in this alloy. Accordingly, this manuscript combines superplastic property results with microstructural observations to provide evidence for the supposition that superplastic metal flow in fine grain Inconel 718 progresses through cycles of diffusion control and dynamic recrystallization.

### Fine Grain Inconel 718

Fine grain Inconel 718 was specially fabricated to 0.05 cm thick by the Huntington division of INCO Alloys International. Fabrication procedures to produce the very fine grain size are proprietary to INCO Alloys and as such are not presented in this manuscript. Metallography illustrating the fine grain size microstructure is presented in Figure 1a where grain size, measured by a linear intercept technique, is  $< 6 \mu\text{m}$ .

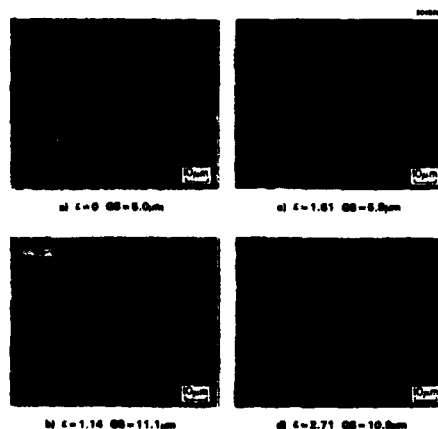


Figure 1 - Grain morphology for increasing strain in SPF tested Inconel 718, strain and grain size are shown.

### Results

In previous work (1), superplastic flow characteristics were determined by a number of approaches including step strain-rate tests, whereby strain rate was incrementally increased each time the load reached a maximum, by constant strain rate tests to measure total elongation and by measurement of  $m$  as a function of strain by periodically increasing the strain rate 40% and establishing the flow stress and again returning to the original strain rate. Evaluation of these results indicated that Inconel 718 did not respond in a manner characteristic of classical superplastic alloys.

Testing under superplastic conditions for the  $< 6 \mu\text{m}$  grain size Inconel 718 showed elongations to be relatively limited with an average true strain at fracture of  $\sim 1.8$ . Even

at this low level of strain, necking occurred along the gage length indicating only moderate strain rate sensitivity. This result is shown quantitatively in Figure 2 where  $m$  is shown to decrease rapidly as a function of accumulated strain. This rapid decrease in strain rate sensitivity behavior is not characteristic of a highly superplastic material and indicates that a change in flow behavior might be occurring with increasing strain.

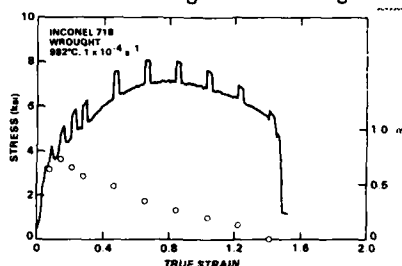


Figure 2 - Strain rate sensitivity of fine grain Inconel 718 with increasing strain at  $2 \times 10^{-4} \text{ s}^{-1}$ .

Optical microscopy shown in Figure 1a-d illustrates a sequence of micrographs with increasing strain for a sample tested at  $980^\circ\text{C}$  and a strain rate of  $2 \times 10^{-4} \text{ s}^{-1}$ . This constant strain rate test was interrupted at an intermediate level of strain (0.8) where the sample was aged at  $980^\circ\text{C}$  for 1 h prior to continued loading at  $2 \times 10^{-4} \text{ s}^{-1}$ . This aging step was introduced to enhance any recrystallization process occurring under these conditions. From this series of micrographs, a number of observations can be made concerning the changing microstructural morphology. The initial grain size is small with an approximately equiaxed grain shape. At low levels of strain (0.68) grains begin to increase in size and continue to increase in size up to a true strain of  $\sim 1.14$ . At higher levels of strain (1.39) the grain size decreases reaching a minimum at a strain of  $\sim 1.61$ . At even higher levels of strain (2.12) grains again increase in size and continue to increase up to the fracture strain of 2.71. The grain shape remains essentially equiaxed throughout the test but the micrograph in Figure 1c shows a bimodal grain size distribution indicating initiation of grain refinement.

A note concerning data collection is in order. It is not possible to quantitatively equate the results in Figures 1 and 2 because of the different way the data were collected. Data in Figure 2 were continuously and analytically derived during testing assuming uniform flow, i.e., no necking. These results illustrate an average true strain over the entire gauge length. Strain measurements from Figure 1 were measured directly from the sample and accurately reflect the local level of strain for the microstructure shown at that precise location. Since necking did occur, Figure 2 can be used only to illustrate a trend, i.e., true strains are higher than shown for a given value of  $m$ .

In superplastic materials, it is common for grains to grow and to elongate in the stress direction. This grain growth and shape change have been explained by diffusional processes whereby vacancies diffuse to grain boundaries approximately parallel to the tensile axis, while there is a corresponding counterflux of atoms to boundaries perpendicular to the tensile axis. Results illustrated in Figure 1 show grain growth up to some intermediate level of strain, where grain refinement occurs, followed again by grain growth. Initial grain growth behavior can be explained by diffusional flow but to explain the equiaxed grain structure and grain refinement other mechanisms must also become active.

To explain an equiaxed and smaller grain size, other investigators have suggested that dynamic recrystallization can be an important component of superplastic deformation (2,3). In fact, there is evidence that in a few cases recrystallization may be important (4,5). Dynamic recrystallization can occur in materials with low stacking fault energies which have limited dislocation mobility and tend to develop localized, high dislocation densities during deformation. When local differences in dislocation density are sufficiently high, recrystallization proceeds by the migration of high angle boundaries (6). Results from the present study show that dynamic recrystallization is active in

superplastic flow of Inconel 718. The transmission electron micrographs in Figure 3, for a sample strained to a true strain of 1.6, show high angle boundaries of recrystallized grains bowed into the grain (on the lower left) which contains a relatively large number of dislocations. This is typical of dynamic recrystallization where dislocation densities drop to very low levels just behind moving boundaries.



Figure 3 - Grain boundary morphology in SPF tested (1.63 true  $\epsilon$ ) Inconel 718.

Further evidence for dynamic recrystallization is shown by comparing Figures 4 and 5. Figure 4 illustrates grain boundary misorientation in as received Inconel 718 while Figure 5 provides misorientations after a true strain of 1.63. The number of twin boundaries ( $59$  to  $60^\circ$ ) decreases but also there is an increase in the number of low angle boundaries, illustrating stored energy available for dynamic recrystallization.

Referring back to Figure 1, it should be remembered that only the portion of the sample strained above  $\sim 1.4$  true strain exhibited dynamic recrystallization. This can be explained by the results of Sakai and Jonas (7). They have shown that the strain to initiate dynamic recrystallization in Inconel 718 is high ( $0.7$  at  $975^\circ\text{C}$ ) and to produce complete recrystallization is much higher than that for less heavily alloyed materials.

The above results have shown grain refinement (Figure 1) and yet the strain rate sensitivity continues to decrease (Figure 2). If recrystallized grain boundaries are high angle boundaries, then flow should again be controlled by diffusion with a corresponding increase in  $m$ . This apparent inconsistency can possibly be explained in two ways. First, with a bimodal grain distribution, as shown in Figure 1c, Ghosh and Raj (8) suggest that a distributed grain size in a polycrystal can lead to mixed mode deformation. In this case, the microstructure may not be conducive to diffusion control because of the bimodal grain size and the increased number of small angle boundaries (compare Figures 4 and 5). Another explanation could be the test procedure itself. Because of necking in the gauge, the sample is unable to re-establish a uniform strain rate. Thus nonuniform strain continues even after grain refinement. If in fact superplasticity can be enhanced in situ via dynamic recrystallization, then novel forming procedures could possibly be developed to accumulate strain when the microstructure is most receptive to uniform elongations.

#### Conclusions

Metallographic and properties results show that dynamic recrystallization is active during superplastic flow of fine grain Inconel 718. During superplastic strain, stored energy associated with high localized dislocation densities becomes sufficient to activate dynamic recrystallization, resulting in grain refinement. This results in superplastic metal flow in Inconel 718 that progresses through cycles of diffusion control and dynamic recrystallization.

#### Acknowledgments

The author would like to acknowledge the support of the Dept. of the Air Force, Flight Dynamics Laboratory, Wright-Patterson AFB and Rockwell International IR&D for sponsorship of this work. The authors also gratefully acknowledge the support of Mr. M. Calabrese for metallography and Dr. A. Ghosh for helpful discussions.

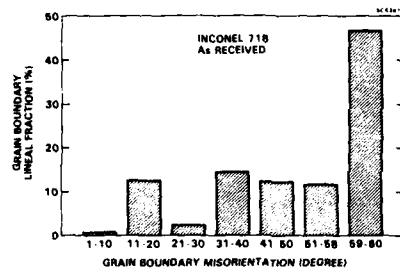


Figure 4 - Grain boundary misorientation distribution in as received Inconel 718.

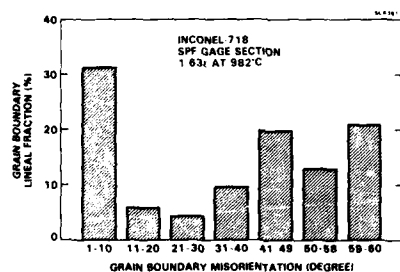


Figure 5 - Grain boundary misorientation distribution in SPF tested wrought Inconel 718.

#### References

1. M.W. Mahoney and R. Crooks, "Superplastic Forming of Inconel 718," Proceedings, Superplasticity in Aerospace AIME 117th Annual Meeting, Phoenix, Arizona, 25 January 1988, Editors, T. McNelley and C. Heikkinen, to be published.
2. C.M. Packer, R.H. Johnson and O.D. Sherby, "Evidence for the Importance of Crystallographic Slip During Superplastic Deformation of Eutectic Zinc-Aluminum," Trans. AIME, 242 (1968) 2485.
3. R.H. Johnson, C.M. Packer, L. Anderson and O.D. Sherby, "Microstructure of Superplastic Alloys," Phil. Mag., 18 (1968) 1309.
4. G. Herriot, M. Suery and B. Baudalet, "Superplastic Behavior of the Industrial Cu7W&%P Alloy," Scripta Met., 6 (1972) 657-662.
5. M.J. Stowell, J.L. Robertson and B.M. Watts, "Structural Changes During Superplastic Deformation of the Al-Cu Eutectic Alloy," Metal Sci. J., 3 (1969) 41.
6. D. Apelian, B.H. Kear, H.W. Schadler, "Spray Deposition Processes," Rapidly Solidified Crystalline Alloys, (Warrendale, PA, the Metallurgical Society, AIME, 1985) 93-109.
7. T. Sakai and J.J. Jonas, "Dynamic Recrystallization: Mechanical and Microstructural Considerations," Acta. Metall., 32 (1984) 189-204.
8. A.K. Ghosh and R. Raj, "The Evolution of Grain Size Distribution During Superplastic Deformation," Superplasticity, Ed. B. Baudalet and M. Suery (Paris, France, Centre National de la Recherche Scientifique, 1985), 11.1-11.19.

**MICROSTRUCTURAL  
DYNAMICS**

## MICROSTRUCTURAL INSTABILITY DURING SUPERPLASTIC FLOW

D. S. Wilkinson

Department of Materials Science and Engineering  
and  
Institute for Materials Research  
McMaster University  
Hamilton, Ontario L8S 4L7  
Canada

### Abstract

Superplasticity relies on the development and maintenance of a fine-grained microstructure. However, such microstructures tend to be unstable. In particular, many materials undergo strain-enhanced grain growth during superplastic deformation. This is a process whereby the rate of grain growth is greatly enhanced over that which occurs in the absence of deformation. The process is thought to be linked directly to grain boundary sliding, and models have been developed which are consistent with the bulk of the experimental data. Some new experiments on the effect of strain reversal during superplastic deformation shed additional light on the operative mechanisms. We find that strain reversals inhibit grain growth in a microduplex alloy but not in "quasi" single phase alloys. A model to explain this behaviour has been developed by assuming that grain growth is enhanced by the effect of sliding on the Zener drag process. The model predicts a delay in the onset of grain growth following each strain reversal for a strain of  $1/D$ ,  $1$  being the particle spacing and  $D$  being the grain size. The model accounts qualitatively for the difference in behaviour between the two types of materials.

Superplasticity and Superplastic Forming  
Edited by C.H. Hamilton and N.E. Paton  
The Minerals, Metals & Materials Society, 1988



## Introduction

Structural superplasticity is exhibited only in materials of fine grain size. Typically a grain size of less than 10  $\mu\text{m}$  is required, although in many materials much more refined grain structures are used. It remains one of the major challenges then in superplasticity, to find processing methods which enable the development and stabilization of a fine grained structure. Two basic approaches have been taken. The first involves the development of a suitable microstructure prior to superplastic forming by an appropriate thermomechanical treatment, typically involving extensive plastic deformation combined with static recrystallization. The other method involves the development of a heavily deformed microstructure which is then recrystallized during the early stages of superplastic deformation.

The first of these approaches has been traditionally used to develop superplastic behaviour in a wide range of materials, including dispersion and precipitation strengthened alloys, microduplex alloys, and ceramic materials. However, it does not lend itself to all materials. For example, it is found that the first method works well for a range of age hardenable alloys including the 7075 and 7475 Al alloys (1). However, the same method does not work nearly as well when applied to Al-Li alloys. Instead, Ghosh and Ghandi (2) have shown that by eliminating the final recrystallization step, a fine subgrain structure can be developed by means of dynamic recrystallization shortly after the onset of high temperature deformation. Continued deformation leads to both an increase in the subgrain misorientation and a continuous increase in the (sub)-grain size.

Whichever of the two processing routes is used it is clear that a fine grain size eventually develops, and that this is responsible for the superplastic behaviour. However, this structure is not generally stable during deformation. Both grain growth and grain refinement are known to occur depending on the material and the test conditions. In particular, it is now clear that in most materials deformed at strain rates below that at which the peak strain rate sensitivity is observed, strain-enhanced grain growth occurs. There is now considerable evidence that at higher strain rates, in excess of the peak strain rate sensitivity, grain refinement by dynamic recrystallization occurs. At intermediate strain rates (one imagines) both processes will occur simultaneously.

It is the main purpose of this paper to review our current understanding of these processes and to consider a range of models which are available to explain this behaviour.

## Tensile Stability

One of the prime motivations for the use of superplasticity comes from the high degree of stability which is exhibited. This allows the forming of parts in which relatively large strains (and strain variations) are achieved without developing large variations in part thickness. The most important consideration in achieving tensile stability and gradual neck

development is a high strain sensitivity,  $m$  (as illustrated by Woodford's classical  $m$  vs. ductility plot) (3). However, other factors are also important. For example, two commercial Zn-Al alloys containing different minor alloy additions exhibit very different tensile stability at low strain rates (in region I of superplasticity). One alloy, containing about 0.5% copper exhibits much greater tensile stability at low strain rates than a copper-free alloy. It has been shown (4) that this is due to the greater degree of strain-enhanced deformation in the copper-containing alloy. The reason for this can be traced to the effect of grain size on flow strength through a simple model.

We start by adopting a constitutive law for superplastic deformation of the form

$$\sigma = K \dot{\epsilon}^m D^{pm} \quad (1)$$

where  $D$  is the grain size, while  $K$ ,  $m$  and  $p$  are measured material parameters. If, as is commonly found, the grain size increases at a rate which depends on strain then the flow itself becomes strain-dependent. To model this, we adopt the simplest possible relationship for grain growth, namely

$$D = D_0 + C\epsilon \quad (2)$$

This relationship is both simple and (based on experimental observation) justifiable (5). By substituting eq. (2) into eq. (1) it is possible to determine the rate of strain hardening  $\tau$ , due to grain growth alone, namely

$$\tau = Cpm / (D_0 + C\epsilon) \quad (3)$$

It is clear from eq. (3) that the hardening rate due to grain growth is initially high but that it diminishes as deformation continues. The tensile stability can be analyzed to a first approximation by an instability parameter of the form (6)

$$I = (1 - \tau - m) / m \quad (4)$$

The larger the value of  $I$  the more unstable deformation will be. Thus at low strain rates (i.e. region I) a large value of  $\tau$  can compensate for the relatively low strain rate sensitivity. Thus grain growth decreases tensile instability at low strain rates. On the other hand, as noted by Hamilton (7), it can increase the tensile instability at higher strain rates near the region I/II boundary. This is due the effect of grain size on flow stress and strain rate sensitivity in this region.

The development of tensile instabilities during superplastic flow, incorporating both strain and strain rate dependent effects, has been analyzed in considerable detail by Hamilton (7) and by Senkov and Likhachev (8). These models are now capable of predicting the development of necks within a tensile specimen under a range of testing conditions. It should therefore be possible to use a detailed knowledge of strain-enhanced grain growth and of the grain-size sensitivity of the flow stress to develop computer codes which will set the optimum conditions for superplastic forming with regard to minimizing the forming time while ensuring the best final

microstructure and the most uniform part thickness. It is therefore of both practical and fundamental value to develop a sound understanding of strain-enhanced grain growth.

### Experimental Observations

There is now a very large body of experimental work in which strain-enhanced grain growth during superplastic flow has been observed. The effect is seen in both metals and ceramics. Moreover, the vast majority of superplastic materials appear to show this behaviour. Several recent reviews can be consulted to obtain a complete list of these materials (5,9,10,11,12). It contains a wide range of materials, including microduplex alloys, single phase alloys containing a fine dispersion of either precipitates or dispersoids, and a range of ceramic materials. There are however, a significant number of materials in which significant strain-enhanced grain growth is not observed. The most notable amongst these are ceramic materials containing a layer of glass along the grain boundaries (13).

In materials which do exhibit strain enhanced grain growth, the main observations can best be summarized by a plot such as Fig. 1.

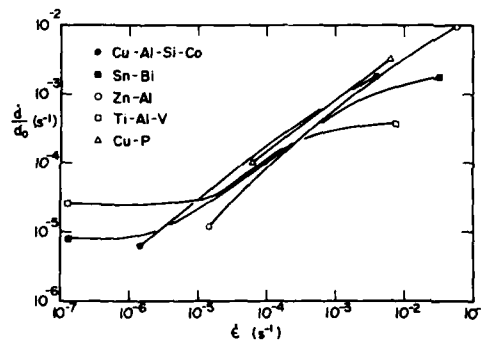


Fig. 1: A plot of the grain growth rate normalized by the initial grain size, as a function of the strain rate, for a range of metallic systems.

This illustrates the three regions of behaviour typically observed. At intermediate strain rates the rate of grain growth depends linearly on the strain rate. Moreover, the grain growth seems to obey a very simple relationship of the form

$$\dot{D} = \alpha D_0 \dot{\epsilon} \quad (5)$$

At low strain rates the rate of grain growth is very low. At sufficiently low strain rates it becomes dominated by the static annealing grain growth rate (i.e. the rate of grain growth at the same temperature in the absence of deformation). At high strain rates there is a decrease in the rate of grain growth per unit strain, denoted on Fig. 1 by a decrease in the slope of the curves. It is interesting to note that this decreasing slope occurs at relatively modest strain rates. This is clearly seen in Fig. 2, in which the strain-enhanced grain growth per unit strain is shown. The strain rates at which the peaks in the strain rate sensitivity are observed are marked by arrows on the plot. Thus it is clear that the strain rate

independent regime occurs in region I of superplastic behaviour.

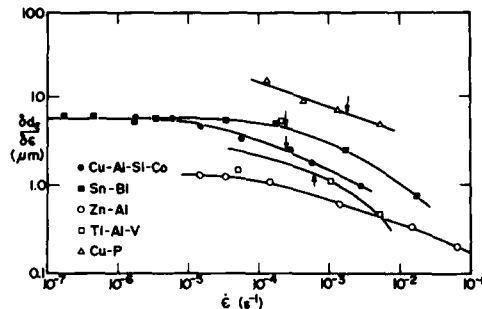


Fig. 2: A plot of the strain-enhanced grain growth rate per unit strain as a function of strain rate, obtained by subtracting the static grain growth rate from that observed during deformation.

Plots of the type just shown, obscure much of the detailed behaviour that is useful for understanding the mechanisms involved. For example the plotted grain growth rates are actually average values measured over relatively large strains. Detailed observations indicate that the grain growth rate is not constant. Moreover the variation in the rate of grain growth with strain differs for different materials. Some of the models for this process (discussed in the next section) suggest that in the intermediate strain rate regime, the grain growth rate should increase linearly with the current grain size. Thus  $\delta \ln(D/D_0)/\delta \epsilon$  should be constant. Our observations on the Zn-Al eutectoid alloy suggest that this is indeed the case (14). However, similar work on Coronze 638 (a single phase copper alloy containing a fine dispersion of CoSi particles) shows a gradual decrease in  $\delta \ln(D/D_0)/\delta \epsilon$  with increasing strain (14). A similar decreasing grain growth behaviour has been documented by Nes (12) for a range of aluminum alloys. The reason for this behaviour is not clear. It is possible however that the distribution of particles which pin grain boundaries may be altered by deformation. In particular, if particles are swept up by the grain boundaries as they migrate then they will act as increasingly effective barriers to grain boundary migration. Detailed electron microscopy is required to resolve this question.

Additional insight into the mechanism of strain-enhanced grain growth is obtained from tests in which samples are cyclically loaded. The first experiments of this type were performed by Clark and Alden (15) on Sn containing 1% Bi. More recently we have performed an extensive series of such tests on two superplastic alloys - Coronze 638 and Zn-22%Al (14). The results are interesting, primarily because of the difference in behaviour between the microduplex alloy (Zn-Al) and the quasi-single phase alloys (Coronze and Sn-Bi). In the latter case, there is no effect of cyclic deformation on grain growth. After each test the measured grain size is the same as that which would have resulted in a monotonic test taken to the same cumulative strain. No effect of strain amplitude, for values between 0.05 and 0.65, was observed. The Zn-Al alloy on the other hand, showed a marked influence of cyclic deformation on the grain growth behaviour. The results are summarized in Fig.

3, in which the grain growth trajectories for different strain amplitudes are shown.

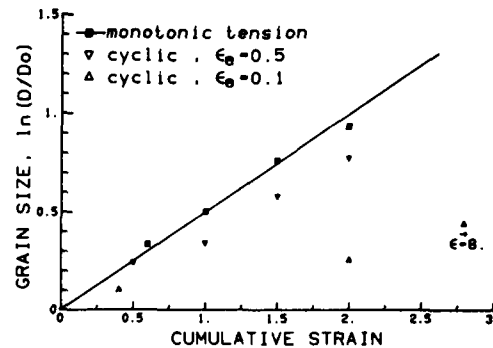


Fig. 3: A plot showing the amount of grain growth in the Zn-Al eutectoid alloy after cyclic deformation with different strain amplitudes. The monotonic result is also shown for comparison.

It is clear that cyclic deformation retards the process of strain-enhanced grain growth in this alloy and that the effect is stronger for small strain amplitudes. The effect is still significant for rather large strain amplitudes of 0.5. The nature of the effect is seen more clearly in Fig. 4.

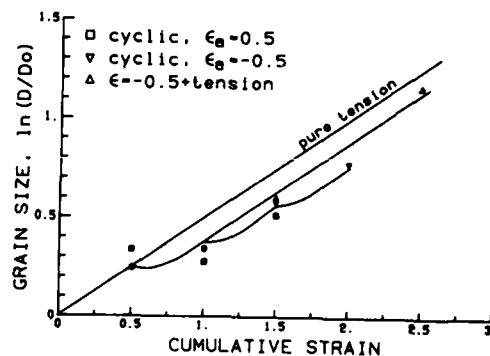


Fig. 4: Grain growth is plotted vs. cumulative strain for a set of experiments in which cyclic deformation is followed by monotonic tensile deformation. These tests were always begun in compression.

From these tests it is clear that on each reversal of the direction of straining, grain growth is interrupted. In this particular case of strain rate equal to  $10^{-4}/s$  and a strain amplitude of 0.5, the strain required to restart the grain growth process is about 0.3. Clearly any model for the process of strain-enhanced grain growth must be able to explain this effect and to rationalize the difference in behaviour between single phase and microduplex alloys.

#### Mechanisms of Strain-Enhanced Grain Growth

It is clear from data of the type presented in Fig. 1, that strain-enhanced grain growth during superplastic flow is governed by the deformation process itself, at least during the intermediate regime on the plot. The process appears to be athermal in the sense that the rate of grain growth depends only on the current strain rate and not directly on temperature. The results conform to a relationship of the form given by eq. (5), and any model for the process must lead to a result of this type. In fact such a model is rather easy to

fabricate, and one can obtain the correct result by a simple dimensional analysis along the following lines. Superplastic deformation is known to be due to grain boundary sliding, and thus the strain rate is proportional to the sliding rate divided by the grain size. Any geometrical model of sliding induced grain growth results in a rate of grain growth proportional to the sliding rate. Putting these two ideas together leads to an equation of the form of eq. (5). The actual physical mechanism merely influences the parameters which make up  $\alpha$ , which must be of order. Previous work on modelling supports this idea (6).

The experiments on strain reversal offer more insight into the operative mechanisms. In particular, it is clear that the behaviour of single phase and microduplex alloys are quite different. The most logical cause of a difference in grain growth on strain reversal lies in the difference in the size and spacing of the particles which pin grain boundaries. The "quasi" single phase alloys such as Coronzé 638 contain fine particle dispersions in which the size and spacing of the particles is much less than the grain size. The microduplex contain particles whose size and spacing is comparable to the grain size of the matrix. A model which incorporates particle size and spacing into grain growth can be developed based on the Zener drag process. Zener, through a private communication with C. S. Smith (16), developed the first model for the grain boundary pinning force exerted by particles. According to this picture, grain boundaries moving towards their centre of curvature must bow out in order to escape from particles, as illustrated in Fig. 5. We now imagine what happens when this boundary undergoes rapid sliding during the stochastic process associated with superplastic deformation. Since there is insufficient time for relaxation to occur sliding distorts the grain boundary - particle interaction as illustrated in Fig. 6. The angle  $\theta$  subtended by the grain boundary at the particle decreases during sliding and eventually, the grain boundary is pulled from the particle and migration occurs. When the direction of strain is reversed the direction of grain boundary sliding also changes. A delay will therefore occur before the grain boundary is again in a position to undergo unpinning and grain growth. This requires a boundary displacement  $s$ , which must be comparable to the particle spacing  $l$ . Since the strain rate is proportional to the sliding rate, the strain increment during which no grain growth will occur is about  $l/D$ , where  $D$  is the grain size. For materials containing a fine particle dispersion  $l/D$  is very small and the effect on strain reversal will be insignificant. However, for microduplex materials, in which  $l$  and  $D$  are roughly equal, a significant delay should be experienced, as indeed occurs.

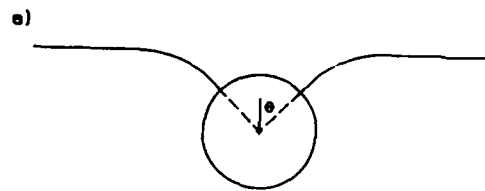
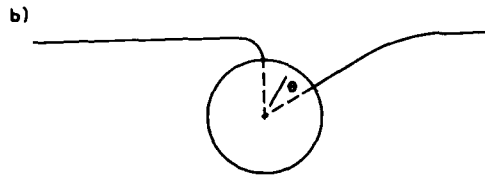


Fig. 5: a) A schematic illustration of a grain boundary bowing away from a particle.



b) A schematic illustration of a sliding grain boundary pinned by a particle.

This model may also provide the explanation for the lack of strain-enhanced grain growth in some materials. If the operative process involves Zener drag then only those materials in which grain growth is controlled by particles (or porosity) should exhibit this effect. For example, glassy ceramics do not contain grain boundaries as such. Instead, the grains are separated by a thin glass film. Grain growth therefore requires the diffusion of matter through this film, a process which should not be deformation sensitive. In other high density-high purity ceramics which contain neither porosity nor particles to pin grain boundaries, the grain size may simply be kinetically limited, and no enhancement of grain growth by deformation may occur.

#### Summary

Superplasticity relies the development and maintenance of a fine-grained microstructure. However, such microstructures tend to be unstable, and undergo strain-enhanced grain growth during superplastic deformation. The process is thought to be linked directly to grain boundary sliding. Experiments on the effect of strain reversal during superplastic deformation suggest that grain growth is enhanced by the effect of sliding on the Zener drag process. A model for this process has been developed which accounts qualitatively for the difference between "quasi" single phase and microduplex alloys.

#### Acknowledgements

This work was performed with funding from the Natural Sciences and Engineering Research Council of Canada.

### References

1. N. E. Paton and C. H. Hamilton, Method for Imparting Fine Grain Size to Aluminum Alloys Containing Precipitating Constituents, U. S. Patent 4,092,181 (1978).
2. A. K. Ghosh and C. Ghandi, "Superplasticity in Al-Li Alloys", Proc. ICSMA7, vol. 3 (Pergamon, 1985), 2065-2072.
3. D. A. Woodford, Trans. ASM, 62 (1969), 291.
4. C. H. Caceres and D. S. Wilkinson, Metall. Trans., 17A (1986), 1873-76.
5. C. H. Caceres and D. S. Wilkinson, J. Mater. Sci. Lett., 3 (1984), 395-99.
6. D. S. Wilkinson and C. H. Caceres, Acta Metall., 32 (1984), 1335-45.
7. C. H. Hamilton, Proc. ICSMA7 (Pergamon Press, 1986), vol. 3, 1831-57.
8. D. N. Senkov and V. A. Likhachev, Phys. Stat. Solidi (a), 98 (1986), 441-52.
9. D. S. Wilkinson and C. H. Caceres, Acta Metall., 32 (1984), 1335-45.
10. M. C. Pandey, J. Wadsworth and A. K. Mukherjee, Scripta Metall., 19 (1985), 1229-34.
11. D. S. Wilkinson, Proc. Intl. Conf. on Superplasticity (Edition du CNRS B. Baudalet and M. Suery, ed.; 1985), paper no. 6.
12. E. Nes, Proc. Intl. Conf. on Superplasticity (Edition du CNRS; B. Baudalet and M. Suery, ed.; 1985), paper no. 7.
13. J.-G. Wang and R. Raj, J. Am. Ceram. Soc., 67 (1984), 399-409.
14. X. Wu, V. D. Campenni, C. H. Caceres and D. S. Wilkinson, Mater. Sci. Techn. (1988), in press.
15. M. A. Clark and T. H. Alden, Acta Metall., 21 (1973), 1195.
16. C. S. Smith, Trans. Metall. Soc. AIME, 175 (1948), 15.



DYNAMIC RECRYSTALLIZATION  
AND SUPERPLASTICITY OF A MAGNESIUM ALLOY

N. G. Zaripov and R. O. Kaibyshev

Institute of the Metal Superplasticity Problems  
USSR Academy of Sciences, Ufa 450001 USSR

Abstract

The Mg-6 Zn-0.6 Zr alloy mechanical properties and structural changes during the hot straining have been studied. The nonhomogeneous character of dynamic recrystallization well correlates with the irregularity of multiple slip. It has been shown that when the volume fraction of recrystallized grains reaches 40%, the material in question becomes superplastic (SP).

Superplasticity and Superplastic Forming  
Edited by C.H. Hamilton and N.E. Paton  
The Minerals, Metals & Materials Society, 1988

## Introduction

One of the ways of obtaining a fine grain microstructure in a magnesium alloy is hot straining (1), the microstructure formation being conditioned by the dynamic recrystallization (2-4).

This paper deals with the study of the alloy mechanical properties and microstructure changes during hot straining and determination of the conditions of the Mg-6 Zn-0.65 Zr alloy conversion to the SP state.

An alloy casting with the mean grain size of 140  $\mu\text{m}$  was used as a blank, subjected to the homogenization annealing in order to increase its manufacturing plasticity. Mechanical testing was performed on the INSTRON dynamometer. Metallographic investigations were conducted on the NEOPHOT-2 microscope and EPIQUANT automatic structure analyser. The electron-microscopic studies were performed on the TESLA BS-540 microscope.

## Experimental Results

The strain-stress curves in the 150-500°C interval are shown in Fig.1. One can see that the alloy deformation is accompanied by a slight hardening which decreases with the rising temperature.

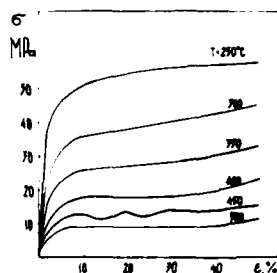


Fig.1 Flow stress-deformation curves  
( $\dot{\epsilon} = 4.3 \cdot 10^{-3} \text{s}^{-1}$ )

The magnesium alloy mechanical properties after different deformations are shown in Fig.2. After the 25% preliminary straining at 450°C the alloy shows the linear dependence of flow stress on strain rate:  $m$  does not exceed 0.25. When preliminary deformation reaches 40% SP features are displayed. The value of  $m$  at  $\dot{\epsilon} = 10^{-3} \pm 2 \cdot 10^{-2} \text{s}^{-1}$  is 0.3. When the strain rate decreases the  $m$  value becomes 0.38, and at the 85% straining and  $10^{-3} \text{s}^{-1}$  strain rate a maximum value of  $m$  is reached. The alloy displays a high SP performance. Flow stresses change with the temperature and preliminary straining.

The metallographic analysis of specimens has been performed in order to establish the regularities of microstructural changes under hot straining (Table I-III). The volume fraction of recrystallized grains and their mean grain sizes depend to a great extent on the temperature and strain rate, this dependence being of an ordinary character (5). The volume fraction of recrystallized grains increases in proportion to deformation, but even after the 75% straining recrystallization does not embrace the whole volume of material. At the 80% straining only the most active de-

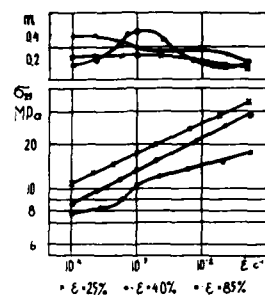


Fig.2 Flow stress ( $\sigma$ ) and rate sensitivity factor ( $m$ ) dependence on strain rate during the Mg-6 Zn-0.65 Zr alloy upsetting.

formation zone, i.e. the specimen center is recrystallized.

Significant changes in the microstructure can be observed already after the 5% straining. Grain boundaries in the vicinity of some triple points become undulated, and new grains appear with the orientation close to that of the original ones. At the original boundaries the growth of deformation results in the nucleation of new grains with a large misorientation as referred to the matrix. A mixed structure is produced, consisting of original grains stretched in the direction of deformation and surrounded by fine grains.

Table I. The Recrystallized Grains Mean Size ( $d_{rec}$ ) and Volume ( $V_{rec}$ ) at Different Temperatures of Deformation ( $\epsilon = 50\%$ )

The Microstructure Parameters	Temperature of Deformation, C°					
	250	300	350	400	450	500
$d_{rec}$ , m*	2.5	$\frac{5.0}{3.5}$	$\frac{7.5}{5.5}$	$\frac{10}{7.5}$	$\frac{14}{9}$	$\frac{16.5}{11}$
$V_{rec}$ , %	20	24	30	43	52	54

Table II. The Recrystallized Grains Mean Size ( $d_{rec}$ ) and Volume ( $V_{rec}$ ) at Different Degrees of Deformation

The Microstructure Parameters	Degree of Deformation, %					
	5	15	25	40	50	75
$d_{rec}$ , m*	-	$\frac{17}{14}$	$\frac{15}{12}$	$\frac{14}{10}$	$\frac{14}{9}$	$\frac{10.5}{7.5}$
$V_{rec}$ , %	-	14	28	42	52	72

\* numerator is longitudinal size, denominator is lateral size

Table III. The Recrystallized Grains Mean Size ( $d_{rec}$ ) and Volume ( $V_{rec}$ ) at Different Strain Rates ( $T=450^{\circ}C$ ,  $\epsilon=50\%$ )

The Microstructure Parameters	Strain Rates, $s^{-1}$					
	$2 \cdot 10^{-4}$	$4 \cdot 10^{-4}$	$8 \cdot 10^{-4}$	$4 \cdot 10^{-3}$	$9 \cdot 10^{-3}$	$2 \cdot 10^{-2}$
$d_{rec}$ , $m^*$	$\frac{28}{17}$	$\frac{24}{15}$	$\frac{19}{11}$	$\frac{14}{9}$	$\frac{12}{8}$	$\frac{10}{7}$
$V_{rec}$ , %	61	60	57	52	46	38

\* numerator is longitudinal size, denominator is lateral size

The specimen surface during deformation displays a single slip developing inside coarse grains. Multiple slip develops mainly in the vicinity of boundaries. The process is characterized by the shift of marks in neighbouring grains when a large number of recrystallized grains is formed.

The fine structure analysis after deformation has indicated that at the initial stage of deformation a 2-3  $\mu m$  cell structure is produced. When deformation increases the dislocation walls are formed in the majority of grains, the spacings between them being 1-2  $\mu m$ . During deformation the shift of one part of fine grains against the other occurs, the density of dislocations entering subgrain boundaries increases, the twisted character of the latter becomes more pronounced. Subgrain boundaries are found in the recrystallized grains too.

The character of microstructural changes during the deformation under the optimum temperature-rate conditions ( $\dot{\epsilon}=4.3 \cdot 10^{-3}$ ,  $T=450^{\circ}C$ ) depends on the original structure of material. The deformation of specimens, with recrystallized grains making 25% of their original structure, results in the further increase of the volume fraction of newly formed grains, but the structure remains partially recrystallized.

Structural changes, observed in the specimens after the 40% preliminary straining, produce a fully recrystallized structure. No significant changes in the microstructure of the specimens cut from the center of the upset blanks ( $\epsilon=80\%$ ,  $T=450^{\circ}C$ ) have been observed.

#### Discussion

The mechanical testing and microstructural studies of the Mg-6 Zn-0.65 Zr alloy have indicated that the fine grain microstructure formation under the considered hot straining conditions is due to the dynamic recrystallization. The dependence of the size of recrystallized grains on temperature and strain rate may be accounted for by the different sizes of the nuclei and different rates of their growth. The experimental data presented in this paper may be interpreted by means of the well known scheme of fine-grain microstructure formation (3), which implies the creation of a developed subgrain structure in the boundary regions and a gradual transformation of low angle boundaries into high angle ones.

The local stresses in the vicinity of grain boundaries cause the development of multiple slip there. The interaction of different slip system dislocations results in the formation of subgrain boundaries which are gradually transformed into high angle ones. When the 25% deformation is reached, the chains of fine grains are formed round the original ones. Under these conditions the development of grain boundary sliding becomes possible, which results in the sharp decrease of local stresses at the original and recrystallized grain boundaries due to the acceleration of the absorption of dislocations in grain boundaries. Multiple slip in the boundary region is impeded. However, a small volume of recrystallized grains is not enough to provide for the SP flow of material. Only at the 40% straining (Vr.g.  $\approx 40\%$ ) the alloy SP deformation starts, localized in the fine grain regions. The absence of local stresses during the SP flow impedes the subgrain structure formation, because dislocation sliding occurs mainly over the basal plane. The transition from the ordinary hot straining to the SP deformation hinders the development of recrystallization.

The application of magnesium alloys in the SP state is possible when their structure contains no less than 40% of recrystallized grains. Blanks with homogeneous microstructures are needed in case a low flow stress and homogeneous deformation are required to produce parts by forming.

#### References

1. O. A. Kaibyshev, Superplasticity of Commercial Alloys (Moscow: Metallurgia Publ., 1984), 264 p. (in Russian).
2. S. E. Burrous, F. G. Humphreys, and S. H. White, "Dynamic Recrystallization and Textural Development in Magnesium Deformed in Compression at Elevated Temperature," Strength Metals and Alloys. Proc. 5th Int. Conf. Aachen, 1979, Vol.1 (Toronto, 1979), 607-612.
3. S. E. Ion, F. J. Humphreys, and S. H. White, "Dynamic Recrystallization and the Development of Microstructure during the High Temperature Deformation of Magnesium," Acta Met., 30(10) (1982), 1909-1919.
4. N. G. Zaripov, A. G. Vagapov, and R. O. Kaibyshev, "The Magnesium Alloy Dynamic Recrystallization," Fizika Metallov i Metallovedenie, 63(4) (1987), 774-781 (in Russian).
5. T. Sakai and J. J. Jonas, "Dynamic Recrystallization: Mechanical and Microstructural Consideration," Acta Met., 32(2) (1984), 189-209.

# GRAIN REFINEMENT BY TORSION AND SUPERPLASTICITY

## IN HIGH STRENGTH AL-ALLOY

Jin Quanlin   Bai Bingzhe   Lai Weihua  
Guo Xusheng   Zhang Hong

Beijing Research Institute of Mechanical and Electrical  
Technology of SIME, Beijing, China

### Abstract

A hot torsion method of grain refinement and realizing superplasticity for two kinds of high strength AL-alloys LC4(close to 7075) and LC9(close to 7475) has been studied experimentally. It is observed that initial coarse columnal grains are gradually changed into the near-equiaxial grains with about 15 micrometer dia.. The tensile tests of specimen machined from torqued rod show that the maximum elongation of LC4 and LC9 is 580% and 470% respectively, the value  $n$  is over 0.5 in a wide range of strain rate, the flow stress is only as 1/5 as that of the original materials under the same tensile conditions, and the fine grains are very stable at the elevated temperature.

Based on the investigation into refinement mechanisms, it is pointed out that the grain refinement is a process of dynamic recrystallization. The effects of torsion temperature, torsion speed and shear strain on refinement result are discussed.

Superplasticity and Superplastic Forming  
Edited by C.H. Hamilton and N.E. Paton  
The Minerals, Metals & Materials Society, 1988

### Introduction

It is well known that fine grain is necessary for the structure superplasticity. The warm rolling method developed first by Hamilton (1) is being used for grain refinement of the commercial high strength aluminium alloy, and an excellent superplastic behavior: total elongation of 1200% for alloy 7475 and total elongation of 1550% for alloy LC4(close to 7075) (2) has been obtained. But this method is applicable only for the sheet, so it is desired to find a new refinement method to apply for the materials in other shapes. Erdmann reported that grain refinement of AL and Cu can be realized by means of hot torsion (3) which is suitable for rod and tube.

The presented investigation aims to propose a hot torsion method of grain refinement in order to realize superplasticity for two kinds of high strength aluminium alloys LC4(close to 7075) and LC9(close to 7475), and to discuss the refinement mechanism and the influences of torsion deformation conditions on refinement and superplasticity.

### Experimental Details

The torsion specimen with diameter of 14mm and gauge length of 150mm was machined from the commercial aluminium alloys LC4 and LC9, whose chemical components are shown in Table 1. After a solution treatment at 753K for 3 hrs and over-aging at 673K for 8 hrs, the specimen was hot torqued and then was quenched into cold water as soon as it was removed from the split furnace.

Table 1                      Chemical Components(%)

materials	Cu	Mg	Zn	Cr	inclusions
LC4	1.4-2.0	0.2-0.6	5.0-7.0	0.10-0.25	< 1.1
LC9	1.2-2.0	/	5.1-6.1	0.16-0.30	/

Further microscopic analysis of a specimen cut from torqued rod was made to determine the precise grain size. Finally, at 793 K, the superplastic tensile test of specimen, with diameter of 5 mm and gauge length of 15 mm, machined from torqued rod was carried out in order to observe superplasticity of above alloys after refinement.

### Results and Discuss

#### Experimental Results

After torsion at the angular speed of 0.02/s and at the temperature of 719K (for LC4) or 763K-773K (for LC9), the initial coarse columnar grain with diameter more than 100 micrometer has become finer grain(with average diameter of 15 micrometers for LC9 after torsion at 773K). From two sectional views of grain(Fig.1), it can be seen that the refined grain looks like an elliptical cake with a thickness-to-length ratio of 1:2, and its long axis is parallel to the tensile direction.

The tensile tests of torqued specimens show that at 793K and at cross-head speed 0.2mm/min, the maximum elongation of LC9 and LC4 is 580% and 470% respectively, the strain rate sensitivity index  $m$  is over 0.5 in a wide

range of strain rates and the flow stress is  $1/5$  of that of the original material under the same tensile conditions. The microstructure of extended specimens shows that the fine grain is rather stable in the elevated temperature, and original near-equiaxial grains have been changed into equiaxial.

#### Refinement Process

A group of microstructures corresponding to different torsion deformations shown in Fig.2 explains the grain refinement process by means of hot torsion. At the beginning, the coarse columnar grain is twisted and the substructure near coarse grain boundary increases. When increasing deformation, number of finer grain formed along coarse grain boundary increases gradually. The finer grain is developing from the boundary to the center of the coarse grain. At last the coarse grain boundary disappears and is replaced by a great deal of finer grains arranged parallel with each other. The refinement is found to develop from surface to center of the rod. Since shear strain increases with radius, the refinement result is directly dependent on shear strain.

#### Grain Refinement Mechanism

Obviously, both deformation and recrystallization take place concurrently during the hot torsion, which is exactly a dynamic recrystallization. In addition, the higher temperature and the lower strain rate, at which the specimen is torqued, provide the conditions for recrystallization.

During the hot torsion, subgrains are produced from coarse grain's breaking. As the nucleus of recrystallization, they can develop into finer grains, that is just as general recrystallization process. On the other hand, in superplastic deformation grain boundary sliding, grain rotation, subgrain boundary sliding and subgrain rotation may be concurrent. Then subgrain movement can change the low angle grain boundary into high angle grain boundary, and subgrains into finer grains. The change from subgrain to finer grain is gradually developing from boundary to the interior of the coarse grain. The coarse grain may be also broken up into several finer grains. Fig.3 shows some finer grains formed from subgrains near the coarse grain boundary and that formed through breaking coarse grain up.

#### Temperature Effect

Fig.4 shows the effect of torsion temperature on the refinement result. Fig.4(a) indicates that the torsion at room temperature caused only extension of the coarse grains in the deformation direction and an increase of the density of the substructure on the grain boundary. From Fig.4(b) and (c) it can be seen that under the same deformation the grain refinement at 673K is not so significant as at 773K, but the cavities produced at 673K are much more serious than at 773K.

A dynamic recrystallization is a complex process where the coarse grain breaking, subgrain moving, finer grain forming and other variations must be coordinated by some external conditions, among which a good match of temperature and strain rate, especially higher temperature, is principle. Only at such high temperature, atoms have stronger diffusion capability for aiding the speed of forming finer grains keep up with the speed of deformation and breaking of coarse grains. Thus, the internal stress accumulated during deformation is released, and uniform refinement process continues. But at lower temperature, it is very easy to cause stress concentration and to form a great deal of cavities too early. The release of the internal stress by the cavities interrupts the refinement process.



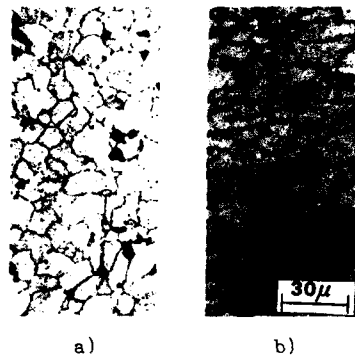


Fig.1 Microstructure of torqued specimen (753K, 21.12 turns)  
a) cross section,  
b) vertical section.

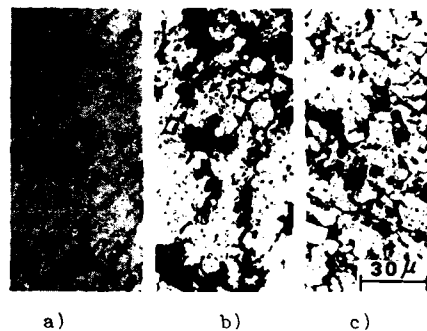


Fig.4 Effect of temperature on grain refinement (1 mm from specimen surface)  
a) room temp., 2 turns, b) 673K, 6 turns.  
c) 773K, 6 turns.

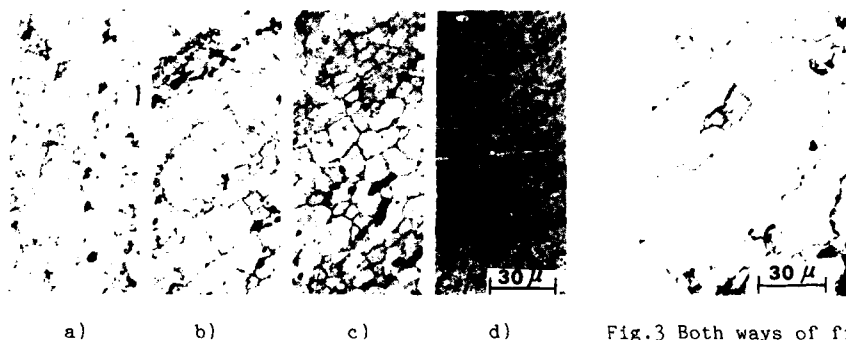


Fig.2 Refinement sequence.

Fig.3 Both ways of fine grain forming being shown (753K, 21.12 turns).

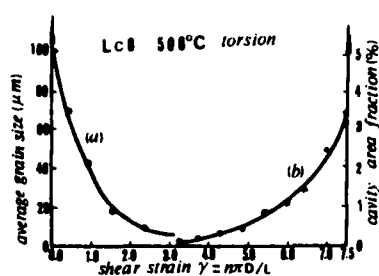


Fig.5 Variation of grain size (a) and cavity growth (b) with shear strain.

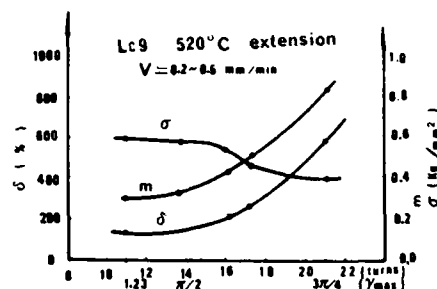


Fig.6 Effect of shear strain on elongation, value  $m$  and flow stress in tensile test.

### Deformation Effect

Not only temperature and torsion speed but also deformation are rather important parameters which effect grain refinement and cavity formation for above cavity sensitive alloys. Fig.5 presents the variations of average grain size and cavity area fraction with shear strain. The curves show that grain refinement needs certain deformation; but when deformation is over a certain value it is no longer significant. On the other hand, an excessive deformation would cause cavity growth and an increase of their number. Therefore it is important to control the torsion deformation in such way that grain refinement is better and cavities are not too serious. In fact, the optimal range of strain is existential. The deformation effect has been supported by tensile test results shown in Fig.6, where the curves demonstrate three basic superplastic parameters are improved with the increasement of shear strain.

### The Possibility of Omitting Heat Treatment

Table 2 gives a comparison of tensile test results after three different refinement processes. The comparison shows that the contribution of hot torsion for grain refinement is much greater than that of heat treatment. Omitting heat treatment before torsion would not make final superplasticity drop too much.

Table 2 Effect of Refinement Process on Superplasticity (LC9)

heat treatment	shear strain	elongation(%)	flow stress(Kg/mm <sup>2</sup> )	M
yes	2.37	580	0.28	0.58
No	2.13	400	0.36	0.42
yes	0.00	155	1.10	0.29

### Conclusions

From presented experimental study, it is concluded that:

- 1.For high strength aluminium alloy, the hot torsion under proper conditions can change the original coarse columnar grains into the stable near-equiaxed grains. The refined alloy has excellent superplasticity.
- 2.The technical process of the grain refinement is  
solid solution ----- over-ageing ----- hot torsion
- 3.The mechanism of the hot torsion refinement is dynamic recrystallization.

### References

1. C.H.Hamilton, C.C.Bampton and N.E.Paton, "Superplasticity in High strength Aluminium Alloys", pp.173-189 in Superplastic Forming of Structural Alloys, N.E.Paton and C.H.Hamilton ed., the Metallurgical Society of AIME, 1982.
2. Wu Qingling et al., "Research on Superplasticity of Commercial Structural Aluminium Alloy LC4", pp.91-94 in Proceeding of JAPAN-CHINA JOINT SYMPOSIUM ON SUPERPLASTICITY, 1986, YOKOHAMA.
3. F.Erdmann-Jesnitzer and T Rahaman, "Dynamic Recorvy and Grain Refinement for Increased Strength of Copper by Suitable Warm Torsion", Metall, Nov., 1978,32,(11).

## THE TRANSFORMATION OF Ti ALLOY

### LAMINAR MICROSTRUCTURE INTO A MICRODUPLEX ONE

G. A. Salishchev and R. Ya. Lutfullin

Institute of the Metal Superplasticity Problems  
USSR Academy of Sciences, Ufa 450001 USSR

#### Abstract

The study of the laminar microstructure evolution into an equiaxial one during hot straining has been performed on the  $\alpha$ -titanium Ti-5.4 Al-2.8 Sn alloy. The acceleration of the alloy microstructure transformation during hot straining as against annealing is shown to be conditioned by the formation of high angle grain and interface boundaries, accompanied by the enhancement of diffusion and  $\alpha \rightarrow \beta$  polymorphous conversion. A microstructure transformation scheme based on the dislocation slip, diffusion creep, and boundary sliding operating during the alloy straining has been suggested, the relation between the said mechanisms changing in favour of the latter during the plastic flow.

Superplasticity and Superplastic Forming  
Edited by C.H. Hamilton and N.E. Paton  
The Minerals, Metals & Materials Society, 1988

## Introduction

Laminar microstructures in Ti-alloys, contrary to the perlite in steels, are thermodynamically equilibrated (1). This is indicated by the laminar shape being preserved in the  $\alpha$ -phase, and its being approached by the original globular phase, subjected to a prolonged annealing in the  $(\alpha + \beta)$  region. The stability of laminar microstructures is accounted for by the low energy semicoherent boundaries existing in the alloys.

The laminar microstructure transformation in titanium alloys is considerably accelerated during hot straining. Meanwhile it should be admitted that the main stages and mechanisms of microstructure globularization during hot straining, especially its kinetics in different alloys, have been studied insufficiently. The results of the laminar microstructure evolution study during the  $\alpha$ -titanium Ti-5.4 Al-2.8 Sn alloy hot straining are presented in this paper.

## Experimental Details

Specimens with the diameter of about 10 mm, and 15 mm high, were upset on the dynamometer and then quenched in water to room temperature in 1 second or less.

## Materials

According to Fig.1, the flow stress ( $\sigma$ ) in the  $\alpha$ -region decreases monotonously with the rise of temperature of deformation. In the alloy duplex state, the reduction of  $\sigma$  is pronounced, but in the  $\beta$ -region it becomes monotonous again. Extrapolating the alloy  $\alpha$ -state curve onto the  $\beta$ -region temperature, one can evaluate the flow stress of each phase during the alloy deformation in the duplex phase region:  $\sigma_\alpha$  almost six times exceeds  $\sigma_\beta$ .

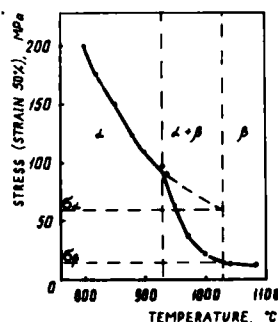


Fig.1 The flow stress dependence on temperature at  $\dot{\epsilon} = 8.5 \cdot 10^{-4} \text{ s}^{-1}$  and  $\epsilon = 50\%$ .

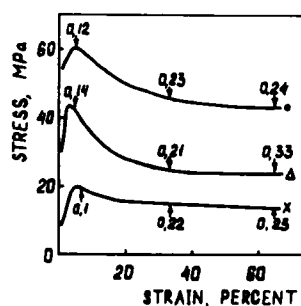


Fig.2 The flow stress and  $m$  factor dependence on straining at the following strain rates:  $\bullet$  -  $5.5 \cdot 10^{-3} \text{ s}^{-1}$ ;  $\Delta$  -  $5.5 \cdot 10^{-4} \text{ s}^{-1}$ ;  $\times$  -  $5.5 \cdot 10^{-5} \text{ s}^{-1}$ .

The study of the  $\sigma = f(\epsilon)$  curves at  $1000^\circ\text{C}$  has revealed the existence of the flow stress peak at the initial stage of deformation (Fig.2). Further increase of straining reduces  $\sigma$ , which

is followed by the steady flow stage. At the same time, it is evident that at  $\dot{\epsilon}=5.5 \cdot 10^{-4} \text{s}^{-1}$  the decrease of  $\sigma$  due to softening is much greater than at other strain rates. It turned out that at this rate and with increasing deformation, the  $m$  factor permanently increases reaching 0.33 at the 70% straining. At higher and lower strain rates the  $m$  values decrease.

In the original state, the alloy microstructure grain size is about 500  $\mu\text{m}$ . At 1000°C the microstructure is two phase with about 12  $\mu\text{m}$  thick  $\alpha$ -laminae.

Consider the alloy microstructure evolution at 1000°C and  $\dot{\epsilon}=8.5 \cdot 10^{-4} \text{s}^{-1}$ . At the initial stage of deformation ( $\epsilon=15\%$ ),  $\alpha$ -laminae become curved and divide into fragments, and some of them shift against the others. Recrystallized grains appear in the  $\beta$ -phase (Fig.3a).

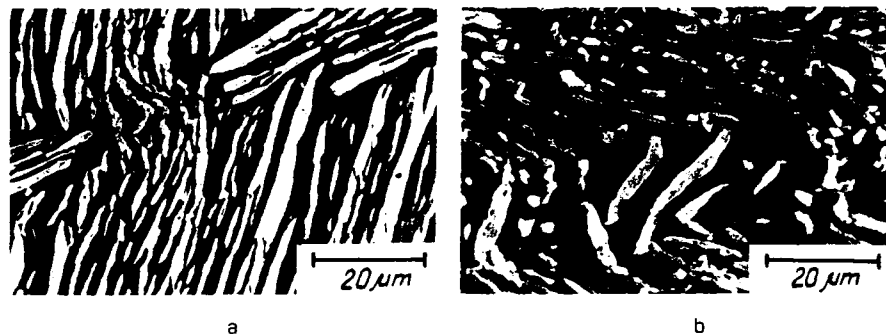


Fig.3 The as-strained alloy microstructure:  
a)  $\epsilon=15\%$ ; b)  $\epsilon=30\%$ .

With further straining ( $\epsilon=30\%$ ) the amount of recrystallized grains in the  $\beta$ -phase considerably increases. The  $\alpha$ -phase displays recrystallization features. The laminae turn in the direction of deformation. Interface boundaries become curved. The bending of laminae occurs at the site where they enter the interface of cross grain boundaries formed during the  $\alpha$ -phase recrystallization. Besides,  $\beta$ -particles which are not connected with the matrix  $\beta$ -phase by means of grain boundaries, are found in the  $\alpha$ -phase (Fig.3b). At the 50% straining a strong metallographic texture is produced. Recrystallization embraced practically the whole of the  $\beta$ -phase volume, as well as much of the  $\alpha$ -phase. In the course of deformation the  $\alpha$ - and  $\beta$ -phase grains will grow and reach the interface boundaries. The bending of the latter towards both the  $\alpha$ - and  $\beta$ -phase regions increases. The laminae fragments shift against one another. The volume fraction of equiaxial  $\alpha$ -precipitations considerably increases. By  $\epsilon=80\%$  a globular microstructure is produced in the alloy, the volume fraction of equiaxial  $\alpha$ -phase particles reaches 78%. The alloy hot straining is accompanied by the changes in the  $\alpha$ -phase volume. At the 50% straining it decreases from 42 to 30%, while at the 80% straining it increases up to 35%.

### Results and Discussion

From the above described experiments it follows that, due to the formation of a microduplex microstructure at the final stage of deformation, the alloy displays superplastic (SP) features, and its flow stresses increase. The laminar microstructure transformation is conditioned by the dislocation slip (DS) and grain boundary sliding (GBS), the relation between them changing in the course of plastic flow in favour of the latter alongside with the enhancement of diffusion.

Due to the difference of deformation characteristics of phases, at the initial stage of deformation DS concentrates in a "softer"  $\beta$ -phase. That is why the  $\alpha$ -phase recrystallization starts with some delay. The growth of the  $\beta$ -phase grains, followed by that of the  $\alpha$ -phase ones, results in the interaction of high angle grain boundaries with interface ones, and transformation of the latter into noncoherent boundaries. The formation of high energy interface and grain boundaries accelerates the diffusion processes and sharply increases the boundary mobility, which makes them curved. On the other hand such boundaries provide a better site for GBS, which is indicated by the turn and shift of both the laminae and their fragments, and the SP flow is observed in the alloy.

The  $\alpha \rightarrow \beta$  phase conversion, occurring during the alloy deformation, is probably a mechanism of DS and GBS accommodation. This conversion may be induced by different causes (4,5), though none of them can account for the  $\beta$ -phase developing inside the  $\alpha$ -phase particles.

The data available makes it possible to suggest a scheme of the alloy laminar microstructure conversion to an equiaxial one during hot straining. Consider the behaviour of  $\alpha$ - and  $\beta$ -phase fragments oriented normal to the load applied (P) (Fig.4). It is evident that due to the difference in the deformation characteristics of phases the plastic flow mostly effects a "softer"  $\beta$ -phase. The aggregate of  $\alpha$ - and  $\beta$ -phase fragments will certainly be effected by contraction and compression stresses. Then, according to the Nabarro-Herring diffusion creep mechanism, vacancies from a more contracted  $\beta$ -phase will flow in the interface boundary, and the basic alloy element atoms (i.e. Al) which are the most mobile in both  $\alpha$ - and  $\beta$ -phase will have to move towards the  $\beta/\beta$  grain boundary. The withdrawal of the Al atoms from the interface will produce, firstly, the  $\alpha \rightarrow \beta$  polymorphous conversion and, secondly, their diffusion in the boundary regions in order to restore the original concentration. The latter process may eventually deplete the Al  $\alpha$ -laminae body and convert some isolated regions to  $\beta$ -phase. It is only natural that Al atoms most actively withdraw from the interface-grain boundary junctions where the increase of surface energy is observed, which results in the formation of "grooves". The shift of fragments along the grain boundary also accelerates conversion, for it enlarges the interface and, consequently, causes the local increase of its energy. With the formation of equiaxial microstructure the GBS contribution sharply increases, which diminishes the role of diffusion creep in deformation (3).

The discussed mechanisms may also be used with the laminar aggregates of other alloys. The comparison of the presented data

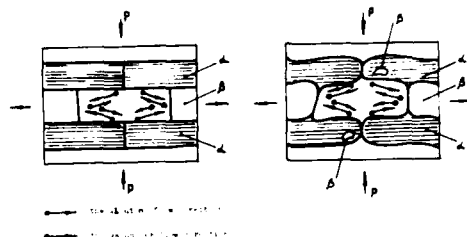


Fig.4 The  $\alpha$ - and  $\beta$ -phase laminae division scheme.

with those in (1) indicates that the basic difference in the behaviour of  $\alpha$ - and ( $\alpha + \beta$ ) alloys is determined by the difference of the high energy interface and grain boundary formation mechanisms. This is accounted for by the peculiarities of their alloying and its influence on the deformation characteristics of phases.

#### References

1. O. A. Kaibyshev, R. Ya. Lutfullin, and G. A. Salishchev, "Microstructural Changes of the VT9 Laminar Titanium Alloy When Subjected to Thermal Treatment and Hot Straining," Fizika Metallov i Metallovedenie, 3(59)(1985), 378-383 (in Russian).
2. I. Wiess et al., "Modification of  $\alpha$ -Morphology in Ti-6 Al-4 V by Thermomechanical Processing," Met. Trans.(A), 11(17)(1986), 1935-1947.
3. O. A. Kaibyshev, Superplasticity of Commercial Alloys (Moscow: Metallurgia Publ., 1984), 55-208 (in Russian).
4. H. Gegel et al., "Dynamic Effects on Flow and Fracture during Isothermal Forging of a Titanium Alloy," Scripta Met., 2(14) (1980), 241-246.
5. P. Dadras and I. F. Thomas, "Characterization and Modelling for Forging Deformation of Ti-6 Al-2 Sn-2 Mo-0.1 Si," Met. Trans.(A), 11(12)(1981), 1867-1876.

THE ROLE OF MATRIX DISLOCATIONS  
IN THE SUPERPLASTIC DEFORMATION

P. Lukáč

Department of Metal Physics, Charles University,  
Ke Karlovu 5, 121 16 Praha 2, ČSSR

Abstract

In the paper the results of the deformation behaviour and microstructural study in a fine-grained Zn-1.1 wt% Al and in an Al-6wt% Cu-0.5 wt% Zr alloy are presented. The influence of strain rate ranging from  $1.2 \times 10^{-5}$  to  $4.2 \times 10^{-2} \text{ s}^{-1}$  on ductility and the strain rate sensitivity of the flow stress was investigated over a wide temperature range. The increase in temperature improved the superplastic properties and shifted the region of the superplastic flow to higher strain rates. The best superplastic properties of a Zn-1.1 wt% Al alloy ductility  $A = 1020\%$  and parameter  $m = 0.72$  were established at 520 K in a sample with the grain size  $d = 17 \mu\text{m}$  deformed at  $\dot{\epsilon}_0 = 10^{-4} \text{ s}^{-1}$ . The grain size was observed to increase during the deformation at higher temperatures. Taking into account the effect of grain growth a satisfactory correction of flow stresses is possible. The grain growth was also found to be responsible for differences in the strain rate sensitivity parameter obtained from the  $\log \sigma$  vs  $\log \dot{\epsilon}$  plots and from the strain rate changes. Experiments on the Zn-1.1 wt% Al were completed by a study of the texture changes accompanying superplastic flow and by an investigation of acoustic emission associated with strain for samples with different grain size deformed at various strain rates. These experimental results confirm the contribution of lattice dislocations to deformation in the superplastic region. The microstructural investigation of the Al-6wt% Cu - 0.5 wt% Zr showed evidence for intergranular dislocation movement. The most important mechanisms in the superplastic deformation seem to be the grain boundary sliding and the movement of matrix dislocations.

Superplasticity and Superplastic Forming  
Edited by C.H. Hamilton and N.E. Paton  
The Minerals, Metals & Materials Society, 1988



## Introduction

A great deal of attention has been paid the past decades to the problem of superplasticity. Generally, it is assumed that superplastic behaviour is observed in materials having a stable fine-grained structure (usually  $d \leq 10 \mu\text{m}$ ) deformed at temperatures  $T > 0.4 T_m$ ,  $T_m$  being the melting point, in a certain strain rate range. The total elongation and the strain rate sensitivity of the flow stress,  $m$ , are considered as a measure of superplasticity. The parameter  $m$  is defined as

$$m = (d \log \sigma) / (d \log \dot{\epsilon})$$

where  $\sigma$  is the stress and  $\dot{\epsilon}$  is strain rate.

Experimental results (1,2) indicate that extensive grain boundary sliding is dominant during optimal superplastic flow. Some evidence for diffusional flow have been reported (2). It has been established that dislocation slip occurs during superplastic deformation (3). In the present paper we have made an attempt to have a better insight into the role of a intergranular dislocation motion in the superplastic deformation.

## Material and experimental procedure

Zn-1.1 wt% Al alloy was prepared from very pure metals (99.999% Zn and 99.999% Al). In order to avoid structure changes that could occur at room temperature the material was set immediately after rolling into dry ice. The mean grain size  $d$  was  $1.1 \mu\text{m}$  (4). Annealing at various temperatures for a certain time was used to prepare samples with variations in grain size (5, 12, 21, and  $55 \mu\text{m}$ ). Tensile tests were carried out on an Instron testing machine at an initial strain rate  $\dot{\epsilon}_0$  from the range of  $1.2 \times 10^{-5}$  to  $4.2 \times 10^{-2} \text{s}^{-1}$ .

The acoustic emission pulses were detected by piezoelectric transducer with a resonance frequency of 180 kHz. The whole amplification was about 82 dB. Acoustic emission was characterized by parameter  $N_C$ - number of pulses higher than definite threshold voltage (5).

The mechanical properties of Al-6 wt% Cu-0.5 wt% Zr were investigated at temperatures between 573 and 777 K (i.e.  $0.6 - 0.85 T_m$ ). Samples (with  $d = 1.5 - 10 \mu\text{m}$ ) were deformed at the initial strain rate  $\dot{\epsilon}_0 = 1.4 \times 10^{-3} \text{s}^{-1}$ . The microstructure of specimens was investigated by means of TEM.

## Results and discussion

The fine grained Zn-1.1 wt% Al alloy exhibits superplastic behaviour already at room temperature. The maximum ductility  $A = 600\%$  and the maximum value of  $m = 0.36$  were observed. Figure 1 shows the strain rate dependence of ductility  $A$  for Zn-1.1 wt% Al samples deformed at two temperatures (6). The increase in deformation temperature to 375 K caused an increase in ductility ( $A = 700\%$ ) and in the parameter  $m (= 0.48)$ . Figure 2 shows the temperature dependence of the maximum values of the strain-rate sensitivity parameter  $m$  obtained by strain rate changes for Zn-1.1 wt% Al samples deformed at various initial strain rates (7). The value of  $m$  obtained from the slope of the  $\log \sigma$  vs  $\log \dot{\epsilon}$  plot are smaller than those estimated from strain rate changes. The parameter  $m$  increases with the strain (4,6,7). The maximum values of  $m$  seem to be independent of the strain rate at higher temperatures. Superplastic behaviour of this alloy is observed in a broad interval of temperatures between  $0.4$  and  $0.9 T_m$ . The best superplastic characteristic  $A = 1020\%$  and  $m = 0.72$  were established at  $T = 520 \text{ K}$  in a sample with the grain size  $d = 17 \mu\text{m}$  deformed at the strain rate  $\dot{\epsilon}_0 = 10^{-4} \text{s}^{-1}$  (6,7). The true stress vs true strain curves at various temperatures for several strain rates exhibit

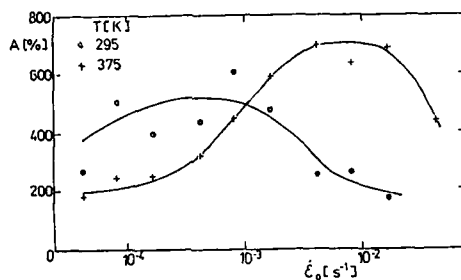


Figure 1 - The strain rate dependence of ductility A.

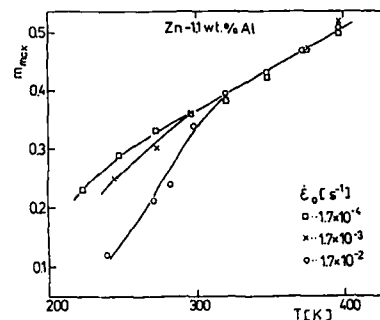


Figure 2 - The temperature dependence of the parameter m.

a nearly steady state character. The deviations from the steady state character of these curves may be explained considering the grain growth and the decrease in the true strain rate during the deformation. The grain growth is also found to be responsible for differences in the values of  $m$  obtained by different techniques.

Considering the experimental data one may suggest that the superplastic deformation of the Zn-1.1 wt% Al alloy results probably from a combination of more deformation mechanisms rather than from a single one. The study of deformation structure revealed typical marks of grain boundary sliding (7). On the other hand, slip lines were observed in some grains (7), which gives evidence for the motion of lattice dislocations.

The influence of grain size on ductility is shown in Fig. 3 (5). It is seen that ductility of samples with grain size of  $5\text{ }\mu\text{m}$  and  $12\text{ }\mu\text{m}$  is high. Ductility of samples with grain sizes of  $21\text{ }\mu\text{m}$  and  $55\text{ }\mu\text{m}$  has values corresponding to the plastic deformation of polycrystals. In all cases the values of parameter  $m$  decrease with increasing grain size.

Figure 4 shows a variation of acoustic emission with strain (at the beginning of deformation) for samples with different grain size deformed at room temperature (5). Acoustic emission is increasing with increasing grain size. Our experimental observations are in agreement with the observation of acoustic emission during the superplastic deformation (8). The experimentally observed grain size dependences can be explained assuming the microstructural mechanisms change with the variation of grain size. The main deformation mechanisms of samples with grain size of  $21\text{ }\mu\text{m}$  and  $55\text{ }\mu\text{m}$  is dislocation glide. Superplasticity occurs for samples with grain size smaller than  $12\text{ }\mu\text{m}$ .

These experimental results confirm the contribution of lattice dislocations to deformation in the superplastic region, too. This conclusion is also in agreement with texture studies on this alloy. The formation of the new texture peak in the centre of the (0002) pole figure may be explained as a result of some intergranular dislocation movement in basal plane. The movement of lattice dislocations in the superplastic region is in accordance with other measurements (9,10). It should be mentioned that in the non-superplastic region at very high temperatures no signs of grain boundary sliding were observed.

The above mentioned observations and conclusions may be further supported by the detailed measurements of the microstructure prior to deformation and after testing in the Al-6wt% Cu - 0.5 wt% Zr alloy examined by TEM (11). Figure 5 shows the strain rate dependence of ductility for samples deformed

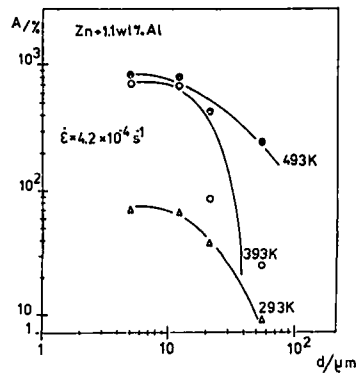


Figure 3 - Ductility as a function of grain size.

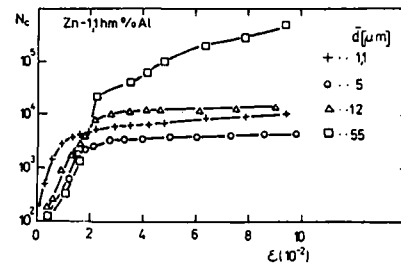


Figure 4 - Variation of AE with strain for different grain size.

at 698 K. The maximum ductility achieved at strain rate of  $1.4 \times 10^{-3} \text{ s}^{-1}$  is a strain of 508%. A typical dislocation configuration for samples deformed at strain rate of  $1.4 \times 10^{-3}$  at 698 K at the strain of 200% is shown in Fig.6. The dislocation density measured in sample deformed at 698 K is about  $2 \times 10^{13} \text{ m}^{-2}$ . Measurements of the dislocation density show that the numbers of dislocations in the matrix increase with increasing deformation. Thus, the microstructural investigations show evidence for intergranular dislocation movement.

On the basis of the experimental results we can conclude that the rate-controlling mechanisms in the superplastic deformation are grain boundary sliding and the movement of lattice dislocations.

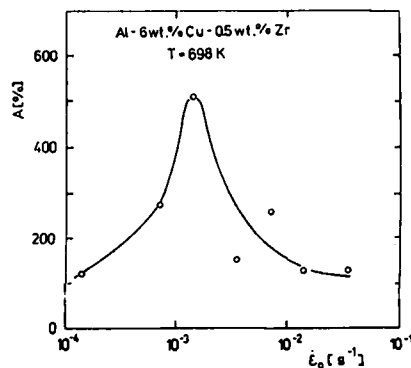


Figure 5 - The strain rate dependence of ductility for an Al alloy.



Figure 6 - Dislocation structure for an Al alloy ( $T=698 \text{ K}$ ,  $\epsilon=200\%$ ).

#### References

1. Oskar A. Kaibyshev, Plastichnost i sverkhplastichnost metallov (Moscow: Metallurgiya, 1975).
2. Kupposwamy A. Padmanabhan and Graeme J. Davies, Superplasticity (Berlin: Springer-Verlag, 1980).
3. O.A. Kaibyshev, R.Z. Valiev, and V.B. Astanin, "On the Nature of Superplastic Deformation", Physics status solidi (a), 35 (1976) 403-413.
4. P. Lukáč, and P. Málek, "Effect of Temperature on the Deformation Behaviour of a Superplastic Zinc Alloy", Czechoslovak Journal of Physics, B 31 (1981) 228-230.
5. Z. Trojanová, P. Lukáč, and F. Chmelík, "The Effect of Grain Size on the Deformation Behaviour of Zn-Al Alloy" 5th International Congress on Heat Treatment of Materials, vol. III (Budapest: Scientific society of Mechanical Engineers, 1986), 1885-1890.
6. P. Málek, and P. Lukáč, "Superplasticity in a Zn-1.1 wt% Al Alloy, I.", Czechoslovak Journal of Physics, B 36 (1986) 498-508.
7. P. Málek, and P. Lukáč, "Superplasticity in a Zn-1.1 wt% Al Alloy, II.", Czechoslovak Journal of Physics, B 37 (1987) 975-992.
8. R. Frydman, R. Pascual, and R.M. Volpi, "Acoustic Emission due to Dislocations and Grain Boundaries", Scripta Metallurgica, 9 (1975) 1267-1270.
9. O.A. Kaibyshev, "Mechanisms of Superplastic Flow of Metals and Alloys", Czechoslovak Journal of Physics, B 31 (1981) 223-227.
10. L.K.L. Falk et al., "The Role of Matrix Dislocation in the Superplastic Deformation of a Copper Alloy", Acta Metallurgica, 34 (1986) 1203-1214.
11. M. Hyža, "Superplasticity of Aluminium Alloys" (Diploma thesis, Charles University, Prague, 1987).

## **SUPERPLASTIC DEFORMATION INDUCED GRAIN GROWTH**

### **IN MICRODUPLEX AND SECOND PHASE DISPERSED ALLOYS**

**Eiichi Sato, Kazuhiko Kuribayashi and Ryo Horiuchi**

The Institute of Space and Astronautical Science,  
3-1-1, Yoshinodai, Sagami-hara-shi, Kanagawa 229,  
Japan

#### **Abstract**

The behavior of grain growth during superplastic deformation is studied, which consists of a deformation induced component and a static component. The former stabilizes the deformation itself through flow hardening. A method to separate these components is developed analytically. The grain growth behavior is examined experimentally using microduplex Zn-22%Al alloy and second phase dispersed Al-5%Mg-0.6%Mn alloy. The deformation induced grain growth in these alloys is independent of strain rate, initial grain size and deformation temperature, and can be expressed by  $\ln(\bar{D}/\bar{D}_0) = \alpha \epsilon$ , where the values of  $\alpha$  are 0.3 and 0.6 in Zn-Al and Al-Mg-Mn alloys, respectively.

Superplasticity and Superplastic Forming  
Edited by C.H. Hamilton and N.E. Paton  
The Minerals, Metals & Materials Society, 1988

### Introduction

In structural superplasticity, it is desirable that the material has fine and equiaxed grain structure. Many superplastic alloys, therefore, have two-phase or second phase particle dispersed structures, whose grain growth rate is relatively small. Rapid grain growth, however, has often been observed during superplastic deformation. As flow stress of superplasticity is sensitive to grain size, Caceres et al [1] pointed out that grain growth influences and stabilizes deformation itself. Their suggestion is important in clarifying the role of grain growth, but lacks consideration to the static grain growth.

Recently, Hamilton [2] pointed out that only the strain dependent component (deformation induced grain growth) has an effect on the stability. He also pointed out that flow stress increase due to the deformation induced grain growth is distinguished as "flow hardening" from the usual work hardening. Nevertheless, he has not given a method to separate the whole grain growth into these two components.

In the present study, at first, the separation of the two components are discussed analytically. To examine the grain growth behavior experimentally, two types of alloys are prepared, that is, microduplex and second phase dispersed alloys. Zn-22%Al eutectoid alloy is used as an example of the former, and Al-5%Mg-0.6%Mn alloy for the latter. The deformation induced grain growth behaviors of both alloys are not affected by the magnitude of the static grain growth, and they are similar to each other except the magnitude per unit strain. Behavior of stress increase is examined under constant strain rate condition.

### Separation of the Two Grain Growth

In this section, a method is developed analytically to separate the whole grain growth into the two components. If these two components are independent of each other, the rate of the latter is equal to the rate in static annealing without deformation, which can be predicted theoretically according to the rate control process. As for the former, an experimental equation (eq.4) is used. The whole grain growth rate is the summation of these two and expressed as

$$\frac{d\ln\bar{D}}{dt} = \left(\frac{\partial \ln\bar{D}}{\partial \dot{\epsilon}}\right)_t \dot{\epsilon} + \left(\frac{\partial \ln\bar{D}}{\partial t}\right)_\epsilon = \alpha \dot{\epsilon} + \frac{k}{t} \bar{D}^{-r}, \quad (1)$$

where  $\bar{D}$ ,  $\epsilon$ ,  $\dot{\epsilon}$  and  $t$  are grain size, strain, strain rate and time, respectively, and  $k$ ,  $r$  and  $\alpha$  are constants. In a two-phase alloy,  $r$  is 3 or 4, and in a second phase particle dispersed alloy,  $r$  is 2 or 3 for bulk or grain boundary diffusion control, respectively.

Equation 1 is a differential equation with respect to  $\bar{D}$ , and can be solved under the boundary condition of constant strain rate as

$$\left(\frac{\bar{D}}{\bar{D}_0}\right)^r = e^{\alpha \dot{\epsilon} t} + \left(\frac{1}{\bar{D}_0}\right)^r \frac{k}{r \alpha \dot{\epsilon}} (e^{r \alpha \dot{\epsilon} t} - 1) = \left(\frac{\bar{D}_d}{\bar{D}_0}\right)^r + \left(\left(\frac{\bar{D}_s}{\bar{D}_0}\right)^r - 1\right) \left(\left(\frac{\bar{D}_d}{\bar{D}_0}\right)^r - 1\right)^{-1} (r \ln \frac{\bar{D}_d}{\bar{D}_0})^{-1}, \quad (2)$$

where  $\bar{D}_0$ ,  $\bar{D}$ ,  $\bar{D}_s$  and  $\bar{D}_d$  are grain sizes before deformation, after deformation, after static annealing without deformation and after deformation in absence of static grain growth, respectively.

If it is possible to ignore the interaction between the first and second terms of eq.1, the approximation

$$\ln\left(\frac{\bar{D}}{\bar{D}_0}\right) \approx \ln\left(\frac{\bar{D}_d}{\bar{D}_0}\right) + \ln\left(\frac{\bar{D}_s}{\bar{D}_0}\right) \quad (3)$$

is obtained. Of course, this approximation is perfectly accurate when the static grain growth is absent. The calculated deviation between eqs.2 and 3 is shown in Table I for both cases of  $r=3$  and 4. Comparing the exact

Table I Deviation of the approximation

$\frac{\bar{D}_d/\bar{D}_0}{\bar{D}_s/\bar{D}_0}$	r = 4			r = 3			
	1.2	1.6	2.0	1.2	1.6	2.0	
1.2	1.38 1.44	1.77 1.92	2.16 2.40	1.39 1.44	1.79 1.92	2.19 2.40	$\frac{\bar{D}}{\bar{D}_0}$ $\frac{\bar{D}_d/\bar{D}_0 \cdot \bar{D}_s/\bar{D}_0}{\bar{D}_d/\bar{D}_0 \cdot \bar{D}_s/\bar{D}_0}$
1.4	1.58 1.68	1.97 2.24	2.37 2.80	1.59 1.68	1.99 2.24	2.40 2.80	$\frac{\bar{D}}{\bar{D}_0}$ $\frac{\bar{D}_d/\bar{D}_0 \cdot \bar{D}_s/\bar{D}_0}{\bar{D}_d/\bar{D}_0 \cdot \bar{D}_s/\bar{D}_0}$

solution ( $\bar{D}/\bar{D}_0$ ) and the approximation ( $\bar{D}_s/\bar{D}_0$ )( $\bar{D}_d/\bar{D}_0$ ), it is recognized that the deviation becomes greater when both grain growth become greater, but that the error of the approximation is within about 10% at least in the region of this table.

The deformation induced component ( $\bar{D}_d/\bar{D}_0$ ) can be estimated as ( $\bar{D}/\bar{D}_s$ ) using eq.3 in case the static grain growth is not so great.  $\bar{D}$  and  $\bar{D}_s$  can be measured at the gage length and the shoulder of a specimen, respectively.

#### Experimental

In this section, deformation induced grain growth is evaluated experimentally. One of the specimen used here is microduplex Zn-22%Al eutectoid alloy, which is a well known superplastic alloy and was made from 99.99% Zn and Al. The other is second phase dispersed Al-4.8%Mg-0.6%Mn-0.6%Cu-0.15%Cr alloy, which is newly developed superplastic alloy [3]. Both alloys had fully recrystallized equiaxed structures before deformation.

Deformation was carried out for both constant elongation rate and constant strain rate conditions using a programmed stepping motor. During deformation, the microstructure maintained equiaxed, and no structural change except grain growth was observed in both alloys.

#### Results and Discussions

##### Grain Growth Behavior

Figures 1 and 2 show the deformation induced component of grain growth ( $\bar{D}/\bar{D}_s$ ) against the given strain in Zn-Al and Al-Mg-Mn alloys, respectively. In Fig.2, since no static grain growth is observed,  $\bar{D}_s$  equals to  $\bar{D}_0$ . The grain growth behavior in these figures are expressed by respective lines independent of strain rate, initial grain size and deformation temperature. It means that the deformation induced grain growth is independent of the magnitude of the static grain growth.

The dependence of grain growth on strain is expressed by

$$\ln(\bar{D}/\bar{D}_s) = \alpha \epsilon, \quad (4)$$

where the values of  $\alpha$  are 0.3 and 0.6 in Zn-Al and Al-Mg-Mn alloys, respectively. This discrepancy is probably ascribed to the difference between two-phase and second phase dispersed structures.

Equation 4 is valid up to the strain rate where  $m$  shows the peak value. Above that strain rate, the deformation induced grain growth becomes small due to the change of deformation mechanism.

Figure 3 shows the evaluated values of deformation induced grain growth in Zn-Al alloy based on eq.3 using the data reported previously [4-6]. They

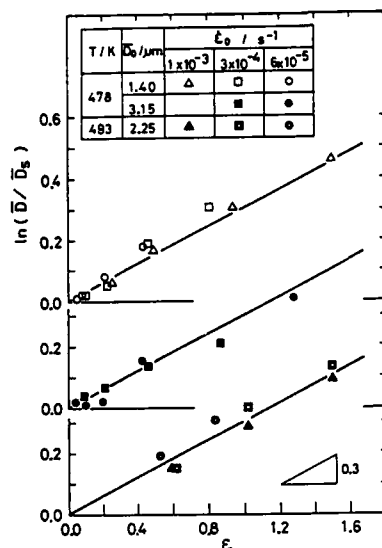


Fig.1 The deformation induced grain growth in Zn-Al alloy.

Fig.3 The deformation induced grain growth in Zn-Al alloy measured by Senkov et al [4], Kaybyshev et al [6] and Mohamed et al [5].

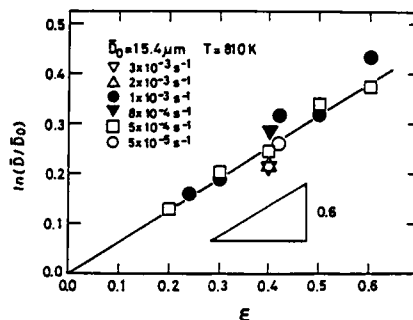
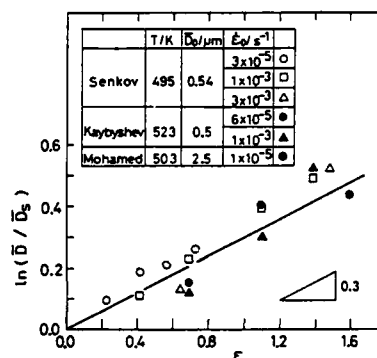


Fig.2 The deformation induced grain growth in Al-Mg-Mn alloy, where no static grain growth is observed.



are expressed by a common line with a slope of 0.3, which is consistent with Fig.1. On the other hand, Caceres et al reported that the deformation induced grain growth is large in Cu containing Zn-Al alloy [7]. In the present study, however, there is no difference in the grain growth behavior between Zn-22%Al and Zn-22%Al-0.5%Cu alloys.

### Flow Hardening

The experiments of different initial grain size shows that flow stress is proportional to  $\bar{D}^{mp}$ , where  $mp=1.3$  and  $2.0$  in Zn-Al and Al-Mg-Mn alloys, respectively. From eq.4, the flow hardening parameter  $\gamma$  is given by

$$\gamma = \left( \frac{\partial \ln \sigma}{\partial \ln \bar{D}} \right)_t = mp \alpha. \quad (5)$$

In Zn-Al and Al-Mg-Mn alloy, the expected values of  $\gamma$  from grain growth are 0.4 and 1.2, respectively.

Figures 4 and 5 shows the stress-strain curves at constant strain rate tests in Zn-Al and Al-Mg-Mn alloys, respectively. As for Al-Mg-Mn alloy, because the static grain growth can be ignored, observed flow hardening has constant value of 1.2. On the other hand in Zn-Al alloy, which has rather small grain size, the apparent stress increase becomes greater when strain rate becomes smaller. The flow hardening, however, must have constant value of 0.4. The great discrepancy of the values of  $\gamma$  is deduced from the



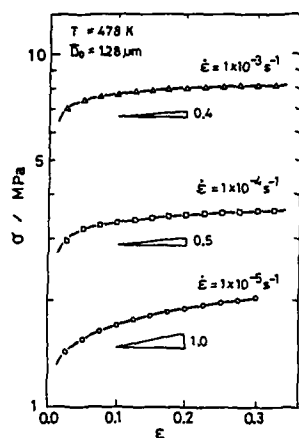


Fig.4 Stress-strain curves of Zn-Al alloy.

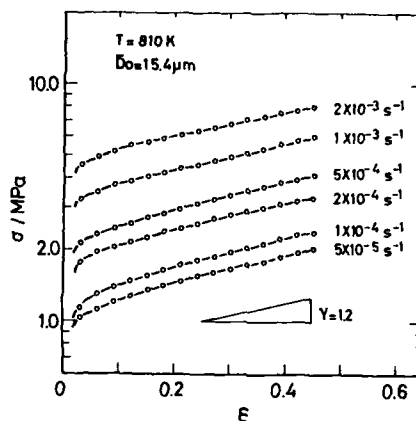


Fig.5 Stress-strain curves of Al-Mg-Mn alloy.

differences of the values of  $\alpha$  and  $m_p$  between these alloys.

#### Conclusions

- 1) Grain growth during superplastic deformation can be divided into two components, and the deformation induced grain growth can be estimated approximately by  $(\bar{D}/\bar{D}_0)$ .
- 2) Deformation induced grain growth is independent of strain rate, initial grain size and temperature, and is expressed as  $\ln(\bar{D}/\bar{D}_0) = \alpha t$ , in both Zn-Al and Al-Mg-Mn alloys, though the values of  $\alpha$  are different of each other.
- 3) Stress increase under constant strain rate condition is consistent with the result deduced from the grain size dependence of flow stress.

#### References

1. C.H.Cáceres and D.S.Wilkinson, "Large Strain Behavior of a Superplastic Copper Alloy," *Acta Metall.*, 32(1984),415-422.
2. C.H.Hamilton, "Superplasticity," *Strength of Metals and Alloys*, Ed.by H.J.McQueen and J.P.Bailon, (Pergamon Press, 1986),1831-1857.
3. H.Watanabe et al., "Development of New Superplastic Aluminum Alloy NEOPRAL," *Bulletin of the Japan Inst.Metals*, 24(1985),313-315.
4. O.N.Senkov and M.M.Myshlyaev, "Grain Growth in a Superplastic Zn-22%Al Alloy," *Acta Metall.*, 34(1986),97-106.
5. F.A.Mohamed et al., "Factors Influencing Ductilities in the Superplastic Zn-22 Pct Al Eutectoid," *Metall.Trans.*, 8A (1977),933-938.
6. O.A.Kaybyshev et al., "Structural Changes and Peculiarities of Crystallographic Slip during Superplastic Deformation of the Alloy Zn-22%Al," *Fiz.Metall. Metalloved*, 36(1973),1235-1241.
7. C.H.Cáceres and D.S.Wilkinson, "Superplastic Behavior of a Zn-22 Pct Al-0.5 Pct Cu Alloy," *Metall.Trans.*, 17A(1986),1873-1875.

**THE MICROSTRUCTURAL CHARACTERISTICS OF AN  
Al-Li-Cu-Mg-Zr ALLOY  
DURING THE INITIAL STAGE OF SUPERPLASTIC DEFORMATION**

**Binyan Ren and C. H. Hamilton  
Department of Mechanical and Materials Engineering  
Washington State University  
Pullman, WA 99164-2920**

**ABSTRACT**

The dynamic recrystallization process of an Al-Li-Zr based alloy ( Al-2.4Li-1.2Cu-0.6Mg-0.1Zr ) was investigated by performing constant strain rate tensile tests. The microstructural changes which occur during the initial stage of superplastic deformation were examined by general optical metallography and transmission electron microscopy (TEM). Particular attention was given to the parameters of high temperature deformation under which the dynamic recrystallization process is expected to occur. The effect of the finely dispersed intermetallic compound particles on recrystallization process was considered. The result of experiments demonstrated that the dynamic recrystallization behavior of the material is effected mainly by the parameters of deformation. Strain-enhanced dynamic recrystallization was observed under high temperature and constant strain rate tensile tests. The strain rate was found to have a strong effect on the dynamic recrystallization behavior.

**INTRODUCTION**

It has been found that aluminum-based alloys may be superplastically deformed in one of two microstructural conditions: 1. a fully recrystallized condition(1-6) and 2. a cold worked or warm worked condition(7-10).

In the second case, the Al alloys generally contain Zr which forms a fine dispersoid of  $Al_3Zr$  particles which interfere with static recrystallization. It has recently been shown that Al alloys containing Li as well as Zr also can exhibit this characteristic(7-10). These alloys undergo recrystallization during the superplastic deformation, and do so usually by a continuous reaction which has been termed continuous dynamic recrystallization (11,12). It has been observed that these alloys develop a small sub-grain on heating to the superplastic temperature; and subsequently the sub-grain structure grows during deformation and the boundary misorientation angle increases, resulting in fully recrystal-

Superplasticity and Superplastic Forming  
Edited by C.H. Hamilton and N.E. Paton  
The Minerals, Metals & Materials Society, 1988

lized microstructure after about 40 to 100% deformation (13,14). While the continuous recrystallization can also take place in the absence of superplastic deformation, little information is available on the kinetics of this recrystallization process under both static and deformation conditions.

In the research reported here, the recrystallization kinetics as evidenced by optical metallographic techniques were determined. It was the objective to determine the extent of full recrystallization observed to take place after exposure to both static and superplastic deformation conditions, and to indicate the affect of the deformation on this recrystallization characteristic.

## EXPERIMENTAL PROCEDURE

The commercial Al-Li-Zr based alloy used in this study was produced by British ALCAN Co., was processed by hot and warm working. The final thickness of the alloy sheet is 2.5mm. The chemical composition of the alloy supplied is: Al-2.4Li-1.2Cu-0.6Mg-0.1Zr.

The high temperature constant strain rate tensile tests were performed in air using a computer-controlled screw-driven Instron testing machine, equipped with a three-zone furnace capable of heating test specimens to temperatures in excess of 600°C. The temperature was controlled to within  $\pm 1^\circ\text{C}$  by an ATS series 2010 three zone furnace control system. The experimental test parameters are as follows: strain rates of  $10^{-2}$  to  $10^{-4} \text{ sec}^{-1}$ , strains of 0.1 to 0.9, and temperatures of 450°C to 500°C. To determine the effect of the deformation on the microstructure and to understand the relationship among strain, strain rate, temperature and dynamic recrystallization, the changes that occurred during the initial stage of deformation were studied in detail. This was achieved by interrupting the tensile test and unloading the specimens after deformation to a pre-determined strain for different constant strain rates and temperatures.

Both optical and electron microscopy were utilized in this study for evaluating the microstructural changes during the recrystallization processes. After the conventional metallographic sample preparation procedure, the specimens were electrochemically etched to create an optically active anodized surface, and the microstructures were examined under polarized light on the Olympus MG optical microscope. The Hitachi H-300 transmission electron microscope operating at 75KV was utilized to view the internal structure of the aluminum foil.

## RESULTS AND DISCUSSION

The structure of the as-received alloy sheet was that of a heavily deformed alloy as shown in the electron micrograph in Figure 1. On heating to the superplastic test temperature, 500 C, the structure recovered and a small sub-grain structure developed which was approximately 2 microns average diameter. While this sub-grain structure formed quickly on heating to this temperature, it was apparently stabilized by the presence of second phase particles, and further growth under static conditions was comparatively quite slow.



Figure 1. Electron micrograph of the internal structure of the as-received alloy.

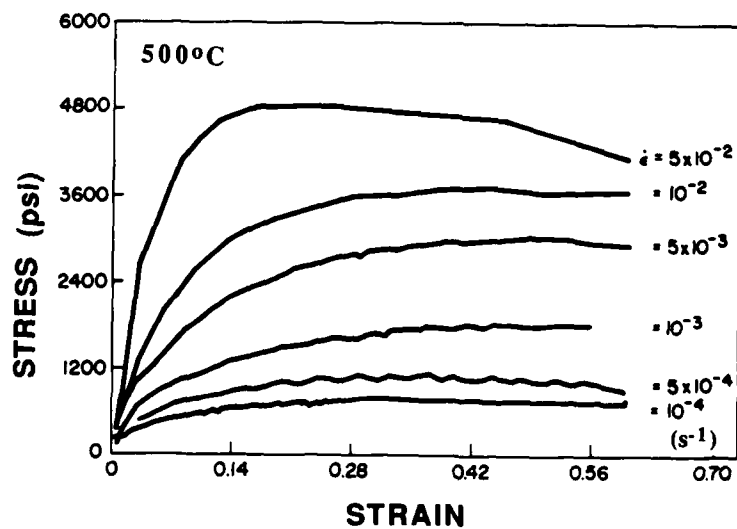


Figure 2. Stress vs. strain curves at various constant strain rates for the alloy tested in tension at 500°C.

Figure 2 shows a series of typical stress-strain curves of this alloy deformed at different strain rates. The stress rises initially with strain exhibiting strain hardening, and subsequently the flow stress stabilizes showing little change with continuing deformation. Figure 3 presents the sequence of the microstructural change with increasing strain at strain rate of  $10^{-2} \text{ sec}^{-1}$ , a sequence which is similar at strain rate of  $10^{-3}$  and  $10^{-4} \text{ sec}^{-1}$ . The characteristics of the alloy and the results of the microstructural examination indicate that, under the conditions of constant strain rate, this alloy exhibits "deformation-induced" dynamic recrystallization occurring during high temperature deformation. The microstructural change during high temperature deformation is closely related to the change of the mechanical behavior.

The recrystallization kinetics of the alloy under both static and deformation conditions are shown in Figure 4 where the percent recrystallization is graphed as a function of time for the various deformation conditions. It is clear that the superplastic deformation has a very strong influence on the rate of recrystallization. Also noteworthy is the observation that static recrystallization will proceed in the absence of deformation, and the superplastic characteristics of the statically recrystallized material may be expected to differ from that of the dynamically recrystallizing material.

The deformation-induced recrystallization was found to be strongly dependent on the strain as shown in Figure 5, and the strain for apparent nucleation was about 0.1 to 0.2. The recrystallization does occur at slightly increasing strains with increasing strain rates.

Examination of the intermetallic compound particle density indicated that there was some dissolution of the particles and an increase in *inter-particle spacing* with time and strain. It is these changes that are believed to be the source of the onset of recrystallization. During the high temperature deformation, the subgrain size increases while the density of the intermetallic compound particles decreases with increasing strain. The finely dispersed intermetallic compound particles within the alloy hinder both the rearrangement of the dislocations necessary for recrystallization, as well as the migration of the recrystallization fronts. Nes(4) reported that the decrease in particle density was caused by a discontinuous dissolution of these particles at a migrating sub-boundary. Nes suggest that the migrating boundary force the  $\text{Al}_3\text{Zr}$  particles to loss coherency, and thereby redissolve, driven by the surface tension of the particle. The high temperature deformation forces thereby cause small particles to dissolve into matrix, further destabilizing the boundaries, and further facilitating subgrain boundary migration. This enhances the dynamic recrystallization process during the initial stage of high temperature deformation, resulting in the relatively rapid kinetics observed under deformation conditions.

## CONCLUSIONS

a. At a temperature of  $500^\circ\text{C}$  and strain rate ( $10^{-4}$  to  $10^{-2} \text{ sec}^{-1}$ ), the recrystallization is significantly accelerated by deformation. There is a critical strain value of about 0.2 at which the dynamic recrystallization nucleates. The higher the strain rate, the higher the critical strain value although the difference is not large.

b. The finely dispersed intermetallic compound particles play important role in effecting the recrystallization process of the alloy, and recrystallization proceeds as these

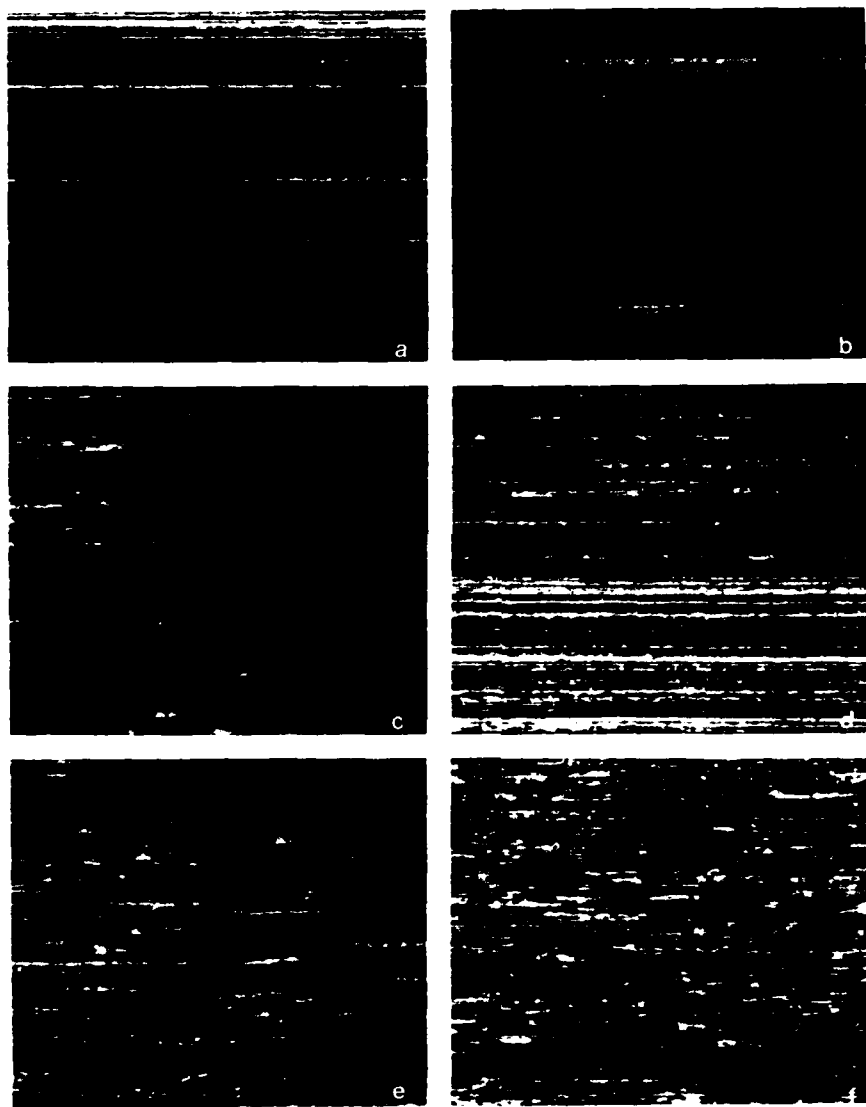


Figure 3. Microstructural change with strain at constant strain rate of  $10^{-2} \text{sec}^{-1}$  and  $500^{\circ}\text{C}$ . (a).  $\epsilon=0.1$  (b).  $\epsilon=0.2$ . (c).  $\epsilon=0.3$ . (d).  $\epsilon=0.4$ . (e).  $\epsilon=0.5$ . (f).  $\epsilon=0.9$ .  $100X$ .

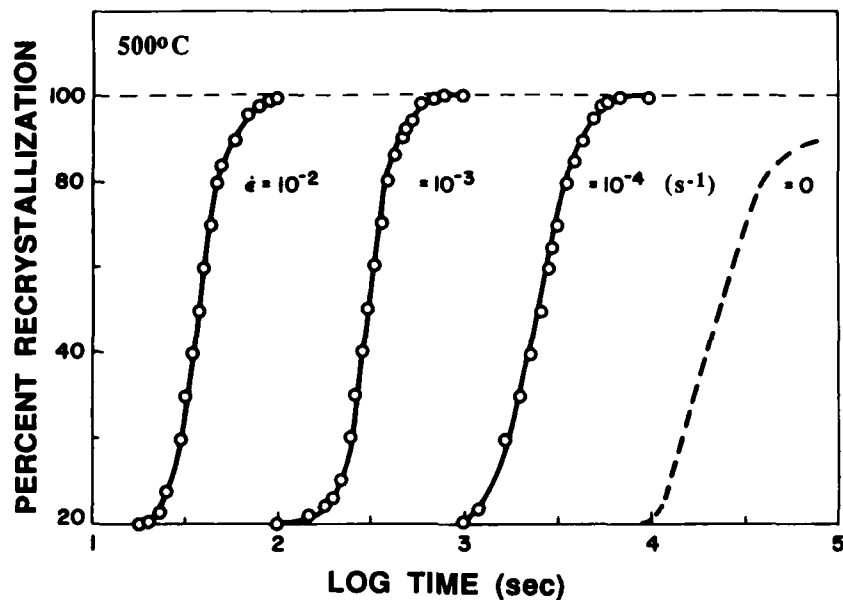


Figure 4. Percent recrystallization as a function of time for various strain rates at 500°C.

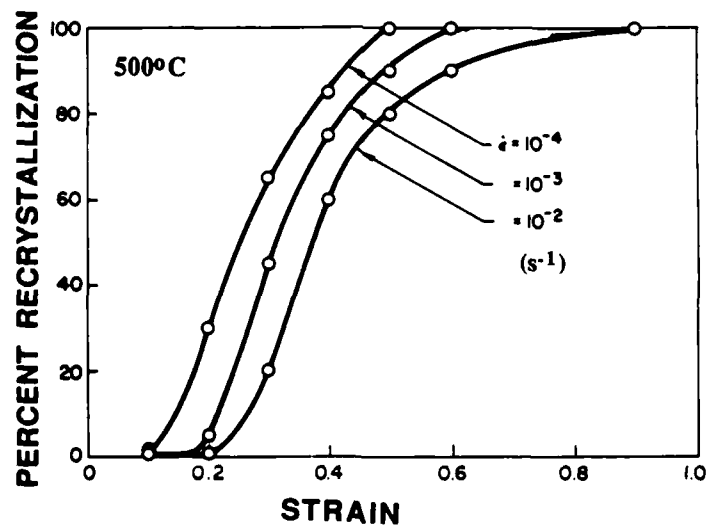


Figure 5. Percent recrystallization as a function of strain for various strain rates at 500°C.

particles are decreased in volume fraction or interparticle spacing is increased.

## REFERENCES

1. Grimes, R., Stowell, M. J. and Watts, B. M., *Met. Tech.*, **3** (1976) 154-160.
2. Hamilton, C. H., Ghosh, A. K., and Wert, J. A., *Metal Forum*, **8** (1985) 172-190.
3. Stowell, M. J. et al. *Met. Sci. J.* **3** (1969) 41-45.
4. Wert, J. A. 1982. *Superplastic Forming of Structural Alloys*. ed. Paton, N. E. and Hamilton, C. H. AIME. Warrendale, Pa. (1982) pp69-84.
5. Wert, J. A., Paton, N. E., and Hamilton, C. H., *Met. Trans. A*, **12A** (1981) 1267.
6. Paton, N. E., Hamilton, C. H., Wert, J. A. and Mahoney, M. W. *J. Metal.* **34** (1982) 21.
7. Wadsworth, J. et al. *Scripta Met.* **17** (1983) 347.
8. Wadsworth, J. et al. *Aluminum-Lithium Alloys*. ed. by Sanders, T. H. Jr. and Starke, E. A. Jr. (1984) 111-135.
9. Wadsworth, J. and Pelton, A. R., *Scripta Met.* **18** (1984) 387.
10. Wadsworth, J. *Superplastic Forming*. Ed. by Agrawal, S. P. ASM. Metal Park, OH. (1985) 43-57.
11. R. Grimes, C. Baker, M. J. Stowell, and B. M. Watts, *Aluminium* **51** (1975) 720.
12. E. Nes, *J. Mater. Sci.* **13** (1978) 2052.
13. Nes, E., *Superplasticity*. B. Baudelet and M. Suery eds., Proceedings, International Conference, Grenoble, France, Editions Du Centre National De La Recherche Scientifique, Paris, (1985) 7.
14. Ash, B. A. and Hamilton, C. H. *Scripta Met.* **22** (1988) pp277-282.



DETAILS OF THE ALPHA GRAIN BOUNDARIES IN ANNEALED

AND SUPERPLASTICALLY DEFORMED Ti-6Al-4V ALLOY

L. R. Zhao, S. Q. Zhang, and M. G. Yan

Institute of Aeronautical Materials, Beijing, China

Abstract

A great number of alpha grain boundaries in annealed and superplastically deformed Ti-6Al-4V alloy were examined with transmission electron microscope. There are lack of extrinsic dislocations in most of the annealed boundaries. And the near-coincidence grain boundaries are characterized by straight and well lined intrinsic grain boundary dislocations (GBDs). A variety of extrinsic dislocation moving configurations were observed in the deformed alpha grain boundaries. The local reactions between intrinsic GBDs have been noticed. It is suggested that a local grain boundary structure transformation followed by its spreading could induce grain boundary sliding and migration in superplastic deformation.

Superplasticity and Superplastic Forming  
Edited by C.H. Hamilton and N.E. Paton  
The Minerals, Metals & Materials Society, 1988

## Introduction

It is well known that grain boundary sliding and migration play an important role in superplastic deformation. The contribution of grain boundary sliding to total superplastic strain is typically 50%-70%(1), and almost all theoretical models are based on the presumptions of grain boundary sliding accommodated by different mechanisms(2,3). Grain boundaries and interfaces are also the preferential sites for cavitation(1). However only less attention was paid to the details of grain boundary in superplasticity. Using transmission electron microscope, we examined a great number of alpha grain boundaries in annealed and superplastically deformed Ti-6Al-4V alloy to approach a better understanding about the mechanisms of grain boundary sliding and migration.

## Observation Results and Analyses

### Annealed State

Most of the annealed alpha grain boundaries are lack of extrinsic dislocations. The straight and well lined intrinsic grain boundary dislocations can be observed in near-coincidence grain boundaries, see Figure 1. Only small amounts of relaxed dislocations exist in a few annealed boundaries. These facts imply that most of the annealed alpha grain boundaries have a well periodic structure.

### Superplastically Deformed State

The specimen was tensiled at 900°C and at initial strain rate of  $4.25 \times 10^{-4} \text{ sec}^{-1}$  to 100%, then quenched to room temperature.

Figure 2 -Figure 4 show the curved alpha boundaries in which the extrinsic grain boundary dislocations were emitted from triple-boundary point and moved along these boundaries. It can be noticed that this movement induced a grain boundary migration in the arrow direction. It is suggested that such process could effectively relax the stress concentration at the triple-boundary point caused by grain boundary sliding. Further examine shows that in Figure 4 there also exist intrinsic GBDs which however may not be directly involved in the migration inducement.

The movement of extrinsic lattice dislocations along a near-coincidence alpha grain boundary is shown in Figure 5. The intrinsic GBDs were absorbed by these moving lattice dislocations, which results in a series of deviations in the boundary plane from near-coincidence orientation. Hence some grain boundaries may partly twist with sliding to meet a geometric requirement.

Figure 6 and Figure 7 show the reactions between intrinsic GBDs happened in the deformation. In the small angle boundary shown in Figure 7, some of the grain boundary dislocations were partly combined to form stronger defects. In Figure 6, the intrinsic GBDs reacted forming dislocation network. It is suggested that such reactions imply a local grain boundary structure transformation.

The emission of lattice dislocations from a near-coincidence grain boundary ledge is indicated in Figure 8. It can be noticed that the boundary ledge consists of facets A, B and boundary plane C, in which the intrinsic GBDs oriente in different derections. The emitted lattice dislocations were generated by the interaction between GBDs at the intersections of A-B and B-C. Stress concentration at the boundary ledge can be relaxed by such dislocation emission.

## Discussion and Summary

The TEM investigations indicate that there exist a variety of extrinsic dislocation moving configurations which may be related to grain boundary sliding and migration. However the most interesting results are the reactions between intrinsic grain boundary dislocations. We have also noticed that there are a lot of deformed alpha grain boundaries which are still lack of extrinsic or even intrinsic grain boundary dislocations. It is hard to say that such grain boundaries will maintain unmovable during superplastic deformation. In general, a local grain boundary structure transformation followed by its spreading which may effectively occur at both the superplasticity temperature ( $0.5 T_m$ ) and the applied stress could induce grain boundary sliding and migration. And such process would be accompanied with vacancy absorption or emission. The observed extrinsic dislocation moving along grain boundary is only one special case of the process.

The investigation results are summarized as:

1. There is a well structure state in annealed alpha grain boundaries.
2. There exist a variety of extrinsic dislocation moving configurations which may be related to grain boundary sliding and migration.
3. Local reactions between intrinsic grain boundary dislocations occurred during superplastic deformation.

#### References

1. A. H. Chokshi and T. G. Langdon, Superplasticity (15, Quai Anatole France, PA: Centre National de la Recherche Scientifique, 1985), 2.1-2.15.
2. R. C. Gifkins, Superplastic Forming of Structural Alloys (New York, NY: The Metallurgical Society of AIME, 1982), 3-26.
3. B. P. Kashyap and A. K. Mukherjee, Superplasticity (15, Quai Anatole France, PA: Centre National de la Recherche Scientifique, 1985), 4.1.

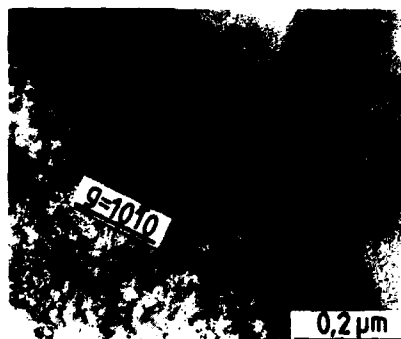


Figure 1 - Annealed grain boundaries in which there exist straight and well lined intrinsic GBDs.

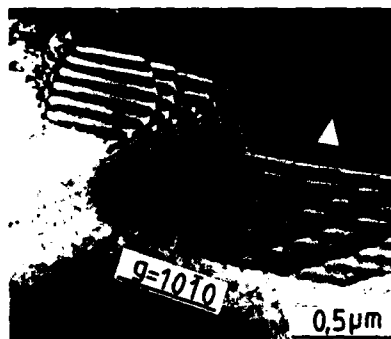


Figure 2 - Grain boundary migration through extrinsic GBD moving (dark field image).



Figure 3 - Grain boundary migration through extrinsic GBD moving.



Figure 4 - Grain boundary migration through extrinsic GBD moving.



Figure 5 - Intrinsic GBD absorption by lattice dislocation moving, which induced deviations in the grain boundary orientation.

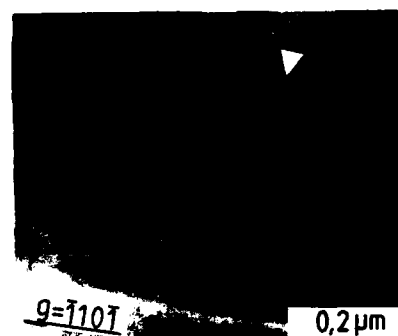


Figure 6 - Reactions between intrinsic GBDs forming dislocation network.

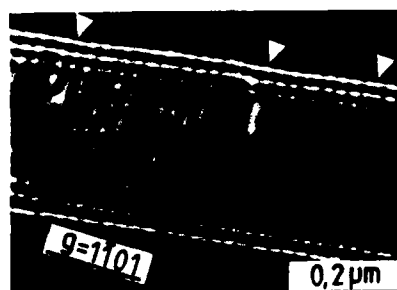


Figure 7 - Reactions between intrinsic GBDs in a small angle grain boundary (dark field image).

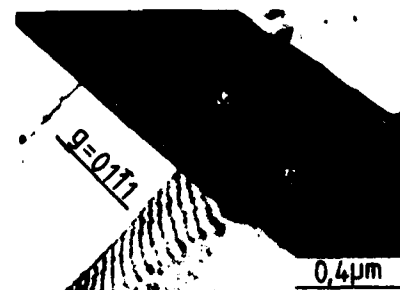


Figure 8 - Emission of lattice dislocations from a grain boundary ledge.

**RHEOLOGY  
AND  
CAVITATION**

## PLASTIC STABILITY AND STRAIN TO FRACTURE

### DURING SUPERPLASTIC DEFORMATION

B. Baudalet and M. Suéry

Institut National Polytechnique de Grenoble  
E.N.S. de Physique de Grenoble  
Génie Physique et Mécanique des Matériaux  
(Unité Associée au CNRS n° 793)  
BP.46 - 38402 - SAINT MARTIN D'HERES CEDEX (France)

#### Abstract

Superplastic alloys are highly resistant to macroscopic neck development owing to their high strain rate sensitivity of stress ( $m$ ) and this leads generally to large tensile elongations. High  $m$  values are however not sufficient and several factors can influence greatly the ductility. These factors include the geometry of the specimen, the uniformity of temperature along the gauge length and the structural evolutions of the alloy such as grain growth and cavitation. The aim of this paper is to analyse the influence of several of these factors on plastic stability and strain to fracture with particular attention to cavitation. Uniaxial and biaxial deformations are considered and quantitative prediction of tensile elongation on thinning development during circular sheet bulging is given. The effect of superimposed pressure on fracture is also examined. It is shown that the fracture mode can be changed by superimposed pressure, from fracture without external necking for cavity sensitive alloys at zero pressure, to fracture with necking development and extensive thinning at pressure large enough to completely suppress cavity growth. Fracture mechanism diagrams are then presented which enable prediction of the fracture mode as a function of material parameters and pressure conditions for uniaxial tension and bulging.

*Superplasticity and Superplastic Forming*  
Edited by C.H. Hamilton and N.E. Paton  
The Minerals, Metals & Materials Society, 1988

### Introduction

Superplastic alloys are now used quite extensively in several applications and one main problem is concerned with the fabrication of parts with an uniform thickness distribution and a low level of internal defects. A high strain-rate sensitivity value of stress ( $m$ ) is one key parameter which has to be controlled for obtaining a high plastic stability of flow during forming but several other factors can influence greatly the ductility, essentially the uniformity of temperature and grain size in the specimen and the structural evolutions (grain growth and cavitation) that are taking place during deformation. The influence of some of these factors has already been studied quite extensively in our laboratory and elsewhere so that the aim of this paper is essentially to summarise what was done on the subject very recently but also to present some new results. Uniaxial tension is considered first by analysing the influence of the previously mentioned factors on plastic stability and neck development. Thinning of the sheet during bulging is studied thereafter with particular reference to cavitation, temperature uniformity and thickness distribution in the sheet.

#### Influence of material parameters under uniaxial stress state (1)

The Hart's expression :

$$\delta (\ln \sigma) = \gamma \delta \epsilon + m \delta (\ln \dot{\epsilon}) \quad (1)$$

will be used in the present analysis (2) ; in the derivation, both  $m$  and  $\gamma$  are considered to be constant except for the final equations where  $\gamma = n/\epsilon_f$  is used for a power law hardening material.

#### Geometrical defect

In a specimen under tension the initial cross section and length are  $A_0$  and  $L_0$  respectively and the corresponding instantaneous values are  $A$  and  $L$ . On the assumptions that there is an initial geometrical defect  $f (= \frac{\delta A_0}{A_0})$  and that only the plastic deformation is considered, from the constant-volume condition and the load equilibrium condition, it is obtained from (1) :

$$m \delta (\ln \dot{A}) = (m + \gamma - 1) \delta (\ln A) - \gamma \delta (\ln A_0) \quad (2)$$

$\delta$  expresses the differential along the tensile axis.

At the stable or quasi-stable stage of deformation, as the difference between the two sections (the homogeneous section and the neck section) is not great, the difference in  $\gamma$  between these two section (if  $\gamma = n/\epsilon$  is accepted) is also not great ; therefore, it can be considered that both the homogeneous section and the necking section have the same  $\gamma$  and  $m$  values. So we integrate eqn. (2) along the tensile axis from the homogeneous section  $A$  to the necking section  $A_N$  and define the integral constant by putting  $\dot{A} = \dot{A}_N$  while  $A = A_N$ . This integration gives :

$$\left( \frac{\dot{A}}{\dot{A}_N} \right)^m = \left( \frac{A}{A_N} \right)^{m+\gamma-1} \left( \frac{A_{N0}}{A_0} \right)^\gamma \quad (3)$$

and by introducing  $f$ ,  $\epsilon_N$  and  $\epsilon$  :

$$(1 - f)^{1/m} \exp\left\{-\frac{\epsilon_N(1 - \gamma)}{m}\right\} d\epsilon_N = \exp\left\{-\frac{\epsilon(1 - \gamma)}{m}\right\} d\epsilon \quad (4)$$

For the description of necking development, assuming also that  $\gamma$  is constant during the deformation (see later for comments) by integration from  $\epsilon = \epsilon_N = 0$  :

$$(1 - f)^{1/m} \left[ \exp\left\{-\frac{\epsilon_N(1 - \gamma)}{m}\right\} - 1 \right] = \exp\left\{-\frac{\epsilon(1 - \gamma)}{m}\right\} - 1 \quad (5)$$

Equation (5) shows that, when there is a geometrical defect  $f$ , the necking will develop but will be controlled by  $m$  and  $\gamma$ .

When failure occurs at  $\epsilon_N \rightarrow \infty$  (3-6), the strain in the homogeneous section to failure is obtained :

$$\epsilon_f = \frac{m}{\gamma - 1} \ln\{1 - (1 - f)^{1/m}\} \quad (6)$$

This is an  $m$ - $\gamma$ - $\epsilon_f$  relationship. For a power-law hardening material, the final  $\gamma$  ( $= n/\epsilon_f$ ) value is used in eqn. (6) as an "average"  $\gamma$  value (4). We obtain :

$$\epsilon_f = n - m \ln\{1 - (1 - f)^{1/m}\} \quad (7)$$

Because  $f$  is very small, we have a simpler expression :

$$\epsilon_f \approx n + m \ln\left(\frac{m}{f}\right) \quad (8)$$

If the contribution of the neck section to elongation is neglected, the total elongation (the engineering strain) for both eqn. (7) and (8) is :

$$e_f = \{1 - (1 - f)^{1/m}\}^{-m} \exp(n) - 1 \quad (9)$$

$$\text{or} \quad e_f = \left(\frac{m}{f}\right)^m \exp(n) - 1 \quad (10)$$

#### Deformation defect

All the derivations carried out for a geometrical defect are repeated using for a deformation defect  $\delta\epsilon = -\delta \ln A$  (2, 6, 7). This gives :

$$\exp\left(-\epsilon_N \frac{1 - \gamma}{m}\right) d\epsilon_N = \exp\left(-\epsilon \frac{1 - \gamma}{m}\right) d\epsilon \quad (11)$$

A deformation defect can be considered as a predeformation in a local region of the specimen, which is the initial place for necking. So eqn. (11) is integrated beginning at  $\epsilon = 0$  and  $\epsilon_N = \epsilon_0$ , this gives :

$$\epsilon_f = \frac{m}{\gamma - 1} \ln\left\{1 - \exp\left(-\epsilon_0 \frac{1 - \gamma}{m}\right)\right\} \quad (12)$$



or, with a power-law material,

$$\epsilon_f = n - m \ln \left\{ 1 - \exp \left[ - \epsilon_0 \frac{\epsilon_f - n}{m \epsilon_f} \right] \right\} \quad (13)$$

Comparison between eqn. (12) and (6), shows that the difference between the equation for a geometrical defect and that for a deformation defect is that the former has a  $(1 - f)^{1/m}$  term and the latter an  $\exp\{-\epsilon_0 (1 - \gamma)/m\}$  term.

#### Comparison with other theories and experiments

Table shows the various relationships given by other theoretical analyses and the present one. From the viewpoint of theoretical analysis, those of Hutchinson and Neale (8) or Ghosh and Ayres (3) are accurate integral analyses of the "long-wavelength approximation" of one dimension. However, unfortunately, the resultant equation of Hutchinson and Neale is an integral one which cannot be solved in an analytical form. The analyses given by Nichols (4), Lin et al. (5), Semiatin and Jonas (9) or Lian and Baudalet (1) based on Hart's approach are a linearized or first-order perturbation in which the necking phenomenon is described by a gradient approach. The present analysis is based on Hart's constitutive equation of differential form.

Table. Various relationships of theoretical analyses

Relationship	Reference	Year
$e_f = \{(1-f)^{1/m}\}^{-m} - 1$	Ghosh and Ayres (3)	1976
$\exp(-s\epsilon_f) \sum_{k=0}^p \frac{(s\epsilon_f)^k}{k!} = (1 - (1-f)^s)$	Hutchinson and Neale (8)	1977
$s = \frac{1}{m}, p = \frac{n}{m}$		
$e_f = \left(\frac{1}{f}\right)^{m/(1-\gamma)} - \gamma$	Nichols (4)	1980
$e_f = (1 + e_0)\lambda^{m/(1-\gamma)} - 1; \lambda = 67$	Lin et al. (5)	1981
$e_f = \left(\frac{1}{f}\right)^m \exp(n) - 1$	Semiatin and Jonas (9) Lian and Baudalet (1)	1984 1986
$e_f = \{1 - (1-f)^{1/m}\}^{-m} \exp(n) - 1$	present work (when $n=0$ , this gives the relationship of Ghosh and Ayres)	
$e_f = \left(\frac{m}{f}\right)^m \exp(n) - 1$	present work	
$\epsilon_f = n - m \ln \left\{ 1 - \exp \left[ - \epsilon_0 \frac{\epsilon_f - n}{m \epsilon_f} \right] \right\}$	present work	

Figure 1 is plotted using eqn. 10 and eqn. (13) with  $n = 0$  and  $n = 0.2$  labelled L-B ; Woodford's experimental data (10) and Hutchinson and Neale's theoretical results (labelled H-N) are also plotted for comparison. From fig. 1, we can define that for  $m > 0.1$ , the strain-hardening exponent  $n$  has a small influence on the elongation, and both theoretical lines are in agreement with the experimental data of Woodford. For  $m < 0.1$ , the strain-hardening effect has an increasing influence on total elongation and the lines for  $n = 0$  and  $n = 0.2$  include most of the experimental data.

Figure 1 shows that the present analysis gives the same result as that of Hutchinson and Neale when  $n = 0$  (which is also the same as that given by Ghosh and Ayres), and for  $n = 0.2$  this analysis gives a good approximation to Hutchinson and Neale's integral analysis. When  $m$  is small (e.g. between 0.01 and 0.1), eqns. (10) and (13) do contain some errors in contrast with Hutchinson and Neale's results. The errors may arise from the assumption in the integrations of the above derivation that  $\gamma$  is constant, especially in the integration of eqn. (4), which is in fact not true.

However, for a material having a large strain rate sensitivity, the strain at fracture is larger than the strain-hardening exponent  $n$  ; for the deformation process where  $\epsilon > n$ , the variation in  $\gamma$  with  $\epsilon$  becomes smooth and in this case the assumption that  $\gamma$  is a constant is quite reasonable. This is why, for large  $m$ , the result of this analysis give quite a good approximation in comparison with Hutchinson and Neale's numerical results.

#### Influence of variation of strain rate sensitivity on limit strain - case of geometrical defect (11)

Ghosh and Ayres (3) have shown that an Al-Cu alloy with an initial  $m$ -value of 0.9 exhibits only a 700% elongation while an alloy with an initial 0.2  $m$ -value exhibits a 1200% elongation. Ghosh and Ayres indicated that these two elongations are more related to their final  $m$ -values, 0.28 and 0.49 respectively. Based on this fact, they suggested that the terminal  $m$  is the most important parameter in controlling total elongation.

To obtain a quantitative estimate of the effect of the variation of  $m$  on limit strain,  $\epsilon_f$  has been numerically calculated with variable  $m$  in the form of either a linear or an arbitrary variation.

Figure 2 shows that a good agreement is observed between the numerically calculated limit strain ( $\epsilon_f$ ) and the final average  $m_f$  ( $= (m_{Hf} + m_{Nf})/2$ ), where  $m_{Hf}$  and  $m_{Nf}$  are the final values of  $m$  in the homogeneous and necked zones respectively. Furthermore, it seems that the relation between  $\epsilon_f$  and  $m_f$  follows approximately the relation (7), assuming  $n$  equal to 0.

#### Influence of the other parameters under uniaxial stress state

The first part of the paper was concerned with the prediction of the strain to failure as function of the strain-rate sensitivity coefficient by considering the development of an initial geometrical imperfection in the cross section of the specimen. However, other factors than  $m$  can greatly influence the ductility. These factors are the geometry of the specimen, the uniformity of temperature and grain size along the gauge length and the structural evolutions of the alloy such as grain growth and cavitation. Analysis of the influence of these factors on plastic stability and strain to fracture in uniaxial tension is the aim of this part.

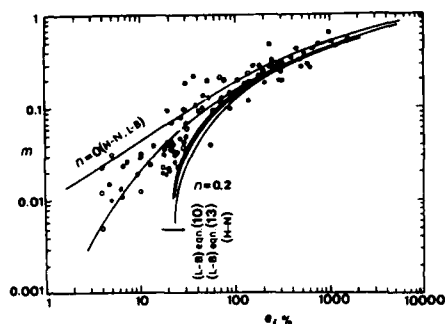


Figure 1 - The theoretical results of the  $m$ - $\epsilon_f$  relationship calculated from eqns. (10) and (13) (Lian-Baudelet (L-B)) and from Hutchinson and Neale's (8) analysis (H-N) in comparison with the experimental data collected by Woodford (10) ( $f = 0.005$  for  $n = 0.2$  (eqn. (13)) ;  $\epsilon_0 = 0.005$ ). (from (1))

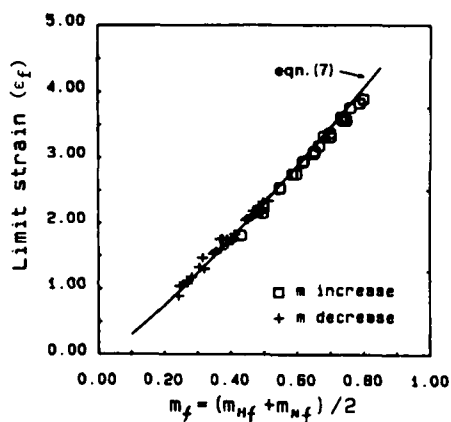


Figure 2 - Relation between limit strain and final average value of  $m$  (from (11))

#### Geometry of the specimen

The influence of the geometry of the specimen on strain to failure is often ignored and no detailed investigation has been performed to quantify it. The importance of this parameter was first recognized by Morrison (12) who expressed the elongation to failure in the case of Sn-Pb eutectic alloy, by the relation :

$$\epsilon_f = b m^2 \left( \frac{D_0}{l_0} \right) \quad (14)$$

where  $b = \text{constant } (\sim 280)$   
 $D_0 = \text{initial diameter}$   
 $l_0 = \text{initial gage length}$

The elongation is thus greater for large diameter and small gage length. In this case, a non negligible part of the elongation comes generally from the heads of the sample which can introduce some error in the determination of the real strain experienced by the specimen. Another empirical relation for failure strain in sheet specimens has been proposed (13) in the case of the Ti-6Al-4V :

$$\epsilon_f = \frac{B m(\epsilon_f)}{(w/t)} \quad (15)$$

Where  $w$  and  $t$  are the width and thickness of the specimen respectively,  $m(\epsilon_f)$  is the strain rate sensitivity measured just before failure and the constant  $B \approx 32$  for this alloy.

#### Non uniformity of temperature and grain size

One source of inhomogeneity of deformation which can be considered to be likely in superplastic forming is that due to some temperature gradient along the gauge length of the specimen. Since the strain-rate is a

strong function of temperature, such gradient can result in a significant inhomogeneity of deformation. Another source of inhomogeneity can be that induced by a localized grain size variation. This variation may result either from inhomogeneous recrystallization as in the case of alloys which become superplastic after some prestraining or from abnormal local grain coarsening.

The analysis of plastic stability taking into account these two types of inhomogeneity was performed recently (14) and equivalence between geometrical defect and a local temperature or grain size imperfection was established. Indeed, the geometrical defect  $f_{eq,T}$  equivalent to a temperature difference  $\delta T/T$  for the same limit strain is :

$$f_{eq,T} = \left(1 + \frac{\delta T}{T}\right)^m \exp \left(-m C \frac{\delta T}{T}\right) \quad (16)$$

where  $C = \frac{Q}{RT}$ ,  $Q$  being the activation energy.

Similarly for the grain size inhomogeneity, we have :

$$f_{eq,d} = 1 - \left(1 - \frac{\delta d}{d}\right)^{mp} \quad (17)$$

Where  $p$  is the grain size exponent in the grain size dependence of the strain-rate.

The comparison between these defects is given in figure 3 for  $m = 0.5$  where it is shown that  $\delta d/d$  (with  $p = 1, 2$  and  $3$ ) has approximately the same effect on limit strain as the geometrical defect  $f$ . The limit strain is also very sensitive to a local temperature variation  $\delta T/T$ . Indeed, a small local increase of temperature of  $0.1\%$  has the same effect as a geometrical defect of about  $1\%$ . This result leads to the conclusion that precise control of temperature along the gauge length is necessary to get large elongation. This control is easier on short samples which confirms the importance of the gauge length on strain to fracture.

#### Grain growth

As deformation of superplastic materials takes place at elevated temperatures, grain coarsening frequently occurs which results in apparent hardening in the stress strain curves. However, such an hardening can be compensated by some flow softening when straining is performed not at constant strain-rate but at constant extension rate. The influence of grain-growth and strain-rate path was detailed recently by Hamilton (15) and Baudalet and Suéry (16) so that this parameter will not be considered in details in this paper.

Grain growth may thus have a stabilizing effect in the tensile deformation by introducing a strain hardening parameter in the equation (9). It may also lead to earlier fracture especially when the imposed strain-rate is close to region III. In this case, grain growth will lead to a rapid decrease of the  $m$  value and according to the results presented in the first part of this paper, smaller elongations will be obtained. It is however possible to avoid this problem by deforming the material while decreasing continuously the strain-rate (or the stress) so that deformation will always take place under optimum conditions of superplasticity. This procedure was applied to  $\alpha/\beta$  brasses and found to be successful for

increasing elongation to rupture compared to usual tests at constant strain-rate (16).

### Cavitation

One of the main problem of superplastic deformation of many alloys is the development of internal cavities which have an important influence on strain to fracture. This phenomenon was considered by Jonas and Baudalet (17) who demonstrated that the generation of spherical cavities during straining increases the tendency towards tensile instability by reducing the effective values of the strain-rate sensitivity and the strain hardening coefficient. Cavity generation also diminishes the reduction in area at fracture, so that failure of the material can occur when the external cross-section is still appreciable.

The influence of cavitation on neck development was studied recently by Lian and Suéry (18) assuming that the volume fraction of cavities increases with strain according to the relation :

$$C_v = C_{v0} \exp(\eta \epsilon) \quad (18)$$

Where  $C_{v0}$  is assumed to be the initial cavity volume fraction in the specimen.  $\eta$  is a parameter which depends on material and testing conditions namely the stress state.

The model of neck development assumes a geometrical defect to be present. However, since cavity growth decreases the effective area of the cross-section of the specimen, the basic equation (4) must take into account the evolution with strain of the cavity volume fraction which is different in the necked region and outside the neck. The following expression was thus obtained when the strain-hardening coefficient is zero:

$$\exp(-\epsilon/m) \epsilon^{1/m} [1 - C_{v0} \exp \eta \epsilon]^{1/m} d\epsilon = (1-f)^{-1/m} \exp(-\epsilon_N/m) \epsilon_N^{1/m} \times (1 - C_{v0} \exp \eta \epsilon_N)^{1/m} d\epsilon_N \quad (19)$$

In the calculations, specimen failure was assumed to occur when either  $\epsilon_N/\epsilon = 2$  or  $C_v = 0.30$  in the necked region.

Figure 4 shows the influence of  $m$  on the variation of fracture strain  $\epsilon_f$  vs cavity growth rate  $\eta$ . The value of  $m$  greatly affects  $\epsilon_f$ , but only when  $\eta$  is not too great. As  $\eta$  increases,  $\epsilon_f$  decreases whatever the value of  $m$  and it becomes almost completely independent of  $m$  in the range  $m > 0.5$ , if  $\eta$  is greater than  $\sim 3$ . This value of  $\eta$  corresponds approximately to the transition between the region where fracture occurs with pronounced external necking (low  $\eta$ ) and that where the fracture mode is controlled by cavity growth (great  $\eta$ ), as shown in figure 5. This figure represents the variations of the necking parameter  $\beta = (A_f - A_{Nf})/A_f \times 100, \%$  and the cavity volume fraction outside the necked region as a function of the cavity growth rate  $\eta$ .  $A_f$  and  $A_{Nf}$  are respectively the area of cross-section in the uniform region and the necked region of the specimen when fracture occurs. At low  $\eta$  value, the fracture criterion  $\epsilon_N/\epsilon = 2$  is satisfied whereas that corresponding to  $C_v = 0.30$  holds at large  $\eta$  values.

The transition from fracture by external necking to fracture by cavity growth can be easily visualized on fracture mechanism diagrams in which isostrain curves at fracture are plotted as functions of  $m$  and  $\eta$ . An example of this diagram is shown in figure 6 taking for  $C_{v0}$  an  $f$  typical

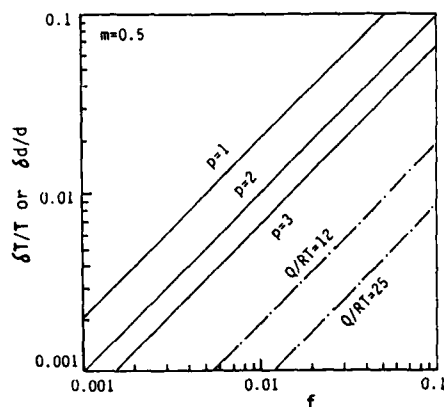


Figure 3 - Comparison between initial grain size inhomogeneity or temperature difference and initial geometrical imperfection for their influences on limit strain (from (14)).

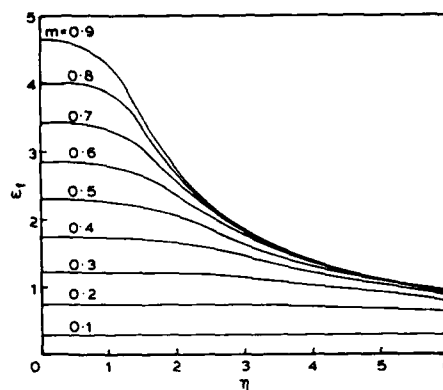


Figure 4 - Calculated fracture strain  $\epsilon_f$  versus cavity growth rate  $\eta$  for various values of  $m$ ;  $C_{v0} = 10^{-3}$ ,  $f = 5 \times 10^{-3}$  (from (18)).

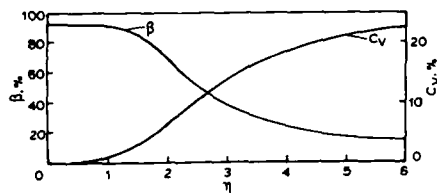


Figure 5 - Influence of cavity growth rate  $\eta$  on external necking and internal cavity volume fraction outside neck section ( $\beta = (A_f - A_{nf})/A_f \times 100, \%$ ) (from (18)).

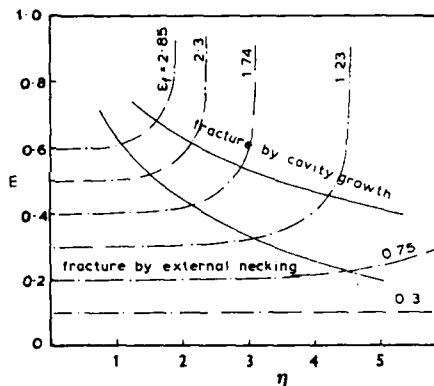


Figure 6 - Superplastic fracture mechanism diagram,  $C_{v0} = 10^{-3}$ ,  $f = 5 \times 10^{-3}$  (from (18)).

values for superplastic alloys,  $10^{-3}$  and  $5 \times 10^{-3}$  respectively.

The previous analysis thus clearly demonstrates that cavity growth has a strong influence on the fracture strain of superplastic materials which justifies the various attempts which were experimented to eliminate or at least reduce cavitation during straining, essentially by using superimposed hydrostatic pressure. Indeed, theoretical models of cavity growth (when it is plasticity controlled) predicts that  $\eta$  will be zero when pressures greater than  $\sigma_0/3$  are superimposed to the tensile stress  $\sigma_0$ . Figure 7 shows the influence of the pressure on the position of the isostrain curves in the fracture mechanism diagrams. The cavity growth rate  $\eta_0$  is defined here as  $\eta = \eta_0 F$  where  $F$ , function of the stress state, is

assumed to be given by the Rice and Tracey model (19) (0.3 in uniaxial tension). It is shown that increasing superimposed pressure increases the fracture strain for given values of  $m$  and  $\eta_0$  and consequently shifts the region of fracture by external necking towards greater  $\eta_0$  values.

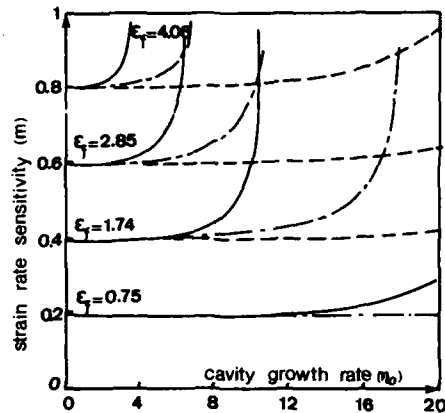


Figure 7 - Influence of pressure  $P_h$  on the position of the isostrain curves in the fracture mechanism diagram ;  $C_{v0} = 10^{-3}$  ;  $f = 5 \times 10^{-3}$ . (from results of (21)).  
 $P_h$  : — 0 ; - - -  $.2\sigma_e$  ; - - -  $.4\sigma_e$

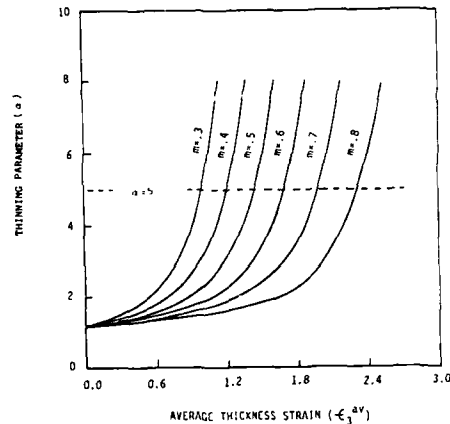


Figure 8 - Calculated thinning parameter  $\alpha$  versus average thickness strain  $(-\epsilon_3^{av})$  for various  $m$ -values. No cavitation. (from (21)).

#### Influence of some parameters under biaxial stress state

Since superplastic forming is now quite extensively used for aerospace applications, deformation is not only limited to uniaxial tension but often performed under more complex stress states. In fact, the basic superplastic forming operation is the bulging of a clamped sheet into a shaped mould by applying one-side gas pressure and for this process a number of theoretical and numerical analyses have been developed. The main calculations have been concerned with the influence of the  $m$  value on the thickness profile for the free bulging of a circular diaphragm and it was shown that the larger the  $m$  value, the more uniform is the thickness distribution. However, as for uniaxial tension, other parameters may influence this distribution and lead to premature failure of the material. In this part, cavitation and temperature inhomogeneities are considered together with initial thickness distribution of the sheet. The basic results for the free bulging of an homogeneous circular clamped sheet will be first briefly reported.

#### Influence of $m$ in superplastic bulging

The more recent calculation dealing with this problem is that developed by Zhou and Lian (20) using the rigid-viscoplastic element method, the material being isotropic with a constant value of  $m$ . Figure 8 shows the influence of this parameter on the thinning development during bulging. This thinning development is described here by a parameter  $\alpha = \dot{\epsilon}_3^p / \dot{\epsilon}_3^v$  where  $\dot{\epsilon}_3^p$  is the thickness strain-rate at the pole and  $\dot{\epsilon}_3^v$  is the average thickness strain-rate along the meridian. It can be seen from

this figure that the non-uniform thinning process is restrained by a large  $m$  value. Moreover the thinning rate increases very rapidly with average thickness strain leading to heavy strain localisation at the pole and then rupture of the material. As for uniaxial tension, an arbitrary criterion for the prediction of limit strain during bulging was used, namely that failure occurs when  $\alpha = 5$ .

### Cavitation

The previous prediction was made assuming that no cavitation develops in the material so that failure occurs by local thinning. For cavitating alloys, fracture can be due also by cavity growth and for its prediction the same criterion as for uniaxial tension have been used that is the cavity volume fraction at the pole  $C_V^p = 30\%$  (21). The influence the cavity growth rate  $\eta_0$  on the limit thickness strain ( $-\epsilon_{3f}$ ) is shown in figure 9 for various values of  $m$ . When  $\eta_0$  is small ( $\eta_0 < 4$ ) large limit thickness strains can be obtained depending on the value of  $m$ . In this case, the failure criterion  $\alpha = 5$  is satisfied which means that the failure of the sheet occurs by geometrical thinning. When  $\eta_0$  is large ( $\eta_0 > 8$ ) a smaller and almost constant limit strain is obtained by the criterion  $C_V^p = 30\%$ . The influence of both  $m$  and  $\eta_0$  on limit strain allows fracture mechanism diagrams to be constructed for superplastic bulging (figure 10). The diagram is divided into three regions corresponding to thinning fracture, mixed fracture and cavitation fracture respectively.

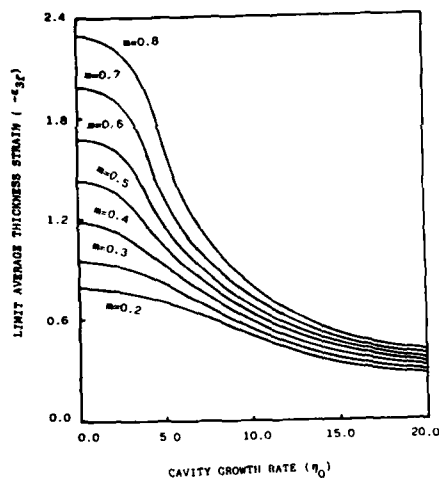


Figure 9 - Calculated limit average thickness strain  $-\epsilon_{3f}$  versus cavity growth rate  $\eta_0$  for various  $m$ -values.  $C_{V0} = 10^{-3}$  (from (21)).

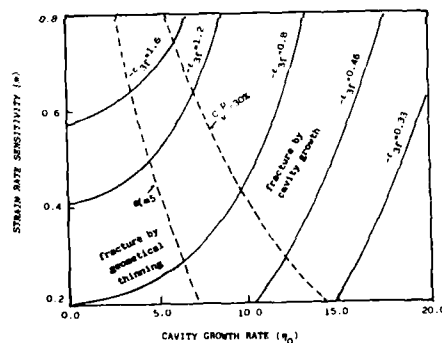


Figure 10 - Superplastic bulging fracture mechanism diagram.  $C_{V0} = 10^{-3}$  (from (21)).

In order to reduce cavitation, bulging can be carried out with superimposed back pressure  $P_h$ , the effect of which is predicted in figure 11. In this figure, the isostrain curves ( $-\epsilon_{3f} = \text{constant}$ ) at fracture are plotted as function of  $\eta_0$  and  $P_h/\sigma_0$ . For a given value of  $\eta_0$ , fracture by cavity growth progressively changes to fracture by thinning when pressure



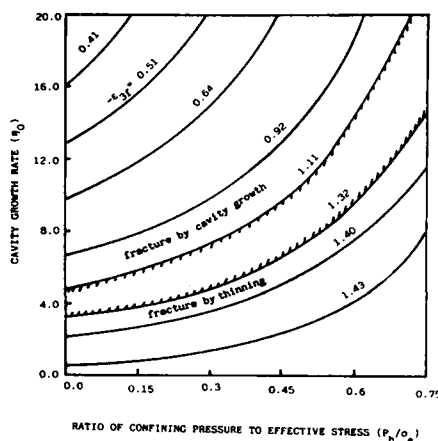


Figure 11 - Superplastic fracture mechanism for bulging for various superimposed hydrostatic pressures and cavity growth rates.  $m = 0.5$ ,  $C_{v0} = 10^{-3}$ . (from (21)).

increases with a corresponding increase of the limit strain. Moreover, it has been shown that, when the pressure exceeds  $2/3 \sigma_e$ , cavity growth is theoretically suppressed and the material behaves as without cavitation.

#### Non uniformity of temperature

As for uniaxial tension, non uniformity of temperature in the sheet plane has a very strong influence on the thinning development and it is then interesting to get an idea of the difference of temperature between the edge ( $T_e$ ) and the pole ( $T_p$ ) which may either lead to earlier fracture ( $T_e < T_p$ ) or inversely to more uniform thickness distribution ( $T_e > T_p$ ).

This problem was considered recently (22) for the case of the circular bulging of Al-7475 sheets, assuming that the deformed sheet is always a portion of a sphere. The temperature  $T_p$  and  $T_e$  are maintained constant during the process with a temperature distribution in agreement with the Fourier's law. Figure 12 shows the results of the calculation, the optimal temperature for superplasticity being  $516^\circ\text{C}$ , taken as the temperature at the pole  $T_p$ . A higher temperature at the edge by only  $10^\circ\text{C}$  is sufficient to obtain almost complete homogeneity of deformation whereas a lower temperature by  $10^\circ\text{C}$  leads to heavy strain localization at the pole. This result thus demonstrates that precise control of temperature is necessary to reduce the thinning development during bulging.

#### Thickness distribution

In the same way as controlled temperature distribution, difference of thickness between the edge and the center of the sheet can delay strain localization at the pole and lead to more uniform thickness distribution during bulging. Experiments with sheets of Ti-6Al-4V of non-uniform thickness were performed (23) and figure 13 shows the various initial thickness profiles used and the corresponding thickness distribution after forming of half a sphere. With profile (3), almost homogeneous thinning is obtained which needs only little machining for complete uniform thickness. Moreover the process allows weight reduction of the starting material since the maximum initial thickness is only 7 mm.

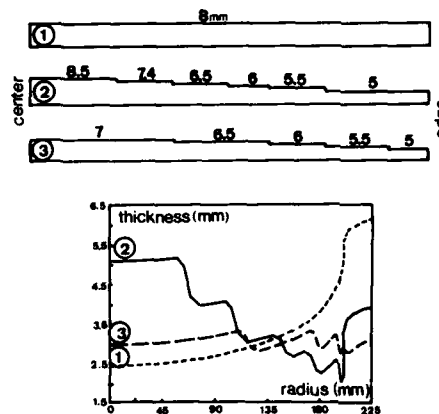
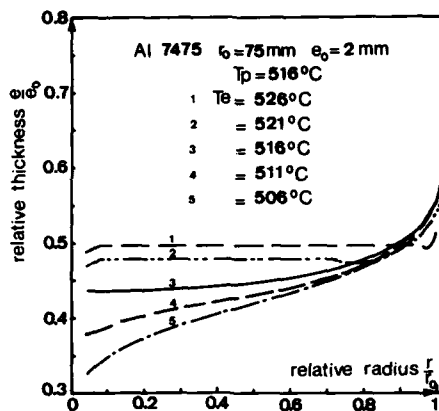


Figure 12 - Influence of temperature  $T_e$  at the edge of the sheet on the thickness distribution after bulging of half a sphere.  $T_p$  is the temperature at the pole. (from (22)).

Figure 13 - Influence of the initial thickness distribution on the thickness after bulging of half a sphere for Ti - 6 Al - 4 V sheets of 450 mm diameter. (from (23)).

### Conclusion

Other factors than the strain-rate sensitivity parameter  $m$  influence greatly the ductility of superplastic materials. In this paper, the uniformity of temperature and grain size and the structural evolutions, mainly cavitation, were considered in uniaxial and biaxial deformations. Temperature gradient dramatically reduces tensile ductility whereas it can have either a stabilizing or destabilizing effect during sheet bulging. Cavitation always reduces strain to fracture which justifies the use of superimposed pressure during deformation for eliminating cavity growth and increasing failure strain in alloys particularly prone to cavitation.

### References

1. J. Lian and B. Baudalet, "Necking Development and Strain to Fracture under Uniaxial Tension", *Mat. Sci. Eng.* **84** (1986) 157-162.
2. E.W. Hart, "Theory of the Tensile Test", *Acta Metall.* **15** (1967) 351-355.
3. A.K. Ghosh and R.A. Ayres, "On Reported Anomalies in Relating Strain-Rate Sensitivity ( $m$ ) to Ductility", *Metall. Trans.* **7A** (1976) 1589-1591.
4. F.A. Nichols, "Plastic Instabilities and Uniaxial Tensile Ductilities", *Acta Metall.* **28** (1980) 663-673.
5. I.-H. Lin, J.P. Hirth and E.W. Hart, "Plastic Instability in Uniaxial Tension Tests", *Acta Metall.* **29** (1981) 819-827.
6. A.K. Ghosh, "Tensile Instability and Necking in Materials with Strain Hardening and Strain-Rate Hardening", *Acta Metall.* **25** (1977) 1413-1424.

7. J.J. Jonas, R.A. Holt and C.E. Coleman, "Plastic Stability in Tension and Compression", Acta Metall. 24 (1976) 911-918.
8. J.W. Hutchinson and K.W. Neale, "Influence of Strain-rate Sensitivity on Necking under Uniaxial Tension", Acta Metall. 25 (1977) 839-846.
9. S.L. Semiatin and J.J. Jonas, in "Formability and Workability of Metals", American Society for Metals, Metals Park (1984) p.155.
10. D.A. Wordford, "Strain Rate Sensitivity as a Measure of Ductility", Trans. of the ASM. 62 (1969) 291-293.
11. J. Lian and B. Baudalet, "Influence of Variation of Strain Rate Sensitivity on Limit Strain of Superplasticity", Scripta Metall. 21 (1987) 331-334.
12. W.B. Morrison, "The Elongation of Superplastic Alloys", Trans. Met. Soc. AIME 242 (1968) 2221-2227.
13. A. Arieli and A.K. Mukherjee, "Factors Affecting the Ductility of the Superplastic Ti-6Al-4V Alloy in Proc" "5th. International Conference on the Strength of Metals and Alloys", Aachen, August 27-31, 1979 (Ed. P.Haasen et al). 1 (1979) 375-380.
14. J. Lian, B. Baudalet and M. Suéry, "Numerical Analysis of the Influence of Various Defects on Superplastic Fracture Under Uniaxial Tension" Computational Methods for Predicting Material Processing Defects (Ed. M. Predeleanu) Elsevier Science Publishers B.V., Amsterdam, 1987, 213-220.
15. C.H. Hamilton, "Superplasticity" In Proc. "7th. International Conference on the Strength of Metals and Alloys", Montréal, August 12-16 1985 (Ed. H.J. McQueen et al) Pergamon Press 3 (1985) 1831-1857.
16. B. Baudalet and M. Suéry, "Temporary Superplasticity", Superplasticity, Ed. B. Baudalet and M. Suéry (Editions du CNRS, Paris, 1985) 17.1 - 17.21.
17. J.J. Jonas and B. Baudalet, "Effect of Crack and Cavity Generation on Tensile Stability", Acta Metall. 25 (1977) 43-50.
18. J. Lian and M. Suéry, "Effect of Strain Rate Sensitivity and Cavity Growth Rate on Failure of Superplastic Material", Mater. Sci. Technol. 2 (1986) 1093-1098.
19. J.R. Rice and D.M. Tracey, "On the Ductile Enlargement of Voids in Triaxial Stress Fields", J. Mech. Phys. Solids 17 (1969) 201-217.
20. D.-J. Zhou, J. Lian, "Numerical Analysis of Superplastic Bulging for Cavity-Sensitive Materials", Int. J. Mech. Sci. 29 (1987) 565-576.
21. D.-J. Zhou, J. Lian and M. Suéry, "Numerical Study of Superplastic Deformation with Superimposed Pressure for Cavity Sensitive Materials", Mater. Sci. Technol. to be published (April 1988).
22. S. Yang, "Mise en Forme par Gonflement de l'Alliage d'Aluminium 7475 Superplastique", M.Sc. Thesis I.N.P.Grenoble (1987).
23. M. Bellet, "Modélisation Numérique du Formage Superplastique de Tôles", Thesis, Ecole Nationale Supérieure des Mines de Paris (1988).

## THE ROLE OF CAVITATION IN THE FAILURE OF SUPERPLASTIC ALLOYS

Atul H. Chokshi and Amiya K. Mukherjee  
Division of Materials Science and Engineering  
Department of Mechanical Engineering  
University of California  
Davis, CA 95616

### Abstract

Superplastic alloys generally exhibit very large elongations to failure by virtue of their high strain rate sensitivities,  $m$ . A high value of  $m$  provides these alloys with a considerable resistance towards flow localization, and it has been shown that the total elongation to failure is influenced also by the occurrence of strain hardening due to concurrent grain growth and specimen geometry. Most superplastic alloys cavitate during deformation, and in some materials extensive cavitation may lead to premature failure. The experimental observations on cavity nucleation and growth are summarized and compared with the relevant theoretical mechanisms. Techniques to reduce cavitation during superplastic deformation are outlined, with emphasis on the superimposition of hydrostatic pressure during superplastic deformation and alloy design considerations.

*Superplasticity and Superplastic Forming*  
Edited by C.H. Hamilton and N.E. Paton  
The Minerals, Metals & Materials Society, 1988

## 1. Introduction

Most metals and alloys exhibit elongations to failure of less than ~50% when pulled in tension at elevated temperatures. Superplastic alloys are capable of exhibiting very large elongations to failure, typically greater than ~500%. Although superplasticity was demonstrated strikingly by Pearson [1] as early as in 1934, with an elongation of 1950% in a Sn-Bi eutectic alloy, and there have been many detailed studies on the mechanical properties of these alloys since the 1960's, it is only recently that the possibility of using this phenomenon to form complex shapes for aerospace applications, with substantial savings in both weight and costs, has aroused commercial interest in this process [2].

It is now widely recognized that there are three major requirements for superplasticity: (i) a fine and reasonably stable grain size, typically less than ~10  $\mu\text{m}$ , (ii) an elevated testing temperature, typically greater than ~0.5  $T_m$ , where  $T_m$  is the absolute melting temperature, and (iii) a high value of strain rate sensitivity, typically greater than ~0.3. The requirement of a fine and stable grain size at elevated testing temperatures has restricted the observation of superplasticity to microduplex alloys based typically on a eutectic or eutectoid composition, and quasi-single phase alloys with fine precipitates pinning the grain boundaries. Most commercial applications of superplasticity involve alloys with a quasi single phase microstructure.

Superplastic alloys usually exhibit a sigmoidal relationship between the flow stress and the strain rate, on a logarithmic scale, and these data may be divided conveniently into three regions, each of which is represented frequently in the form  $\sigma = B\dot{\epsilon}^m$ , where  $\sigma$  is the flow stress,  $B$  is a constant,  $\dot{\epsilon}$  is the strain rate and  $m$  is the strain rate sensitivity. Superplastic elongations to failure are obtained at intermediate strain rates in region II, where the value of  $m$  is typically greater than ~0.4, and the elongations to failure decrease at lower strain rates in region I and at higher strain rates in region III, where the respective values of  $m$  are typically less than ~0.3.

At elevated testing temperatures, failure in tension may occur by two processes: (a) external necking and (b) internal cavitation. It is now widely known that a high value of  $m$  provides superplastic alloys with a resistance towards external flow localization [3]. It is also being recognized increasingly that most superplastic alloys cavitate during deformation [4-7], and although these materials are generally capable of withstanding extensive cavitation before failure, recent studies have shown that even small levels of cavitation lead to a deterioration in the subsequent room temperature properties of superplastically formed components [8]. Clearly, in order to decrease the rate of cavitation damage accumulation during superplastic deformation, it is necessary to develop a good understanding of the processes leading to cavitation failure; this is particularly important for many of the more recently developed marginally superplastic commercial quasi-single phase Al-based alloys.

This paper reviews briefly the processes involved in the failure of superplastic alloys. The following section describes the occurrence of flow localization in superplasticity, and the subsequent section deals with the important role of cavitation in the failure of superplastic alloys. The final section discusses some experimental procedures and alloy design considerations that may inhibit the occurrence of cavitation during superplastic deformation.

## 2. Flow Localization during Superplastic Deformation

In general, superplastic alloys do not exhibit much external necking when tested under optimum conditions, so that even in specimens exhibiting elongations to failure of several thousands of percent, there is very little evidence of flow localization [4]. The importance of strain rate sensitivity in imparting superplastic alloys with resistance towards flow localization has been demonstrated experimentally by measuring with increasing deformation the variation in the local strain along the gauge length [9].

Mohamed and Langdon [9] conducted experiments to determine the onset and degree of flow localization in a superplastic Zn-22% Al eutectoid alloy. Tensile specimens were tested at strain rates representative of region I ( $m = 0.22$ ), region II ( $m = 0.5$ ) and the onset of region III ( $m \sim 0.2$ ), respectively. The specimen gauge lengths were divided into equal segments, with an initial length  $l_0$ , and the local strain along the gauge length,  $\Delta l/l_0$ , was measured at different total specimen elongations  $\Delta L/L_0$ , where  $\Delta l$  is the change in the length of a given segment,  $\Delta L$  is the change in the total gauge length and  $L_0$  is the initial gauge length of a specimen. The variation in the local elongation at different sections along the gauge length is shown in Figs. 1 and 2 for specimens tested in regions I and II, respectively. Inspection of Figs. 1 and 2 reveals that, in contrast to region I where the deformation becomes non-uniform at elongations of  $>100\%$ , the deformation in region II is fairly uniform up to elongations of  $\sim 800\%$  and non-uniform flow is observed only at large elongations of  $>1000\%$ . These results demonstrate clearly that an increase in the strain rate sensitivity delays the onset of flow localization to higher strains.

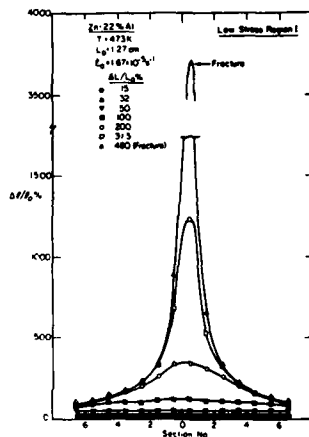


Figure 1 - Variation in local strain during deformation in region I ( $m = 0.22$ ) [9].

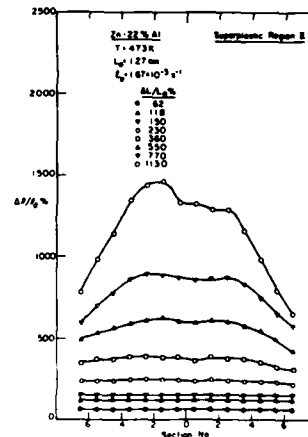


Figure 2 - Variation in local strain during deformation in region II ( $m = 0.5$ ) [9].

Following the general analyses of flow localization during testing, it is anticipated that the occurrence of strain hardening may also contribute to the stability of tensile deformation [3]. The overall stability of tensile deformation is related to a combination of  $m$  and  $\gamma$ , where  $\gamma$  is the strain hardening coefficient. Caceres and Wilkinson [10] examined in detail the

influence of strain hardening due to grain growth on fracture in a superplastic quasi single phase Cu alloy, and they demonstrated that concurrent grain growth at low strain rates in region I may provide a substantial contribution to the stability of tensile deformation. However, concurrent grain growth also tends to decrease the strain rate for a transition from region II to region III. Therefore, as emphasized recently by Hamilton [11], concurrent grain growth may also have a destabilizing effect on tensile deformation if the tensile experiments are conducted close to the transition from region II to III.

Several attempts have been made to express the elongation to failure in a tensile test analytically in terms of the specimen dimensions and parameters such as  $m$  and  $\gamma$ , and they were summarized recently by Hamilton [11]. It suffices to note here that, while most of these expressions predict the correct trend in increasing ductility with increasing  $m$ , they do not predict the exact ductility of any given material satisfactorily. In this context, it is to be noted that some recent experimental studies suggest that the ductility is affected not only by the size of a geometrical defect (local neck) but also by the defect gradient [12].

### 3. Cavitation Failure in Superplastic Alloys

Although a high value of  $m$  is generally considered to be a pre-requisite for the observation of superplasticity, a close inspection of the available data suggests that cavitation frequently plays an important role in the failure of superplastic alloys to such an extent that in some alloys excessive cavitation may lead to premature failure [4,5]. In addition, it is now reasonably well established that even small levels of cavitation have a deleterious effect on the subsequent room temperature properties of superplastically formed components, and this may impose a substantial limitation on the commercial use of superplastic alloys.

It is clear that a fundamental understanding of cavitation in superplasticity may lead to the development of better materials, processing or experimental conditions, so that cavitation damage may be controlled, if not eliminated. Cavitation failure involves the nucleation, growth and interlinkage of cavities. Cavity interlinkage will not be discussed in the present paper, except to note that a recent model study has shown that an increase in the strain rate sensitivity delays the onset of interaction effects and the interlinkage of cavities in a direction perpendicular to the tensile axis [13].

#### 3.1 The Nucleation of Cavities

It has been suggested in many investigations on cavitation failure that cavities may pre-exist prior to deformation in many alloys because of the extensive thermo-mechanical treatment used to develop a fine grain size in superplastic alloys [5-7]. It is shown below that there is very little direct or indirect evidence regarding pre-existing cavities.

Indirect evidence on the occurrence of pre-existing cavitation was reported in some studies from an extrapolation to zero strain of semi-logarithmic plots of the variation in the total level of cavitation with imposed strain [5]. However, as noted elsewhere [14], since cavitation is plotted on a logarithmic scale, an extrapolation of such plots to zero strain will always give a positive offset, irrespective of whether cavities pre-existed or not. Thus, it is noted that, while such plots may be useful in examining the increase in the total level of cavitation damage with strain, they do not provide any evidence for pre-existing cavitation.

An important point to note in this context is that, although there have been numerous microstructural studies on superplastic alloys, there have been no direct observations of pre-existing cavities. However, in view of the sampling and resolution limitations of the available microstructural techniques, it is not possible to rule out the presence of very small cavities with dimensions of less than  $\sim 0.1 \mu\text{m}$  prior to superplastic deformation. If very small cavities are present in the material, it is important to evaluate their stability at elevated temperatures, prior to superplastic deformation. It is known that only cavities with dimensions greater than a critical value  $r_0$  ( $=2\gamma/\sigma$ , where  $\gamma$  is the surface energy) are stable at elevated temperatures, so that cavities with radii less than  $r_0$  will tend to sinter under the action of surface tension. The time necessary to sinter out cavities completely,  $t$ , in the absence of any internal gas pressure, may be determined from the following expression [15]:

$$t = \frac{r^4 k T}{\phi \Omega \delta D_{gb} \gamma} \quad (1)$$

where  $\Omega$  is the atomic volume,  $\delta$  is the grain boundary width,  $D_{gb}$  is the grain boundary diffusion coefficient,  $\phi$  is a constant equal to 1.6,  $k$  is Boltzmann's constant,  $T$  is the absolute temperature and  $r$  is the radii of pre-existing cavities. This equation was developed by using the Speight and Beere [16] expression for diffusion cavity growth under conditions where cavities are small and fairly well separated, and by putting  $\sigma = 0$ .

An evaluation of Eqn. 1 under typical superplastic conditions reveal that the cavities with radii less than  $0.1 \mu\text{m}$  will be completely sintered at the test temperatures in time intervals of less than  $\sim 1$  second [15]. Since most superplastic alloys are maintained at test temperatures for a period of  $\sim 30$  minutes to allow for temperature stabilization, in addition to any annealing treatment, it is clear from these calculations that all small cavities will be completely sintered prior to superplastic deformation.

In view of the above analysis it is noted that, cavities generally do not pre-exist prior to superplastic deformation, so that it may be concluded reasonably that all of the microstructurally observed cavities are nucleated during superplastic deformation. Furthermore, the observed range of cavity sizes at a given strain, the increase in the number density of cavities with increasing strain and the volumetric size-distribution of cavities at different strains, as determined from Quantimet analyses, all suggest that cavities nucleate continuously during superplastic deformation.

It is well known that grain boundary sliding (GBS) plays an important role in the deformation of superplastic alloys and careful measurements reveal that GBS contributes more than  $\sim 50\%$  of the total strain during superplastic deformation [13]. It is clear that GBS will lead to the development of stress concentrations at irregularities along a boundary, such as particles, ledges and triple points, and cavities may nucleate if these stress concentrations are not relieved sufficiently rapidly.

Quasi single phase alloys, which are stabilized against grain growth by a distribution of fine precipitates, frequently contain coarse agglomerated precipitates, such as  $\text{ZrAl}_3$  in Al-Cu-Zr alloys, or other coarse constituent or impurity particles, such as the Al-Fe-Si particles in some 7000 series Al alloys. In these alloys, cavity nucleation occurs predominantly at coarse grain boundary particles. It is important to note that cavities are not nucleated at fine precipitates pinning the grain boundaries, presumably



because the stress concentrations at these sites are relieved rapidly by local diffusion. A detailed investigation of cavitation in a copper alloy revealed cavities at coarse particles and also a tendency for some cavities to form at grain boundary triple junctions [17]. These observations are consistent with a transmission electron microscopy study that revealed dislocation pile-ups at grain boundary particles and triple grain junctions [18].

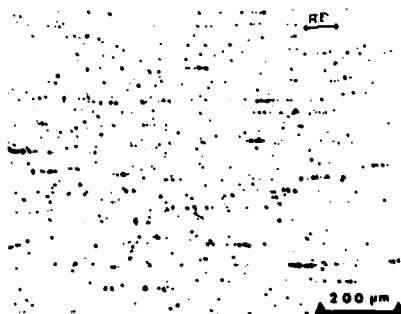


Figure 3 - Cavitation in a copper alloy tested with gauge length parallel to rolling direction:  $\dot{\epsilon} = 1.3 \times 10^{-3} \text{ s}^{-1}$ ,  $\epsilon = 125\%$  [19].



Figure 4 - Cavitation in a copper alloy tested with gauge length transverse to rolling direction:  $\dot{\epsilon} = 1.3 \times 10^{-2} \text{ s}^{-1}$ ,  $\epsilon = 245\%$  [17].

Microstructural inspection of superplastically deformed alloys reveals, in many instances, the alignment of cavities in stringers parallel to the tensile axis [19]. A possible explanation for this observation is that large agglomerated particles are broken up along the extrusion or rolling direction and cavities are nucleated subsequently at these sites [20]. In order to examine this possibility critically, experiments have been conducted on a quasi-single phase Cu alloy with specimen gauge lengths either parallel or perpendicular to the rolling direction (R.D.) [17,20]. It was shown that the mechanical properties of the Cu alloy were not influenced significantly by the change in the orientations of the tensile specimens [17], but there was a marked difference in the orientation of cavity stringers, as shown in Figs. 3 and 4. The tensile axis is horizontal in both these micrographs, and R.D. is horizontal in Fig. 3 but vertical in Fig. 4. These micrographs clearly support the conclusion that the alignment of cavity stringers is caused by the nucleation of cavities at coarse grain boundary particles, which are aligned in stringers along the rolling direction.

Cavities have been observed also in microduplex superplastic alloys which do not contain coarse particles. The observation of cavities in a high-purity laboratory grade, 15 ppm impurity content, Zn-Al eutectoid alloy by Miller and Langdon [21] suggests that grain boundary particles are not always necessary to nucleate cavities. In a recent study, Zn-22% Al eutectoid alloy specimens were tested with gauge lengths perpendicular to the rolling direction [22]. Figure 5 is a micrograph of a specimen pulled to failure; here, the tensile axis is horizontal and R.D. is vertical. Inspection of Fig. 5 reveals that, in contrast to the quasi-single phase Cu alloy, the cavities remain aligned in stringers parallel to the tensile axis. This observation, in conjunction with previous reports of cavity stringers parallel to the tensile axis in specimens with gauge lengths parallel to R.D. [4], suggests strongly that cavities are not nucleated at

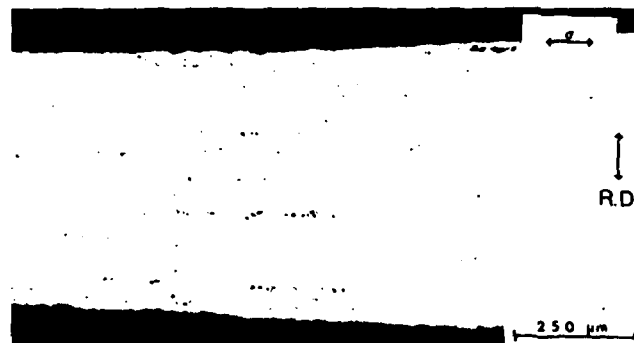


Figure 5 - Cavitation in the Zn-22% Al alloy tested with the gauge length transverse to the tensile axis:  $\dot{\epsilon} = 3.3 \times 10^{-4} \text{ s}^{-1}$ ,  $\epsilon = 1400\%$  [22].

aligned grain boundary particles. Microstructural inspection of the Zn-Al eutectoid alloy revealed the presence of cavities at triple points and at interphase boundaries, without any apparent association with impurity particles [22]. Recently, the nucleation of cavities at ledges was modeled theoretically and conditions favorable for cavity nucleation at grain boundary ledges were identified [15]. It was demonstrated that the analysis is consistent with the experimental results on the Zn-Al eutectoid alloy. It is therefore concluded that, in the absence of grain boundary particles, cavity nucleation in microduplex alloys occurs at grain boundary ledges and at triple points.

### 3.2 Cavity Growth in Superplastic Alloys

Cavity growth has been modeled extensively for conditions of high temperature creep deformation, and the process is reasonably well understood [23]. In general, cavity growth may occur by the stress-directed diffusion of vacancies into cavities or by the plastic (power-law) deformation of the material surrounding a cavity.

For superplastic deformation, the relevant cavity growth mechanisms are quasi-equilibrium diffusion [16] and power-law growth [24]. Analyses of these mechanisms indicate that below a critical radius,  $r_c$ , cavities grow by a diffusion mechanism whereas, above  $r_c$ , cavities grow by a power-law mechanism [4,13]. In fine-grained superplastic alloys, cavities are observed frequently with dimensions substantially larger than the grain size. Under these conditions, cavity growth may occur also by a superplastic diffusion mechanism, in which vacancy diffusion into cavities occurs along the many grain boundaries intersected by large cavities [25].

The cavity growth rate equations for the diffusion, superplastic diffusion and the power-law growth mechanisms have been presented elsewhere [7,13,25,26]. Analyses of these mechanisms and inspection of the appropriate cavity growth maps [26] indicate that the superplastic diffusion mechanism is important only in fine-grained alloys, typically with grain sizes of  $< 5 \mu\text{m}$ , deformed at low strain rates, typically  $< 10^{-3} \text{ s}^{-1}$ . For most alloys deformed under typical superplastic conditions, cavities with dimensions greater than  $\sim 2 \mu\text{m}$  grow predominantly by a power-law mechanism.

Several attempts have been made to quantitatively compare the

experimental observations with the theoretical predictions [4-7]. In this context it is important to note that the theoretical cavity growth mechanisms do not take into account the experimental observations of either continuous cavity nucleation or cavity interlinkage.

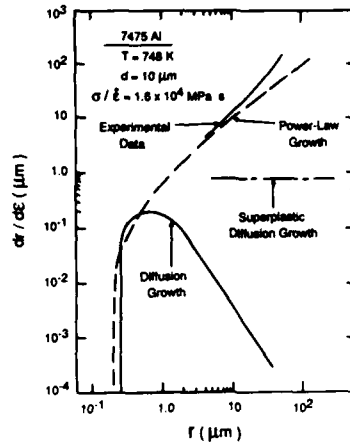


Figure 6 - Comparison between theoretical cavity growth mechanisms and experimental results in a superplastic 7475 Al alloy.

Recently, Franklin *et al.* [27] examined cavitation in detail in a commercial quasi-single phase 7475 Al alloy. Tensile specimens were tested to different strains at 748 K and a strain rate of  $5 \times 10^{-4} \text{ s}^{-1}$ . The size-distribution of cavities at different strains was obtained using a Quantimet, and the experimental cavity growth rates were determined from the slopes of a plot of the variation in the average radii of the largest 1% population against the true strain. Figure 6 shows the variation in cavity growth rate with cavity radius for the theoretical diffusion, superplastic diffusion and power-law mechanism along with the experimental data. Inspection of Fig. 6 shows that there is good agreement between theory and experiment at low cavity radii, corresponding to low strains. At radii greater than  $10 \mu\text{m}$ , the experimental cavity growth rates are higher than the theoretical predictions due to the occurrence of interaction effects and extensive cavity interlinkage.

For microduplex alloys, with the two phases having substantially different flow properties, Shang and Suery [28] developed a power-law cavity growth model, where cavity growth is controlled by deformation in the softer phase. This model leads to a cavity growth rate equation having the same form as that determined by Hancock [24] for single phase alloys. Pilling [29] modeled the influence of cavity interlinkage on cavity growth and cavity size distributions, and obtained good agreement with the experimental results. Caceres and Wilkinson [30] examined the effect of strain hardening on cavity growth by a power-law mechanism.

#### 4. Techniques to reduce cavitation during superplasticity

Several different procedures have been developed to reduce cavitation damage during superplasticity; these include (a) annealing superplastically formed components at elevated temperatures, (b) hot isostatically pressing superplastically formed components and (c) superimposition of hydrostatic

pressures during superplastic forming. The first technique listed above relies on the sintering of cavities at elevated temperatures to reduce the cavitation damage. However, as shown by Eqn. 1, the time to completely sinter cavities is proportional to  $r^3$ ; this Eqn. implies that although small cavities may be conveniently sintered by this procedure, larger cavities cannot be removed because of the prohibitively long time intervals required. Hot isostatic pressing essentially enhances the sintering rate by the addition of stress at elevated temperatures, and it may be somewhat more effective in reducing the sizes of larger cavities. However, it is to be noted that in the presence of gas pressure within cavities, the collapsed cavities may grow again at elevated temperatures.

By far, the most effective and commercially viable technique to reduce cavitation substantially is to superimpose hydrostatic pressure during superplastic forming. Following the work of Bampton et al. [31], there have been many experimental investigations using this technique, and the results were reviewed recently by Pilling and Ridley [7]. The experimental results suggest that hydrostatic pressures reduce both the number density of cavities and the sizes of the largest cavities, thereby implying that this procedure reduces both the cavity nucleation rate and the cavity growth rate [27]. Although the precise role of hydrostatic pressures on cavitation is not completely understood, this procedure offers a simple and attractive means of reducing cavitation damage and it is being utilized in the commercial applications of superplastic forming. Pilling and Ridley [7] have examined in detail the influence of stress state on experiments conducted under hydrostatic pressures, but an examination of their analysis shows that the stress state has a rather minor effect, and hydrostatic pressures of the order of the flow stress are necessary to decrease cavitation during superplastic forming.

While the imposition of hydrostatic pressures of the order of  $\sim 4$  MPa to reduce cavitation is satisfactory for many of the current Al-based alloys, it is anticipated that the development of higher strength Al-based alloys, which may be superplastic at higher strain rates, will require significantly higher levels of hydrostatic pressures, and this may not be commercially feasible for many large components. Therefore, it is useful to consider alternative techniques, such as superplastic alloy design [15], to reduce cavitation damage. Theoretical studies of cavity nucleation at elevated temperatures predict a cavity nucleation rate that depends very strongly on the shape factor,  $F_v$  [32]. The shape factor essentially defines the volume of a critical cavity nucleus, and its value depends on the energies of the interfaces involved in cavity nucleation. Analysis of cavity nucleation in superplasticity reveals that in commercial quasi-single phase alloys,  $F_v$  may be decreased by designing superplastic alloys with a low energy particle/matrix interface, and this will tend to reduce the cavity nucleation rate substantially [15]. Also, a decrease in the sizes of large particles will tend to reduce cavitation because local diffusion across particles may alleviate stress concentrations and prevent cavity nucleation [5,15].

## 5. Summary and Conclusions

A high value of strain rate sensitivity  $m$  enhances the resistance to flow localization and leads to large elongations to failure in superplastic alloys. The elongation to failure is influenced also by the strain hardening coefficient and the gradient in geometric defects (local necks). Cavitation plays an important role in the failure of many superplastic alloys, and even small levels of cavitation lead to a deterioration in the subsequent properties of superplastic alloys. It is shown that most cavities observed in superplastically deformed alloys nucleate during the deformation process,

although there is a possibility that cavities may pre-exist in some commercial alloys. In quasi-single phase alloys, cavities tend to nucleate predominantly at coarse grain boundary particles. Experimental results indicate that, in microduplex alloys, cavities nucleate at grain boundary ledges and at triple points. In general, cavity growth may occur by the diffusion, superplastic diffusion and power-law mechanisms. In commercial quasi-single phase superplastic alloys, the growth of cavities with dimensions greater than  $\sim 2 \mu\text{m}$  is controlled by the power-law mechanism. The level of cavitation may be decreased substantially by superimposing hydrostatic pressures of the order of the flow stress. Cavitation damage may be reduced also by suitable alloy design considerations.

#### Acknowledgement

This work was supported by the Air Force Office of Scientific Research under Grant No. AFOSR 860091 monitored by Dr. A. Rosenstein.

#### References

1. C.E. Pearson, "The Viscous Properties of Extruded Eutectic Alloys of Lead-Tin and Bismuth-Tin," J. Inst. Metals, 111 (1934) 111-144.
2. Superplastic Forming, Ed. S.P. Agrawal (ASM, Metals Park, Ohio, 1985).
3. F.A. Nichols, "Plastic Instabilities and Tensile Ductilities," Acta Metall., 28 (1980) 663-673.
4. T.G. Langdon, "Fracture Processes in Superplastic Flow," Metal Sci., 16 (1982) 175-183.
5. M.J. Stowell, "Failure of Superplastic Alloys," Metal Sci., 17 (1983) 1-11.
6. B.P. Kashyap and A.K. Mukherjee, "Cavitation Behavior During High Temperature Deformation of Micrograined Superplastic Materials - A Review," Res Mechanica, 17 (1986) 293-355.
7. J. Pilling and N. Ridley, "Cavitation in Superplastic Alloys and the Effect of Hydrostatic Pressure," Res Mechanica, 23 (1988) 31-63.
8. C.C. Bampton and J.W. Edington, "The Effect of Superplastic Deformation on Subsequent Service Properties of Fine Grained 7475 Al," J. Engng. Mater. Tech., 105 (1983) 55-60.
9. F.A. Mohamed and T.G. Langdon, "Flow Localization and Neck Formation in a Superplastic Metal," Acta Metall., 29 (1981) 911-920.
10. C.H. Caceres and D.S. Wilkinson, "Large Strain Behavior of a Superplastic Copper Alloy," Acta Metall., 32 (1984) 415-434.
11. C.H. Hamilton, "Superplasticity," Strength of Metal and Alloys (ICSMA 7), vol. 3, Eds. H.J. McQueen et al. (Pergamon Press, Oxford, 1986) 1831-1857.
12. P. Shariat and T.G. Langdon, "The Influence of Specimen profile and Notch Geometry on Superplasticity in Zn-22% Al," this volume.
13. A.H. Chokshi and T.G. Langdon, "The Role of Interfaces in Superplastic Deformation," Superplasticity, Eds. B. Baudalet and M. Suery (Centre National De La Recherche, Paris, 1985) 2.1-2.15.

14. A.H. Chokshi and A.K. Mukherjee, "The Cavitation and Fracture characteristics of a Superplastic Al-Cu-Li-Zr Alloy," Mater. Sci. Engng., to be published (1988).
15. A.H. Chokshi and A.K. Mukherjee, "An Analysis of cavity Nucleation in Superplasticity," to be published.
16. M.V. Speight and W. Beere, "Vacancy Potential and Void Growth on Grain Boundaries," Metal Sci., 9 (1975) 190-191.
17. A.H. Chokshi and T.G. Langdon, "to be published.
18. L.K.L. Falk et al., "The Role of Matrix dislocations in Superplastic Deformation of a Copper Alloy," Acta Metall., 34 (1986) 1203-1214.
19. A.H. Chokshi, "An Experimental Study on the Alignment of Cavities in a Superplastic Commercial Copper Alloy," Metall. Trans., 18A (1987) 63-67.
20. C.H. Caceres and D.S. Wilkinson, "Large Strain Behavior of a Superplastic Copper Alloy - II. Cavitation and Fracture," Acta Metall., 32 (1984) 423-434.
21. D.A. Miller and T.G. Langdon, "Evidence for Cavitation in Superplastic Zn-22Pct Al of Very High Purity," Metall. Trans., 9A (1978) 1688-1690.
22. A.H. Chokshi and T.G. Langdon, "The Influence of Rolling direction on the Mechanical Properties and Formation of Cavity Stringers in the Superplastic Zn-22% Al Alloy," submitted for publication (1988).
23. A.C.F. Cocks and M.F. Ashby, "On Creep Fracture by Void growth," Prog. Mater. Sci., 27 (1982) 189-244.
24. J.W. Hancock, "Creep Cavitation without a Vacancy Flux," Metal Sci., 10 (1976) 319-325.
25. A.H. Chokshi and T.G. Langdon, "A Model for Diffusional Cavity Growth in Superplasticity," Acta Metall., 35 (1987) 1089-1101.
26. A.H. Chokshi, "The Development of cavity Growth Maps for Superplastic Materials," J. Mater. Sci., 21 (1986) 2073-2082.
27. J.E. Franklin, A.H. Chokshi and A.K. Mukherjee, to be published.
28. H.M. Shang and M. Suery, "Modelling of Cavitation in Two Phase Superplastic Alloys under Uniaxial Tension," Metal Sci., 18 (1984) 143-152.
29. J. Pilling, "Effect of Coalescence on Cavity Growth during Superplastic Deformation," Mater. Sci. Tech., 1 (1985) 461-465.
30. D.S. Wilkinson and C.H. Caceres, "Mechanism of Plastic Void Growth during Superplastic Flow," Mater. Sci. Tech., 2 (1986) 1086-1092.
31. C.C. Bampton, M.W. Mahoney, C.H. Hamilton, A.K. Ghosh and R.Raj, "Control of Superplastic Cavitation by Hydrostatic Pressure," Metall Trans., 14A (1983) 1583-1591.
32. R.Raj and M.F. Ashby, "Intergranular Fracture at Elevated Temperatures," Acta Metall., 23 (1975) 653-666.

## HIGH RATE SUPERPLASTIC BEHAVIOR OF MECHANICAL ALLOYED ALUMINUM IN90211

T.R. Bieler\*, T.G. Nieh\*\*, J. Wadsworth\*\*, and A.K. Mukherjee\*

\*Division of Materials Science, Department of Mechanical Engineering,  
University of California, Davis, CA 95616

\*\*Lockheed Missiles and Space Co., Inc., Research and Development,  
Palo Alto, CA 94304

### Abstract

The tensile behavior of IN90211 was characterized at strain rates between 0.0001/sec and 340/sec at temperatures between 425 and 475 °C. At strain rates below 0.1/sec, the strain rate sensitivity  $m$  is low ( $< 0.03$ ), with corresponding low elongation ( $< 100\%$ ). At strain rates above 0.1/sec, the strain rate sensitivity increases to 0.3 ( $n=3-4$ ). A maximum elongation of 500% was obtained at 475 °C at a strain rate of 2.5/sec. Fracture surfaces of the highly elongated specimens exhibits intergranular fracture and cavitation. Grain boundary sliding and rotation was observed in the deformed specimens. Analysis of the experimental data in the high strain rate regime (superplastic) revealed the existence of a temperature dependant threshold stress. The analyzed results are also consistent with direct measurements from stress relaxation experiments. The results differ from the kind of behavior expected from established superplasticity and creep theories.

Superplasticity and Superplastic Forming  
Edited by C.H. Hamilton and N.E. Paton  
The Minerals, Metals & Materials Society, 1988

### Introduction

Superplastic forming of commercial alloys usually occurs at relatively slow strain rates. In general, this strain rate is inversely related to grain size. It was recently discovered [1] that composites of Al-2124 containing 20 vol% of SiC whiskers behave in a superplastic-like manner with up to 300% elongation at a high strain rate of 0.3/s. Similarly, a high strain rate superplasticity phenomenon was observed in an ultrafine grained, mechanically alloyed IN9021 alloy [2], where maximum elongations were found at strain rates greater than 1/s. The observation of superplastic like behavior at these unusually high strain rates is nonetheless believed to be consistent with the extremely fine (submicron) grain sizes in these complex composites and alloys. The micromechanisms that govern superplastic deformation of the IN90211 specimens reported in [2] are discussed below.

### Experimental Procedures

Specimens of IN90211 were produced by Novamet Aluminum, further processed and then deformed between 425°C and 475°C at strain rates between 0.0001 and 340/sec, as described in [2]. The alloy contains about 7 vol% oxide and carbide dispersions of approximately 30 nm in diameter with an interparticle spacing of about 60 nm, as well as the Al<sub>2</sub>Cu  $\theta$  phase precipitates. Selected specimens were examined using optical, scanning and transmission electron microscopy, and X-ray diffraction prior to and after deformation.

### Results and Discussion

The elongation-to-failure for IN90211 alloy, as a function of strain rate, is shown in Figure 1a for temperatures between 425 and 475°C. A maximum elongation-to-failure of 505% was recorded at a test temperature of 475°C and a strain rate of 2.5/s. The peak true stress is plotted as a function of true strain rate in Figure 1b. Each of these regimes has a particular value of stress dependence upon strain rate. For superplastic studies it is convenient to use the simple equation  $\sigma = k\dot{\epsilon}^m$  where  $\sigma$  is the true flow stress at a true strain rate,  $\dot{\epsilon}$ ,  $k$  is a constant, and  $m$  is the strain rate sensitivity exponent. At strain rates between 0.0001 and 0.1/sec,  $m \approx 0.027$ , but at strain rates above 0.1/s  $m \approx 0.26$ . The exponent changes to  $m \approx 0.15$  at strain rates above 50/s.

Threshold stresses are commonly invoked in the analysis of stress-strain behavior of ODS materials, especially at low stress and strain rates. Theoretically the strain rate can be expressed in terms of an applied stress  $\sigma$ , and a threshold stress  $\sigma_0$ :

$$\frac{\dot{\epsilon} k T}{D_1 E b} = A \left( \frac{\sigma - \sigma_0}{E} \right)^n \quad (1)$$

where  $\dot{\epsilon}$  is strain rate,  $kT$  are Boltzman's constant times the absolute temperature,  $D_1$  is the temperature dependant lattice bulk diffusivity (145 kJ/mol),  $E$  is temperature dependant Young's modulus,  $b$  is the Burger's vector,  $A$  is a mechanism dependant constant that includes the grain size, and  $n$  is the stress exponent (where  $n=1/m$ ). An effort was made to determine whether a threshold stress is operative by conducting a stress relaxation experiment at 450°C. After a few seconds, an apparent steady state stress of  $9 \pm 1$  MPa was reached and it remained constant for several hours.



A threshold stress can also be estimated from the data of Figure 1b using the approach suggested by Mohamed [3]. A threshold stress can be obtained from a plot of the cube root (i.e.  $n=3.0$ ) of strain rate versus stress [2], using the data from the high strain rate regime of Figure 1b (the low strain rate data fell off the extrapolated line). These data were linear, providing extrapolated threshold stress values of 5 and 16 MPa for the 475°C and 425°C data, respectively. These extrapolated values are consistent with the 9 MPa value obtained from the stress relaxation measurement at 450°C. The introduction of this temperature dependant threshold stress (to replace the flow stress with an effective stress) in the normalized plot of Figure 2 caused the data in the high strain rate regime to superpose with a slope of  $n=3$ . The apparent activation energy of the superplastic-like regime was estimated using constant strain rate data, and the value of  $n=3$ . The activation energy thus determined is  $160 \pm 40$  kJ/mol using the peak true stresses and  $125 \pm 25$  kJ/mol using the effective stress data (including temperature dependant shear modulus corrections). The bulk diffusion activation energy for pure aluminum is 145 kJ/mol, within the tolerances given. Also, the threshold stress does not affect the abrupt change in the stress exponent at lower strain rates, contrary to the results of others [3].

The change in stress sensitivity at high stresses and strain rates occurs at a stress near 200 MPa. An Orowan stress of about 200 MPa can be estimated from 30 nm particles 60 nm apart. The change in deformation mechanism in the highest rate data suggests a stress exponent around 8, a value consistent with other dispersion strengthened alloys [4]. Thus the change in the stress exponent may result from dislocation generation and motion by Orowan looping. The change in behavior may also be due to power-law breakdown. More data are needed to confirm the deformation behavior at high stresses.

Microscopy was reviewed in detail in [2], and is summarized as follows: Transmission electron microscopy of an undeformed sample revealed 30 nm oxides and carbides, and S phase ( $\text{Al}_2\text{CuMg}$ ) precipitates notably on grain boundaries. The grain size was determined to be  $0.5 \pm 0.3$   $\mu\text{m}$ . The grain size and microstructure of samples after deformation appeared to be similar to the undeformed microstructure, indicating high stability at elevated temperatures. Grain boundary sliding and rotation was observed by placing markers on highly polished specimen surfaces and observing the deformed specimen surface in SEM. Fracture surfaces from superplastically deformed IN90211 specimens exhibited an intergranular fracture mode. The sizes of the granular features were similar to the grain size of the untested material observed by TEM. This fracture surface is quite different from the observation in IN9021 by Shaw [5], where a fibrous fracture surface was observed. This difference is difficult to explain since the testing temperature used by Shaw was 400°C, close to the temperatures of the specimens in the present study.

X-ray analysis was conducted on a Siemens Diffraktometer using Cu-K $\alpha$  radiation. Specimens were oriented so that the X-ray beam was perpendicular to the tensile axis, with diffraction from the originally rolled surfaces. In addition to the strong peaks for aluminum, about 35 small peaks were noted.  $\text{Al}_2\text{Cu}$  ( $\theta$  phase), was clearly identified, and correspondence was made for  $\text{Al}_4\text{C}_3$ ,  $\text{Al}_2\text{O}_3$ , and  $\text{Al}_2\text{CuMg}$  (S phase, accounting for no more than 20% of the Mg). Although energetically favored over  $\text{Al}_2\text{O}_3$ , MgO was not observed, as has been reported for other aluminum-magnesium alloys with oxide phases [6].

Mg reacts with  $\text{Al}_2\text{O}_3$  in the presence molten Al to form MgO at interfaces, which was precluded by the solid state processing. The 2 wt% Mg did not appear in X-ray or TEM diffraction, except for the small amount associated with the  $\text{CuMgAl}_2$ . Its absence indicates that it is dissolved in the matrix, as phase diagrams would indicate. Auger spectroscopy of Al-Mg alloys indicate that Mg increasingly segregates to boundaries with decreasing temperature [7]. This is consistent with the TEM observation of the S phase on grain boundaries. With increasing temperature, the Mg concentration in the lattice increases, dissolving the S phase. Mg Solute atoms can cause locking and unlocking behavior of dislocations, resulting in serrated flow curves. Serrations occur in solution treated samples deformed at room temperature [8] and elevated temperature deformation. The high relative intensity of {200} planes in the IN90211 sample indicated that rolling caused a preferred orientation of {001} poles parallel to the rolling direction, increasing the number of {111} planes oriented for slip. The {200} peak intensity increased to twice the usual {200} peak intensity with superplastic deformation, indicating that slip plays an important role in the superplastic-like deformation. The value of  $n=3$  from the high temperature superplastic-like regime thus seems to be associated with solute drag mechanisms.

The exact deformation mechanisms that operate at high strain rates in materials like MA alloys, such as ODS materials, are generally uncertain. Shaw [5] suggested that the elongation phenomenon may not be related to a fine grain size, but rather the result of dynamic recrystallization during the high rate of deformation. His theory however, does not explain the observation of grain boundary sliding and the retention of the same grain size distribution before and after superplastic deformation. Gregory, et al., [9] have argued that a combination of slip with Coble creep (in which the Coble creep exhibits a threshold stress) can explain the phenomenon in a mechanically alloyed nickel based superalloy. However, the IN90211 has a stress dependence of 3 where superplastic behavior was observed, while Gregory measured a slope near 1, consistent with Coble creep theory. The majority of superplastic deformation theories have grain boundary sliding as a major feature, but predict a stress dependence of 2 [10]. The behavior of IN90211 differs from the behavior predicted by superplastic deformation theories.

### Conclusions

Tensile elongation in excess of 500% were obtained with IN90211 mechanically alloyed aluminum at strain rates between 1 and 10/s at 475°C. The superplastic-like behavior at high strain rates appears to be associated with the fine grained (0.5  $\mu\text{m}$ ) microstructure in the alloy. There was evidence for a threshold stress associated with superplastic behavior, but this threshold stress is apparently unrelated to the observed low stress-low strain rate behavior. Grain boundary sliding was clearly observed, but instead of the stress exponent usually associated with grain boundary sliding, a stress exponent of 3 was obtained in the superplastic-like regime. This stress exponent is consistent with the serrated flow observed and solute drag from Cottrell atmospheres. Current superplastic theories do not fully account for the combination of slip with solute drag and grain boundary sliding observed in this alloy. At the highest stresses, the change in mechanism to  $n \approx 8$  is consistent with Orowan bowing around dispersions as commonly seen in ODS materials.

### Acknowledgements

The authors (TRB and AKM) acknowledge the support of the Air Force Office of Scientific Research under grant No. AFOSR-860091 monitored by Dr. Alan Rosenstein. TGN and JW acknowledge the support of the Lockheed independent research program. The authors also gratefully acknowledge R. Shelton and T. Folkerts of the UCD Physics Department for use of the X-ray diffractometer.

### References

1. T.G. Nieh, C.A. Henshall and J. Wadsworth, "Superplasticity ... in an SiC Whisker Reinforced Al Alloy", *Scripta Met.*, 18, (1984) 1405-1410.
2. T.R. Bieler, T.G. Nieh, J. Wadsworth, A.K. Mukherjee, "Superplastic-like ... in Mechanically Alloyed Aluminum", *Scripta Met.*, 22, (1988) 81-86.
3. F.A. Mohamed, "Interpretation of Superplastic Flow in Terms of a Threshold Stress", *J. Mat. Sci.*, 18, (1983) 582-592.
4. J.E. Bird, A.K. Mukherjee, J.F. Dorn, "Correlations Between High-Temperature Creep Behavior and Structure", *Quantitative Relation Between Properties and Microstructure*, Proceedings of International Conference in Haifa, Israel, (Israel University Press, July 1969), p. 255.
5. W.J.D. Shaw, "Microsuperplastic Behavior", *Mat. Letters*, 4, (1985) 1.
6. J.E. Hack, R.A. Page, R. Shermann "The Influence of Thermal Exposure on Interfacial Reactions on Interfacial Reactions ... in Aluminum Oxide Fiber Reinforced Magnesium Alloy Composites", *Met. Trans.*, 16A, (1985) 2069.
7. C. Lea, C. Molinari, "Magnesium diffusion, surface segregation and oxidation in Al-Mg alloys", *J. Mat. Sci.*, 19, (1984) 2336.
8. S.J. Bane, J. Bradfield, M.R. Edwards, "Tensile behavior of mechanically alloyed ... IN 9021", *Mat. Sci. & Tech.*, 2, (1986) 1025-1030.
9. J.K. Gregory, J.C. Gibeling and W.D. Nix, "High Temperature Deformation of Ultra-Fine-Grained Oxide Dispersion Strengthened Alloys", *Met. Trans.*, 16A, (1985) 777.
10. M. Suery and A.K. Mukherjee, "Superplasticity-Correlation Between Structure and Properties", *Creep Behavior of Crystalline Solids*, B. Wilshire and R.W. Evans, eds., (Swansea, U.K., Pineridge Press, 1984), 154.

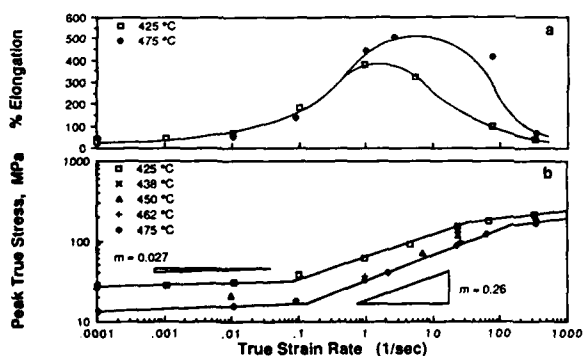


Figure 1--Experimental Data

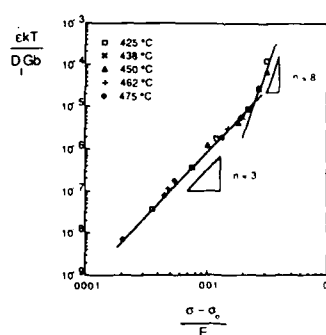


Figure 2--Normalized strain rate-stress plot

EFFECT OF ACCELERATED/DECELERATED STRAIN RATE

ON SHEET FORMABILITY OF  $\sigma = K \dot{\epsilon}^m \epsilon^n$  -MATERIALS

H. Ohsawa

Department of Mechanical Engineering  
Faculty of Technology, Hosei University  
Tokyo, Japan

Abstract

An extension of diffuse necking criterion to materials obeying  $\sigma = K \dot{\epsilon}^m \epsilon^n$  predicts a delay of the attainment to the maximum load point when the rate of change of the strain rate is positive, that is, testing for accelerated strain rate. Experimental verification for the prediction was made on some non-ferrous metal sheets including superplastic alloy. Extended analysis of Hill's local necking and Stören-Rice theory to  $\sigma = K \dot{\epsilon}^m \epsilon^n$ -materials also reveals a significant role of accelerated strain rate for increasing fracture strain. Much dependency of ductility upon the rate of change of the strain rate was demonstrated, while the evaluation on the effect of acceleration on fracture strain involves cumbersome and complex factors such as G.L. for measuring strain, variation of  $m$  value with the strain rate and non-uniform deformation in G.L..

In deep drawing, on the other hand, where the elongation of materials is of little concern, the influence of accelerated/decelerated punch speed on Limiting Drawing Ratio (LDR) was also examined. Improved Instron machine with revised die assembly was used. It was found that the rise of formability due to continuous change of punch speed was not so remarkable.

Superplasticity and Superplastic Forming  
Edited by C.H. Hamilton and N.E. Paton  
The Minerals, Metals & Materials Society, 1988

### Introduction

Sheet metal forming problem has been investigated so far with respect to strain hardening index  $n$  and anisotropy  $r$ . The prediction of formability from these material characteristics, however, is not necessarily complete and in Al and Al alloys, for instance, poor correlation between  $r$  value and formability is found in many works. An constitutive equation  $\sigma = K \dot{\epsilon}^m \epsilon^n$  expressed in explicit form for flow stress was adopted in this work consistently. Swift's diffuse necking criterion for strain hardening materials was extended to this material. The analytical prediction emphasizes the earlier occurrence or the delay of the attainment to the maximum load point in uniaxial tensile test according to the rate of change of the strain rate (1).

Local instability strain for  $\sigma = K \dot{\epsilon}^m \epsilon^n$ -materials, on the other hand, can be also estimated by applying Hill's (2) or Stören-Rice theory (3), which shows again the significant role of the rate of change of the strain rate in the discussion on ductility measured. When the rate of change of the strain rate is positive, testing for accelerated strain rate, the higher the rate, the more the elongation measured. Caution should be paid, however, that these modified analyses do not involve any diffuse necking process, therefore the nature of predicted local instability strain may be experimentally verified in detail.

In uniaxial tensile testing ductility of materials may be examined, while formability in deep drawing by means of flat headed punch is not directly related to ductility. Although the factors which control deep drawing process are quite evident, they interact in such a complex way that precise mathematical description is not possible in simple terms. It is of practical interest to consider deep drawability, Limiting Drawing Ratio (LDR) representing the largest blank that can be drawn without tearing, in relation to the magnitude of punch speed or the rate of change of punch speed. The discussion of deep drawability will be limited to the effect of punch speed and continuous change of punch speed.

### Theoretical Remark

In uniaxial tensile test, if the constitutive equation

$$\sigma = K \dot{\epsilon}^m \epsilon^n \quad (1)$$

holds, the maximum load point  $dP=0$  leads to instability strain

$$\epsilon_u = n / (1 - \gamma m) = n + \bar{\gamma} m, \quad (2)$$

where

$$m = \partial \ln \sigma / \partial \ln \dot{\epsilon}, \quad n = \partial \ln \sigma / \partial \ln \epsilon, \quad (3)$$

and

$$\gamma = d \ln \dot{\epsilon} / d \epsilon, \quad \bar{\gamma} = d \ln \dot{\epsilon} / d \ln \epsilon, \quad (4)$$

are both strain rate paths specifying the rate of change of the strain rate during deformation. Whichever the strain is taken in Eq.(2), instability strain can be influenced by strain rate path. For positive  $m$  value, accelerated strain rate can delay the onset of the instability limit.

It should be noticed that

$$\bar{\gamma} = \epsilon \gamma. \quad (5)$$

Both local necking theories of Hill and Stören-Rice state that the larger  $n$  value makes Forming Limit Diagram (FLD) larger. Even if  $\sigma = K \dot{\epsilon}^m \epsilon^n$ , by using the value of  $n'$  instead of simple  $n$

$$n' = d \ln \sigma / d \ln \epsilon = n + \bar{\gamma}_m, \quad (6)$$

these analyses can be reserved as they are. Simple conclusion, therefore, can be obtained that in this materials acceleration/deceleration of the strain rate is much responsible for total ductility measured.

### Tensile Test

#### Testing Mode

The experiment was carried out by computer-aided Instron testing machine (20tonf). The system block diagram is shown in Fig.1. Four types of testing mode were taken; 1) the pulling rate becomes higher gradually according to

$$\Delta l / l_0 = A (\tau / t)^2 \text{ (accelerated)}, \quad (7)$$

where  $\Delta l / l_0$  is engineering strain  $\epsilon_0$  in Gauge Length (G.L.= $l_0=10, 25\text{mm}$ ), A is a arbitrary constant specified prior to the test (%),  $\tau$  is testing duration (sec) and t total testing time specified prior to the test (sec), 2) the pulling rate becomes lower continuously,

$$\Delta l / l_0 = -A (\tau / t - 1)^2 + A \text{ (decelerated)}, \quad (8)$$

3) engineering strain  $\epsilon_0$  in G.L. increases lineally,

$$\Delta l / l_0 = A (\tau / t) \text{ (constant extension rate)}, \quad (9)$$

in this case strain rate path  $\gamma$  in Eq.(4) takes a constant value of -1, 4) conventional constant cross head speed ranging from 5 to 200mm/min.

The use of extensometer is an essential element when controlling the system and two strain gauge type extensometers,  $l_0=10\text{mm}$  Max.strain 50% and  $l_0=25\text{mm}$  Max.strain 100%, were used.

#### Materials

Supplied sheet materials are pure aluminum A1050-0 ( $m=0.003-0.011$ ,  $n=0.275$ ,  $r=0.68$ ), superplastic alloy SP22 (Zn-22Al-0.5Cu-0.01Mg,  $m=0.087-0.165$ ,  $n=0.013$ ,  $r=0.40$ ) and pure zinc ( $m=0.056-0.085$ ,  $n=0.116$ ,  $r=0.25$ ).

#### Strain Rate Path

The test results are shown in Fig.2. The displacement of the maximum load point can be experimentally confirmed. Strain rate path should be considered as a kind of material properties when cross head speed is not controlled, but it takes a certain value and changes as specified when controlled. Bold lines were determined for only constant cross head speeds. In comparison with constant cross head speed, acceleration according to Eq.(7) did not make  $\gamma$  larger and the highest value of  $\gamma$  for

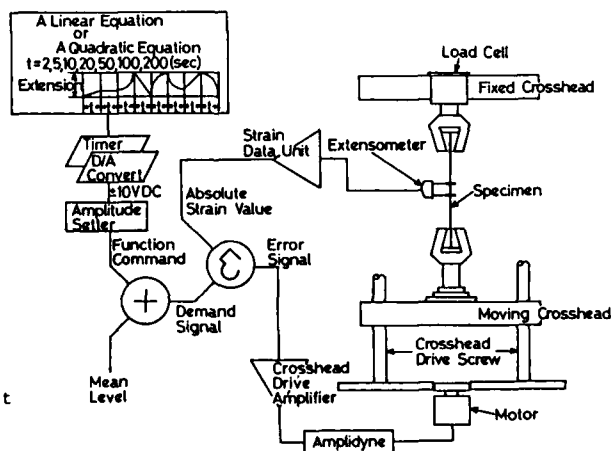
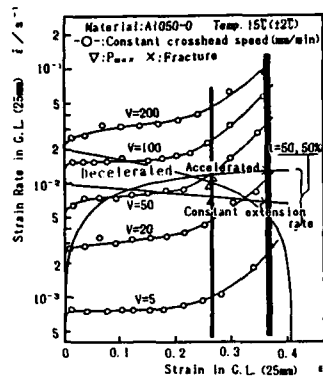
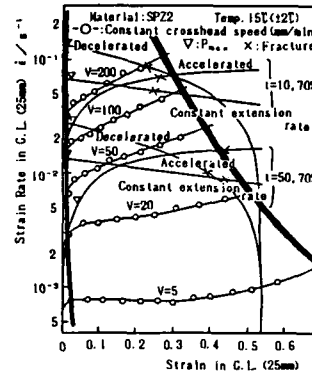


Fig.1 The system block diagram.



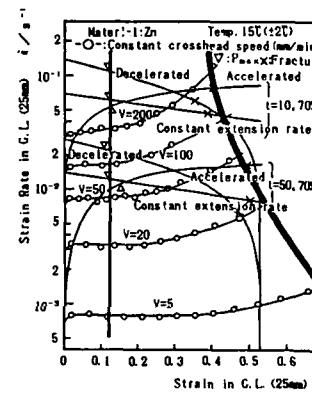
a) pure aluminum, annealing



b) superplastic material

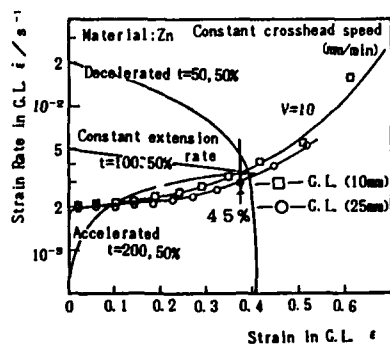
constant cross head speed near the fracture limit makes fracture strain highest in the result.

At the same strain ( $\epsilon = 45\%$ ) and strain rate ( $\dot{\epsilon} = 3-4 \times 10^3 \text{ sec}^{-1}$ ) but the different strain rate path, the non-uniform strain distributions along the length of the specimen were measured (Fig. 3 a), b)). The ductility evaluation from the strain distributions can be more explicitly if caution is paid to the back ground component and the difference between peak strain value and the back ground component of the strain distribution. It readily can be seen that the excellent strain distribution is the one for constant cross head speed and the inferior for decelerated. Good correlation between these observation and the strain rate paths at  $\epsilon_0 = 45\%$  can be found.

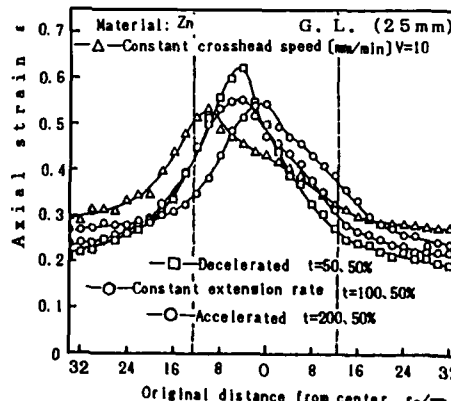


c) pure zinc

Fig.2 Instability, fracture limits and strain rate paths.



a) the tests were interrupted at the same strain



b) measured axial strain distributions

Fig.3 Influence of strain rate path on axial strain distributions.

## Deep Drawing

### Testing Mode

The apparatus shown in Fig.1 was improved so that controlling punch speed was made by using the extensometer ( $l=25\text{mm}$ ). The maximum punch stroke was 250mm. Chosen punch speeds and changes of punch speed are; Low speed, 2 mm/min; High speed, 200mm/min; Accelerated, 2-200mm/min,  $A=50\%$ ,  $t=50\text{sec}$ ; Decelerated, 200-2mm/min,  $A=40\%$ ,  $t=50\text{sec}$ .

### Materials

Materials are pure aluminum A1100-O ( $m=0.005$ ,  $n=0.236$ ,  $\bar{r}=0.95$ ), pure half hard aluminum A1100-H24 ( $m=-0.015$ ,  $n=0.076$ ,  $\bar{r}=1.07$ ) and superplastic alloy SPZ (Zn-22Al,  $m=0.113$ ,  $n=0.084$ ,  $\bar{r}=0.53$ ).

### LDR

Fig.4 shows the relationships between probability  $P_r$  and drawing ratio DR. Acceleration/deceleration of punch speed does not exhibit any increases of LDR. The transition range of  $P_r$  from 100 to 0% which means uncertainty in success of deep drawing, is broader in SPZ, especially for high speed. It can be deduced that one of features in deep drawing of rate dependent materials is broader transition range due to unstable strain rate field in the circular blank at each trial.

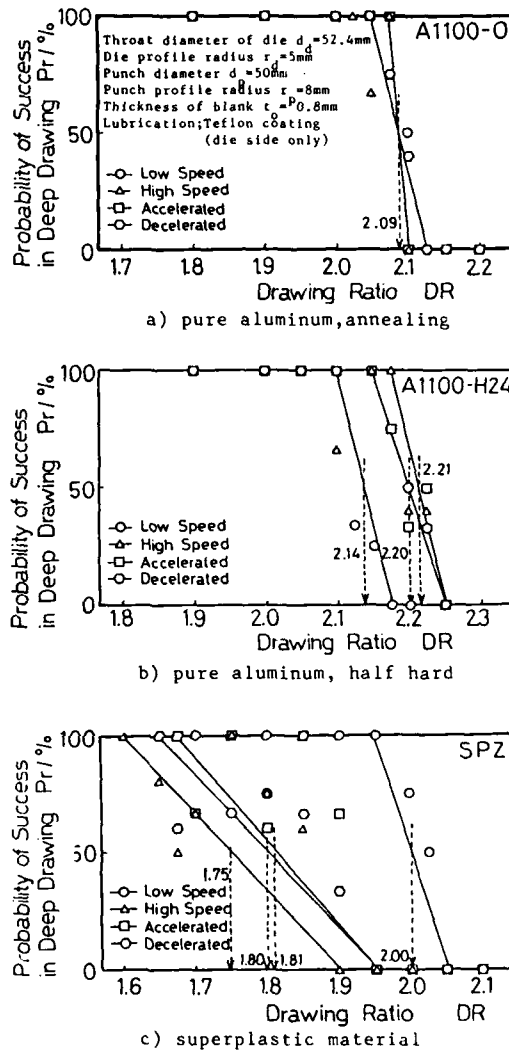


Fig.4 Probability  $P_r$  and drawing ratio DR.

### References

1. H. Ohsawa, S. Yamazaki and H. Nishinura, "The Role of Strain Hardening and Strain Rate Sensitivity in Uniaxial Tension and Hemispherical Punch Stretching", *Advanced Technology of Plasticity*, 1(1984)640-645.
2. R. Hill, "on Discontinuous Plastic States, with Special Reference to Localized Necking in Thin Sheets", *Journal of the Mechanics and Physics of Solids*, 1(1953)19-30.
3. S. Stören and J.R. Rice, "Localized Necking in Thin Sheets", *Journal of the Mechanics and Physics of Solids*, 23(1975)421-441.



AN INVESTIGATION OF THE CHARACTERISTICS OF CAVITATION  
IN SUPERPLASTIC MATERIALS

Yan Ma and Terence G. Langdon

Departments of Materials Science and Mechanical Engineering  
University of Southern California  
Los Angeles, CA 90089-1453, U.S.A.

Abstract

There are three standard growth processes for the growth of internal cavities in superplastic materials: diffusion growth, superplastic diffusion growth and plasticity controlled growth. Observations on several different superplastic materials show that there is also an additional cavity growth process in which the cavities grow in a crack-like manner along the grain boundaries. This process is illustrated with reference to a superplastic Al-Li alloy, and the crack-like growth mechanism is incorporated in a plot of cavity growth rate versus cavity radius for the two conditions of long cylindrical crack growth and axisymmetric crack growth, respectively.

Superplasticity and Superplastic Forming  
Edited by C.H. Hamilton and N.E. Paton  
The Minerals, Metals & Materials Society, 1988

## Introduction

Superplastic alloys exhibit very high elongations to failure under optimum conditions, and in early investigations it was generally considered that void formation was not prevalent in these materials [1]. More recently, it has been established that internal cavities are formed during the superplastic deformation of most materials, even including highly superplastic alloys such as the Zn-22% Al eutectoid [2] and the Al-33% Cu eutectic [3]. As a result of these observations, it is now considered that the requirement for optimum superplasticity is the suppression of significant cavity interlinkage rather than the suppression of cavity nucleation [4].

To date, the experimental observations of cavitation in superplastic materials have related almost exclusively to the nucleation and growth of isolated cavities [5]. Early experiments on a superplastic Cu alloy showed that the appearance of the cavities was markedly dependent upon strain rate, with many small cavities elongated along the tensile axis at high strain rates and a small number of large rounded cavities at low strain rates [6]. The change in cavity morphology with strain rate was interpreted in terms of a transition in the dominant cavity growth process from diffusion growth (DG) at low strain rates to plasticity controlled growth (PCG) at high strain rates [7]. This approach has been used in many subsequent analyses and, more recently, the model for diffusion growth was improved for superplastic materials by noting that the growth rate is enhanced when the cavity size exceeds the grain size. The latter process, termed superplastic diffusion growth (SPDG), leads to a growth rate which is independent of the instantaneous cavity radius and inversely proportional to the square of the grain size [8].

The present experiments were designed to investigate in more detail the occurrence of cavitation in four different superplastic materials: the two-phase Zn-22% Al eutectoid alloy, a Cu alloy containing a Co-rich phase, an Al-Li alloy containing  $\text{Al}_3\text{Li}$  precipitates and an Al-Cu-Zr alloy with a dispersion of  $\text{Al}_3\text{Zr}$ . The observations show that there is also an additional cavity growth process in superplastic materials, not previously recognized, whereby the cavities grow by the propagation of cracks along the grain boundaries to form reasonably stable crack networks. This process of growth was observed in each of the four experimental materials selected for this investigation but, due to space limitations, this paper will be restricted specifically to a description of some of the results obtained using the Al-Li alloy.

## Experimental Material and Procedures

The material used for this investigation was an Al-Li alloy containing, in wt %, 2.32% Li, 1.3% Cu, 0.8% Mg, 0.13% Zr, 0.056% Fe, 0.04% Si, 0.016% Ti and the balance Al. The alloy was received in the form of a sheet, 1.6 mm in thickness, and tensile specimens were machined parallel to the rolling direction with a gauge length of 6.4 mm and a gauge width of 5.1 mm.

Prior to testing, specimens were solution heated at 793 K for 45 minutes, quenched in cold water, and then annealed at a temperature of 463 K for 3 hours. This procedure produced a banded structure with grains which were essentially pancake-shaped: the linear intercept grain sizes were estimated as  $\sim 5\text{--}300\text{ }\mu\text{m}$  in the longitudinal direction along the tensile axis,  $\sim 5\text{--}300\text{ }\mu\text{m}$  in the long transverse direction, and  $6.3 \pm 0.5\text{ }\mu\text{m}$  along the short transverse direction through the thickness of 1.6 mm. The large range of sizes in the longitudinal and long transverse directions is due to the non-uniformity of the microstructure, and these measurements exclude the layer of exceptionally large grains at the upper and lower specimen surfaces

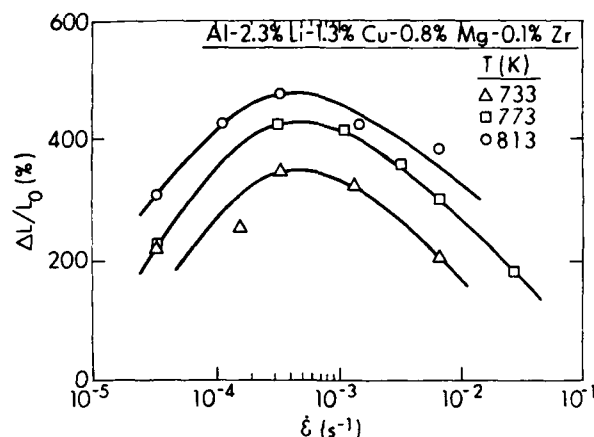


Figure 1 - Elongation to failure versus initial strain rate for three different testing temperatures.

due to the depletion of Li and, to a lesser extent, Mg.

All specimens were pulled to failure on an Instron testing machine operating at a constant rate of cross-head displacement. The tests were conducted at initial strain rates from  $3.33 \times 10^{-5}$  to  $2.67 \times 10^{-2} \text{ s}^{-1}$  and at temperatures in the range from 733 to 813 K. After failure, specimens were carefully examined using optical and scanning electron microscopy.

#### Experimental Results and Discussion

Figure 1 shows the variation in the elongation to failure,  $\Delta L/L_0$ , with the initial strain rate,  $\dot{\epsilon}$ , for the three absolute testing temperatures,  $T$ , of 733, 773 and 813 K, where  $\Delta L$  is the total change in the gauge length at fracture and  $L_0$  is the initial gauge length. Each point represents a different specimen, and the plot shows that (i) the maximum elongations occur at intermediate strain rates in the vicinity of  $\sim 3 \times 10^{-4} \text{ s}^{-1}$  and (ii) the elongations to failure increase with increasing temperature at any selected strain rate. The maximum elongation under the present experimental conditions was  $\sim 475\%$  at 813 K with  $\dot{\epsilon} = 3.33 \times 10^{-4} \text{ s}^{-1}$ .

An examination of specimens after testing revealed the occurrence of extensive dynamic recrystallization so that the banded structure was replaced by a reasonably equiaxed configuration of grains having a linear intercept size of  $\sim 10\text{--}60 \mu\text{m}$ . There was also evidence for extensive cavitation and, by lightly etching, it was established that cavities were nucleated at the grain boundaries and especially at triple points.

An example of cavitation is shown in the photo-montage in Fig. 2 for the specimen tested at  $\dot{\epsilon} = 6.67 \times 10^{-3} \text{ s}^{-1}$  at the highest testing temperature of 813 K. This specimen failed at  $\Delta L/L_0 = 382\%$  and Fig. 2 is a top view of the polished fracture tip with the tensile axis lying horizontal. This specimen shows many large cavities near the fracture tip but there is a decrease in the density of cavities with increasing distance from the tip. There is also evidence for cavity interlinkage in Fig. 2, with the interlinkage occurring both along the tensile axis and, in the vicinity of the fracture tip, in a direction perpendicular to the stress axis.

The cavities in Fig. 2 appear to be reasonably isolated from each other



Figure 2 - Cavitation in the specimen pulled to failure at  $\dot{\epsilon} = 6.67 \times 10^{-3} \text{ s}^{-1}$  at 813 K: the tensile axis is horizontal.

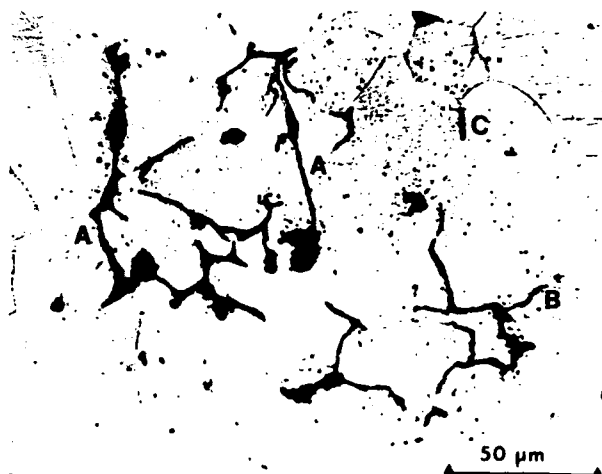


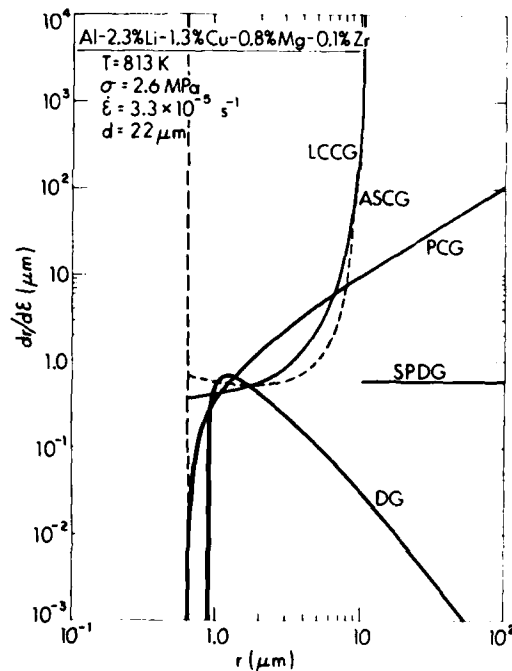
Figure 3 - Internal cavitation and grain boundary cracking in the specimen pulled to failure at  $\dot{\epsilon} = 3.33 \times 10^{-5} \text{ s}^{-1}$  at 813 K: the tensile axis is horizontal.

but inspection of several specimens at higher magnifications revealed also the development of cracking along some of the grain boundaries. An example of boundary cracking is shown in Fig. 3 for the specimen tested to failure at  $\dot{\epsilon} = 3.33 \times 10^{-5} \text{ s}^{-1}$  and 813 K with  $\Delta L/L_0 \approx 312\%$ : this photomicrograph was taken on the polished top surface of the specimen after lightly etching and again the tensile axis is horizontal. Figure 3 shows several examples of the development of cracks along the grain boundaries. By inspection of Fig. 3 and other similar photomicrographs, it was possible to identify three specific crack configurations: there are cracks which appear to propagate between adjacent cavities along grain boundaries lying approximately perpendicular to the tensile axis (as at points A in Fig. 3), there are cracks originating at cavities but apparently not influenced by adjacent

cavities (as at B), and there are grain boundary cracks which appear to exist in isolation and without association with any rounded cavities (as at C).

It is a standard procedure in investigations of cavitation in superplasticity to plot the rate of change of the cavity radius,  $r$ , with the total strain,  $\epsilon$ , as a function of the instantaneous cavity radius. As noted earlier, there are three basic mechanisms of cavity growth: diffusion growth (DG) where  $dr/d\epsilon$  is primarily proportional to  $1/r^2$  [9], superplastic diffusion growth (SPDG) where  $dr/d\epsilon$  is independent of  $r$  but proportional to  $1/d^2$  where  $d$  is the grain size [8], and plasticity controlled growth (PCG) where  $dr/d\epsilon$  is primarily proportional to  $r$  [10]. However, it is clear from the evidence in Fig. 3 that a plot of these three mechanisms is incomplete because it fails to include the possibility of grain boundary cracking. The latter mechanism may be incorporated into the plot by using the non-equilibrium model for the growth of a cavity in a narrow crack-like manner [11]. The result is shown in Fig. 4 for the Al-Li alloy tested at  $\dot{\epsilon} = 3.33 \times 10^{-5} \text{ s}^{-1}$  and at a temperature of 813 K: the corresponding value of the maximum stress,  $\sigma$ , under these conditions was 2.6 MPa, the grain size was taken as the average of the measured recrystallized grain size after 100% deformation ( $\sim 10.4 \mu\text{m}$ ) and the final grain size at failure ( $\sim 32.7 \mu\text{m}$ ), and the experimental conditions correspond to Fig. 3. The plot shows the curves for DG, SPDG and PCG, and, in addition, crack-like growth for the two conditions of long cylindrical crack growth (LCCG) and axisymmetric crack growth (ASCG), respectively [11]. In practice, the rates for LCCG and ASCG are similar, and they become infinite at  $r = d/2 \approx 11 \mu\text{m}$  because it is assumed that the cavities are located at adjacent triple points on a grain boundary lying perpendicular to the tensile axis and that they grow towards each other in a crack-like manner along the boundary. This type of growth appears reasonably consistent with the cracks labelled A in Fig. 3.

Figure 4 - Cavity growth rate versus cavity radius for the experimental conditions shown in Fig. 3: the growth processes are diffusion growth (DG), superplastic diffusion growth (SPDG), plasticity controlled growth (PCG), long cylindrical crack growth (LCCG) and axisymmetric crack growth (ASCG).



### Summary and Conclusions

1. Experiments on several superplastic alloys show the possibility of cavities growing in a crack-like manner along the grain boundaries. This process is illustrated for an Al-Li alloy.

2. The standard plot of  $dr/de$  versus  $r$  incorporates diffusion growth (DG), superplastic diffusion growth (SPDG) and plasticity controlled growth (PCG), where  $r$  is the cavity radius and  $\epsilon$  is the total strain. This plot is extended to include crack-like growth under the two conditions of long cylindrical crack growth (LCCG) and axisymmetric crack growth (ASCG), respectively.

### Acknowledgement

This work was supported by the National Science Foundation under Grant No. DMR-8503224.

### References

1. R.H. Johnson, "Superplasticity", Metall. Rev., **15** (1970) 115-134.
2. H. Ishikawa, D.G. Bhat, F.A. Mohamed and T.G. Langdon, "Evidence for Cavitation in the Superplastic Zn-22 Pct Al Eutectoid", Metall. Trans., **8A** (1977) 523-525.
3. A.H. Chokshi and T.G. Langdon, "Cavitation and Fracture in the Superplastic Al-33% Cu Eutectic Alloy", J. Mater. Sci. (in press).
4. T.G. Langdon, "Fracture Processes in Superplastic Flow", Metal. Sci., **16** (1982) 175-183.
5. B.P. Kashyap and A.K. Mukherjee, "Cavitation Behavior During High Temperature Deformation of Micrograined Superplastic Materials - A Review", Res Mechanica, **17** (1986) 293-355.
6. S.-A. Shei and T.G. Langdon, "The Fracture Characteristics of a Superplastic Single Phase Copper Alloy", J. Mater. Sci., **13** (1978) 1084-1092.
7. D.A. Miller and T.G. Langdon, "An Analysis of Cavity Growth During Superplasticity", Metall. Trans., **10A** (1979) 1869-1874.
8. A.H. Chokshi and T.G. Langdon, "A Model for Diffusional Cavity Growth in Superplasticity", Acta Met., **35** (1987) 1089-1101.
9. W. Beeré and M.V. Speight, "Creep Cavitation by Vacancy Diffusion in Plastically Deforming Solid", Metal Sci., **12** (1978) 172-176.
10. J.W. Hancock, "Creep Cavitation Without a Vacancy Flux", Metal Sci., **10** (1976) 319-325.
11. T.-J. Chuang, K.I. Kagawa, J.R. Rice and L.B. Sills, "Non-equilibrium Models for Diffusive Cavitation of Grain Interfaces", Acta Met., **27** (1979) 265-284.

# RHEOLOGICAL CRITERIA FOR RATIONAL USE OF SUPERPLASTICITY

## IN METAL WORKING BY PRESSURE

O. M. Smirnov

Superplastic Materials Deformation Laboratory  
Moscow Steel and Alloys Institute  
Moscow, 117936, U.S.S.R.

### Abstract

A theory of superplastic deformation (SPD) processes based on the suggested rheological model of elastoviscoplastic (EVP) medium allows to estimate an expedience of SPD advantages use in metal working by means of rheological parameters from the corresponding constitutive equation. These advantages as simple analysis shows are rather the consequences of viscous behaviour of superplastic (SP) materials. This paper reports general results of analysis of some SPD processes obtained with the application of mathematical and physical simulation methods and use of various modeling materials including special polymers. Possibility of proportioned application of superplasticity based on estimation of expedience of structure refining and control of temperature / strain rate regimes of SPD is discussed.

Superplasticity and Superplastic Forming  
Edited by C.H. Hamilton and N.E. Paton  
The Minerals, Metals & Materials Society, 1988

### Introduction

The use of SP regimes in drop forging, sheet forming as well as in specialized metal forming processes is known to provide essential metal saving, reduction of necessary pressure and energy consumption, better quality of produced parts (1,2). At the same time realization of SP state in metal forming makes working techniques more complicated and expensive because of necessity to provide ultrafine grain structure of preforms (3) and to control temperature and strain rate regimes of SPD. The latter problem deals with creation of expensive equipment and instruments (4).

Therefore in order to use superplasticity in metal working more efficiently it is important to discuss principles which should be taken into consideration when making decision concerning an expedience to realize technology based on use of SPD advantages in proportioned manner. These advantages as analysis shows (1,4) are rather the consequences of SP materials viscous behaviour.

### Rheological Criteria of SPD

Rheological model of EVP medium suggested to describe SPD (1,5) allows to formulate the relation between effective stress  $\sigma_e$  and effective strain rate  $\dot{\epsilon}_e$  by SPD of a material with stable structure and constant temperature for any complex deformation scheme as follows:

$$\sigma_e = \sigma_s (\sigma_0 + K_v \dot{\epsilon}_e^{m_v}) / (\sigma_s + K_v \dot{\epsilon}_e^{m_v}) \quad (1)$$

where  $\sigma_s$ ,  $\sigma_0$ ,  $K_v$ ,  $m_v$  are invariant to strain rate rheological parameters of the material deformed.

The capability of a material for viscous flow can be estimated with the value of strain rate hardening coefficient  $m_v$  which for SP materials exceeds .3 and in some cases approaches the unity.

The influence of SP material structure state on the relationship between  $\sigma_e$  and  $\dot{\epsilon}_e$  can be described in the first approach (5) by the parameter  $K_v$  if it would be introduced as a function of the mean grain size  $L$  by:

$$K_v = \{ \dot{\epsilon}_{eq} \exp[\alpha L (\sigma_{eq} - \sigma_e)] \}^{-1/m_v} \quad (2)$$

where  $\dot{\epsilon}_{eq}$ ,  $\sigma_{eq}$  are parametric values of strain rate and stress which correspond to the equicohesive state of SP material.

At least three consequences of SP materials viscous flow can be considered as advantages of SPD used for metal working: 1) The greater the  $m_v$  value the greater is the ability to reduce deformation force and consequently energy consumption by reducing strain rate. 2) Deformation stability in form of localization resistance during linear and plane tension also increases with  $m_v$ . 3) Equation (1) shows that SP material flow begins when  $\sigma_e \geq \sigma_0$ . The threshold stress  $\sigma_0$  of SP material seems to be at least 100...1000 times less than its standard yield stress  $\sigma_s$ . Therefore yield criterion should be modified for SP material as follows:

$$\sigma_e = (1/\sqrt{2}) \sqrt{(\sigma_1 - \sigma_2)^2 + (\sigma_2 - \sigma_3)^2 + (\sigma_3 - \sigma_1)^2} = \sigma_0 \quad (3)$$

It results in significant reduction of "dead" zones area in vicinity of contact surfaces between SP workpiece deformed and the instrument compared with deformation field of plastic material workpiece which begins to flow when  $\sigma_e \geq \sigma_s$ . It makes deformation more homogeneous and facilitates filling deep die cavities e.g. sharp corners by metal deformed, see Fig. 1.



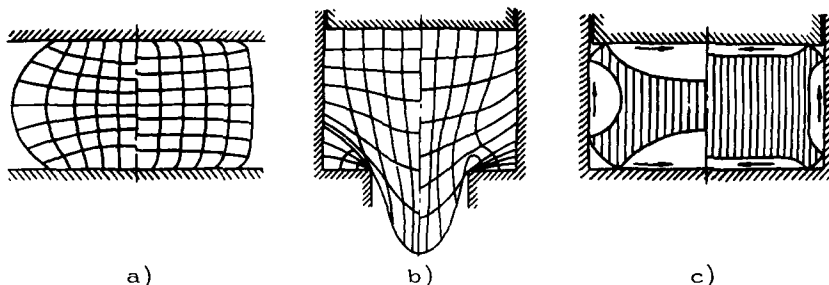


Figure 1 - Schematic illustration of the deformation inhomogeneity in different processes of drop forging of plastic (left) and SP (right) materials: a) upsetting (grid distortion), b) extrusion (grid distortion), c) filling of closed die corners ("dead" zones are white).

These regularities have been confirmed by the results of mathematical and physical simulations of SPD processes. Polymers such as monodisperse polyisoprene, monodisperse polybutadiene and its modifications are proved to be promising modelling materials for such cases.

#### Types of SPD Processes

All metal working processes using SPD can be divided into two groups: non-traditional processes of metal working by pressure which can be realized exclusively on the basis of SPD and traditional processes such as isothermal drop forging using SPD regimes to increase their efficiency. There are also processes based on combinations of different deformation schemes both traditional and non-traditional.

There is a certain tendency to use working schemes of nonmetallic viscous materials (hot glass, thermoplastics) in development of non-traditional SPD processes. Thus one of the early SPD processes of dieless drawing (1,6) is similar to production of optical fibres. Some of non-traditional processes such as SP forming of sheets (2), thermoelastic stamping of thin ribbed shells (1,4), multichannel extrusion into closed cavities (4,6) seem to have good prospects for a wide application in metal working industry.

SP Forming of Hollow Parts has been performed by bulding of sheets and tubes with compressed gas using negative and positive schemes of thermoplastics working processes as prototypes. A relatively small gas pressure (usually less than .1 MPa) as well as extremely high localization resistance of SPD at plane tension resulting in high local elongations is required to form SP sheets into complicated parts. These processes have been widely used for production of complex components in machinery and construction industry, tricky wares of applied art (see Fig. 2) etc. The combination of SP forming and diffusion bonding seems to be especially promising for fabrication of big advanced complex parts and structures (2).

Thermoelastic Stamping of Ribbed Shells is based on the high fluidity of SP materials resulting in their ability to fill in deep die cavities (4). Thermoelastic press, see Fig. 3, right, is a special stamping device where thermal energy transforms directly into mechanical deformation energy. The working stroke comes as a result of thermal expansion of mandrel inside the heated container. SPD regime in this case makes forming of ribs perfect without defects, see Fig. 3, left. Traditional fabrication of such parts by machining leads to material waste of 80 to 95%.



Figure 2 - Decorative ash-tray-formed from Zn-22%Al alloy.

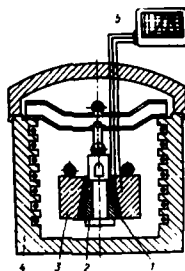


Figure 3 - Thermo-elastic stamping of a ribbed shell from aluminium alloy (left); scheme of thermo-elastic press (right): 1) stamped part, 2) mandrel, 3) container, 4) furnace, 5) thermocontroller.

Multichannel Extrusion Processes appear to be rational for fabrication of extremely complex parts such as turbine disk with blades as a unit (7) by filling in deep die cavities through radial channels. Obvious similarity of such processes to foundry schemes allows to call them "solid state foundry".

Isothermal Drop Forging in Hydraulic Presses can also be made more efficient by utilization of SPD rheological advantages such as decreasing deformation force, more precise forming of parts and lower material waste. The best result can be achieved thus by drop forging of big thin-wall parts from less ductile materials such as the panel shown in Fig. 4.

#### SPD Rational Use Principles

The expedience of SPD use in metal working can be estimated by the comparison of expenses and profits related to realization of certain SPD processes. The following ideas could be taken into consideration in this case.

The expenses for preparation of ultrafine-grain structure is known to be proportional to the refining grade. Thus it would be rational in some cases to avoid structure preparation and to arrange SPD regime for the material as supplied, i.e. the temperature/strain rate regimes related to maximum  $M_V$  for this structure state. In other cases such as SP forming there is essentially necessary ultrafine-grain structure which allows to reach absolute maximum of  $M_V$  value and maximum efficiency of SPD for a given material.

The control of temperature regime is carried out by means of isothermal set (8) which is very expensive equipment. But the drop forging of big parts from light alloys can be arranged isothermally without such sets utilizing accumulated heat in massive changeable die blocks.

Low strain rate of SPD is considered as a disadvantage telling on productivity of SPD processes. But it has been already experienced that SPD strain rate is necessary only during the final stage of working process when an ordinary regime results in excessive deformation pressure or lack of the material plasticity. Thus the rational strain rate regime seems to be of two stages, as shown in Fig. 5: the first stage is carried out with standard cross-head speed and the second relatively short one should be accomplished with SPD strain rate by

means of programmed cross-head speed controller.

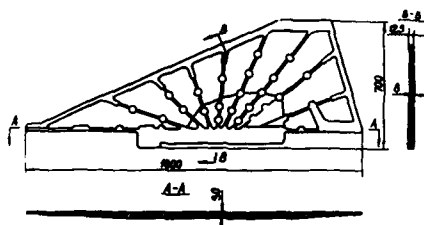
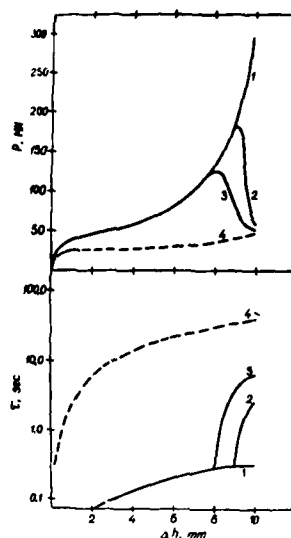


Figure 4 - Thin-wall panel stamped from magnesium alloy MA 2-1 in SPD regime.

Figure 5 - Variation of stamping force  $P$  and stamping time  $\tau$  of the panel, see Fig. 4, with press stroke  $\Delta h$  (computed curves): 1) ordinary deformation rate, 2) and 3) two stages regimes with different durations of stages, 4) full scale SPD regime



#### References

1. Oleg M. Smirnov, Metal Working by Pressure in Superplastic State (Moscow: Mashinostroyenie, 1979), 44-160.
2. "Superplastic Forming Processes and Applications", Superplastic Forming of Structural Alloys, ed. N. E. Paton and C. H. Hamilton (Warrendale, PA: The Metallurgical Society, 1982), 257-317.
3. Ilya I. Novikov and Vladimir K. Portnoy, Superplasticity of Ultrafine Grain Alloys (Moscow: Metallurgia, 1981), 128-158.
4. O. M. Smirnov, "Problems of Rational Use of Superplasticity in Metal Forming Processes", Kuznechno-Shtampovochnoye Proizvodstvo, 1987, No. 9: 3-6.
5. A. N. Yershov, M. A. Tsepin, A. M. Afrikantov, "Structure Factor Account in Constitutive Equation of Superplastic State", (Paper presented at the 2nd All-Union Conference "Superplasticity of Metals", Moscow, 1981), 134-135.
6. "The Current Status of Applied Superplasticity", Ultrafine-Grain-Metals, ed. J. J. Burke and V. Weiss (Syracuse, NY: Syracuse University Press, 1970), 325-343.
7. O. A. Kaibyshev and Yu. K. Kolehkin, "Complex Profile Parts Fabrication in Superplastic State", Kuznechno-Shtampovochnoye Proizvodstvo, 1981, No. 3: 2-4.
8. S. Z. Figlin et al., Isothermal Deformation of Metals (Moscow: Mashinostroyenie, 1978), 29-62.

# EFFECT OF STRAIN RATE DEPENDENCE OF $m$ ON DUCTILITY

## IN SUPERPLASTIC MATERIALS

Takuji Okabe\*, Tomei Hatayama\*\* and Hideo Takei\*\*\*

\* Kure National College of Technology, Kure 737, Japan

\*\* Faculty of Engineering, Hiroshima University,  
Higashi-Hiroshima 724, Japan

\*\*\* Hiroshima Institute of Technology, Itsukaichi,  
Hiroshima 731-51, Japan

### Abstract

Superplastic materials show very high fracture elongations when pulled in tension under optimum conditions. It has been widely observed that the fracture elongations are closely related with the strain rate sensitivity  $m$  and increase with increasing  $m$ . It has been observed that the  $m$ -value depends not only on a given strain rate but on the width ( $\sqrt{(\Delta \log \dot{\epsilon})^2}$ ) and the sign of the change in strain rate ( $\pm \sqrt{(\Delta \log \dot{\epsilon})^2}$ ) from the given strain rate when the  $m$ -value is measured by the strain rate change method. The strain rate in a necking portion of a specimen increases one after another from start of deformation to fracture, and it has been proposed that fracture occurs when the necking portion gets the strain rate where the  $m$  is equal to zero on the higher strain rate side. So, the  $m$ -value ( $m^+$ ) for the positive change in strain rate ( $+\sqrt{(\Delta \log \dot{\epsilon})^2}$ ) should be taken into consideration when the fracture elongation is analyzed. It has been observed in several superplastic alloys that the greater part of the fracture elongation is produced in the strain rate region where the  $m$  is not so much different from that for the given strain rate. Based upon the result the fracture elongation ( $\epsilon_f$ ) is analyzed by using the  $m^+$ -value. Then the following expression is obtained:

$$\epsilon_f = A m [\exp(m^+/(1 - m^+)) - 1],$$

where  $m^+$  is the  $m$ -value for the maximum strain rate deviation within the limits of the possibility (i.e.  $\log 2/m$ ),  $m$  is that for the strain rate change ratio ( $N=1.5-2$ ), and  $A$  is a constant which depends on the strain rate dependence of  $m$ . The calculated results are compared with experimental ones for Zn-22%Al eutectoid and Al-33%Cu eutectic (mass%) alloys.

Superplasticity and Superplastic Forming  
Edited by C.H. Hamilton and N.E. Paton  
The Minerals, Metals & Materials Society, 1988

## INTRODUCTION

The fracture elongations in superplastic materials are closely related with the strain rate sensitivity,  $m$ , and it is well known that they increase with increasing  $m$  (1)-(3). The strain rate change method is one of the methods of  $m$ -measurement, and it has been proposed that this method is the favorable one in accordance with the definition of  $m$  (4). The  $m$ -values measured by this method, however, depend not only on the given strain rate but on the width and the sense of the change in strain rate (4). Therefore, we cannot judge which  $m$ -value should be used, for example, when the fracture elongation is calculated as a function of  $m$ . In this study, the fracture elongation is calculated in consideration of the characteristic of  $m$  and the calculated results obtained are compared with the experimental results and discussed.

## FRACTURE ELONGATION AND $m$ -VALUE

There are many deriving methods for the  $m$ -value in superplastic materials. In this study, the  $m$ -value means the one for the strain rate change method. The strain rate in the local portion (i.e. necking portion) of a specimen increases one after another from start of deformation to fracture, and it has been proposed that fracture occurs when the necking portion gets the strain rate,  $\dot{\epsilon}_\infty$ , where the  $m$  is equal to zero on the higher strain rate side (5). Therefore, it is considered that the  $m$ -value ( $m^+$ ) for the positive strain rate change ( $\Delta \log \dot{\epsilon}^+ = +\sqrt{(\Delta \log \dot{\epsilon})^2}$ ) takes an important role in the deformation process. From this, it is necessary to obtain the width of the change in strain rate in the local portion of a specimen.

Now consider the case where the strain rate in the local portion of a specimen changes macroscopically. Figure 1 shows the schematic stress-strain curve in the local portion. If the barrier energy ( $\Delta F$ ) for the change is larger than the driving energy ( $F$ ) for the change, no macroscopic strain rate change takes place. The generating condition of macroscopic strain rate change can be expressed as:

$$\Delta F / F < 1 \quad (1)$$

Using the stress-strain rate equation  $\sigma = K \dot{\epsilon}^m$  and the elastic energy-stress relation  $F = (1/(2E)) \sigma^2$  ( $E$ : Young's modulus), Eq.(1) is rewritten as follows:

$$\sigma_2 / \sigma_1 = (\dot{\epsilon}_2 / \dot{\epsilon}_1)^m < 2 \quad (2)$$

From this, the strain rate change  $\Delta \log \dot{\epsilon}^+$  is written in the form:

$$\Delta \log \dot{\epsilon}^+ = \log(\dot{\epsilon}_2 / \dot{\epsilon}_1) < \log 2 / m, \quad (3)$$

where the  $\log$  means not common logarithms but a logarithm.

As mentioned before, it is considered that fracture occurs at the strain rate where  $m$  is equal to zero on the higher strain rate side. If the strain rate change in the local portion is the utmost limit of deviation ( $\log 2 / m$ ), the local portion can reach the point of fracture

most quickly, but the energy density in the local portion increases most quickly, so that the force which prevents the change is the largest of all the strain rate change processes. The actual change is considered to be smaller than the utmost limit of deviation ( $\log 2/m$ ). However, it is expected that the change which is about to occur is the utmost limit of deviation ( $\log 2/m$ ). Therefore, the value of  $m$  ( $m^+$ ) for the utmost limit of deviation ( $\log 2/m$ ) is considered an important parameter which controls the deformation process.

In this study, for simplicity, the  $m^+$ -value is measured using the normal  $m$ - $\log \dot{\epsilon}$  curve with the strain rate ratio  $N$  of 1.5-2 (we call it the reference curve of  $m$ ) as shown in Fig.2 since the strain rate dependence of  $m$  ( $J = \partial m / \partial \log \dot{\epsilon}$ ) and the dependence of  $m$  on the width of the change in strain rate ( $J^* = \partial m / \partial \sqrt{(\Delta \log \dot{\epsilon})^2}$ ) show a similar tendency (6). In this figure, for example, the  $m$ -value for the strain rate change ( $\log 2/m$ ) from  $\dot{\epsilon}_1$  is indicated with  $m^+(\dot{\epsilon}_1)$  and it is plotted for the  $\dot{\epsilon}_1$ .

The fracture life time can be obtained if we can calculate the residence time for each state of strain rate. The residence time  $t_i$  in a strain rate state is given by the following form using the expression,  $m^+/(1-m^+)$ , instead of the expression,  $m/(1-m)$ , as the energy barrier for the state change (5):

$$t_i = CoGT_i^* [\exp\{m_i^+/(1-m_i^+)\} - 1], \quad (4)$$

where  $Co$  is a proportional constant,  $G$  the reciprocal of the element number of a specimen ( $= 1/(n+1)$ ),  $T_i^*$  the period of deformation (i.e. the period of the fluctuation in strain rate). The fracture lifetime  $t_f$  is the sum total of the residence time  $t_i$  in each strain rate state up to fracture. Using eq.(4), the fracture lifetime  $t_f$  can be expressed as the following equation:

$$t_f = \sum t_i = \sum CoGT_i^* [\exp\{m_i^+/(1-m_i^+)\} - 1]. \quad (5)$$

Therefore, the fracture elongation can be expressed as:

$$\epsilon_f = Vt_f/L_0 = (V/L_0) \sum CoGT_i^* [\exp\{m_i^+/(1-m_i^+)\} - 1], \quad (6)$$

where  $L_0$  is the initial length of a specimen,  $V$  the tensile speed. The values of  $T_i^*$  and  $m_i^+$  change one after another up to fracture because of their dependence on the strain rate. Therefore, the estimation of  $\epsilon_f$  cannot readily be carried out.

Since the greater part of the fracture elongation is produced in the strain rate region where the  $m$  is not so much different from that for the given strain rate, the fracture elongation  $\epsilon_f$  can be estimated by the elongation which is produced in the strain rate region. Then, the  $\epsilon_f$  can be expressed as (5):

$$\epsilon_f = A m [\exp\{m^+/(1-m^+)\} - 1], \quad (7)$$

where  $A$  is a constant which depends on the strain rate dependence of  $m$ ,

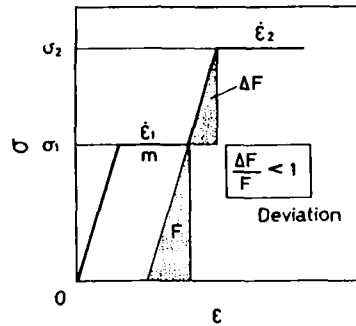


Figure 1 - Schematic stress-strain curve in local portion of specimen when the strain rate changes macroscopically.

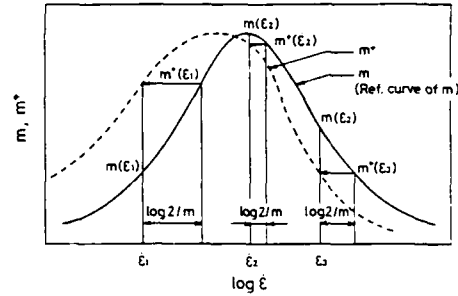


Figure 2 - Method of measurement of  $m^+$ , where  $m^+(\dot{\epsilon}_1)$  is the  $m$ -value for the strain rate change ( $\log 2/m$ ) from  $\dot{\epsilon}_1$ .

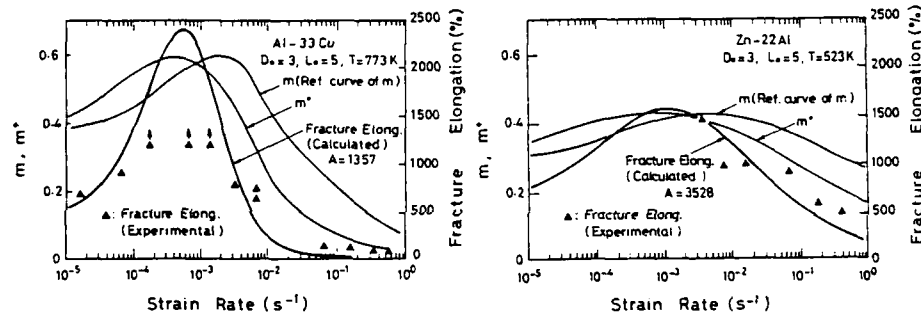


Figure 3 - Dependence of  $m$ ,  $m^+$  and fracture elongation on strain rate for (a) Al-33%Cu eutectic and (b) Zn-22%Al eutectoid alloys.

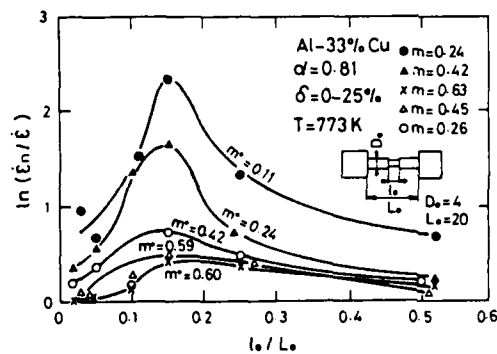


Figure 4 - Dependence of the ratio of strain rate,  $\ln(\dot{\epsilon}_n/\dot{\epsilon})$ , on the length of non-uniform region,  $l_0/L_0$ , for various  $m$ -values.

and it becomes larger, the lower the strain rate dependence of  $m$ .

#### RESULTS AND DISCUSSION

The calculated results of eq.(7) is shown in Fig.3(a) and (b) for Al-Cu eutectic and Zn-Al eutectic alloys, respectively. From this, it can be seen that the  $m^+ - \log \dot{\epsilon}$  curve shifts to the lower strain rate side compared with the  $m - \log \dot{\epsilon}$  curve (the reference curve of  $m$ ), and the strain rate at the maximum point of fracture elongation is lower than that of  $m$ -value. The calculated values agree quite well with the experimental results. The constant  $A$  for the Zn-Al eutectoid alloys which have a smaller strain rate dependence of  $m$  is higher than that for Al-Cu eutectic alloys. This also agrees quite well with the theoretical prediction.

Figure 4 shows the relationship between the strain rate ratio  $\ln(\dot{\epsilon}_n/\dot{\epsilon})$  and the length of non-uniform region  $l_0/L_0$  in non-uniform specimens (4), where  $\alpha (=0.81)$  is the initial ratio of the cross-sectional area of non-uniform region to that of uniform region,  $\dot{\epsilon}_n$  is the average value of strain rate over the elongation interval  $0 \leq \delta \leq 25\%$ , the solid and open symbols represent the results obtained under the condition of the higher and the lower strain rate side than the strain rate at the maximum  $m$ -value, respectively, and the  $m^+$ -value for each  $m$ -value is added in this figure. Compared with the same  $m$ -value, the strain rate deviation in the non-uniform region from a given strain rate,  $\Delta \ln \dot{\epsilon} (= \ln(\dot{\epsilon}_n/\dot{\epsilon}))$ , is smaller in the lower strain rate side (open symbol), but compared with the  $m^+$ -value, there is a good correlation between the  $\Delta \ln \dot{\epsilon} (= \ln(\dot{\epsilon}_n/\dot{\epsilon}))$  and the  $m^+$ -value. It is suggested from these results that the  $m^+$ -value is the important parameter which controls the fracture elongation and the uniformity of deformation.

#### REFERENCES

1. W. B. Morrison, "The Elongation of Superplastic Alloys," Trans. Met. Soc. AIME, 242(1968), 2221-2227.
2. D. A. Woodford, "Strain-Rate Sensitivity as a Measure of Ductility," Trans. ASM, 62(1969), 291-293.
3. G. L. Dunlop, and D. M. R. Taplin, "The Tensile Properties of a Superplastic Aluminum Bronze," J. Mat. Sci., 7(1972), 84-92.
4. T. Hatayama, T. Okabe, and H. Takei, "Dependence of the  $m$ -value on Strain Rate in Superplastic Al-Cu Alloys," Trans. Japan Inst. Metals, 27(1986), 576-583.
5. T. Okabe, T. Hatayama, H. Takei, and M. Ikeda, "The Fracture Processes in Superplastic Materials," Proc. 2nd Int. Conf. on Creep and Fracture of Engineering Materials and Structures, University College, Swansea, U.K., (1984), 211-222.
6. T. Hatayama, T. Okabe, and H. Takei, "A Kinematical Approach to Deformation Behaviour in Superplastic Materials," Proc. 2nd Int. Conf. on Creep and fracture of Engineering Materials and Structures, University College, Swansea, U. K., (1984), 211-222.



## EVOLUTION OF CAVITATION DURING SUPERPLASTIC DEFORMATION

J.J. Blandin and M. Suéry

Institut National Polytechnique de Grenoble  
E.N.S. de Physique de Grenoble  
Génie Physique et Mécanique des Matériaux  
Unité Associée au C.N.R.S. n° 793  
BP 46 - 38402 Saint Martin d'Hères Cedex (FRANCE)

### Abstract

The nucleation of cavities during superplastic deformation is difficult to point out since it is necessary to distinguish between truly nucleated cavities and preexisting cavities formed during prior processing treatments. In order to quantify the impact of strain-induced nucleation on cavitation, the evolution with strain of an initial distribution of cavities is calculated. From the discrepancy between predicted change of the shape of the distribution and the experimental results obtained with aluminum alloys, the importance of the nucleation process during straining can be concluded. However most models of plasticity controlled cavity growth were developed for creeping materials and did not include grain boundary sliding which can modify cavity growth rate. This process must therefore be taken into account in the modelling of damage development during superplastic deformation. Such an approach leads then to emphasize on the average number of moving grains during straining, the viscosity of the grain boundaries and the ability of cracks to nucleate and grow by diffusion.

Superplasticity and Superplastic Forming  
Edited by C.H. Hamilton and N.E. Paton  
The Minerals, Metals & Materials Society, 1988

### Introduction

Cavitation during superplastic straining can cause the premature failure of many commercial alloys when forming is performed under atmospheric pressure. From the numerous studies dealing with this topic the following points were concluded:

- 1) There are three stages in cavity development: nucleation, growth and coalescence.
- 2) The nucleation process remains quite unknown owing to the difficulty of obtaining experimental data. Laws for nucleation rate have been proposed, dealing with thermodynamical probability of vacancy condensation (1,2).
- 3) There are two main controlling processes in cavity growth. When the cavity radius is small, the diffusion controlled growth is predominant. When the cavity radius reaches a critical value, the cavity growth is then controlled by plasticity of the matrix.
- 4) Several criteria for coalescence have been proposed (3), based on interspacing distances between cavities, but none of them are fully satisfactory.

However, cavities may preexist in the material as a consequence of the thermomechanical treatment applied to develop a fine grain structure. Such cavities are present in aluminum alloys (4). Another problem is concerned with strain-induced nucleation. This phenomenon occurs concurrently with cavity growth so that measurements of the change in cavity volume fraction with strain can not easily be compared with theoretical prediction of cavity growth rate which usually assumes that cavities are all the same size. Moreover modelling of cavity growth in superplastic alloys does not generally take into account the effect of grain boundary sliding which can be another source of disagreement between experimental data and theoretical prediction.

The aim of this paper is the two-fold - first to theoretically quantify the influence of continuous nucleation on the variation of the cavitation level with strain by considering the evolution of an initial distribution of cavities; second to propose an approach of the cavitation problem in superplastic alloys which takes into account grain boundary sliding. Results of cavitation obtained with Al-alloys will be considered for comparison with theoretical prediction.

### Evolution of an initial damage

Cavities are assumed to preexist in the material with an initial distribution given by a gaussian law:

$$dN/dr = \phi \exp[-A(r-r_{mean})] \quad (1)$$

However the cavities whose radius is smaller than the critical one defined as  $r_c = 2\tau/\sigma$ , are not taken into account. The cavity growth is supposed to be controlled by lattice diffusion (1) and plasticity of the matrix (5), according to the relations:

$$dr/dt = [2\Omega\beta D_v / \pi k T r^2] \{ (\sigma - 2\tau/r) / (4Ln(\beta/2r) - [1 - (2r/\beta)^2][3 - (2r/\beta)^2]) \} \quad (2)$$

$$dr/d\epsilon = [m+1/2m] \sinh[(2-m/2+m)(1/3 - P/\sigma_0)] r \quad (3)$$

In these relations,  $\tau$  is the surface tension,  $\beta$  is the cavity spacing, and all the other parameters have their usual meaning. Grain boundary diffusion is assumed to be negligible compared to lattice diffusion, as shown for a 7475-Al alloy superplastically deformed at optimum temperature (6).

Figure 1 shows the evolution with strain of the shape of an initial distribution of cavities if nucleation does not occur. This initial distribution was chosen according to experimental observations assuming a mean radius equal to  $0.75\mu m$  and a maximum radius of  $1.5\mu m$ . It can be seen that the variance of the distribution decreases with strain. Such a result is obtained because the initial distribution deals with cavities whose radius is smaller than the transition radius  $r_t$  between diffusion controlled and plasticity controlled growth.  $r_t$  is defined as:

$$(dr/dt)_{diff} = (dr/dt)_{plast} \text{ for } r=r_t \quad (4)$$

and is equal to about  $3 \mu\text{m}$  for Al-alloys. This narrowing of the distribution is not observed experimentally and this can be explained by strain-induced nucleation. A confirmation of the importance of nucleation can be obtained by image analysis of superplastically deformed samples. Figure 2-a-b-c shows experimental results of the variation with strain of cavity area fraction  $C_a$ , equivalent radius  $R_{eq}$  and number of cavities per unit area  $n_a$  for 7475 Al-alloy deformed under optimum conditions.  $R_{eq}$  is defined here as the radius of the spherical cavities which would have the same volume as that determined experimentally from the measure of the area and the perimeter of the cavity (7). The main result shown in the figure is the constancy of  $R_{eq}$  with increasing strain whereas  $C_a$  and  $n_a$  continuously increase, which can be explained by continuous nucleation during deformation. This constancy of  $R_{eq}$  with increasing strain is also observed from the results of Cho and al. (8).

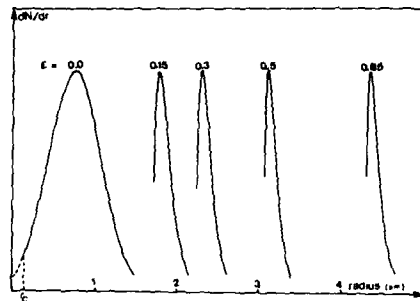


Figure 1 - Change in the shape of cavity size distribution with deformation.

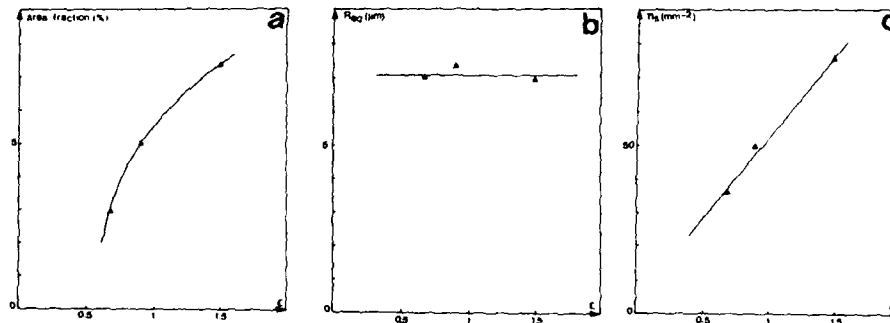


Figure 2 - Variation with strain of experimental parameters concerning cavitation: a) area fraction of cavities; b) equivalent radius; c) number of cavities per unit area.

Another experimental confirmation of the importance of cavity nucleation can be given by considering the calculated cavity volume fraction and its variation with strain. Figure 3 shows the result of such a calculation for an Al-Cu-Li-Mg alloy together with the experimental results. For the calculation, the previous distribution was considered and the parameter  $\Phi$  in relation (1) was determined according to the initial level of cavitation. Moreover, the effect of the heating time of the sample before deformation on possible cavity sintering was taken into account (7). An important gap is observed between the calculated and the experimental curves beyond a strain  $\approx 0.5$ . Figure 3 shows also the variation with strain of  $C_a$  including continuous nucleation. For this curve, the following law of nucleation rate (1,2) was used:

$$dN/dt = C(N_{max} - N) \quad (5)$$

where  $N_{max}$  is the total number of possible nucleation sites (taken as the number of grains) and  $C$  is a parameter. Good agreement with experimental results is obtained with a value of  $C \approx 10^{-3}$ . This parameter in fact depends on the flow stress and several expressions have been proposed for this dependence (1,2). They show that stress concentrations are needed to reach non-zero  $C$ -values, even if cavities are assumed to nucleate with non-spherical shape. However, no stress evaluation is possible from the knowledge of the value of the nucleation-rate coefficient  $C$  owing to the steplike dependence of  $C$  on stress.

The previous results demonstrate that continuous nucleation of cavities is very important in superplastically deformed Al-alloys, in opposition for example to  $\alpha/\beta$  brasses for which growth only occurs during deformation as soon as cavities have been nucleated in the first stage of straining (9). This continuous nucleation allows an interpretation of the discrepancy observed between the experimentally determined cavity growth rate and that expected through theoretical models. However, it has to be noted that these theoretical models used for superplastic materials, were initially developed for creeping materials. One main deformation process is thus completely ignored, i.e. grain boundary sliding which can reach 70% of the total strain. This process can influence cavity growth.

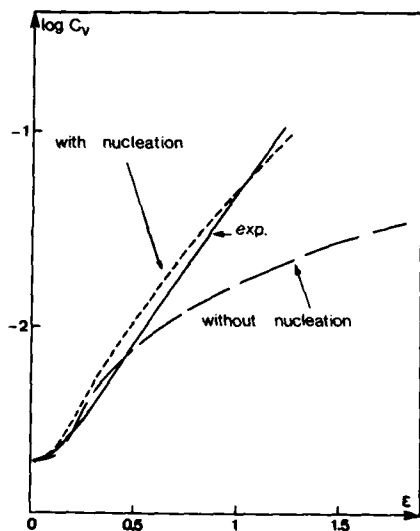


Figure 3 - Comparison between predicted and experimental results of damage evolution.

Figure 4 shows a cavity in an Al-Cu-Li-Mg alloy and it is clear that the growth of this cavity is correlated with the motion of the grains in its neighbourhood and sliding along grain boundaries. A damage process dealing with grain movement has thus to be considered. Figure 5 depicts schematically this process with a group of five grains. Sliding at [1-2] interface generates normal tractions on [1-3] grain boundary. This stress profile generates an elastic crack at the triple junction (fig. 5-a). Because of stress concentration on [1-3] grain boundary, growth of the crack occurs. The evolution of the shape of the crack depends on respective values of surfacic and grain boundary diffusivities. Moreover the presence of precipitates in grain boundary can affect the development of the void. Whatever the conditions, the kinetics of growth is controlled either by vacancy emission and annihilation or by vacancy diffusion if the grain boundary is assumed to operate as perfect source and sink of vacancies. If the crack reaches the triple junction /1-3-4/, grain {1} separates from grain {3}. If the same process occurs at interface [1-4], damage evolution is then controlled by the motion of grain {1} (fig. 5-b), which strongly depends on viscosities of [1-2] and [1-5] grain boundaries. Another important parameter affecting macroscopic damage evolution is

therefore the average number of moving grains at every moment during superplastic deformation. Calculations are now underway to get quantitative evaluation of local damage evolution according to this approach.



10 μm

Figure 4 - Correlation between cavitation and grain boundary sliding in a superplastically deformed Al-Cu-Li-Mg alloy.

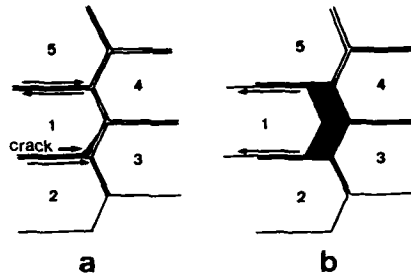


Figure 5 - a) Development of a crack at a triple junction; b) Control of damage growth by sliding rate of grains.

#### Conclusion

The evolution of an initial distribution of cavities during superplastic straining was calculated according to classical laws for diffusion and plasticity controlled growth. The comparison with experimental results confirms the importance of strain-induced nucleation for superplastic aluminum alloys. Cavity growth can also be affected by grain boundary sliding. In order to account for this process, an approach of damage development during superplastic deformation is proposed, pointing out structural parameters which are generally ignored in cavity evolution.

#### References

1. R. Raj and M.F. Ashby, "Intergranular fracture at elevated temperature", *Acta Met.*, 23 (1975) 653-666.
2. M.H. Yoo and H. Trinkaus, "Crack and cavity nucleation at interfaces during creep", *Metallurgical Transactions*, 14A (1983) 547.
3. M.J. Stowell, D.W. Livesey and N. Ridley, "Cavity coalescence in superplastic deformation", *Acta Met.* 32 (1984) 35-42.
4. A. Varloteaux, J.J. Blandin and M. Suéry, "How to control cavitation in aluminum alloys", To be published.
5. A.C.F. Cocks and M.F. Ashby, "Intergranular fracture during power-law creep under multiaxial stresses", *Met. Sci.* 14 (1980) 395-402.
6. A. Varloteaux, "Superplasticité et endommagement des alliages d'aluminium à haute résistance - 7475-" (Thesis, Institut National Polytechnique de Grenoble, 1987).
7. J.J. Blandin, "Endommagement des alliages d'aluminium au lithium lors d'une déformation superplastique" (Thesis, Institut National Polytechnique de Grenoble, 1988).
8. C.W. Cho, B.A. Cheney, D.J. Lege and J.I. Petit, "Superplastically of 2090 SPF sheet at hot rolled gauge", Proc. of the 4th International Al-Li Conference, Paris (F), 10-12 June 1987, 277-283.
9. J. Belzunce and M. Suéry, "Analysis of cavity growth and fracture in superplastic  $\alpha/\beta$  brasses", *Acta Met.*, 31 (1983) 1497-1504.

AN EXPERIMENTAL INVESTIGATION OF HOLE GROWTH AND INTERLINKAGE

IN THE SUPERPLASTIC Zn-22% Al EUTECTOID ALLOY

Norio Furushiro<sup>†</sup> and Terence G. Langdon<sup>§</sup>

<sup>†</sup>Department of Materials Science and Engineering  
Faculty of Engineering, Osaka University  
Suita, Osaka 565, Japan

<sup>§</sup>Departments of Materials Science and Mechanical Engineering  
University of Southern California  
Los Angeles, CA 90089-1453, U.S.A.

Abstract

Experiments were conducted to investigate the growth and interlinkage of holes in the superplastic Zn-22% Al eutectoid alloy by testing specimens with small holes machined in the gauge lengths prior to testing. Specimens were tested without holes, with a single hole machined in the center of the gauge length, and with two holes oriented so that their centers were on a line perpendicular to the tensile axis. The results show that there is an interaction effect between adjacent holes such that the holes in the double hole configuration increase in size more rapidly than the single holes. The interlinkage of the two holes occurs at the highest elongation in the superplastic region II, thereby demonstrating that, under optimum superplastic conditions, there is a resistance to internal necking in the inter-cavity ligaments.

### Introduction

Superplastic materials generally exhibit a logarithmic relationship between the maximum flow stress,  $\sigma_m$ , and the initial strain rate,  $\dot{\epsilon}_0$ , which is sigmoidal [1]. By relating  $\sigma_m$  to  $\dot{\epsilon}_0$  through an empirical equation of the form

$$\sigma_m = B \dot{\epsilon}_0^m \quad (1)$$

where B is a constant and m is termed the strain rate sensitivity, it follows that the flow behavior divides into three regions: the value of m is high ( $\sim 0.5$ ) at intermediate strain rates in region II but m decreases to a low value ( $\sim 0.2$ ) at both low and high strain rates in regions I and III, respectively. Since there is a correlation between the value of m and the total elongation to failure [2], the maximum superplastic elongations occur in region II and there is a decrease in the elongations in regions I and III.

Although early experiments suggested that cavity formation was not important in superplasticity [3], more recent work has demonstrated that internal cavities develop in many (if not most) superplastic alloys [4]. Indeed, the requirement for optimum superplasticity appears to be the suppression of significant cavity interlinkage rather than the elimination of cavity nucleation and growth [5].

It is possible to model the growth and interaction effects between adjacent cavities by using specimens containing machined holes which are inserted prior to testing. The first experiments of this type were conducted by Tait and Taplin on an Al-Mg alloy exhibiting extended ductility [6] and on a superplastic aluminum alloy [7], respectively. For both sets of experiments, specimens were tested at a single strain rate in region II either with a single machined hole or with two holes machined perpendicular to the tensile axis with a range of center-to-center spacings. More recently, Wilkinson and Cáceres [8] tested specimens of a superplastic Cu alloy containing a single hole near one end of the gauge length and two holes perpendicular to the tensile axis near the other end, and using strain rates which, based on earlier experiments on this alloy under similar conditions [9], correspond to region I and the lower end of region II. The present paper describes some of the results obtained in similar experiments conducted over a range of strain rates on the superplastic Zn-22% Al eutectoid alloy.

### Experimental Material and Procedures

The tests were conducted on the Zn-22% Al alloy using specimens cut from sheets, 2.54 mm in thickness, with the tensile axes parallel to the rolling direction. Specimens were tested in three different configurations: (i) without machined holes, (ii) with one hole, 0.33 mm in diameter, machined in the center of the gauge length ("single hole configuration"), and (iii) with two holes, each 0.33 mm in diameter, machined in the center of the gauge length with a center-to-center spacing, perpendicular to the tensile axis, of 1.0 mm ("double hole configuration"). For all specimens containing holes, the gauge width was 6.4 mm and the holes were machined perpendicular to the tensile axis and in the short transverse direction. After machining the holes, all specimens were annealed to give a spatial grain size, d, of  $\sim 2.1 \mu\text{m}$ , where d is defined as  $1.74 \times \bar{L}$  where  $\bar{L}$  is the mean linear intercept grain size. Specimens were tested at strain rates from  $1.33 \times 10^{-5}$  to  $1.33 \text{ s}^{-1}$  using an Instron testing machine operating at a constant rate of cross-head displacement. A testing temperature of  $473 \pm 2 \text{ K}$  was attained using a bath of silicone oil stirred with bubbling

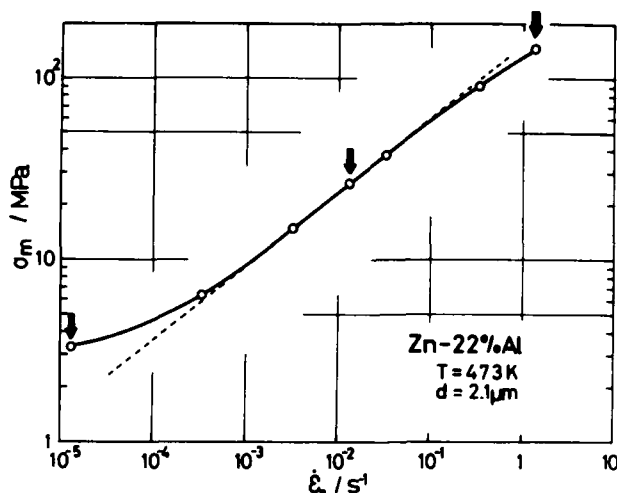


Figure 1 - Maximum flow stress versus initial strain rate, showing the three strain rates (arrowed) selected for testing of the single and double hole configurations.

argon. For the specimens containing holes, each test was discontinued at a selected elongation and the specimen was carefully removed from the testing machine, photographed, and then measurements were taken to determine the hole shape and, for the double hole configuration, the hole spacing.

#### Experimental Results and Discussion

Figure 1 shows the logarithmic plot of  $\sigma_m$  versus  $\dot{\epsilon}_0$  for specimens without holes tested at single strain rates. These results are consistent with the data reported earlier for Zn-22% Al tested under similar conditions [10] and they show the division into region I at  $\dot{\epsilon}_0 \lesssim 10^{-3} \text{ s}^{-1}$ , region II at  $\dot{\epsilon}_0 \approx 10^{-3} \text{ to } 10^{-1} \text{ s}^{-1}$ , and region III at  $\dot{\epsilon}_0 \gtrsim 10^{-1} \text{ s}^{-1}$ . The broken line denoting the slope in region II gives  $m \approx 0.41$ , and this is also similar to the earlier data [10,11].

Specimens having the single and double hole configurations were tested at initial strain rates of  $1.33 \times 10^{-5}$ ,  $1.33 \times 10^{-2}$  and  $1.33 \text{ s}^{-1}$  corresponding to regions I, II and III, respectively: these three strain rates are indicated in Fig. 1 by the solid arrows. Figures 2 and 3 give examples of the specimens in the single hole and double hole configurations, respectively.

In Fig. 2, the top specimen is untested and shows the machined hole in the center of the gauge length. The lower six specimens were tested in region II to elongations of 19%, 40%, 69%, 133%, 234% and 394%, respectively. An examination of these specimens shows that the hole pulls out along the tensile axis and ultimately, at elongations above  $\sim 200\%$ , the deformation is concentrated in the two ligaments of material on either side of the elongated hole. In Fig. 3, the three specimens have the double hole configuration and they were pulled to fracture in regions I (upper), II (center) and III (bottom) with corresponding fracture elongations of  $\sim 135\%$ ,  $\sim 400\%$  and  $\sim 65\%$ , respectively. Since the anticipated fracture elongation in region II is  $>2500\%$  under these experimental conditions in the absence of a machined hole in the gauge length [10], it is clear that the overall



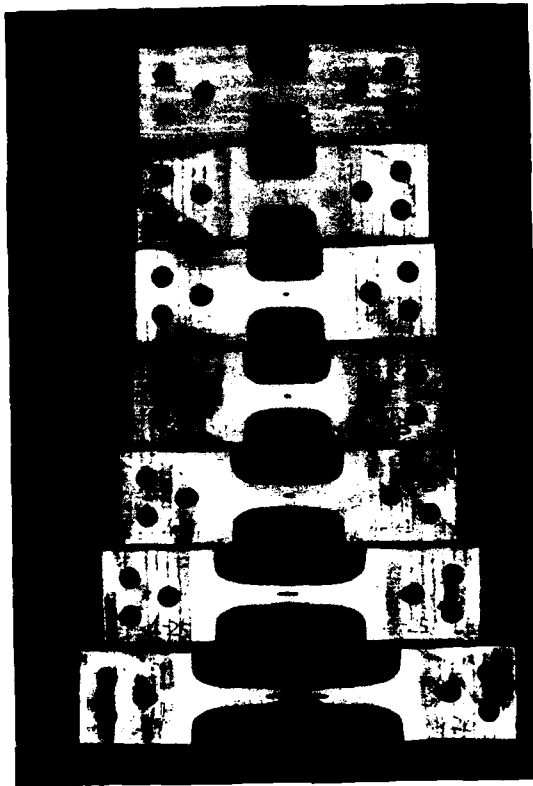


Figure 2 - Specimens with a single hole configuration. The top specimen is untested and the other specimens were pulled in region II to elongations of 19%, 40%, 69%, 133%, 234% and 394%, respectively.

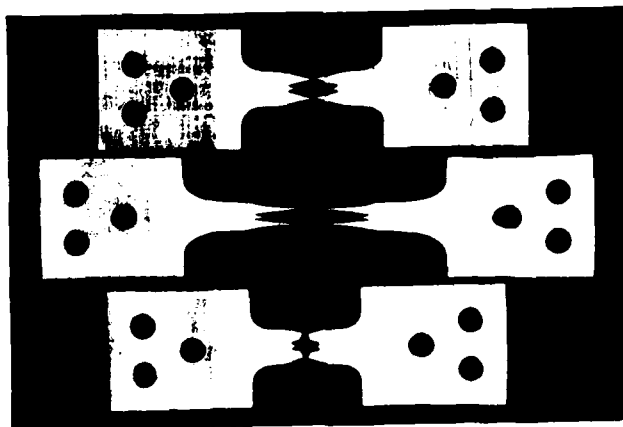


Figure 3 - Specimens with a double hole configuration pulled to fracture in regions I (upper), II (center) and III (bottom).

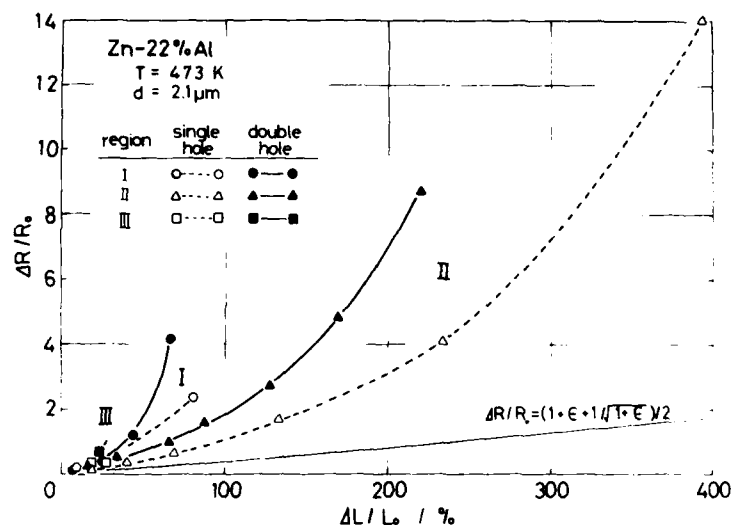


Figure 4 - Change in hole radius versus elongation for the single and double hole configurations.

ductility has been very much reduced because of the presence of the two holes.

The growth of the holes during deformation is illustrated in Fig. 4, where the change in radius,  $\Delta R/R_0$ , is plotted against the overall elongation,  $\Delta L/L_0$ , where  $\Delta R$  and  $\Delta L$  are the change in hole radius and the change in specimen gauge length and  $R_0$  and  $L_0$  are the initial hole radius and the initial specimen gauge length, respectively. Initially, the machined holes were circular so that  $R_0 = 0.165$  mm. However, reference to Figs 2 and 3 shows that the holes become elongated along the tensile axis during deformation, so that the effective radius,  $R$ , at any selected elongation may be defined as  $R = (\alpha + \beta)/2$  where  $2\alpha$  and  $2\beta$  are the diameters measured in the plane of the specimen surface parallel and perpendicular to the tensile axis, respectively. Datum points are shown in Fig. 4 for both the single hole and the double hole configurations, and for measurements at the three different strain rates in regions I, II and III. For the double hole configuration, the measurements do not continue beyond the elongations where the two holes interlink. For a single hole, since the measurements are taken on the flat surface of the tensile specimens, there would be an apparent change in the value of  $\Delta R/R_0$  with elongation even if there was no growth of the hole. Assuming that the total volume of the hole in the thickness of the specimen remains constant with elongation, the value of  $\Delta R/R_0$  varies with strain,  $\epsilon$ , according to the lower solid line in Fig. 4.

Inspection of Fig. 4 shows that there is an interaction effect such that the holes in the double hole configuration increase in size more rapidly than the single holes. For all situations, there is a genuine increase in the size of the holes with increasing elongation, and this growth occurs most rapidly in regions I and III. The interlinkage of the two holes occurs at an elongation of  $>200\%$  in the superplastic region II, but the holes interlink at elongations of  $<100\%$  in regions I and III. The delay in interlinkage in region II demonstrates that, under optimum superplastic conditions, there is less interaction between adjacent holes. This is consistent with the concept that the fracture of inter-cavity ligaments

is difficult under highly superplastic conditions because of the high value of  $m$  and the consequent resistance to internal necking [5].

#### Summary and Conclusions

1. Specimens of the Zn-22% Al alloy were tested containing either a single hole or two holes machined prior to testing.
2. The single hole pulls out along the tensile axis with increasing elongation and ultimately deformation is concentrated in the two ligaments on either side of the hole.
3. For the double hole configuration, there is an interaction effect such that the holes increase in size more rapidly than the single hole. Hole interlinkage occurs at the highest elongation in region II, thereby demonstrating that, under optimum superplastic conditions, there is a resistance to internal necking in the inter-cavity ligaments.

#### Acknowledgement

This work was supported in part by the National Science Foundation under Grant No. DMR-8503224.

#### References

1. T.G. Langdon, "The Mechanical Properties of Superplastic Materials", Metall. Trans., **13A** (1982) 689-701.
2. D.A. Woodford, "Strain-Rate Sensitivity as a Measure of Ductility", Trans. ASM, **62** (1969) 291-293.
3. R.H. Johnson, "Superplasticity", Metall. Rev., **15** (1970) 115-134.
4. B.P. Kashyap and A.K. Mukherjee, "Cavitation Behavior During High Temperature Deformation of Micrograined Superplastic Materials - A Review", Res Mechanica, **17** (1986) 293-355.
5. T.G. Langdon, "Fracture Processes in Superplastic Flow", Metal Sci., **16** (1982) 175-183.
6. R.A. Tait and D.M.R. Taplin, "Interaction Effects During the Growth of Holes in a Superplastically Deforming Medium", Scripta Met., **13** (1979) 77-82.
7. R.A. Tait and D.M.R. Taplin, "The Growth and Interlinkage of Holes During Hot Tensile Deformation of Two Strain-Rate Sensitive Aluminium Alloys", Mechanical Behaviour of Materials, vol. 2, ed. K.J. Miller and R.F. Smith (Oxford: Pergamon Press, 1980), 663-674.
8. D.S. Wilkinson and C.H. Cáceres, "Mechanism of Plastic Void Growth During Superplastic Flow", Mater. Sci. Tech., **2** (1986) 1086-1092.
9. C.H. Cáceres and D.S. Wilkinson, "Grain Growth at Low Strain Rates in a Superplastic Cu Alloy", Scripta Met., **16** (1982) 1363-1365.
10. H. Ishikawa, F.A. Mohamed and T.G. Langdon, "The Influence of Strain Rate on Ductility in the Superplastic Zn-22% Al Eutectoid", Phil. Mag., **32** (1975) 1269-1271.
11. F.A. Mohamed, M.M.I. Ahmed and T.G. Langdon, "Factors Influencing Ductility in the Superplastic Zn-22 Pct Al Eutectoid", Metall. Trans., **8A** (1977) 933-938.

CAVITATION BEHAVIOR AND DISLOCATION STRUCTURE  
OF COMMERCIAL MANGANESE-BRASS DURING SUPERPLASTIC DEFORMATION

Zhao You-Chang Li Xiu-Qing

Institute of Material Science, Jilin University  
Changchun China

Abstract

In this paper we have studied features of superplasticity for commercial manganese-brass (HMn58-2). Experiments show that elongation of the alloys was reached 520% in tensile deformation at 600 °c and an initial strain rate of  $7.7 \times 10^{-4}$ /s, these specimens were not given any pre-treatments. The roles of cavity nucleation and growth have been researched during superplastic deformation. The volume fractions of metastable cavities were determined at different initial strain rate ( $\dot{\epsilon}$ ) and reduction of area ( $\psi$ ) using small angle X-ray scattering method. The relationship between volume fraction of cavity and strain has been studied using scanning electro microscopy and metallography. The parameters of cavity growth rate ( $\eta$ ) were determined at different  $\dot{\epsilon}$ . At higher strain rate the whole volume fraction of metastable cavity decreases with increasing  $\psi$ ,  $\eta$  value is higher, superplasticity of this specimen is badly. At lower strain rate the whole volume fraction of metastable cavity increases with increasing  $\psi$ ,  $\eta$  value is lower, superplasticity of that specimen is better.

Dislocations and stacking faults of this alloy were observed using transmission electron microscopy (TEM). Experiments show that interaction of dislocation with stacking fault and interaction of grain boundary with lattice dislocation are presented.

Superplasticity and Superplastic Forming  
Edited by C.H. Hamilton and N.E. Paton  
The Minerals, Metals & Materials Society, 1988

## Introduction

Cavitation has been studied in a wide range of superplastic alloy (1-6). The problem of cavity nucleation has been researched in some papers, but there is a difficulty for direct observation, therefore understanding the roles of cavity nucleation in detail is subjected to some restrictions. Occurrence and growth of cavity affected by strain rate have been researched in some works, but the conclusions were not clean. In this paper we have used the small angle X-ray scattering analysis (SAXS). Scanning electron microscopy (SEM) and metallography to study systematically the cases of micro cavity ( $R < 100\text{nm}$ ) nucleation and roles of cavity ( $R > 100\text{nm}$ ) growth. The parameters of cavity growth rate ( $\dot{\gamma}$ ) were measured. The models of dislocation accommodation in grain boundary sliding (GBS) were developed by some authors (7,11). There were some works which supported those models (8,9). Change of stacking fault during superplastic flow and interaction of stacking fault and dislocation are seldom reported. In this paper we have observed the interaction of stacking fault and dislocation.

## Experimental details and discussion

For commercial plates without pretreatment the maximum elongation can reach 520% under  $600^\circ\text{C}$  and  $\dot{\epsilon} = 7.7 \times 10^{-4}/\text{s}$ .

The cavities were observed in grain boundaries and interphase boundaries (Fig 1). The aspects of voids are spherical under lower strain rate (Fig 2), observed by SEM that radius of minimum



Figure 1 - Cavities formed in boundaries



Figure 2 - Small granular cavities, SEM.

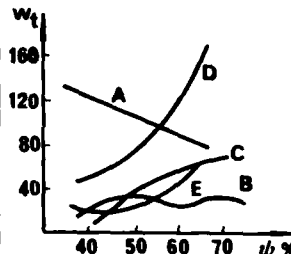


Figure 3 - Curves between  $W_t$  and  $\psi$ .

voids is  $\sim 40\text{nm}$ . The distribution of micro cavities ( $R < 40\text{nm}$ ) was determined using X-ray small angle scattering (10) under various strain rate and  $600^\circ\text{C}$ . The volume fraction distribution of micro cavities is shown in table 1. Which is separated in seven regions for different  $R$ ,  $W$  shows volume fraction of micro cavities in various region. The value of ( $W_t$ ) presents summation of individual parts (i. e.  $R$  from  $3.5\text{nm}$  to  $39\text{nm}$ ). For different  $\dot{\epsilon}$  the curves of relationship between  $W_t$  and  $\psi$  is shown in Fig 3. Some roles can be seen from Fig 3: (1) the volume fraction of micro cavities ( $W_t$ ) decreases with increasing  $\psi$  under larger  $\dot{\epsilon}$  (specimen A); which elongation is minimum ( $\delta = 133\%$ ); (2) under intermediate  $\dot{\epsilon}$ ,  $W_t$  appears in wave shape with increasing  $\psi$  (specimen B) which elongation ( $\delta = 273\%$ ) is larger than specimen A; (3) when  $\dot{\epsilon}$  decreases continuously (specimen C and D),  $W_t$  increases with increasing  $\psi$ , whereas specimen D appears more obviously (elongation is maximum); (4) for minimum  $\dot{\epsilon}$ ,  $W_t$  (specimen E) also increases with increasing  $\psi$ , but increment (specimen E) is less than specimen C and D, corresponding value of  $\delta$  is also less than the latter. These results can be analysed

Table 1 The Volume Fraction Distribution of Micro Cavities by SAXS

$\dot{\epsilon}$	$2.7 \times 10^{-3}/s$		$1.0 \times 10^{-3}/s$		$4.6 \times 10^{-4}/s$		$1.9 \times 10^{-4}/s$		$8.3 \times 10^{-5}/s$	
$\delta$	133%(A)		273%(B)		293%(C)		330%(D)		283%(E)	
	$\psi\%$	Wt	$\psi\%$	Wt	$\psi\%$	Wt	$\psi\%$	Wt	$\psi\%$	Wt
	59.2	86.80	69.4	27.00	64.3	62.72	68.4	174.12	63.3	62.40
	32.7	132.84	64.3	20.64	59.1	52.59	61.2	138.21	59.2	52.90
	19.4	152.22	59.1	7.45	55.1	41.66	58.2	114.08	54.1	21.44
			54.1	31.69	53.1	37.81	53.1	71.36	53.1	19.03
			46.9	24.60	49.0	22.37	50.0	61.37	50.0	17.46
			39.8	9.08			43.9	55.49		

as follows. According to the theory of cavitation nucleation, when a cavity of radius  $R$  is formed, the energy will be changed

$$\Delta G = 4\pi R^2\gamma - 4/3\pi R^3\sigma \quad (1)$$

where  $\gamma$  is surface energy of cavity,  $\sigma$  is located flow stress, thus critical radius of nucleation  $R_c$  may be written as  $R_c = 2\gamma/\sigma$ . The calculated value of  $R_c$  is larger than 100nm. Therefore the size of cavity determined by SAXS is placed in a metastable condition. When the cavity size is larger than stable cavity ( $R > R_c$ ), energy of system will decrease with growing of cavity. It is similar to that energy of system decreases with growing of stable grains. To increase energy of system and to maintain high energy condition, superplasticity of materials can be developed. According to this analysis, increase of metastable cavity quantity will promote the superplasticity to develop.

When the cavity size is over the critical radius  $R_c$ , generally cavity growth has two mechanisms: i.e. vacancy diffusion mechanism (2) and plastic deformation mechanism (3). In fact, Beere and Speight (4) have indicated that these two mechanisms are both to act. Stowell (6) has put forward that cavity growth obeys a relationship

$$\phi = \phi_0 \exp(\eta \epsilon) \quad (2)$$

where  $\eta$  is a parameter, which expresses the growth rate of cavity,  $\phi$  is cavity volume fraction under strain of  $\epsilon$ ,  $\phi_0$  is cavity volume fraction under strain of zero. We have measured the relation lines between  $\ln \phi$  and  $\epsilon$ . The experimental results conform to formula (2) basically. From these lines the values of  $\eta$  can be obtained. The experimental results are shown in table 2. We have obtained that values of  $\eta$  increase with increasing  $\dot{\epsilon}$  except minor  $\dot{\epsilon}$ . For larger  $\dot{\epsilon}$  (specimen A), value of  $\eta$  is maximum, value of  $\delta$  is minimum. For intermediate strain rate (D)  $\eta$  is minimum,  $\delta$  is maximum.

In HMn 58-2 brass the numerous dislocations are activated and moved after superplastic deformation. It is shown that alloys present dislocation accommodation of GBS. Fig 4 shows three sets of dislocations paralleled to slip plane which were activated in grain boundary ledges and piled up the opposite grain boundary. From Fig 5 it seems possibly

Table 2. Volume Fraction of Cavities and Value of  $\eta$ 

$\dot{\epsilon}$	$2.7 \times 10^{-3}/s$		$1.0 \times 10^{-3}/s$		$4/6 \times 10^{-4}/s$		$1.9 \times 10^{-4}/s$		$8.3 \times 10^{-5}/s$	
	$\epsilon$	$\phi \times 10^3$	$\epsilon$	$\phi \times 10^3$	$\epsilon$	$\phi \times 10^3$	$\epsilon$	$\phi \times 10^3$	$\epsilon$	$\phi \times 10^3$
	0.24	2.44	0.66	2.61	0.78	2.77	0.69	2.33	1.00	3.11
	0.47	3.99	0.83	3.50	0.96	3.35	1.00	3.35	1.13	3.39
	1.45	16.61	1.19	4.95	1.23	4.36	1.39	5.42	1.18	3.63
			1.44	7.24	1.44	6.11	1.58	6.53	1.45	4.56
			1.79	12.70	1.79	8.85	1.80	8.27	1.73	5.69
$\eta$	1.69		1.44		1.22		1.00		1.11	

that stacking faults change to partial dislocations and stacking faults at below part, and change to full dislocations at over part. Of course this process may occur in the opposite direction. Fig 6 shows the interaction between stacking faults and dislocations. The stacking faults obstruct the dislocations to slip, when the dislocations accross the stacking fault, it causes the structure of stacking fault to change.



Figure 4 - Activited dislocation Sets in Grain Boundary.



Figure 5 - Stacking Faults and Partial Dislocations.



Figure 6 - Interaction Between of Dislocations and Stacking Faults.

#### Conclusions

1. The commercial plate specimens of HMn 58-2 brass tensile in superplastic condition under 600 °C without pretreatment, elongation can be reached 520%.

2. For large strain rate (A) volume fraction of metastable cavities ( $W_t$ ) decreases with increasing  $\psi$ , the parameter  $\eta$  is maximum elongation  $\delta$  is minimum. For minimum strain rate (E)  $W_t$  increases with increasing  $\psi$ , value of  $\eta$  is minor, value of  $\delta$  is large. For intermediate strain rate (D)  $W_t$  increases obviously with increasing  $\psi$ , value of  $\eta$  is minimum, value of  $\delta$  is maximum. The present of metastable cavity is beneficial to accomodate action of GBS. The growth of stable cavity is not beneficial to GBS.

3. In this alloys dislocations are activated and moved during superplastic deformation, which play the accomodate role in GBS. The interaction of stacking faults and dislocation is presented, which produces the change of stacking fault and dislocation.

#### References

1. S. Sagat et al., "A Metallographic Study of Superplasticity and Cavitation in Micro-duplex Cu-40%Zn," J. Inst. Met. 100 (1972), 268-274.
2. R. Raj et al., "Correction to: Intergranular Fracture at Elevated Temperature," Scripta Metallurgica, 11 (1977) 839-842.
3. J.W. Hancock, "Creep Cavitation without a Vacancy Flux," Metal Science 10 (1976) 319-325.
4. W. Paere and M.V. Speight, "Creep Cavitation by Vacancy Diffusion in Plastically Deforming Solid," Metal Science, 12 (1978), 172-176.
5. D.A. Miller and T.G. Langdon, "An Analysis of Cavity Growth During Superplasticity," Met. Trans., 10A (1979), 1869-1874.
6. M.J. Stowell, "Cavity Growth in Superplastic Alloys," Metal Science, 14 (1980), 267-272.
7. R.C. Gifkins, "Grain-Boundary Sliding and Its Accommodation During Creep and Superplasticity," Met. Trans., 7A (1976) 1225-1232.
8. K. Matsuki et al., "Superplastic Behavior in Nominally Single-Phase and Two-Phase Al-Cu Alloys," Metal Science, 13 (1979) 619-626.
9. Y.C. Zhao et al., "A Study of Al-6Cu-0.5Zr Alloy Microstructure After Superplastic Deformation," Metal Science and Technology, (China), 5 (1986), 7-13.
10. J.Y. Zhang and C.L. Liu, "Small Angle X-Ray Scattering Analysis of Particle Size Distribution of Ultrafine Powder," Modern Development in Powder Metallurgy, Washington 12 (1981), 47-51.
11. B.P. Kashyap and A.K. Mukherjee, "On the Models for Superplastic Deformation," International Conference on Superplasticity, Grenoble, September 1985.



DEFORMATION OF Ti-6Al-4V BAR AND EXTRUSION

UNDER SUPERPLASTIC FORMING CONDITIONS

D. V. Dunford and P. G. Partridge

Royal Aircraft Establishment  
Farnborough, Hants, UK

Summary

There is increasing interest in the use of conventional product forms such as bar and extrusions for superplastic forming (SPF) of pressure vessels and tubular body shells. Tests have been carried out to compare the superplasticity of Ti-6Al-4V bar and extrusion with that reported for sheet. The flow stresses,  $m$ -values and plastic anisotropy were measured and related to the microstructure. Resulting anisotropy occurred in specimens machined both parallel (L) and perpendicular (T) to the extrusion major axis. Anisotropy also occurred in specimens machined perpendicular (T), but not parallel (L) to the bar major axis. The anisotropy can be explained in terms of the directionality of the microstructure. It is concluded that for limited strains these conventional product forms, although having non-ideal microstructures can be suitable for superplastic forming of components.

Superplasticity and Superplastic Forming  
Edited by C.H. Hamilton and N.E. Paton  
The Minerals, Metals & Materials Society, 1988

### Introduction

The superplastic forming (SPF) of titanium alloys in sheet form is well established and the emphasis has moved towards optimum processing for particular structures [1], and on the post-formed mechanical properties [2]. Meanwhile the need to reduce costs and weight has directed attention to other product forms such as rolled bar and extruded sections for superplastic forming into bottles or pressure vessels. Previous work on textured rectangular rolled bar [3-4] showed texture had negligible effect but the aligned contiguous  $\alpha$ -microstructure caused stress and strain anisotropy during deformation under superplastic conditions. Further tests have been carried out to compare the behaviour of round bar, and of an extruded U-channel section in Ti-6Al-4V alloy under superplastic conditions. The results obtained are described in the paper.

### Experimental Details

The Ti-6Al-4V (IMI 318) extruded section (Fig 1) was produced by conventional extrusion at 950°C and had dimensions of 120 mm wide x 18 mm thick in the web section. The rolled bar was 50 mm diameter. Tensile test pieces aligned parallel to the principal orthogonal directions L and T were machined from the web of the extrusion as shown in Fig 1 and from the axis (L) and diameter (T) of the bar; the gauge lengths of test pieces were 20 mm long and 9 mm diameter. Uniaxial tensile tests were carried out at 925°C at strain rates of  $3 \times 10^{-4} \text{ s}^{-1}$  (extrusion) and  $9 \times 10^{-5} \text{ s}^{-1}$  (bar) to elongations up to 400%. The flow stresses and m-values were determined within the range 4-25% elongation and compared with data reported for IMI 318 sheet [5].

### Results

The microstructures of the extruded and bar materials were examined after annealing for 2h at 925°C and cooling at 25°C/minute to simulate the thermal cycle experienced under superplastic conditions. The microstructures are shown in Figs 2a and 3a. The  $\alpha$ -phase dimensions varied up to 16  $\mu\text{m}$  in the L-direction with the  $\alpha$ -phase contiguous and aligned in this direction. The  $\alpha$ -phase dimensions were generally much less in the T-directions. The microstructures after deformation to strains of 2.24 (bar) and 1.2 (extrusion) are shown in Fig 2b and 3b; the microstructure was much less aligned and the  $\alpha$ -phase appeared to be more equiaxed and broken up into isolated grains.

The shape of the cross-sections in the test piece gauge lengths after deformation to area strains of 2.07-2.24 are shown for the bar in Fig 4; a circular cross-section was obtained for the L-oriented test piece and an elliptical cross-section for the T-oriented test piece, with the maximum diameter parallel to the T-direction. The corresponding cross-section for the extruded material after deformation to strains of 1.2-1.36 is shown in Fig 4; for both L and T orientation test pieces the cross-sections become elliptical during deformation, with the maximum diameter in the T-direction (L oriented test piece) and the L-direction (T oriented test piece). The elliptical shaped cross-section indicated a resistance to deformation in the direction of the larger diameter compared with the orthogonal direction. In all cases the maximum diameter was parallel to the direction of the aligned microstructure in the initial bar and extrusion.

The flow stress v strain rate curves for the extrusion and bar L-oriented test pieces are shown in Fig 5. Over the whole strain rate range the flow stresses were in the order  $\sigma_f \text{ extrusion} > \sigma_f \text{ bar} > \sigma_f \text{ sheet}$ . The corresponding m-values v strain rate curves are plotted in Fig 6. The coarser microstructure in the bar and extrusion caused a shift in the peaks of the curves to lower strain rates compared with the curve for sheet. The extruded material

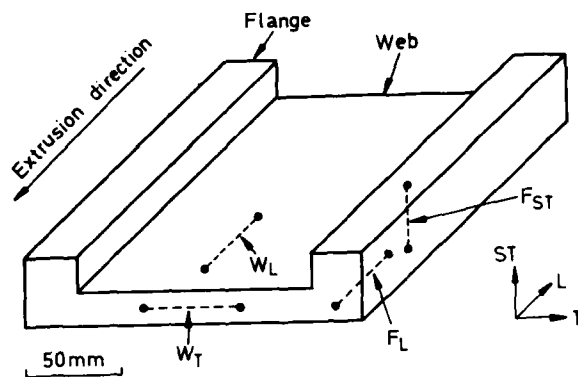


Fig 1 Position of test piece in extruded section

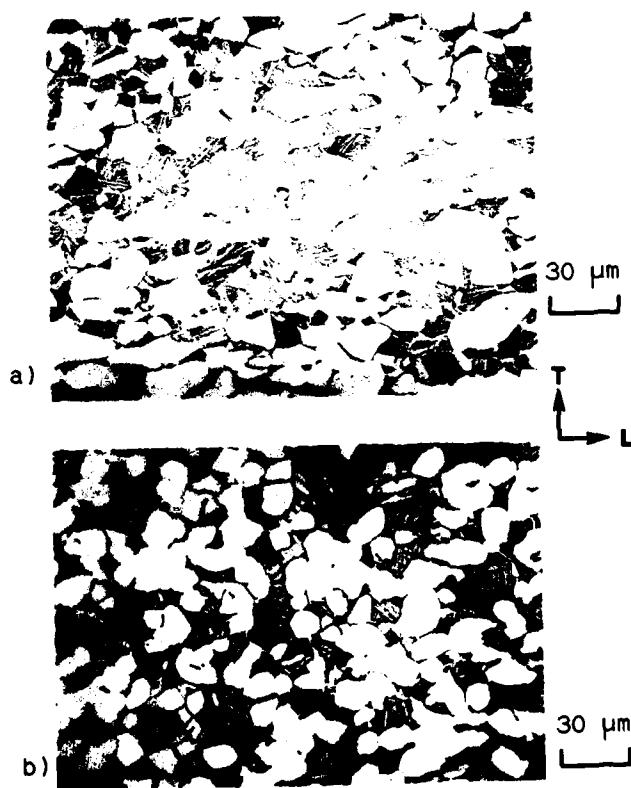


Fig 2 Microstructures of IMI 318 bar (a) after thermal cycle, (b) after superplastic strain (area strain,  $\bar{\epsilon} = 2.24$ )

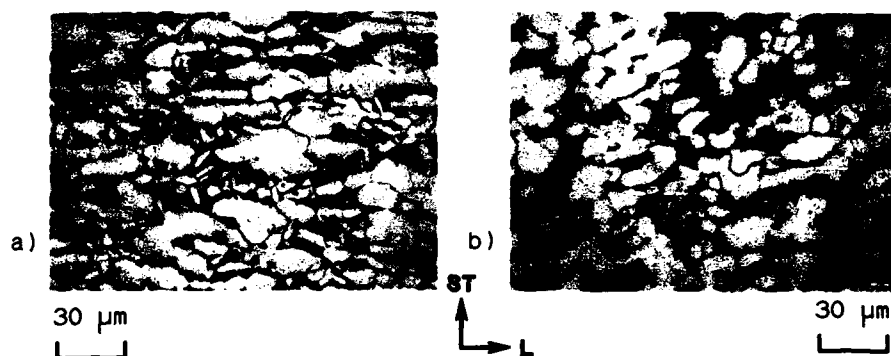


Fig 3 Microstructures of IMI 318 extrusion,  $W_T$  test piece  
(a) after thermal cycle, (b) after superplastic strain  
(area strain,  $\epsilon = 1.20$ )

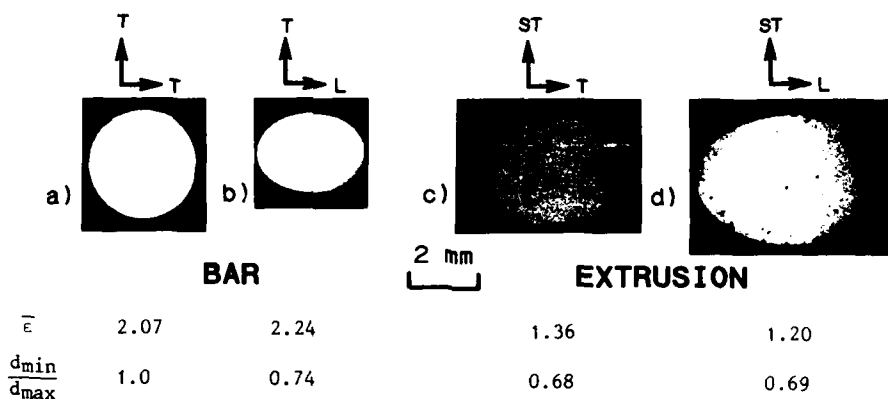


Fig 4 Cross-sections after deformation. Round bar  
(a) L-direction, (b) T-direction and extrusion  
(c)  $W_L$  test piece, (d)  $W_T$  test piece. Minimum  
diameter,  $d_{min}$ , maximum diameter,  $d_{max}$

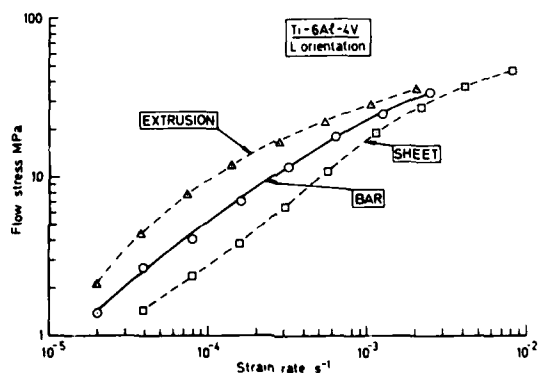


Fig 5 Flow stress v strain rate for IMI 318 bar,  
extrusion and sheet at 925°C

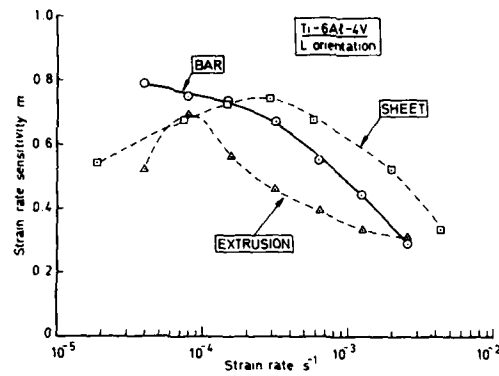


Fig 6 m-values v strain rate for IMI 318 bar, extrusion and sheet at 925°C

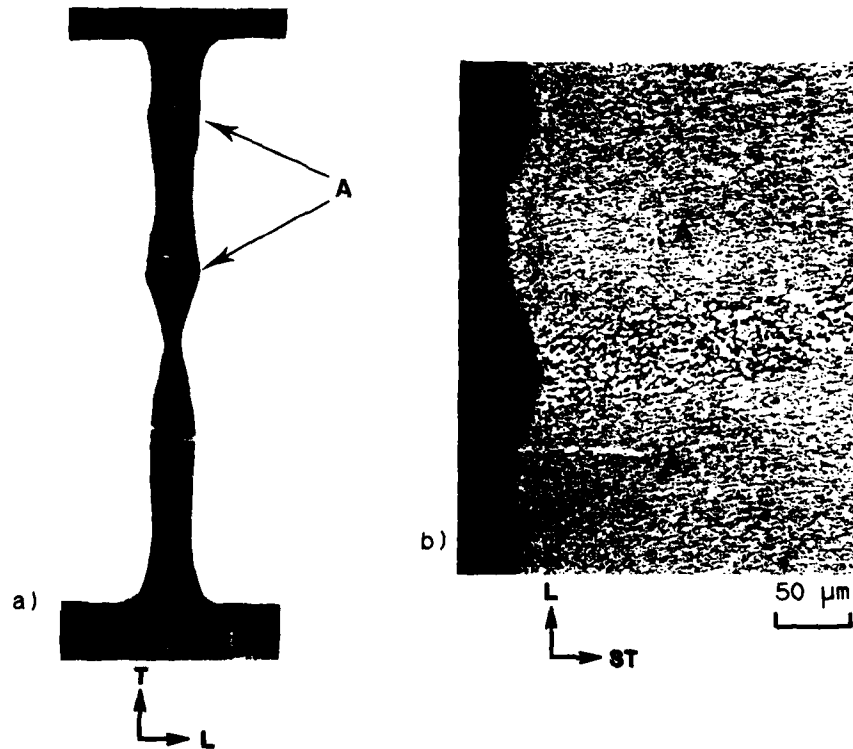


Fig 7 Ti-6Al-4V sheet machined from bar (a) test piece, (b) microstructure, after 273% extension at 875°C,  $\dot{\epsilon} = 3 \times 10^{-4}$

also showed a sharper peak compared with the other materials. Although for extrusions the uniaxial tests were carried out at strain rates corresponding to maximum  $m$ -value for the sheet ( $3 \times 10^{-4} \text{ s}^{-1}$ ) whilst the bar was tested at a lower strain rate ( $9 \times 10^{-5} \text{ s}^{-1}$ ) which gave a similar  $m$ -value to that of sheet ( $m > 0.70$ ); anisotropic deformation occurred for bar and extrusion under both test conditions.

#### Discussion and Conclusions

The results show that for bar and extrusions high  $m$ -values and low flow stresses can be obtained with microstructures which were not ideal for superplasticity. To obtain the same flow stress as used for superplastic sheet, with  $m > 0.6$  the ratio of the strain rates ( $\dot{\epsilon}$ ) would be  $\dot{\epsilon}_{\text{sheet}} : \dot{\epsilon}_{\text{bar}} : \dot{\epsilon}_{\text{extrusion}} \approx 2.4 : 2.1 : 1$ . A fivefold increase in forming time for the extruded material is likely to impose a severe cost penalty on processing. The other characteristic of the bar and extruded material was the tendency to deform anisotropically under superplastic conditions. This behaviour has also been reported in thin sheet test pieces when the microstructure was strongly aligned [6]. This is illustrated in Fig 7 for sheet test pieces machined from rolled bar [6] the non-uniform deformation in Fig 7a was caused by the banding shown in Fig 7b; note the minimum transverse strain occurred at the position of the aligned microstructure at A. This behaviour has been explained in terms of the resistance to sliding in  $\alpha/\alpha$  phase grain boundaries compared with  $\beta/\beta$  grain boundaries [3,4,7].

Although isotropic strain and high  $m$ -values can be obtained in conventionally processed material in a particular direction of stressing, eg rolled bar in the  $L$ -direction, for more homogeneous deformation at higher strain rates some modification to the rolling, extrusion or heat treatment operations will be required. This may involve some cost increases in exchange for subsequent reduced component manufacturing costs by SPF.

#### References

1. D. Stephen, Designing with Titanium, Inst.Metals, (1986), 108
2. P. G. Partridge et al, Superplasticity, AGARD Lecture Series No 154, (1987), 6
3. D. S. McDarmaid et al, J.Mater.Sci., 19, (1984), 2378
4. D. S. McDarmaid et al, J.Mater.Sci., 20, (1985), 1976
5. C. D. Ingelbrecht, Designing with Titanium, Inst.Metals, (1986), 252
6. C. D. Ingelbrecht, P. G. Partridge, J.Mater.Sci., 21, (1986), 4071
7. P. G. Partridge et al, Acta Met., 33, (1985), 571

EFFECT OF SUPERPLASTIC DEFORMATION ON THE SURFACE ROUGHNESS OF SHEET

P. G. Partridge and D. V. Dunford

Royal Aircraft Establishment  
Farnborough UK

Abstract

Superplastic deformation increased the surface roughness of Al and Ti-alloy sheet. The implications for SPF/DB processing are discussed.

Superplasticity and Superplastic Forming  
Edited by C.H. Hamilton and N.E. Paton  
The Minerals, Metals & Materials Society, 1988

### Introduction

SPF/DB [1] involves in situ diffusion bonding after the sheet has undergone large superplastic strain. Bond quality depends primarily on precise process control which is based upon the forming and bonding parameters [2]. Surface roughness is one of the most important parameters affecting solid state bonds since in practice increased surface roughness requires an increase in the bonding time. Plastic deformation is known to increase the surface roughness of CP titanium sheet [3], but although an increase in surface roughness has been reported during superplastic deformation of Ti-alloy sheet [4,5], no roughness measurements were made. Ra values\* have therefore been determined for Ti and Al alloy sheets before and after SPF and are reported in this paper. Their significance for forming and bonding of sheet is discussed.

### Experimental Details

The alloys in sheet form had the compositions (wt%) of Ti-6Al-4V, Ti-15V-3Cr-3Al-3Sn, Al-2.4Li-1.2Cu-0.7Mg-0.1Zr (LITAL A) and Al-6Zn-2.3Mg-1.7Cu-0.11Zr (7010). Sheet thicknesses and grain sizes are given in Table 1.

Table 1  
Effect of Superplastic Strain on Grain Size and Surface Roughness Ra

Material	Sheet Thickness mm	SPF Strain $\bar{\epsilon}$	Grain Size $\mu\text{m}$	Ra $\mu\text{m}$
LITAL A	1.6	0	5	0.35
		1.33	12	2.69
		at 540°C		
7010 (Unclad)	3.2	0	8-12	0.35
		1.61	12-24	4.42
		at 500°C		
Ti-6Al-4V	3.2	0	6	0.29
		1.38	15	1.44
		at 925°C		
Ti-15V-3Cr-3Al-3Sn	2.0	0	38	0.44
		1.1	60	2.62
		at 910°C		

The Ti-alloys were tested at 910-925°C at an initial strain rate of  $3 \times 10^{-4} \text{ s}^{-1}$  and the Al-alloys at 500-540°C in the range  $3 \times 10^{-5} - 8.3 \times 10^{-4} \text{ s}^{-1}$ . Surface roughness in terms of Ra were determined using a Taylor Hobson Talysurf machine with a truncated diamond pyramid stylus having a 2  $\mu\text{m}$  radius and a length in the direction of movement of 5  $\mu\text{m}$ . Total length sampled was 1.25 mm.

### Results

The surface of Ti-6Al-4V sheet in the as received state showed ridges with smooth regions between (Fig 1a). After a strain of 1.38 grain boundary sliding was apparent (Fig 1b) and the grain size increased (Table 1) coincident with an increase in Ra value from 0.29  $\mu\text{m}$  to 1.44  $\mu\text{m}$ . A larger Ra value

\* Ra is the arithmetic mean of the departure of the profile from the mean line.



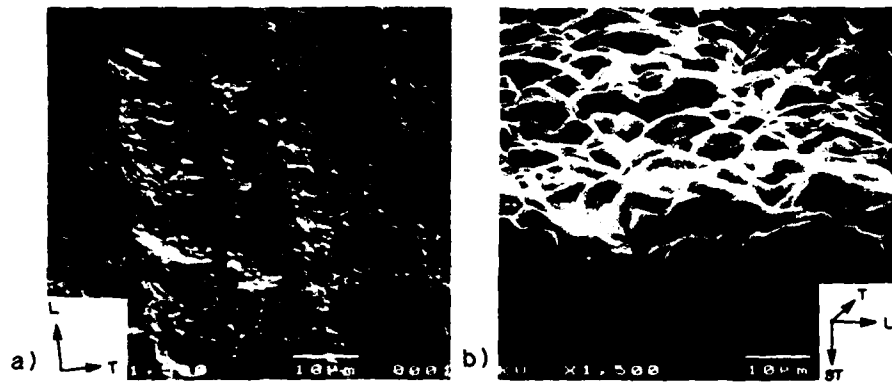


Fig 1 SEM of Ti-6Al-4V surface (a) as received and (b) after superplastic ( $\bar{\epsilon} = 1.38$ )



Fig 2 SEM of Ti-15V-3Cr-3Al-3Sn surface after superplastic strain strain ( $\bar{\epsilon} = 1.1$ )



Fig 3 SEM of aluminium alloy (7010) surface after superplastic strain ( $\bar{\epsilon} = 1.61$ )

of 2.62  $\mu\text{m}$  was obtained for the coarser grained Ti-15-3-3 alloy (Table 1). This alloy is less superplastic and showed less grain boundary sliding but numerous transgranular shear bands (Fig 2). Surface detail on LITAL A tested in air was obscured by oxidation products, but during SPF the increase in the Ra value was much greater than for Ti-6Al-4V (Table 1). The less superplastic 7010 alloy had a larger grain size and showed a greater increase in the Ra values (Table 1). There was evidence of large grain boundary shear with deep local depressions (Fig 3). Unlike Ti-6Al-4V alloy surface, in the Al-alloys the short wavelength roughness was superimposed on a longer wavelength roughness as shown in Fig 4.

Plots of change in surface roughness ( $\Delta\text{Ra}$ ) v strain are shown in Figs 5-6. The  $\Delta\text{Ra}$  values increased with strain and with grain size. Biaxially strained LITALA appeared to have a lower rate of roughening than uniaxially strained material. For the fine grained alloys the rate of roughening ( $\Delta\text{Ra}/\epsilon$ ) was 1.8-2.3  $\mu\text{m}$  for LITALA and 0.46-1.1  $\mu\text{m}$  for Ti-6Al-4V.

#### Discussion

The results show that the surface roughness increased by a factor 5-8 in Ti and Al-alloys during SPF. This increase is significant compared with the surface finish specified for SPF quality Ti-alloy sheet of  $\text{Ra} = 0.5 \mu\text{m}$  [1], although much higher values are implied by other workers [5]. The maximum Ra values produced in the present tests lie at the upper limit for ground surfaces and at the lower limit for turned or milled surfaces [2]. It should also be noted that roughness or surface area generated by grain boundary sliding may be underestimated by Ra values since the dimensions of the stylus prevented it recording the very narrow grooves between grains.

An increase in surface roughness can affect:

- a) reactions between the sheet surface and the environment
- b) diffusion bonding of the sheet
- c) mechanical properties of the sheet.

Reactions at the sheet surface may be between liquids or gases. For Ti-alloys the most common contaminant is oxygen, sometimes derived from water vapour, which can dissolve in titanium to produce brittle surface layers with a thickness up to 4-5 grain diameters under normal processing conditions. Such layers can be removed by pickling but the depth of contamination would be greater for rougher surfaces and contamination or metal removal to these depths could be severe for thin sheet eg  $\sim 0.25 \text{ mm}$  thick after SPF. Al-Li-Mg alloys are subject to both magnesium and lithium loss by oxidation at the surface [6] and this would be enhanced by the increase in surface area and accentuated by the back pressure of gas required to suppress cavitation. The narrow grain boundary grooves associated with grain boundary sliding may increase the difficulty in cleaning such surfaces with liquids, especially when access is restricted in for example fuel tanks or pressure vessels.

An obvious practical consequence of increased surface roughness would be an increase in time required to diffusion bond such surfaces. Theoretical studies [7] suggest the time increase could be greater for the longer wavelength roughness found in the Al-alloys. Other implications for bonding are thicker oxide contamination at both Ti and Al-alloy interfaces which is known to adversely affect bond strength [2], a greater tendency to trap gas at the interface and greater disruption of coatings placed on sheet surfaces either to act as a diffusion aid or as a barrier layer to prevent diffusion bonding. Any contamination or solute loss prior to bonding leads to a double layer at the bond interface. This interface may then remain planar and the joint may be susceptible to delamination or low impact properties [2]. The shear strength of diffusion bonded joints in 7010 Al-alloy was particularly sensitive

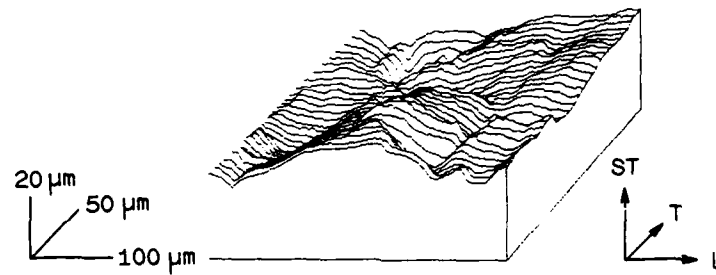


Fig 4 Simulated three-dimensional surface contours of Lital A after superplastic strain ( $\epsilon = 1.33$ )

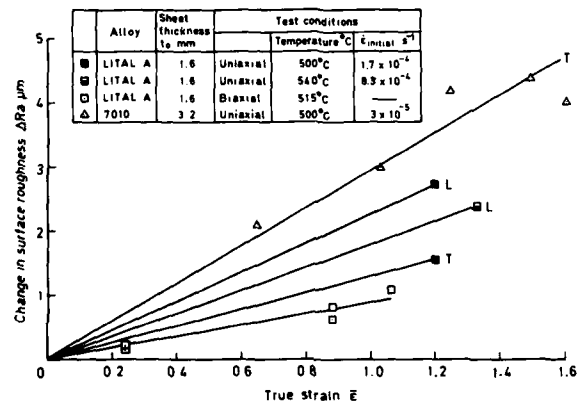


Fig 5  $\Delta R_a$  v true strain for aluminium alloys tested under superplastic conditions

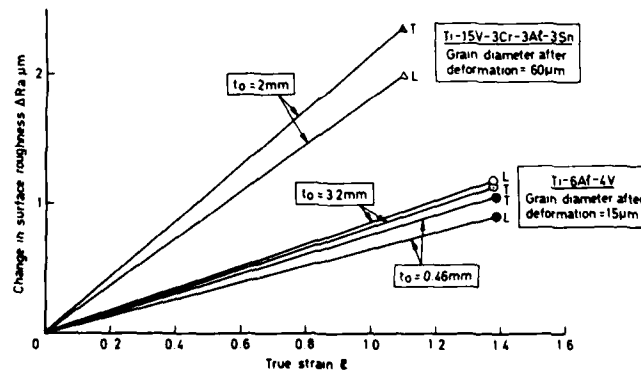


Fig 6  $\Delta R_a$  v true strain for titanium alloys tested under superplastic conditions

to roughness for values of  $R_a < 0.20$  (clad sheet). For greater  $R_a$  values the shear strength appeared to be insensitive to roughness but the width of the scatter band for bond strength was increased to  $\pm 15\%$  [8].

The potential effect of surface finish on the mechanical properties of sheet is less clear. Roughness on the scale of 1-3 grain diameter might be considered to be equivalent to short cracks. These could reduce the time for crack nucleation in low stress/long life fatigue or at least increase the scatter in test data. This effect might be avoided by pickling, but where this is not possible and if sharp radii give rise to local thinning [1] the roughness effects could become important under fatigue loading conditions. Note that the beneficial effects conferred by residual stresses in machined or worked surfaces are normally absent in SPF sheet.

#### Conclusions

The surface roughness of thin sheet increases with increase in superplastic strain and with increase in grain size. The increase is greater in Al-alloys than in Ti-alloys. The increase in roughness could have implications for surface reactions, diffusion bonding and for fatigue properties, especially for very thin sections.

#### References

- 1 D. Stephen, Designing with Titanium, Institute of Metals, 1986, 108-124
- 2 P. G. Partridge, Superplasticity, AGARD Lecture Series No 154, 1987
- 3 W. T. Roberts, D. V. Wilson, Titanium Science and Technology, Vol 2, 1985, 539-546
- 4 C. D. Ingelbrecht, P. G. Partridge, Journal of Materials Science, 21 (1986), 4071-4080
- 5 W. Beck, P. Knepper, DVS, 98 (1985), 63-66
- 6 S. Fox et al, Scripta Met., 20 (1986), 71-74
- 7 G. Gormong et al, Metallurgical Transactions, 6A (1975), 1269-1279
- 8 J. Harvey et al, Materials Science and Engineering, 79 (1986), 191-199.

© Controller, Her Majesty's Stationery Office, London, 1988

## SUPERPLASTICITY AND CAVITATION OF THE 2091 AL-CU-LI-MG ALLOY

J.J. Blandin\*, J.Y. Lacroix\*\* and M. Suéry\*

\* Institut National Polytechnique de Grenoble  
E.N.S. de Physique de Grenoble  
Génie Physique et Mécanique des Matériaux  
Unité Associée au C.N.R.S. n° 793  
BP 46 - 38402 Saint Martin d'Hères Cedex (FRANCE).

\*\* Centre de Recherches et Développement  
Cégédur-Pechiney  
38340 Voreppe (FRANCE).

### Abstract

Superplastic properties of Al-Li alloys can be obtained either by dynamic recrystallization or by a special thermomechanical treatment producing a fine grain structure before forming. Both ways are studied in this work.

In the first case small elongations to failure are obtained due to inhomogeneity of recrystallization and insufficient misorientation between the new grains which persists during straining.

In the second case, small deformations to failure are observed in optimal superplastic conditions during tests under atmospheric pressure, whereas elongations higher than 1500% without rupture are reached with superimposed pressure. This behavior is mainly explained by extensive cavitation which develops during deformation. Particular attention is given on the influence of lithium on diffusional processes which occur during deformation and on differences of cavitation behavior between Li-depleted and non Li-depleted regions.

Superplasticity and Superplastic Forming  
Edited by C.H. Hamilton and N.E. Paton  
The Minerals, Metals & Materials Society, 1988

### Introduction

A large variety of Al-Li alloys has been developed recently for superplastic properties with the goal of using superplastic forming for aeronautical parts. Two procedures were experimented and both were found satisfactory depending on the alloy. The first one generates a superplastic behavior through strain-induced recrystallization as for SUPRAL, whereas the second one starts superplastic forming with a fine grain recrystallized structure produced by appropriate thermomechanical treatments as in the case of 7475.

The aim of this work is to investigate these two procedures on a 2091 Al-alloy not yet known as superplastic and to study the resultant superplastic properties. This alloy was chosen for its ability of being easily rolled.

### Material

The alloy used in this investigation is a 2091 (2.2Cu-2.0Li-1.6Mg-.08Zr) produced by an ingot metallurgy route. It was provided by Cégédur-Pechiney in the form of sheets of 2 mm thick either with an unrecrystallized or a recrystallized structure and both materials were processed to get superplastic properties.

### Experimental results

#### Unrecrystallized structure

The material was tested at various strain-rates and temperatures ranging from 460°C to 520°C, but whatever the straining conditions, only small elongations were obtained (less than 250 %) with  $m$ -values always smaller than .25.

Two reasons can be given to explain this poor superplastic behavior: heterogeneous strain-induced recrystallization and insufficient misorientation between adjacent recrystallized grains thus hindering grain boundary sliding. The heterogeneity of recrystallization can be clearly shown in figure 1. Some areas are fully recrystallized while some others are not yet affected. This heterogeneity can be due to the development of static recrystallization which has taken place during the heating time of the specimen before straining. Indeed the kinetics of static recrystallization can be enhanced in this alloy compared to other Al-Li alloys exhibiting strain-induced recrystallization, due to the presence of high level of Mg and Cu. These elements are known to decrease the temperature of recrystallization of aluminum alloys. Insufficient misorientation between grains may be the result of small amount of copper compared with SUPRAL, due to its little stacking fault energy.

#### Recrystallized structure

In order to get a fine grain recrystallized structure before straining, the material was subjected to an appropriate thermomechanical treatment. This treatment produces an equiaxed structure with grains of 12  $\mu\text{m}$  in diameter as shown in figure 2, which remains stable during deformation.

The material was first tested at various temperatures using crosshead velocity jumps in order to determine the optimum conditions for superplasticity. These were found at 500°C at about  $10^{-3} \text{ s}^{-1}$  with maximum  $m$ -values of 0.4. Elongations to rupture of about 400 % were obtained under atmospheric pressure.

The main reason for this quite early failure is the development of cavitation during deformation. Figure 3 shows the variation with strain of the relative density change of the specimen. If it is assumed that this density change is due only to cavitation, an equation of the form  $C_v = C_{v0} \exp \beta \epsilon$  can be fitted with the experimental results with values of  $C_{v0}$  and  $\beta$  equal to  $2 \cdot 10^{-3}$  and 3.7 respectively. Such an equation agrees with general models for plasticity controlled growth of cavities (1) with however a  $\beta$ -value larger than expected. This discrepancy can be explained by strain-induced nucleation of cavities as confirmed by (2), but it may be due also partly to the fact that the observed density change is not solely related to cavitation but to lithium depletion as discussed later.

Tensile tests were performed in the same conditions of strain-rate and temperature with superimposed hydrostatic pressure in order to suppress cavitation. The results of density change measurements are given in figure 4 which shows that a pressure of 5 MPa is high enough to completely suppress cavitation. With this pressure, elongations without failure of

1500% were obtained. This pressure is larger than that theoretically required ( $\sigma_w/3$ ) to suppress plasticity controlled growth since the tensile stress at the beginning of deformation is about 10 MPa and it continuously decreases during straining due to constant velocity testing with almost no grain growth. One reason of this discrepancy could be the particular importance of both diffusion controlled cavity growth and continuous nucleation in this alloy which require pressure of the order of the flow stress to be suppressed.



50 μm

Figure 1 - Heterogeneity of recrystallization during deformation.



50 μm

Figure 2 - Structure of the recrystallized alloy before deformation.

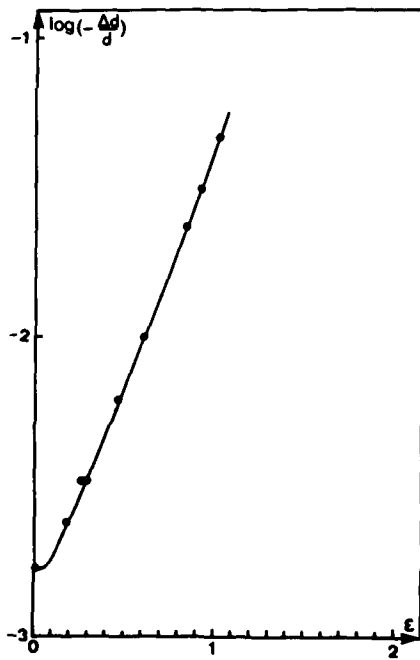


Figure 3 - Change of density vs strain for straining under atmospheric pressure.

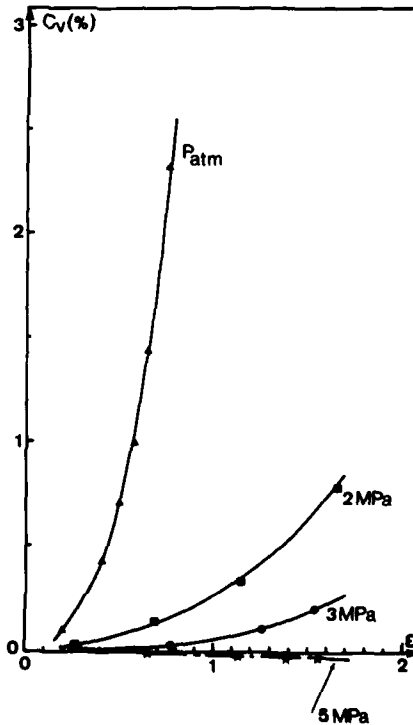


Figure 4 - Influence of superimposed pressure on cavitation behavior.

### Discussion

The interpretation of density variation measurements is difficult since it can be due partly to the loss of elements, particularly lithium, from the near surface region of the specimen during high temperature treatments. Due to the large density difference between Al ( $2.7 \text{ g/cm}^3$ ) and lithium ( $.5 \text{ g/cm}^3$ ), density variations can be thus generated which can be of the same order of magnitude as those produced by cavitation. The influence of lithium depletion must then be taken into account. Papazian and al. (3) have studied this phenomenon of lithium loss during heat treatment of 8090 and 8091 alloys. They have shown that the depth of the Li-depleted zone increases with time according to the relationship:

$$x = 1.5 (D_{Li}t)^{1/2} \quad (1)$$

with  $D_{Li} \text{ (m}^2\text{.s}^{-1}\text{)} = 3.6 \cdot 10^{-4} \exp(-Q/RT)$  and  $Q = 136 \text{ kJ.mol}^{-1}$ . Measurements of this depth were performed in 2091 in static conditions and are in good agreement with theoretical predictions as shown in figure 5.

Figure 6 shows the cross-section of a specimen deformed up to 1.5 at  $500^\circ\text{C}$ . The holding time at this temperature is about 2 hours. The depth of the Li-depleted zone is  $\approx 130 \mu\text{m}$  whereas it was only  $\approx 80 \mu\text{m}$  for static annealing at  $500^\circ\text{C}$ . Superplastic deformation seems therefore to accelerate lithium loss from the surface. This result must however be carefully considered since other parameters can affect Li-depletion such as the thickness of the sample. Moreover the figure shows a close correlation between cavitation and Li-loss. Cavitation is much more important close to the surface than in the center of the specimen. Since this increase of cavitation near the surface was not observed in a 7475 superplastic aluminum alloy (4), it can be concluded that it is not correlated with a different stress state at the surface from that in the center but associated with some physical phenomena involved in Al-Li alloys. The main problem is thus to determine in which way cavitation and Li-loss interact, in other words how cavitation can promote Li-depletion on one hand and how lithium loss can affect cavitation on the other.

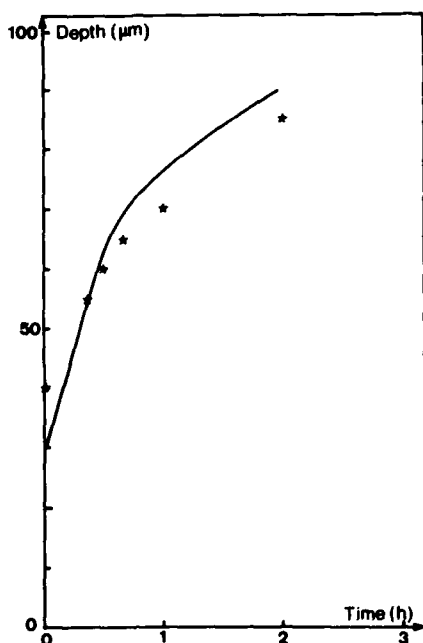


Figure 5 - Depth of the Li-depleted zone vs annealing time at  $500^\circ\text{C}$  :  
\* experiments, --- calculated curve (3).

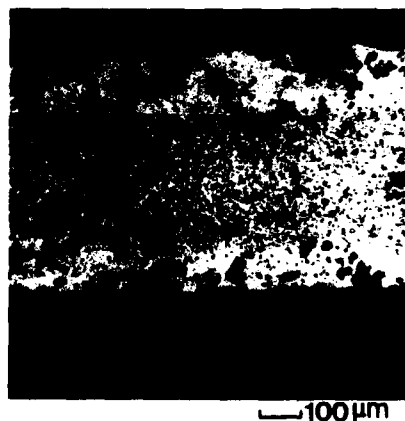


Figure 6 - Cross-section of a superplastically deformed specimen showing the difference in cavitation behavior between the center and the periphery.



#### Effect of cavitation on lithium depletion

The development of cavitation increases the area of free surfaces in the material, some of them being in connection with the outer periphery of the specimen. Consequently a larger area of the sample is concerned with lithium loss. This effect is particularly important when coalescence of the cavities occurs and promotes the propagation of intergranular damage from the surface.

#### Effect of lithium depletion on cavitation

Lithium has an influence on the diffusion coefficients in aluminum owing to its large energy of interaction with vacancies, equal to 0.25 eV (5). This influence is weakly dependent of Li amount, because, even at high temperature, the vacancy concentration is always smaller than the Li atomic concentration. In these conditions, the equilibrium vacancy concentration in Li containing Al-alloys is much larger than in pure aluminum. Moreover the jump frequency of a vacancy is also affected by the neighbourhood of a lithium atom. From these remarks, new values of diffusion coefficients can be obtained. The self-diffusion coefficient of aluminum is increased while the vacancy diffusion coefficient is decreased when lithium amount is sufficient.

It is known that stress concentrations are one of main causes of strain-induced nucleation and growth of cavities. These concentrations are developed on inhomogeneities which inhibit grain boundary sliding, such as triple junctions or second phase particles. The relaxation phenomenon involves matter diffusion through lattice or grain boundaries. If the vacancy flow required for lithium migration is neglected, it can be predicted that the stress concentrations which develop in depleted regions will be more difficult to relax due to the smaller self-diffusion coefficient of aluminum than in non-depleted regions.

#### Conclusion

A 2091 Al-alloy was tested in tension for characterization of superplastic behavior. The following results were obtained:

- \* dynamic recrystallization of the initially unrecrystallized alloy does not occur homogeneously, leading to poor superplastic properties
- \* a fine grain recrystallized structure can be produced by an appropriate thermomechanical treatment
- \* the as-produced material is superplastic with however only small elongations due to extensive cavitation
- \* superimposed pressure can completely suppress cavitation, leading to 1500% elongations.
- \* Li-loss occurs at the periphery of the specimen and interacts with cavitation.

*The authors acknowledge Direction des Recherches, Etudes et Techniques (DRET) of Ministère de la Défense for financial support.*

#### References

1. A.C.F. Cocks and M.F. Ashby, "Intergranular fracture during power-law creep under multiaxial stresses", Metal Science (1980) 395-402.
2. J.J. Blandin and M. Suéry, "Evolution of cavitation during a superplastic deformation", This conference.
3. J.M. Papazian, J.P.W. Wagner and W.D. Rooney, "Porosity development during heat treatment of Al-Li alloys", Proc. of 4th International Al-Li Conference, Paris 10-12 June 1987 513-519.
4. A. Varloteaux, "Superplasticité et endommagement des alliages d'aluminium à haute résistance - 7475-", (Thesis, Institut National Polytechnique de Grenoble, 1987).
5. S. Cesara, A. Giarda and A. Sanchez, "Annealing of vacancies and ageing in Al-Li alloys", Philosophical Magazine 35 (1977) 97-110.

THE INFLUENCE OF SPECIMEN PROFILE AND NOTCH GEOMETRY

ON SUPERPLASTICITY IN Zn-22% Al

Parvin Shariat<sup>†§</sup> and Terence G. Langdon<sup>†</sup>

<sup>†</sup>Departments of Materials Science and Mechanical Engineering  
University of Southern California  
Los Angeles, CA 90089-1453, U.S.A.

<sup>§</sup>Now at Division of Aerospace, Mechanical and Civil Engineering  
Northrop University, 5800 W. Arbor Vitae Street  
Los Angeles, CA 90045-4770, U.S.A.

Abstract

Experiments were conducted to investigate the influence of specimen profile and notch geometry on the elongations to failure in the superplastic Zn-22% Al eutectoid alloy at a testing temperature of 473 K. The results show that the elongations to failure are reduced significantly at all strain rates when a taper is introduced into the gauge length. At any selected strain rate, the fracture elongations decrease as the ratio  $A_{\min}/A_{\max}$  decreases but they are essentially independent of the precise value of  $A_{\min}$ , where  $A_{\min}$  and  $A_{\max}$  are the minimum and maximum cross-sectional areas within the gauge length, respectively. There is a further significant reduction in the fracture elongations when a notch is introduced into the gauge length, and in these specimens there is a sharp concentration of plastic deformation within the region of the notch.

Superplasticity and Superplastic Forming  
Edited by C.H. Hamilton and N.E. Paton  
The Minerals, Metals & Materials Society, 1988

## Introduction

Although superplastic materials are characterized by very high elongations to failure, it is well known that the precise magnitudes of the fracture strains depend both on microstructural features such as the average size and stability of the grains and on external parameters such as the testing temperature and the experimental strain rate. In addition, there is evidence that the overall fracture elongations are influenced by the precise configuration of the testing samples. For example, early work by Morrison [1] on the Pb-62% Sn eutectic alloy demonstrated that the fracture strain is proportional to  $\delta_0/L_0$  in specimens machined from round bars, where  $\delta_0$  and  $L_0$  are the initial gauge diameter and initial gauge length of the specimens, respectively. In addition, Morrison [1] showed that the elongations to failure were reduced by the presence of notches in the gauge lengths, and this effect was confirmed in subsequent experiments on Al-33% Cu [2] and Pb-62% Sn [3].

The purpose of this paper is to describe some of the results obtained in a detailed investigation of the influence of specimen profile and notch geometry on the elongations to failure in the superplastic Zn-22% Al eutectoid alloy.

## Experimental Material and Procedures

The tests were conducted on the Zn-22% Al alloy obtained in superplastic form from The New Jersey Zinc Company. The material was supplied in sheets with a thickness of 2.54 mm and with an as-received grain size of  $\sim 1 \mu\text{m}$ . Tensile specimens were machined from the sheets parallel to the rolling direction. Three representative specimen configurations are depicted schematically in Fig. 1: these configurations, labelled (b), (f) and (j), are examples of the smooth, tapered and notched profiles, respectively. All specimens were annealed in argon for 1 hour at 523 K to give a spatial grain size,  $d$ , of  $2.5 \mu\text{m}$ , where  $d = 1.74 \times \bar{L}$  and  $\bar{L}$  is the mean linear intercept grain size. The specimens were pulled to failure in tension over a range of strain rates at  $473 \pm 2 \text{ K}$  using an Instron testing machine operating at a constant rate of cross-head displacement.

## Experimental Results and Discussion

Typical results are shown in Fig. 2 in a plot of the elongation to fracture,  $\Delta L/L_0$  %, versus the initial strain rate,  $\dot{\epsilon}$ , where  $\Delta L$  is the total change in the gauge length at the point of failure. The upper curve is for a smooth specimen of type (b) in Fig. 1, where the ratio of the minimum to maximum cross-sectional areas within the gauge length,  $A_{\min}/A_{\max}$ , is 1.0. The four lower curves are for tapered specimens having values of  $A_{\min}/A_{\max}$  from 0.9 to 0.7: the specimen of type (f) is shown in Fig. 1 and, since the central width is 6.4 mm and the outer width adjacent to the specimen shoulders is 7.2 mm, the value of  $A_{\min}/A_{\max}$  for this sample is  $6.4/7.2 \approx 0.9$ . The specimens of types (f), (g) and (h) had central widths of 6.4 mm and  $A_{\min}/A_{\max}$  values of 0.9, 0.8 and 0.7, respectively. The specimens of type (i) were used to check on the effect of the total amount of material within the gauge length: these specimens were machined with central and outer widths of 3.3 and 4.8 mm, respectively, to give  $A_{\min}/A_{\max} \approx 0.7$ . For all of these samples, the effective gauge length was 12.7 mm.

The upper curve for the smooth profile in Fig. 2, for specimens of type (b), is typical of the superplastic Zn-22% Al alloy with maximum elongations in the vicinity of  $\dot{\epsilon} \approx 10^{-2} \text{ s}^{-1}$  and decreases in the elongations to failure at both higher and lower strain rates [4,5]. The flow stress,  $\sigma$ , is related to the imposed strain rate by an empirical equation of the form

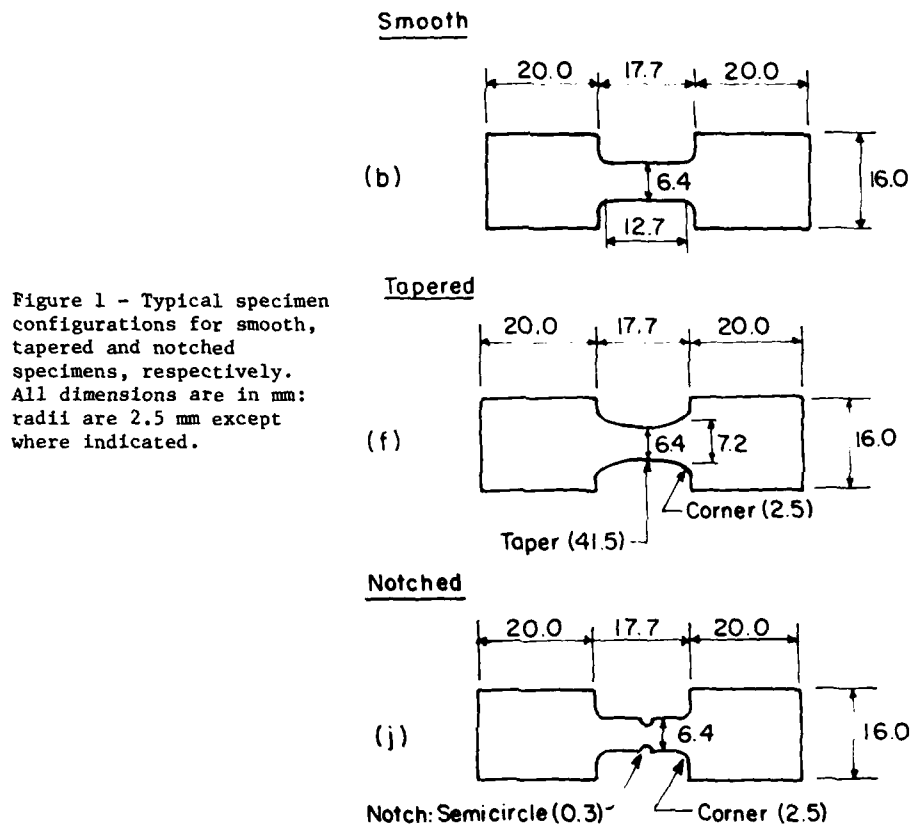


Figure 1 - Typical specimen configurations for smooth, tapered and notched specimens, respectively. All dimensions are in mm: radii are 2.5 mm except where indicated.

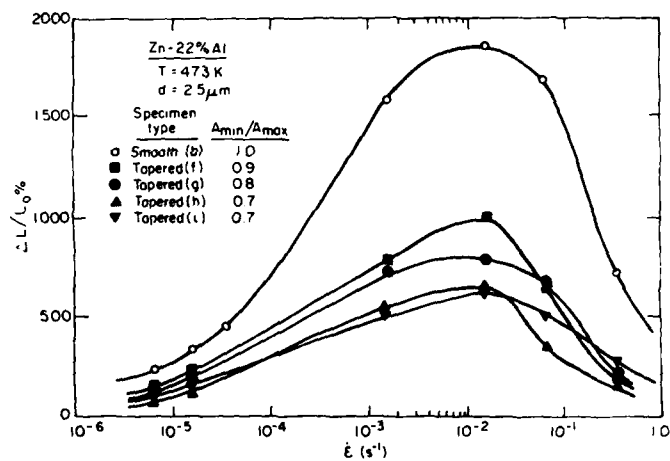


Figure 2 - Elongation to failure versus initial strain rate for smooth and tapered specimens.

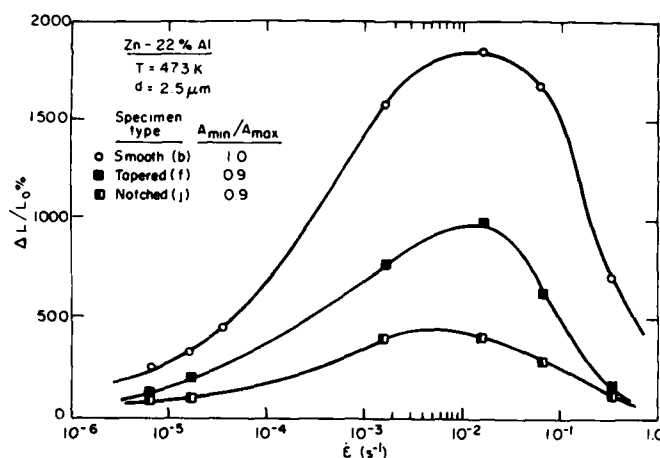


Figure 3 - Elongation to failure versus initial strain rate for smooth, tapered and notched specimens.

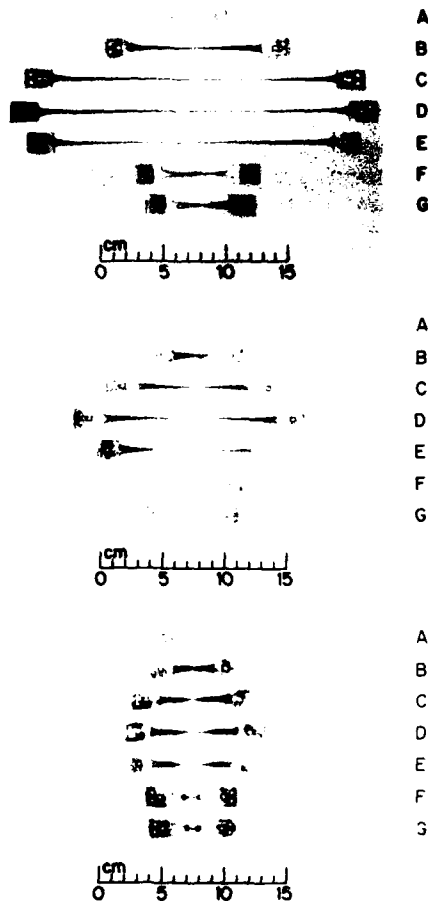
$$\sigma = B\dot{\epsilon}^m \quad (1)$$

where  $B$  is a constant and  $m$  is the strain rate sensitivity. It is well established that the logarithmic relationship between  $\sigma$  and  $\dot{\epsilon}$  is sigmoidal for Zn-22% Al tested under the present experimental conditions, with  $m \approx 0.5$  at intermediate strain rates in the vicinity of  $10^{-2} \text{ s}^{-1}$  (region II) and  $m \approx 0.2$  at both slower (region I) and faster (region III) strain rates [6]. Since there is both an experimental [7] and a theoretical [8] correlation between the elongation to failure and the value of  $m$ , it follows that the elongations are a maximum in region II and there are decreases in the elongations to failure in regions I and III. The maximum elongation recorded for the smooth configuration in Fig. 2 is  $<2000\%$  under optimum conditions, and this contrasts with an earlier report on the same alloy, using the same testing temperature and grain size, where the maximum elongation was  $\sim 2900\%$  in region II [4]. This difference arises because the early work was conducted using specimens with a gauge length of 6.35 mm and the present experiments used a gauge length of 12.7 mm. When tests were conducted in the present investigation using a gauge length of 6.35 mm, the maximum elongation to failure was also increased to  $\sim 2900\%$ .

An examination of Fig. 2 shows that the presence of a taper in the gauge length leads to significant decreases in the overall ductilities at all strain rates. In region II, the maximum elongation is reduced to  $\sim 1000\%$  for specimen type (f) with  $A_{\min}/A_{\max} = 0.9$ , and it is further reduced to  $\sim 640\%$  for specimen type (h) with  $A_{\min}/A_{\max} = 0.7$ . However, the difference between the two tapered profiles having  $A_{\min}/A_{\max} = 0.7$ , specimen types (h) and (i), is fairly minor.

Figure 3 provides a direct comparison between the tapered and notched profiles, and it is clear that the elongations to failure are very much reduced when there is a notch in the gauge length. The profile of the notched specimens of type (j) is shown in Fig. 1. These specimens contained a concentrated neck in the middle of the gauge length, in the form of a notch having a radius of 0.3 mm, so that  $A_{\min}/A_{\max} = 5.9/6.4 \approx 0.9$ . The maximum recorded elongation to failure for specimens of type (j) was  $\sim 420\%$ . Thus, although the specimens of types (f) and (j) have the same values of  $A_{\min}/A_{\max}$ , the elongations to failure are higher at all strain rates when

Figure 4 - Appearance of smooth specimens of type (b) (upper), tapered specimens of type (f) (center), and notched specimens of type (j) (lower). The specimens labelled A are untested and the specimens labelled B to G were pulled to failure at initial strain rates of  $3.33 \times 10^{-1}$ ,  $6.67 \times 10^{-2}$ ,  $1.67 \times 10^{-2}$ ,  $1.67 \times 10^{-3}$ ,  $1.67 \times 10^{-5}$  and  $6.67 \times 10^{-6} \text{ s}^{-1}$ , respectively.



the area difference is gradual within the gauge length (as in a taper) compared with when it is concentrated (as in a notch).

The appearance of the specimens is shown in Fig. 4 for the three configurations given in Fig. 1: smooth type (b) (upper), tapered type (f) (center) and notched type (j) (lower). The specimens labelled A are untested, and the other specimens were pulled at initial strain rates decreasing from  $3.33 \times 10^{-1} \text{ s}^{-1}$  for the specimens labelled B to  $6.67 \times 10^{-6} \text{ s}^{-1}$  for the specimens labelled G, respectively.

For the smooth profile, the fractured specimens in Fig. 4 have pulled out reasonably uniformly at the intermediate strain rates in region II (specimens C to E) but there is evidence for necking in specimens F and G tested at the lower strain rates in region I. For the tapered specimens, there is evidence for the development of non-uniform deformation associated with the presence of the taper. This non-uniformity is visible in all of the tapered specimens taken to fracture in Fig. 4 but it is especially apparent in specimens B, F and G. From the lower photograph in Fig. 4, it is clear that the introduction of a pre-machined notch into the gauge length

leads to a very sharp concentration of plastic deformation within the region of the notch. When tested in region II, the notched region behaves as a very short tensile specimen and it pulls out to a thin point as in specimens D and E.

#### Conclusions

1. The introduction of a taper into the gauge length of the superplastic Zn-22% Al alloy leads to a significant decrease in the overall elongations to failure at all strain rates. The fracture elongations decrease at any initial strain rate as the ratio  $A_{\min}/A_{\max}$  decreases, where  $A_{\min}$  and  $A_{\max}$  are the minimum and maximum cross-sectional areas within the gauge length, respectively. The fracture elongations are essentially independent of the precise value of  $A_{\min}$ .

2. The introduction of a notch into the gauge length leads to a further significant reduction in the elongations to failure at all strain rates, even by comparison with tapered specimens having the same value of  $A_{\min}/A_{\max}$ . For the notched specimens, there is a sharp concentration of the plastic deformation within the region of the notch.

#### Acknowledgement

This work was supported in part by the National Science Foundation under Grant No. DMR-8503224.

#### References

1. W.B. Morrison, "The Elongation of Superplastic Alloys", Trans. Met. Soc. AIME, **242** (1968) 2221-2227.
2. T. Hatayama and O. Izumi, "Deformation Behaviours of an Al-33Cu Superplastic Material with Non-Uniform Cross-Sections", J. Japan Inst. Metals, **45** (1981) 1326-1332.
3. T. Tozawa, H. Kato, Y. Takayama, N. Furushiro and S. Hori, "Influence of Notch Shape on Elongation in a Sn-Pb Superplastic Alloy", J. Japan Inst. Metals, **49** (1985) 614-619.
4. H. Ishikawa, F.A. Mohamed and T.G. Langdon, "The Influence of Strain Rate on Ductility in the Superplastic Zn-22% Al Eutectoid", Phil. Mag., **32** (1975) 1269-1271.
5. F.A. Mohamed, M.M.I. Ahmed and T.G. Langdon, "Factors Influencing Ductility in the Superplastic Zn-22 Pct Al Eutectoid", Metall. Trans., **8A** (1977) 933-938.
6. T.G. Langdon, "Experimental Observations in Superplasticity", Superplastic Forming of Structural Alloys, ed. N.E. Paton and C.H. Hamilton (Warrendale, PA: The Metallurgical Society, 1982), 27-40.
7. D.A. Woodford, "Strain-Rate Sensitivity as a Measure of Ductility", Trans. ASM, **62** (1969) 291-293.
8. F.A. Nichols, "Plastic Instabilities and Uniaxial Tensile Ductilities", Acta Met., **28** (1980) 663-673.

THE RELATIONSHIP BETWEEN STRAIN-RATE  
SENSITIVITY INDEX AND STRAIN IN SUPERPLASTICITY

Chen Hechun      Yang Zhenheng

Department of Materials Science and Engineering  
Northwestern Polytechnical University  
Xian, Shaanxi, PRC

Abstract

The relation of strain-rate sensitivity index  $m$  to strain in H62 brass and TC9 titanium alloys has been studied. The value of  $m$  is strain-dependent, after the maximum  $m$  value, the  $m$  value decreases with strain. It is showed that there are different mechanisms at different stages of deformation for the effect of cavities. The cavity nucleation and growth have been discussed. The Mclean's mistakes about the cavity nucleation have been corrected. The formulas of cavity nucleation and growth and critical strain are derived. The theories correspond with experiments not only in qualitative, but also in quantitative analysis. The model proposed can explain satisfactorily the follows phenomena: the cavity nucleation at boundaries and at particles; the cavity elongation in direction perpendicular to the tensile axis; the formation of neck; the effects of hydrostatic pressure on cavity growth and the exterior tensile stress on cavity alignment.

Superplasticity and Superplastic Forming  
Edited by C.H. Hamilton and N.E. Paton  
The Minerals, Metals & Materials Society, 1988



## Introduction

Recently, interest in superplasticity focused on its applications and changes of structure and properties in superplastic deformation. Recent studies have demonstrated that even a small volume fraction of cavities can lead to a serious deterioration in the mechanical properties of superplastically formed components (1,2). It is necessary to propose the model about the relation of the changes structure and properties in superplastic deformation to the cavity nucleation and growth. In Mclean's formulas(3) only the volume elastic energy of voids was considered. In fact, it has been shown that during superplastic deformation, cavities form at the dislocation pile-up boundaries and particles and the effect of dislocation pile-up stress on cavity nucleation is greater than that of volume elastic energy of cavity. Therefore the relaxation of dislocation pile-up stress would be considered.

## Experimental Details

The nominal compositions of two alloys, H62 brass and TC9 titanium alloy, were supplied in form of 100mm dia, form which uniform bars were produced by hot forging. Tensile specimens, 5 mm dia by 35 mm gauge length were machined after annealed. Both constant crosshead-speed tests and variable crosshead-speed tests were conducted at the temperature 750°C and 900°C (H62 brass at 750°C, TC9 alloy at 900°C) by using Instron 1195 and Instron 1122 Testing Machine. during testing the temperature was kept constant within  $\pm 1K$ , variable-speed tests were carried out by straining a single specimen through a sequence of crosshead speed range 0.02-2 mm min<sup>-1</sup> in cycle, speed was then increased by a factor 2.0 - 2.5.

## Results

Typical sets of curves relations of strain to  $m$  in both constant-speed and variable-speed tests are shown in Fig 1-2.

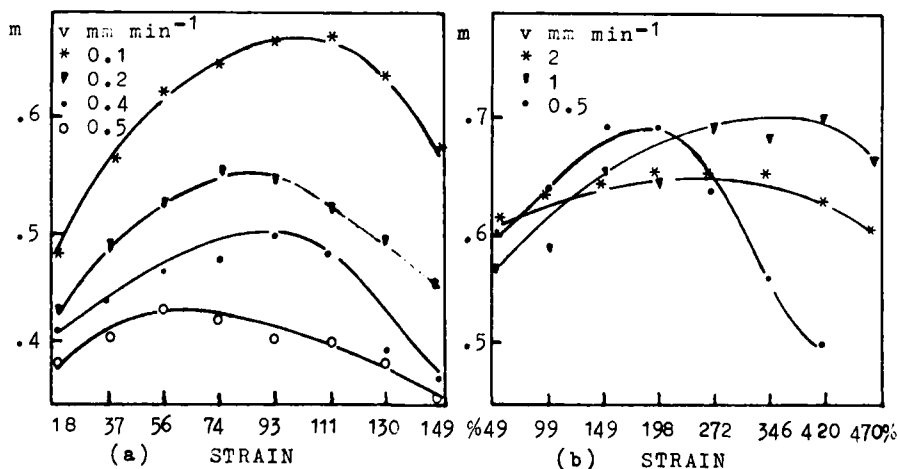


Fig 1. The relation of  $m$  value to strain in cycles variable crosshead-speed. (a) H62 brass, (b) TC9 alloy.

Over a wide range of strain rate both alloys showed a distinct peak. It is also apparent that strain-rate sensitivity index  $m$  is strain-dependent and the changes of  $m$  value concern with the structure and properties in metal superplastic deformation. A lot of cavities were observed at the fracture surface of H62 brass specimens Fig. 3.

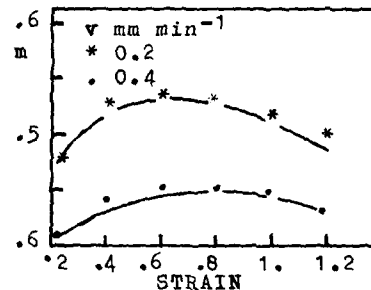


Fig.2. The curves of  $m$ - $\epsilon$  in H62 brass in constant speed



Fig.3. The cavities of H62 brass at fracture surface.

#### Discussions

The  $m$  value of the alloys in superplasticity depends not only on strain-rate; grain size; temperature, but also to a certain degree on strain, so it is difficult to ascertain the elongation of the materials in superplasticity only according to the initial  $m$  value in deformation. Fig.1 (a) and (b) illustrate that almost the same initial  $m$  value of H62 and TC9, since the effect of strain on  $m$  value for H62 brass is stronger than that for TC9 alloy, the specimens of H62 brass fractured much earlier than that of TC9. A lot of cavities were observed in H62 brass specimens after superplastic deformation. It is clear that varies of  $m$  value with strain concern with the cavity nucleation and growth.

#### Cavity Nucleation and Growth

In plastical deformation, because of the nonconservation motion of grain boundary dislocation (GBD) and grain boundary slip (GBS), a lot of supersaturated vacancies are produced, they are thermodynamic unstable defects and tend to precipitate into cavities under the action of dislocation pile-up stress at boundaries or particles. Suppose cavity nucleus are spherical, the changed free energy can be written:

$$W = 4R^2\gamma\pi - LSr^2/G - (4R^3\pi kT\ln C/C_e)/3b^3 \quad (1)$$

R is radius,  $\gamma$  is surface energy,  $\tau$  is shearing stress, G is elastic modulus, L is length of dislocation pile-up, S is area of slip plane, b is Burger's Vector, T is temperature, K is Boltzman's constant, C is vacancy density,  $C_e$  is equilibrium vacancy density. According to the publication (4), we suppose:  $C = C_e + B\varepsilon$ , B is constant,  $\varepsilon$  is strain. The critical radius  $R^*$  and critical nucleation energy  $W^*$  can be express:

$$R^* = 2b^3\gamma \ln(C/C_e)/kT \quad (2)$$

$$W^* = 4\gamma\pi/3(2b^3\gamma/(kT\ln C/C_e))^2 - LSr^2/G \quad (3)$$

while  $W^*=0$  all the nucleus with  $R \geq R^*$  will grow spontaneously, then critical strain ( $\varepsilon^*$ ) can be also estimated from:

$$\varepsilon^* = (\exp(2b^3\gamma(4G\gamma\pi/3LS)^{-1/2}/\tau kT) - 1)/B \quad (4)$$

If  $\tau = 8 \times 10^8 - 6 \times 10^7$  Pa,  $C/C_e = 1.05 - 2$ , the nucleation of cavities will be possible. If the coordinate origin is at cavity nuclear, exterior stress is there equiaxed tensile stress, average stress is  $\bar{\sigma}$ , the differential value of tangential stress ( $\sigma_e$ ) and radius stress ( $\sigma_r$ ) could be written:

$$\sigma_e - \sigma_r = \sigma(R/r)^2 \quad (5)$$

r is radius coordinate, The differential stress value result in differential migration rate of vacancies or atoms to tangent and to radius in the same manner as N-H creep. If  $r = 3R$ , the average differential stress value ( $\bar{\sigma}$ ) and the migration rate of vacancies to cavities can be expressed by:

$$\bar{\sigma} = 1/2R \int_R^{3R} (\sigma R^2/r) dr = \sigma/3 \quad (6)$$

$$I = A D (1 - \exp(-H/kT)) \quad (7)$$

A is constant, D is the diffusion coefficient. H is free energy changed by  $\bar{\sigma}$ , we could write the growth rate of cavities (dV/dt):

$$dV/dt = 4DR^2\pi\Omega(\sigma/3 + h\varepsilon / -3\gamma/R)/kT \quad (8)$$

$\Omega$  is the atomic volume, h is constant,  $\gamma$  is surface energy. In fact, because the difference of every tensile axis stress ( $\sigma_x \sigma_y \sigma_z$ ) causes differential migration rate, the cavities tend to be elongated along the tensile axis. For the interaction of surface tensile stress ( $\gamma$ ) of cavity and exterior stress ( $\sigma_x \sigma_y \sigma_z$ ), the atoms nearby cavities diffuse from the direction perpendicular to the tensile axis to the direction parallel to the tensile axis. Finally the interlinkage of cavities in a direction perpendicular to the tensile axis and neck could be observed. The tensile stress will be of advantage to cavity growth, the hydrostatic pressure can be of no

advantage to cavity growth. The higher strain rate (or tensile stress), the greater effect on the cavity shape and alignment.

#### The Relation of m Value to Cavity

The change of m value during deformation shows that are different deformation mechanisms at different stages of deformation. In initial deformation, the m value increasing with strain could be explained by the ratio of diffusion creep increasing with strain, it is because as the strain increase, nonconservative motion of dislocation increases the free supersaturated vacancies which are of great advantage to diffusion creep and GBD. However, after the maximum m value, most of the free supersaturated vacancies precipitate into cavities. Actually free supersaturated vacancies in metal, the both ratio of diffusion creep and GBS decrease, for the cavity nucleation and growth affect the continuity of GBS, the climb of GBD and atom diffusion. Therefore, m value decreases with strain after maximum m value. If critical strain is correspond to maximum m value, the strain correspondent maximum m value can be expressed equ.(4). It can be seen from equ.(4) that strain correspondent maximum m value depends on the surface energy of materials, exterior shear stress and grain size. If  $h=0.0049$ , the values of calculated critical strain from equ. (4) correspond with that of experiment strain correspondent maximum m value in publication (5).

#### Conclusions

The m value is significantly dependent on strain during superplastic deformation. There are different deformation mechanisms at different deformation stages. The changes of m value during deformation relate with the cavity nucleation and growth. The cavity nucleation and growth model proposed can explain satisfactorily the cavity nucleation at boundaries and particles; the interlinkage of cavities in direction perpendicular to the tensile axis; the formation of neck; the effects of hydrostatic pressure on cavity growth and the exterior tensile stress on cavity alignment.

#### References

1. J.Pilling and N.Ridley, "Effect of Hydrostatic Pressure on Cavities in Superplasticity Aluminium Alloys" Acta. Metall. 34 (1986), 669-679.
2. Atul H. Chokshi, "An Experimental Study on the Alignment of Cavities in a Superplastic Commercial Copper Alloy" Metall. Trans. 18A (1987), 63-67.
3. D. Mclean, Mechanical Properties of Metals. (Copyright (c) 1962, by John Wiley & Sons, Inc.) P.334.
4. J. Belzunce, Scr. Metall. 15 (1981), 895-898.
5. C.I.Smith, B.Norgate and N.Ridley; Met. Sci. 5 (1976), 182.

# FACTORS AFFECTING SUPERPLASTIC STABILITY

IN AN Al-Li-Cu-Zr ALLOY

B. Ash\*

Rockwell International/Rocketdyne Division  
Canoga Park, California 91303

C. H. Hamilton

Department of Mechanical and Materials Engineering  
Washington State University  
Pullman, Washington 99164-2920

## Abstract

An analysis of the mechanical behavior of a superplastic Al-Li-Cu-Zr alloy was conducted to understand the geometric stability offered by the material during deformation. In conjunction with this, the microstructural evolution with strain was monitored and found to change with deformation. Analysis of the flow properties from constant and variable strain-rate tensile tests shows that the mechanical parameters reflect the altering microstructure. It was determined that the strain-rate hardening was initially low and increased, while the strain hardening was initially high and decreased with strain. Thus, the material was dependent on strain hardening for necking resistance in the early stages of deformation. Since it was also found that the strain hardening was comparable at all strain rates, it follows that the critical strain rate could be quite high without loss of superplastic ductility, provided that subsequent strain rates correspond to a high strain-rate hardening. Thus, it is the combination of these two parameters that provide the mechanical stability essential for superplastic deformation. From this information, optimum forming parameters could be predicted that would decrease forming time without sacrificing ductility.

\*Work reported herein was accomplished while Ms. Ash was attending graduate school at Washington State University.

Superplasticity and Superplastic Forming  
Edited by C.H. Hamilton and N.E. Paton  
The Minerals, Metals & Materials Society, 1988

### Introduction

A number of alloys based on the composition of Al-Li-Zr have been shown to be superplastic<sup>(1-6)</sup> either through static recrystallization to a fine, stable grain size prior to deformation, or dynamic recrystallization during deformation. Alloys displaying the latter, reportedly undergo structural coarsening during initial deformation with a corresponding increase in misorientation angle.<sup>(6,7)</sup> This leads to a continuous evolution from subgrains to grains.

Previous work on an Al-Li-Cu-Zr alloy indicates that both static and dynamic recrystallization occur.<sup>(3)</sup> However, the strain hardening and strain-rate hardening have not yet been studied in detail, as they relate to the microstructural evolution during superplastic deformation. Since it is to be expected that these properties will reflect the changing microstructure, a study was conducted to (1) determine the flow properties for a warm-worked and unrecrystallized Al-Li-Cu-Zr alloy and (2) assess their relationship to the development of necking resistance, which is necessary for achieving superplastic deformation.

### Experimental

The Al-2.4Li-2.6Cu-0.2Zr alloy utilized in this study was provided by Reynolds Aluminum Company and was specifically processed for superplastic forming.<sup>(4)</sup> Specimens with a 1.27-cm gage length was machined from a single sheet for superplastic tensile testing in the as-received condition.

Tensile tests were conducted on an Instron testing machine that was interfaced with a computer to provide complete control of the crosshead velocity.<sup>(8)</sup> Superplastic temperature was maintained to within  $\pm 2^\circ\text{C}$  in a 10-inch range by a 3-zone split furnace; heatup time to  $500^\circ\text{C}$  took an average of 25 minutes.

Constant strain-rate tests were conducted over a range of strain rates from  $10^{-4}$  to  $2 \times 10^{-2} \text{ sec}^{-1}$  and test temperatures from  $450$  to  $510^\circ\text{C}$ . Since the test condition was that of constant strain rate, the flow stress changes were due to hardening only and not a result of strain-rate variations. The strain hardening exponent ( $n$ ) and hardening parameter,  $\gamma (=1/\sigma \cdot \partial\sigma/\partial\epsilon)$ <sup>(9)</sup> were calculated as a function of strain directly from the stress-strain data. Determination of the strain-rate sensitivity was conducted from jump strain-rate tests in a manner reported previously.<sup>(8)</sup>

Thin foil specimens were made for observation under a Transmission Electron Microscope (TEM) from a variety of strain rate and strain conditions as well as select time at temperature conditions. Primary thinning to a thickness of 0.13 mm was conducted mechanically on both sides of the specimen. Disks, 2.175 mm in diameter, were punched from the thinned sheet and jet thinned with a Metal Thin Jet Thinner in a 20% nitric acid in methanol solution at  $-15^\circ\text{C}$ . TEM was employed using a Hitachi Model H-600 Microscope to monitor the structural evolution with strain. From TEM, the structure size was determined for various thermal exposure and deformation conditions. However, measurements reflect the intercept distance between boundaries without distinguishing whether they are high or low angle (i.e., grain or subgrain) boundaries.

### Results and Discussion

It was found that each strain rate results in comparable strain hardening exponents ( $n$ ) during the initial stages of deformation.<sup>(8)</sup> The initial  $n$  ranges from 0.41 at a strain rate of  $10^{-4} \text{ sec}^{-1}$  to 0.3 at a strain rate of  $2 \times 10^{-2} \text{ sec}^{-1}$ . Hardening diminishes after this, and the flow stress appears to approach a relatively constant value after a strain of approximately 0.5, as shown in Fig. 1. These results imply that mechanical stability offered by strain

hardening is significant and approximately equivalent for each strain rate in the initial stages of deformation. Strain-rate sensitivity is low initially (0.3) and rises with strain to approximately 0.5 to 0.6 depending on the strain rate imposed. This value is maintained after a strain of 0.5 (Fig. 1) for a strain rate of  $0.001 \text{ sec}^{-1}$ . It is therefore clear that there are components of both strain hardening and strain-rate hardening, but their trends with strain are counter to one another. The m-value is low initially, then increases, whereas n is high initially, then decreases. Thus the superplastic stability of this material is initially dependent upon the strain hardening for its necking resistance. This, coupled with the fact that roughly comparable strain hardening was observed at all strain rates, suggests that the initial strain rate can be quite high without loss of superplastic ductility, provided that subsequent strain rates correspond to a high strain-rate sensitivity. Therefore, an instability parameter, "I" ( $= 1 - m - \gamma/m$ )<sup>(10,11)</sup> was determined for a variety of strain rates that incorporate the

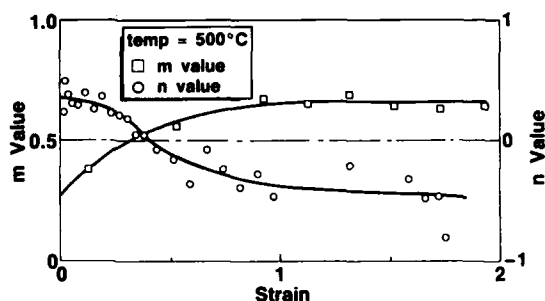


Figure 1 - m and n values vs strain for a strain rate of  $0.001 \text{ sec}^{-1}$ .

effects of both strain and strain-rate hardening on the geometric stability of the material under tension. Since an exponential increase in the growth rate of the neck is shown to occur when "I" rises above 0<sup>(12)</sup>, "I" can be examined as a function of strain to determine the relative stability to be expected from different conditions, such as strain rate (Fig. 2).<sup>(8)</sup> From this, variable strain-rate paths were predicted that optimized superplastic ductility and reduced forming time.<sup>(8)</sup> An example of the relative elongations resulting from the variable strain-rate tests is illustrated by the test samples in Fig. 3.<sup>(8)</sup> The specimen tested at a strain rate of  $2 \times 10^{-2} \text{ sec}^{-1}$  (Fig. 3B) shows significantly less ductility than the specimen tested at  $10^{-3} \text{ sec}^{-1}$  (Fig. 3C). However, when the strain rate is reduced from a constant strain rate of  $2 \times 10^{-2}$  to a constant strain rate of  $10^{-3} \text{ sec}^{-1}$  at a strain of 0.74 (Fig. 3D), the high ductility is retained. Therefore, by imposing a variable strain rate path, the testing time was decreased from 35 to 20 minutes with no sacrifice in ductility.

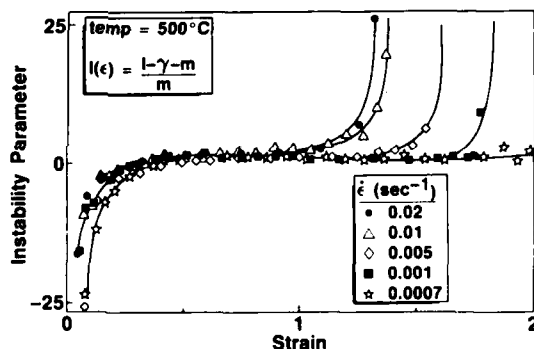


Figure 2 - Instability parameter vs strain rates between  $0.02$  and  $0.001 \text{ sec}^{-1}$ .

The microstructural evolution was monitored in order to understand the mechanical behavior during superplastic deformation. The alteration of the as-received material with time at temperature as well as the microstructural changes with deformation were observed through TEM.

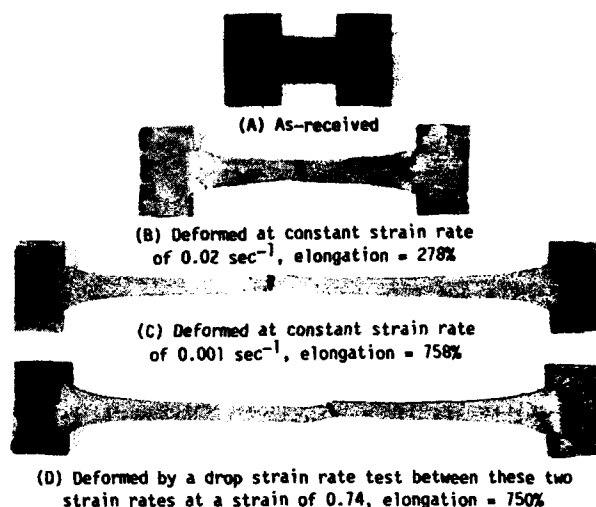


Figure 3 - Tensile specimens.

The as-received material (Fig. 4) is heavily dislocated and the size of the structure was determined to be  $0.8 \mu\text{m} \pm 0.2$ . The effects of static annealing on the size of the structure is observed in Fig. 5 where a sample was held at  $500^\circ\text{C}$  for 1 hour and water quenched. There is a coarsening of the structure to approximately  $2 \mu\text{m} \pm 0.2$  with no evidence of dislocation activity. The grain size was constant up through 4 hours at temperature, and after 8 hours, increased to 4 to  $5 \mu\text{m}$ .



Figure 4 - TEM of as-received material heavily dislocated with size of structure at  $0.8 \mu\text{m} \pm 0.2$ .



Figure 5 - TEM of specimen statically annealed at  $500^\circ\text{C}$  for 1 hour, average grain =  $2 \mu\text{m} \pm 0.2$ .

Deformation substantially altered the microstructure from that of static conditions, which is consistent with previous observations of superplastic materials. This is seen in a plot between grain size versus exposure time for static and deformation conditions (Fig. 6). Grain size is approximately equivalent at 2.5 to  $3.0 \mu\text{m}$  for strain rates between  $0.02$  and  $0.0001 \text{ sec}^{-1}$  at the start of deformation.



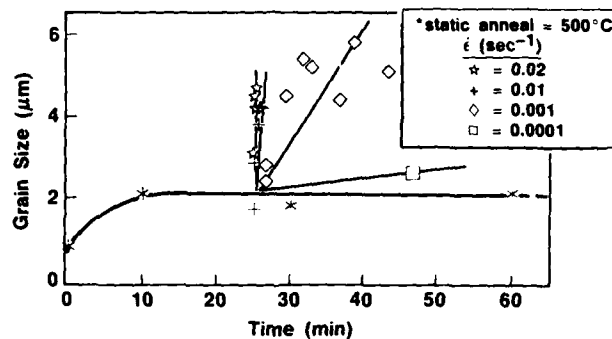


Figure 6 - Grain size vs exposure time for static and deformation conditions.

Figure 7 is a plot of grain size versus strain for various constant strain rates between 0.02 and 0.0001  $\text{sec}^{-1}$ , which indicates that the grain size is less than 3.0  $\mu\text{m}$  up through strains of 0.1. By a strain of 0.2, it increases to about 4.5  $\mu\text{m}$  and remains fairly constant through strains of 0.9 to 1.0. Above this strain, differences were seen to emerge between strain rates. At a strain rate of 0.02  $\text{sec}^{-1}$ , there was no significant change. However, strain rates between 0.001 and 0.0001  $\text{sec}^{-1}$  resulted in an increase in grain size to 5 microns after a strain of 1.2.

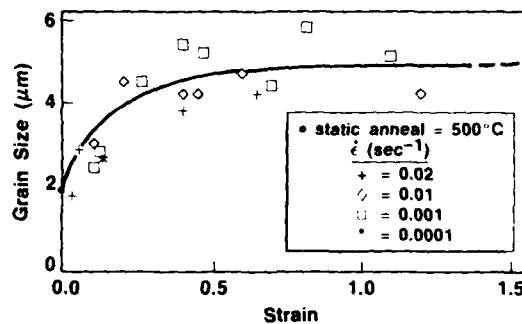


Figure 7 - Grain size vs strain for constant strain rates between 0.02 and 0.0001  $\text{sec}^{-1}$ .

The mechanical behavior and microstructural evolution are interrelated as observed in Fig. 8 where the strain-rate sensitivity, strain hardening, and grain size are plotted together versus strain for a strain rate of 0.01  $\text{sec}^{-1}$ . Strain-enhanced grain growth up through strains of 0.4 correlates with the observed strain hardening in the early stages of deformation. Stable grain size after this point corresponds to the diminished strain hardening and stable strain-rate sensitivity.

#### Conclusions

1. Initial strain hardening is important in the development of superplastic ductility in the alloy under consideration.
2. An "instability parameter" that considers both  $m$  and  $\gamma$  provides good indication of the relative tensile stability and shows equivalent necking resistance for all strain rates through strains of 1.0.

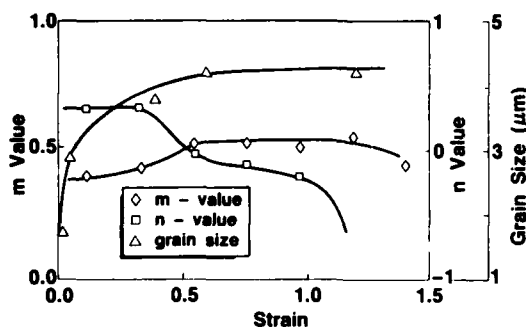


Figure 8 - Strain rate sensitivity, strain hardening exponent, and grain size vs strain rate of  $0.01 \text{ sec}^{-1}$ .

3. A high strain rate can be imposed initially to strains of approximately 1.0, which decreases deformation time without sacrificing ductility.
4. The mechanical behavior was seen to reflect the microstructural evolution during deformation.

#### Acknowledgement

Work reported herein was conducted through grants from Washington State University and General Dynamics, Fort Worth Division under the direction of Charles Heikkenen. Appreciation is also extended to Benny Ward of Reynolds Aluminum Company for providing the sheet materials.

#### References

1. Wadsworth, J., Superplastic Forming, S.P. Agrawal, ed. ASM, 32 (1985).
2. Grimes, R., Superplasticity, B. Baudalet and M. Suery, eds., Centre National de la Recherche Scientifique, Paris, 13.1 (1985).
3. Chokshi, A. H., J. Wadsworth, and A. K. Mukherjee, Scripta Metall., 21, 1347 (1987).
4. Navrotsky, G. and B. R. Ward, paper presented at the Conference on Al-Alloys, University of Virginia (June 1986).
5. Wadsworth, J., C. A. Henshall, and T. S. Nieh, Aluminum-Lithium Alloys III, C. Baker, P. J. Gregson, S. J. Harris, and C. J. Peel, eds., The Institute of Metals, London, p. 199 (1986).
6. Ghosh, A. K. and C. Gandhi, Strength of Metals and Alloys 3, J. P. Bailon, H. J. McQueen, J. I. Dickinson, J. J. Jonas, and M. G. Akben, eds., Pergamon Press, p. 2065 (1986).
7. Nes, E., Superplasticity, B. Baudalet and M. Suery, eds., Editions Du Centre National de la Recherche Scientifique, Paris, p. 7.1 (1985).
8. Ash, B. and C. H. Hamilton, Scripta Metall., 22, 277 (1988).
9. Hart, E. W., Acta Metall., 15, 415 (1984).
10. Nichols, F. A., Acta Metall., 28, 663 (1980).
11. Caceres, C. H. and D. S. Wilkinson, Acta Metall., 32, 415 (1984).

# EFFECT OF GRAIN SIZE ON REGION TRANSITION BEHAVIOR

## IN SUPERPLASTIC DEFORMATION

Jianzhong Cui, Qinling Wu and Longxiang Ma

Department of Metals Forming, Northeast  
University of Technology, Shenyang, P.R.C

### ABSTRACT

An essential phenomenon in superplastic deformation—region transition is studied in this paper. Experimental and theoretical analyses were made to search into the reason and conditions of the transition. It is suggested that the region transition is caused by the change of the deformation mechanisms. Effects of grain size, temperature on the transition behaviors were worked out. The conditions for superplasticity were studied which can be represented by some new concepts—critical grain size and critical temperature.

Key words: superplastic deformation, region transition, grain size, temperature.

*Superplasticity and Superplastic Forming*  
Edited by C.H. Hamilton and N.E. Paton  
The Minerals, Metals & Materials Society, 1988

### Introduction

The variation of  $\lg \dot{\epsilon}$  with  $\lg \dot{\epsilon}$  is sigmoidal in superplastic deformation ( $\dot{\epsilon}$  is stress,  $\dot{\epsilon}$  is strain rate). The curve was divided into three regions. Many experiments showed that the main deformation mechanism in each region is different from that in the others. The main mechanism in region II is grain boundary sliding, that in region III is dislocation creep and that in region I is diffusion creep. So far, many theories have been proposed to explain the behaviour in region II. little effort has been made to study the region transition though it is of great importance to the theory and application of superplasticity (1). In this paper, we will discuss the conditions of the region transition. Emphasis is put on the effects of grain size on the region transition strain rate.

### Experiments

The chemical composition of the alloy used in this investigation is as follows:

Zn	Mg	Mn+Cr+Ti	Fe	Si	Al	Wt%
4--5	2-3	—0.5	<0.15	<0.1	BAL.	

The alloy was processed by thermomechanical treatment. Ingots were hot rolled at 400 °C into plates 10 mm thick. Then the plates were solution treated at 480 °C, overaged at 350--400 °C for 0--48h, given a 50--95% cold rolling reduction and annealed in a salt bath at 480 °C for 20--720 min. After the above processing the grain size of the alloy ranged from 9.4 to 32  $\mu\text{m}$ , aspect ratio was 1.1--7.5.

The grain size measurements were performed by the line intercept method on a microscope. The grain size,  $d$ , was calculated by

$$d = 3 ( 2H^{-1} + W^{-1} )^{-1}$$

where  $H$  is the grain size in the longitudinal (rolling) direction and  $W$  is that in the short transverse direction.

Specimens of aspect ratio  $R$  less than 1.17 were used in studying the effects of grain size to avoid interference of grain shape. The Backfen method (2) was used to measure  $m$  values. The contribution of each mechanism to the total strain was measured by the method suggested by K. Matsuoka (3)

### Results and discussion

#### The essence of region transition

There is a multiple mechanism effect in superplastic deformation. The total strain rate,  $\dot{\epsilon}_t$ , could be represented by the sum of strain rates of three mechanisms, diffusion creep (D.C), grain boundary sliding (G.B.S) and dislocation creep (d.c). So the total strain is given by (4)

$$\dot{\epsilon}_t = \dot{\epsilon}_{dc} + \dot{\epsilon}_{gbs} + \dot{\epsilon}_{dc} \quad (1)$$

Detailed measurements and analyses confirmed that strain rates of these mechanisms, which cooperate in superplastic deformation, could be expressed respectively by (4)

Diffusion creep:

$$\dot{\epsilon}_{dc} = A_1 \bar{\sigma} / k T d^2 \exp(-Q_L / RT) \quad (2)$$

Grain boundary sliding:

$$\dot{\epsilon}_{gbs} = A_2 \bar{\sigma}^2 / k T d^2 \exp(-Q_{gb} / RT) \quad (3)$$

Dislocation creep:

$$\dot{\epsilon}_{dc} = A_3 \bar{\sigma}^{4.5} / k T \exp(-Q_L / RT) \quad (4)$$

where  $A_1, A_2$  and  $A_3$  are constants,  $\bar{\sigma}$  is stress,  $d$  is grain size,  $Q_L$  is activation energy for lattice diffusion,  $R$  is the gas constant,  $Q_{gb}$  is the activation energy for grain boundary diffusion,  $T$  is the absolute temperature and  $k$  is Boltzmann's constant.

If  $\lambda_{dc}$ ,  $\lambda_{gbs}$  and  $\lambda_{dc}$  are used to represent contributions of diffusion creep, grain boundary sliding and dislocation creep to the total strain respectively, then

$$\lambda_{dc} = \dot{\epsilon}_{dc} / \dot{\epsilon}_t, \quad \lambda_{gbs} = \dot{\epsilon}_{gbs} / \dot{\epsilon}_t$$

$$\lambda_{dc} = \dot{\epsilon}_{dc} / \dot{\epsilon}_t$$

An equation was deduced to calculate the  $m$  value in superplastic deformation (4).

$$m = (1 - \bar{\sigma}_0 / \bar{\sigma}) / (\lambda_{dc} + 2 \lambda_{gbs} + 4.5 \lambda_{dc}) \quad (5)$$

where  $\bar{\sigma}_0$  is the threshold stress.

Contribution of each mechanism to the total strain ( $\lambda_{dc}$ ,  $\lambda_{gbs}$ ,  $\lambda_{dc}$ ) changes with change of deformation conditions because  $\dot{\epsilon}_{dc}$ ,  $\dot{\epsilon}_{gbs}$  and  $\dot{\epsilon}_{dc}$  have different dependence on  $\bar{\sigma}$ ,  $T$ , and  $d$ , therefore the  $m$  value changes correspondingly with change of  $\bar{\sigma}$ ,  $T$  and  $d$ . The experimental results in this study are shown in Fig 1.  $\lambda_{dc}$  and  $\lambda_{gbs}$  increase and  $\lambda_{dc}$  decreases with decrease of the strain rate. When a certain strain rate,  $\dot{\epsilon}_{c2}$ , is reached  $\lambda_{dc} = \lambda_{gbs} = 1/2$  and  $\lambda_{dc} = 0$ ,  $\bar{\sigma}_0$  is much smaller than  $\bar{\sigma}$  so  $\bar{\sigma}_0 / \bar{\sigma} = 0$ . Inserting these values into Equation (5) we obtain  $m = 0.3$ . We define the strain rate,  $\dot{\epsilon}_{c2}$ , as the transition strain rate between region II and region III. In low strain rate,  $\lambda_{dc} = 0$ ,  $\lambda_{dc}$  increases with decreasing

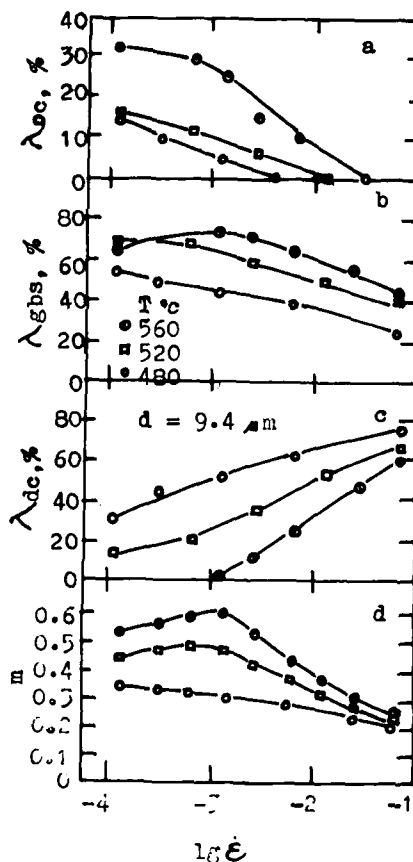


Fig.1. Dependence of  $\lambda_{dc}$  (a),  $\lambda_{gbs}$  (b),  $\lambda_{dc}$  (c) and  $m$  (d) on strain rate.

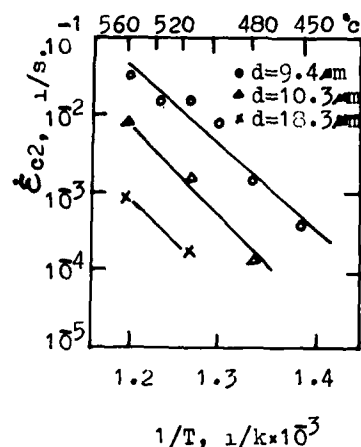


Fig. 2. Dependence of  $\dot{\epsilon}_{c2}$  on temperature.

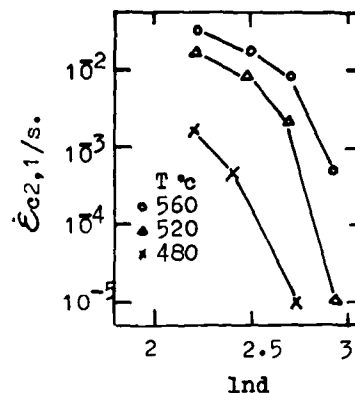


Fig. 3. Dependence of  $\dot{\epsilon}_{c2}$  on grain size.

strain rate. When  $\dot{\epsilon}_t = \dot{\epsilon}_{c1} \cdot \lambda_{oc} = gbs = 1/2$ , the strain rate decreases again, diffusion creep becomes the main mechanism. Then we define  $\dot{\epsilon}_{c1}$  as the transition strain rate between region I and region II. In region I  $\dot{\epsilon}_{c1}$  increases with decreasing strain rate because the efficiency of grain boundaries serving as source and sink for vacancies lowers, so that  $m$  drops. The above discussion shows that the region transition is caused by the change of the main mechanism.

#### Effect of grain size on region transition

An essential requirement for superplasticity is fine grain size, therefore grain size also have a strong effect on the behavior of the region transition. When the transition between region II and region III occurs,  $\dot{\epsilon}_{dc} = \dot{\epsilon}_{gbs} = \dot{\epsilon}_t / 2$ . Combining Equations (3) and (4), we obtain

$$\dot{\epsilon}_{c2} = 2A_2 / A_3 d^{-5/2} \exp((-9/5 Q_{gb} - 4/5 Q_L) / RT) = A_{c2} d^{-5/2} \exp(-Q_{c2} / RT) \quad (6)$$

This equation shows that  $\dot{\epsilon}_{c2}$  decreases with the increase in grain size and decrease in temperature. The dependence of  $\dot{\epsilon}_{c2}$  on grain size and temperature were measured as shown in Fig. 2 and 3. The measured results are identical to the theoretical predictions. In the same way the transition strain rate between region I and region II can be derived.

$$\dot{\epsilon}_{c1} = A_{c1} d^{-2} \exp(-Q_{c1} / RT) \quad (7)$$

$\dot{\epsilon}_{c1}$  decreases with increasing grain size and decreasing temperature. The  $\dot{\epsilon}_{c1}$  was not measured because of the limitation of the strain rate range of the testing machine.

Upon careful examination of Equations (6) and (7), one will find that  $\dot{\epsilon}_{c1}$  and  $\dot{\epsilon}_{c2}$  have different dependence on grain size. When  $d = d_c$ ,  $\dot{\epsilon}_{c1} = \dot{\epsilon}_{c2}$ . If the  $d$  is larger than  $d_c$ , region II disappears so that the materials don't exhibit superplasticity. We define  $d_c$  as the critical

grain size for superplasticity. Combining Equation (6) and (7) we obtain:

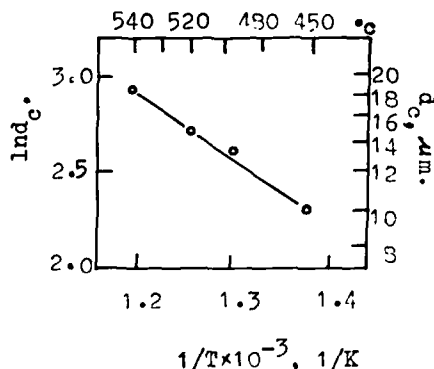


Fig.4. Dependence of  $d_c$  on temperature.

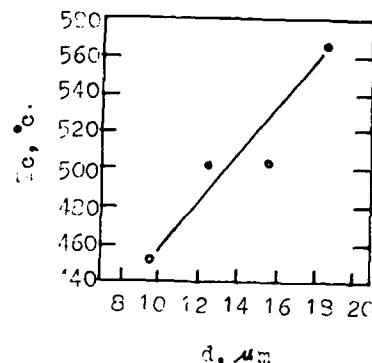


Fig.5. Dependence of  $T_c$  on grain size.

$$d_c = (A_{c2}/A_{c1})^{-\frac{5}{8}} \exp(5(Q_{c2} - Q_{c1})/8 RT)$$

$$= A_c \exp(-Q_c/RT) \quad (8)$$

In the same way we can discuss the effect of temperature. A critical temperature,  $T_c$ , can be deduced as shown in Equation(9). If  $T > T_c$  the materials do not exhibit superplasticity.

$$T_c = Q_c / (R \ln(A_c / d)) \quad (9)$$

The dependence of  $d_c$  on temperature and of  $T_c$  on grain size was measured as shown in Fig.4 and 5. The experimental results are identical to the theoretical predictions.

### Conclusions

1. The region transition in superplastic deformation results from a change of the main mechanism.
2. Grain size and temperature have a strong influence on the region transition. Transition strain rates decrease with increasing grain size and decreasing temperature.
3. There exist a critical grain size,  $d_c$  and a critical temperature,  $T_c$ .  $d > d_c$  or  $T < T_c$  the materials do not exhibit superplasticity.

### References

1. R.C.Gifkings, Superplastic Forming of Structural Alloys, ed by N.E. Paton and C. H.Hamilton, Metallurgical Society AIME,(1982), 3-26.
2. W.A.Backofen, I.R.Turner and D.H.Avery. Superplasticity in an Al-Zn alloy,Trans. ASM, 57 (1964),980.
3. K.Matsuki, N.Hariyama and M.Tokarawa.The role of grain boundary sliding in superplastic deformation, J.Jap.Met.Inst.38,(1974),219-226.
4. Jianzhong Cui and Longxiang Ma, Characteristic parameters in superplastic deformation, Acta Metall.Sin. 24,(1988),B22-26.

INFLUENCE OF UNI- AND BI-AXIAL STRAINING ON CAVITATION IN A  
SUPERPLASTIC ALUMINUM ALLOY

A. Varloteaux, J.J. Blandin and M. Suéry

Institut National Polytechnique de Grenoble  
E.N.S. de Physique de Grenoble  
Génie Physique et Mécanique des Matériaux  
Unité Associée au C.N.R.S. n° 793  
BP 46 - 38402 Saint Martin d'Hères Cedex (FRANCE).

Abstract

This paper investigates uniaxial and biaxial superplastic deformation of 7475 Al-alloys, with particular attention to the effect of superimposed pressure on cavity development. Pressure reduces cavitation but its efficiency depends on the flow hardening behavior of the material which suggests to adapt the testing conditions in order to have always a sufficient  $P/\sigma$  ratio. Pressure, however, does not affect the thickness distribution during bulging which is primarily influenced by the strain rate sensitivity parameter of the material and by the uniformity of temperature in the sheet plane. Precise control of temperature is thus necessary to avoid extensive strain localization and delay fracture of the sheet.

Superplasticity and Superplastic Forming  
Edited by C.H. Hamilton and N.E. Paton  
The Minerals, Metals & Materials Society, 1988



### Introduction

Superplastic high strength aluminum alloys are highly sensitive to cavitation which leads to early fracture by extensive growth and coalescence of voids. Such cavitation is usually characterized by the cavity volume fraction whose variation with strain strongly depends on the stress state applied to the material. This has led to the development of a procedure for cavity suppression by applying superimposed gas pressure during deformation. Critical pressure conditions were thus defined which are not always in agreement with theoretical predictions, depending on material and testing conditions.

The aim of this paper is to present some experimental results dealing with cavitation during uniaxial and biaxial deformation of superplastic 7475 Al-alloy and attention is particularly given to the effect of superimposed pressure.

### Uniaxial deformation

Cavity growth is assumed to be usually controlled by plastic deformation of the matrix and in this case theoretical prediction shows that superimposed pressure equal to  $\sigma/3$  is sufficient to suppress cavity development. Experimental results confirm generally the prediction but sometimes higher pressures seem to be required (1,2). One explanation is the importance of strain-induced nucleation and diffusion controlled growth which need pressures of the order of the flow stress to be completely suppressed. Another source of disagreement can be due to strain-hardening during deformation. Indeed, the value of the necessary pressure is usually determined in comparison with the level of the flow stress at the beginning of the tensile test. If strain hardening occurs during deformation, the as-chosen pressure can become insufficient to suppress cavity growth. Such a situation is presented in figure 1 which compares the cavitation behavior of two superplastic 7475 Al-alloys referred as A and B under atmospheric pressure and under a superimposed pressure of 2 MPa. Alloy A was tested at constant crosshead velocity corresponding to an initial strain rate equal to  $5.5 \cdot 10^{-4} \text{ s}^{-1}$ , close to the optimum condition for superplasticity (3). It has a coarse grain structure and its tensile curve obtained in atmospheric pressure is shown in figure 2. The flow stress at the beginning of deformation is equal to 7 MPa and almost no strain hardening is observed during straining. Figure 1 shows that a pressure of 2 MPa is sufficient to suppress cavitation, which is in agreement with theoretical prediction. Alloy B exhibits a fine grain structure and it was tested at a constant strain rate of  $1.6 \cdot 10^{-3} \text{ s}^{-1}$ , close also to the optimum condition (4).

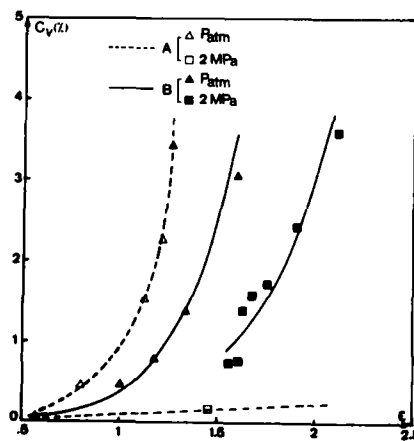


Figure 1 - Variation with tensile strain of cavitation level for two superplastic 7475 Al-alloys.

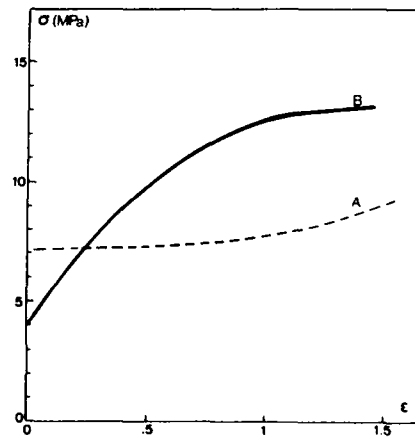


Figure 2 - Stress-strain curves for the two alloys used in uniaxial straining.

The variation with strain of the flow stress is given in figure 2. Despite the greater strain-rate, its flow stress at the beginning of deformation is only 4 MPa but an important hardening occurs during straining. Figure 1 shows that, in this case, a pressure of 2 MPa is not large enough to suppress cavity development. The effect of such a pressure is in fact to shift the strain beyond which the cavitation level becomes important since the applied pressure is only efficient at the beginning of deformation. At large strain, the pressure becomes small compared to the flow stress and the cavity growth rate is almost identical to that observed during tests under atmospheric pressure.

The different hardening behavior of alloys A and B is partly due to the testing conditions (constant crosshead velocity for alloy A and constant strain rate for alloy B) but also to the different behavior of the two alloys in terms of structural evolution. Alloy B is sensitive to strain-induced grain coarsening and this can explain at least partly, the important hardening. Inversely the coarse grain structure of alloy A is more stable during straining and almost no strain hardening occurs. These results suggest that reduction of cavitation can be obtained even with limited pressure levels by adapting the testing conditions in order to maintain a sufficient  $P/\sigma$  ratio.

#### Biaxial tests

Circular sheet bulging tests were performed with alloy B by applying either one-side or two-side gas pressure. A cylindrical vessel was used as the female tool so that the deformed sheet is composed by a portion of a cylinder and half a sphere (as verified by measuring the radius of curvature after forming - see figure 5). The radius of the sheet  $r_0$  is 75 mm and its initial thickness  $e_0$  is 2.13 mm. After forming, specimens were taken along a meridian and thickness and density measurements were carried out to determine the local thickness strain  $\epsilon_3 = \ln[e_0/e]$  and the cavitation level  $C_v$  respectively. Figure 3 shows the results of such measurements for two forming pressures  $\Delta P$ , the back pressure being one atmosphere. The cavitation behavior is similar for both pressures but the cavity volume fraction is increased by about 2 when  $\Delta P$  increases from 0.1 to 0.15 MPa. 0.15 MPa corresponds to an average thickness strain-rate at the pole of  $1.6 \cdot 10^{-3} \text{ s}^{-1}$  corresponding to the optimum conditions for superplasticity whereas for 0.1 MPa, the strain-rate is about  $5 \cdot 10^{-4} \text{ s}^{-1}$ . This result thus shows that cavitation is sensitive to strain-rate, which can be due to the influence of strain-induced nucleation. It is to be noted that each thickness strain corresponds to a different stress state so that comparison is neither possible with theoretical prediction nor with the tensile test results.

Figure 4 shows the same type of results for sheet bulging with various back pressures,  $P_{\text{atm}}$ , 2 MPa and 3 MPa. In this case also, the forming pressure corresponds to the optimum conditions for superplasticity at the pole. Increasing back pressure reduces substantially the cavitation level but a pressure of 3 MPa is found to be insufficient to completely suppress cavitation. This result can be explained, as for uniaxial deformation, by strain hardening which occurs during deformation.

The decrease of the cavitation level measured along the meridian of the sheet with the increase of the back pressure is not associated with an appreciable change of the thickness distribution as shown in figure 5. For this figure, the thickness variation was determined taking as reference the thickness  $e_1$  at the junction between the cylindrical and the spherical portion of the deformed sheet. The constancy of the thickness profile seems to be logical since the cavitation level remains rather small so that it is essentially controlled by the value of the strain rate sensitivity coefficient (5) as far as temperature is carefully controlled.

Indeed, non uniformity of temperature in the sheet plane can strongly influence the thinning development leading either to earlier fracture if the temperature at the edge of the sheet  $T_e$  is smaller than that at the pole  $T_p$  or to more uniform thickness distribution in the inverse case. Theoretical prediction of the thickness distribution was performed in the case of Al-7475 alloys assuming that the deformed sheet is always a portion of a sphere. Figure 6 shows the results of the calculation, with a temperature at the pole equal to the optimal temperature for superplasticity. A higher temperature at the edge by only 10°C is

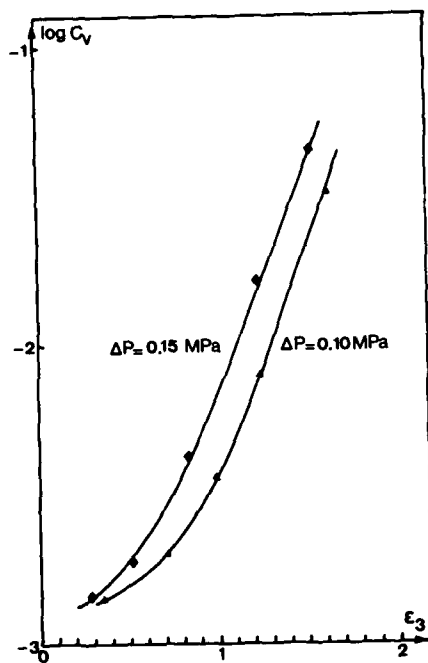


Figure 3 - Influence of forming pressure on the variation with thickness strain of cavity development during bulging under atmospheric back pressure.

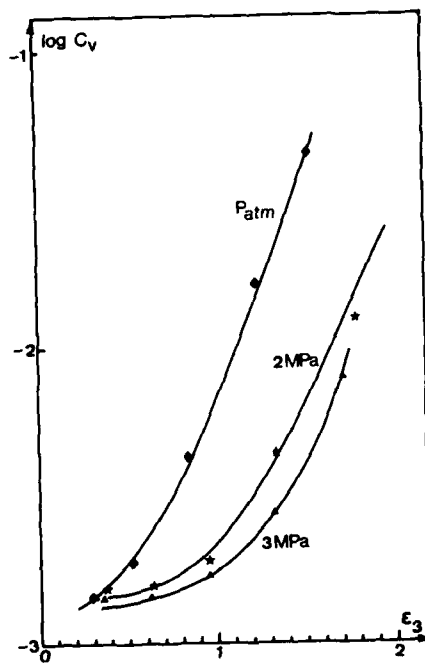


Figure 4 - Influence of back pressure on the variation with thickness strain of cavity development during bulging.

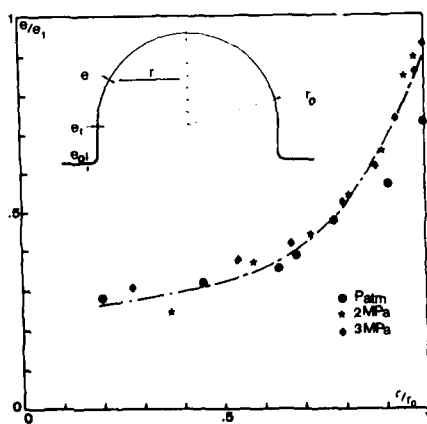


Figure 5 - Distributions of thickness along a meridian of a deformed sheet for various back pressures.

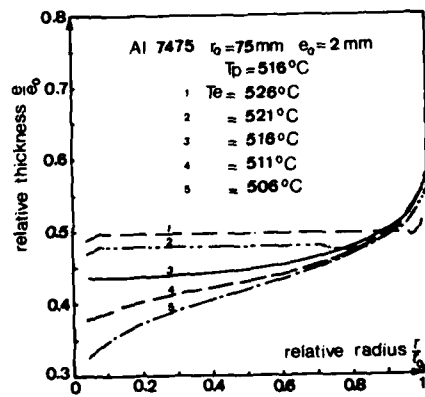


Figure 6 - Influence of temperature  $T_e$  at the edge of the sheet on the thickness distribution after bulging of half a sphere.  $T_p$  is the temperature at the pole.

sufficient to obtain almost complete homogeneity of deformation whereas a lower temperature leads to important strain localization near the pole. Comparison between theoretical profiles and experimental ones suggests that non perfect uniformity of temperature was present in the sheet plane during the experiments.

#### Conclusion

Superimposed pressure is efficient for reducing cavitation during deformation of superplastic 7475 Al-alloys. However the value of the pressure has to be either continuously adjusted during forming or chosen large enough at the beginning in order to be always sufficient in reference to the flow stress, this flow stress depending on testing conditions and structural evolutions.

#### Acknowledgements

The authors acknowledge Cégédur-Pechiney for providing the alloys. They are grateful to D. Weichel and G. Boutet for technical assistance in the bulging experiments and density measurements.

#### References

1. J.Pilling and N.Ridley, "Effect of hydrostatic pressure on cavitation in superplastic aluminum alloys", Acta Met. 34 (1986) 669-679.
2. C.C. Bampton and R. Raj, "Influence of hydrostatic pressure and multiaxial straining on cavitation in a superplastic aluminum alloy", Acta Met. 30 (1982) 2043-2053.
3. A. Varloteaux, "Superplasticité et endommagement des alliages d'aluminium à haute résistance - 7475 -", Thesis, Institut National Polytechnique de Grenoble (1987).
4. S. Yang, "Mise en forme par gonflement d'un alliage d'aluminium 7475 superplastique", M. Sc. Thesis, INP Grenoble (1987).
5. D.-J.Zhou, J. Lian and M. Suéry, "Numerical study of superplastic deformation with superimposed pressure for cavity sensitive materials", Mater. Sci. Technol. To be published (April 1988).

EFFECTS OF SECOND PHASE PARTICLES ON  
THE CAVITY OF SUPERPLASTICITY

J.F.Yang, Peng Xu and H.Wang

Department of Metals and Technology  
Harbin Institute of Technology  
Harbin, China

Abstract

In this paper, the effects of second phase particles on formation and extension of cavities in the tensile superplastic specimens of the Al-13Si and Al-4.7Si-8.2Mg alloys were investigated. The quantitative analysis of the formation and extension of the cavities was carried out, and the effecting factors, such as the shape and size of the second phase particles and the difference of high temperature hardness between the particles and the  $\alpha$ -phase matrix, were examined in detail. It was found that the effects of the Si and  $Mg_2Si$  particles on the morphology, distribution, and extending rate of the cavities are different. The  $Mg_2Si$  particles are globular in the Al- $Mg_2Si$  quasi-eutectic alloy, and the high temperature hardness difference between the particles and the matrix is very small. During the superplastic tension, the cavities are round and distributed along the tension direction, the extending rate of the cavities are low. However, the Si particles

in the Al-Si alloy are prismatic ones with axis ratio of 2/1, and the hardness difference between the particles and the matrix at high temperatures is very large, leading to an incompatible deformation at the interface. There is a stress concentration at edges of the Si particles. The cavities extended around the Si particles rapidly, especially along the edge directions. Therefore, an early failure occurred during superplastic tension in the specimens of Al-13Si alloy.

Superplasticity and Superplastic Forming  
Edited by C.H. Hamilton and N.E. Paton  
The Minerals, Metals & Materials Society, 1988

## Introduction

It is well known that cavities appear during superplastic flow in the superplastic alloys. Influencing superplasticity and the other properties of the alloys, the cavities have aroused a great interest of many researchers all over the world. A lot of research work has shown that the superplastic cavities may be divided into two kinds: one is produced by the incoordinate sliding either at the grain boundaries or at the triple junctions (1), and another occurs at the interfaces between the second particles and the matrix (2). A thorough investigation has been done on the former and many models were developed (3,4), but little attention has been paid to the latter. In this paper, we lay out stress on the observation and analysis of the effects of the large second phase particles on the formation and growth of the cavities. Two alloys were selected which have different properties.

## Experimental Procedure

### Specimens

Al-13Si and Al-4.7Si-8.2Mg alloys were melted in a resistance furnace, and modified by 0.2% Na. Ingots were made by chill-casting into a copper mold. After annealing at 500°C for 1 hour, the alloys were rolled to sheets of about 1 mm thick under the hot and cold conditions. Tensile samples of 10 X 6 X 1 mm were cut down along the rolling direction.

### Superplastic Test

Superplastic tension was performed in a LSS-10T-S machine at temperatures varied from 300-500°C. The strain rates are in the range of  $8.33 \times 10^{-4}$ - $8.33 \times 10^{-1}$ . The values of the elongation of the specimens to failure were recorded for each test. Under the optimum superplastic conditions, the elongations to failure were 248% for Al-13Si and 650% for Al-4.7Si-8.2Mg, respectively.

### High-temperature Microhardness

After polished, specimens were etched by 0.5% HF. The microhardness of Si, Mg and alpha-phase at 20°C, 100°C, 300°C and 450°C were examined on HM-800 model microscope.

### Microstructure Observation

The microstructural aspects including the size, shape and percentage of particles and cavities in the two alloys at different amount of deformation were examined by TEM, SEM and quantitative metallography.

## Results and Discussion

In the two eutectics, the percentages of Si and Mg<sub>2</sub>Si particles are nearly equal, about 20%. The shape of the Si particles is rhombohedral, their ratio of axis is 2:1 (5), and the average diameter of the particles is 1.85 μm in diameter.

### Microcavity Formed during Rolling

It was argued whether and where the microcavities would occur in the superplastic alloys during predeformation (6). In this study, the result of examining with TEM indicated that the predeformation led to formation of microcavities on the edge of Si and Mg<sub>2</sub>Si particles in the two alloys (see Fig.1). By the same pretreatment, the microcavities in the alloys are quite different in size, shape and volume percentage. In the Al-13Si alloy, microcavities occur mostly on the sharp angles of Si particles, and they were 0.1-0.3 μm in



(a)



(b)

Figure 1 - Cavities around (a) the Si and (b)  $Mg_2Si$  particles in preformed specimens

width and much more in number. However, in the Al-4.7Si-8.2Mg alloy, the mean size of cavities was about 0.05-0.2  $\mu m$  and the percentage of them is small.

#### Quantitative Analysis of Cavities

By means of quantitative metallography, the developing process of cavities and differences in the two alloys are evaluated. It was found that a large amount of smaller cavities were formed in the initial stage of the deformation. With increasing the amount of deformation, the cavities developed to large size shown an inhomogenous distribution in size. Comparing with the cavities in the Al-13Si alloy, the cavities in the Al-4.7Si-8.2Mg alloy were less and their growth rates were slower. Fig 2 shows the volume percentage of cavities against elongation. It can be seen that the growth

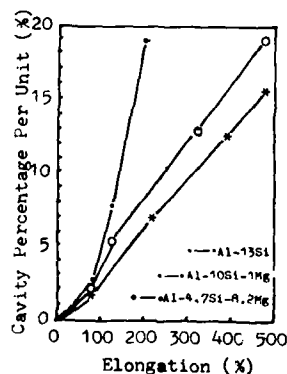


Figure 2 - Curve of the volume percentage of cavity against elongation

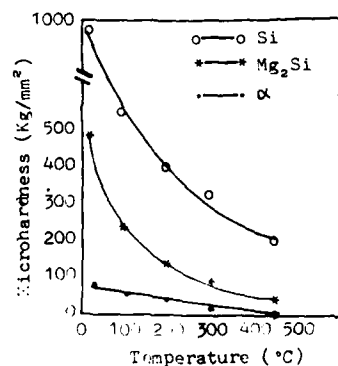


Figure 3 - The temperature dependence of hardness for the Si,  $Mg_2Si$  and alpha-phase.

of cavities followed different laws in the two alloys: the volume percentage in the Al-Si-Mg alloy increased linearly, while in the Al-Si alloy it increased rapidly and exponentially in the late stage of deformation.

Effect of Hardness Difference at High Temperatures between the Matrix and Second Phase Particles on the Formation of Cavity

Fig.3 shows the high-temperature hardness of the Si, Mg<sub>2</sub>Si and  $\alpha$  phase decrease with temperature increasing and there are much higher values of hardness difference between the Si and  $\alpha$  phases compared with that between the Mg<sub>2</sub>Si and  $\alpha$  phases. Obviously, the disparity in hardness accounts for the incoordinate superplastic flow of the two phase. After some superplastic flow in the Al-Si alloy, accumulation of dislocations around the large and hard Si particles incoordinate with the matrix during the flow. Thus, the stress concentration was created at the Si particles, and resulted in nucleation of cavities.

Effect of the Second Phase on Formation of Cavity

Although cavities were commonly observed on edges of second phase particles in the two alloys, the cavity morphology was quite different (see Fig 4). The cavities in the Al-Si alloy are more in number than that in the Al-Si-Mg alloy. The cavities in the Al-Si-Mg alloy are spherical and less in number, but the cavities in Al-Si alloy are with sharp angles and show a radiating distribution. The difference of the cavity morphology is associated with the shapes of second phase particles. The homogenous stress distribution around Mg<sub>2</sub>Si particles due to their spherical shape can retard the formation of the cavity. The cavities emerging around Mg<sub>2</sub>Si are also spherical,

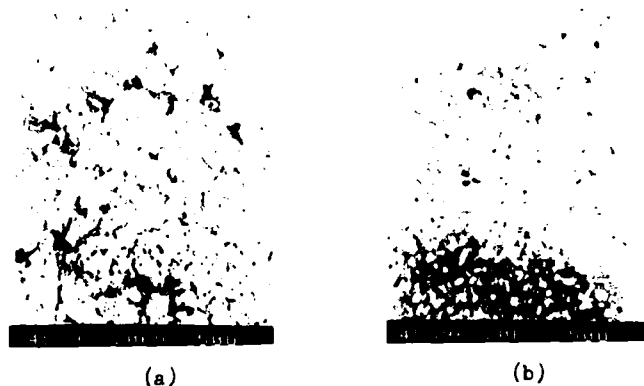


Figure 4 - The size and shape of cavities in (a) the Al-Si and (b) the Al-Si-Mg alloys after superplastic flow ( $\dot{\epsilon}$  = 140%).

they grow slowly, and expand along the tension. Gradually, a new, larger and elliptical cavity forms. But the Si particles are rhombohedral, which leads to an inhomogeneous stress distribution during tension. The rhomb angles of the particles result in the stress concentration and cause the cavities to nucleate at the interfaces between the particles and the matrix, and make the cavities expand along all the directions of the angles of the Si particles in the subsequent tension. The cavities grow quickly and present an irregular shape. Thus, the cavities can expand both along the longitudinal and the traverse direction, resulting in the Al-13Si alloy early failure.



### Conclusion

(1) The cavities are formed easily during predeformation and superplastic flow in the Al-13Si and the Al-4.7Si-8.2Mg alloys which contain large second phase particles ( $\geq 2 \mu\text{m}$ ).

(2) The formation and volume percentage of cavities are related to the hardness difference between the second phase and the matrix. The cavities are formed easily in the Al-13Si alloy due to the greater high temperature hardness difference between the two phase.

(3) The shape of second phase particles has great influence on the morphology and growing of cavities. The cavities in the Al-13Si alloy are distributed radiately. The fast growing of the cavities attributed to the presence of the rhomb Si particles.

### References

1. C.W. Humphries and N.Ridley, "Cavitation during the Superplastic Deformation of an  $\alpha/\beta$  Brass", Journal of Materials Science, 13, (1978), 2477-2482.
2. R.G.Fleck, D.M.R.Taplin and C.J.Beevers, "An Investigation of the Nucleation of Creep Cavities by 1 MV Electron Microscopy", Acta Metallurgica, Vol.23, 1975, 415-424.
3. D.W.Livesey and N.Ridley, "Cavitation and Cavity Growth during Superplastic Flow in Microduplex Cu-Zn-Ni alloys", Metallurgical Transactions A, Volume 13A, September 1982, 1619-1626.
4. M.J.Stowell, "Cavity Growth and Failure in Superplastic Alloys", Metal Science, Vol 17, February 1983, 92-98.
5. J.F.Yang and Peng.Xu, "Analysis on the Superplastic Fracture of Al-13Si Eutectic Alloy and Physic-Mathematical Model for Cavity Failure in Superplastic Deformation", Proceeding of Japan-China Joint Symposium on Superplasticity, November 18-21, 1986. 37-40.
6. N.Ridley, D.W.Livesey and A.K.Mukherjee, "Effect of Cavitation on post-deformation Tensile Properties of a Superplastic Copper-Base Alloy", Metallurgical Transactions A, Volume 15A, July 1984, 1443-1450.

# SUPERPLASTICITY IN Ti-10V-2Fe-3AL ALLOY

Pan Ya qin, Liu Weimin and Song Zuozhou

Department of Materials Science and Engineering  
Beijing Institute of Aeronautics and Astronautics  
Beijing, China

## Abstract

This paper studied the effects of temperature, strain rate, grain size, various processing parameters and heat-treatment on superplasticity ( $\delta, m, \sigma$ ) of this alloy. The results show that specimens with a grain size of 5-10 $\mu$ m possess excellent superplasticity in which  $\delta$  equals approximately 830-910%, and  $m$  equals approximately 0.45-0.57 when the temperature range is 700-750°C, and strain rate range is  $8.25 \times 10^{-4}$  -  $1.2 \times 10^{-3}$  s $^{-1}$ . For specimens of a grain size of 50 $\mu$ m,  $\delta$  equals approximately 200-240%,  $m$  equals 0.31 in the same conditions as above. The activation energies during deformation were calculated, for fine grain specimens  $Q=171$ KJ/mol, and for coarse grain specimens  $Q=267$ KJ/mol.

Superplasticity and Superplastic Forming  
Edited by C.H. Hamilton and N.E. Paton  
The Minerals, Metals & Materials Society, 1988

## Introduction

Ti-10V-2Fe-3Al is a new type of near-beta titanium alloy. With high strength, high toughness and high hardenability, it can be used for the manufacture of structural components of airplanes and engines working below the temperature of 316°C. The alloy is suitable for superplastic forming and isothermal forging because of its low beta-transus temperature. Now lots of research has been done on heat treatment(1), but much less on superplasticity which will be discussed in this paper. Superplasticity of metal appears at a certain forming condition. Its main characters are high elongation, low flow stress and high strain rate sensitivity  $m$ . During superplastic deformation the correlation among  $\dot{\epsilon}$ ,  $\sigma$  and  $m$  obeys:  $\sigma \propto \dot{\epsilon}^m$ ,  $m$  represents the resistance ability to local necking. The larger the value of  $m$ , the higher the resistance necking ability. Hence  $m$  is also related to elongation  $\delta$ .  $\delta$  and  $m$  are two of the most important parameters in superplastic deformation.

## Experiment

The material used in our test is an ingot twice smelted by vacuum consumable-electrode melting. Its beta-transus temperature is 805°C. The ingot is bloomed at 1050°C and forged into 20mm plates at 900°C, then they are hot-rolled to 2-3mm sheets at 760°C. After being annealed at 740°C/1hr, the 3mm sheets are cold-rolled, the deformation extent is separately 10%, 20% and 40%. The superplastic tensile tests are done with a 5T testing machine.

## Results and Discussions

### 1. The Effects of Deformation Temperature

Superplasticity appears at a temperature range. Ti-1023 alloy possesses excellent superplasticity at 700-750°C, in which elongation is high and stress is low (see fig.1). This temperature range is much lower than other titanium alloys(4). In fig.1 we can also see that when deformation temperature is below 700°C, the stress increases rapidly and elongation decreases; when temperature is in 800-850°C, stress is low and elongation is also very low. The deformation temperature is related closely to the structure. The annealing state of the alloy is  $\alpha + \beta$  equilibrium structure. Below the beta-transus temperature the volume fraction of  $\alpha$  phase particles, decreasing as the raising of temperature, is 30% at 700°C, and is 15% at 750°C (1,2). In superplastic deformation at 700-750°C a large number  $\alpha$  particles resist the migration of  $\beta$  grain boundary, the grain size enlarges slowly. The average diameter of grain is still smaller than 10 $\mu$ m (see fig.2). When deforming at 800°C which is near the beta-transus temperature, most  $\alpha$  particles dissolve in  $\beta$  phase, grain size tends to grow obviously,  $\delta$  is very low. When deforming at 650°C, though grain is very fine,  $\delta$  is much lower and stress is higher, because lower temperature makes the diffusion of atoms and vacancies difficult.

### 2. The Effects of Strain Rate

The strain rate is an important factor affecting superplasticity. The results of superplastic tensile test at different strain rate are in fig.3. The optimal  $\delta$  and  $m$  occur when strain rate equals about  $10^{-3} \text{ s}^{-1}$ . The maximum  $\delta$  is 910% at 700°C, and 830% at 750°C, the corresponding values of  $m$  are 0.45 and 0.57.

Superplastic deforming is an even flow process, work hardening contends with dynamical recover softening. When local necking occurs, local harden-

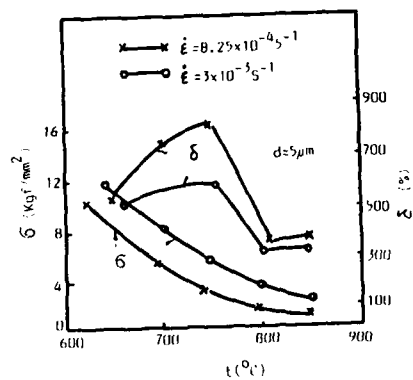


Fig.1 Effect of temperature on elongation and stress

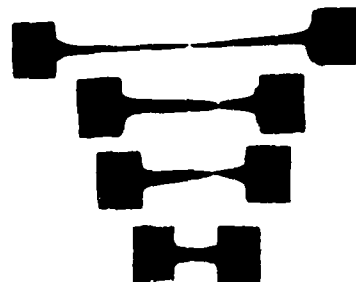


Fig.4 Superplastic deformed Specimens

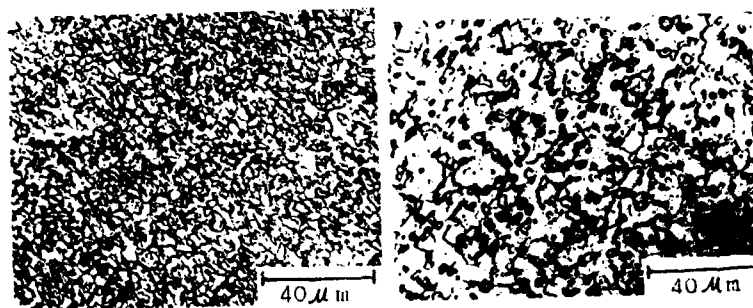


Fig.2 Superplastic deforming microstructures a) 700°C, b) 750°C.

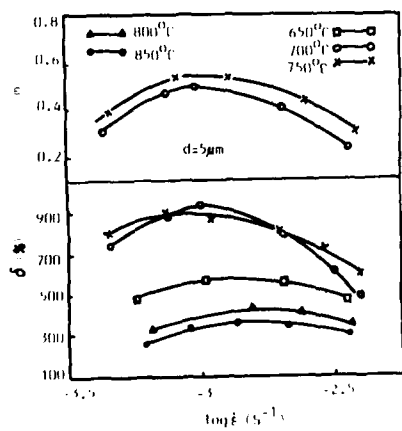


Fig.3 Relationship among strain rate, elongation and m

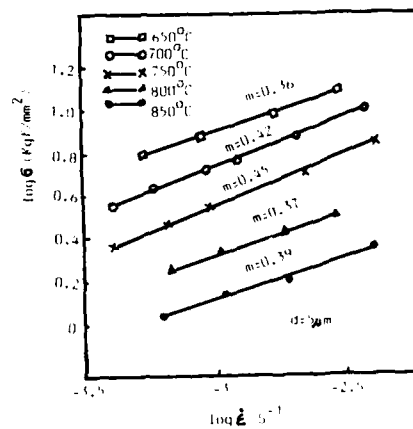


Fig.5  $\log \dot{\epsilon} - \log \sigma$  curves

ing happens in the necking part because of the raising of strain rate, while other part deforms continuously. Then another necking appears, and so on. This is an even flow process in microscopic view, and a local necking move process in microscopic view. So there are many local necks in deformed specimens (see fig.4). The  $\log \sigma$ - $\log \dot{\epsilon}$  correlation curves are showed in fig.5. The slope of each curve represents the average values of  $m$ . Just as in fig. 3,  $m$  takes maximum value at 700°C and 750°C.

### 3. The Effects of Structures

The results of tensile test at 750°C are showed in table 1. The elongations are higher for the specimens which are cold-rolled 40% and the specimens which are hot-rolled and solution treatment at 740°C/1hr and aging at 510°C/8hr. Lower  $\delta$  for the specimens which are cold-rolled 10% may be caused by the low reduction and the inhomogeneity of structure. The elongation of the hot rolled specimens in transverse is very low, and it has been improved after being annealed at 740°C/1hr, but still lower than in longitudinal. This illustrates that annealing at 740°C/1hr can not thoroughly dispel anisotropy produced by rolling. The various specimens are equiaxial grain after superplastic deformation. The average grain diameter of hot-rolled sheets is 50 $\mu$ m after being annealed at 790°C/1hr. For specimens of a grain size of 50 $\mu$ m, equals 200-240%,  $m$  equals approximately 0.3 in the same condition as above.

Table. Superplastic Properties of Sheets

condition	$\dot{\epsilon}$ (S <sup>-1</sup> )	$\sigma$ (kgf/mm <sup>2</sup> )	$\delta$ %	$m$
cold roll 40% d=5 $\mu$ m	6.7X10 <sup>-4</sup>	2.0	640	0.495
	9.0X10 <sup>-4</sup>	2.6	760	
	2.1X10 <sup>-3</sup>	3.8	520	
cold roll 10% d=5 $\mu$ m	6.2X10 <sup>-4</sup>	1.9	570	0.401
	8.7X10 <sup>-4</sup>	2.4	580	
	2.1X10 <sup>-3</sup>	3.4	490	
	2.9X10 <sup>-3</sup>	4.0	370	
hot roll+740°C/1hr. +510°C/8hr.	5.7X10 <sup>-4</sup>	2.0	520	0.446
	9.4X10 <sup>-4</sup>	2.4	700	
	2.3X10 <sup>-3</sup>	3.4	700	
	3.5X10 <sup>-3</sup>	4.3	670	
hot roll transvers test	6.2X10 <sup>-4</sup>	2.1	310	0.351
	9.1X10 <sup>-4</sup>	2.5	360	
	1.7X10 <sup>-3</sup>	3.0	340	
	2.6X10 <sup>-3</sup>	3.4	340	
hot roll+740°C/1hr. transvers test	5.9X10 <sup>-4</sup>	1.9	370	0.42
	9.2X10 <sup>-4</sup>	2.5	405	
	1.6X10 <sup>-3</sup>	3.0	450	
	2.5X10 <sup>-3</sup>	3.7	360	
hot roll+790°C/ 1hr. d=50 $\mu$ m	6.2X10 <sup>-4</sup>	4.0	240	0.314
	8.7X10 <sup>-4</sup>	4.5	240	
	1.9X10 <sup>-3</sup>	5.6	200	
	2.6X10 <sup>-3</sup>	6.3	200	

#### 4. The Relationship among Strain Rate, Temperature and Stress

When forming at high temperature, the correlation among strain rate, temperature and stress obeys the following formula:

$$\dot{\epsilon} \propto \sigma^n \exp(-Q/RT)$$

Where  $n=1/m$ ,  $R$  is gas constant and  $T$  is absolute temperature. The apparent activation energy  $Q$  can be calculated by the above formula.  $Q$  and  $n$  are related to the deformation mechanism (3,4). Being used the data in fig.1, the activation energies during deformation are calculated, for fine grain specimens  $Q=171\text{KJ/mol}$ , which is approximate to grain boundary diffusion activation energy of beta titanium (3,5,6). This illustrates that grain boundary gliding is the main mechanism in superplastic forming. The relationship between  $\log \sigma$  and  $\log \dot{\epsilon}$  for coarse grain specimens is showed in fig. 6, by which we can calculate the activation energy,  $Q=267\text{KJ/mol}$ . This is approximate to the self-diffusion activation energy of beta titanium (3). So the deforming mechanism for coarse grain structure differs greatly from that for fine grain structure.

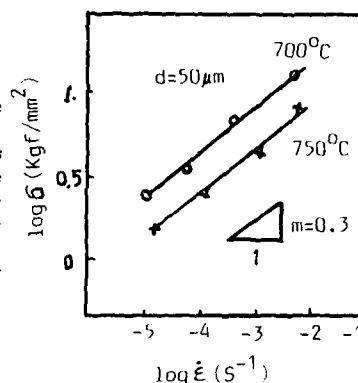


Fig.6 Log  $\sigma$  - log  $\dot{\epsilon}$  curves

#### Conclusions

A. Ti-1023 alloy possesses excellent superplasticity. For fine grain specimens  $\delta = 830-910\%$ ,  $m=0.45-0.57$  when  $T=700-750^\circ\text{C}$ ,  $\dot{\epsilon}=8.25 \times 10^{-4} - 1.2 \times 10^{-3} \text{ S}^{-1}$ , and  $Q=171\text{KJ/mol}$ .

B. For coarse grain specimens  $\delta = 200-240\%$ ,  $m=0.31$  when  $T=750^\circ\text{C}$ , and  $\dot{\epsilon}=6.2 \times 10^{-4} - 1.2 \times 10^{-3} \text{ S}^{-1}$ , and  $Q=267\text{KJ/mol}$ .

C. The hot-rolled sheets possess poor superplasticity in transvers,  $\delta$  and  $m$  increases after annealing.

#### References

1. T.W. Duering, et al., Met. Trans., 11A (1980) 1987-1998.
2. J.I. Shannon, Aerospace Structural Metals Handbook, Vol.4, 1987 Code 3726
3. N.E. Paton and C.H. Hamilton, Superplastic Forming of Structural Alloys (The Metallurgical Society of AIME, 1982), 3, R.C. Gifkins.
4. Terence G. Langdon, OP. cit. 27.
5. J.A. Wert and N.E. Paton, Met. Trans. 14A, (1983), 2535.
6. P.M. Sargent and M.F. Ashby, Soripta Metallurgica, Vol.16, (1982), 1415.

**FUNDAMENTALS  
OF  
FORMING**

## Novel Processing Methods for Superplastic Alloys

Masaru Kobayashi

Department of Mechanical Engineering,  
Technological University of Nagaoka, Nagaoka, 940-21 JAPAN

### Abstract

A variety of processing techniques have been proposed to obtain a uniform structure of equiaxed grains as small as a few micrometers in accordance with alloy compositions. The present paper reviews the recent developments in processing for superplastic alloys such as superalloys, 25%Cr-6.5%Ni-3.2%Mo duplex stainless steel, and high-strength aluminum alloy.

(1) Superalloy. Superheated molten metal was injected onto the rim surface of copper roller rotating at a speed of 1500 revolutions per min in a protective atmosphere and solidified into 10-mm wide ribbons with a thickness between 30 and 100  $\mu\text{m}$ . For consolidation, bundles of the ribbons were cold pressed, sealed in vacuum in a 70-mm diameter can of stainless steel, and extruded at 1200°C. Extruded bars have a fine structure of duplex  $\gamma+\gamma'$  and  $\gamma'$ . The material was superplastic at 1050 °C to have an elongation of 800% at an initial strain rate of  $3.5 \times 10^{-4} \text{ s}^{-1}$ . The strain rate sensitivity,  $m$ , is above 0.6 at 950°C.

(2) Delta-gamma duplex stainless steel (25%Cr-6.5%Ni-3.2%Mo). A strip, 300-mm width and 1.2-mm thickness, was cast in a rotating two-drum strip caster and cooled in air. The strip that was cold rolled 50% showed a large  $m$ -value and an elongation of 700 to 1000% at 950°C with an initial strain rate below  $1.67 \times 10^{-4} \text{ s}^{-1}$ . The microstructure has a dispersion of secondary austenite with a grain size below 1  $\mu\text{m}$  in ferrite and of sigma phase around both primary and secondary austenite.

(3) High strength aluminum alloy. A 4-mm thick sheet of type 7475 aluminum alloy was processed by solution treatment at 480°C for 3 h, warm rolled at 200-260°C and annealed at 400 °C for 1h, rolled at -150°C to 1-mm thickness and annealed at 150°C for 5 min, and finally rolled at -150°C to 0.95 mm in a single pass. The specimen rolled at the cryogenic temperature showed an extremely large elongation and a small flow stress at 517°C with an initial strain rate of  $5 \times 10^{-3} \text{ s}^{-1}$ . This superplastic behavior is caused by the presence of very small recrystallized grains produced in the sequence of processing of heavy and skin-pass rolling at cryogenic temperatures with an intermediate annealing at low temperature. Generation of the very fine grain structure was observed and analyzed with transmission electron microscopy. The fine grain structure was retained during superplastic deformation and suppressed the cavitation.



## Introduction

A uniform and equiaxed grain structure with a size as small as a few micrometers is indispensable for rendering superplasticity. A variety of processing techniques have been proposed in accordance with the alloy composition: (1) formation of duplex structures by eutectoid reaction; (2) recrystallization after heavy deformation in hot or cold working of eutectic alloys; (3) optimum combination of heavy deformation, precipitation and static recrystallization; (4) thermomechanical treatments; (5) thermal cycling to intersect the eutectoid temperature; (6) spray atomization, compaction and sintering through hot, cold or combined hot and cold isostatic pressing; (7) spray deposition and controlled spray deposition of gas-atomized powder and others. The present paper reviews the innovative processing techniques to produce superplastic materials and to improve the superplasticity.

### Development of processing methods for superplastic superalloys

#### 1. Overview

Preparation of block materials for superplastic forging is usually made by Gatorizing which processes canned gas-atomized powder by hot extrusion. A big atomization machine is necessary to obtain a large amount of powder for manufacturing a large block. Melt spinning for practical production of amorphous alloy ribbons is a very promising method to apply to superalloys, because the method can bring a fine cell structure, as shown in Fig. 1, to render superplasticity after heat treatment<sup>(1)</sup>. The processing can be made in a relatively small machine equipped with a single roller or twin rollers for rapid cooling. Ishikawajima-Harima Heavy Industries Ltd. has developed a method to produce block materials by hot extrusion of bundles of the ribbons<sup>(2,3)</sup>.

#### 2. Manufacturing process

Superheated melt of MAR-M247LC (Ni-8.0%Cr-3.0%Ta-9.2%Co-0.5%Mo-9.4%W-5.55%Al-1.4%Hf-0.7%Ti-0.07%C) was continuously injected onto the rim surface of a copper roller rotating at a speed of 1500 revolutions/min and rapidly solidified in the form of ribbon. Ribbons can be controlled their thickness in the range of 30 to 100  $\mu\text{m}$  by the change in circumferential speed of the roller and their width by the opening of injection nozzle. The processing was made for ribbons with 30- $\mu\text{m}$  thickness and 10-mm width. The ribbons were bundled without cutting and packed by cold pressing to be canned and vacuum sealed in a stainless steel capsule of 70-mm diameter.



Fig. 1 Transmission Electron micrograph of roll-quenched IN738LC ribbon.

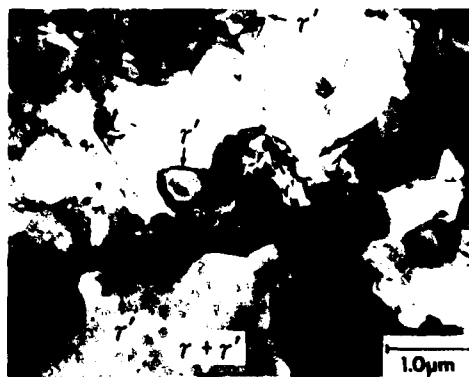


Fig. 2 Transmission electron micrograph of extrusion-consolidated MAR-M247LC.

Consolidation was performed by extrusion at 1200°C with an extrusion ratio of 8:1. The extruded 8-mm diameter product had an ideal full density.

### 3. Microstructure

The ribbons have a structure of 1- $\mu$ m columnar grains growing from the roll contact surface and the secondary dendrites are refined and inhibited their growth. A fine dispersion of M<sub>23</sub>C<sub>6</sub> type carbides is observed along grain boundaries. Microstructure of the bar consolidated by extrusion consists of a duplex structure of  $\gamma'$  (about 1.5 $\mu$ m) and  $\gamma+\gamma'$  (0.1 to 0.5 $\mu$ m), as shown in Fig. 2, and grain growth is strongly inhibited to produce the extremely fine structure.

### 4. Superplastic behavior

Tensile test specimens of 2.5-mm diameter were taken from the extruded bars. Figure 3 shows the flow stresses at a temperature between 900 and 1050°C; testing at 1050°C shows a low flow stress of about 1.5 MPa and an elongation of above 800%. The strain rate sensitivity as a measure of superplasticity is higher than 0.6 in the test temperature range, as shown in Fig. 4, indicating the possibility of superplastic forming of the extruded product in the range of 900 to 1050°C.

### 5. Evaluation of rapid solidification method

Cast superalloys melt partially at temperatures significantly below the solidus of the alloys because of a high degree of segregation among the arms of dendrite. Figure 5(a) shows an incipient melting during heating of a cast alloy at 1300°C, while rapidly solidified (RS) ribbons as well as atomized powder shows no trace of partial melting after solution treatment at 1300°C, as shown in Fig. 5(b). Table 1 compares the cast material and ribbon; the melting temperature of RS product is 30°C higher than that of the conventional cast alloy.

Table 1 Comparison between RS ribbon and cast sample of MAR-M247Lc

Properties	Cast sample	RS ribbon
Tensile strength (MPa)	1078	1274
Ductility (%)	10	15
Melting temperature (°C)	1295	1325
Grain size (mm)	5	0.001
Dendrite spacing ( $\mu$ m)	500	1

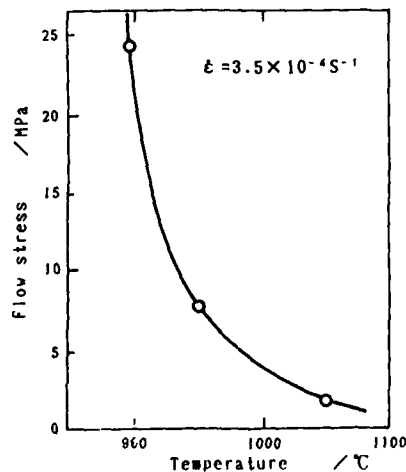


Fig. 3 Temperature dependence of flow stress of extruded M247LC bar.

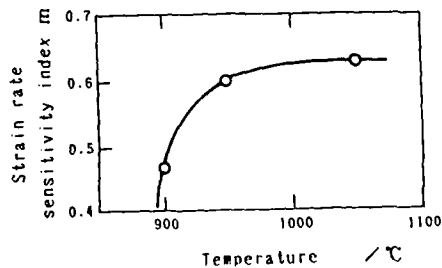


Fig. 4 Temperature dependence of m-value of extruded M247LC bar.

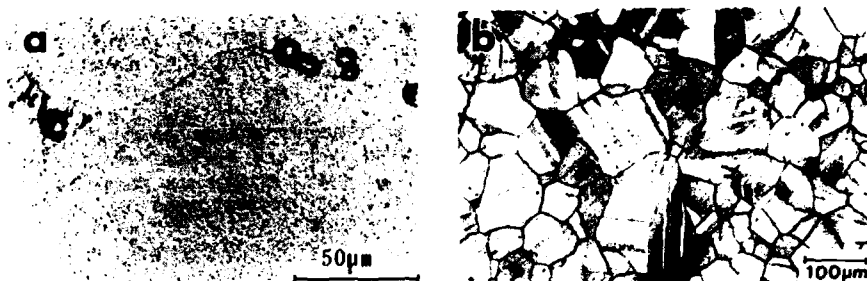


Fig. 5 Microstructure of solution treated MAR-M247LC: (a) ingot, and (b) extrusion-consolidated bar.

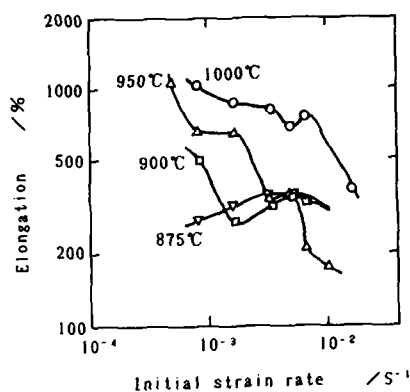


Fig. 6 Elongation vs. strain rate in cold rolled duplex stainless steel.

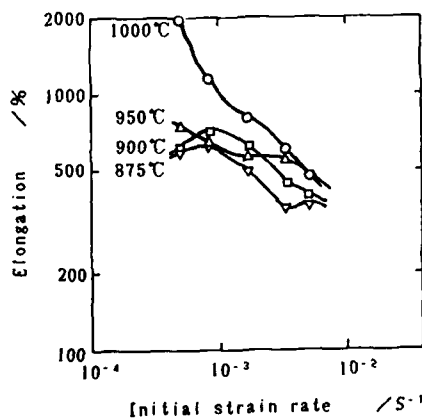


Fig. 8 Elongation vs. strain rate in cold rolled and annealed duplex stainless steel.

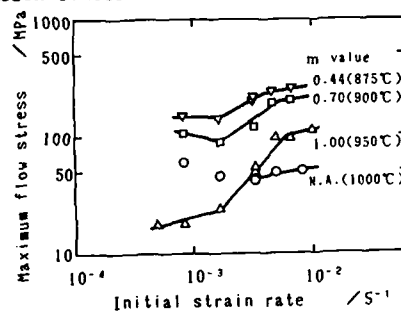


Fig. 7 Maximum flow stress vs. strain rate in cold rolled duplex stainless steel.



Fig. 9 As-cast structure on transverse section of directly cast duplex stainless steel strip.



Fig. 10 Microstructure of directly cast duplex stainless steel strip deformed at 875°C with a strain rate of 3.33x10<sup>-3</sup> s<sup>-1</sup>.

## Improved processing method for superplastic $\delta/\gamma$ duplex stainless steel

### 1. Overview

Corrosion resistive  $\delta/\gamma$  duplex stainless steel is poor in workability because of embrittlement due to the precipitation of  $\sigma$ -phase in hot working process. However, fine dispersion of  $\sigma$ -particles in the matrix improves the workability. Superplasticity arises at temperatures between 850 and 1100°C and at strain rates between  $10^{-2}$  to  $10^{-3}$  s $^{-1}$  through the following processing; hot forging and rolling of an ingot into a 12-mm thick plate, quenching after solution treatment at 1250°C ( $\delta/\gamma$  duplex phase region) for 30 min, and 50% reduction in cold rolling<sup>(4,5)</sup>. Extremely low-carbon ingots processed by argon oxygen decarburization (AOD) process also show superplasticity after the similar sequence of hot and cold working<sup>(6)</sup>. The favorable initial microstructure is a fine dispersion of  $\gamma$  particles in refined  $\delta$  matrix. The  $\delta$ -ferrite precipitates  $\gamma$  during deformation above 1000°C and decomposes into  $\gamma/\sigma$  structure below 1000°C; the final microstructure is the duplex structure of  $\delta/\gamma$  or  $\gamma/\sigma$ . The precipitation and decomposition during deformation are thought to bring high ductility. A direct strip casting technique for production of duplex stainless steel has been developed by Nippon Yakin Kogyo Co. Ltd<sup>(7)</sup>.

### 2. Manufacturing process

Corrosion resistive  $\delta/\gamma$  duplex stainless steel (Fe-24.79%Cr-6.36%Ni-3.10%Mo-0.74%Mn-0.57%Si-0.014%C-0.12%N-0.028%P-0.002%S) was continuously cast into a strip of 1.2 mm-thickness and 300 mm-width by direct strip casting with a two-drum strip caster. The strip was cold rolled 50%.

### 3. Superplastic behavior

The cast strip shows an elongation of 404% at 1000°C with a strain rate of  $8.33 \times 10^{-4}$ . The superplastic behavior is enhanced by cold rolling to achieve an elongation of 1029%. Figure 6 shows the relationship between elongation and strain rate; elongations above 500% can be obtained in the strain rate range less than  $10^{-2}$  s $^{-1}$  for 1000°C and  $1.67 \times 10^{-3}$  s $^{-1}$  for 950°C. Figure 7 shows the dependence of flow stress on strain rate, which is sigmoidal except for the scattered data of 1000°C. Figure 8 shows the superplastic characteristics of 2-mm thick fully annealed sheets made from the AOD processed ingots. Directly cast strips are comparatively less in superplasticity, however by cold rolling, they are rendered higher elongations at higher strain rates than the strips made from the AOD processed ingots.

### 4. Microstructural changes

The cast structure of directly cast strip has a network of austenite precipitates along boundaries of coarse  $\delta$ -ferrite grains, as shown in Fig. 9. The structure deformed by cold rolling recrystallizes during heating for high temperature tensile testing. At temperatures between 800 and 900°C,  $\delta$ -ferrite decompose into  $\sigma$  and  $\gamma$ . The  $\sigma$  particles and the secondary austenite grains as small as 1  $\mu$ m are formed rapidly on the slip planes to enhance the superplasticity at high strain rates around  $5 \times 10^{-3}$  s $^{-1}$ . The microstructure of the directly cast product is a fine and equiaxed structure of  $\gamma$ ,  $\delta$  and  $\sigma$  phases at the fracture stage in tensile deformation at 875°C with a strain rate of  $3.33 \times 10^{-3}$  s $^{-1}$ , as shown in Fig. 10.

### 5. Evaluation of direct strip casting technique

Very low carbon contents achieved by the AOD process permit the cold rolling of 1.2-mm thick direct cast strips. The continuous casting of strip is a highly productive process. Although the cast strips are now cooled in air, rapid cooling will surely provide a fine grain structure more favorable to superplasticity.

## Improvements of superplasticity in 7475 aluminum alloy

### 1. Overview

Grain refinement of 7475 aluminum alloy is limited down to  $12\text{ }\mu\text{m}$  by the conventional thermomechanical processing. Therefore, formation of voids is unavoidable at triple grain points and leads to internal defects by the growth, coalescence and interlinkage of the voids. This cavitation imposes the secularity of infalliable performance in the structural use of superplastically formed materials. Cavitation can be suppressed by superposition of a back stress<sup>(9)</sup>, however, an extra cost is needed for instrumentation and operation for the back pressure imposition. Recently superplasticity was reported in the 8-mm thick sheets processed to achieve a fine grain size of  $3.7\text{ }\mu\text{m}$  through spray deposition of gas-atomized powder, thermomechanical processing and subsequent recrystallization. However, an ideal starting material is thought to be cast products because of the poor productivity of atomized powder<sup>(10)</sup>.

The present author has observed in face-centered cubic metals that cryogenic working at liquid nitrogen temperature produces a higher density of dislocations than room-temperature working and results in formation of a fine cell structure as small as  $1\text{ }\mu\text{m}$ <sup>(11)</sup>. It is anticipated that the fine cell structure will enhance the superplasticity, if misorientations can be controlled at a certain level between recrystallization grains formed in the high dislocation density regions of cell structure<sup>(12)</sup>.

### 2. Manufacturing process

Type 7475 (Al-5.45%Zn-2.34%Mg-1.4%Cu-0.2%Cr) alloy sheets were warm rolled and annealed at  $400^\circ\text{C}$  for 1h. Four types of rolling procedure, (a) to (d) shown in Fig. 11, were applied in the subsequent process: the product thickness was 1.0 mm in the processes (a) and (c) and 0.9 mm in (b) and (d).

The process (a) is conventionally evaluated as the best and the process (d) is newly developed by the present author.

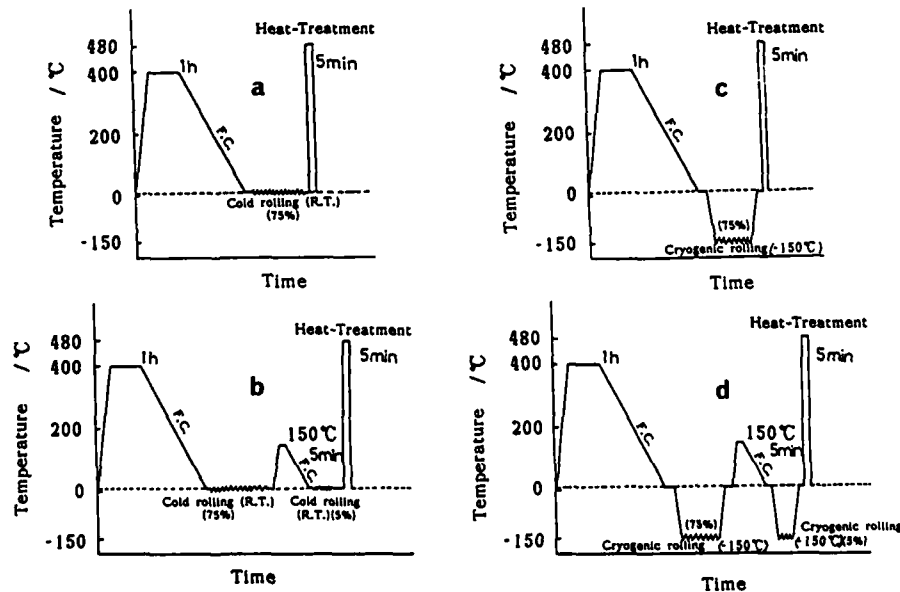


Fig. 11 Types of thermomechanical processing for 7475 Al alloy sheet: (a) rolling at room temperature; (b) rolling and skin pass at room temperature; (c) rolling at cryogenic temperature; and (d) rolling and skin pass at cryogenic temperature.

### 3. Superplastic behavior

Figure 12 shows the flow stress (conventional stress)-strain curves in tensile deformation at  $517^{\circ}\text{C}$  with a strain rate of  $5 \times 10^{-4} \text{ s}^{-1}$ , the optimum condition for the conventional superplastic materials. The specimen processed in (d), consisting of rolling and skin-pass at liquid-nitrogen temperature, rapid heating, brief annealing and quenching, has a flow stress of  $0.15 \text{ kgf/mm}^2$ , which remains constant with increasing strain and is one-third of the specimens (a) and (b) rolled at room temperature. The (d) process provides an elongation seven times higher than the (a) process and the maximum elongation of  $815\%$  at  $517^{\circ}\text{C}$  with an initial strain rate of  $5 \times 10^{-4} \text{ s}^{-1}$ , as seen in Figs. 13 and 14. In Fig. 15 the flow stresses of (c) and (d) processed specimens are found to vary more significantly with the strain rate than the (a) and (b) specimens. The strain-rate sensitivity index  $m$  is relatively low in the (c) and (d) specimens at  $517^{\circ}\text{C}$ , the temperature bringing the highest elongation, as shown in Fig. 16. Figure 17 indicates the change in  $m$ -value with increasing strain during tensile deformation at  $517^{\circ}\text{C}$  with interrupted changes of strain rate. The  $m$ -values are shown to remain constant up to higher strains in the (c) and (d) specimens that have relatively low  $m$ -values, however, they increase in the final stage to fracture probably because of work-hardening.

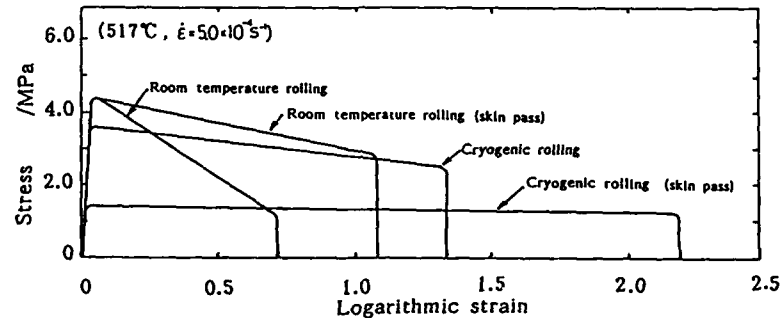


Fig. 12 Comparison of four processes: stress-strain relationship.

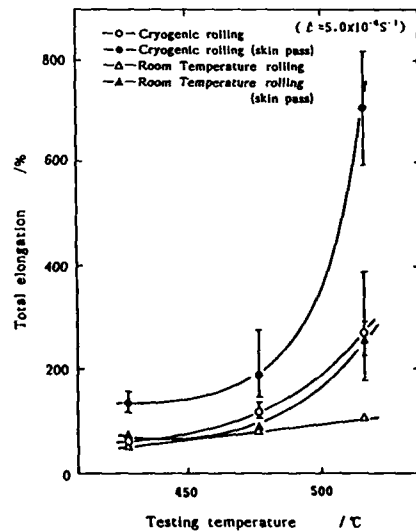


Fig. 13 Comparison of four processes: elongation vs. testing temperature.

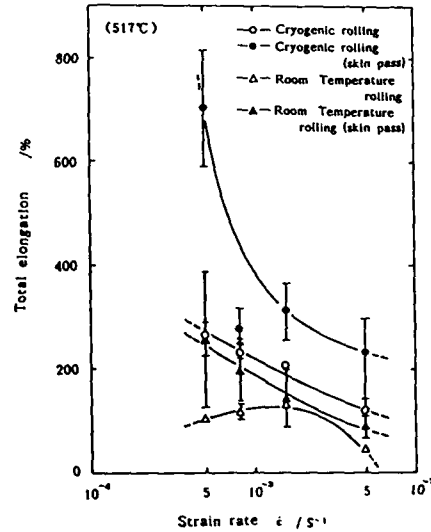


Fig. 14 Comparison of four processes: elongation vs. strain rate.

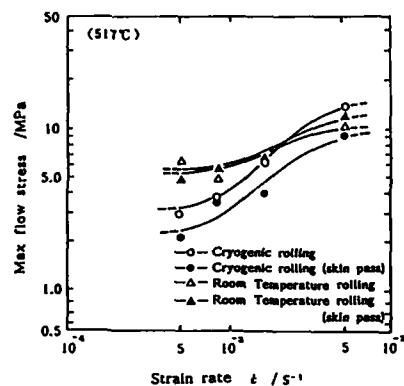


Fig. 15 Comparison of four processes: flow stress vs. strain rate.

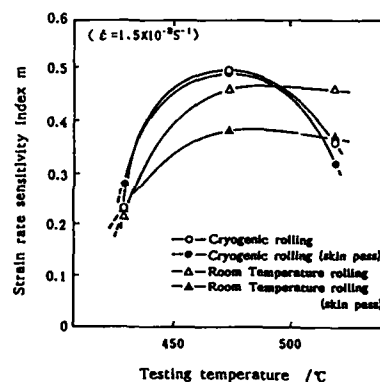


Fig. 16 Comparison of four processes: m-value vs. testing temperature.

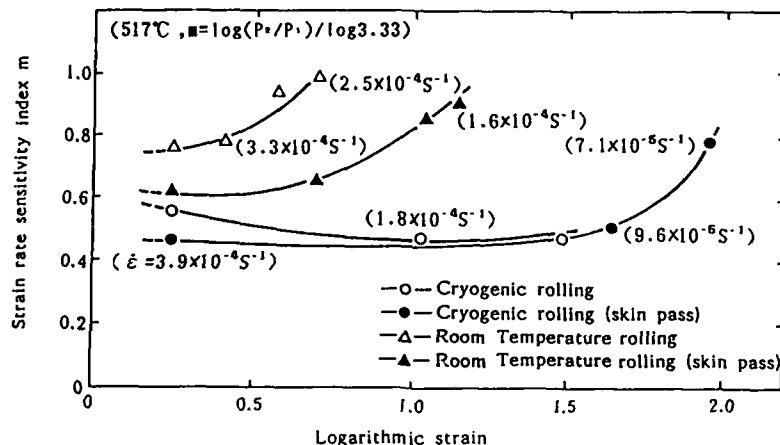


Fig. 17 Variation of m-value with superplastic deformation.

#### 4. Microstructural changes and cavitation in superplastic deformation

Figure 18 shows the microstructural evolution during superplastic deformation. The (a) specimens are accompanied by strain-induced grain growth and the (d) specimens substantially retain the initial grain size which is relatively large. The slight microstructural change in the (d) specimen is thought to bring a large elongation and is consistent with the constancy of m-value above mentioned. Figure 19 shows the cavitation in the specimen (a) deformed 70% and in the specimen (d) deformed 150%. The specimens (a) as well as (b) reach to the stage of nucleation, growth, coalescence and interlinkage of cavity, while the specimens (d) as well as (c) generate only a dispersion of small cavities. Bampton has reported an increase of cavitation above 200% strain<sup>(13)</sup>, however, the evolution of cavity through nucleation, growth, coalescence and interlinkage to fracture seems different in the present cryogenic process products from the conventional superplastic materials.

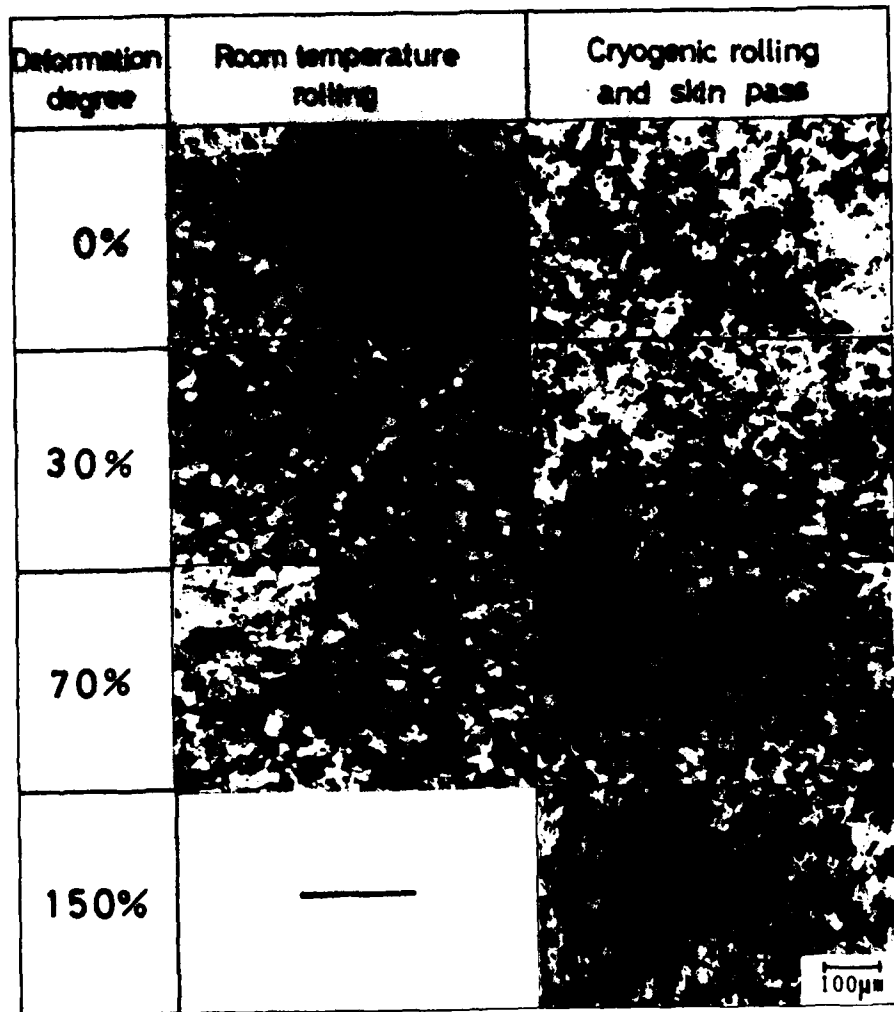


Fig. 18 Microstructural change during tensile deformation with the axis in horizontal direction of the figure.



Fig. 19 Difference of cavitation due to prior processing: (a) room temperature rolling (at the stage of 70% tensile strain) and (b) cryogenic rolling (at the stage of 150% tensile strain).



### 5. Mechanism of high ductility

Figure 20 shows a transmission electron micrograph and electron diffraction patterns of the specimen (d). Analysis of the diffraction spots indicates that the misorientation between grains is  $18.5^\circ$  for grains (1) and (2),  $13.3^\circ$  for (2) and (3), and  $12.9^\circ$  for (3) and (1). The grain (1), 3 to 4  $\mu\text{m}$  in size, is a recrystallization grain originating from the site of high dislocation density at a triple point of cell structure. Such a characteristic fine structure, which has not been observed in the materials produced by conventional thermomechanical processes, is thought to contribute to the stabilization of microstructure and the suppression of cavitation during superplastic deformation.

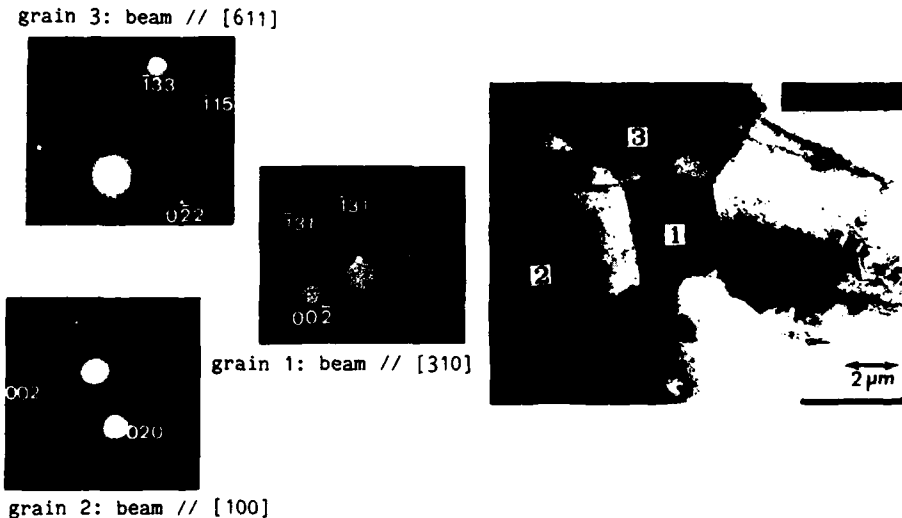


Fig. 20 Transmission electron micrograph with diffraction patterns (grains 1, 2 and 3) for 7475 Al alloy rolled and skin passed at cryogenic temperature.

### 6. Proposal

As proved in the present experiment, the formation of a fine cell structure of high dislocation density is an effective means for obtaining fine grain structures and consequently for superplastic forming. Therefore, working at cryogenic temperatures together with preliminary thermomechanical processing including cryogenic working is a very promising procedure for obtaining the fine structure and also an inexpensive process applicable to a variety of materials.

### Conclusion

Among future technological advances in development and application of superplastic materials, the manufacturing processes should be explored on the basis of sound understanding on the mechanism and the microstructural characteristics of superplastic deformation. Furthermore, for the reliability of superplastically formed materials, retardation of cavity formation in superplastic forming must be considered in the designing of an integrated process including the manufacturing processes for rendering superplasticity.

#### Acknowledgement

The author's thanks are due to Mr. Nakagawa of Ishikawajima-Harima Heavy Industries, Ltd., Mr. K. Yasuda of Hitachi Ltd., and Mr. K. Osada of Nippon Yakin Kogyo Co. Ltd. for permission of the reference to their papers.

#### References

- 1) K. Yasuda, M. Tsuchiya, T. Kuroda, and M. Suwa: "Mechanical Properties and Microstructure of Melt-spun Superalloy Ribbons", (Proceedings of 5th International Symposium on Superalloys, Pennsylvania, October 7 - 11, 1984), p.477-486.
- 2) Y. G. Nakagawa, H. Yoshizawa, and H. Terashima: "Superplastic MAR-M247LC Superalloy Made by Compaction of Rapidly Solidified Ribbons", Mater. Sci. Technol., 2(1986), 637-639.
- 3) F. Pierre, H. Yoshizawa, H. Terashima, and Y. G. Nakagawa: "Characterization of Nickel Base Superalloy Consolidated from rapidly Solidified Ribbons", Ishikawajima-Harima Engineering Review, 28(1988).
- 4) Y. Maehara: "Superplasticity of  $\delta$ -ferrite/Austenite Duplex Stainless Steels", Trans. Iron Steel Inst. Jpn., 25(1985), 69-76.
- 5) Y. Maehara: "Superplastic Deformation Mechanism of  $\delta/\gamma$  Duplex Stainless Steels", Trans. Iron Steel Inst. Jpn., 27(1987), 705-712.
- 6) K. Osada, S. Uekoh and K. Ebato: "Superplasticity of As-rolled Duplex Stainless Steel", Trans. Iron Steel Inst. Jpn., 27(1987), 713-718.
- 7) K. Osada, S. Uekoh, T. Tohge, M. Noda, and K. Ebato: "Superplasticity of a Duplex Stainless Steel Produced by a Direct Strip Casting Technique", Trans. Iron Steel Inst. Jpn., 28(1988), 16-22.
- 8) C. H. Hamilton, C. C. Bampton and N. E. Paton: "Superplasticity in High Strength Aluminum Alloys", Superplastic Forming of Structural Alloys, eds. N. E. Paton and C. H. Hamilton (Metallurgical Society of AIME, 1982), 173-189.
- 9) J. M. Story, J. I. Petit, D. J. Lege and B. L. Hazard: "Forming Process Variable Effects on Cavitation in the Superplastic Forming of Commercially Produced 7475 Aluminum", (Paper presented at "Superplasticity in Aerospace-Aluminum Conference", Cranfield, U. K., July 12-15, 1985).
- 10) K. Matsuki, M. Tokizawa and H. Nakagawa: to be published.
- 11) M. Kobayashi, A. Kamada, T. Terabayashi and H. Asao: "Pressformability of Face-centered Cubic Metals at Cryogenic Temperatures", Proceedings of the 20th International M. T. D. R. Conference, (Birmingham, U. K., September 10-14, 1979), 239-246.
- 12) M. Kobayashi, Y. Hirotsu, Y. Ohtani and T. Takahashi: "Superplasticity of 7475 Al Alloy Sheet Processed by Cryogenic Rolling and Heat Treatment", (Paper presented at MRS International Meeting on Advanced Materials, Symposium E; Superplasticity, Tokyo, May 31-June 1, 1988).
- 13) C. C. Bampton, A. K. Ghosh, and M. W. Mahoney: "The Causes, Effect and Control of Cavitation in Superplastic 7475 Aluminum Airframe Structures", (Paper presented at "Superplasticity in Aerospace-Aluminum Conference", Cranfield, U. K., July 12-15, 1985), 1-31.

# MEMBRANE ELEMENT ANALYSIS OF AXISYMMETRIC AND NON-AXISYMMETRIC SUPERPLASTIC METAL FORMING PROCESSES

N. Chandra and B. Roy

Department of Mechanical Engineering  
FAMU/FSU College of Engineering  
Florida State University  
Tallahassee, FL 32316

## Abstract

Superplastic properties of certain structural materials are increasingly used for the advanced fabrication processes in aerospace and automotive industries. In such processes the optimum forming conditions are achieved when the strain-rate of deformation is held constant typically within a narrow range specific to the material. Analytical modeling of the manufacturing processes is very important in the successful forming and overall economy of the method. The prime interest in modeling superplastic forming process is to predict the optimum rate of pressurization to control the strain-rate and to predict the resulting thickness distribution. A new method of solution for the superplastic forming of axisymmetric parts is presented in this paper in which the sheet is divided into a finite number of segments. Force equilibrium is imposed on each of the segments at any given instant by balancing the forces due to applied pressure and induced stress field. The results of the method are compared with that of other models and experiments.

## Introduction

The commercial development of titanium and aluminum based superplastic alloys has provided very economical methods to produce complex components in the automotive and aerospace industries using forming techniques which were not previously possible. Several methods and techniques have been reported for forming superplastic materials, e.g., blow (pressure) forming, vacuum forming, thermo-forming, deep drawing and superplastic forming with concurrent diffusion bonding (SPF/DB). In the blow or pressure forming process, the dies and sheet are normally maintained at the forming temperature, and the gas pressure is imposed over the sheet causing it to form into the lower die. The gas within the lower die chamber is either vented to atmosphere or is subjected to a vacuum or positive back pressure. The pressure forming process has the advantage of no moving components and does not require male die member. Production rates can also be increased by forming multiple components in a single process cycle. Processing information required for a successful design and fabrication include:

- (1) Rate of pressurization to maintain the constant strain-rate required for optimum superplastic forming, and
- (2) Thickness distribution and maximum thinning on the part after superplastic forming,

The pressure-time cycles required for constant strain-rate, and the resulting thickness distribution are generally determined by trial-and-error techniques except for certain simple geometries like domes, cones and long rectangular boxes (1-10). A mathematical model in which geometry, equilibrium and constitutive laws for the material

This research effort was partially supported by ALCOA Technical Center, PA, U.S.A

Superplasticity and Superplastic Forming  
Edited by C.H. Hamilton and N.E. Paton  
The Minerals, Metals & Materials Society, 1988

are all satisfied at each incremental time step will provide a fairly accurate description of the process. Such *process models* are important in the numerical representation and the design of the processing methods. The models described in the above references for the simple configurations basically use the membrane theory to predict optimum pressure-time cycles and thickness distribution that occur during superplastic forming. For more complex geometries and the consideration of friction at the sheet-tool interface, the use of non-linear finite element analysis offers a potentially viable approach (11-15). However, the analysis using finite element solution method involves high computational effort and is uneconomical for a general iterative design process. Hence a two stage design methodology with the *preliminary design* using simplified analysis followed by the finite element method as a *final design stage* offers an attractive solution to the complex problem.

The constitutive equation for the material is a necessary component of the process model and is essential for an accurate description of the manufacturing process. This phenomenological equation is determined experimentally and different forms are used by different investigators. The most common equation for the superplastic flow is given by  $\sigma = K\dot{\epsilon}^m$  where  $\sigma$  is the flow stress of the material,  $K$  is the strength parameter,  $\dot{\epsilon}$  is the strain rate and  $m$  is the strain rate sensitivity. This relationship is based upon the properties at constant temperature required for superplastic forming and assumes no work hardening during deformation. Other equations include that of Story (8), who used the form  $\sigma = K_1\epsilon^n$  where  $\epsilon$  is the effective strain. The material parameters  $K_1$  and  $n$  are both functions of strain-rate given by  $K_1 = K_0\dot{\epsilon}^\alpha$  and  $n = n_0\dot{\epsilon}^\beta$  where  $K_0, n_0, \alpha$  and  $\beta$  are all material parameters. Ghosh and Hamilton developed the Constitutive relationship of the form  $\log \sigma_0 = A_0 + A_1 \log \dot{\epsilon} + A_2 (\log \dot{\epsilon})^2 + A_3 (\log \dot{\epsilon})^3 + A_4 (\log \dot{\epsilon})^4$ , and  $\sigma = \sigma_0 + B\epsilon$ , where  $A_0, A_1, A_2, A_3, A_4$  and  $B$  are material constants. This equation represents the combined effect of strain hardening and strain-rate sensitivity. All the above relationship can be generalized in the form

$$\bar{\sigma} = \bar{\sigma}(\bar{\epsilon}, \dot{\bar{\epsilon}}, d)$$

where  $d$  is the grain size, and  $d$  can be conveniently replaced by  $t$  the elapsed time.

In this paper a numerical model called *Membrane Element Model* is developed based on the concepts of finite element and finite difference analyses. No thickness distribution is assumed in this model, as against the earlier works (1-10). The formulation is applied to solve the problem of axisymmetric dome forming of sheet metal. The method is also extended to non-axisymmetric pan forming and some preliminary results are presented.

#### Theory of the membrane element model

An analytical method to model superplastic sheet metal forming is presented here which uses the concepts of finite elements in space and finite difference in time. The sheet metal is divided into a number of linear segments in the case of plane strain and axisymmetric problems. When complex geometries are to be modeled, the sheet is divided into either triangles or rectangles. The one-dimensional line and the two-dimensional plane stress elements are called as membrane elements. The deformation at any given time is first approximated based on the kinetic and the kinematic quantities in the earlier time step. Force equilibrium is imposed in each of the elements and the resulting stress quantities are used to predict a new approximation. The numerical iterative scheme is carried out until the known boundary conditions at the pole and at the edges are satisfied.

The assumptions made in the analysis are: (1) The shape of the deformed unsupported segment is spherical. Experimental evidence shows that this is a valid assumption (16). (2) The sheet is in a state of plane stress. (3) The thickness at any point within an element depends on the thickness at the nodes. (4) The deformation at the pole (geometric center) is balanced biaxial in axisymmetric parts, and is a function of edge dimensions (length and width) in non-axisymmetric parts. (5) The edges are tightly held, and are thus in a state of plane strain. The theory is developed first for axisymmetric configuration and later extended to non-axisymmetric case.

The sheet metal is made up of material with constitutive equations of the form  $\bar{\sigma} = \bar{\sigma}(\bar{\epsilon}, \dot{\epsilon})$  with  $\bar{\sigma} = \sqrt{\frac{3}{2} \hat{\sigma}_{ij} \hat{\sigma}_{ij}}$  and  $\bar{\epsilon} = \sqrt{\frac{2}{3} \hat{\epsilon}_{ij} \hat{\epsilon}_{ij}}$ , where  $\bar{\sigma}$  and  $\bar{\epsilon}$  are the equivalent quantities. A hat denotes that the quantity is deviatoric. With the plane stress assumption the equivalent quantities at each material point can be written as

$$\bar{\sigma} = \sqrt{\sigma_1^2 + \sigma_2^2 - \sigma_1 \sigma_2} \quad \text{and} \quad \bar{\epsilon} = \sqrt{\frac{4}{3} (\epsilon_1^2 + \epsilon_2^2 + \epsilon_1 \epsilon_2)}$$

where subscripts 1 and 2 indicate that the quantities are principal in the plane of the sheet metal. In axisymmetric configurations they refer to meridional and circumferential directions. Since the material is assumed to be incompressible

$$\epsilon_1 + \epsilon_2 + \epsilon_3 = 0 \quad \text{or} \quad \dot{\epsilon}_1 + \dot{\epsilon}_2 + \dot{\epsilon}_3 = 0$$

where the subscript 3 refers to the thickness direction. The constitutive equation can be written in Lévy-Mises form as:

$$\hat{\sigma}_{ij} = \frac{2}{3} \frac{\bar{\sigma}}{\bar{\epsilon}} \hat{\epsilon}_{ij} \quad \text{with} \quad \sigma_{ij} = \hat{\sigma}_{ij} + \frac{\sigma_{kk}}{3} \quad \text{and} \quad \dot{\epsilon}_{kk} = 0$$

with the boundary condition at the pole

$$\bar{\sigma} = \sigma_1 = \sigma_2 = \frac{p\rho}{2s} \quad \text{and} \quad \sigma_3 = 0$$

$$\dot{\epsilon}_1 = \dot{\epsilon}_2 = \frac{\dot{\bar{\epsilon}}}{2} \quad \dot{\epsilon}_3 = -\dot{\bar{\epsilon}}$$

and at the edge:

$$\dot{\epsilon}_2 = 0 \quad \dot{\epsilon}_1 = -\dot{\epsilon}_3 \quad \dot{\bar{\epsilon}} = \frac{2}{\sqrt{3}} \dot{\epsilon}_1 \quad \bar{\sigma}^2 = \sigma_1^2 + \sigma_2^2 - \sigma_1 \sigma_2$$

The problem can be formulated as an incompressible non-linear viscous material subjected to a time dependent pressure loading with a set of boundary conditions. The loading is to be determined for a specified strain rate  $\dot{\bar{\epsilon}}^*$  at the critical location. The critical location is at the pole of a freely forming axisymmetric part. Once the pole contacts the die, the critical location shifts to the geometric center of the largest undeformed segment.

Consider the discretization of a sheet metal in a radial direction as shown in Figure 1.

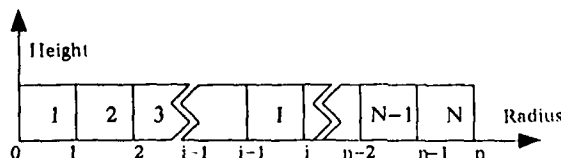


Figure 1. Membrane element discretization of sheet metal

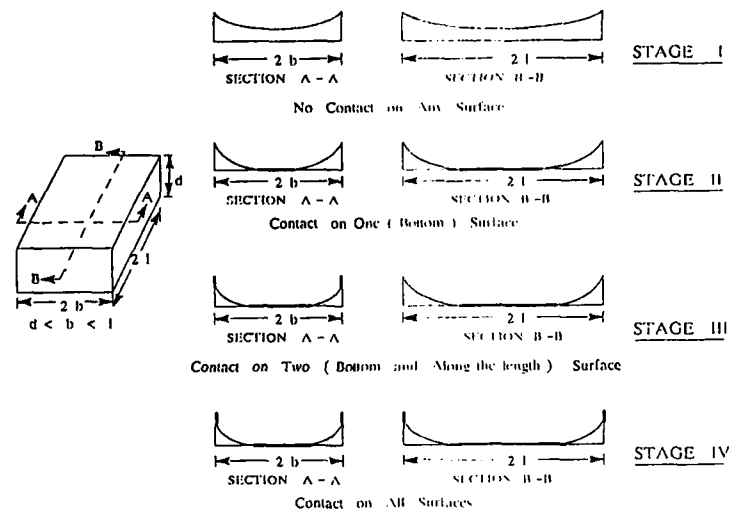


Figure 2. Stages of formation of a box with finite dimensions.

The sheet metal is divided into  $N$  elements with node numbers 0 to  $n$ . For a detailed description of the numbering scheme refer to (16). Assume that the equilibrium configuration, stress, and strain-rate quantities are all known at time  $t$ . It is required to determine all these quantities at time  $t + \Delta t$ , where  $\Delta t$  is the chosen time increment. Using the incompressibility conditions and definition of thickness strain, the change in surface area  $\delta A_I$  of element  $I$  can be written as,

$$\delta A_I = -\frac{\dot{\bar{\epsilon}}}{2\bar{\sigma}}({}^t\sigma_1 + {}^t\sigma_2)({}^tA_I)\Delta t$$

where the left superscript indicates the time of reference. In the above equation, all the data refer to quantities at time  $t$  and the latest iteration.

Total change in surface area  $\Delta A$  of the sheet metal in the incremental time  $\Delta t$  can be determined by summing  $\delta A_I$  over all the elements 1 to  $N$ . The global quantities like radius of curvature  $\rho$ , angle  $\alpha$  and height  $H$  can be calculated from the new area. The pressure  $P$  is calculated from the equivalent stress at the pole using  $\bar{\sigma} = \frac{P\rho}{2s}$ . Since  $\bar{\epsilon}^*$  is specified at the pole,  $\bar{\sigma}$  at the pole can be evaluated using the functional form of the constitutive equation. The thickness  $s_I$  is calculated based on a linear variation of thickness within an element. From the force equilibrium of a spherical segment subjected to uniform pressure we have,

$$\sigma_{1,p}s_p = \sigma_{1,l}s_l$$

where the  $p$  refers to the pole and  $l$  refers to the meridional direction.  $\sigma_1$  in each element can be evaluated from the above equation. From the geometry of deformation, thickness at each node, and force equilibrium the new stress and strain-rate quantities are calculated in each element. The updated values of stress and strain-rate quantities are used to recalculate the area, and other geometric quantities till the boundary condition at the pole and edge are satisfied. This procedure is repeated until the dome height reaches any specified value.

The concepts described above is extended to model *non-axisymmetric* problems. As an illustrative example the formation of a square box as shown in Figure 2 is considered.

In this case, a further assumption is made that every line segment passing through the geometric center deforms as a part of a sphere with maximum height at the pole and radius of curvature corresponding to half the edge to edge distance. An additional geometric constraint is that the vertical deflection and the thickness at the geometric center are identical to each of the domes. Thus every material point can be considered as a part of a radial line from the geometric center through the point under consideration. The deformation at the point is determined based on the history of stress and the depth at the geometric center. The contact of the sheet with any of the surfaces is determined from the geometry of each node and equation of surface. Thus a square box (or box with finite dimension) is formed in four stages with free forming in the first stage and in unsupported regions in the subsequent stages.

### Results and discussion

The above method was used to model axisymmetric dome forming. The model is compared to the published experimental results of dome forming of Al 7475. The details of the experiment can be found in reference (17). The material is represented by the equation of the form  $\sigma = K\dot{\epsilon}^m \epsilon^n$  in which  $n$  is given by  $n = n_0 \dot{\epsilon}^\beta$ , with the material constants  $K = 67,500$ ,  $m = 0.55$ ,  $n_0 = 0.0477$  and  $\beta = -0.24$ . The pressure time loading used to form the dome (radius = 1.75 in.) in the actual experiment is shown in Figure 3. This data does not correspond to any constant value of strain-rate as predicted by the model, but falls within the range given by  $\dot{\epsilon}^* = 0.0002$  to  $0.0004/\text{sec}$ . It can be concluded that in the actual experiment the strain-rate varied within this range. Though the pressure loading and the total time of formation varies for different  $\dot{\epsilon}^*$  the thickness distribution at a given height of formation is not affected. Hence the experimental data at specific heights are plotted in Figure 4, along with the numerical results from the present model and the data agree very well. For comparison purposes the thickness distribution predicted by some other model is also shown (5). It is to be noted that this (Ghosh) model assumes a parabolic variation of meridional strain, whereas no such assumption here.

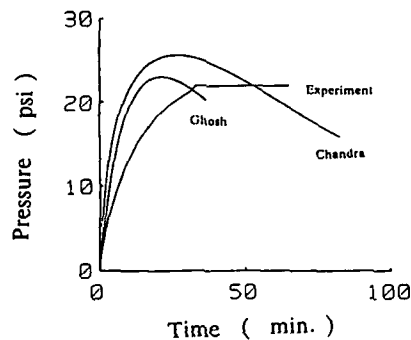


Figure 3. Pressure-time loading

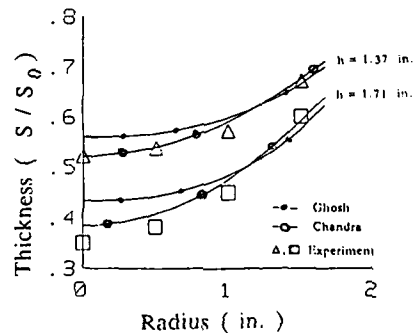


Figure 4. Thickness variation in the dome.

In general the material constants in the constitutive equations are evaluated based on limited experiments, and there is always some uncertainty involved in the exact value of parameters. Figure 5 shows the effect of strain-rate sensitivity  $m$  on variation of peak pressure, total time to dome forming, and minimum thickness. The figure shows

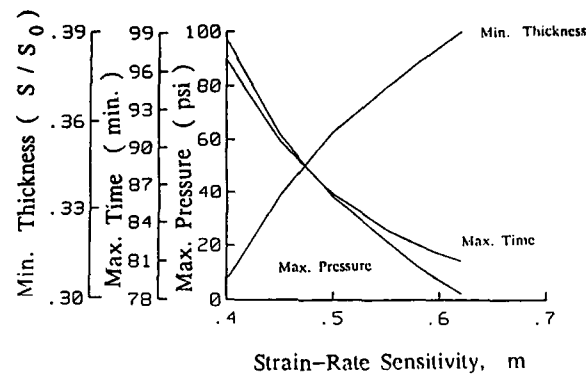


Figure 5. Effect on  $m$  on forming

significant changes in these process parameters; it implies that accurate determination of material properties is very critical.

The concepts of non-axisymmetric forming described earlier are applied to the formation of a square box. The progressive deformation in box forming is shown in Figure 6. The deformation shown in this figure is based on pure kinematics and is shown at various depths in the first stage. Further work on the model development and experimental verification using physical model (16), and superplastic materials is in progress.

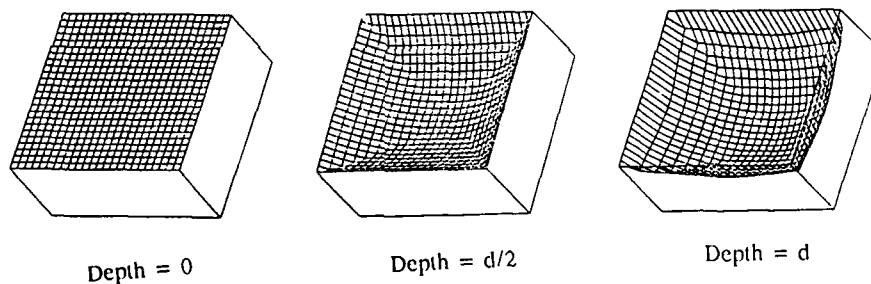


Figure 6. Kinematics of box in stage I.

#### Summary and Conclusion

A numerical *Membrane Element Model* using the concepts of finite element in space and finite difference in time has been developed to solve the problem of axisymmetric superplastic sheet metal forming problems and compares well with experimental results. The method has also been extended to model non-axisymmetric problems. More numerical and experimental work needs to be done for a complete validation and further extension of the model.



### References

1. F. Jovane, "An Approximate Analysis of the Superplastic Forming of a Thin Circular Diaphragm: Theory and Experiments," International Journal for Mechanical Sciences, (10) (1968), 403-427.
2. G.C. Cornfield and R.H. Johnson, "The Forming of Superplastic Sheet Metal," International Journal for Mechanical Sciences, (12) (1970), 479-490.
3. D.M. Woo, "The Analysis of Axisymmetric Forming of Sheet Metal and the Hydrostatic Bulging Process," International Journal for Mechanical Sciences, (6) (1964), 303-317.
4. D.L. Holt, "An Analysis of the Bulging of a Superplastic Sheet by Lateral Pressure," International Journal for Mechanical Sciences, (12) (1970), 491-497.
5. A.K. Ghosh and C.H. Hamilton, "Influences of Material Parameters and Microstructure on Superplastic Forming," Metallurgical Transactions A, (13A) (1982), 733-743.
6. A.K. Ghosh and C.H. Hamilton, "Superplastic Forming of a Long rectangular Box Section-Analysis and Experiment," Proceedings of American Society for Metals on Process Modeling - Fundamentals and Applications to Metals (1978) 303-231.
7. Yu-Quan, S, "Technological Analysis of the Superplastic Bulging of a Metal Sheet," Materials Science and Engineering, (86) (1987), 179-189.
8. J.M. Story, J.I. Petit, D.J. Lege, and B.L. Hazard, "The Effect of Forming Process Variables on Cavitation in the Superplastic Forming of 7475 Aluminum," Proceedings of International Conference on Superplasticity in Aerospace-Aluminum, Cranfield, England (1985).
9. Z.J. Luo, N.C. Guo, and Q.Y. Gong, "A numerical Method for Simulating the Bulging of Superplastic Sheet Metal," Proceedings of the 14th North American Research Council, (1986) 420-425.
10. S.S. Gavrishun and O.C. Zienkiewicz, "A simple Algorithm for the Analysis of Axisymmetric Thin Shell Metal Forming," International Journal for Numerical Methods in Engineering, (23) (1986), 1179-1194.
11. N. Chandra, W.E. Haisler and R.E. Goforth, "A Finite Element Solution Method for Contact Problems with Friction," International Journal for Numerical Methods in Engineering, (24) (1987), 477-495.
12. N. Chandra, R.E. Goforth and W.E. Haisler, "Finite Element Analysis of Hertz Problem with Friction," Finite Elements in Analysis and Design, (3) (1987), 39-56.
13. N. Chandra, R.E. Goforth and W.E. Haisler, "Finite Element Formulation of Superplastic Metal Forming Processes," 1985 ASM Metals Congress, Toronto, Canada, ASM Paper No. 8511-004, (1985).
14. N.M. Wang and M.L. Wenner, "Elastic-viscoplastic Analysis of Simple Stretch Forming Problems," Proceedings of the General Motors Symposium on Mechanics of Sheet Metal Forming, (1977) 367-402.
15. N. Chandra, "Finite Element Analysis of Superplastic Metal Forming Processes," to be published in International Journal for Numerical Methods in Engineering, (1988).
16. N. Chandra and R. E. Goforth, "An Analytical Model for Axisymmetric Superplastic Metal Forming Process," TMS Technical Paper No. A87-11.
17. K.N. Shah, J.M. Story, and N. Chandra, "Modeling of Superplastic Forming Under Axisymmetric and Plane Strain Conditions," Proceedings of 1988 TMS Conference on Superplasticity, Phoenix, AZ, January 1988.

# FINITE ELEMENT MODELLING OF THE SUPERPLASTIC

## FORMING OF THIN SHEET

J. Bonet<sup>1</sup>, R.D. Wood<sup>2</sup> and O.C. Zienkiewicz<sup>2</sup>

Civil Engineering Department  
University College of Swansea  
Singleton Park, Swansea SA2 8PP  
U.K.

### Summary

Superplastic forming of thin sheet into complex, often diffusion bonded, components is an important manufacturing process. In particular, products formed from the titanium alloy Ti-6Al-4V are light, strong and resistant to adverse environmental conditions. The success of the process relies, in part, on the ability to be able to predict the relationship between the forming pressure cycle and the final product shape and thickness distribution.

This paper discusses a finite element technique for the computer simulation of the superplastic forming of a sheet of arbitrary shape. The method is capable of predicting a forming pressure cycle in order to achieve a given maximum strain rate. A new implicit solution scheme is introduced and examples are presented to demonstrate the potential of the formulation.

Superplasticity and Superplastic Forming  
Edited by C.H. Hamilton and N.E. Paton  
The Minerals, Metals & Materials Society, 1988

1. Research Student, 2. Staff member.

## Introduction

Superplastic forming of thin sheet components is an important manufacturing process but the problems of predicting the relationships between the pressure cycle and the final product shape, thickness distribution and grain size distribution are difficult. It is in this respect that the predictive capabilities of a numerical simulation using the finite element method, [1-7], can make a valuable contribution to the industry. This paper outlines a membrane element based finite element formulation of the superplastic forming problem; briefly introduces a new implicit solution scheme and presents two examples to validate and demonstrate the general capabilities of the technique.

## Governing Equations and their Solution

The sheet is modelled as a non-Newtonian viscous membrane for which the constitutive relation between the Von Mises equivalent stress  $\bar{\sigma}$  and the equivalent strain rate  $\dot{\epsilon}$  is given in terms of viscosity  $\mu$  as, [8],

$$\bar{\sigma} = 3\mu\dot{\epsilon}; \quad \mu = (K\dot{\epsilon}^{m-1})/3; \quad g = g_0(t/10)^N; \quad t > 10 \text{ min.} \quad (1a,b,c)$$

where the constant  $K$  and the sensitivity index  $m$  are both functions of the grain size  $g$ , see Figure 1. The variable  $N$  is a function of the strain rate, [9] and  $g_0$  is the initial grain size for  $0 < t \leq 10$  min. Incorporating plane stress and incompressibility assumptions enables the constitutive relations for a membrane shell to be written as,

$$\sigma_m^{\alpha\beta} = 2\mu t C^{\alpha\beta\lambda\delta} D_{\lambda\delta}^m \quad (2)$$

where, in terms of convected coordinates  $\xi^\alpha$  ( $\alpha=1,2$ )  $\sigma_m^{\alpha\beta}$  is the membrane stress resultant over thickness  $t$ ,  $D_{\lambda\delta}^m$  is the membrane rate of deformation and  $C^{\alpha\beta\lambda\delta}$  is a function of the metric tensor.

The governing equilibrium expression is the virtual velocity equation,

$$\int_A \sigma_m^{\alpha\beta} \delta D_{\alpha\beta}^m dA - \int_A p \delta v_3 dA = 0 \quad (3)$$

where  $A$  is the current sheet surface area,  $p$  the pressure and  $v_3$  the velocity normal to the sheet. In order to introduce pressure control, the equilibrium equation is augmented by an equation that constrains the maximum effective strain rate  $\dot{\epsilon}_0$  as,

$$L(\underline{D}(\underline{v})) = \dot{\epsilon}_0 \quad (4)$$

where  $L$  is a suitable function weighting the strain rates  $\underline{D}$ . Discretization of the virtual velocity equation, using 3-node constant stress triangular elements, yields a system of non-linear differential equations in time as,

$$\underline{I}(\underline{x}, \underline{v}) - \underline{F}(\underline{x}, t) = 0 \quad (5)$$

which represents the equilibrium balance between the internal stresses, discretized as  $\underline{I}$  and the applied pressure discretized as  $\underline{F}$ . Equations (5)

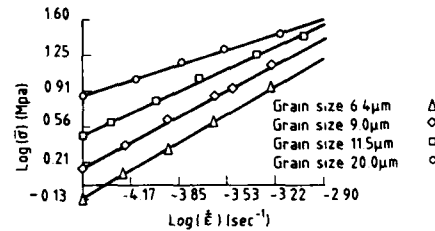


Figure 1 Linearized stress-strain relation for Ti-6Al-4V

are solved using an implicit time stepping scheme, see Figure (2) which on account of the geometric and material non-linearity involved requires the use of a Newton-Raphson iteration, summarized, in conjunction with Figure 2 for iteration  $k$  and time step  $(n+1)$  as,

$$\underline{K}_{n+1}^T \Delta v_{n+1}^k = \underline{F}(\underline{x}_{n+1}^k, t_{n+1}) - \underline{T}(\underline{x}_{n+1}^k, v_{n+1}^k); \quad v_{n+1}^{k+1} = v_{n+1}^k + \Delta v_{n+1}^k \quad (6a,b)$$

where the tangent stiffness matrix,

$$\underline{K}_{n+1}^T = \frac{\partial \underline{T}}{\partial v_{n+1}^k} + \left[ \frac{\partial \underline{T}}{\partial \underline{x}_{n+1}^k} - \frac{\partial \underline{F}}{\partial \underline{x}_{n+1}^k} \right] \frac{\partial \underline{x}_{n+1}^k}{\partial v_{n+1}^k} \quad (6c)$$

A full account of the implicit solution procedure will be presented in [10].

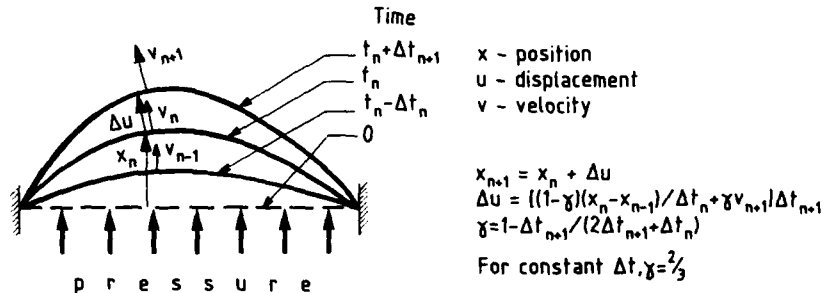


Figure 2 Implicit time stepping scheme

#### Applications

Both examples refer to the forming of Ti-6Al-4V sheet, at a constant temperature of 927°C, with an initial 1mm. thickness and initial grain size  $g_0$  of 8 $\mu$ m. The grain size evolves according to equation (1,c) with parameters  $K$  and  $m$  being interpolated from Figure (1). The dies are represented by a mesh of triangular elements and sticking friction is assumed.

**Truncated cone** The base and top diameters of the cone are 120 mm. and 60 mm. respectively and the height is 55 mm. A quarter mesh comprising 648 elements and 361 nodes was used to model the sheet, see Figure 3(a). Experimental and computed pressure cycles were used in the analyses, the latter being for a constrained maximum  $\bar{\epsilon}_0$  of  $3.5 \times 10^{-4}$ , see Figure 3(d). For both pressure cycles the final shape and thickness distribution were identical, see Figures 3(b) and (c), where an excellent agreement between experimental and computed thicknesses is observed. The effectiveness of the pressure control is clearly demonstrated in Figure 3(e) where the experimental pressure cycle causes a dramatic rise in the strain rate in the region of the corner, after contact is made with the top of the die. In addition, with pressure control the forming time is reduced by 13.4% from an experimental value of 4400 secs. On a VAX 11/750 the CPU times were 3042 and 2400 secs, with and without pressure control, respectively.

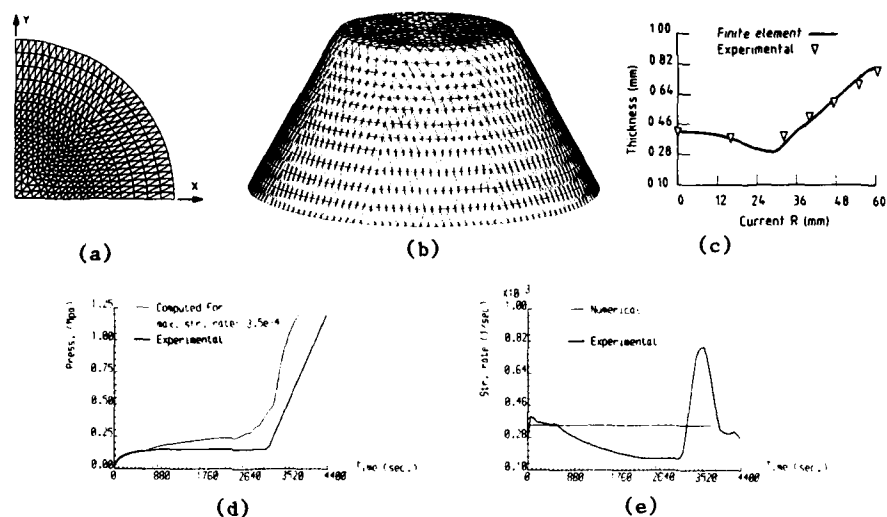


Figure 3 Superplastic forming of a truncated cone (a) finite element mesh, (b) final deformed shape, (c) final thickness distribution, (d) experimental and computed pressure cycles, (e) numerical and 'experimental' maximum strain rates.

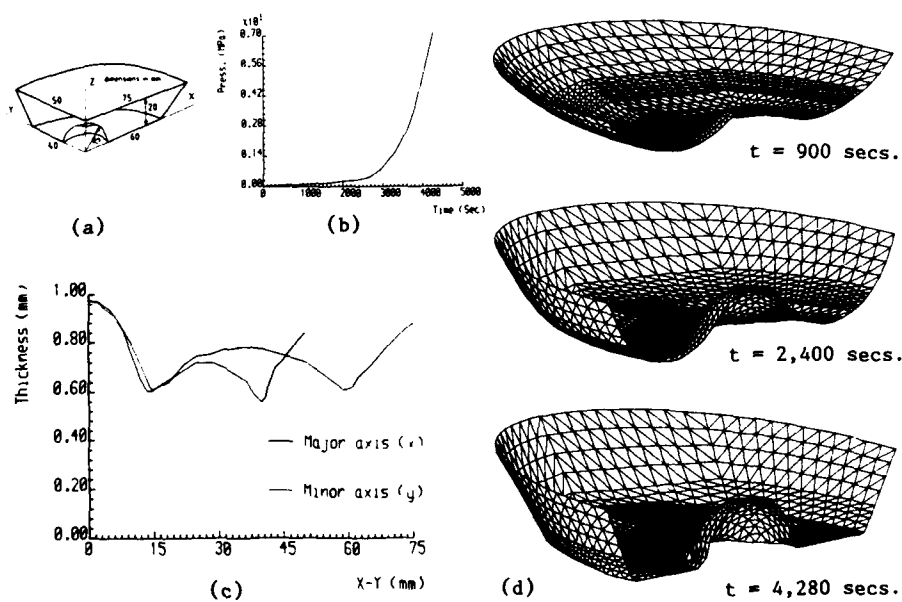


Figure 4 Superplastic forming of a truncated ellipsoid with a spherical indent; (a) geometry, (b) pressure cycle, (c) final thickness distributions, (d) deformed shapes at various forming times.

Truncated ellipsoid with a spherical indent In this hypothetical example a 150 mm. by 100 mm. elliptical sheet is formed into the die as shown in Figure 4(a). Due to symmetry a quarter mesh comprising 856 elements and 465 nodes is used to model the sheet. The pressure cycle, shown in Figure 4(b) was computed for a constrained maximum  $\bar{\epsilon}_0$  of  $3.5 \times 10^{-4}$ . Figure 4(c) shows the thickness distributions along the major (x) and minor (y) axes for the final forming time of 4280 secs. The minimum final thickness was 0.53 mm. and the maximum final grain size was 12.8  $\mu\text{m}$ . The problem took 7800 CPU secs. on a VAX 11/750.

#### Conclusions

Close agreement with the experimental results together with the ability to simulate the forming of complex shapes indicates the potential of finite element analysis for predicting the behaviour of superplastically forming thin sheet.

#### Acknowledgement

This work is associated with a contract between British Aerospace Civil Division and the Institute for Numerical Methods in the Civil Engineering Department at Swansea University.

#### References

1. J.H. ARGYRIS and J. ST. DOLTSINIS, "A primer on superplasticity in natural formulation", Compt. Meths. Appl. Mech. Engrg., 16, (1984), 83-132.
2. N. CHANDRASEKARAN, R.E. GOFORTH and W.E. HAISLER, "Finite element formulation of superplastic metal forming processes", American Society for Metals, Metals/Materials Technology Series, Materials Week, Paper 8511-004, (1985), 1-8.
3. W.C. ZHANG, R.D. WOOD and O.C. ZIENKIEWICZ, "Superplastic forming analysis using a finite element viscous flow formulation", Aluminium Technology '86, Book 4, Session C, (1986), 111.1-111.6, The Institute of Metals, London.
4. J. ST. DOLTSINIS, J. LOGINSLAND and S. NOLTING, "Some developments in the numerical simulation of metal forming processes", Proc. Int. Conf. on Computational Plasticity : Models, Software and Applications, Part 2, (1987), 875-899.
5. M. BELLET, E. MASSONI and J.L. CHENOT, "A viscoplastic membrane formulation for 3-dimensional analysis of thin sheet metal forming", Ibid., 917-926.
6. J. BONET and R.D. WOOD, "Solution procedures for the finite element analysis of superplastic forming of thin sheet", Ibid., 927-939.
7. J. BONET, R.D. WOOD and O.C. ZIENKIEWICZ, "Finite element analysis of thin sheet superplastic forming", Mathematical Models for Metals and Materials Applications, Institute of Metals, London (1988), 2.1-2.7.
8. Superplasticity, AGARD-LS-154, Advisory Group for Aerospace Research and Development, NATO, Aug. 1987, pp. 204.
9. A.K. GHOSH and C.H. HAMILTON, "Mechanical behaviour and hardening characteristics of a superplastic Ti-6Al-4V alloy", Metallurgical Trans., A, 10A, (1979), 699-706.
10. J. BONET, R.D. WOOD and O.C. ZIENKIEWICZ, "An implicit solution procedure for the finite element analysis of thin sheet superplastic forming", to be submitted for publication.

INCORPORATION OF SLIDING FRICTION INTO A CLOSED-FORM MODEL OF

PLANE STRAIN SUPERPLASTIC FORMING

J. M. Story

Aluminum Company of America  
Alcoa Technical Center  
Alcoa Center, PA 15069

Abstract

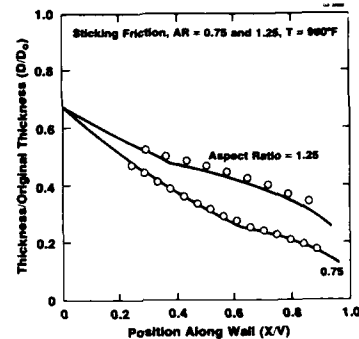
An incremental approach based on equilibrium of a wedge-shaped segment of the wall of a long rectangular pan was used to incorporate sliding friction into a closed-form model of superplastic forming (SPF). Using a constitutive relationship where flow stress depends on both strain and strain rate, strain rate was shown to have a very small effect on the distribution of thickness. It was also found that a critical length exists along the die sidewall within which sticking will occur. The magnitude of this critical length depends upon the coefficient of friction and the aspect ratio of the die. It was found that sticking can occur over most of the die sidewall even when the coefficient of friction is low. Experiments were performed where the depth of the bulge, for deforming sheet which has not yet touched bottom, was measured at various forming times with boron nitride as a lubricant and compared with depths predicted for perfect sticking and perfect sliding. Both the model described above and the experimental results showed that the assumption of sticking used in simpler models will not result in significant error in predicting thickness when boron nitride is used as a lubricant.

Superplasticity and Superplastic Forming  
Edited by C.H. Hamilton and N.E. Paton  
The Minerals, Metals & Materials Society, 1988

### Introduction

A model of the superplastic forming (SPF) of a long, rectangular box section was developed and verified.<sup>1,2</sup> The model assumes a plane strain condition, a cylindrical bulge profile, that only unsupported metal deforms (sticking friction) and uniform thinning in the deforming sheet. Improvements to the earlier model of Ghosh and Hamilton<sup>3</sup> include the use of a constitutive relationship incorporating both strain and strain rate hardening and a modification accounting for deviation from plane strain resulting from a less than infinitely long die.

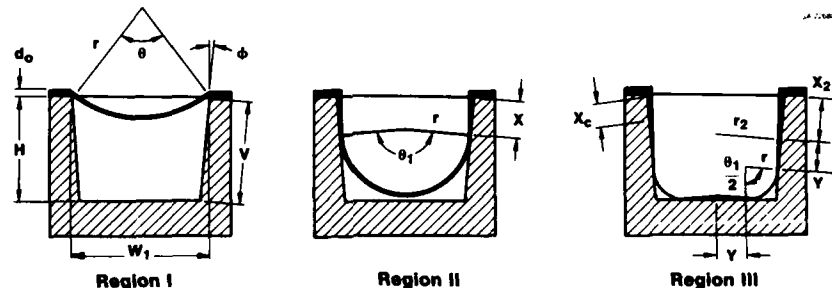
The good agreement, shown in Fig. 1, between the predicted and measured thickness distributions, for rectangular pans of two aspect ratios formed without lubrication, demonstrates that the sticking friction assumption is not unreasonable when no lubricant is used. However, the time to form a pan of a given geometry would be expected to be less and the thickness gradients in the pan walls and bottom less severe when an effective lubricant is used. Therefore, a method to incorporate sliding friction into the plane strain model of SPF was developed.



Predicted and Measured Thickness Distribution - Plane Strain Superplastic Forming of 7475 Aluminum  
Figure 1

### Model Description

The forming operation is considered to occur in three geometrical phases. The first phase, called Region I, shown in Fig. 2, consists of bulging the sheet into a cylindrical shape, with no contact with the die



Geometry of SPF  
Figure 2

walls. The radius of curvature of the cylinder decreases and the contact angle increases with time during Region I. Region I ends when the sheet first becomes tangent to the die walls. The second phase, called Region II, begins with tangency to the die walls and ends with contact with the die bottom. The radius of curvature decreases slowly with time and the contact angle remains constant during Region II. Region III begins with contact with the bottom. The radius of curvature decreases more rapidly with time and the contact angle still remains constant.

Friction results in a thickness gradient along the die walls and bottom, as shown in Fig. 2. When sliding is allowed at the wall/sheet interface, metal is allowed to "feed in" to the unsupported region from the region of contact, so that not only the unsupported metal is deforming.



This reduces the severity of the thickness gradient. If the SPF operation were perfectly frictionless, then at any instant the thickness would be the same at any location in the pan.

Thickness strain,  $\epsilon_3$ , can be related to thickness,  $d$ , and original thickness,  $d_0$ , and, for plane strain, true effective strain,  $\bar{\epsilon}$ , can be related to thickness strain as shown below.

$$\epsilon_3 = \ln\left(\frac{d}{d_0}\right) \quad [1] \quad \bar{\epsilon} = \frac{2}{\sqrt{3}} \epsilon_3 \quad [2]$$

True effective strain can also be obtained by integrating the true effective strain rate,  $\dot{\bar{\epsilon}}$ , over time,  $t$ . Combining [3] with [1] and [2] and rearranging yields

$$\bar{\epsilon} = \dot{\bar{\epsilon}} t \quad [3] \quad d = \frac{d_0}{\exp\left(\frac{\sqrt{3}}{2} \dot{\bar{\epsilon}} t\right)} \quad [4]$$

The constitutive law used assumes that the true effective stress,  $\bar{\sigma}$ , is dependent on both true effective strain rate and true effective strain. Expressing strain by [3]

$$\bar{\sigma} = K \dot{\bar{\epsilon}}^m (\dot{\bar{\epsilon}} t)^n \quad [5]$$

where  $K$ ,  $m$  and  $n$  are material parameters called the flow stress, the strain rate sensitivity exponent and the strain hardening exponent, respectively. The strain hardening exponent is a function of strain rate in the present model for 7475-O2 aluminum.

From geometry in Region II (see Fig. 2), considering the unsupported metal as a cylindrical, thin-walled pressure vessel

$$r = r_1 - X \tan \phi \quad [6] \quad p = \frac{2}{\sqrt{3}} \frac{\bar{\sigma} d}{r} \quad [7] \quad \sigma_1 = \frac{pr}{d} \quad [8]$$

where  $r$  is the radius of curvature,  $r_1$  is the radius of curvature at the end of Region I,  $X$  is the distance along the die wall from the top theoretical sharp corner,  $\phi$  is the draft angle,  $p$  is the forming pressure and  $\sigma_1$  is the hoop stress.

If the SPF operation is frictionless, the position,  $X$ , can be calculated according to

$$X = \frac{d_1 - d}{d} \frac{r_1 \theta_1}{2 - \theta_1 \tan \phi} \quad [9]$$

where  $\theta_1$  and  $d_1$  are the contact angle and thickness at the end of Region I. Values at the end of Region I can be calculated from geometry and volume constancy.

#### Incremental Approach

At a given time  $t$ , such that the process is in Region II, the incremental scheme is as follows.

1. calculate  $d$  from [4]
2. calculate  $X$  for frictionless conditions from [9]
3. calculate  $r$  from [6]
4. calculate  $\bar{\sigma}$  from [5]
5. calculate  $p$  from [7]
6. calculate  $\sigma_1$  from [8]

Friction is incorporated by using the free body diagram shown in Fig. 3. At the point of tangency with the die, the hoop stress times the thickness gives the force per unit length for the first element. The

force at the other end of the element can then be calculated from equilibrium. The new thickness depends on the stress-strain relationship as shown below:

$$\frac{\sqrt{3}}{2} \frac{F(I+1, J)}{d(I+1, J)} = \bar{\sigma}(I+1, J) \quad [10]$$

where  $J=1$  means that the first estimate of pressure was based upon the frictionless thickness distribution and  $I$  is the element number.

$$\bar{\sigma}(I+1, J) = K \dot{\epsilon}^m \left[ \frac{2}{\sqrt{3}} \left| \ln \left( \frac{d(I+1, J)}{d_0} \right) \right| \right]^n \quad [11]$$

which leads to

$$d(I+1, J) = \frac{\sqrt{3} F(I+1, J)}{2 K \dot{\epsilon}^m} \left[ \frac{2}{\sqrt{3}} \left| \ln \left( \frac{d(I+1, J)}{d_0} \right) \right| \right]^{-n} \quad [12]$$

which is solved numerically. The volume of each element in contact with the die wall is subtracted from the initial volume, and this remainder is used to calculate the new uniform thickness in the unsupported region. If there are  $n$  elements, this is called  $d(n, 2)$ . A new hoop stress is calculated using steps 4-6 of the six step procedure outlined above. A new force  $F(n, 2)$  is then calculated, [12] is applied and  $d(n, 3)$  is calculated. This procedure is repeated 20 times, although convergence usually occurs in 15 iterations. A similar procedure is described by Ghosh and Hamilton.<sup>3</sup>

For frictionless condition the six step procedure can be applied without incrementation or iteration. For perfect sticking, an analysis was made based on another procedure of Ghosh and Hamilton.<sup>4</sup> Assuming that only unsupported metal deforms, the procedure is the same, except

$$X = \frac{r_1}{\tan \phi} \left[ 1 - \left( \frac{d}{d_1} \right) \right]^{1/\beta} \quad [13] \quad \text{where} \quad \beta = \frac{2 - \theta_1 \tan \phi}{\theta_1 \tan \phi} \quad [14]$$

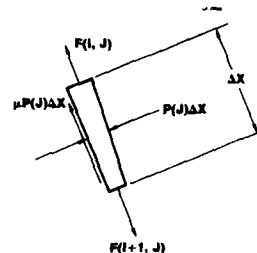
An incremental, iterative approach is not required in the case of perfect sticking.

#### Results

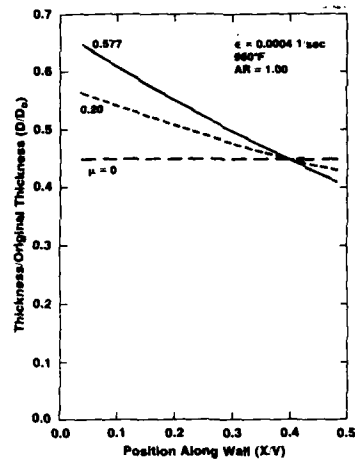
The strain distribution is shown for perfect sliding ( $\mu=0$ ), perfect sticking ( $\mu=0.577$ ) and for  $\mu=0.20$  for a pan with an aspect ratio of 1.00 in Fig. 4. (Aspect ratio is used to define the geometry of the pan. For aspect ratios greater than 2 the sheet will touch bottom before touching the sides. For aspect ratios less than 2, the reverse is true.)

The distributions shown in Fig. 4 are up to the end of Region II only. As expected, the perfect sliding case shows no thickness gradient. It was found that, for  $AR=1.00$ , for a coefficient of friction,  $\mu > 0.24$  there exists a critical length along the die wall within which sticking will occur (see  $X$  in Fig. 2). This critical length is a function of aspect ratio and coefficient of friction. A similar phenomenon occurs in forging.<sup>5</sup> It was shown analytically that sticking can occur over a majority of the contact region, even for very low coefficients of friction.

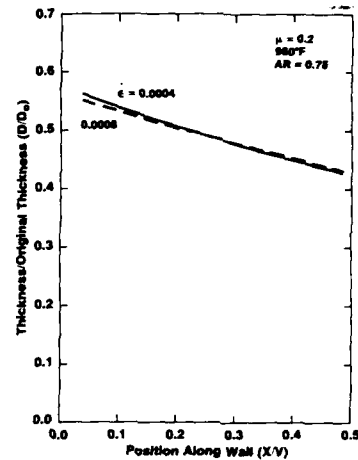
The material properties of strain rate sensitivity,  $m$ , and flow stress,  $K$ , were found to have no effect on the strain distribution. Strain rate affected the strain distribution slightly, as shown in Fig. 5, when the coefficient of friction was 0.2. For sticking friction, strain rate has no effect on the strain distribution, nor do strain rate sensitivity, strain hardening or flow stress. Only geometry affects strain distribution for sticking conditions.



Free Body Diagram  
Figure 3



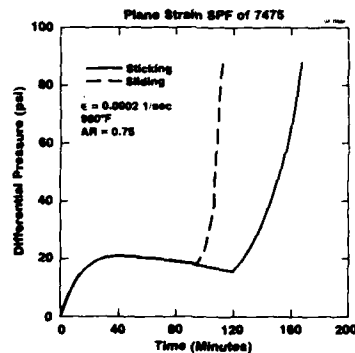
The Effect of Friction on Strain Distribution  
Plane Strain SPF Model Predictions with  
Sliding Friction Incorporated  
Figure 4



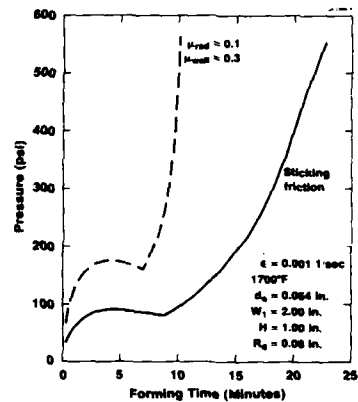
The Effect of Strain Rate on Strain Distribution  
Plane Strain SPF Model Predictions with  
Sliding Friction Incorporated  
Figure 5

The pressurization schedule required to maintain a constant true strain rate for a pan with an aspect ratio of 1.00 is shown in Fig. 6 for perfect sticking and perfect sliding.

There is no difference in pressure at a given time until Region III. However, the depth of the pan at a



The Effect of Friction on Pressurization Schedule  
Figure 6



The Effect of Friction on Pressurization Schedule  
for Ti-6Al-4V Plane Strain SPF Model Predictions  
(From Ghosh & Hamilton)  
Figure 7

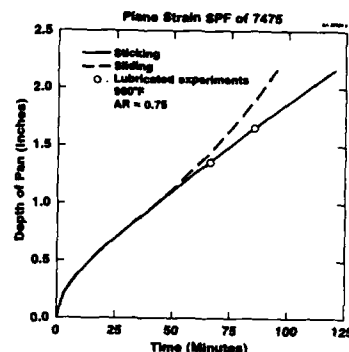
given time will vary with friction. Most failures during forming occur during Region III, so the pressure profile during that stage is important.

The effect of friction on the pressure profile predicted by the model of Ghosh and Hamilton is shown in Fig. 7 for a shallow pan. The difference in pressure profile during Regions I and II is due to sliding over the die profile radius on metal feeding into the die from outside the die, but in-board of the clamping bead. The current model assumes a zero die radius (sharp) and that clamping occurs at these theoretical sharp corners.

### Experimental Results

The pressurization schedule which must be maintained in order to result in a true effective strain rate of  $0.0002 \text{ sec}^{-1}$  and an aspect ratio of 0.75 is shown in Fig. 6 for perfect sliding. These curves are nearly coincident up to the point where contact with the bottom of the die first occurs. Fig. 8 shows the depth of the formed pan, for the same forming conditions, as a function of time, up to contact with the die bottom for perfect sliding and perfect sticking. These curves start to diverge when the sheet first contacts the die wall.

SPF tests were performed following the pressure/time schedules shown in Fig. 6 up to times less than that at which contact with the bottom would occur. Boron nitride was used as a lubricant. The results of the experiment, shown in Fig. 8, indicate that the sticking model accurately simulates the SPF process, even when a lubricant is used. The effect of friction on forming time predicted by Ghosh and Hamilton<sup>3</sup> does not necessarily contradict this result. This result may only mean that the low coefficients of friction used by Ghosh and Hamilton in their model cannot be achieved experimentally for aluminum, even with a good lubricant.



The Effect of Friction on Forming Time  
Figure 8

### Conclusions

Because strain rate has little effect on strain distribution, the pressurization schedule used during SPF will affect producibility only through the effect of strain rate on superplastic formability. Since a sample well coated with boron nitride was shown not to violate the sticking assumption, any overspray of the sealing flange area, which must be coated to aid in removing the part from the die, will not result in changes in the thickness distribution which could cause a deviation from the desired strain rate when a pre-specified pressure-time relationship is used. The validity of the assumption that sticking occurs whenever the sheet touches the die will greatly simplify the development of models to analyze more complex shapes. Demonstration that sticking can occur even with low coefficients of friction indicates that efforts to develop a high temperature lubricant will not likely have much effect on strain distribution in SPF parts.

### References

1. J. M. Story, J. I. Petit, D. J. Lege and B. L. Hazard, "The Effect of Forming Process Variables on Cavitation in the Superplastic Forming of 7475 Aluminum," *Proc. NAMRC-XIII*, Berkeley, CA, 1985, pps. 252-259.
2. J. M. Story, J. I. Petit, D. J. Lege and B. L. Hazard, "Forming Process Variable Effects on Cavitation in the Superplastic Forming of Commercially Produced 7475 Aluminum," *Superplasticity in Aerospace - Aluminum*, *Proc. Int. Conf.*, Cranfield, U.K., 1985, pps. 67-104.
3. A. K. Ghosh and C. H. Hamilton, "Superplastic Forming of a Long Rectangular Box Section - Analysis and Experiment," *Process Modeling*, ASM, T. Altan and H. Gegel, editors, 1979, p. 303.
4. A. K. Ghosh and C. H. Hamilton, "On Constant Membrane Stress Test for Superplastic Metals," *Met. Trans.*, 11A, 1980, pps. 1980-1915.
5. E. G. Thomsen, C. T. Yang and S. Kobayashi, *Plastic Deformation in Metal Processing*, MacMillan, 1965, p. 236.

BULGE-FORMING OF DOMES; A COMPARISON OF THEORETICAL  
PREDICTION AND EXPERIMENT

Z.X. Guo,<sup>†</sup> J. Pilling<sup>\*</sup> and N. Ridley<sup>†</sup>

<sup>†</sup> Manchester Materials Science Centre  
University of Manchester/UMIST  
Grosvenor Street  
Manchester, M1 7HS, England.

<sup>\*</sup> Department of Metallurgical Engineering  
Michigan Technological University  
Houghton, Michigan 49931, U.S.A.

Abstract

Bulge forming of domes has been performed to investigate the superplastic behaviour of aluminium alloy 7475 sheet material under biaxial stress conditions. The variations of dome height, thickness distribution, and dome geometry have been examined experimentally. It was observed that dome height varied with time in a non-linear manner at a constant forming pressure. Both the thickness distribution and dome geometry were a function of dome height. The strain-rate sensitivity parameter,  $m$ , has been found to play an important role in thickness distribution. Modelling of the forming process has been carried out to predict the bulging behaviour. The variation of thickness at any point on a dome has been analytically expressed as a function of strain rate sensitivity,  $m$ , and dome height. A significant improvement in thickness distribution along the dome profile, in the variation of thickness distribution with dome height, and in the forming time-height relationship has been obtained in the present model, compared with the predictions of previous theoretical models of the forming process.

Superplasticity and Superplastic Forming  
Edited by C.H. Hamilton and N.E. Paton  
The Minerals, Metals & Materials Society, 1988

### Introduction

In recent years superplastic forming (SPF) has become a well established advanced shaping technique (1). Commercial SPF processes usually involve, at least in the early stages, the bulge-forming of simple domes. It is, therefore, of significance to examine, both experimentally and theoretically, the forming process. Early work on the bulge forming of domes has shown an important feature to be the non-uniform thickness along the dome profile (2,3). The distribution of thickness varies with dome height and with strain rate sensitivity,  $m$ . However, previous theoretical analyses have not considered the variation of thickness (4,5), are based on the incorrect assumption of a balanced biaxial stress state (2,6-8), or require extensive and tedious calculations using iterative or numerical methods (3).

The present work has involved an experimental and theoretical investigation of the bulge-forming of aluminium alloy 7475 at constant pressure, with particular interest in the following: (a) The variation of dome height with forming time. (b) Thickness non-uniformity and factors influencing the non-uniformity. (c) The geometry of dome profiles (experimental only).

### Experimental

Discs of 65 mm in diameter were machined from sheet material, with a thickness of 1.5 mm. Each specimen was clamped between two hollow dies and was bulged at 516°C using gas pressure, which was automatically maintained to an accuracy of  $\pm 3\%$  by a microcomputer through a control system (9). Domes were formed into the die cavity, which was 40 mm in diameter, to various heights up to 30 mm. The domes were sectioned through a meridian plane, and the dimensions were measured using an optical microscope.

### Theoretical

As seen in Fig. 1, bulge forming involves an equibiaxial stress state at the dome apex, with the principal stresses  $\sigma_c$ ,  $\sigma_t$  and  $\sigma_s$ , given by:

$$\sigma_c = \sigma_t = \frac{PB}{4S_a} \left[ H + \frac{1}{H} \right]; \quad \sigma_s = 0 \quad (1)$$

where subscripts c, s, and t, refer to the circumferential, thickness, and tangential directions, respectively;  $P$  is the forming pressure;  $B$  is the die radius;  $h$  and  $S_a$  are the height and the apex thickness, respectively, of a dome, and  $H$  is the relative dome height ( $h/B$ ).

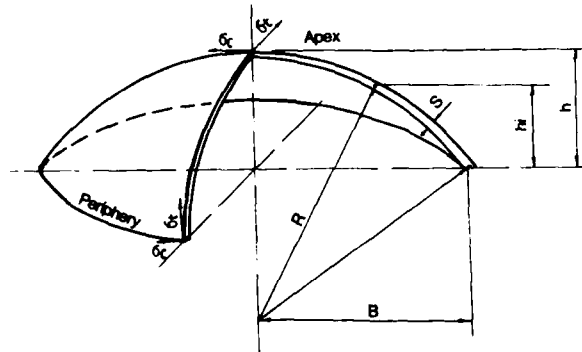


Fig.1. Schematic of bulged dome.

If a dome is assumed to be spherical, and the bending and shearing effects are ignored, the stresses at the dome periphery can be determined from the condition of plane strain deformation which may be expressed as,

$$\sigma_c = \frac{\sigma_t}{2} = \frac{PB}{8S_p} \left[ H + \frac{1}{H} \right] ; \sigma_s = 0 \quad (2)$$

where  $S_p$  is the thickness at the periphery. At other positions on a dome,  $\sigma_c$  needs to be determined.

A study of plastic hole growth along a dome profile has shown that the ratio of hole dimensions in the circumferential and tangential directions increases logarithmically with the relative position (height),  $h_i/h$ , of the hole on the dome profile (9);  $h_i$  is the height of the hole above the dome periphery. Since the plastic holes are stress related, it may be assumed that the ratio of the circumferential and tangential stresses also varies with  $h_i/h$  in a logarithmic manner. By using the boundary conditions given by equations (1) and (2) we have

$$\frac{\sigma_c}{\sigma_t} = \lambda = \log_M \left[ (M - \sqrt{M}) \frac{h_i}{h} + \sqrt{M} \right] \quad (3)$$

where  $M$  is a positive integer larger than 1, and may depend on the strain rate sensitivity of a material;  $M = 10$  has been found to be appropriate for the alloys employed here (9).

From the constitutive equation for superplasticity,  $\dot{\epsilon} = A\dot{\epsilon}^n$  ( $n = 1/m$ ), and the concepts of effective stress and effective strain rate, and the von Mises flow rule, the thickness strain rate,  $\dot{\epsilon}_s$ , at any point on a dome can be obtained as

$$\dot{\epsilon}_s = -A \left[ \frac{PB}{4} \left[ H + \frac{1}{H} \right] \right] \left[ \frac{1+\lambda}{2} \right] \left[ 1 - \lambda + \lambda^2 \right]^{\frac{n-1}{2}} \cdot S^{-n} \quad (4)$$

The above equation shows that the variation of thickness along the dome profile not only depends on the dome height,  $H$ , but also on the material parameter  $n$  or  $m$  ( $=1/n$ ), and the sub-structure related parameter,  $A$ . By further considering a group of geometric relationships for a spherical dome, and regarding the dome as consisting of a series of annuli with the thickness being constant in each annulus, the forming process can be predicted. The values used in the model are:  $m = 0.53$  and  $A = 3.17 \times 10^{-5}$ , for the corresponding strain rate range of  $10^{-4} - 10^{-3} \text{ s}^{-1}$ .

### Results

The variation of relative dome height,  $H$ , with time  $t$ , for different pressures is shown by the experimental data points in Fig. 2, where a sigmoidal trend of variation of height is observed. Theoretical predictions of Al-Hassani et al (A-H model) (6), Ragab (7) and the present analysis are also shown. The agreement between the theories and experiment is reasonable, with a small improvement being observed for the present model. Moreover, the A-H model is only valid for  $H < 1$  and Ragab's model produces a discontinuous variation of dome height at  $H = 1$ .

A dome cross section is shown in Fig. 3, and it is seen that thickness decreases from the periphery of the dome to its apex. A thin section observed at the clamped (bottom) corner is due to bending and stretching effects. The variation of the absolute value of thickness strain,  $\epsilon$ , along the dome profile is plotted against relative position,  $h_i/h$ , on the dome, Fig. 4. It appears that the thickness strain (absolute value) increases

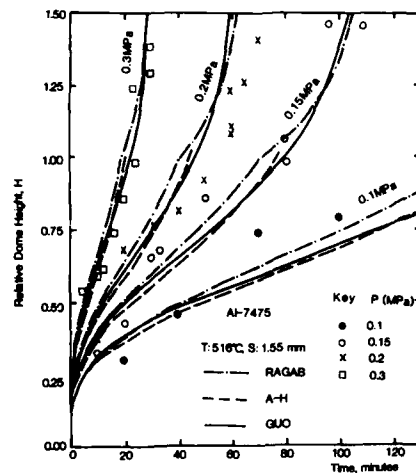


Fig. 2. Relative dome height versus forming time. Experimental and theoretical.

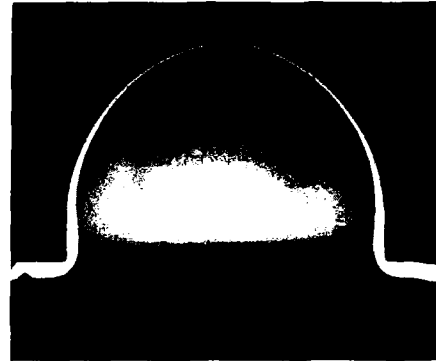


Fig. 3. Dome profile of bulged sheet.

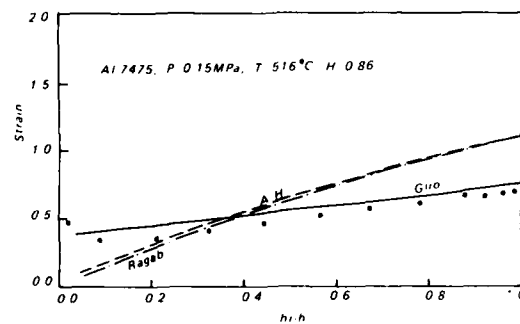


Fig. 4. Variation of thickness strain with relative height for sheet bulged at 0.15 MPa. Experimental (points) and theoretical.

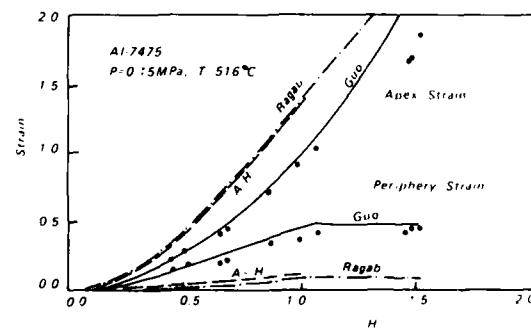


Fig. 5. Variation of thickness strain at apex and periphery for sheet bulged at 0.15 MPa. Experimental (points) and theoretical.

linearly with  $h_i/h$ . The predictions of the present analysis, and of the Ragab and A-H models are also shown in Fig. 4. Good agreement has been achieved between the present theory and experiment. The other two models predict too high a thickness gradient, quite different from the experimental observations. To further evaluate the thickness non-uniformity, both the apex strain and periphery strain are shown in Fig. 5, as a function of relative dome height,  $H$ . It is clearly seen that the



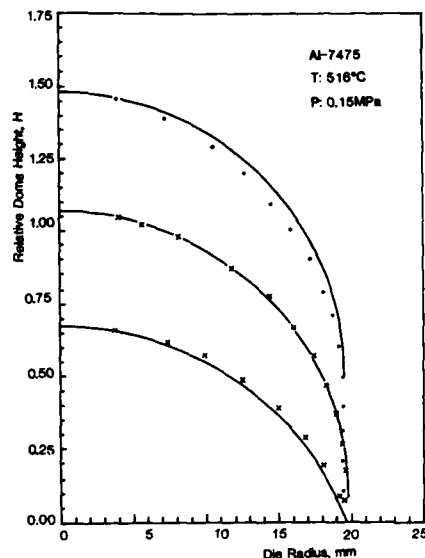


Fig. 6. Dome geometry versus relative height.

#### Discussion

As noted in equations (1) and (2), relatively higher stresses are encountered both in the early stages of forming, because  $H$  is very small, and in the later stages of forming, due to the large decrease in thickness. This leads to high strain rates in these stages, and so results in a sigmoidal variation of dome height with time, Fig. 2.

Due to the constraint at the dome periphery, different stress levels are observed even in the initial stages of forming, as indicated in equation (1) and (2). It is the stress difference which is responsible for the occurrence of the non-uniformity of dome thickness, as observed in Fig. 4. This thickness gradient leads to further differences in the stresses. Therefore, the greater the dome height, the larger the non-uniformity of thickness, Fig. 5.

From equations (3) and (4), the ratio of the thickness strain rates at the dome apex,  $\dot{\epsilon}_a$ , and dome periphery,  $\dot{\epsilon}_p$ , can be shown as

$$\frac{\dot{\epsilon}_a}{\dot{\epsilon}_p} = \left[ \frac{2}{\sqrt{3}} \right]^{\frac{1}{m}} \left[ \frac{S_p}{S_a} \right]^{\frac{1}{m}} \quad (5)$$

Hence, the higher the value of  $m$ , the smaller the strain rate difference and the less the non-uniformity of thickness.

The main difference between the present model and the two models examined is that the former has taken account of the effect of  $m$  value on thickness distribution. The latter two analyses only predict a geometry-related variation of thickness (6,7). The satisfactory agreement between the present theory and experiment indicates that: (a) the model is relatively suitable for the forming process and (b) the strain rate sensitivity parameter,  $m$ , plays an important role in the dome thickness distribution. The variation of dome profile is probably due to the effects of the large initial stresses, the superplastic characteristics of the

non-uniformity reflected by the difference of apex and periphery strains, increases with dome height. The present model gives improvement with experiment, compared with the earlier analyses.

The actual geometry of dome profiles varies with dome height (9). The profile is flatter than a spherical shape when  $H < 1$ , sharper than a spherical form when  $H > 1$ , and spherical at  $H = 1$ . An example is shown in Fig. 6, where data points outline half of a dome profile; the adjacent curve is a circular arc through the dome apex and the last point of contact with the die wall.

material, and the geometry of stress state (9).

#### Conclusions

- (1) For a constant bulging pressure, the dome height increases sigmoidally with time. The geometry of the dome profile is a function of dome height, and can be flatter or sharper than, or equivalent to, a spherical shape.
- (2) For a bulge formed dome, the thickness strain seems to vary linearly with the height of a reference point measured from the dome periphery. The non-uniformity of thickness increases with dome height.
- (3) The strain rate sensitivity parameter,  $m$ , plays an important role in the thickness distribution of bulge-formed shapes. The higher the value of  $m$ , the less the non-uniformity of thickness.
- (4) A model for the bulge forming of domes has been established, which takes account of the effect of  $m$  value on the forming process and yields satisfactory agreement with experiment. Improvement upon previous analyses has been achieved (6,7). The present model can be easily modified for use in the bulge forming of other shapes.

#### References

1. Superplastic Forming of Structural Alloys, ed. N.E. Paton and C.H. Hamilton (Warrendale, P.A.: TMS-AIME, 1982)
2. D.L. Holt, "An Analysis of the Bulging of a Superplastic Sheet by Lateral Pressure", Int. J. Mech. Sci., 12 (1970) 491-497.
3. G.C. Cornfield and R.H. Johnson, "The Forming of Superplastic Sheet Metal", Int. J. Mech. Sci., 12 (1970) 479-490.
4. F. Jovane, "An Approximate Analysis of the Superplastic Forming of a Thin Circular Diaphragm: Theory and Experiments", Int. J. Mech. Sci., 10 (1968) 403-427.
5. J.A. Belk, "A Quantitative Model of the Blow-Forming of Spherical Surfaces in Superplastic Sheet Metal", Metals Technol., 17 (1975) 505-511.
6. S.T.S. Al-Hassani, G.G.W. Clemens and T.Y.M. Al-Naib, "The Free Bulge Forming of Zn-Al Superplastic Sheet from a Circular Die", Proc. 18th Int. Machine Tool Design and Research Conference, ed. J.M. Alexander, (London, 1977) 361-368.
7. A.R. Ragab, "Thermoforming of Superplastic Sheet in Shaped Dies" Metals Technol., 10 (1983) 340-348.
8. Y.Q. Song and J. Zhao, "A Mechanical Analysis of the Superplastic Free Bulging of Metal Sheet", Mater. Sci. Eng., 84 (1986) 111-125.
9. Z.X. Guo, Ph.D. Thesis, University of Manchester, 1988.

# A STUDY ON SUPERPLASTIC ALLOY SHEET BULGING

## UNDER THE MICROCOMPUTER CONTROL

Tao Shuxue Ma Longxiang

Department of Metal Forming  
Northeast University of Technology  
Shenyang, China

### Abstract

In our investigation, a simple approach to derive the optimal forming pressure vs. forming time relationship for constant strain rate bulging(C.S.R.B) process including free bulging of a circular membrane, bulging into a cylindrical die, and bulging into a v shaped groove was presented. A microcomputer system was set up to fulfill the smooth and automatic controlling of the changing of pressure with time to maintain strain rate constant during a forming process. Experiment was conducted for both free bulging and cavity bulging(bulging into a top hat) of two different superplastic alloy sheets, 7075 and ZnAl5 eutectic. Comparison of thickness distribution of the bulged profile was made between constant pressure and constant strain rate forming. The reason of the more uniform thickness distribution achieved by C.S.R.B was explained with emphasis on the effect of dynamic strain rate hardening caused by small fluctuation of strain rate.

### Introduction

Since Jovane (1) presented the concept of constant strain rate bulging(C.S.R.B) and indicated that constant pressure forming was unacceptable due to the wide variation of strain rate during the forming process, the method and mathematical analysis have been well developed by Hamilton, etc.(2,3) for C.S.R.B process. The constant pressure bulging can cause severe strain rate variation in some areas of the bulging profile and so the severe thinning or even fracture in these areas because  $m$  is not constant and the strain rate hardening effect has not been fully utilized during the bulging process. While, on the other hand, the C.S.R.B can control the superplastic alloy sheet to deform in its optimal superplastic conditions by maintaining a optimal constant strain rate at the critical point so a sufficiently high  $m$  value is maintained, and this results in that forming times are saved, formability improved and more uniform thickness distribution of the bulged profile obtained.

Fields and Stewart (4) had given an interesting analysis  
Superplasticity and Superplastic Forming  
Edited by C.H. Hamilton and N.E. Paton  
The Minerals, Metals & Materials Society, 1988

of strain hardening and softening effect on  $m$  value and thickness distribution of the superplastically formed components. In this paper, we first established the optimal pressure vs.  $t$  relationship by a simple theoretical approach. Bulging experiments were then conducted under the control of a microcomputer system. By extending the explanation made by Fields, we can explain the effect of dynamic strain rate hardening on the thinning characteristics of the bulging profile during the C.S.R.B process.

### Theoretical Approach

As shown in Fig. 1, the optimal pressure vs. time relationship for these three stages was derived under the assumption of constant volume, uniform thinning (except for those parts contacted the die in the second and third stages), and Von Mises criterion being valid for the tested materials. The familiar relationship  $\sigma = K\dot{\epsilon}^m$  was used in which the  $\sigma$  and  $\dot{\epsilon}$  were substituted by effective stress  $\bar{\sigma}$  and strain rate  $\dot{\bar{\epsilon}}$  respectively. The detailed description was presented elsewhere (5).

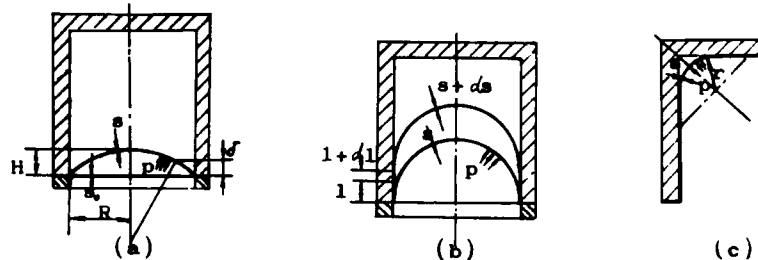


Fig 1 - Diagram of sections of the bulged profile of a top hat at three different stages (a) free bulging, (b) bulging into a cylindrical die (c) corner filling.

The so derived  $p$  vs.  $t$  relationships are as follow

$$p_1 = 4K\bar{\epsilon}^m \frac{S_0}{R} \frac{(\exp(\bar{\epsilon}t) - 1)^{1/2}}{\exp(2\bar{\epsilon}t)} \quad (1)$$

$$p_2 = K\bar{\epsilon}^m \frac{S_0}{R} \exp(-\bar{\epsilon}t) \quad (2)$$

and

$$p_3 = K\bar{\epsilon}^m \frac{S_0}{R} \exp(2.3034\bar{\epsilon}t) \quad (3)$$

Where  $R$  is the radius of the die,  $S_0$  is the initial thickness of the bulged sheet. These equations can be connected to produce a profile similar to that by Hamilton or Bampton (6), with or without backpressure.

### Experimental

#### Materials

The Zn-5Al-0.03Mg eutectic which has a very good capacity for electroplating was prepared by homogenizing and hot then cold rolling of ingots with dimensions of 80×200×300 mm into 2.0 mm thick superplastic sheets. The alloy has a maximal  $m$  value of 0.65 at the strain rate of  $8.33 \times 10^{-3}$  1/s and 330°C.

The 7075Al was prepared by TMTA method (7) into final thickness of 2.0 mm with  $m$  value about 0.82 at a strain rate of  $8.33 \times 10^{-4}$  1/s and 516 °C.

### Testing Set

The testing set was made up with a microcomputer system and a superplastic bulging set as shown in Fig. 2. The control

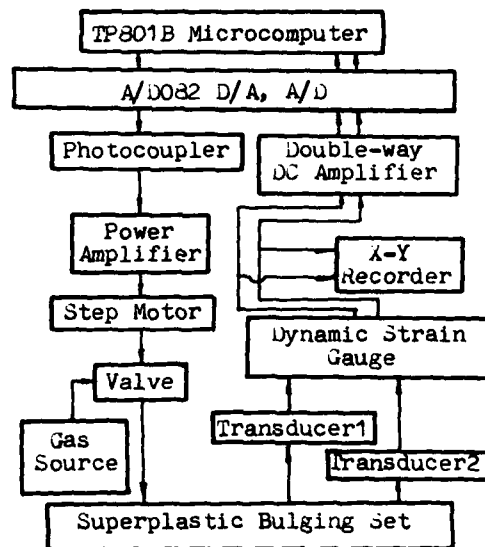


Fig. 2 - The scheme of the testing set

system is a real-time, closed-loop system. After the parameters of  $\dot{\epsilon}$ ,  $m$ ,  $K$ ,  $S_0$  were input into the computer, the computer began to compute according to the equations (1), (2) and (3), thus a  $p$  vs.  $t$  profile was built up in the computer. When the control system began to work, the computer drove the step-motor to open the valve of the gas source. Transducer 1 and 2 (for monitoring the backpressure) were used to receive feedbacks and to provide gas pressure information to the computer. The bulging set consisted of a furnace, a die with 50 mm radius and a moveable depth and a temperature control unit.

### Bulging Test

Bulging tests were made with the prepared ZnAl5 and 7075 alloy sheets at constant pressure and different constant strain rates. The sheets were cut into 140 mm diameter blanks. Blanks were clamped against the die and held for 15 min. prior to bulging. Thickness measurements along the profile of the formed parts were made.

### Results and Discussion

We select some typical test results here as shown in Fig. 3, 4, 5. It is obviously seen that the thickness distribution of the hemispheres and top hats formed by C.S.R.B is much more

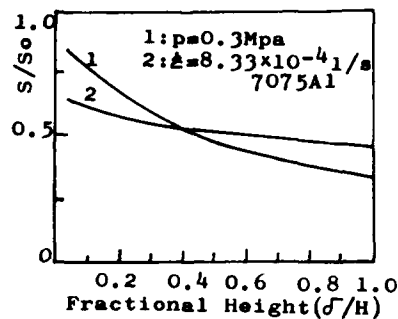


Fig. 3-Final thickness over original thickness vs. fractional height for hemisphere formed at constant pressure and constant strain rate.

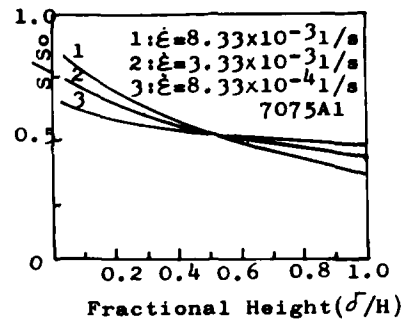


Fig. 4-Thickness distribution of hemispheres formed at three different constant strain rates.

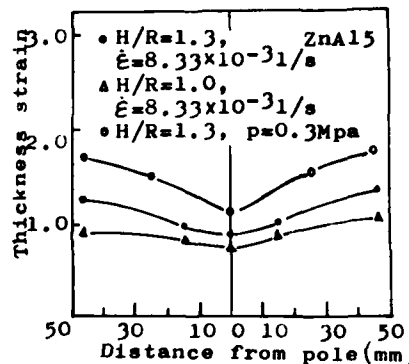


Fig. 5-Thickness strain of top hats of different depths formed by constant pressure and constant strain rate.

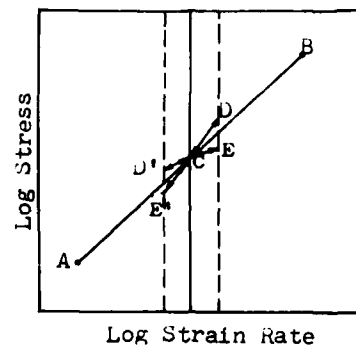


Fig. 6-Schematic representation of the effect of strain hardening and small strain rate fluctuation on flow stress.

uniform than that formed by constant pressure. While for C.S.R.B, the thickness distribution of the components formed at optimal constant strain rate which represents a higher  $m$  value has advantage over that formed at other strain rates lower  $m$  value.

The uniform thickness achieved by C.S.R.B has been generally explained as a result of maintaining the sheet deforming in optimal superplastic conditions. However, if the strain rate is maintained absolutely constant in the critical area during forming process and the flow stress is also constant, this area should deform more easily than other areas. We would have not expected the uniform thickness distribution being achieved. A dynamic process should be involved for the explanation of this phenomena.

As shown in Fig. 6 after Fields and Stewart mainly, We

assume that, because of the accuracy of the control system and this is really the case in our research, the forming strain rate is not maintained constant at point C, but a small fluctuation of strain rate occurs, i.e., the strain rate is only quasi-constant. Therefore, for alloys exhibiting strain hardening during the superplastic deformation process as ZnAl5 and 7075 in our research, the flow stress will go through a C-D and a C-D' cycle. The dynamic strain rate hardening effect occurs in the C-D cycle. The increase of flow stress and  $m$  value will slow up the critical area of the bulged profile to deform and, relatively, to drag the areas close to the clamped edge to deform. This results in the increased uniformness of the thickness distribution of the formed parts. For alloys that exhibit no strain hardening and strain softening, the stress will change along A-B line, and the  $m$  value under this condition would be constant. If the alloy exhibits strain softening the flow stress will go through C-E and C-E' cycles. At the last two cases, the level of the dynamic strain rate hardening effect would be lower than that in alloys exhibiting strain hardening.

#### Summary

A simple approach to derive the optimal forming pressure vs. time relationship for C.S.R.B process was presented in our investigation with a microcomputer control system setting up to fulfill the control process. The aim of which was to develop a way for industrial application of the C.S.R.B method.

The thickness distribution of the parts formed by the optimal Constant strain rate bulging process was more uniform than that formed by constant pressure and non-optimal constant strain rates. This has been explained by the effect of dynamic strain rate hardening.

#### References

1. F. Jovane, "An approximate analysis of the SPF of a thin circular diaphragm: theory and experiments", Int. J. Mech. Sci., 10(1968), 403-427.
2. C.H. Hamilton and N.E. Paton, U.S. Patent 4181000.
3. A.K. Ghosh and C.H. Hamilton, "Influence of materials parameters and microstructure on SPF", Met. Trans. A, 5(1982) 733-743.
4. D.S. Fields and T.J. Stewart, "Strain effects in superplastic deformation", Int. J. Mech. Sci., 13(1971), 63-75.
5. Tao Shuxue, "The optimal relationship of pressure vs. time for C.S.R.B process and the fulfillment of its control" (Accepted by the Journal of the Northeast University of Technology).
6. C.C. Bampton, A.K. Ghosh and M.W. Mahoney, "The cause, effects, and control of cavitation in superplastic 7475 Aluminum airframe structures" ("Superplasticity in Aerospace-Aluminium" Conference, Cranfield, England, 1985).
7. Jiang Xinggang, "Research on the superplasticity of conventional 7075Al", (M.S. thesis, Northeast University of Technology, 1987).

## SUPERPLASTIC FORMING OF TI-ALLOY VESSEL

Chen Bingkin\*    Hai Jintao\*\*

\*Research Institute of Astronautic Standard of China

\*\*Beijing Research Institute of Mechanical & Electrical  
Technology, SCMI, Beijing, China

### Abstract

Based on the study of forming method and superplasticity of Ti-6Al-4V alloy, a superplastic forming procedure of Ti-alloy global spherical vessel is suggested in this paper. The experimental results point out that the suggested superplastic forming procedure is better than other process in product quality and decreasing consumed materials. The method details of forming global seamless spherical container is also introduced here.

Superplasticity and Superplastic Forming  
Edited by C.H. Hamilton and N.E. Paton  
The Minerals, Metals & Materials Society, 1988



### Introduction

Because of its higher strength, lower density and better corrosion resistance, Ti-alloy is used widely for chemical industry, navigation, airspace and other industries. But, on the other hand, the application is limited by its disadvantages, such as larger deformation resistance, lower formability and difficulty of working.

It is found that the Ti-alloy with finer grain has better plastic deformation capability, and its elongation is over 1000% under proper temperature and strain rate. It is also found that the effect of grain size on its superplasticity is small. This fact provides a new method to make Ti-alloy parts, i.e. superplastic forming.

The Ti-alloy spherical vessels are very useful parts because of its significant advantages due to its shape, such as the largest volume and the best stress state. The shape of the vessel is shown in Fig.1. A type of materials used for making the vessel is Ti-6Al-4V alloy.

### Some Forming Methods

The small spherical vessel with pipe joint can be made by means of forging, and its technological process is shown in Fig.2. That is the die forging of two half spherical vessels, cutting by copy lathe and welding them into a global spherical vessel. The characters of this method are simple process, accurate part size and finer part exterior, but it also has some disadvantages: wasting a lot of material, lower production efficiency, no uniform microstructure and instability of product quality.

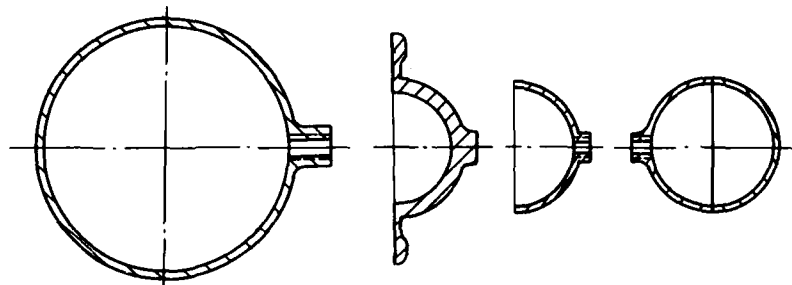


Fig.1 Spherical vessel

Fig.2 Process of die forging

For the spherical vessel without pipe joint or the vessel allowing welding the pipe joint, the deep drawing is often adopted, its technological process is shown in Fig.3. The procedure includes punching sheet, deep drawing two half-spherical shells and welding them into a global spherical vessel. High use factor of material and simple operation are advantages of this method. But it is difficult to obtain more accurate size of products.

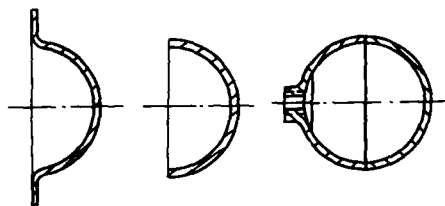


Fig.3 Process of drawing forming

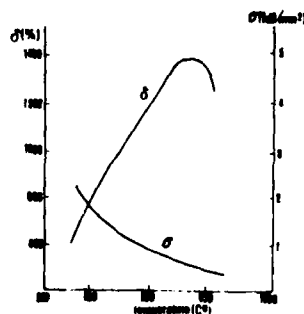


Fig.4 Flow stress and elongation

#### Superplastic Forming

The development of superplastic technology provides convenience for making Ti-alloy parts. The experimental curves of flow stress  $\sigma$  and tensile elongation  $\delta$  vs temperature under strain rate  $\dot{\epsilon}=1 \times 10^{-3}$  /second are shown in Fig.4. From this figure it can be seen that a optimal temperature corresponding to the best plasticity is 1193-1213K, the largest tensile elongation is 1300-1400%.

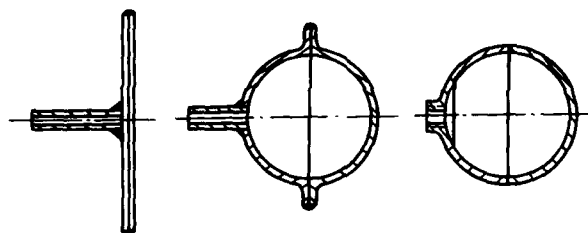


Fig.5 Process of superplastic forming using sheet

The technological process of superplastic forming the spherical vessel using sheet is shown in Fig.5. Based on the diameter of spherical vessel the blank dimensions can be determined, and a experimental formula is

$$D_b = (1.4 \sim 1.5) D_s$$

where  $D_b$  is the diameter of blank, and  $D_s$  is the diameter of the sphere. A circular hole of dia. 6mm is made at the centre of a blank, and then a pure titanium pipe with outer dia. 6mm is connected to the hole by argon arc welding. Put the blank with the pipe on another blank and weld them along their outer edges for sealing by argon arc welding. Thus a global blank is completed. Putting it into a special die, it is heated up to 1203±10K in a special press for superplastic forming. Argon with pressure of 6-14kg/cm<sup>2</sup> from the Ti-pipe comes into the blank and the bulging

begins. After a period of time the part is formed and is taken out from the die, its profile is shown in Fig.6, the two half spherical shells are welded into a spherical vessel we wanted. The pipe joint machined according to the technological requirements will be welded in other methods.



Fig.6 Profiles of half spherical vessels

The development of the spinning technology provides a new way for making spherical vessel. A suggested procedure is that taking a seamless tube as the blank, machining it according require dimensions, spinning at its two ends. One of the ends is sealed by argon arc welding, and another end is connected with a pure titanium pipe of  $\phi 6 \times 1 \text{ mm}$ . Such machined blank is put into a spherical die and is heated up to  $1203 \pm 10 \text{ K}$ . As soon as the temperature reaches the set value, entering argon, pressing in the vertical direction and the bulging begins. This technological process is shown in Fig.7. The formed part can be seen in Fig.8.

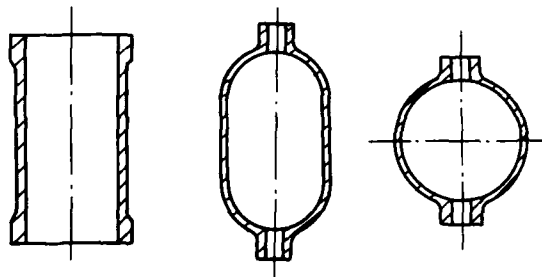


Fig.7 Process of superplastic forming using seamless tube

Using the technological procedure the spherical seamless container can be manufactured and the quality and reliability of product can be increased. It is emphasized that the superplastic forming can give uniform deformation and stable product quality, and the degree of uniformity of wall thickness is also improved significantly. For the spherical container with special requirements in quality and nonspherical containers in shape of revolution, these advantages are more distinctive.

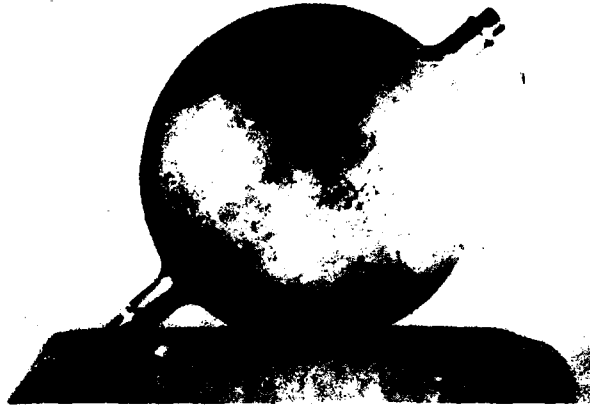


Fig.8 Spherical vessel produced by superplastic forming

#### Conclusions

Above mentioned various forming process of Ti-alloy container is applicable for different products, but the experimental results point out that the superplastic forming is better than other methods in the aspect of the product dimensions accuracy, product microstructure, quality stability of product and other overall index.

THEORETICAL AND EXPERIMENTAL STUDIES ON THE  
PRESSURE THERMOFORMING OF HEMISPHERES OF ALLOY Ti-6Al-4V

D. Viswanathan\*, S. Venkataswamy\*\* and K. A. Padmanabhan

Department of Metallurgical Engineering  
Indian Institute of Technology  
Madras - 600036, India

Abstract

The thickness distribution, thickness strain and thinning factor in a hemispherical dome, formed by pressure thermoforming, were predicted by a modified form of an earlier analysis due to Holt, in which the plane strain condition existing at the clamped edge and the strain rate dependence of the strain-rate sensitivity index  $n$  and the material constant  $k$  are incorporated. It is shown that good correlation exists between the theoretical predictions and experimental results obtained at a forming temperature of 927°C.

\* Permanent address: Department of Mechanical Engineering, A.C. College of Technology, Anna University, Madras - 600025

\*\* Permanent address: Department of Production Technology, Madras Institute of Technology, Anna University, Madras - 600044

### Introduction

Superplastic forming of the alloy Ti-6Al-4V has already emerged as a specialised technique in the aerospace industries. The effects of the material and process parameters on the pressure thermoforming of superplastics have been considered (1-11). Theoretical predictions have also been made (5-12). The alloy Ti-6Al-4V has excellent superplastic properties in the range 800°C to 1000°C and the properties are optimal at 927°C in a strain rate range of  $10^{-5} \text{ s}^{-1}$  to  $10^{-3} \text{ s}^{-1}$ . In an analysis of the pressure thermoforming of thin sheets into shaped dies, the thickness distribution and the forming time are of considerable importance.

The influence of the process parameters on forming, e.g. on the thinning factor, thickness strain and bulge profile development, has been reported (5-7). Jovane (6) has analysed the bulging of a circular sheet clamped at its perimeter. His assumption of uniform sheet thickness throughout restricts the usefulness of his analysis. Holt (5) has analysed the same process and has estimated the distribution of thickness in the formed component as a function of the process parameters. He has used the approximation that the stress and strain states are 'balanced biaxial'. Also, Holt has assumed the material parameters of the strain-rate sensitivity index,  $m$  and  $k$  (a material constant) to be constant throughout deformation, whereas in practice they vary as functions of strain rate. Cornfield and Johnson (7) have, on the other hand, assumed that at any instant the dome is part of a sphere.

In this paper, the thickness distribution and bulge profile development are predicted for an optimum temperature of 927°C. Both  $m$  and  $k$  have been allowed to vary as functions of strain rate. The predictions have been compared with the experimental results obtained at 927°C.

### Bulge Profile Development: An Analysis

A Ti-6Al-4V alloy sheet, with an initial thickness  $S_0$  and diameter  $D$ , is considered. Initially the blank is assumed to be slightly curved (as in the earlier analyses) and  $\alpha$  is the inclination of the sheet. Let  $\sigma_\theta$  be the circumferential stress and  $\sigma_\phi$  the tangential stress, Fig.1. At the pole of the spherical cap, the stress and strain states are assumed to be 'balanced biaxial'. Since the flow behaviour of superplastic alloys obeys for all practical purposes the von Mises Criterion (11), the effective stresses at the pole ( $\sigma_p$ ) and the edge ( $\sigma_e$ ) (plane strain condition) of the spherical cap can be expressed as  $\sigma_p = \sigma_\phi$  and  $\sigma_e = 0.87 \sigma_\theta$  (9). The pertinent equation due to Holt (5) is

$$2\dot{p}/D = \frac{1}{2} (pD/4S_0k)^{1/m} (2p/D)^{(1+3/m)} (2p_0/D)^{(-2/m)} (\sin\alpha)^{-1/m} \quad (1)$$

which can be solved as follows:

$$\text{Let } C_1 = [(D/4)(pD/4k)^{1/m} (2/D)^{1+1/m}] \Delta t/s^{1/m} \quad (2)$$

$$C_2 = C_1 p_0^{1+1/m} / (\sin\alpha_0)^{1/m}; \quad C_3 = 1 - [(C_2/p_0)^{(m+3)/m}] \quad (3)$$

(To obtain equation (3),  $p$  was expanded in terms of  $p_0$  using the binomial theorem and the higher order terms were ignored.) Then,

$$\Delta p = C_2 / C_3 \quad \text{and} \quad p = p_0 + \Delta p \quad (4)$$

The dome surface was divided, as in the earlier analyses, into 10 concentric rings. For each increment of time, the new surface area of the dome, thickness at each ring of the dome, inclination of the sheet and stress in each ring were calculated for constant  $m$  and  $K$ . The procedure up to here is similar to that used by Holt (5), except for the correction made for the presence of plane strain at the clamped edge. A modification was made at this stage by introducing  $m$  and  $k$  as variables (functions of strain rate).

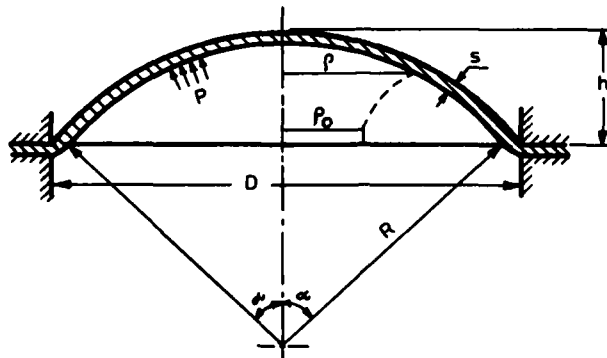


Figure 1 - Bulge profile development: Definition of symbols used.

#### Calculation of $m$ and $k$ as functions of strain rate

The flow properties of alloy Ti-6Al-4V tested at 927°C (4) are used to obtain  $m$  as the instantaneous slope at different strain rates of the  $\log \sigma - \log \dot{\epsilon}$  plot (derived from a polynomial fit between  $\log \sigma$  and  $\log \dot{\epsilon}$ ). Also  $\log k$  vs.  $\log \dot{\epsilon}$  was predicted from the above data (using the instantaneous values of  $m$  and  $\dot{\epsilon}$  and the observed stress value). From the above,  $m$  and  $k$  could be obtained as functions of strain rate by a polynomial regression analysis and the use of the forward selection procedure (13).

These functional forms of  $m$  and  $k$  were used in the theoretical analysis. A bulge profile was predicted, Fig.2. From the computer program, the sheet thickness at different intervals of time for different forming pressures was obtained. The stress gradient during forming was also predicted and plotted against the fractional dome height, Fig.3. It is observed that the stress variation in the different rings for small bulge heights lay within a narrow range but when the bulge height increased, the stress gradient from the pole to the edge of the dome became sharper.

#### Experimental Programme

The experimental set-up which consists of a hydraulic press and heating system has been described earlier (2,14). Pressure thermoforming of Ti-6Al-4V alloy sheets into hemispheres was carried out following earlier procedure (2,14). Experiments were conducted at temperatures of 830°C, 880°C, 927°C and 980°C. The forming pressure at each temperature was varied from 0.2 MPa to 0.8 MPa. The increase in the bulge height was recorded through an LVDT arrangement. The thickness at different points of the formed component was measured using an ultrasonic thickness gauge, which has an accuracy of  $\pm 0.001$ mm.

Many of these experimental results will be considered in detail elsewhere. Only those results that are relevant to the theoretical analysis presented above are discussed here.

#### Results and Discussion

##### Thickness distribution

The experimentally observed thickness distribution along the dome cross section at a forming temperature of 927°C and a gas pressure of 0.4 MPa is

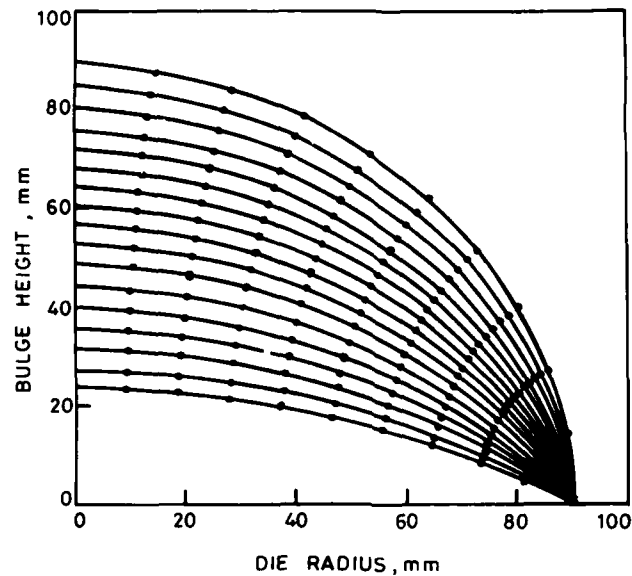


Figure 2 - A theoretically predicted bulge profile for a Ti-6Al-4V alloy sheet deformed at 927°C, with  $m$  and  $K$  varying as functions of strain rate. Forming pressure: 0.4 MPa.

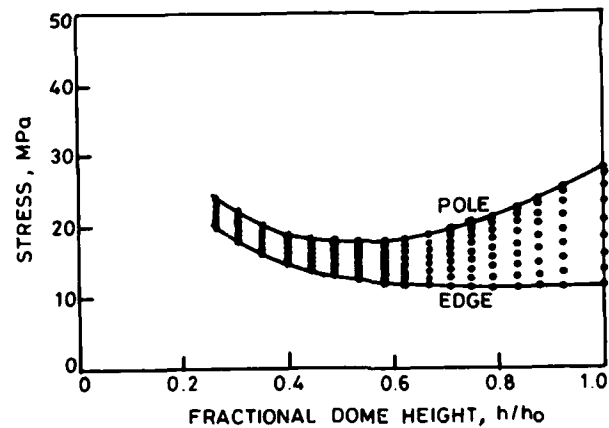


Figure 3 - Stress distribution predicted at each ring as a function of the fractional height of the dome. Temperature: 927°C. Pressure: 0.4 MPa.

shown in Table I, along with the theoretically predicted values. Evidently the correlation is good.

#### Thickness Strain

Thickness strain,  $\ln (S/S_0)$ , was computed from the measured thickness at various points along the circumference of the formed component ( $s$  is the measured thickness at a given point and  $S_0$  is the initial thickness). In



Table I. Thickness along the dome cross section

	Pole	Thickness in mm					Edge
Experimental	0.651	0.691	0.752	0.807	0.937	1.021	
Predicted	0.643	0.655	0.744	0.816	1.170	1.370	

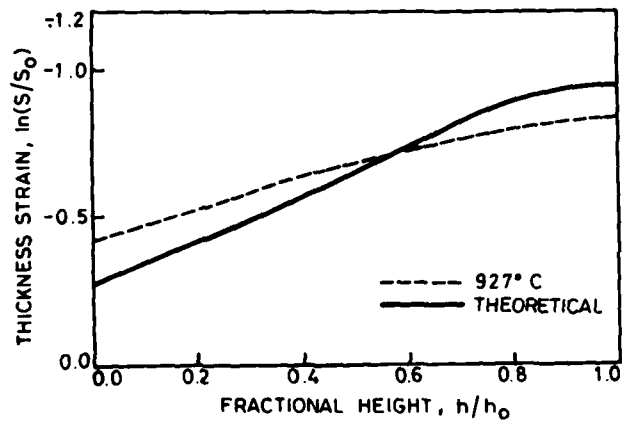


Figure 4 - Thickness strain as a function of fractional height. Forming temperature 927°C. Forming pressure 0.4 MPa.

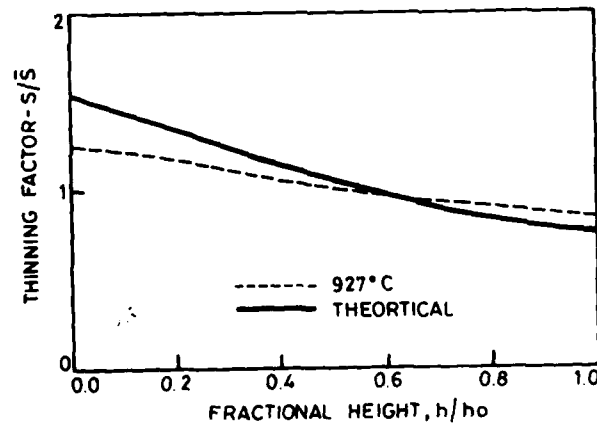


Figure 5 - Thinning factor as a function of fractional height. Forming temperature 927°C. Forming pressure 0.4 MPa.

Fig.4 the thickness strain is plotted against the non-dimensional fractional height,  $(h/h_0)$ , where  $h_0$  is the height of the pole and  $h$  is the height of the given point above the base line. The theoretically predicted values are also given in the same plot. The thickness strain of the hemisphere formed at 927°C is in fair agreement with the theoretical predictions.

### Thinning Factor

The thinning factor,  $S/\bar{S}$ , following forming at 927°C is plotted as a function of the fractional height (where  $S$  is the local thickness and  $\bar{S}$  is the average thickness following a given deformation) in Fig.5. The theoretically predicted thinning factor is also shown in this figure. It is found that the experimentally observed thinning factor of the hemisphere formed at 927°C is very close to that predicted theoretically.

### Conclusions

It is possible to predict the formation of the hemispherical shape during pressure thermoforming by making suitable assumptions with regard to the stress and strain states.

The stress gradient developed during the pressure thermoforming of hemispheres causes more rapid thinning at the pole compared to the edge and the intervening regions and this is confirmed by the theoretical and experimental results obtained at 927°C.

Thickness distribution and thickness strain of the hemispheres formed at 927°C were very close to the theoretically predicted values. The thinning factor for the hemispheres formed at 927°C is very close to that predicted theoretically.

### Acknowledgements

The authors thank the Aeronautics Research and Development Board, Ministry of Defence, Government of India, for financial support and Mr. Helmut Wolf for his help in computer programming.

### References

1. K.A. Padmanabhan and G.J. Davies, Superplasticity, (Springer-Verlag, Berlin, Germany, 1980)
2. K.S.K. Chokalingam et al, "On the Pressure Forming of Two Superplastic Alloys", J. Materials Science, 20 (1985) 1310-1320
3. C.H. Hamilton and G.W. Stacher, "Superplastic Forming of Ti-6Al-4V Beam Frames", Metal Progress, 20 (1985) 34-37
4. C.H. Hamilton, NATO/AGARD Lect. Series 154, Superplasticity, (9/87) 2.1-2.23
5. David L. Holt, "An Analysis of the Bulging of a Superplastic Sheet by Lateral Pressure", Int. J. Mech. Sci., 12 (1970) 491-497
6. F. Jovane, "An Approximate Analysis of the Superplastic Forming of a Thin Circular Diaphragm: Theory and Experiments", Int. J. Mech. Sci., 10 (1968) 403-427
7. G.C. Cornfield and R.H. Johnson, "The Forming of Superplastic Sheet Metal", Int. J. Mech. Sci., 12 (1970) 479-490
8. C.D. Ingelbrecht, "Prediction of the Optimum Pressure Cycle for the Superplastic Forming of Hemispheres from Ti-6Al-4V Sheet", J. Mat. Sci. Let., 4 (1985) 1021-1025
9. A.K. Ghosh and C.H. Hamilton, "Influences of Material Parameters and Microstructure on Superplastic Forming", Met. Trans. A, 13A (1982) 733-743
10. A.R. Ragab, "Thermoforming of Superplastic Sheet in Shaped Dies", Metals Technology, 10 (1983) 340-348
11. A.K. Ghosh and C.H. Hamilton, "On Constant Membrane Stress Test for Superplastic Metals", Met. Trans. A, 11A (1980) 1915-1918
12. J.A. Belk, "A Quantitative Model of the Blow-Forming of spherical Surfaces in Superplastic Sheet Metal", Int. J. Mech. Sci., 17 (1975), 505-511
13. K.A. Padmanabhan and G.J. Davies, "Numerical Analysis of Superplasticity Data for use in Metal Forming Applications", J. Mech. Phys. Solids, 18 (1970) 261-275
14. K.S.K. Chokalingam et al., "Investigation on The Pressure Thermoforming of Superplastic Alloys" Conference Proceedings on Metal Forming (ASM International, Bombay, India, 1987, in press)

## NEW ADVANCE OF SUPERPLASTIC

### FORMING PROCESS FOR COMMERCIAL STRUCTURAL ALLOYS

Wang Cheng and Luo Ying-She

Xiangtan University, Xiangtan, Hunan, China

#### Abstract

This paper states the new advance of superplastic forming for commercial structural alloys, and mainly introduces the newest research achievement the superplastic rheological forming. What is called the superplastic rheological forming is a new superplastic forming method which is obtained by using a theory of rheology to research the forming method of the commercial structural alloys. It is more representative of the actual situation than other theories. It is discovered by us that commercial structural alloys (Lc4, Ly-12, Ti-6Al-4V and 30CrMnSiA) manifest evidently viscosity in plastic forming stage. What is called the viscosity is that deformation of the materials in the act of a force field is a function of time. The effect of the dependent variable (time) in the rheology's theory is used to calculate rheological strain, in which exists an essential distinction as compared with the conventional theory which is used to calculate plastic forming of metal. Viscosity has been considered, being introduced through a time variable in visco-elastic theory, corresponding to the visco-elastic principle what is usually used is only suitable for small deformation and which is restricted by basis hypotheses of elastic mechanics. However, the material of superplastic rheological forming is an elastic-visco-plastic material which is suitable for large deformation. When a material of superplastic rheological characteristic is pressed in the dies at the high temperature, the elastic effect may be neglected. Therefore, it may be considered as a visco-plastic material. Tests show that because the materials can exhibit good filling character, the pre-heat-treatment and refined treatment for superplastic rheological forming may not be needed and the workpieces of complex shape and high properties with thin wall, high webs and long blades can be obtained in one deformation step.

Superplasticity and Superplastic Forming  
Edited by C.H. Hamilton and N.E. Paton  
The Minerals, Metals & Materials Society, 1988

### Introduction

The effect of the dependent variable (time) is not considered formerly when the strain of superplastic forming is calculated. In this paper, the effect of the dependent variable (time) upon superplastic forming is mainly introduced. In recent years, the superplastic rheological forming has been researched and tested by the authors during the period of cooperative work together with some plants. The complex workpieces with gears, thin and long blades, screws, rolling figures and holes, which are made of commercial structural materials are shown in Figure 1. This achievement now is being extended for solving the practical problems appearing in production.

The advantages of superplastic rheological forming are introduced as follows:

(1) because the cavity filling properties of superplastic rheological alloy are very good, the complex workpieces can be obtained in one deformation, such as the helicopter's impeller which is made of Ti-6Al-4V alloy (see Fig.1-6); (2) under the action of stress field and the activation energy, eliminating point-line defects in the internal of material, high strength workpieces can be obtained, such as the missile bracket which is made of Lc4 alloy (see Fig.1-5); (3) using a  $k_3$  high temperature alloy as die material, elastic deformation of die and nonhomogeneity of deforming temperature and residual stress in structural workpieces are lessened, so the accuracy of workpiece dimension is much higher; (4) it improves the surface finish smoothness of the structural workpieces; (5) compared with the other methods of forming, the kinds of alloys are not restricted, and the preheat treatment and reheat treatment are not needed. Because the superplastic rheological forming has unique advantages, we believe that the application of rheological theory to superplastic forming will bring great changes to the metal forming technique today.

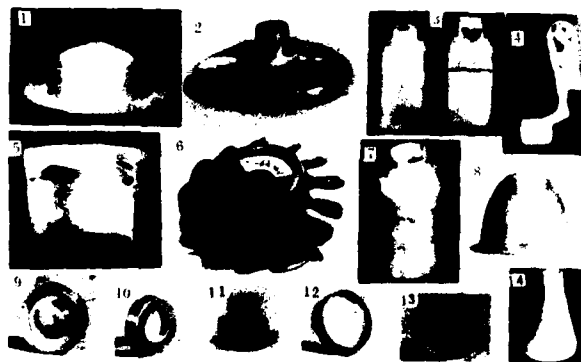


Figure 1 - Superplastic rheological forming workpieces made of commercial structural alloy.

### Experimental Details

The experimental details of superplastic rheological forming is introduced as follows:

#### Materials

The materials (extrusion bars, rolling sheet) were used to study the superplastic rheological forming and are listed in Table 1.

Table 1. Chemical Constituent of Commercial Structural Alloys

Materials	Chemical Constituent (%)										
	Ti	Al	V	Cu	Mg	Mn	Zn	Cr	C	Fe	Si impurity
Ti-6Al-4V	re.*	50-65	35-45								
Ly-12		re.		38-49	12-18	03-09					≤1.5
Lc4		re.		14-20	18-28	02-06	50-70	001-025			≤1.5
30CrMnSiA					08-11		08-11	027-034	re.	09-12	

\* re. is remainder.

#### Equipments

The hydropress (50-500T) was used for forging and extrusion; the double-acting drawing machine is used for powder forming.

#### Dies

The dies are illustrated in Figure 2. In Figure 2-a): 1 is the heat plate; 2, the plate of heat insulation; 3, the cooling plate; 4, the die stand; 5, the positioning sleeve; 6-7, the hollow die; 8, the sleeve of heat insulation; 9, the cooling sleeve; 10, the fixture sleeve; 11, the protruding die (upper die); 12, the ejector (or positioning sleeve); 13, the fixture plate; 14, the heater; 15, the fixture plate; 16, the plate of heat insulation. In Figure 2-b): 1 is the lower die; 2, the special holder; 3, the talcum powder; 4, the superplastic sheet; 5, the hollow die and 6 is the heater.

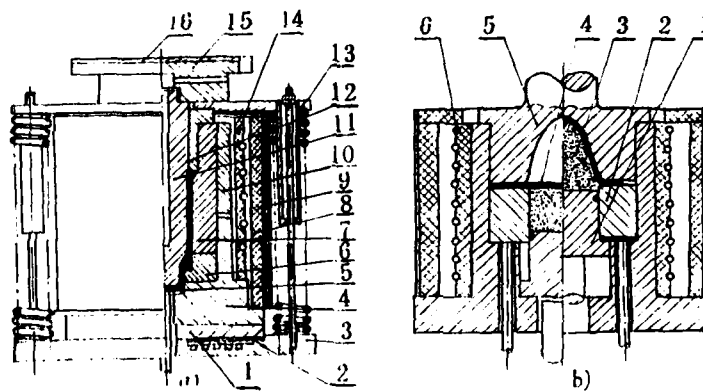


Figure 2 - The dies are used forging (or extrusion) a) and powder forming b).

#### The Principle of Superplastic Rheological Forming

The principle of superplastic rheological forming can be expressed by

$$\epsilon = f_1(\sigma)f_2(T)f_3(t) \quad (1)$$

where  $\epsilon$  is the strain;  $f_1(\sigma)$ , the stress function;  $f_2(T)$ , the temperature function, and  $f_3(t)$  is the time function. If  $f_1(\sigma)$  is kept steady in forming stage, this is referred as superplastic creep forming; if  $f_1(\sigma)$  is not steady, this is referred as superplastic rheological forming. The  $f_1(\sigma)$ ,  $f_2(T)$  and  $f_3(t)$  are established as follows, we use the Bingham Model to describe the elastic visco-plastic metal materials. It is a three-element compose model. According to Maxwell Model, the constitutive equation of Bingham may be obtained as follows

$$\epsilon = \frac{\sigma}{2G} - \frac{\sigma - \sigma_s}{2\eta_r} t \quad (2)$$

where  $\epsilon$  is the total strain;  $\sigma$ , the stress;  $G$ , the shear modulus;  $\sigma_s$ , the yield stress of materials;  $\eta_r$ , the viscosity of viscous materials; and  $t$  is the time. Because the metal forming which is pointed out here takes place under a thermocompression state, the elastic effect may be neglected and the action of activation energy must be considered. The equation is given by

$$\epsilon = \frac{\sigma - \sigma_s}{2\eta_r} \exp\left(\frac{U}{RT}\right)t \quad (\sigma > \sigma_s) \quad (3)$$

where  $U$  is the activation energy;  $R$ , the gas constant, and  $T$  is the absolute temperature. The relationship curve between the forming time,  $t$ , and the load,  $p$ , may be shown in Figure 3. The line 1 is the curve for conventional forming; line 2, the curve for superplastic forming and the curve 3 is the curve for superplastic rheological forming. It has been shown that curve 3 can be divided into three stages. In first stage ( $t_1$ ), the forming procedure is simulated to conventional forming; the cavity is filled fundamentally (from upper die contract billet to fill cavity fundamentally). In second stage ( $t_2$ ), the workpiece is pressed enough, using extra load to close dies and the small, thin parts on the workpiece can be filled completely, in which the  $\sigma$  is not steady. In third stage ( $t_3$ ) the  $\sigma$  is kept steady (it is referred as constant-stress creep stage). Under the action of stress field and the activation energy, the point-line defects in the internal of workpiece can be eliminated and the high property workpieces can be obtained. We refer to ( $t_2+t_3$ ) stage as the stage of constant pressure.

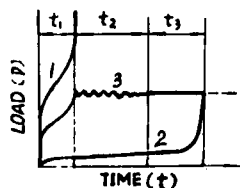


Figure 3 - Different curve of the metal forming



Figure 4 - Forming procedure of impeller (1,2 and 3)

## The Application of Superplastic

### Rheological Forming in the Practical Producing

To bring the advantages of superplastic rheological forming into full play, the holes screws, keys, rolling patterns, gears, blades and inserts if the workpiece must be developed as much as possible in the forming procedures. The machining may be reduced greatly, and even may be eliminated. In this statement the helicopter's impeller made of Ti-6Al-4V alloy is mainly introduced (2). It is well known that titanium alloy are attractive structural materials because of their high strength to density ratio, fatigue and fracture toughness etc. However, they are not only very costly materials for many applications, but also very difficult to forge and extrude. As shown from tests, the most promising method to reduce production costs, to increase yields, to improve their properties and surface quality is using superplastic rheological forming. The helicopter's impeller is an example of superplastic rheological forming. It is made in the high temperature dies made of  $k_2$  high temperature alloy. It is seen from Figure 4-3 that the die-filling properties are very good and its surface is bright, clean and artistic.

### Summary

It has been proved by experiment that the method of superplastic rheological forming has following characters:

- a) Because the die-filling properties of commercial structural alloys are very good, the high property complex workpieces with holes, threads, keys, rolling patterns, gears, blades and inserters can be made out and machining of workpiece may be reduced greatly, even without being machined.
- b) Successful tests have been made in which powder has been used by authors as medium for conveying force to produce workpieces with thick walls and complex shapes during the process of the superplastic rheological forming. It is found that the process is superior to using other forming methods, such as using liquid and gas as mediums for conveying force to produce complex workpieces.

### REFERENCES

1. L.W. Yuan, Rheological Mechanics (Beijing, Science Public House, 1986)
2. J.T. Hai, "The Application of Superplasticity in Press Working", Magazine of Forging and Stamping Technology, 2(1980)
3. C. Wang, etc., "The Experiment and Exploration on Creep Forming Principle of High Strength Aluminum Alloy," Magazine of Hot-Working Technology, 5 (1985)
4. Y.S. Luo, "The Application of Rheological Mechanics in the Metal Hot Rheological Forming," (paper presented at the First Annual Meeting of the Society of Young Mechanics, 1987).

SUPERPLASTIC FORMABILITY TO DISTINGUISH  
THE METALLIC THIN WALL COMPONENT BY CRITERIA AND CRITERION-MODEL

Wang Chunrong, Song Hailong, Qu Li and Chao Shuzhi  
Institute of Metal Research, Academia Sinica, Shenyang,  
P.R.China

Abstract

This paper deals with an evaluation of the relation between two type of press close to die (blank comes in die and blank covers die) and four criteria by means of studying superplastic forming of the metallic thin wall components. Also, writers estimated the formability of metallic thin wall components before forming the components by using the criteria and criterion-model recommended by writers. It follows that the formability of components is good but in many form-groove because of  $Q \geq 1$ , ( $Q$  is computing a value of criterion-model) and it is no possible to form in few individual form-groove because of  $Q < 1$ . Addition to a used mathematical model formula as follow:

$$\frac{1}{r} = 0.0844T + \frac{0.0948}{\sqrt{V}} + 1.9850P - 0.0076TP - 21.800$$

We carry out to with objective the control of superplastic forming even though the forming is very difficult, and we were successful in producing the components more than one hundred by superplastic air bulge.

We judged again the formability of superplastic air bulge, good or bad, through four criteria and criterion-model after getting the dissection-part of the components. The result showed that the estimation for the formability of superplastic air bulge prior to the superplastic forming was correct. We consider that this kind of prediction can be used to evaluate the superplastic formability beforhand.



## Introduction

According to the use, loading the condition, and the rotational situation of the part on machine, we decided to form this part by means of superplastic air bulge technology. This process not only allows forming components of complex shape, but also allows for weight reduction. This technology for the production of components will provide a new processing method.

The prediction of form-groove on forming the difficult of components by the criteria and criterion-model. The metallic thin wall component has an external groove-curve of the left-right cross duplex helix. The width, depth of the groove-curve and outline of section vary with the helix angle change. The narrowest width is 3.5 mm. and the widest width is 15.3 mm. The shallowest depth is 1.5 mm, and the deepest depth is 16.6 mm. But the narrowest width is not always following by the shallowest depth. The width is very narrow while the depth is very deep at some locations. Consequently, many difficulties will have been encountered for superplastic forming. In order to decide whether the superplastic air bulge forming method can be used, we sought to carry out an analysis on the basis of the form-groove of every groove of an outside section of part at first. We supposed that the component had been cut along the axis, if we cut the component on each 10 degree, there were 377 form-grooves. We used the four criteria proposed to carry out prediction of the formability of one by one for 377 form-groove. The four criteria are respectively the criterion of ratio of width to depth,  $W/H$ , the angle difference,  $\theta-\varphi$ , the ratio of rotary to bottom angle,  $r/r_0$ , the distribution of material formed,  $F/S$ , and the criterion-model:

$$Q = \frac{WS}{HF} + \frac{\pi}{180} (\theta - \varphi) - \frac{r}{r_0} + 0.55 \quad (1)$$

where:

- Q---The dimensionless model of combined criterion,  $Q \geq 1$  formability good,  $Q < 1$  formability bad.
- W---The narrowest width of forming part (mm)
- H---The deepest depth of forming part (mm)
- S---All area of plate face before forming ( $\text{mm}^2$ )
- F---All area of plate face after forming ( $\text{mm}^2$ )
- $\theta$ ---A least angle between flank side with bottom side of forming part (deg)
- $\varphi$ ---A much angle between level face of entrance with flank side of forming part (deg)
- $r_0$ ---A datum rotary angle to bottom angle  $r_0 = 1$  (mm)
- r---A rotary angle to bottom angle ( $r = r_2 - r_1$ , where  $r_2$  is the value of practice. and  $r_1$  is the value of plan)

Because the prediction was carried out before forming, there is no the value of practice-measuring, therefore the  $r$  value was offered to the critical value of 1 and substituted in formula (1). The result of prediction showed that the most of  $Q$  value were more than one, which indicated the superplastic formability is good. Many position can carrying out superplastic forming. A few of specifical positions have some  $Q < 1$ . In superplastic air bulge forming of metallic component, as the form of section with type of press close to die, the forming differentate both blank comes in die and blank covers die. The blank comes in die shows in figure 1(a,b). The blank covers die shows in figure 1(c). In reference 1 we had discussed only blank comes in die, had no discussed blank covers die. Blank covers die except the angle of entrance and bottom have the change, others every parameter are in agreement with blank comes in die.

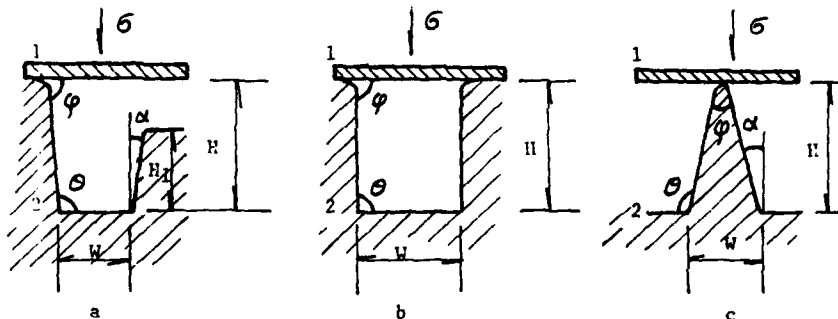


Fig.1, The opposite position of blank with die and both difference form of press close to die

1--blank 2--die  
a, b--blank comes in die  
c--blank covers die

Blank covers die as for cone, the angle of entrance is the angle between entrance position of component and two flank side of it. As to other form, the angle of entrance is the largest between surface of blank on entrance position and flank side of component. The bottom angle is the last blank into position, which is out angle between flank side and bottom side. Three criteria, the ratio of width to depth,  $W/H$ , the angle difference,  $\theta - \varphi$ , the ratio of rotary angle to bottom angle,  $r/r_0$ , can be computed directly. Because the part to be formed is continuous part instead of single form, therefore the fourth criterion  $F/S$ , was computed to take the half of common side along axial two flank or to take a common side. In addition, along circumferential direction the every form-grooves is a annular body, without any surface before and after it, therefore the counting didn't include them. We take unit body for step of  $W$  for operate convenience, and look curved surface like plane. Therefore, all area on outer surface of blank, look like figure 1(a), to use following formula carry out computing

$$S = W^2$$

All area on outer surface of part after forming to use following formula carry out to computer

$$F = W^2 + W[(H_1 \tan \alpha)^2 + H_1^2]^{\frac{1}{2}}$$

Distribution criteria of blank for blank comes in die, to use following formula compute.

$$\frac{F}{S} = \frac{W + [(H_1 \tan \alpha)^2 + H_1^2]^{\frac{1}{2}}}{W} \quad (2)$$

for figure 1(c)

$$S = W^2$$

$$F = W[(H \tan \alpha)^2 + H^2]^{\frac{1}{2}}$$

Distribution criterion of blank for blank covers die to use following formula compute

$$\frac{F}{S} = \frac{[(H \tan \alpha)^2 + H^2]^{\frac{1}{2}}}{W} \quad (3)$$

The distribution of blank is the process of dynamic strain during metallic components of superplastic forming. Any similar form of figure 1(c), the first contact is blank with protrusile die. The process of forming has three procedures. First pressing close to die, second, crooking pressure close to die, and finally filling bottom angle to the full. The position where the blank contact with die thined a little. Because of the effect of friction resistance on the forming, moreover, pulled the neighbour blank to come here easily, therefore this position lossed thickness less than other place. All similar form to figure 1(a,b), blank is forming after to crook of it. The process of forming has three procedures too. First, to crooked, second, pressing close to die, and finally filling bottom angle to the full.

#### Experiment

The relation of between form temperature, no continuous provide the rate of flow of air press, from press and form bottom angle  $r$ , to apply that we had been proposed formability mathematics-model to control 2.

$$\frac{1}{r} = 0.0844T + \frac{0.0948}{V} + 1.9850P - 0.0676TP - 21.800 \quad (4)$$

where:

T---form temperature ( $^{\circ}\text{C}$ )

V---no continuous provide the rate of flow of air press (atm/min)

P---form press (atm)

r---rotary angle to form bottom angle (mm)

The relation of between keeping time of press to form component with a rotary angle to bottom angle  $r$ , to apply the result of reference 3 show:

$$r = 1.2 \exp(4.17/\tau)$$

where:

$\tau$ ---time of keep press to form component

The form component is showed in figure 2. The components of 140 by superplastic air bulge forming and the component to dissect of one of where show in figure 3.



Fig.2, The metallic thin wall component by superplastic air bulge forming

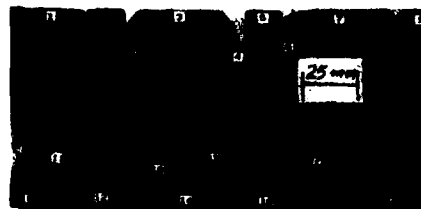


Fig.3, The dissection part of component by superplastic air bulge forming

The parameter of every position is listed by four criteria way in table 1. At the same time, the result to compute Q value by formula (1) and rate to diminish thin is listed together in table 1 too.

Table 1 The every parameter of dissection part a on component of metallic thin wall and the result to compute Q value by syuthetecal criterion-model

form position	forming way*	W/H	F/S	$\theta - \varphi$ deg.	$r/r_0$	Q	rate to diminish thin %	formability
1	1	3.34	1.32	6	0.60	2.59	56-46	good
2	2	0.35	2.83	86	0.50	1.68	62-24	good
3	1	2.33	1.57	8	0.40	1.77	56	good
4	2	0.67	1.60	69	0.60	1.57	61-31	good
5	1	0.92	2.20	6	0.50	0.57	70	bad
6	2	0.79	1.47	80	0.40	1.74	64-46	good
7	1	2.37	1.52	10	0.60	1.68	56	good
8	2	0.34	2.94*	85	0.50	1.65	57-49	good
9	1	1.56	1.74	6	0.50	1.09	66	good
10	1	1.66	1.71	12	0.50	1.23	67	good
11	2	0.37	2.74	84	0.60	1.55	67-43	good
12	1	2.21	1.50	0	0.40	1.62	59	good
13	2	0.66	1.53	80	0.40	1.98	68-27	good
14	1	0.97	2.16	0	0.40	0.69	72	bad
15	2	0.68	1.57	70	0.50	1.71	48-41	good
16	1	1.94	1.55	8	0.70	1.24	68	good
17	2	0.43	2.37	81	0.50	1.65	60	good
18	1	3.46	1.31	18	0.60	2.91	59-43	best

\* 1 blank comes in die                      2 blank covers die

#### Discussion

- a) It will be see from figure 3 and table 1 form position 8  $Q=1.65>1$  show superplastic formability good. Although value Q of form position 5 and 14 is 0.57 and 0.6 respectively, rate to diminish thin of form part after forming is 70% and 72% respectively. It is not achieved the limit value. Therefore, it did not crack, just forming difficulty is large.
- b) It will be see from table 1, the blank comes in die expect form position 5 and 14 the others  $W/H>1$ , and blank covers die  $W/H<1$  (between 0.34-0.79) to distinguish just from criterion of ratio of width to depth, the superplastic formability of blank cover die of component is very bad. At the angular difference criterion  $\theta - \varphi$  of blank covers die of component, all position more than  $60^\circ$ , superplastic forming is better, therefore the model of combined criterion  $Q>1$ . Formability of component at blank covers die is better than that at blank comes in die.

#### Conclusion

- a) Although the rate of width to depth of the metallic thin wall components is small, the angular difference quite big. Therefore the value of combined criterion of superplastic formability demonstrate that the superplastic formability of components of blank cover die is better than blank comes in die. And we had also confirmed that combined criterion-model has more value than the single criterion in practice.
- b) It can be identified whether the formability is good or bad by carrying out the prediction can supply a basis for the designer to correct the design of a component as soon as early.

#### References

1. Wang Chunrong and Chao Shuzhi, "Criteria of formability of components by superplastic air bulge", Acta Metallurgica Sinica, 23(4)(1987), B185-189.
2. Wang Chunrong et al., "Mathematical model of r criterion of formability by superplastic air bulge" Technology for metal Forming 1984, No.4:10-16.
3. Wang Chunrong et al., "Study of formability by superplastic air bulge of metallic material" Forging & Stamping Technology, 9(4)(1984), 4-9.

An Experimental Study of Yield Criterion Using Superplastic

Thin-walled Tubes Subjected Tension-torsional Combined Loads\*

Z.R. Wang Xu Yanwu Guo Dianjian

Harbin Institute of Technology Harbin

Yin Changkui

Beijing Agricultural Engineering University

Abstract

The superplastic yield criterion is one of the basic problems on superplastic mechanics. It is very important for analysing engineering problems as well.

To find out superplastic yield criterion, the high precision tension-torsional combined tests have made first. Both unequal section and uniform section thin walled tubes of typical superplastic material Sn-38Pb alloy deformed under room temperature. Depending on the experimental results, the superplastic yield criterion has been given.

Its physical meaning is that the unit work-rate equals the constant value during superplastic deformation. Its geometric meaning is curved-side hexagon cylinder. The experimental results show that yield criterion of initial yield surface and subsequent yield surface are coincident in region II ( $\dot{\epsilon} = 10^{-4} \sim 10^{-2}$ ); and the yield surfaces expand out homogeneously with superplastic unit work-rate increasing. This shows the phenomenon of superplastic strain-rate hardening.

The experimental results show also that in the case of superplastic deformation, the superplastic yield locus is located between the locuses of Mises and Tresca criteria. It is nearer to Tresca Yield Locus.

The Project Supported by National Natural Science Foundation of China

Superplasticity and Superplastic Forming  
Edited by C.H. Hamilton and N.E. Paton  
The Minerals, Metals & Materials Society, 1988

### Introduction

With the wide applications and research developments of superplasticity, it becomes urgent to develop superplasticity theory and to find a superplasticity equation of universal significance to describe the relationship among various parameters. Thus a reliable mechanics foundation for superplastic forming (1) can be provided. The yield criterion, which is of important significance in engineering, is a principal topic in the research of the fundamental theory of superplasticity mechanics. The references (2), (3) made an investigation of superplasticity under the condition of fixed principle stress axes (P-experiment). The physical meaning, geometrical meaning and the characteristics of subsequent yield surface were also investigated.

Using the MTS Model 809 Tension-Torsional Material System, the authors have made a detail investigation of the yielding characteristics of superplastic material under the stress state of tension (compression) — torsion. A yield criterion is formulated.

### Experiment

The experimental material is Sn-38Pb alloy made of thin-walled tubes which is stable in superplastic properties, isotropic and without strain hardening. As shown in Fig.1, a set of combined callipers is designed for the convenience of experiments of tension-torsion, compression-torsion, tension, compression and torsion are made on the MTS System, see Fig2, Fig3.

### Investigation of yield criterion

The yield function is determined through the analysis and conclusion of experimental results. The stable superplastic yield surface is determined through the treatment of measured shear stress  $\tau$  and normal stress  $\sigma$ , as shown in Fig.4. Fig.5. shows its projections on the  $\pi$ -plane. The measured points forms a hexagon of curved sides. An approximate approach can be made by the following equation,

$$f = J_2 \left( 1 - A \frac{J_3^2}{J_2^3} \right) - k^2 = 0 \quad (1)$$

where,  $A$  — Constant  
 $J_2$  — Second invariant of stress deviator;  
 $K$  — The flow shear stress of pure shear for a certain plastic energy rate,  
 $J_3$  — third invariant of stress deviator.

It lies between the Mises and Tresca criteria, near to the latter.

For ordinary materials, plastic potential is often used to describe the yield function while for the rate-sensitive materials, the yield function (surface) should be the collection of the states when the rates of plastic power are equal. This is the physical meaning of the yield function for stable superplastic deformation.

According to the physical meaning of the yield function, the selection of yield points should depend on the rate of plastic power,

$$\dot{W} = \sigma_{ij} \dot{\epsilon}_{ij} \quad (2)$$

When the rates of plastic power of different stress states satisfy equation (2), and remain constant, the corresponding points lie on the same yield surface. The value of A can be determined by using two yield points (one of which is pure shear) of one of the plastic power. Take a typical set of experimental data, shown in table 1. The value can be calculated,  $A=1.477$ , it is independent of stress states and the rate of plastic power. Correspondingly, K changes with the changes of strain rate. Geometrically, the yield surface expands outward uniformly with the increase of the rate of plastic power, which is verified through experimental results and theoretical analysis. Therefore arises the phenomenon of isotropic strain rate hardening with the increase in strain rate during superplastic deformation.

Table 1. Experimental Data

Parameters	Sample No. 1	Sample No. 2
$\dot{W} \times 10^3$	8.77785	8.77870
$J_2^2 \times 10^4$	2.2253	1.3927
$J_3^2 \times 10^4$	0.217996	0

#### Discussion

a). It can be known from the research of reference (4) that the subsequent yield surface coincides with the original surface for stable superplastic deformation because of the hardening exponent is zero, or no memory effect. This yield criterion applies, especially within Region II of superplastic deformation, to non-strain-hardening materials. There is a certain error in Region I, III of superplastic deformation. This can be shown in the difference between the original yield surface and the subsequent one. The subsequent yield surface is fairly stable. For strain-hardening superplastic materials, this criterion is not fully applicable and further researches are needed.

b). In the above experiments, character curves of the same strain rate but different stress states are made, as shown in Fig. 6. It can be seen that the  $J_2 - J_3$  ( $J_2$  - second invariant of strain tensor) curves under different stress do not coincide during superplastic deformation. It shows that superplastic deformation does not fully satisfy Mises Criterion. And the flow principle connected with this criterion is not fully applicable either.

c). Compared with the results of references (2), (3), the experimental results are more accurate. What is more, the principal stress axes are changeable. The deformation pattern is universal (5) and therefore the result is of general significance.

### Conclusion

a). In this investigation, the thin-walled tube specimen is first used in high accuracy tension (compression)-torsion complex experiment, the aim of which is to build a yield criterion of superplastic deformation. The advantage of this experiment over the P-p experiment is that the results under changing principal stress axes can be obtained.

b). The experimental results show that the yield trace of superplasticity lies in between Mises criterion and Tresca criterion, but nearer to Tresca criterion. The flow principles connected with Mises criterion (the Odquist equation) are not fully applicable.

c). For non-strain-hardening stable superplastic deformation, the yield criterion is,

$$f = J_2 \left( 1 - A \frac{J_2^2}{J_3} \right) - k^2 = 0$$

Geometrically, it is a curved hexagonal surface. The physical meaning is the collection of all yielding points for a rate of a constant plastic power. The subsequent yield surface coincides with the original yield surface in Region II. (but does not in Region I, III.) Subsequent yield surface is stable. This criterion can well describe the yield characteristics of superplastic deformation.

d). It is proper to describe the yield characters of superplastic deformation by using the rate of the plastic power. As value is calculated according to this theory. The theoretical results corresponds well with experimental ones.

### Reference

- (1). CINO-JAPAN Joint Symposium on Superplasticity, 1985, P1-5.
- (2). Z.R.Wang et al, An Experimental Study of Superplastic Tin-Lead Alloy Thin-walled tubes Subjected to Combined Stress, Journal of Harbin Institute Technology, (2), 1981, P68-72.
- (3). Z.Y.Wang, Research of the Yield Criterion of Zn-22Al Alloy under Tension-Compression Combined Stress at Superplastic Temperature, Journal of Northeast Institute of Technology, (2), 1983, P29-34.

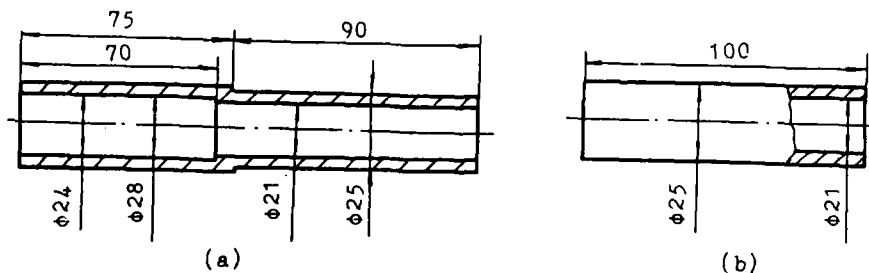


Fig.1-Specimens.



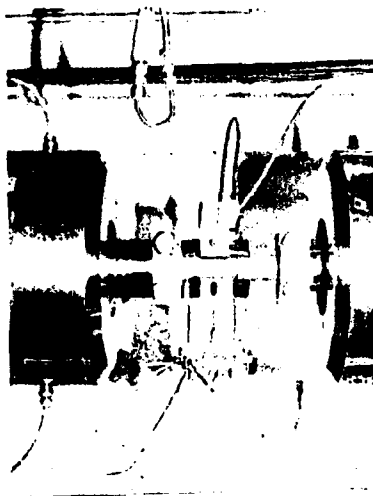


Fig. 2-Experiment with the unequal section thin walled tube.

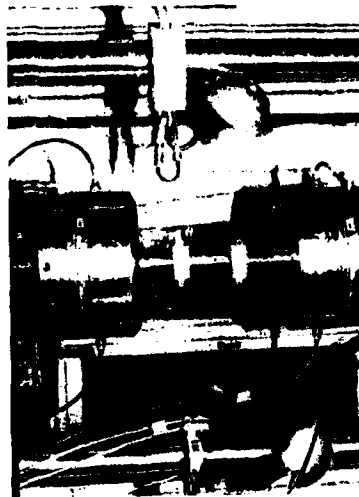


Fig. 3-Experiment with the unique section thin walled tube.

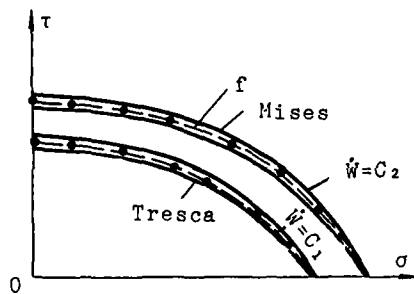


Fig. 4-Yield points on  $\sigma - \tau$  plan.

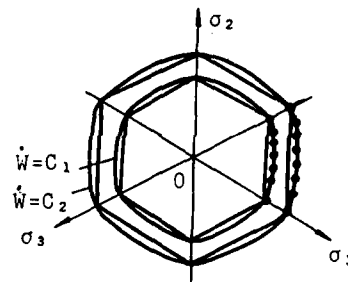


Fig. 5-Yield points on  $\pi$ -plan.

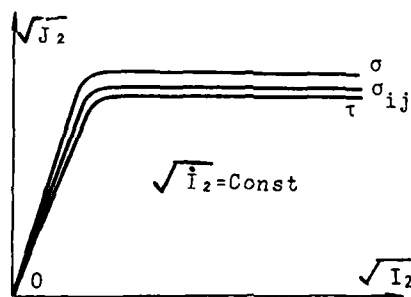


Fig. 6- $\sqrt{J_2}$ ,  $\sqrt{I_2}$  curves under different stress

MECHANICAL ANALYSIS ABOUT DEFORMATION LAWS  
OF SUPERPLASTIC EXTRUSION THROUGH CONE-SHAPED DIES

Song Yu-quan\* Zhang Zhen-jun\*\* Lian Shu-jun\*

Abstract

In this paper, analytical formulae of stress, strain, displacement and strain rate in deformed region about superplastic extrusion are derived through mechanical analysis, based on the fundamental theory in mechanics of continuum media and combined with Backofen's constitutive equation of superplasticity. The theory was proved correct with viscoplasticity method. Then, from the derived theoretical conclusion, the following are obtained, equations of rational displacement and velocity of press slide during steady and non-steady extrusion; equations of extrusion time and flow rate. At last, automobile piston was chosen to be formed according to the rational deformation rule. The results show that the forming time can be shortened by 40 percent and the quality of formed parts are distinctly improved.

\* Department of Metallic Material Engineering, Jilin University of Technology, Changchun, China.  
\*\* Chinese Academy of Agricultural Mechanization Sciences, Beijing, China

Superplasticity and Superplastic Forming  
Edited by C.H. Hamilton and N.E. Paton  
The Minerals, Metals & Materials Society, 1988

## Introduction

The authors have introduced and reviewed the present situation upon mechanics of superplastic extrusion in Ref. [1], and pointed out that some investigators have used rigid-plastic finite element method, flow function method, slip-line method to study the mechanical problems of superplastic extrusion. Moreover, certain success has been achieved. Each theory has its own feature. Here it should be pointed out that the mechanical analysis method is contributive to the analysis of functional relations among mechanical parameters in the deformation process. In Ref. [2], the analytical formulae among mechanical parameters in deformed region of superplastic extrusion through cone-shaped die are theoretically determined. In Ref. [3, 4], both the technological rules and the influence of condition coefficients for superplastic extrusion through cone-shaped die were theoretically discussed according to the conclusions of Ref. [2]. In present paper, the deformation laws of superplastic extrusion through cone-shaped die are briefly discussed based on the work of Ref. [2~4].

## Theory

### Basic Hypothesis

Material is supposed to be isotropic, incompressible and sensitive to strain rate. The material flow in the deformed region of cone-shaped die shown in Fig. 1 can be regarded as a radial flow toward its apex. Materials beyond the two ends of the deformed region are in the rigid regions. The main axis of stress tensor coincides with the main axis of strain rate tensor, that is, it conforms Saint-Venant equation.

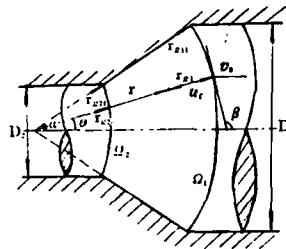


Fig. 1 schematic diagram for deformed region of extrusion through cone-shaped die

### Stress, Displacement, Displacement Rate, Effective Strain and Effective Strain Rate

From the fundamental theory in plastic mechanics of continuum media, combined with the basic hypotheses and Backofen's constitutive equation at three-dimension condition, stress in deformed region can be determined,

$$\sigma_r = \frac{2k(1+\mu \cot \alpha) [2v(t)r_{Q1}^2 \cos^2 \alpha / 2]^m}{2\mu \cot \alpha + 3m} \{r^{-2m} - r_{Q2}^{-2m}\} \quad (1)$$

$$\sigma_\theta = \sigma_r - k[2v(t)r_{Q1}^2 \cos^2 \alpha / 2]^m \cdot r^{-2m} \quad (2)$$

displacement and displacement rate of particle

$$\mu_r = [r_{Q1}^2 + 3r_{Q2}^2 s(t) \cos^2 \alpha / 2]^{1/2} - r_{Q1} \quad (3)$$

$$\dot{\mu}_r = \frac{r_{Q1}^2 v(t) \cos^2 \alpha / 2}{r^2} \quad (4)$$

effective strain and effective strain rate

$$\epsilon_r = \frac{-2r_{Q1}^2 s(t) \cos^2 \alpha / 2}{r^2} \quad (5)$$

$$\dot{\epsilon}_r = \frac{-2r_{Q1}^2 v(t) \cos^2 \alpha / 2}{r^2} \quad (6)$$

Where  $\mu$  is friction coefficient,  $k$  material constant,  $m$  strain rate sensitivity

index,  $s(t)$  and  $v(t)$  is displacement and speed of press slide, and the others are shown in Fig.1.

**Laws of Extrusion with Varying Speed.** For superplastic materials, we must take account of strain rate besides extrusion angle and friction even at the condition of optimal temperature. To forward extrude through cone-shaped die, the most dangerous position is the annular band near die wall shown in Fig.1. If effective strain rate  $\dot{\epsilon}_e$  at any particle in the annular band is equal to strain rate  $\dot{\epsilon}_m$ , which is the strain rate corresponding to maximum  $m$  value, the aim that superplasticity of materials can be made fully use of is reached, that is, when  $\theta = \alpha$ , let  $\dot{\epsilon}_e = \dot{\epsilon}_m$ . Substituting this condition, and when  $\theta = \alpha$ ,  $r_{Q1} = r_{Q11}$ ,  $r = r_{Q11} - \mu_m$  into eqns.(3) and (5), considering initial condition  $s(t)|_{t=0} = 0$ , the rational displacement and velocity of press slide for non-steady extrusion can be determined

$$s(t) = \frac{-D_1}{6 \sin \alpha \cos^2 \alpha / 2} (1 - e^{-\dot{\epsilon}_m / k \cdot t}) \quad (7)$$

$$v(t) = \frac{-D_1 \dot{\epsilon}_m}{4 \sin \alpha \cos^2 \alpha / 2} e^{-\dot{\epsilon}_m / k \cdot t} \quad (8)$$

where  $D_1 = 2r_{Q11} \sin \alpha$  is diameter at entrance of cone-shaped die.

As deformation of blank enters the period of steady extrusion as soon as the blank extrude from die exit, the technological rules for steady extrusion can be obtained as long as time  $t_p$  for non-steady extrusion period is determined. From Fig.1, we know that when  $t = t_p$ ,  $\mu_m = r_{Q11} - r_{Q1}$ . Substitute this condition into eqn.(3), we have

$$r_{Q1}^2 - r_{Q11}^2 = 3r_{Q11}^2 s(t_p) \cos^2 \alpha / 2 \quad (9)$$

Combining eqns. (7) and (9), we obtain

$$t_p = \frac{1}{\dot{\epsilon}_m} \ln k \quad (10)$$

Where  $k = D_1^2 / D_2^2 = r_{Q11}^2 / r_{Q1}^2$  is extrusion ratio. Substitute eqn.(10) into eqn.(9), we can obtain the rational rules for speed and displacement of press slide for steady extrusion

$$v_s(t) = \frac{-D_1 \dot{\epsilon}_m}{4 \sin \alpha \cos^2 \alpha / 2} k^{-t/t_p} \quad (11)$$

$$s(t) = \frac{-D_1 \dot{\epsilon}_m}{4 \sin \alpha \cos^2 \alpha / 2} [1 - (1 + 2/3 \cdot \ln k - 2/3 \cdot \dot{\epsilon}_m t) k^{-t/t_p}] \quad (12)$$

**Extrusion Time and Flow Rate.** Shortening deformation time is one of the key problems that superplasticity develops toward practical application. Extrusion time indicates the time from the beginning of blank deformation to all blank extruded from die exit. For extrusion with varying speed, the extrusion time can be obtained so long as optimal strain rate  $\dot{\epsilon}_m$  in eqn.(11) is replaced by general rate  $\dot{\epsilon}$ . Since the speed at the entrance of die maintains being  $v(t)$  for constant-speed extrusion, replacing  $r$  in eqn.(6) by  $r_{Q1}$  and considering eqn.(10), we can determine  $t_p$ . Therefore, we have

$$t_p = \begin{cases} \frac{\ln k}{\dot{\epsilon}} & \text{(varying speed)} \\ \frac{2(1 - k^{-1/3})}{3\dot{\epsilon}} & \text{(constant speed)} \end{cases} \quad (13)$$

In the field of engineering, extrusion flow rate is generally represented by mean volume flow rate, i.e.

$$Q = \frac{\text{Volume of deformed region (V)}}{\text{extrusion time (tp)}} \quad (14)$$

Determining volume enclosed by three surfaces shown in Fig.1, i.e.  $Q_1$ ,  $Q_2$  and die wall, and substituting eqn.(13) into eqn.(14), we obtain

$$Q = \left\{ \begin{array}{ll} \frac{16\pi}{3}(r_{Q1}^2 - r_{Q2}^2)(\cos^2 \frac{\alpha}{2} - \cos^2 \frac{\alpha}{2}) \frac{\dot{\epsilon}}{\ln k} & \text{(varying speed)} \\ \frac{16\pi}{2}(r_{Q1}^2 - r_{Q2}^2)(\cos^2 \frac{\alpha}{2} - \cos^2 \frac{\alpha}{2}) \frac{\dot{\epsilon}}{(1-k)^{-1/2}} & \text{(constant speed)} \end{array} \right. \quad (15)$$

From eqns.(13) and (15), we know that  $tp$  is the function of  $K$  and  $\dot{\epsilon}$ ,  $Q$  is the function of  $r_{Q1}$ ,  $\alpha$ ,  $K$  and  $\dot{\epsilon}$ , but these two parameters are all not related to friction coefficient  $\mu$ .

### Experiment Results

#### Proof of Stress Distribution

Material is superplastic alloy Zn-4wt%Al. At 300°C,  $m=0.708$  and  $k=50.18$  kg/mm<sup>2</sup> are determined by tensile test. When silicon oil as lubricant,  $\mu=0.16$  is measured by the upsetting method of cylindrical ring. Take  $k=4$ ,  $\alpha=20^\circ$ . Substitute those data into eqns.(1) and (2), the theoretical curves of  $\sigma_r/\sigma_{\theta Q1} = r/r_{Q1}$  and  $\sigma_\theta/\sigma_{\theta Q1} = r/r_{Q1}$  can be drawn by computer, shown in Fig.2 and Fig.3. Then extrusion has been tested. Extrusion specimen is two hemi-cylinder body of dimension  $1/2\phi 40 \times 40$ . Grids for visioelasticity method are etched in the contact plane of any hemi-cylinder body. Lubricant is silicon oil. Extrusion velocity is 3 mm/min. Extrusion step  $\Delta t$  is 1 min, and total number of extrusion steps is 9. After each step of extrusion, distortion of grids is recorded by photograph method. Then the displacement field of particle is measured at the projection instrument JIJ-180 whose magnifying multiple is 50. The Data of displacement field measured

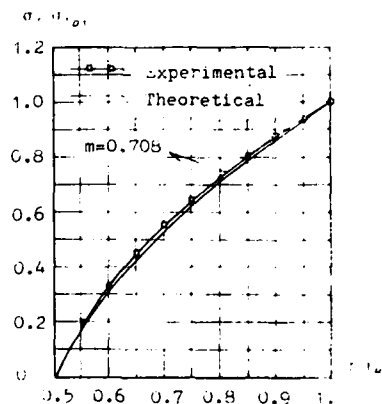


Fig.2 curves of  $\sigma_r/\sigma_{\theta Q1} - r/r_{Q1}$  relation.  $\mu=0.16, k=4, \alpha=20^\circ$

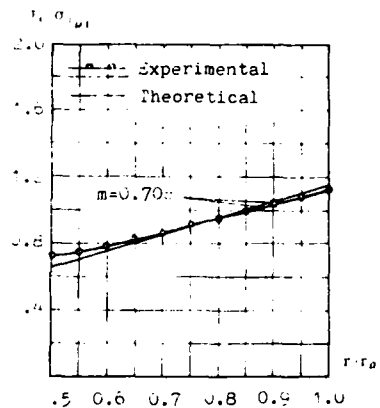


Fig.3 curves of  $\sigma_\theta/\sigma_{\theta Q1} - r/r_{Q1}$  relation.  $\mu=0.16, k=4, \alpha=20^\circ$

are then treated by computer with regress and smooth method. The curves drawn with this method are shown in Fig.2 and Fig.3. Since stresses in deformed region are influenced by every parameters, the identity between the results of theory and the experiment shows that the theory is reliable.

#### Forming Test of Extrusion

The feasibility of the technological rules is verified by forming automobile

piston. Material used is high strength commercial aluminum bar of LD10. Firstly material is preserved at 460°C,  $m=0.49$  is measured by tensile test, the corresponding strain rate  $\dot{\epsilon}=9.33 \times 10^{-3} s^{-1}$ . Extrusion forming is made in oil

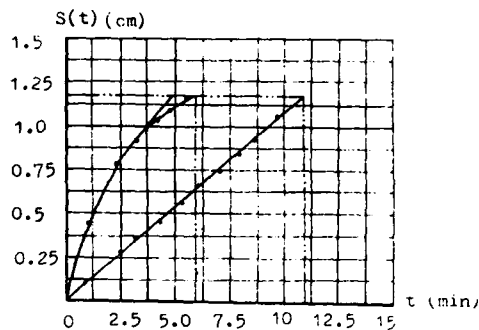


Fig. 4 the recorded curves of forming  
—Theoretical —Experimental

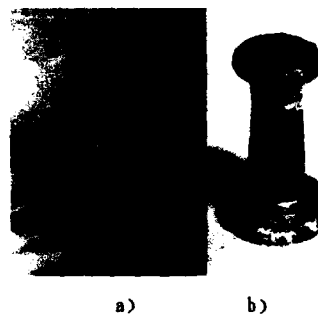


Fig. 5 the pistons extruded  
a. piston extruded with varying speed  
b. piston extruded with constant speed

press Y41-40A at the same temperature. Lubricant used is silicon oil. Displacement is recorded by X-Y recorder associated with 100 mm displacement transducer. The curves recorded are shown in Fig. 4. The curve in this figure represents extrusion with varying speed; the straight line represents constant speed extrusion. The corresponding parts formed are shown in Fig. 5. From this figure, we know that extrusion with varying speed needs 5.6 min, and surface quality of formed part are very high. Constant speed extrusion needs 11 min. Furthermore, inadequate filling and stretch crack appear at the bottom of the formed part.

#### Conclusion

The stress distribution in deformed region for superplastic extrusion through cone-shaped die obtained from theoretical analysis is identical with experimental results. The extrusion time for the forming of automobile piston with varying speed according to the rational technological rule of extrusion derived theoretically is about 40% shorter than that with constant speed. Furthermore, the quality of the formed parts is distinctly improved. This shows that the rational technological rules of extrusion with varying speed can direct the extrusion forming of axial symmetrical parts in principle.

#### References

1. Song Yu-quan and Zhang Zhen-jun, "The present situation for Mechanics of Superplastic Extrusion", *Journal of Jilin University of Technology*, 4(1986) 105-116. (in Chinese)
2. Song Yu-quan and Zhang Zhen-jun, "The theoretical Analysis for Superplastic Extrusion through Cone-shaped Dies," *Journal of Jilin University of Technology*, 2(1987) 77-88. (in Chinese)
3. Song Yu-quan and Zhang Zhen-jun, "The study of Superplastic Extrusion through Cone-shaped Dies", *Transactions of the Chinese Society of Agricultural Machinery*, 3(1987)71-78. (in Chinese)
4. Song Yu-quan and Zhang Zhen-jun, "The Influence of the Condition Coefficients upon the Superplastic Extrusion Parameters of Cone-shaped Dies", *Transactions of the Chinese Society of Agricultural Machinery*, 1(1988)61-70. (in Chinese)

## **ALLOY DESIGN**

## ALLOY DESIGN OF SUPERPLASTIC NICKEL-BASE

### AND TITANIUM-BASE ALLOYS

Michio Yamazaki

National Research Institute for Metals  
Meguro, Tokyo, Japan

#### Abstract

This paper reviews works which have been done by the author and his group on developments of superplastic Ni-base superalloys and superplastic Ti alloys for several years in a national project in Japan. The computer-aided alloy design method previously developed by us for Ni-base gamma/gamma-prime type superalloys is applied to design superplastic nickel-base alloys. The similar alloy design method is contrived for alpha/beta type Ti alloys and is used to develop superplastic titanium alloys. The both alloy design methods deal with two phase alloys; phase compositions are so calculated that the two phases are equilibrium each other, fully solution-hardened, and free from the formation of detrimental phases. Many candidate pairs of the two phases are obtained and the volume fraction of the two phases can be set arbitrarily without changing the phase compositions but for good superplastic properties the volume fractions of the phases are chosen to be about 50%. The tensile strengths and ductilities at use temperatures of the alloys are also important target of the project as well as good superplasticity at forming temperatures.

Superplasticity and Superplastic Forming  
Edited by C.H. Hamilton and N.E. Paton  
The Minerals, Metals & Materials Society, 1988



### Introduction

In a national project of Japan, "Advanced Alloys With Controlled Crystalline Structures" two superplastic alloys are being studied. This project, started in 1981, is one of "Jisedai Projects" planned and sponsored by Agency of Industrial Science and Technology of MITI and will end at March of 1989. For this alloy project three national research institutes and "Research and Development Institute of Metals and Composites for Future Industries" are working together. The latter Institute has been established for this alloy project and other composite materials project in "Jisedai Projects" and seven member companies in this Institute are sharing works for the alloy project.

In the above alloy project the following four alloys are being developed.

- [1] Single crystal Ni-base superalloy
- [2] Superplastic Ni-base superalloy
- [3] Oxide dispersion strengthened Ni-base superalloy
- [4] Superplastic Ti alloy

In this alloy project, the author and his group in National Research Institute for Metals are in charge of alloy design and propose candidate alloys for processing studies by the seven companies as members of the aforementioned specially established Institute. Even in the alloy design stage these companies do appreciable contributions in preparing our specimens.

In this paper will be described only alloy design aspects of the above two superplastic alloys [2] and [4].

### Principle of Alloy Design

The very principle of our alloy design is as follows; phase names before and within parentheses are for Ni-base and Ti alloys, respectively.

- (a) An arbitrary composition of gamma prime (beta) phase is set, in a computer, with restrictions that it can be equilibrated with gamma(alpha) phase and that it is not excessively solid-solutioned.
- (b) Composition of gamma(alpha) phase is calculated from the gamma prime(beta) composition using the partitioning ratio of each element between the two phases.
- (c) The gamma(alpha) phase composition above is checked if it is prone to the formation of detrimental phases such as sigma(alpha-2).
- (d) We can compose alloys with any volume fraction of gamma prime(beta) phase without changing gamma prime and gamma(beta and alpha) compositions.
- (e) We can utilize some property-prediction equations, mostly derived from experimental experiences.

For titanium alloy, the phase calculation method based on thermodynamics, somewhat different from the above, is also tried.

### Alloy Design of Ni-base Superalloy

Figure 1 shows our computer-aided alloy design method for Ni-base gamma/gamma-prime superalloy (1, 2). Some description for this figure was given in the author's previous paper (3). We have been extensively using this method for conventionally cast, directionally solidified

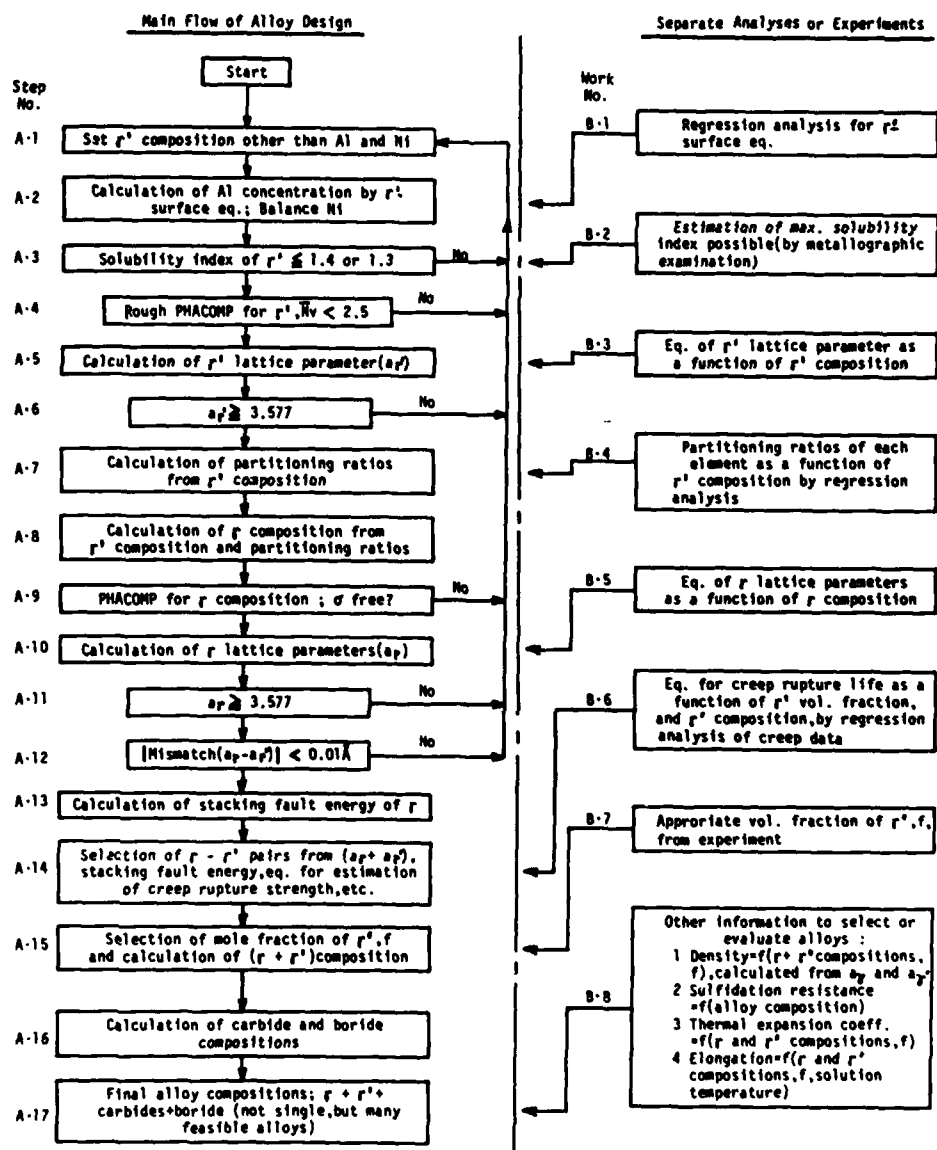


Figure 1 - Computer-aided alloy design method for  $\gamma/\gamma'$  Ni-base superalloy (3). The left column shows alloy design steps and the right preparations for each step of the left.

columnar, and directionally solidified single crystal alloys and ODS alloys as well as for superplastic P/M alloys.

#### Development of Superplastic Ni-base Superalloy

##### Target

The target of the project is that developed alloys have a tensile strength higher than 160 kgf/sq.mm(1569 MPa) and a tensile elongation of 20 % at 760 C and are capable of being superplastically deformed. The elongation of 20 % is not superplastic one. The detailed target for superplasticity is not set up.

The above target tensile property values were found rather too high to be achieved after they had been approved as the official target.

##### Modification of Rene 95 (4, 5)

Alloy Design. The gamma and gamma prime compositions and the volume fraction of the latter of Rene 95, one of typical P/M superalloys, were calculated by a modification of our original alloy design program mentioned above. In the original program we start from setting gamma prime composition and then calculate the gamma composition by using partitioning ratios of each element, the ratios being functions of the gamma prime composition. Consequently, when we start from an overall alloy composition we must do some iteration since we do not have the partitioning ratio values for a particular alloy at the beginning (6).

By using gamma and gamma prime compositions obtained above, we designed a series of Ni-base superalloys with varied amounts of gamma prime phase volume fractions yet with keeping the given phase compositions. In Table I are shown alloys designed. Alloy H (TMP-11), 115 % of gamma prime phase, was derived by extrapolating the tie line connecting the gamma and gamma prime compositions by 15 % across the gamma prime surface. Due to some possible inaccuracy in the alloy

Table I. Nominal Compositions(wt. %) and Contents of Gamma-prime Phase in a Series of Designed Alloys Including Rene 95

Alloy	Co	Cr	Mo	W	Al	Ti	Nb	cgpp
A TMP-1	14.2	25.6	5.8	4.1	1.1	0.6	1.0	0
B TMP-9	11.6	20.5	4.8	3.8	2.1	1.4	2.0	25
C TMP-2	9.0	15.2	3.9	3.6	3.1	2.2	3.0	50
D Rene-95	8.0	13.0	3.5	3.5	3.5	2.5	3.5	60
E TMP-3	6.9	10.8	3.1	3.4	3.9	2.8	3.9	70
F TMP-10	5.3	7.6	2.5	3.3	4.5	3.4	4.5	85
G TMP-4	3.7	4.3	1.9	3.1	5.2	3.9	5.1	100
H TMP-11	2.1	1.0	1.3	3.0	5.8	4.4	5.6	115

Ni:Balance, C:0.07, B:0.01, Zr:0.05. "cgpp":Content of gamma-prime phase. The "cgpp" of 115% means that the designed alloy resides, on the tie line connecting the gamma and gamma-prime compositions, at a point exceeding by 15 % beyond the gamma-prime phase surface into the gamma phase region.

design calculation, Alloy G, designed to have 100 % gamma prime phase contained a small amount of gamma phase, but Alloy H has only gamma prime phase. Alloy A, designed to be 100 % gamma phase has some unknown phase.

**Experimentals.** In the first paper(4), from melting stocks of the alloys were made powders by a rotating disk cooled by liquid helium, and they were extruded after HIP process. Alloys F, G, and H contained many flaws after extrusion. In the second paper(5), powders were made by argon gas atomization and they were superplastically forged after the HIP process without extrusion.

**Results.** Figure 2 shows tensile superplastic properties of the extruded bars. It is seen that Alloy E(TMP-3) designed to have 70 % of gamma prime phase gives better superplastic properties than the original alloy (Alloy F, Rene 95). Figure 3 shows superplastic forging load of HIP-consolidated preforms. Though the loads go through minimum at around 60 - 80 % of gamma prime phase, there is no clear indication of the advantage of 70 % gamma prime phase as in Figure 2.

Figure 4 shows tensile properties at 760 C(not superplastic). We are much behind the target values(hatched), though the target is now believed too high.

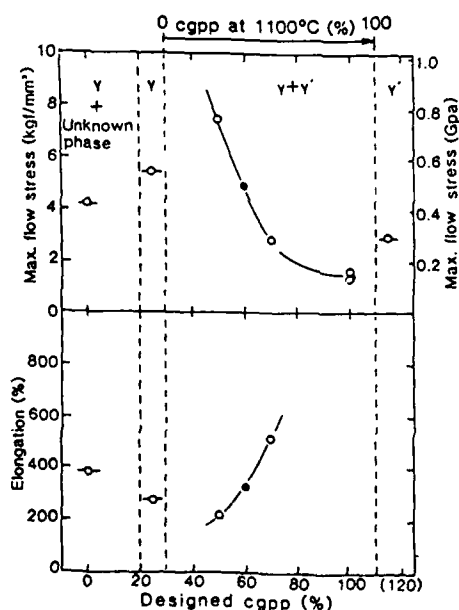


Figure 2 - Tensile superplastic properties of a series of Ni-base superalloys with various amounts of gamma-prime phase after extrusion. "cgpp": content of gamma-prime phase. The upper abscissa indicates rough estimation of "cgpp" at 1100 C. Test temp.: 1100 C. Strain rate: 0.105 %/s of the initial gage length.

#### Other Alloys Developed

Based on the knowledge derived by our developmental work for conventionally cast Ni-base superalloys, several superplastic P/M Ni-

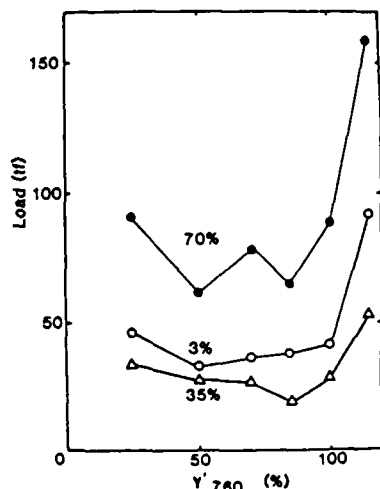


Figure 3 - Superplastic forging load of HIP-consolidated preforms of a series of Ni-base superalloys with various amounts of gamma-prime phase. "cgpp" is content of gamma-prime phase. Forging temp.: 1050 C. Forging rate: 0.02 %/s. Forging strain: 3, 35, and 70 %.

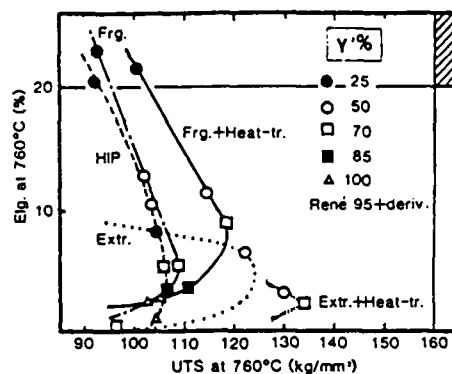


Figure 4 - Tensile properties of a series of Ni-base superalloys with various amounts of gamma-prime phase. Frg.: HIP-consolidated and superplastically forged. Extr.: Extruded after HIP (no forging). HIP: Only HIP-consolidated.

base superalloys have been developed. They are mostly strengthened by Ta and W and the gamma prime phase contents are 60 to 70 %. The improvement in tensile properties at 760 C was not so remarkable. The alloys developed, however, are superplastic if they are designed within gamma plus gamma prime regions and the contents of the latter are about 60 to 70 %.

#### Alloy Design of Ti Alloy

In order to design alpha-beta two phase Ti alloy, the following three computer-aided alloy design methods, A, B, and C were developed.

##### Method A (7)

The method A, based on data of Ti-X (X=Al, Sn, Zr, V, Mo, Cr, and Fe) binary phase diagrams, is made up of the following 6 steps.

**Step 1.** A composition of beta phase, except Al concentration, is set within the solubility limit of each element. The Al concentration of the beta phase will be determined later as a function of the beta phase composition set here. The Ti concentration is the balance.

**Step 2.** The beta-transus temperature,  $T_B$  (C) of Ti-X binary phase diagram is expressed approximately in a quadratic form. That is,

$$T_B = 882 + a_1 \cdot (X_1 \beta)^2 + b_1 \cdot X_1 \beta \quad (1)$$

where 882 is the alpha-beta transition temperature (C) of pure Ti,  $X_j \beta$  is concentration of j element (at %) in the beta phase, and  $a_j$  and  $b_j$  are constants in Table II and obtained from published binary phase diagrams. Then, beta-transus temperature of multi-component system is obtained by the summation of Eq. 1 for each element as

$$T_B = 882 + a_{Al} \cdot (X_{Al} \beta)^2 + b_{Al} \cdot X_{Al} \beta + \sum \{ a_j \cdot (X_j \beta)^2 + b_j \cdot X_j \beta \} \quad (2)$$

where j excludes Al as well as Ti. If we design beta and alpha phase compositions at 900 C,  $T_B$  in Eq. 2 is set as 900 and the concentration of Al in the beta phase,  $X_{Al} \beta$  can be calculated using  $X_j \beta$ 's which have been set in Step 1. Here,

$$X_{Al} \beta = f(X_j \beta)$$

is called, according to our notation, beta surface equation; in Ni-base superalloys, a similar notation, gamma prime surface equation has been used.

Table II. Constants in Eqs.1 and 2

j	Al	Sn	Zr	V	Mo	Cr	Fe
$a_j$	-0.300	0.646	0.152	0.226	0.093	0.630	0.340
$b_j$	18.241	-9.893	-3.107	-17.057	-19.047	-24.430	-18.048

Step 3. The composition of alpha phase, which is in equilibrium with the beta phase set in Steps 1 and 2, is calculated from Eq. 3 using the partitioning ratios,  $C_j$ , which are shown by Eq. 4.

$$X_j \alpha = C_j \cdot X_j \beta \quad (3)$$

$$\begin{aligned} C_{Al} &= 1.426 - 0.0148 \cdot X_{Al} \beta \\ C_V &= 0.731 - 0.263 \cdot X_V \beta \\ C_{Zr} &= 0.914 - 0.032 \cdot X_{Zr} \beta \\ C_{Sn} &= 0.928, \quad C_{Mo} = 0.078, \quad C_{Cr} = 0.081, \quad C_{Fe} = 0.089 \end{aligned} \quad (4)$$

The partitioning ratio of each element,  $C_j$ , is determined either from the binary phase diagram or from the EPMA data of alpha and beta phase compositions.

Step 4. The composition of alpha phase is checked whether it forms alpha-2 phase or not by Eq. 5. Alpha phase composition is converted to wt. % before being put into Eq. 5.

$$X_{Al} \alpha + X_{Sn} \alpha / 3 + X_{Zr} \alpha / 6 + 10 \cdot X_{Oxygens} \alpha \leq 9 \text{ wt\%} \quad (5)$$

Alpha-2 prone alpha phase composition and the coupled beta phase are discarded.

Step 5. The volume fraction of alpha phase,  $V_\alpha$ , is set to be suitable for superplastic forming. The final alloy composition,  $X_j$ , is calculated by Eq.6.

$$X_j = V_\alpha \cdot X_{j, \alpha} + (1 - V_\alpha) \cdot X_{j, \beta} \quad (6)$$

Actually, alpha and beta phase compositions are converted to wt. % and weight fraction of alpha phase is used instead of volume fraction of alpha phase.

Step 6. Alloys are classified according to their estimated strengths. For this purpose, compositional parameters such as the degree of solid-solution strengthening,  $dDE^\alpha$  (Eq.7), for the alpha phase and the electron-atom ratio,  $e/a\beta$ , for the beta phase are calculated from compositions of alpha and beta phases set in Steps 1, 2, and 3.

$$dDE^\alpha = \sum X_{i, \alpha} \cdot |(D_i - D_{Ti}) / D_{Ti}| \cdot 100 + \sum X_{j, \alpha} \cdot \Delta \rho_j \quad (7)$$

where  $i$ : transition metal element,  $j$ : non-transition metal element,  $X_{i, \alpha}$  or  $X_{j, \alpha}$ : at % of solute atom in the alpha phase,  $D_i$  or  $D_{Ti}$ : atomic diameters, and  $\Delta \rho_j$ : electrical resistivity increasing rate with alloying. Parameters in Eq.7 are shown in Table III, where values of  $\Delta \rho_j$  are after Sasano and Kimura(8). In the previous paper(7), the author's group confirmed a roughly linear correlation between Vickers hardness and  $dDE$  in multi-component titanium alloys in the state of alpha'-martensite. Then, in this case, the parameter  $dDE^\alpha$  is used to estimate the degree of solid-solution strengthening of the alpha phase. The author's group have found (9) that in the solution treated and aged condition, the strength of alpha-beta titanium alloys is estimated well by the following regression equation, and in this method the strengths of designed alloys are estimated by using this equation.

$$\sigma_u \text{ (kgf/mm}^2\text{)} = 207.72 - 318.29V_\alpha + 119.43V_\alpha \cdot dDE^\alpha + 178(1 - V_\alpha) \cdot (e/a\beta - 4) - 19(1 - V_\alpha) \cdot T_{\alpha\beta} / 100 \quad (8)$$

Table III. Constants in Eq.7

Element	Transision					Non-transision	
	V	Zr	Cr	Mo	Fe	Al	Sn
$  (D_i - D_{Ti}) / D_{Ti}   \cdot 100$	8.93	9.69	13.56	5.71	14.15	-	-
$\Delta \rho \text{ (}\Omega \cdot \text{cm/at}\%)$						14.40*	17.61*

\*:After H. Sasano and H. Kimura(8)

#### Method B (10)

Compositions of alpha and beta phases measured by EPMA were utilized to construct the alloy design method B similar to that for gamma/gamma-prime two phase Ni-base superalloys explained before. In the method B, the beta surface equation,

$$X_{A, \beta} = f(X_j, \beta), \text{ where } j \text{ excludes Al and Ti,}$$

at 900 C is obtained from beta phase compositions by the regression analysis. Partitioning ratios of each element between alpha and beta phases are expressed, also by regression analysis, as functions of beta phase compositions. The formation of alpha-2 phase is avoided by using Eq.5 as in the method A. The accuracy of the results obtained by the method B is better than that by the method A.

#### Method C (10)

The thermodynamical calculation (method C), based on Hillert's subregular solution model, was performed in order to confirm an applicability of thermodynamical representations to titanium alloys containing eight elements. The calculation by this method predicted very well the tendency of partitioning of each element between alpha and beta phases and the volume fraction of alpha phase at various temperatures (10). These results demonstrate that we have adequate set of parameters to describe the thermodynamics of the alpha and beta phases in multi-component Ti alloys.

#### Development of Superplastic Ti Alloys

##### Target

The target of the project, expressed as tensile properties at 300 C, is shown in Figure 5. Other than that shown in this figure, alloys developed must show good superplastic properties. P/M processes are studied in the project, but for alloy design purpose, specimens are made by melting and forging.

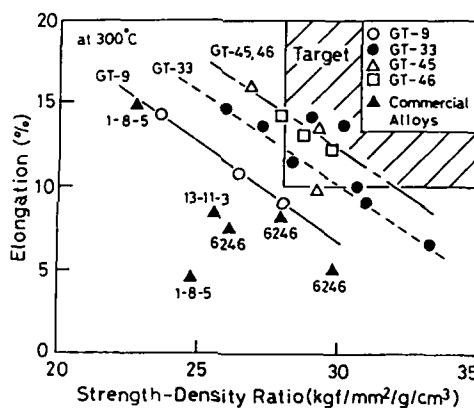


Figure 5 - Tensile properties of developed Ti alloys and commercial Ti alloys at 300 C.

#### Tensile properties of developed alloys at 300 C (9)

It is well known that optimum superplastic behavior is achieved by a fine microstructure with approximately equal fractions of two phases at forming temperatures. Furthermore, most of superplastic experiments for Ti alloys are usually carried out at around 900 C, and thus we designed at first, by the method A, alloys having alpha/beta volume fraction ratio of unity at 900 C. Among them, Alloy GT-9 (Table IV) showed tensile properties at 300 C near the target as shown in Figure 5. By lowering the design temperature, where alpha/beta volume fraction ratio is unity, from 900 C (GT-9) to 850 C (Gt-33), 800 C (GT-45), and 750 C (GT-46), beta-stabilizer content can be increased and age hardening response is expected to be improved. Alloys GT-33, 45, and 46, thus developed, showed tensile properties exceeding the target at 300 C as shown in Figure 5.



Table IV. Chemical Compositions of Some Developed Alloys(wt.%)

Alloy	Al	V	Sn	Zr	Mo	Cr	Fe	O	Ti
GT-9	5.70	0.50	1.40	3.86	0.98	1.29	0.98	0.12	bal.
GT-33	6.54	1.43	1.36	1.03	2.89	2.11	1.65	0.11	bal.
GT-45	6.35	2.85	0.88	1.05	2.48	2.54	1.59	0.11	bal.
GT-46	5.72	1.48	0.94	5.06	2.45	3.49	2.61	0.16	bal.

Superplastic properties of developed alloys (11)

Superplastic properties of these alloys are shown in Figures 6(a) and 6(b). Each alloy shows excellent superplasticity at temperatures between 800 C and 850 C. Total elongation of each alloy is more than 400 % in the temperature range between 750 C and 850 C. On the other hand, the maximum flow stress increases rapidly with decreasing temperature in the temperature range lower than 800 C. From these results, the temperature between 800 C and 850 C is considered to be suitable for superplastic forming of these alloys at the strain rate of 0.067 %/s (11).

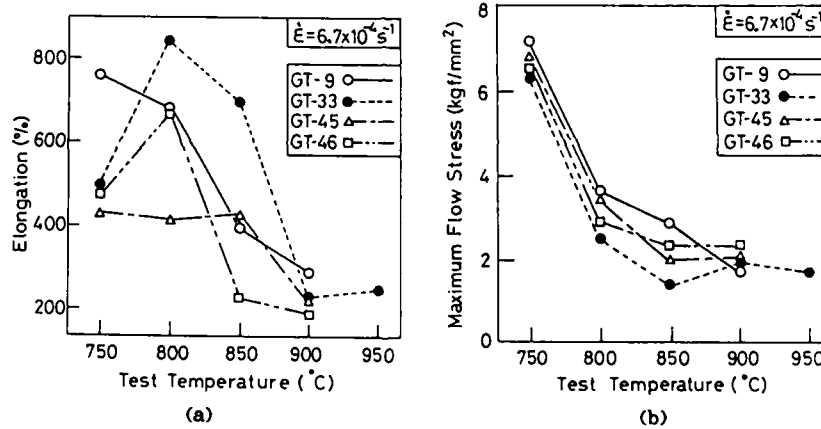


Figure 6 - Superplastic properties of developed Ti-alloys.

By examining the effect of test temperature and volume fraction of alpha phase on superplastic properties, it was concluded that Ti alloys having alpha/beta volume fraction ratio of unity at 850 C gave the best superplasticity at the forming temperature near 850 C (11). Therefore, a program was set up to improve the tensile properties of alloys having alpha/beta volume fraction ratio of unity at 850 C by optimizing the parameters,  $dDE^\alpha$  and  $e/a\beta$  at the solution temperature of 850 C. For that purpose, the method B which is applicable at 850 C is now being developed.

### Acknowledgments

This paper is a summary of many works by the author and some members of his group in National Research Institute for Metals. As is described in Introduction, this work is a part of the project sponsored by AIST of MITI, and the author and his group are indebted to many people participating in the project.

### References

1. H. Harada and M. Yamazaki, "Alloy Design for Gamma Prime Precipitation Hardening Nickel-base Superalloys Containing Ti, Ta, and W", *Tetsu-to-Hagane*, 65(1977)1059-1068.
2. H. Harada, M. Yamazaki, Y. Koizumi, N. Sakuma, N. Furuya, and H. Kamiya, "Alloy Design for Nickel-base Superalloys", *Proceedings of International Conference on High Temperature Alloys for Gas Turbines*, held in Liege, Belgium, Oct. 1982 (Dordrecht, D. Reidel Publishing Co., 1982), 721-735.
3. M. Yamazaki, "Development of Nickel-base Superalloys for a National Project in Japan", *High Temperature Alloys for Gas Turbines and Other Applications 1986*, *Proceedings of a Conference held in Liege, Belgium, 6-9 Oct., 1986* (Dordrecht, D. Reidel Publishing Co.), PART II, 945-954.
4. I. Tomizuka, H. Harada, S. Nakazawa, Y. Koizumi, and M. Yamazaki, "Effects of Gamma-prime Phase Content in Rene 95 and its Derivative Alloys on Parameters of Superplasticity and High Temperature Tensile Properties, I.-- Extruded Bars", submitted for publication to *Proceedings of International Conf. of PM Aerospace Materials*, held on Nov. 2-4, 1987, Luzern, Switzerland.
5. I. Tomizuka, T. Maeda, S. Nakazawa, Y. Koizumi, H. Harada, and M. Yamazaki, "The same as above, II.-- HIP-Consolidated Blocks", *ibid.*
6. K. Kusunoki, M. Yamazaki, and H. Kamiya, "A Phase Decomposition Calculation of Gamma-prime phase Precipitation Hardening Nickel-base Superalloys and Its Application to the Estimation of Alloy Properties", *Tetsu-to-Hagane*, 70(1984)875-881, or *Transactions of National Research Institute For Metals*, 28(1986)103-111.
7. H. Onodera, Y. Ro, T. Yamagata, and M. Yamazaki, "Design of Titanium Alloys", *Proc. of 5th Int. Conf. on Titanium*, G. Lutjering et al., ed., Munich, FRG (1984), 1883-1890.
8. H. Sasano, and H. Kimura, "Solid-Solution Strengthening of Alpha Titanium Alloys", *Proc. of 4th Int. Conf. on Titanium*, H. Kimura et al., ed., Kyoto, Japan (1980), 1147-1154.
9. H. Onodera, K. Ohno, T. Yamagata, and M. Yamazaki, "The Effect of Beta-Stabilizer Content on Tensile Properties of Alpha-Beta Titanium Alloys", *Tetsu-to-Hagane*, 72(1986)284-291.
10. H. Onodera, K. Ohno, T. Yamagata, and M. Yamazaki, "Methods for Calculation of Alpha-Beta Equilibria in Multi-Component Titanium Alloys", *Trans. ISIJ*, to be published.
11. H. Onodera, K. Ohno, T. Yamagata, T. Ohkoshi, and M. Yamazaki, "Design of Titanium Alloys Suitable for Superplastic Forming", *Tetsu-to-Hagane*, 74(1988)123-129.

## DEVELOPMENT OF SUPERPLASTIC BEHAVIOUR

### IN VARIOUS COMMERCIAL MATERIALS

N. Ridley<sup>†</sup> and C. Hammond<sup>\*</sup>

<sup>†</sup>Materials Science Centre,  
University of Manchester/UMIST,  
Grosvenor Street,  
Manchester M1 7HS, UK.

<sup>\*</sup>Department of Metallurgy,  
University of Leeds,  
Leeds LS2 9JT, UK.

#### Abstract

The principles of the development of stable fine grained superplastic microstructures in pseudo-single phase and duplex materials, and the factors which influence cavitation during superplastic flow, are outlined. The procedures used to develop superplasticity in a number of materials of commercial significance are reviewed, as are the resulting superplastic deformation characteristics. Alloys based on aluminium, copper, iron and titanium, are critically examined, and also potentially important ceramic materials. Recent work which shows that exceptional superplastic behaviour can be obtained in copper alloys and stainless steels is reported. It is clear that dynamic recrystallisation is not only an important process in developing superplasticity in aluminium alloys, but also can be applied to duplex titanium alloys and stainless steels. The advantages of duplex titanium alloys is pointed out, but attention is also drawn to the fact that Ti-6/4 is not the only  $\alpha/\beta$  alloy with superplastic forming potential. The similarities between ceramic composites and the particle-stabilised pseudo-single phase alloys are emphasised, and the very recent work on TiO<sub>2</sub> which demonstrates the enormous benefits of reducing grain size is outlined.

Superplasticity and Superplastic Forming  
Edited by C.H. Hamilton and N.E. Paton  
The Minerals, Metals & Materials Society, 1988

### Introduction

It is well established that for the occurrence of superplasticity a fine grain size must be achieved and maintained at a relatively high deformation temperature,  $>0.5T_m$ . Under these conditions a high strain rate sensitivity of flow stress,  $m$ , which is the most important mechanical characteristic of superplastic materials, will be obtained. However, a high  $m$  value does not necessarily lead to large tensile strains, since cavitation during superplastic flow can result in premature fracture in a number of alloys. Hence, an understanding of the principles underlying both grain refinement and the inhibition of grain coarsening, and of the factors which influence cavitation are clearly of importance in the development of superplasticity.

In the last 25 years a large number of superplastic alloys have been discovered, although relatively few of these have any commercial significance. A few alloys have been designed for superplasticity but it is likely that this approach is limited in view of the cautious outlook of designers and metal users, particularly those in the aerospace sector. The dominant current approach is to take an alloy with well established service properties and to process it to develop superplasticity. In the present paper the metallurgical requirements which enable a material to be processed to give a superplastic microstructure are outlined and the procedures used to develop superplasticity in selected alloys based on aluminium, copper, iron, and titanium, and in ceramic materials, will be reviewed.

### Processing of Superplastics

Superplastic alloys may be divided into two main types: pseudo-single phase and microduplex. In the former type of material, precipitates can play an important role both in the development of a fine grain size by thermomechanical processing and in the inhibition of grain growth during subsequent superplastic forming. The precipitation strengthened Al alloys of the 2000 (Al-Cu), 7000 (Al-Zn-Mg) and 8000 (Al-Li) series are important pseudo-single phase, particle stabilised superplastic alloys.

The role of particles in microstructural refinement and grain size control of superplastic materials has been discussed by Wert (1) and by Stowell (2). Large particles provide nucleation sites for recrystallisation following heavy warm deformation, while small particles ( $<0.1\mu m$ ), retard recrystallisation, grain and sub-grain growth by pinning dislocations, sub-grain and grain boundaries. The effectiveness of a particle as a nucleating site for recrystallisation increases both with its size and with the level of imposed work. However, it is important that the imposed warm or cold work does not cause particle cracking or decohesion of the particle-matrix interface, and hence lead to cavity nucleation prior to superplastic forming (SPF) (see next section).

Several procedures have been described for the development of fine equiaxed grain microstructures in duplex alloys (1). Grain refinement may be carried out by hot working in the two-phase field close to the superplastic temperature range. If the phases have different deformation characteristics, such as one being harder or more brittle than the other, then working could fragment the harder phase and redistribute it throughout the softer phase. If the two phases have similar mechanical behaviour, then hot working first elongates the phases and then fragments them by the development of intense shear bands. In these procedures recrystallisation and spheroidisation lead to the required equiaxed grain structures. In

some cases the microduplex structure may be developed by recrystallisation of warm/cold worked material, while annealing of martensitic structures produced by quenching can give the required microstructure e.g.  $\alpha/\beta$  Ti alloys.

In duplex alloys, grain growth is restricted by equilibrium partitioning of alloying elements between the two phases. The microstructure is said to be segregation stabilised. High stability would be predicted for microstructures consisting of equi-volume fractions of two phases which showed little mutual solid solubility and which contained a predominance of interphase boundaries. Important microduplex superplastic materials include  $\alpha/\beta$  titanium alloys and  $\alpha/\gamma$  stainless steels. Materials such as the ultra-high carbon steels and  $\alpha/\kappa$  aluminium bronzes, which contain about 25% volume of second phase particles, may be regarded as pseudo-single phase/particle stabilised since they contain a predominance of boundaries between like phases i.e. grain boundaries rather than interphase boundaries.

#### Cavitation

Cavitation occurs in a wide range of alloys during superplastic tensile flow, and the topic was very recently reviewed by Pilling and Ridley (3). Cavities can either nucleate at grain boundary sites, due to lack of accommodation of grain boundary sliding, or may pre-exist. Their subsequent growth, coalescence and interlinkage can lead to premature failure, while the presence of cavities in superplastically formed components may have an adverse effect on service behaviour.

It is well established that cavity growth is dominated by matrix plastic flow and that coalescence plays an important role in the development of large cavities. Hence, to prevent cavitation it is necessary to inhibit nucleation and to avoid the presence of pre-existing defects by control of the processing required to develop superplastic behaviour in a given material. Factors which influence cavity nucleation include those related to microstructure and those associated with deformation conditions. Important microstructural features may include the average grain size, grain size distribution and grain shape, the type, size, volume fraction and hardness (reflecting the type of bonding) of second-phase particles, and in the essentially duplex alloys the proportions of the major phases and their characteristics.

To minimise cavitation it is necessary to develop a small, stable, equi-axed grain size containing second-phase particles in a finely dispersed form. In practice, it is often difficult to control microstructure and forming conditions so as to inhibit cavitation. However, cavitation can be suppressed by the application of a hydrostatic pressure  $>0.5-0.7$  of the material flow stress (3), although imposed pressures  $>34\text{MPa}$  would be technically difficult to apply.

#### Commercial Superplastic Materials

The procedures used to develop superplastic microstructures in a number of commercially important alloys, and in ceramic materials, will be examined.

##### Aluminium Alloys

The design and processing of a range of aluminium alloys for

superplastic deformation has been discussed by Lloyd and Moore (4). However, only some aspects of the pseudo-single phase materials in which superplastic microstructures develop either by static recrystallisation prior to SPF or dynamic recrystallisation during SPF, will be considered.

The former process is typified by work on the high strength 7475 Al alloy (the Rockwell route) (5). Superplastic microstructures with grain sizes of  $\sim 10\mu\text{m}$  are produced by recrystallisation, using rapid heating rates, of heavily warm worked microstructures containing a bimodal distribution of precipitates. The larger particles,  $1-2\mu\text{m}$ , produced by overageing, lead to localised intense deformation and lattice rotation during working, and provide nucleating sites for discontinuous recrystallisation, while smaller,  $0.1-0.2\mu\text{m}$ , precipitates (Cr-rich) inhibit grain growth during recrystallisation and subsequent SPF. Processed 7475 Al alloy is capable of sustaining large tensile strains  $>1000\%$  elongation under optimum conditions ( $516^\circ\text{C}$ ;  $2 \times 10^{-4}\text{s}^{-1}$ ). Cavitation damage can occur in 7475 during superplastic flow and is often associated with iron and silicon-rich impurity particles. However, because of the low flow stresses ( $<6\text{MNm}^{-2}$ ) cavitation can be eliminated by the application of hydrostatic pressure during SPF if necessary.

Mahoney and Ghosh (6) recently developed superplastic behaviour in a high strength PM aluminium alloy (Kaiser PM64) with and without SiC reinforcement. Processing of the extruded alloys by the Rockwell route led to fine grain,  $6-8\mu\text{m}$ , microstructures. It was observed that oxides from the Al powder and SiC particles provided cavity nucleating sites during superplastic deformation, additional to those associated with impurity particles normally found in 7000 series alloys. However, since flow stresses were low at strain rates of  $2 \times 10^{-4}\text{s}^{-1}$ , cavitation could be prevented by the application of hydrostatic pressures,  $<2\text{MPa}$ .

In alloys such as Supral 100 (Al-6Cu-0.4Zr) and Supral 220 (Al-6Cu-0.4Zr-0.3Mg-0.1Ge-0.1Si) a fine grain structure is developed by dynamic or in-situ recrystallisation in the early stages of SPF. The principles of the processing route have been described by Watts et al (7). During processing the material is heavily warm worked at  $300^\circ\text{C}$ , when recovery and recrystallisation are prevented by a dispersion of fine  $\text{ZrAl}_3$  particles ( $5-10\text{nm}$ ), and to a lesser extent by  $\text{Mg}_2\text{Si}$  particles, and by copper and magnesium in solid solution. During SPF at  $460^\circ\text{C}$  recrystallisation is usually complete after 50% strain, and the faster the strain rate up to  $\sim 10^{-2}\text{s}^{-1}$  the smaller the recrystallised grain size (Fig.1), and the more rapid the recrystallisation process (8). Tensile elongations of  $>1000\%$  can be attained in Supral 220 for optimum conditions ( $460^\circ\text{C}$ ;  $10^{-3}\text{s}^{-1}$ ). Cavitation occurs during SPF and is frequently associated with primary  $\text{ZrAl}_3$  and with coarse  $\text{CuAl}_2$  particles. It is difficult to control cavitation damage with hydrostatic pressure because of the relatively high flow stresses ( $\sim 10\text{MPa}$ ) resulting from the low forming temperature ( $460^\circ\text{C}$ ).

In Al-Li based alloys superplastic microstructures can be developed by static or dynamic recrystallisation, of ingot or PM alloys (9-12). An interesting feature of alloys which develop fine grain microstructures by dynamic recrystallisation is that they show a high resistance to necking in the early stages of deformation before superplasticity has developed. Ash and Hamilton (13) recently examined an Al-Li based alloy which had been processed to develop superplasticity by dynamic recrystallisation. Measurements of strain rate sensitivity,  $m$ , and strain hardening exponent,  $n$ , showed that although  $m$  was low initially,  $\sim 0.3$ , it rises with strain to  $0.5-0.6$ , whereas  $n$  is initially high and then decreases (Fig.2). Thus the stability of the material is initially dependent on strain hardening for

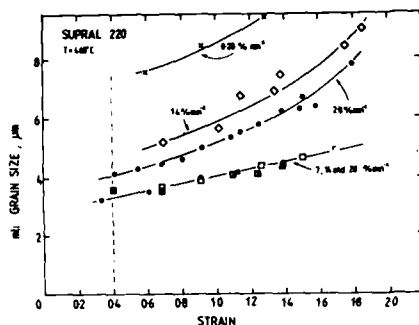


Fig. 1. Effect of strain rate on recrystallised grain size ( $\epsilon \sim 0.4$ ) and grain growth.

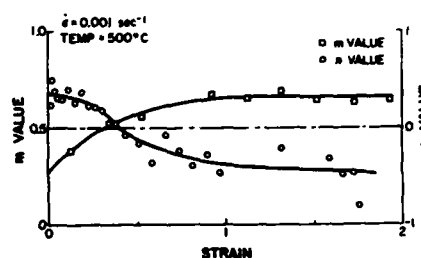


Fig. 2. Variation of strain rate sensitivity,  $m$ , and strain hardening exponent,  $n$ , as function of strain for Al-Li alloy (13).

its necking resistance. Experiments showed that the strain could be quite high ( $\sim 10^{-2} \text{s}^{-1}$ ) in the early stages without loss of superplastic ductility. Hence the material can be rapidly deformed at strains up to  $\sim 1$  to develop a superplastic microstructure, and then reduced to a more optimum strain rate ( $\sim 10^{-3} \text{s}^{-1}$ ) for superplastic flow. Similar procedures have been proposed for Supral 220 (8).

#### Copper Alloys

Superplastic behaviour has been reported for a range of copper alloys, but most of these materials undergo marked grain growth during deformation or have too low an optimum deformation temperature, and are particularly prone to cavitation. Despite these problems, exceptional superplasticity has been observed in a complex commercial Al-bronze of nominal composition Cu-10Al-5Fe-5Ni by Higashi and co-workers (14). A fine stable microstructure can be developed by a processing sequence which involves rolling at  $900^\circ\text{C}$ , annealing at  $700^\circ\text{C}$ , warm rolling at  $640^\circ\text{C}$ , cold rolling and finally recrystallisation at  $\sim 800^\circ\text{C}$ . The room temperature microstructure consists of  $\alpha$ -phase with a grain size of  $2\text{-}3\mu\text{m}$  containing a fine dispersion of aluminide particles ( $\sim 25\%$  vol. of  $\kappa$  phases). The material can be superplastically deformed at  $750\text{-}850^\circ\text{C}$  which spans the  $\alpha+\kappa$  and the  $\alpha+\beta+\kappa$  phase fields. Tensile elongations of  $1000\%$  can be readily obtained at strain rates as high as  $10^{-2}$  to  $10^{-1} \text{s}^{-1}$ , with an elongation of  $5,500\%$  without failure being recorded for an initial strain rate of  $6 \times 10^{-3} \text{s}^{-1}$  at  $800^\circ\text{C}$  (Fig. 3). At this temperature, the microstructure contains about  $40\%$   $\alpha$ ,  $30\%$   $\beta$  and  $30\%$   $\kappa$  by volume and its stability is due to a combination of segregation and particle stabilisation. The superplastic microstructures are highly resistant to cavitation.

#### Iron Alloys

Two types of steels in which substantial superplastic behaviour has been developed include the ultra-high carbon (15), tool and bearing steels studied by Sherby and co-workers, and the microduplex  $\alpha/\gamma$  stainless steels. The processing procedures for the former steels have been outlined in the reviews of superplasticity in iron-base alloys by Ridley (16) and by Walser and Ritter (17).

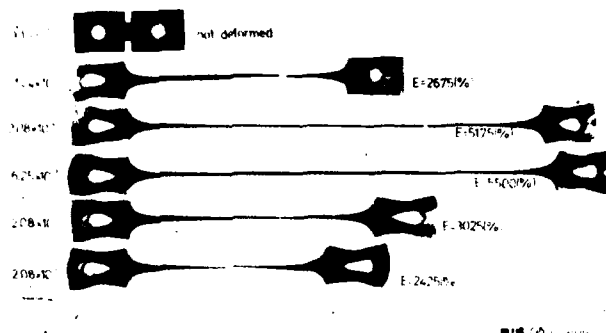


Fig. 3. Cu-10Al-5Fe-5Ni. Profiles of tensile specimens deformed at various strain rates (Courtesy K. Higashi).

There is a wide range of duplex stainless steels which are commercially available and which after normal hot processing to sheet develop a fine grain duplex structure suitable for SPF. The alloys have a 2-phase microstructure from room temperature to  $>1200^{\circ}\text{C}$ , when they become fully ferritic. Previous studies on these materials show that they can exhibit tensile elongations  $>1000\%$ , and that they can be satisfactorily bulge-formed (16).

Maehara and Ohmori (18) have recently reported exceptional superplasticity in a duplex stainless steel of weight % composition: Fe-25Cr-6.5Ni-3Mo-0.14N. The steel was processed by forging and hot rolling to thick plate, then solution treated at  $1250^{\circ}\text{C}$ , when the material contained only a small volume fraction of austenite, before being given a 50% cold rolling reduction. On subsequent deformation at an optimum strain rate of  $\sim 10^{-3}\text{s}^{-1}$ , two peaks of high superplastic elongation ( $\sim 2000\%$ ) were observed at  $900^{\circ}\text{C}$  (1173K) and  $1050^{\circ}\text{C}$  (1323K) (Fig.4). Detailed metallographic studies showed that during deformation at the lower temperature, rapid decomposition of  $\alpha$ -ferrite into  $\sigma$ -phase and austenite occurred. The relatively soft  $\gamma$  grains were subjected to severe deformation adjacent to the hard  $\sigma$ -phase particles and underwent dynamic recrystallisation leading to a fine equiaxed  $\sigma/\gamma$  microstructure (Fig.5). At the higher temperature, fine Widmanstätten  $\gamma$  particles precipitated from the ferrite, and probably inhibited discontinuous recrystallisation, and the pre-existing coarser  $\gamma$  grains were broken into spherical particles, leading to a uniform dispersion of  $\gamma$  precipitates in a ferrite matrix. The softer ferrite phase underwent dynamic recrystallisation to form a fine equiaxed  $\alpha/\gamma$  microstructure.

Osada et al (19) have examined a similar steel which was hot rolled in a planetary mill to 4mm thickness, water cooled to room temperature, cold rolled to various extents and tested. The as-hot rolled plate consisted of coarse elongated  $\alpha/\gamma$  grains and showed significant superplastic behaviour at  $900/950^{\circ}\text{C}$  at strain rates of  $10^{-3}$ - $10^{-2}\text{s}^{-1}$ , which was enhanced after cold rolling ( $\sim 2000\%$  elongation).

#### Titanium-base Alloys

Superplasticity in titanium-base alloys has been reviewed by Hammond (20) and more recently by Hamilton (21). The two-phase duplex titanium alloys, e.g. Ti-6Al-4V (Ti-6/4), Ti-6Al-2Sn-4Zr-2Mo (Ti-6/2/4/2), Ti-4Al-4Mo-2Sn-0.5%Si (IMI550) have the great advantage in that the



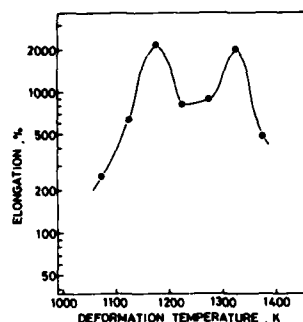


Fig. 4. Variation of elongation with deformation temperature  $\epsilon = 4 \times 10^{-3} \text{s}^{-1}$  (18).

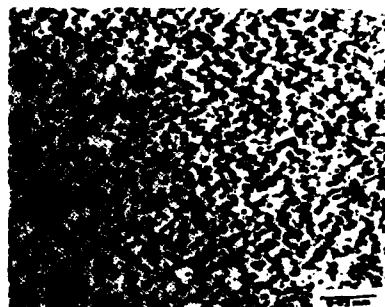


Fig. 5. Duplex  $\alpha/\beta$  structure developed on deformation at  $950^\circ\text{C}$ ,  $\epsilon = 4 \times 10^{-3} \text{s}^{-1}$  (18).

normal duplex processed sheet material possesses superplastic properties without the requirement (and associated cost premium) for complex prior thermomechanical processing. Furthermore, because of the absence of hard second phase particles at grain or interphase boundaries, cavitation is almost wholly absent. The superplastic properties are affected by variations in the initial sheet microstructure ( $\alpha$  and  $\beta$  grain sizes, grain size distribution and volume fractions) and much effort is presently directed towards modifications in the duplex processing routes for the manufacture of 'superplastic grade' sheet material. However, identifying the optimum microstructure is not a straightforward procedure; a simple measurement of an average (fine) grain size and a 50%  $\alpha$ /50%  $\beta$  volume are insufficient criteria. For example, Paton and Hamilton (22) examined six heats of Ti-6/4 with different alloying element and impurity concentrations, grain sizes and grain size distributions. Their results clearly show that non-uniformity of the microstructure, the presence of 'blocky  $\alpha$ ' grains etc., need to be taken into account. The work of Cope et al (23) on Ti-6/4 and Ti-6/2/4/2 also shows that a  $\beta$ -phase volume fraction of ~40% confers maximum elongation, a 50% volume fraction leading to rapid grain coarsening.

The optimum volume fraction will however be determined by the deformation characteristics and distributions of the two phases and how they interact (20). There are two limiting cases. Firstly, it may be assumed that the 'harder', or more creep resistant  $\alpha$ -phase restricts the deformation of the 'softer'  $\beta$ -phase, such that they deform at the same rate - the isostrain rate model. Secondly, it may be assumed that the stress in the two phases is constant and that the  $\beta$ -phase deforms at a faster rate - the isostress model. These two models (which are precisely analogous to the 'parallel' and 'series' models for heat or electrical conductivity in the two-phase materials) predict substantial differences in overall superplastic deformation behaviour, particularly at small volume fractions of  $\beta$ .

Which model is applicable probably depends on the distribution of the  $\alpha$  and  $\beta$  phases in the microstructure; a continuous, interconnected or matrix  $\beta$  phase suggesting the isostress model (and vice-versa). In such microstructures the deformation properties of the  $\beta$  phase dominates; it is in effect a 'mantle' around the  $\alpha$  grains (Fig.6). Hence, it may be expected that additions of  $\beta$ -stabilising alloying elements which increase the effective diffusion coefficients for creep will result in reduced flow stresses and higher strain rate sensitivities. Such has been shown to be

the case for additions of nickel, cobalt and iron to Ti-6/4, although direct comparisons are not straightforward because of concomitant changes in  $\beta$ -phase volume fractions (20,24).

As with the unrecrystallised sheet material of the 7000 and 8000 series aluminium alloys, an initial non-superplastic microstructure, for example a transformed  $\beta$  microstructure consisting of martensitic or Widmanstätten  $\alpha$  platelets in a transformed  $\beta$  matrix, may dynamically recrystallise to a fine grained equiaxed microstructure, superplastic properties thereby being developed as a result of the deformation (25). This is a very important characteristic in that it allows superplastic forming processes to be carried out on sheet materials which contain  $\beta$  transformed regions, e.g. weld structures and heat affected zones. This is clearly an area in which considerably more work needs to be carried out in order to determine the optimum forming conditions to give grain refinement and to avoid localised thinning and cavitation.

The development of superplastic sheet materials must ultimately be assessed in relation to the required mechanical properties of the superplastically formed parts. In the case of Ti-6/4, superplastic forming leads to a decrease in strength which is a result not of the deformation as such, but of the grain growth normally observed during the thermal cycling. There is no reason why this situation should not be reversed, with improved properties being obtained as a result of grain refinement and redistribution and texture changes brought about as a result of modifications to the forming temperatures and strain rates employed. Indeed this is already the situation in the case of certain superplastically formed nickel-base superalloys, e.g. following the 'Minigrain' processing route (26).

#### Ceramics

Microstructural superplasticity of fine-grained ceramics (i.e. in the absence of phase transformations brought about by thermal cycling) was recently reviewed by Carry and Mocellin (27). As in the case of metallic alloys, it is the deformation properties of the material at the grain boundaries which are of importance and, although in ceramics dislocation-climb controlled creep mechanisms are probably of negligible significance, it appears that there is considerably greater scope for modifying grain boundary and lattice diffusional creep mechanisms by modification of the grain boundary chemistry and structure. In addition, the potential for extending the temperature range over which diffusional creep mechanisms are of importance by refinement of the grain size to the order of 1-10nm has been exploited in ceramics, albeit on a very small scale.

Two microstructural situations may be identified: ceramics which have a glassy grain boundary phase and those which do not. The former comprise those 'glass ceramics' which result from the incomplete crystallisation of a glass and those hot pressed 'silicon ceramics' which result from the sintering of  $\text{Si}_3\text{N}_4$  or  $\text{SiC}$  powders to which small amounts of sintering additions have been made, e.g.  $\text{MgO}$  or  $\text{Y}_2\text{O}_3$  for  $\text{Si}_3\text{N}_4$ ;  $\text{Al}$  or  $\text{C}$  for  $\text{SiC}$ . These sintering additives or dopants give rise to small volume fractions of intergranular glassy phases in the form of particles at triple points or near-continuous films. The latter comprise those ceramics which may be single phase oxides such as  $\text{MgO}$ ,  $\text{Al}_2\text{O}_3$ ,  $\text{TiO}_2$ ,  $\text{UO}_2$ ; single phase fluorides, spinels, perovskites, olivines and two-phase dispersion strengthened and toughened oxide composites such as  $\text{Y}_2\text{O}_3$ -stabilised tetragonal  $\text{ZrO}_2$  (Y-TZP), with various volume fractions of  $\text{Al}_2\text{O}_3$  distributed within the  $\text{ZrO}_2$

matrix (Y-TZP/ $\text{Al}_2\text{O}_3$ ).

In the case of glass ceramics it has been proposed (28) that the boundary consists of islands of crystalline material in a glassy matrix which undergo a continuous process of solution-precipitation; the islands supporting the grain boundary shear stresses and the glassy phase providing fast molecular diffusion paths. This model could also apply to those silicon ceramics in which the grain boundary glass phase occurs as near-continuous films.

Most deformation experiments on ceramics have been carried out in bending or compression, but more recently tensile tests have been carried out which allow a direct comparison with metals and alloys to be made in terms of cavitation and neck stability. The most extensively studied single phase oxide ceramics are  $\text{MgO}$  and  $\text{Al}_2\text{O}_3$  with grain sizes normally in the range 1-5  $\mu\text{m}$ . There are two ways in which the superplastic properties may be enhanced: by influencing the effective grain boundary and lattice diffusivities by modifications to the amount and types of dopants, and by decreasing the grain size. The effects of dopants arises as a result of segregation to grain boundaries. There is insufficient transmission electron microscopical evidence to preclude the possibility that small volume fractions of glassy phases are not also generated. A reduction in the grain size of  $\text{TiO}_2$  from  $\sim 10\mu\text{m}$  to  $\sim 10\text{nm}$  (three orders of magnitude) is reported by Karch, Birringer and Gleiter (29) to extend the temperature range over which diffusional creep is effective down to  $\sim 180^\circ\text{C}$ . This is not unexpected since grain boundary diffusional creep is proportional to the third power of the grain size, which indicates an enhancement factor of  $10^9$ !

The Y-TZP- $\text{Al}_2\text{O}_3$  ceramic composites are of course of increasing importance. With respect to their superplastic properties, it is the co-existence of the tetragonal and cubic phases in the  $\text{Y}_2\text{O}_3$ - $\text{ZrO}_2$  system and the presence of the second phase  $\text{Al}_2\text{O}_3$  particles which contribute to their grain stability. Recently, Wakai and Kato (30) have demonstrated the superplastic properties of such a composite with a grain size of 0.5  $\mu\text{m}$  containing 20wt%  $\text{Al}_2\text{O}_3$ . At a temperature of  $1450^\circ\text{C}$  and strain rates below  $1 \times 10^{-3} \text{ s}^{-1}$  the flow stresses were approximately strain independent and uniform elongations up to 200% were achieved (Fig.7). At higher strain rates strain-softening and reduced elongations were observed, which was attributed to cavitation or creep crack growth.



Fig.6. Ti-6Al-4V-1Co alloy superplastically deformed at  $835^\circ\text{C}$ . Shows grain boundary network of  $\beta$ -phase.

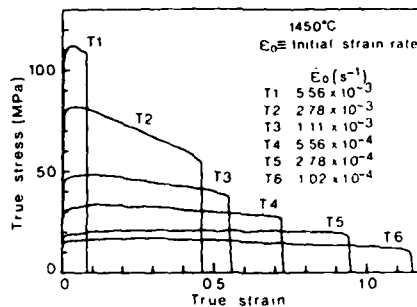


Fig.7. True stress as a function of true strain for constant velocity tensile testing of Y-TZP/ $\text{Al}_2\text{O}_3$  at  $1450^\circ\text{C}$  (30).

### Discussion

It is clear that dynamic recrystallisation of cold or warm worked material is not only of importance in developing superplastic microstructures in aluminium alloys, but can also be applied to duplex titanium alloy and stainless steels. The alternative processing route involving static recrystallisation is used to develop superplasticity in the 7000 series alloys, although Grimes et al (11) have pointed out the practical problems of applying heavy warm rolling reductions to materials of limited working capability, and of applying very high heating rates uniformly to large sheets of material to produce a uniform microstructure. As a consequence, current commercial interest in the development of superplasticity in Al-Li alloys is focused on the dynamic recrystallisation route. Whether the 7000 series alloys could indeed be processed by this route given minor compositional changes e.g. by small additions of Zr, is an area which merits further investigation.

Strain enhanced grain growth occurs in all superplastics, but the problem of maintaining a small stable grain size in aluminium alloys requires special attention because of the high homologous temperatures,  $\sim 0.9T_m$ , at which they exhibit optimum superplasticity. However, McNeilly and co-workers (31) have shown that substantial elongations ( $>500\%$ ) can be obtained at  $300^\circ\text{C}$ , a homologous temperature of  $\sim 0.7T_m$ , in a thermomechanically processed Al-10Mg alloy at strain rates  $2-5 \times 10^{-3}\text{s}^{-1}$ . Warm rolling at  $300^\circ\text{C}$ , below the Mg solvus, leads to a fine sub-grain structure stabilised by a fine dispersion of  $\text{Al}_3\text{Mg}_2$  and  $\text{MnAl}_6$ . On deformation at  $300^\circ\text{C}$  continuous recrystallisation occurs, and misorientation between sub-grains progressively increases. Although measured  $m$  values were relatively high it is likely that the necking resistance of these materials is due to high strain hardening, as identified by Ash and Hamilton (14), rather than conventional superplastic deformation processes. The material shows a low level of cavitation, consistent with lack of grain boundary sliding.

All aluminium alloys tend to undergo cavitation during superplastic flow. Although cavitation can be suppressed by the application of hydrostatic pressure during forming provided the flow stress of the material is not too high, this procedure will clearly influence the cost and competitiveness of SPF as a shaping process. Stowell (32) has pointed out that to minimise cavitation during SPF care must be taken at all stages in the production process. Attention must be paid to the cleanliness of the liquid Al alloy, the minimisation of iron and silicon pick-up, prevention of coarse primary phase formation, and the avoidance of fracture and decohesion of large particles during warm working procedures involved in the production of superplastic microstructures.

Cavitation during superplastic flow in 7475 Al alloy can vary appreciably from batch to batch. It is uncertain whether there is a correlation between cavitation and the Fe + Si content of the alloy, or whether microstructural features other than Fe and Si-rich constituent particles make a significant contribution to cavitation. It may be possible to minimise cavitation by using PM or rapid solidification production routes. However, these would appear to be expensive options for the relatively large scale production of superplastic sheet.

The duplex titanium alloys are in many respects ideal superplastic materials, apart from their high forming temperatures. The normally processed mill products are usually superplastic and the materials contain substantial proportions of b.c.c.  $\beta$ -phase which readily accommodates grain boundary sliding during SPF. The alloys do not cavitate and, in addition,

they readily undergo diffusion bonding.

However, the superplastic forming potentials of  $\alpha+\beta$  titanium alloys other than Ti-6/4 are grossly under-exploited. The concentration of research effort and the increasing experience in the use of superplastically formed Ti-6/4 parts in aerospace engineering has consolidated its position as the 'workhorse' titanium alloy. But workhorses, by their nature, are not evolved to fulfil a specific set of requirements and when the limitations of Ti-6/4 become more widely recognised by designers, the opportunities for the development both of other commercial titanium alloys and alloys of modified compositions, will be greatly increased.

The work of Karch et al (29) on TiO<sub>2</sub> has demonstrated the enormous advantages attainable on reducing the grain size. And although this work was carried out on very small amounts of vapour deposited material, it does indicate the enormous benefits which will follow from the development of processing routes which result in only ten-fold or five-fold decreases in grain size.

The deformation characteristics of the ceramics composites are remarkably similar to those of fine grain alloys which contain a dispersion of hard second phase particles: the harder Al<sub>2</sub>O<sub>3</sub> particles inhibit grain growth but act as nucleation sites for cavitation; the deformation is largely accommodated by grain boundary deformation processes with a small amount of grain elongation; strain rate sensitivities are approximately 0.5 and grain growth is dynamically enhanced by the deformation. Finally, there is again the problem of identifying the appropriate diffusion coefficient for the composites which will be a function of the diffusional and dislocation climb contributions of the phases present. The exploitation of the superplastic potential of ceramics, as well as of metals, will clearly depend on a greater understanding of this function and the ways in which it may be modified by compositional and microstructural design.

#### References

1. J.A. Wert, Superplastic Forming of Structural Alloys, ed. N.E. Paton and C.H. Hamilton, (Warrendale, PA: TMS-AIME, 1982) 69-83.
2. M.J. Stowell Deformation of Multi-Phase and Particle Containing Materials", ed. J.B. Bilde-Sorensen et al., (4th Riso Intl. Symposium, Riso National Lab., Roskilde, Denmark, 1983) 119-129.
3. J. Pilling and N. Ridley, Res. Mechan., 23 (1988) 31-63.
4. D.J. Lloyd and D.M. Moore, in Ref. 1, 147-172.
5. C.H. Hamilton, C.C. Bampton and N.E. Paton, in Ref. 1, 173-189.
6. M.W. Mahoney and A.K. Ghosh, Metall. Trans., 18A (1987) 653-661.
7. B.M. Watts, M.J. Stowell, B.L. Baikie and D.R.E. Owen, Metal Sci., 10 (1976) 189-197; 198-206.
8. B. Geary, J. Pilling and N. Ridley, Superplasticity in Aerospace-Aluminium, ed. R. Pearce and L. Kelly, (SIS, Cranfield, 1985) 127-135.
9. J. Wadsworth et al, Aluminium-Lithium Alloys II, ed. T.H. Sanders and E.A. Starke, (Warrendale, PA: TMS-AIME, 1983) 111-135.

10. R.J. Lederich and S.M.L. Sastry, *ibid*, 137-151.
11. R. Grimes, W.S. Miller and R.G. Butler, 4th International Al-Li Conference, ed. G. Champier et al, (Les Editions de Physique, France 1987) 239-249.
12. H. Yoshida, S. Hirano, Y. Baba, T. Tsuzuku and A. Takahashi, *ibid*, 269-275.
13. B.A. Ash and C.H. Hamilton, Scripta Metal, 22 (1988) 277-282.
14. K. Higashi, T. Ohnishi and Y. Nakatani, Scripta Metall, 19 (1985) 821-824.
15. O.D. Sherby et al, Scripta Met, 9 (1975) 569-574.
16. N. Ridley, in Ref. 1, 191-207.
17. B. Walser and J. Ritter, Superplasticity, ed. B. Baudalet and M. Suery, (Editions CNRS, Paris, 1985) 15.1-15.18.
18. Y. Maehara and Y. Ohmori, Metall. Trans., 18A (1987) 663-672.
19. K. Osada, S. Uekoh and K. Ebato, to be published in Proc. Stainless Steel Conference, York, Sept. 1987, Institute of Metals, London.
20. C. Hammond, in Ref. 1, 131-146.
21. C.H. Hamilton, in Ref. 17, 14.1-14.16.
22. N.E. Paton and C.H. Hamilton, Metall. Trans. 10A (1979) 241-250.
23. M.T. Cope, D.R. Evetts and N. Ridley, J. Mater. Sci, 21 (1986) 4003-4008.
24. J.R. Leader, D.F. Neal and C. Hammond, Metall. Trans, 17A (1986) 93-106.
25. N. Ma, R. Kent and C. Hammond, J. Mater. Sci, 21 (1986) 475-487.
26. H.F. Merrick, in Ref. 1. 209-224.
27. C. Carry and A. Mocellin, in Ref. 23, 16.1-16.19.
28. R. Raj and C.K. Chyung, Acta Metall, 29 (1981) 159-166.
29. J. Karch, R. Birringer and H. Gleiter, Nature, 330 (1987) 556-558.
30. F. Wakai and H. Kato, Adv. Ceramic Mat, 3 (1988) 71-76.
31. T.R. McNelley, E.W. Lee and M.E. Mills, Metall. Trans, 17A (1986) 1035-1041.
32. M.J. Stowell, in Ref. 1, 321-336.

## SUPERPLASTIC OPTIMISATION FOR DIFFUSION BONDING

### APPLICATIONS IN AL-LI ALLOYS

R A Ricks\* and P J Winkler†

\* Alcan International Limited, Southam Road, Banbury, Oxon  
OX16 7SP ENGLAND

† M.B.B. Central Laboratories, D 8000 Muenchen, FEDERAL REPUBLIC OF  
GERMANY

#### Abstract

There is a growing requirement for the development of optimised superplasticity in aluminium-lithium alloys such as 8090, and it is now observed that microstructures obtained through strain-induced recrystallisation give better superplastic performance when compared with statically recrystallised microstructures (1). However, when the development of superplasticity is achieved by a strain-induced recrystallisation route, higher flow stresses are frequently observed, especially during the early stages of the forming operation. In those applications where the requirement is to form simple shapes which are subsequently mechanically or adhesively bonded, this does not present a problem. In other applications however, where intricate shapes are developed from previously bonded (by diffusion or otherwise) arrays, then the limiting forming pressures are set by the bond strengths achieved. Clearly, in this latter case the need is to understand and optimise the superplastic forming operation through the understanding of the superplastic characteristics of the alloy.

This paper describes part of a detailed investigation into the development of superplastic microstructures in 8090 alloy sheet. A combination of techniques has been used to monitor the microstructural evolution as a function of superplastic strain, including transmission electron microscopy, strain rate sensitivity determination and texture measurement. The results indicate that deformation is accommodated by a number of mechanisms, dependent upon the level of strain in the sample and that superplastic performance is critically dependent on the development of a stable sub-grain structure. The implications of these results will be discussed with respect to forming practices.

Superplasticity and Superplastic Forming  
Edited by C.H. Hamilton and N.E. Paton  
The Minerals, Metals & Materials Society, 1988

## Introduction

Superplasticity or superplastic-like deformation in Al-Li alloys has been observed by many research workers in practically all alloy variants currently in commercial production. This behaviour may be induced by developing a statically recrystallised fine grain size capable of superplastic deformation, although in Al-Li alloys this route often leads to disappointing superplastic performance due to strain induced grain growth causing premature cavitation and failure. Better performance may be obtained by the development of an ultrafine-grained microstructure during the initial strain accommodation, provided certain product processing conditions are met (2). One problem with this route is the changing microstructure can cause concomitant changes in both the flow stress and strain-rate sensitivity of the material ("m" value) which may cause difficulties when forming components using gas pressure. Furthermore, the application of diffusion bonding prior to superplastic forming requires a minimisation of flow stress to prevent premature bond failure.

In this paper the development of microstructure during the early stages of deformation in an Al-Li alloy (8090) is described and the subsequent changes in the flow stress and strain-rate sensitivity behaviour are presented and discussed.

## Experimental Details

Material for this investigation was produced via a commercial route designed to optimise superplasticity by strain induced recrystallisation (2). The material was assessed using standard procedures to measure "m" values at various strain rates and also as a function of total specimen prestrain. Optical and transmission electron metallography of similar specimens was performed to evaluate microstructural evolution during straining.

## Results

### Superplastic Testing

Flow stress - strain rate curves as a function of specimen prestrain for the 8090 material used in this investigation are shown in Figure 1. These data essentially show that the flow stress falls, over the entire range of strain rates studied, as the specimen prestrain

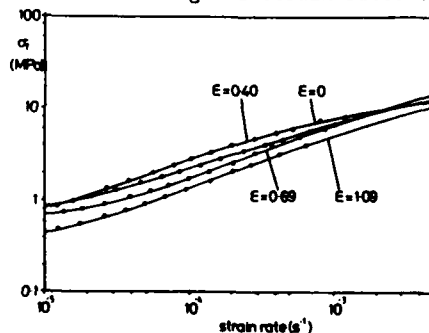


Figure 1 Flow Stress - Strain Rate Curves for 8090

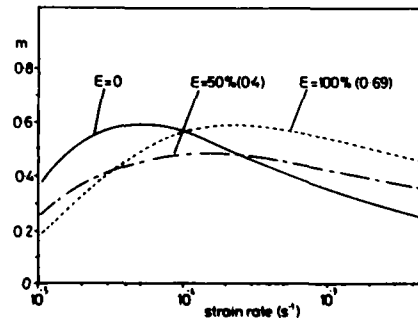


Figure 2 "m" Value Curves as a Function of Total Strain



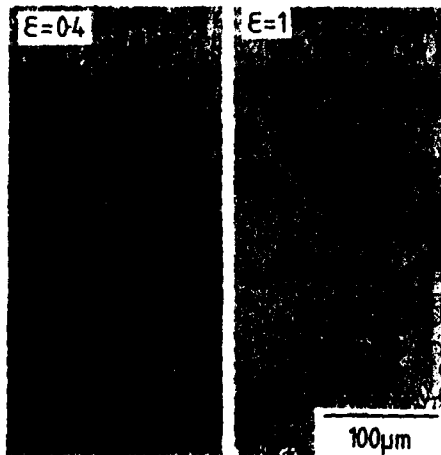
increases. The corresponding derivative curves, displaying "m" value as a function of strain rate and specimen prestrain are shown in Figure 2. Here it may be seen that the starting material initially has a fairly high "m" value maximum of 0.6 located at a strain rate of  $\sim 5.10^{-4} \text{ S}^{-1}$ . As a prestrain of 0.4 is applied (50%) the "m" value peak drops to a value of  $\sim 0.45$  but is now situated at a higher strain rate of  $1.5 \cdot 10^{-4} \text{ S}^{-1}$ . Increasing the prestrain to 0.69 (100%) increases the "m" value maximum to  $\sim 0.59$  at a still higher strain rate of  $3 \cdot 10^{-4} \text{ S}^{-1}$ . Summarising these data it may be stated that:-

- a) the flow stress of the 8090 falls at all strain rates as total specimen strain is increased,
- b) the maximum strain-rate sensitivity index moves to higher strain rates as total specimen strain is increased,
- c) the maximum recorded value of "m" initially drops as strain is applied followed by an increase back to approximately the initial value, albeit at a higher strain rate.

Further prestrain applications (at 0.91, 1.09) maintained the maximum value of "m" at  $\sim 0.6$ , although the peak was observed to shift slightly to slower strain rates. These data have not been plotted in the interests of clarity.

#### Optical Microscopy

Optical metallography was performed on prestrained specimens to evaluate microstructural development during straining. Kellers' reagent was used to accentuate grain boundary development and micrographs are shown in Figure 3. No discernable grain structure was visible in the material which had received strains of up to 0.4 and clearly distinguishable grains could only be seen after straining to 0.69 true strain. At this stage the grain size, measured by mean linear intercept, was  $5.8 \mu\text{m}$ , and the cavity content, measured from an unetched specimen by quantitative metallography was 0.15%. Examination of specimens prestrained to 1.09 true strain (200%) showed clear evidence of grain growth and further cavitation, with a mean grain size of  $7.5 \mu\text{m}$  and cavity content of 0.21% being recorded.



**Figure 3** Grain Boundary Structure Development With Strain



**Figure 4** B.F. T.E.M. Image Showing Sub-Grain Structure

#### Transmission Electron Microscopy

Figure 4 illustrates the microstructure developed by thermal cycling only and as such represents the starting microstructure which experiences hot deformation. The microstructure is seen to consist of a complex series of sub-grain boundaries (sub-grain size  $\sim 0.5 \mu\text{m}$ ) produced as a consequence of recovery of the cold worked sheet microstructure. Close examination of Figure 4 shows that the dislocation spacing in the boundary arrowed is not constant and increases towards a triple junction with another boundary. Such microstructures may be interpreted as the loss of dislocations from low angle boundaries leading to continuous recrystallisation by sub-grain co-alescence (3).

The interior of the sub-grains observed in this microstructure were essentially free from matrix dislocations, implying that the recovery process was essentially complete.

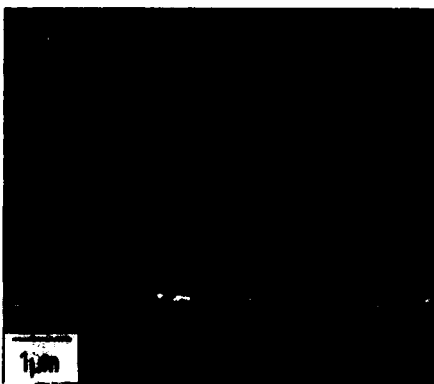
Examination of specimens deformed up to a true strain of 0.4 showed the development of extensive matrix dislocation activity inside the sub-grains, which had increased in size to  $\sim 2 \mu\text{m}$  (Figure 5). The helical nature of these dislocations, brought about by the interaction of trapped vacancies with the line defects, indicates that these dislocations were present during deformation, and were not introduced during specimen preparation.

This build up of matrix dislocation content could be observed to react with sub-grain boundaries as shown in Figure 6. In this Figure the decomposition of a matrix dislocation into two intrinsic sub-grain boundary dislocations can be seen (arrowed). Such observations indicate that sub-grain boundary mis-orientation may be developed by the incorporation of dislocations produced by deformation, thus accelerating the process of recrystallisation and the development of high angle grain boundaries.

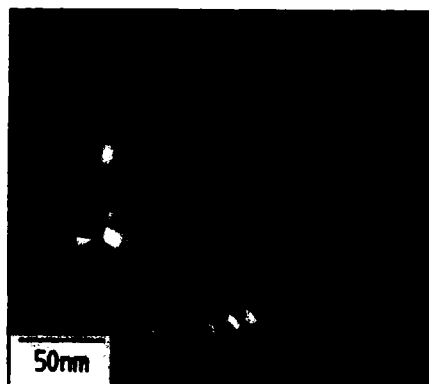
#### Discussion and Conclusions

The microstructural observations described above may be interpreted as follows:-

- a) the initial (heat cycled) microstructure consists of a stable array of sub-grain boundaries which are undergoing co-alescence leading to continuous recrystallisation.



**Figure 5** B.F. T.E.M. Image  
Showing Dislocation  
Activity  $\epsilon = 0.4$   
 $T = 515^\circ\text{C}$



**Figure 6** W.B. T.E.M. Image  
Showing Dislocation  
Reaction at Sub-Grain  
Boundary (Arrowed)

- b) during the initial stages of deformation (0-0.4 true strain) matrix dislocations are produced which decompose into available sub-grain boundaries and accelerate the development of high angle boundaries.
- c) after a strain of  $\sim 0.69$  a high angle grain boundary structure has developed and cavitation of the specimen is observed.

The stability of the sub-grain structure is essential if a fine grain size is to be achieved, since any size advantage displayed at this stage would cause a few grains to grow to a large size.

The results of the superplastic testing can thus be interpreted as a consequence of the microstructural history of the specimen as it undergoes strain. During the early stages of strain, a high "m" value at a low strain rate may be interpreted as a creep-based phenomenon, involving extensive dislocation activity. The relatively high (dislocation creep) strain rates may be attributed to the very fine sub-grain size developed during recovery (4). As strain develops the sub-grain size is seen to increase and consequently the measured "m" value falls. At the same time the misorientation of the sub-grains is increasing as dislocations are decomposed and sub-grain coalescence continues. This mechanism accounts for the development of a high angle grain structure, able to accommodate deformation by grain boundary sliding, and this is responsible for the increase in measured "m" value at a strain rate more consistent with truly superplastic behaviour as seen in specimens deformed to 0.69 true strain. Finally, strain-induced grain growth causes a degradation of this behaviour and the acceleration of cavitation within the specimen.

These observations are substantiated by the development of crystallographic texture as a function of strain. Work done within this study, together with data presented by Partridge et al (5), has shown that texture intensities can increase during the initial stages of deformation before a reduction is observed due to grain boundary sliding effects.

#### References

1. A K Ghosh and C Gandhi, "Superplasticity in Al-Li alloys", proc conf International Conference on Strength of Metals and Alloys (I.C.S.M.A.) 7, Montreal, Canada (1985). Pergamon Press eds H J McQueen, J P Bailon, J I Dickson, J J Jonas and M G Akben. Vol 3, p 2065.
2. R Grimes, W S Miller and R G Butler, "Development of superplastic 8090 and 8091 sheet", proc 4th International Al-Li Conference, Paris (1986) eds G Champier, B Dubost, D Miannay and L Sabetay, p 239.
3. A R Jones, B Ralph and N Hansen, "Subgrain coalescence and the nucleation of recrystallisation at grain boundaries in aluminium", Proc royal Soc Lond A 368 (1979) 345.
4. P Griffiths and C Hammond, "Superplasticity in large grained materials", Acta Met 20 (1972) 935.
5. P G Partridge, A W Bowen and D S McDermid, "The relationship between r-values and superplasticity in aluminium alloy sheet", proc conf Superplasticity in Aerospace Aluminium, Cranfield, UK (1985) eds R Pearce and L Kelly, p 215.

## THE DEVELOPMENT OF LFC-X1 ALLOY

Zhou Tiecheng, Zhang Zhimin and Zhang Yanhui  
Department of Materials Science and Engineering  
Taiyuan Institute of Machinery, Taiyuan  
Tang Defen  
Beijing Nonferrous Metals and Rare Earth Research Institute  
People's Republic of China

### Abstract

A new kind of corrosion-resisting, weldable superplastic aluminum alloy is introduced in this paper.

The component feature of this alloy is that it contains 1-2 wt% Zn in Al-Mg system. through the processes of chill casting, homogenization, rolling at middle temperature and recrystallization, the fine grain structure was obtained.

Up to 800% elongation can be reached with the strain rate sensitivity index,  $m$ , about 0.5 at the condition of 803 K and strain rate  $8.3 \times 10^{-4} s^{-1}$ .

This alloy possesses considerable strength at ambient temperature. It also has good weldability and corrosion resistance which equals to alloy 5083.

The mechanical properties of this alloy are compared with those of alloys of Super-100, Neopral, 5456 and Al-10Zn-1Mg. The testing results are discussed after the investigation of microstructure by Optical Microscope, TEM, X-Ray Diffractometer et al.

This alloy is suitable for making complex structure parts served in damp atmosphere or seawater. It has good prospects of commercial application.

Superplasticity and Superplastic Forming  
Edited by C.H. Hamilton and N.E. Paton  
The Minerals, Metals & Materials Society, 1988

## Introduction

For more than 20 years, the developing tendency of superplastic technology is to try to develop superplastic structure alloys with excellent mechanical properties. We can get marked examples for aluminum alloys through the appearance of Superal series alloys, the realization of superplasticity of high strength 7475 aluminum alloys and its application in aviation industry. But some high strength aluminum alloys have the problems of corrosion resistance and weldability. In order to meet the requirements needed by complex structure parts used in damp atmosphere or the sea, a new kind of superplastic aluminum alloy with high strength, fine corrosion resistance and good weldability has been developed.

## Experimental Details

### 1. Chemical composition of the alloy and the production method of plate

#### Chemical composition.

Mg	Zn	Mn	Cr	Zr	Al	
5-7	1-2	0.5-1	0.1-0.2	0.3-0.5	balance	wt%

The production method of plate. The alloy was melted with normal method and then went through chill casting. After homogenizing treatment, it was rolled into the required plates. Finally recrystallization treatment was carried out on these plates. Figure 1 is the schematic of the thermomechanical processing sequence used for LFC-X1 alloy.

### 2. Material properties

Superplasticity. Tensile tests on samples prepared from rolling and transverse directions were carried out on a Instron testing machine. The results are shown in figure 2. The maximum elongation can reach up to 800%.

#### Mechanical properties at ambient temperature and corrosion tests.

Table I gives the results of mechanical properties and corrosion tests at

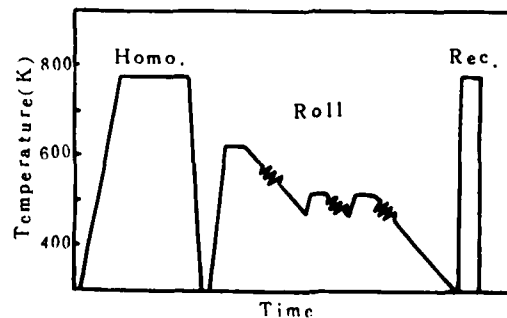


Figure 1 - Schematic of the thermomechanical processing sequence used for LFC-X1 alloy.

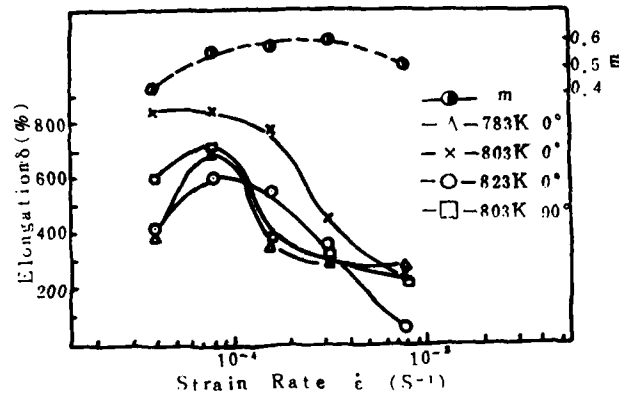


Figure 2 - The variation of elongation and strain rate sensitivity index,  $m$ , with the strain rate in LFC-X1 alloy.

ambient temperature. The data of compared alloys is taken from relevant documents.

Table I. The comparison of mechanical properties at ambient temperature among several aluminum alloys

Alloys	$\sigma_b$ (Mpa)	$\sigma_{0.2}$ (Mpa)	$\delta$ (%)	Lose of weight (g/m <sup>2</sup> h)	Ref.
LFC-X1	400	200	25	0.104	
5456	310	160	24		(1)
Neopral	335	170	25		(2)
Al-6Cu-0.6Zr	265	225	20	1.096	(3)
Al-10Zn-1Mg- 0.5Zr	300	260	20	3.61	(4)

Stress-corrosion tests. Stress-corrosion tests were conducted on recrystallized samples at  $308 \pm 2$  K with stress of  $0.96\sigma_{0.2}$ . The corrosion solution is 3%NaCl plus 0.5%  $H_2O_2$ . After 60 days of tests, the samples did not present any tendency to fracture, indicating that this alloy has good ability to resist stress-corrosion.

Weldability. The strength of jointing part after welding is more than 75% matrix strength. The Weldability of LFC-X1 alloy is evidently better than Al-6Cu-0.5Zr and Al-10Zn-1Mg-0.5Zr alloys by comparing them at the same welding condition.

### 3. Observation and analysis of the structure of LFC-X1 alloy

Microstructural observation. The extent of deformation has strong effect on the growth of grains in LFC-X1 alloy, as shown in Fig. 3. Thin foils were prepared from tensiling samples experienced 600% deformation at 803 K and strain rate of  $8.3 \times 10^{-4} \text{s}^{-1}$ , then observed at H-800 TEM. Higher dislocation densities can be seen in Fig. 4 (a). Cavities appeared and interlinked along grain boundaries during deformation, see Fig. 4 (b).

Texture measurements. Samples were taken respectively from rolling plate, recrystallized plate and the specimen after 500% deformation at about 803 K and  $8.3 \times 10^{-4} \text{s}^{-1}$ , then observed at D/max-rB X-ray Diffractometer. The pole figures are shown in Fig. 5.

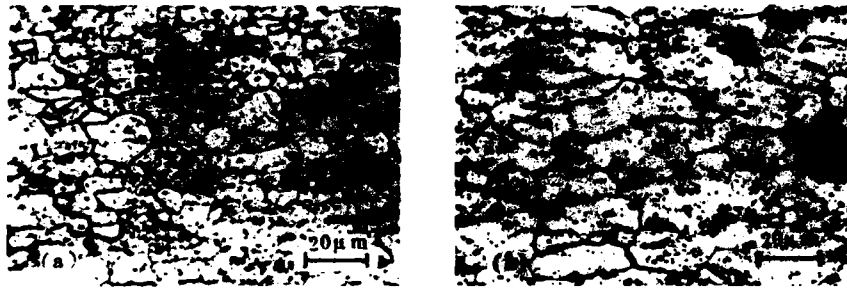


Figure 3 - Optical microstructure of LFC-X1 alloy deformed at 803 K and  $8.3 \times 10^{-4} \text{s}^{-1}$ : (a)  $\delta=200\%$ , (b)  $\delta=600\%$ .

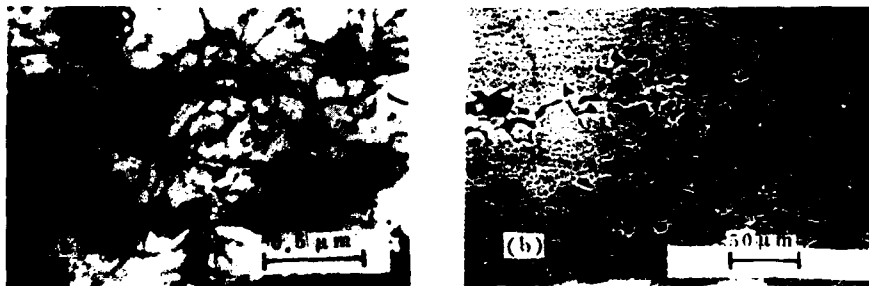


Figure 4 - TEM and SEM micrographs of samples deformed at 803 K and  $8.3 \times 10^{-4} \text{s}^{-1}$ : (a) dislocation structure, (b) interlinkages of cavities.

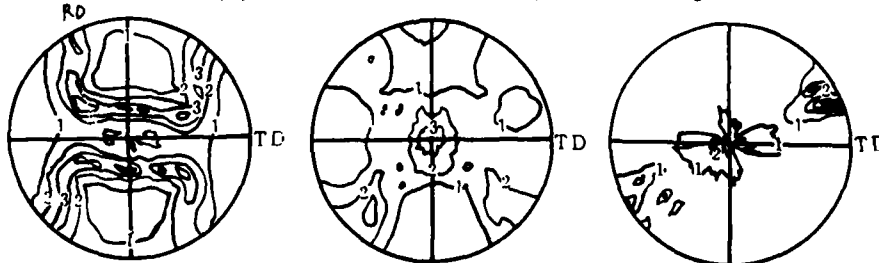


Figure 5 - (200) pole figures: (a) rolling state, (b) after recrystallization, (c) after 500% deformation.

### Discussion

With the addition of proper amount of element Zn in Al-Mg series deforming aluminum alloys, the LFC-X1 alloy can get satisfactory superplasticity on the basis of keeping fine corrosion resistance and weldability, increasing mechanical properties and having good stress-corrosion resistance. This alloy has good prospects of commercial application.

The observation of microstructure indicated the growth and elongation of grains. This decreased the grain boundary slips, caused the activities of dislocations in grains, which were verified by the preferred orientation after deformation and TEM micrographs, and increased the flow stress, as reported by Ghosh (5). In turn, the increase of flow stress promoted the growth of grains and quickened the linkages of cavities, seeming to cause vicious cycle. It is essential to restrict the growth of grains for keeping good superplasticity. In order to stabilize grain sizes during superplastic deformation, elements Zn and Cr were added to form stabler second phase particles to obstruct the motion of grain boundaries. Its role is dependent not only on the quantities of second phase particles, but also on their sizes, shapes and distributions. The elongation of LFC-X1 alloy can be further increased by improving manufacturing technology to keep grains stable.

### Conclusions

1. The addition of 1-2% Zn element in Al-Mg series deforming aluminum alloys can both increase strength and improve stress-corrosion resistance.
2. This alloy can reach up to 800% elongation at 803 K and strain rate of  $8.3 \times 10^{-4} s^{-1}$ .
3. The growth and elongation of grains occurred during superplastic deformation. The linkages of cavities resulted in the fracture of tested samples. Certain preferred orientation was kept following superplastic tensile tests.

### References

1. I. J. Polmear, Light Alloys, (London, Edward Arnold Ltd, 1981), 71.
2. Watanabe et al., Bulletin of the Japan Institute of Metals, 24(1985), 313.
3. B. M. Watts et al., Metal Science, 10(1976), 168.
4. Matsuki, Yamata, Journal of the Japan Institute of Metals, 37(1973), 448.
5. N. E. Paton and C. H. Hamilton eds., Superplastic Forming of structural Alloys, (Warrendale, Pa: The Metallurgical Society of AIME, 1982), 98.  
A. K. Ghosh



**MICROSTRUCTURAL REFINEMENT VIA CONTINUOUS  
RECRYSTALLIZATION IN A SUPERPLASTIC ALUMINUM ALLOY**

R. Crooks<sup>\*</sup>, S.J. Hales<sup>\*\*</sup> and T.R. McNelley<sup>\*\*</sup>

<sup>\*</sup> Rockwell International Science Center  
P.O.Box 1085, Thousand Oaks, CA 91360

<sup>\*\*</sup> Materials Group, Department of Mechanical Engineering,  
Naval Postgraduate School, Monterey, CA 93943-5000

**Abstract**

The microstructural characteristics which account for the superplastic response, at 300°C, of an Al-10Mg-0.1Zr (wt%) alloy produced by controlled thermomechanical processing were evaluated. It was determined that increasing the reheating time between passes during rolling at 300°C increased the superplastic ductility of the material. It was concluded that the refined microstructure resulting from this treatment, which exhibited a uniform, equiaxed grain size (2-5  $\mu\text{m}$ ), evolved by continuous recrystallization during processing. This structure, consisting of predominantly high-angle boundaries, was capable of sustaining a superplastic response (with  $m \approx 0.5$ ) from the onset of deformation. Microstructural investigations determined that the population of coincidence-site-lattice boundaries was shifted towards higher  $\Sigma$  values in the more ductile condition.

Superplasticity and Superplastic Forming  
Edited by C.H. Hamilton and N.E. Paton  
The Minerals, Metals & Materials Society, 1988

## Introduction

A fine-grain size ( $\leq 10 \mu\text{m}$ ) containing a large-area fraction of high-angle grain boundaries is generally considered to facilitate superplasticity. In instances where grain refinement by continuous recrystallization (CRX) is aimed at inducing superplasticity, the distinction between a substructure and a grain structure is often unclear (e.g., Ref. 1). Recent studies of superplastic aluminum alloys have correlated the distribution of grain boundary misorientation angles with thermomechanical processing variations (2) and superplastic deformation (3,4). While descriptions of misorientation angles are adequate to distinguish grain and subgrain structures, more specific information (in the form of axis/angle pairs) allows comparison to grain boundaries reported to have special properties (5) or special geometric attributes, such as certain low  $\Sigma$  coincident site lattice (CSL) types (6). The precise determination of grain boundary geometries presents severe experimental difficulties, and most property related studies have been conducted with bicrystals. The characterization of polycrystalline grain boundary populations has recently become practical with the development of computer-assisted diffraction analysis techniques (7,8). The properties of the component boundaries should be a significant factor in superplastic deformation (SPD), where grain boundary sliding (GBS) is considered to be an important mechanism (9). To develop a preliminary concept of the role of grain boundary type in superplastic deformation, the material selected for the present study was examined in two conditions which exhibit dramatically different superplastic response. Consistent with other studies, the boundaries studied were classified as 1), low-angle ( $\theta \leq 15^\circ$ ), 2), high-angle (CSL), or 3), high-angle (random) (10), and these data were correlated with the corresponding elevated temperature ductility data.

## Experimental Procedure

The nominal composition of the alloy is Al-9.89Mg-0.09Zr (wt%) and details of the thermomechanical processes (TMPs) adopted have been presented elsewhere (11). The eutectic temperature of the alloy is  $\approx 451^\circ\text{C}$  and the  $\beta$  (Al<sub>3</sub>Mg<sub>2</sub>) phase solvus is  $\approx 365^\circ\text{C}$ . The essential features were solution treatment and hot working at  $440^\circ\text{C}$ , followed by rolling at  $300^\circ\text{C}$  to a true strain of 2.5. The reduction per rolling pass was held constant at 10% and isothermal conditions were maintained by reheating between consecutive passes. To evaluate the effect of the length of the reheating interval on subsequent superplastic ductility, times of 4 min. (TMPA) and 30 min. (TMPB) were selected.

During evaluation of superplastic response, samples were equilibrated at the  $300^\circ\text{C}$  test temperature prior to loading. The initial, nominal strain rates were varied from  $6.7 \times 10^{-5} \text{ s}^{-1}$  to  $1.7 \times 10^{-2} \text{ s}^{-1}$ . The data were reduced to elongation and true stress vs strain-rate plots on double logarithmic coordinates and corrected to compensate for the decrease in true strain rate with increasing strain (11).

TEM specimens, with foil normals parallel to the sheet normal, were sectioned from the midplane of bulk material and prepared using conventional means. Groups of approximately 50 contiguous grains or subgrains were chosen for detailed study. Convergent beam Kikuchi patterns obtained with a Philips EM400T were used to determine the axis and angle of misorientation for each boundary (7). These were then used to determine the deviation from exact CSL relationships by the matrix method (12); those with angular deviations less than  $15^\circ/\Sigma$  were considered CSLs, as previously suggested (14). Due to grain size variations, grain boundary data were compiled in terms of lineal fraction of each type, rather than number of boundaries.

## Results

The mechanical property data for the elevated temperature testing at  $300^\circ\text{C}$  are shown in Fig.1, and are the same data as reported previously for this material (13). Maximum ductilities are observed between strain-rates of  $10^{-3}$  and  $10^{-2} \text{ s}^{-1}$ , where the maximum  $m$ -value ( $\approx 0.45$ ) is also seen. The material behaves in a superplastic manner from the onset of deformation with high  $m$ -values being recorded at the

smallest strain (0.02) evaluated. The data indicate that the increase in reheating time leads to a dramatic increase in ductility, from 200% (TMP A) to 600% (TMP B) at a strain-rate of  $1.7 \times 10^{-3} \text{ s}^{-1}$ . In addition, the flow stress has decreased by 20-40% over all strain rates with an increase in the slope (m-value) of the sigmoidal curves.

In the as-rolled condition, the underlying structure of the material is masked by the presence of a large dislocation density, such that differences in the two microstructures are not readily apparent. However, a brief anneal of 4 min at  $300^\circ\text{C}$ , equivalent to the minimum reheat time between passes, was adequate to reveal the differences between the two microstructures. The areas selected for study were located near heavily  $\beta$ -precipitated prior grain boundaries. TEM micrographs (Fig. 2) reveal well-defined boundaries in both conditions. The TMPA condition appears to consist of a recovered substructure, with some larger grains along the continuous  $\beta$  phase boundary. The microstructure of the TMPB material is clearly much coarser. Large,  $0.5\text{--}1.0 \mu\text{m}$  precipitates were found in both samples, and at most of the grain boundaries in the TMPB material. Although these are relatively coarse, the grain dimensions in the TMPB sample were of the order of the interparticle spacing, which suggests a stabilizing influence. The data obtained from subsequent analysis of the boundaries are presented as histograms in Fig. 3. The TMPA process results in a predominantly low-angle boundary structure (Fig. 3a), in contrast to TMPB. The proportion of high-angle boundaries which correspond to CSLs (Fig. 3b) shows a tendency towards low  $\Sigma$  values in the TMPA. The  $\Sigma 3$  CSL, in particular, was frequently observed in the TMPA, but not found in the TMPB.

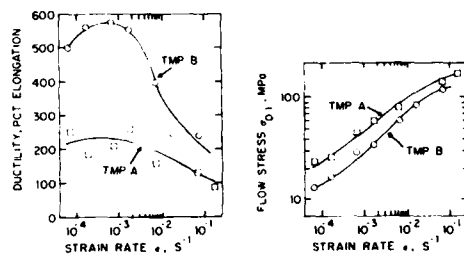


Figure 1 - Mechanical test data for TMP A and TMP B at  $300^\circ\text{C}$ .

SC45340

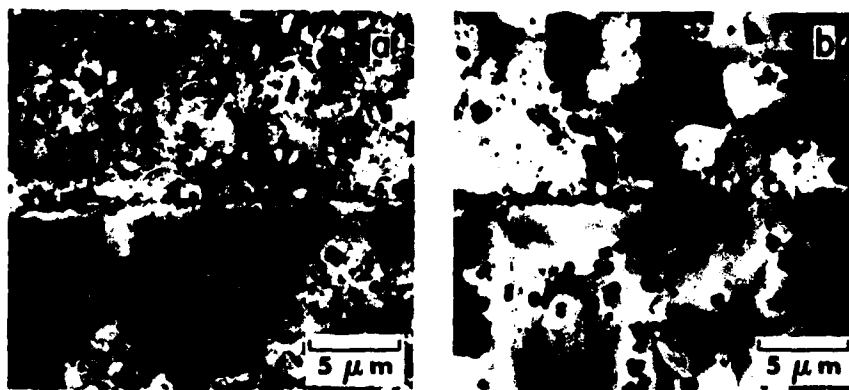


Figure 2 - TEM micrographs showing the microstructure after a brief (4 min) anneal at  $300^\circ\text{C}$  showing well-defined boundaries in both (a), TMP A and (b), TMP B material.

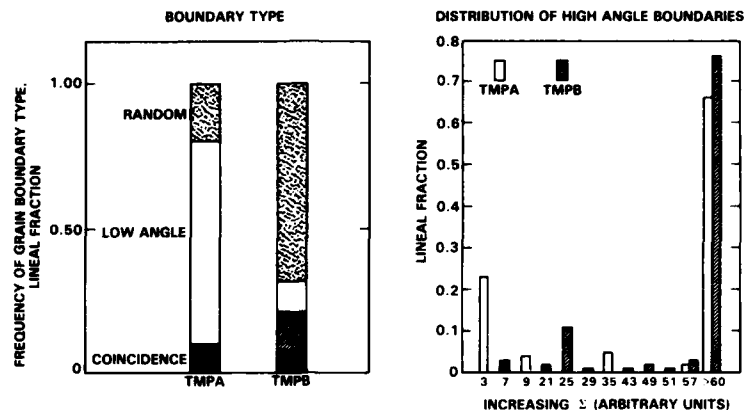


Figure 3 - Frequency of (a) low-angle, coincidence and random boundaries, and (b) high angle boundaries as a function of  $\Sigma$ , in TMP A and TMP B material.

#### Discussion

Superplasticity in alloys of this type relies on a fine, fairly stable grain size, capable of supporting SPD mechanisms, such as GBS. On first inspection of the two microstructures, it is surprising that the coarser one, TMPB, is considerably more superplastic. The advantage of the TMPB process can be attributed to the nature of the grain boundaries developed. The special properties reported for some boundaries may provide some insight into the relative stability of the two microstructures. Incoherent  $\Sigma 3$  boundaries, such as those found on the TMPA sample, have been described by Randle and Ralph (15) as "highly mobile" in solid-solution alloys. The presence of boundaries capable of relatively rapid migration should result in anomalous grain growth and a decrease in superplastic response. In the TMPB condition, the grain boundary population tended towards more random, less ordered orientations. Romeu and Dingley (16) have observed that GBS is controlled by the ease with which lattice dislocations can enter and dissociate into grain boundaries; a process which may be facilitated at random boundaries. The grain boundaries observed in the TMPB material then, may offer advantages in terms of both their stability and compatibility with GBS.

#### Conclusions

1. Increasing the reheating time between passes during rolling at 300°C drastically improves the superplastic response of the alloy at the same temperature. The ductility increased from 200% (4 min) to 600% (30 min) at a strain-rate of  $1.7 \times 10^{-3} \text{ s}^{-1}$  with a corresponding decrease in flow stress of  $\approx 30$  pct.
2. At the completion of rolling, the more ductile material had a larger grain size, but contained mostly (89%) high-angle boundaries. This was in contrast to the predominantly (71%) low-angle boundary structure determined for the other condition.
3. The distribution of CSL types was dominated by low  $\Sigma$  boundaries (especially  $\Sigma 3$ ) in the short reheat sample, and tended towards more random orientations in the more ductile, long reheat material. The improvement in superplastic response can be attributed to the development of boundaries by a CRX mechanism which are less mobile and more likely to support GBS.

### Acknowledgements

This research has been supported by the Naval Air Systems Command with Dr. L.E. Sloter as program monitor, and Rockwell International Internal Research and Development funding. The provision of software by Prof. W.A.T. Clark (of The Ohio State University) for reduction of the diffraction data is gratefully acknowledged. A program to determine the deviation from exact CSL orientations was written for this study by A. Murphy and K. Peppi of the Rockwell Science Center.

### References

1. E. Nes, Superplasticity, Ed. by B. Baudalet, M.Suery, CNRS, Paris (1985), 7.1.
2. S.J. Hales, T.R. McNelley, *Acta Metall.*, (1988), in press.
3. R. Crooks, Proc. Symp. Superplasticity in Aerospace, TMS-AIME, Warrendale, PA. (1988), in press.
4. E. Nes, "Superplastisitet og høydugtillitet i Zr-holdige aluminiumlegeringer," NTNF Report 80 01 52-1, 1980.
5. P.H. Pumphrey, Grain Boundary Structure and Properties, ed. G.A. Chadwick and D.A. Smith, Academic Press, New York (1976), 139.
6. D. Bouchet and L. Priester, *Scripta Metall.*, 21 (1987), 475.
7. P. Heilmann, W.A.T. Clark and D.A. Rigney, *Ultramicroscopy*, 9 (1982), 365.
8. V. Randle, B. Ralph and D. Dingley, *Acta Metall.*, 36 (1988), 267.
9. T.H. Alden, Treatise on Materials Science and Technology, ed. R.J. Arsenault, Academic Press, New York (1975), 225.
10. T. Watanabe, Proc. Symp. Interfacial Structure, Properties and Design, MRS, Pittsburgh, PA., (1988), in press.
11. E.-W. Lee and T.R. McNelley, *Mater. Sci. Eng.* (1988), in press.
12. M. Déchamps, F. Barbier and A. Marrouche, *Acta Metall.*, 35 (1987), 101.
13. S.J. Hales and T.R. McNelley, Proc. Symp. Superplasticity in Aerospace, TMS-AIME, Warrendale, PA. (1988), in press.
14. D.G. Brandon, B. Ralph, S. Ranganathan and M.S. Wald, *Acta Metall.*, 12 (1964), 813.
15. V. Randle and B. Ralph, Proc. Symp. Interfacial Structure, Properties and Design, MRS, Pittsburgh, PA., (1988), in press.
16. L.D. Romeu and D.J. Dingley, Proc. Conf. Electron Microscopy and Analysis, Inst. Phys., Bristol, (1980), 193.

# Superplasticity of Rapidly Solidified 7475-0.7 wt% Zr Alloys

K. Matsuki\*, M. Tokizawa\* and G. Staniek\*\*

\* Department of Mechanical Engineering for Production  
Faculty of Engineering, Toyama University  
3190 Gofuku, Toyama, JAPAN

\*\* Institut für Werkstoff-Forschung, D F V L R  
D-5000 Köln 90, WEST GERMANY

## Abstract

The superplastic 7475-0.7 wt% Zr cold rolled sheets were produced from rapidly solidified powder and tape, and the superplastic properties of the sheets have been examined by tensile tests and microstructure observations using OM and TEM, in comparison with those of an ingot metallurgy processed 7475 Al alloy. The optimum strain rates for superplasticity of the 7475-0.7 wt% Zr cold rolled sheets produced from powder and tape are in the range of  $10^{-2}$  -  $10^{-1}$  s<sup>-1</sup> at 520 °C and are remarkably higher than the optimum strain rate range of  $10^{-4}$  s<sup>-1</sup> of the IM 7475 Al alloy. The void volume of both 7475-0.7 wt% Zr alloys increased gradually with strain, but the cavitation rates of both alloys were slower than that of the IM 7475 Al alloy. During the deformation, both 7475-0.7 wt% Zr alloys exhibited dynamic recrystallization behaviour. The grain refining caused by the dynamic recrystallization is considered to contribute to relatively high cavitation resistance and large elongation at high strain rates in both alloys.

Superplasticity and Superplastic Forming  
Edited by C.H. Hamilton and N.E. Paton  
The Minerals, Metals & Materials Society, 1988

## Introduction

The use of superplastically formed high strength aluminium alloys is currently increasing for industrial applications. Problems in superplastic forming may be slow strain rate and cavitation formation. It is well known that the superplastic strain rate increases and cavitation rate decreases with decreasing grain size of the alloy (1). In this experiment, rapidly solidified 7475 Al tape and powder supersaturated with 0.7 wt% Zr have been used to fabricate improved superplastic alloy sheets. The Zr addition is made to control the recrystallization and to obtain fine microstructure required for superplasticity (2-5). The superplastic properties of the two 7475-0.7 wt% Zr alloy sheets from powder and tape (Powder and Tape 7475-0.7 Zr alloy, respectively) were compared with the result of an ingot metallurgy 7475 superplastic alloy without Zr.

## Experimental

### Materials

The production of 7475 Al tape and powder supersaturated with 0.7 wt% Zr was performed by melt spinning and gas atomization, respectively. The chemical composition of the 7475-0.7wt% Zr ingot used for the production of both rapidly solidified materials is shown in Table 1. The tapes were cold compacted in an aluminium can ( $\phi 45$ mm ID, 65mm in length). The powders finer than 100  $\mu$ m were cold isostatically pressed and canned ( $\phi 70$  mm ID, 210 mm in length). Both cans were degassed at 520 °C for 1 hr and hot compacted at 440 °C. After removing the cans, the hot compacted tape and powder billets were extruded at 440 °C to rectangular bar shapes of 5 $\times$ 25mm and 5 $\times$ 30 mm in cross section, respectively. The extrusions were heat treated at 440 °C for 24 hr, then 300 °C for 8 hr and cold rolled from 5 mm to 1 mm.

On the other hand, the chemical composition of the superplastic 7475 alloy sheet produced by ingot metallurgy is also shown in Table 1. This superplastic sheet (IM 7475 alloy) was fabricated at Kobe Steel Ltd. (6). This sheet has an equiaxed fine grain structure after annealing for 0.5 hr at 480 °C. The average grain size of the sheet is about 11  $\mu$ m.

Table 1 Chemical Composition of Alloys (wt%)

	Zn	Mg	Cu	Zr	Cr	Si	Fe	Mn	Al
7475-0.7Zr	5.90	2.40	1.74	0.72	0.19	0.06	0.08	0.013	bal
7475	5.75	2.27	1.51	-	0.20	0.04	0.09	0.01	bal

### Tensile Test and Metallography

Tensile tests of specimens cut from these cold rolled (Powder and Tape 7475-0.7Zr alloy) or annealed (IM 7475 alloy) sheets parallel to the rolling direction were carried out at a constant temperature at 520 °C, and at constant crosshead speed (initial strain rate  $\dot{\epsilon}=2\times 10^{-4}$  -  $3\times 10^{-1}$  s $^{-1}$ ) by using an Instron type testing machine and an electric furnace. Thin foils for transmission electron microscopy were prepared by Jet polishing in an electrolyte of 20% perchloric acid in methanol. Changes in volume fraction of cavities with superplastic strain were evaluated by density measurements using acetylene tetrabromide.

## Results and Discussion

### Tensile Tests

Fig.1 shows the relationship between total elongation and strain rate at 520 °C for the Powder and Tape 7475-0.7 Zr alloys, in comparison with

those for the IM 7475 alloy. It can be seen from Fig.1 that the Powder and Tape 7475-0.7Zr alloys show high elongations at remarkably higher strain rate range than the IM 7475 alloy.

Fig.2 shows the flow stress-strain curves for the Powder and Tape 7475-0.7 Zr alloy, and the IM 7475 alloy. As shown in Fig.2, the flow stress of the IM 7475 alloy at  $\dot{\epsilon}=2 \times 10^{-4} \text{ s}^{-1}$  tend to increase gradually with super-plastic strain up to about 200% and to reach almost a steady state. However

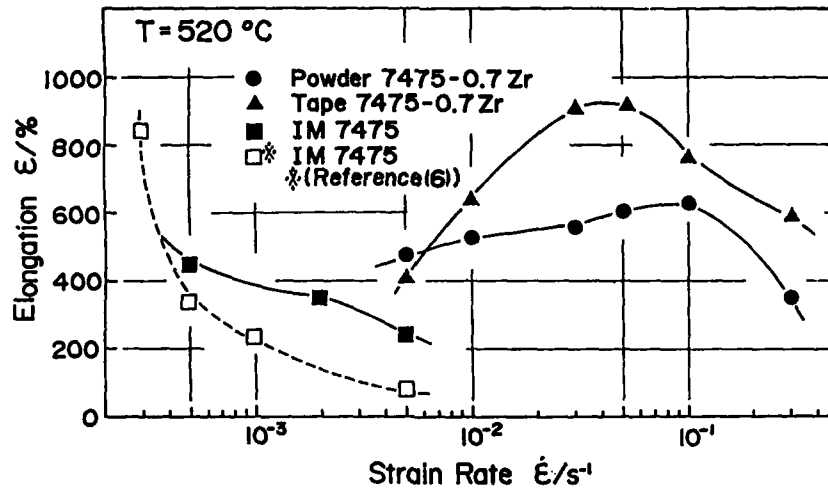


Fig.1 Effect of strain rate on total elongation at 520 °C of 7475-0.7 wt% Zr cold rolled sheet produced from powder and tape, and IM 7475 annealed sheet.

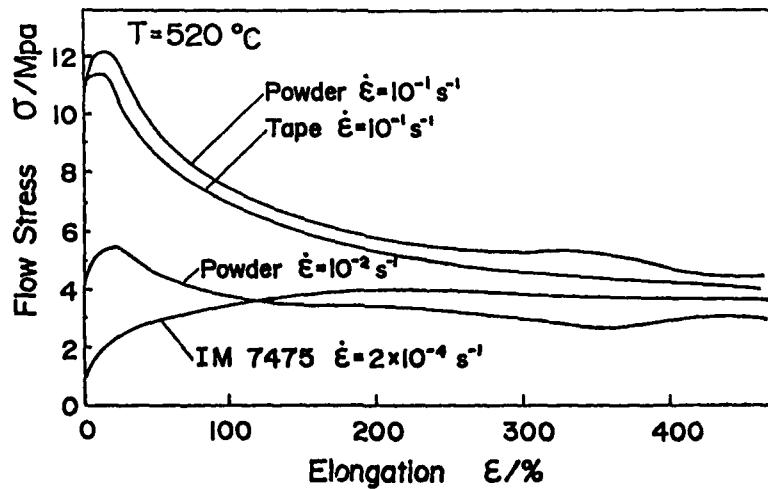


Fig.2 Flow stress-strain curves of 7475-0.7wt% Zr cold rolled sheet from powder and tape, and IM 7475 annealed sheet.



, the flow stress of the Powder and Tape 7475-0.7Zr alloys tend to reach the maximum value at the initial stage of straining, and then to decrease rapidly with increasing strain to a relatively low steady state stress level. The flow stress at  $\dot{\epsilon}=10^{-2} \text{ s}^{-1}$  of the Powder 7475-0.7Zr alloy is lower than that at  $\dot{\epsilon}=2 \times 10^{-4} \text{ s}^{-1}$  of the IM 7475 alloy at the strain range of higher than about 120%. The different flow characteristics shown in Fig.1 and 2 are considered to be closely related to the microstructure change during deformation of these alloys.

#### Metallography

Fig.3(a) and (b) are optical micrographs of the Powder 7475-0.7 wt% Zr with strain at 520 °C and  $\dot{\epsilon}=10^{-1} \text{ s}^{-1}$ . Small regions of equiaxed fine grains can be seen after 29% elongation(Fig.3(a)). With increasing strain, the equiaxed fine grain microstructure was developed progressively (Fig.3 (b)). The average grain size of the specimen after 300% elongation was about 2.8  $\mu\text{m}$ . This grain size is very fine in comparison with the average grain size of about 13.9  $\mu\text{m}$  of IM 7475 alloy deformed to the same elongation of 300% at 520 °C and  $\dot{\epsilon}=2 \times 10^{-4} \text{ s}^{-1}$ .

Fig.4(a) and (b) are transmission electron micrographs of specimens quenched after heating up to 520 °C and holding for 15 min, and deformed to 211% at 520 °C and  $\dot{\epsilon}=10^{-1} \text{ s}^{-1}$ , respectively. During the heating period before tensile test, a fine and equiaxed subgrain structure stabilized by the dispersion of metastable  $\text{Al}_3\text{Zr}$  precipitate particles has been formed, as shown in Fig.4(a). After 211% elongation, well defined grains of 2-4 $\mu\text{m}$  in dia were observed (Fig.4(b)), although subboundaries could still be observed within some grains. The Tape 7475-0.7Zr alloy showed a similar change in microstructure with strain. The microstructure change can be interpreted as the dynamic recrystallization behaviour in which the fine grain structure was stabilized by the fine precipitate particles of  $\text{Al}_3\text{Zr}$ (4,7-9).

On the other hand, void volume of the Powder and Tape 7475-0.7 Zr alloys increased gradually with strain, but the cavitation rates of both alloys were slower than that of the IM 7475 alloy(10).

The grain refining with the dynamic recrystallization contributed to the superplasticity at the higher strain rates of both 7475-0.7 Zr alloys.

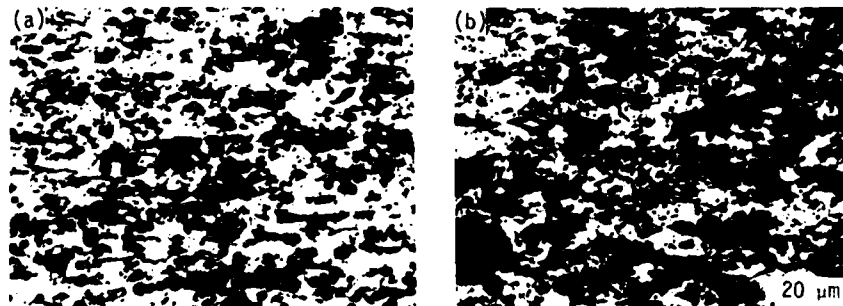


Fig.3 Optical microstructure change of the 7475-0.7wt% Zr cold rolled sheet produced from powder with increasing strain at  $\dot{\epsilon}=10^{-1} \text{ s}^{-1}$  and at 520 °C. Deformed to (a) 29%, and (b) 300%. Tensile axis is horizontal.

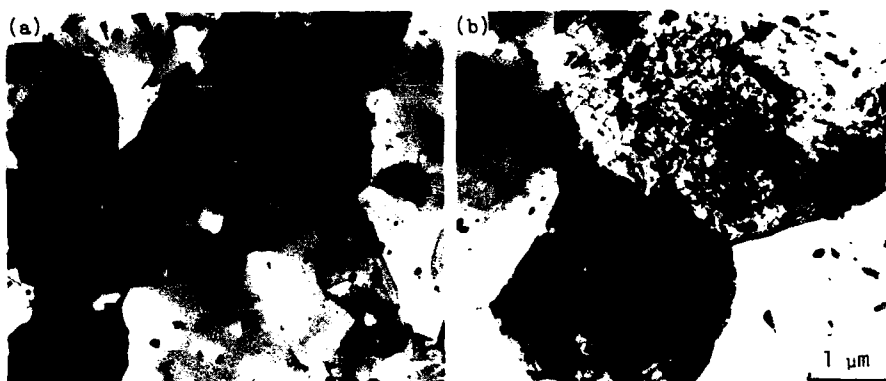


Fig.4 Transmission electron micrographs of the Powder 7475-0.7 Zr specimens (a) quenched after heating up to 520 °C and holding for 15 min, and (b) deformed to 211% at  $\dot{\epsilon}=10^{-1} \text{ s}^{-1}$  and at 520 °C.

#### Acknowledgement

The authors would like to thank Prof.Dr.Murakami, Prof.Dr.Bunk and Dr.Wirth for discussion and support of this work.

#### References

1. C.C.Bampton, A.K.Ghosh and M.W.Mahoney, "The Causes, Effects and Control of Cavitation in Superplastic 7475 Aluminium Airframe Structures" *Superplasticity in Aerospace-Aluminium*, Ed. by R.Pearce and L.Kelly, Ashford Press, Cranfield, England (1985)1-35.
2. K.Matsuki and Y.Yamada, "Superplastic Behaviour of Al-Zn-Mg Alloys," *J.Japan Inst.Metals*, 37(1973)448-455.
3. R.Grimes, M.J.Stowell and B.M.Watts, "Superplastic Aluminium-Based Alloys," *Met. Technol.*, 3(1976)164-160.
4. B.M.Watts, M.J.Stowell, B.L.Baikie and D.G.Owen, "Superplasticity in an Al-Cu-Zr Allys," *Metal Sci.*, 10(1976)189-197.
5. K.Matsuki, Y.Uetani, M.Yamada and Y.Murakami, "Superplasticity in an Al-6 wt% Mg Alloy" *Metal Sci.*, 10(1976)235-242
6. Y.Hirose, Y.Miyagi, M.Hino and T.Eto, "Superplastic Deformation Behavior of High Strength Aluminium Alloy 7475 Sheet," *J.Japan Inst.Light Metals* 36(1986)491-497.
7. R.H.Bricknell and J.W.Edington, "Deformation Characteristics of an Al-6 Cu-0.4Zr Superplastic Alloy," *Met.Trans.*, 10A(1979)1257-1263.
8. K.Higashi, S.Nagai, M.Maeda and T.Ohnishi, "The Superplastic Behaviour and Structure Change during Hot Deformation of Al-Cu-Zr Alloy," *J.Japan Inst. Light Metals*, 36(1986)361-371
9. K.Matsuki, O.Kimura, H.Nakagawa, M.Tokizawa and Y.Murakami, "Superplasticity of a Rapidly Solidified 7475 Aluminium Alloys" *J.Japan Soc.Tech. Plasticity*, 27(1986)415-421.
10. K.Matsuki, C.Stanek, H.Nakagawa and M.Tokizawa, "Superplasticity of Rapidly Solidified 7475 Al Alloys with 0.7 wt% Zr" *Z. Metalkd.*, in press.

OPTIMIZATION OF HETEROGENEITY AS GENERAL PRINCIPLE OF  
CONTROLLING ALLOYS STRUCTURE FOR SUPERPLASTIC FORMING

I. I. Novikov and V. K. Portnoy

Superplastic Materials Deformation Laboratory  
Moscow Steel and Alloys Institute  
Moscow, 117936, U.S.S.R.

Abstract

The principle mechanisms of ultrafine grain structure development are considered for different superplastic alloys. The analysis for the processes of fragmentation of plate-like and rod-like phases at microduplex structure development is made; the role of reversible variations of phase volume ratio in processes of fragmentation is revealed. It is shown that to obtain ultrafine grain structure in any commercial superplastic alloy it is necessary to solve the intermediate task of optimization of heterogeneity parameters of the alloy. The role of optimization of heterogeneity for various alloys with microduplex and matrix structure is illustrated.

Superplasticity and Superplastic Forming  
Edited by C.H. Hamilton and N.E. Paton  
The Minerals, Metals & Materials Society, 1988

### Introduction

The development of the ultrafine grain (UFG) structure is a necessary condition for commercial application of superplasticity (SP). The review (1) generalizes various grain refinement mechanisms, two of which out of four can't be agreed upon. The point is that firstly there is no evidence of breaking of fibres to small segments during severe hot working of  $\alpha + \beta$  titanium alloys and  $\alpha + \beta$  brasses due to extremely high ductility of both phases in these alloys, and secondly phase separation of the monotectoid Zn-22Al alloy is not the result of spinodal decomposition. The grain refinement mechanisms in different groups of alloys will be considered here in brief.

There are two main types of microstructure in SP alloys: microduplex and matrix (2). Grains of two different phases in alloys with microduplex structure occur intermittently in such a manner that in the ideal case of phase volume ratio equals to 50:50 and there is no continuous grain boundary network for each phase. During SP deformation both phases mutually restrict the grain growth. Alloys with matrix structure have continuous grain boundary network of matrix phase with fine dispersoids of second phase (or phases) distributed in matrix. These dispersoids restrict grain growth of matrix phase.

The UFG structure in the alloys with matrix structure is obtained by a continuous or discontinuous recrystallization, while grain refinement in alloys with microduplex structure occurs as a result of: i - fragmentation of initial plate-like or rodlike structures with subsequent spheroidization of the fragments; ii - phase transformation and iii - recrystallization, these mechanisms acting individually or simultaneously.

### Zn-22Al alloy

The classic alloy with microduplex structure is Zn-22Al investigating which prof. A.A. Bochvar introduced the term "superplasticity". Up to the present time there is a widely spread opinion that UFG structure develops in this alloy as a result of spinodal decomposition (1, 3). However, the in situ observation carried out in the column of TEM (4) proved that it was a mistake [see also (2)]. The thin sample was quenched in a cold water and then immediately placed into liquid nitrogen to avoid decomposition and finally the sample was thinned in the solution of  $\text{HClO}_4$  in ethanol at the temperature of  $-60^\circ\text{C}$  and was quickly inserted into the column of 100 kV TEM to observe the phase transformations.

The monotectoid  $\alpha + \beta$  cells spread from the grain boundaries of supercooled  $\alpha'$ -phase. These cells consist of extremely thin branched lamellae with the average lamellar spacing about 1 nm (Fig. 1a). The lamellae are very thin due to high supercooling (about 250 K) and presumably to small lattice misfit on the interphase boundaries. The primary cells are gradually coarsening and at last are replaced by secondary cells having average lamellar spacing created by an order or even more (Fig. 1b). High level of interphase energy and nonequilibrium of phase composition are the driving forces of the primary cells coarsening. Zinc concentration in  $\alpha$ -phase is determined by means of the lattice parameter measurements carried out at the temperature of liquid nitrogen. During holding of quenched alloy at  $20^\circ\text{C}$  for 16 min the concentration of zinc in the initial aluminium phase decreased from 78 to 70%. The exposure referred to above corresponds to the time necessary for the completion of the monotectoid decomposition and the formation of the primary cells. That is why  $\alpha$ -phase lamellae (light in Fig. 1a) are thicker than  $\beta$ -phase lamellae (dark) according to the lever rule. As the holding time at  $20^\circ\text{C}$  increases when the monotec-

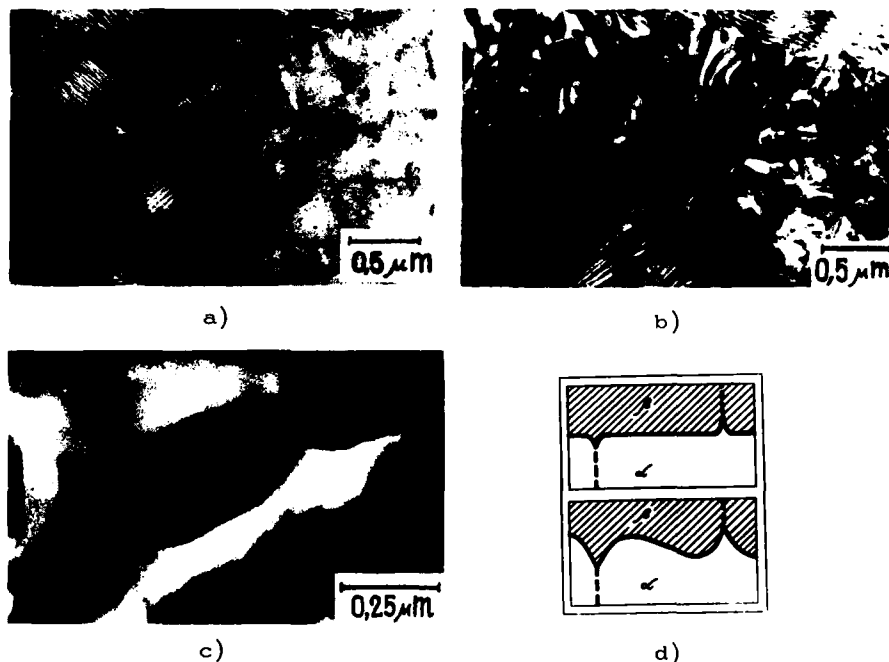


Figure 1 - The structure of Zn-22Al alloy (a-c) at different stages of solution decomposition after quenching (foil) and lamella fragmentation scheme (d): a - the decomposition in TEM column (3 min); b - the same area of the foil after soaking for 15 min at 100°C; c - soaking for 30 min at 120°C.

toid cell coarsening occurs zinc concentration in  $\alpha$ -phase was gradually decreases. After 30 h holding 26% of zinc remains in  $\alpha$ -phase.

The lamellae of the secondary cells have local sharp contractions at subboundaries (Fig. 1c) which point to the development of lamella fragmentation. All the features of the process are in agreement with the mechanism proposed in (5) for the transformation of lamellar pearlite into globular during annealing of steel. The surface tension forces being unbalanced at the outlet of  $\alpha$ -phase subboundary on the lamella surface resulted in local dissolution of  $\alpha$ -lamella until the equilibrium configuration is achieved; thus the dissolution groove in  $\alpha$ -lamella is formed (Fig. 1d, top). The dissolution groove in  $\beta$ -lamella is formed for the same reason. As the curvature radius in such a groove is small the dissolution and groove wall straightening occurs in accordance with Thomson-Freundlich equation. The above described process results in the damage of balance of surface tension forces and this balance is restored by further dissolution of the lamella along the subboundary until the equilibrium configuration is achieved etc. At the same time diffusion mass transfer from the groove and precipitation of the material on the interphase surface with large curvature radius occurs. The development of the grooves due to the solution/precipitation process results in cutting one phase by the other (Fig. 1d, bottom) until full fragmentation takes place (unshown in Fig. 1d).

After the fragmentation is completed a partial spheroidization of lamella fragments develops resulting in the formation of a microduplex structure. The primary cells, the secondary cells and the globular

structure areas are represented in Fig. 1b.

Diffusion processes of fragmentation and spheroidization are accelerated when the alloy is heated including self heating of massive samples to 100–120°C (0.57 Tm) due to latent heat of monotectoid transformation. Self heating of a massive sample intended to SP testing always takes place in contrast to a thin foil. So thin foil was specially heated up to 100–120°C after  $\alpha'$ -phase decomposition was completed (Fig. 1b,c). Thermomechanical treatment of Zn-22Al including quenching and rolling at temperature of self heating when the lamellar structure is transformed into microduplex results in more uniform grain structure due to dislocation piles-up and formation of subboundaries in the lamellae of both phases.

Spheroidization and coalescence of lamella fragments result in microduplex equilibrium structure formation with grain diameter 2–4 times greater than the initial lamella thickness. Thus the thinner the initial lamellae the smaller are the grains in a microduplex structure.

#### Titanium alloys

The  $\alpha + \beta$  titanium alloys with initial lamellar structure as well as Zn-22Al when heated and soaked before SP deformation undergo the same diffusion processes of fragmentation and spheroidization resulting in transformation of lamellar structure into microduplex. If the initial structure consists of coarse plates the transformation doesn't occur during annealing. The  $\alpha + \beta$  deformation promotes such transformation. It is necessary to emphasize that the role of hot working in  $\alpha + \beta$  field consists not in plate breaking as stated in (1,3) but in plate thinning, the rising of dislocation density and in subboundary formation resulting in the acceleration of diffusion process of plate fragmentation according to Fig. 1d.

The development of microduplex structure in titanium alloy with initial martensitic structure is not the result of nucleation of equiaxed grains of equilibrium phases in many sites (1,3) but the result of the same lamellar structure fragmentation processes (see Fig. 1d). The point is that during heating of quenched titanium alloy up to  $\alpha + \beta$  field initially the plates of  $\alpha$ -phase form from the martensite (Fig. 2a) and then they fragmentate in accordance with the mechanism shown in Fig. 1d. The role of quenching in the development of fine grain microduplex structure consists in forming from martensite very thin  $\alpha$ -plates of intermediate structure.

The finest grain structure (about 1  $\mu\text{m}$ ) can be obtained in  $\alpha + \beta$  titanium alloys by thermo-mechanical treatment (TMT) including: hot deformation in  $\beta$ -field, quenching from the deformation temperature and deformation in  $\alpha + \beta$  field (2). The using of TMT for the UFG structure development extends the strain rate range of SP deformation by an order of magnitude towards high values or decreases SP deformation temperature by the score of degrees (2). The quenching from the temperature of  $\beta$ -deformation allows to obtain thinner martensitic plates than simple quenching.

The microstructural study carried out on different stages of TMT revealed an extremely important role of phase transformations affecting phase volume ratio (6). It was determined for the thermo-mechanically treated Ti-5Al-1V-3Mo alloy that when heated to the deformation temperature of 750–800°C in  $\alpha + \beta$  field the volume fraction of  $\alpha$ -phase (44 vol.%) precipitated from the martensite was less than that of equilibrium (Fig. 2b). The working of the alloy with 10% reduction resulted in the volume fraction of  $\alpha$ -phase (64 vol.%) more close to the equilibrium. The transformation of metastable  $\beta$ -phase into  $\alpha$ -phase during

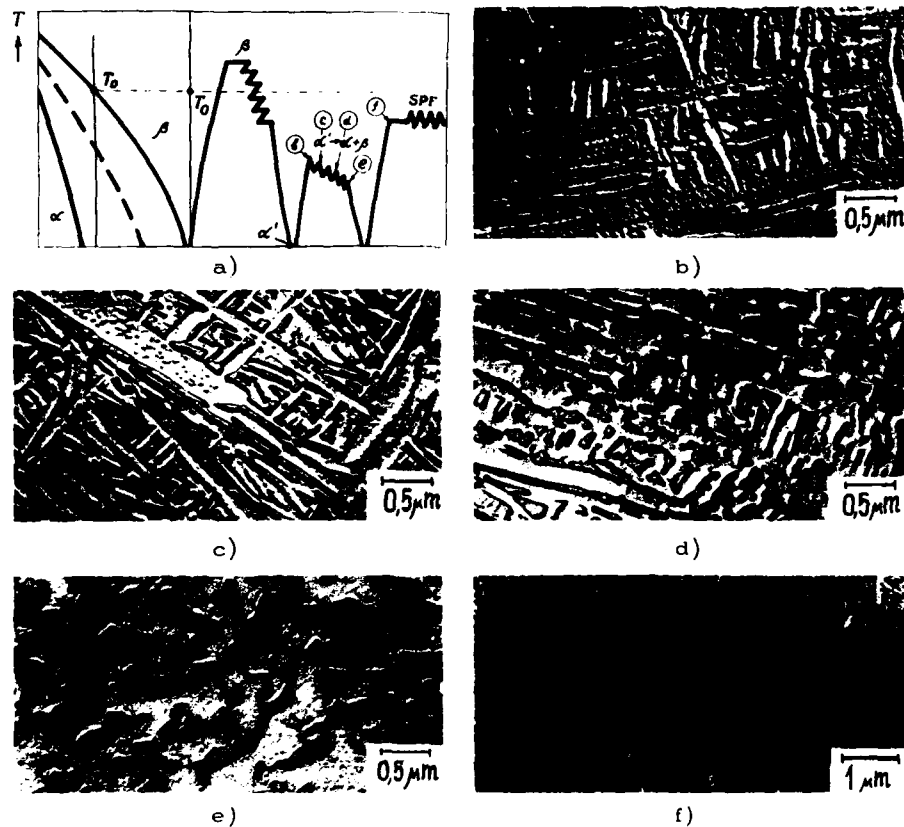


Figure 2 - TMT for obtaining the UFG structure in  $\alpha + \beta$  titanium alloys (a) and structure changes sequence in Ti-5Al-1V-3Mo alloy: b - heating to 750°C for 10 min; c - 10% reduction at 750°C; d - 40% reduction at 750°C; e - 80% reduction at 750°C; f - heating to SPF temperature (replicas, more dark  $\beta$ -phase).

deformation promotes an abrupt separation of the remained  $\beta$ -phase into compartments between  $\alpha$ -phase plates: interphase surface increases almost twice, while the average  $\beta$ -phase intercept decreases from 0.24 to  $0.1 \pm 0.01 \mu\text{m}$ , the average  $\alpha$ -phase intercept being approximately constant. It should be noted here that the phase transformation promotes the separation of the phase with the decreasing volume fraction. While the degree of reduction increases up to 40% the fragmentation of  $\beta$ -phase takes place in accordance with mechanism shown in Fig. 1d. During the increase of the reduction the  $\alpha$ -phase becomes connected (Fig. 2d,e) and the thin plates of  $\beta$ -phase are fragmented. The microduplex structure finally develops during heating to SP deformation temperature of 750-900°C (Fig. 2f): in this case the volume fraction of  $\alpha$ -phase decreases and the volume fraction of  $\beta$ -phase increases until phase volume ratio 50 : 50 is reached. The generated  $\beta$ -phase tends to separate  $\alpha$ -phase and equiaxed microduplex structure with the average grain intercept of about  $1 \mu\text{m}$  is developed.

### Brasses

Nonequilibrium phase ratio may be also obtained in  $\alpha + \beta$  brasses to promote the preferred fragmentation of the selected phase. For example, hot rolling of  $\alpha + \beta$  brass followed by air cooling results in  $\beta$ -phase fraction higher than the equilibrium one. Cold rolling provides dislocation density required for recrystallization and produces a fibrous structure favourable for fragmentation. During the intermediate annealing recrystallization of the  $\alpha$ -phase fibres occurs and the increase of the volume fraction of  $\alpha$ -phase which precipitates inside the polygonized  $\beta$ -fibres accelerates their fragmentation. The repeated cold rolling draws the two phases into still finer fibres. When brass is heated to SP deformation  $\alpha \rightarrow \beta$  transformation occurs again promoting fragmentation of  $\alpha$ -phase and microduplex structure with grain size about 5  $\mu\text{m}$  finally develops (6).

The finest grain structure of  $\alpha + \beta$  brasses (3  $\mu\text{m}$ ) as well as of  $\alpha + \beta$  titanium alloys can be obtained by TMT. When  $\alpha + \beta$  brasses are heated to 300-500°C after quenching the bainitic decomposition of  $\beta$ -phase results in fine lamellar structure, and the following rolling at the same temperature provides microduplex structure development (2).

The microduplex structure development in the above mentioned examples was carried out by solving of the intermediate task namely, to obtain the finest lamellar structure or desired phase volume ratio aiming to control the process of the following fragmentation of plates or fibres. Such an approach can be named as the optimization of heterogeneity because dual-phase structure parameters are optimized. Some other parameters of heterogeneity can be optimized in the alloys of various types. For example, when developing the microduplex structure in ferritic-austenitic steels such as IN 744, the starting moment to ferrite-austenite transformation and the quantity of the austenite which restricts grain growth at discontinuous recrystallization of ferrite are of great importance.

In case of aluminium alloys with matrix structure such as Supral the optimization of heterogeneity consists in the precipitation of dispersoids with size and precipitation density required for a full suppression of discontinuous recrystallization while continuous recrystallization can form the UFG structure (1).

As to aluminium alloys of the 7075 type the optimization of heterogeneity consists in the precipitation of large enough particles which increase the number of discontinuous recrystallization nuclei and also in the precipitation of dispersoids restricting the grain growth during SP deformation (1,3).

Generally optimization of heterogeneity means the control of the UFG structure development by varying volume fraction, size, shape, distribution and the time of precipitation of second phase particles.

### References

1. J. A. Wert, "Grain Refinement and Grain Size Control", Superplastic Forming of Structural Alloys, ed. N. E. Paton and C. H. Hamilton (New York, NY: The Metallurgical Society, 1982), 69-83.
2. I. I. Novikov, V. K. Portnoj, Superplastizität von Legierungen (Leipzig, VEB Deutsche Verlag für Grundstoffindustrie, 1984) 12, 154-171.
3. C. H. Hamilton, A. K. Ghosh, and J. A. Wert, "Superplasticity in Engineering Alloys: A Review", Metals Forum, 8 (4) (1985), 172-190.
4. I. I. Novikov et al., "Mechanism of Structure Development in SP Zn-22Al Alloy", Dokl. Akad. Nauk SSSR, 230(3) (1976), 642-644.
5. A. A. Baranov, "Initial Stages of Cementite Spheroidization in Steel", Izvestija Akad. Nauk SSSR, Metally, 1969, No. 3: 104-107.
6. V. K. Portnoj, "Obtaining Ultrafine Grain in SP Alloys", Tsvetnye Metally, 1987, No. 5: 79-83.



## SUPERPLASTIC PROPERTIES OF THE COLD FORMABLE TITANIUM ALLOY SP35

S. Yamazaki, T. Oka and Y. Mae

Central Research Institute, Mitsubishi Metal Corp.  
Ohmiya, Japan

M. Kobayashi

Technological University of Nagaoka  
Department of Mechanical Engineering  
Nagaoka, Japan

### Abstract

In order to reduce the production cost of titanium alloy products, the development of cold formable and superplastically formable titanium alloy is needed. Presently most widely used Ti-6Al-4V alloy is superplastically formable but not cold formable. On the other hand, cold formable  $\beta$  alloys such as Ti-13V-11Cr-3Al and Ti-15V-3Cr-3Al-3Sn are not superplastically formable. From results of preliminary research we developed a new near  $\beta$  titanium alloy named SP35 with the chemical composition of Ti-9.5V-2.5Mo-3Al. First, thermomechanical processings were investigated. SP35 alloy is quite softened by  $\beta$  processing and subsequent sub-transus annealing and shows good cold workability. The alloy obtains tensile strength of 130kgf/mm<sup>2</sup> and very fine  $\alpha + \beta$  structure of equiaxial  $\alpha$  grains in  $\beta$  matrix by solution treatment and aging. Next, superplastic characteristics were investigated. The alloy shows good superplasticity at 700~750°C, lower temperature than conventional titanium alloys. By utilizing the advantage of near  $\beta$  alloy, in which metastable  $\beta$  phase can be retained at room temperature by air cooling, the strengthening process of direct aging after superplastic working was developed. In this process, tensile strength of 130kgf/mm<sup>2</sup> was obtained. Moreover it is recognized that SP35 is superior in ductility and fracture toughness at age hardened condition.

### Introduction

Although titanium alloys are widely used as a structural material in aerospace industries, their production cost is very high. For the development of titanium industry, cost reduction of titanium alloy products is of great importance. For this purpose authors have developed a cold formable and superplastically formable titanium alloy named SP35 (1). Cold workability, superplasticity and mechanical properties of this alloy are reported.

### Experimental Details

SP35 has a composition of 2.5% Mo, 9.5% V, 3% Al and Balance Ti. This is almost the same composition as Ti-10V-2Fe-3Al alloy when Fe is replaced by Mo. Therefore the difference between these two alloys can be said to be caused from the difference between  $\beta$  eutectoid element Fe and  $\beta$  isomorphous element Mo.

Superplasticity and Superplastic Forming  
Edited by C.H. Hamilton and N.E. Paton  
The Minerals, Metals & Materials Society, 1988

### Cold Workability

Cold rolling and cold drawing tests were conducted on SP35 plate and bar respectively. Cold rollability was evaluated by the maximum reduction until edge cracking occurs and deformation resistance. Cold drawability was evaluated by the hardness change of wire product. Figure 1 shows the change of specific rolling load  $p$  ( $P/b/\Delta h$ ) with increasing rolling reduction, while  $P$  is rolling load,  $b$  is sheet width and  $\Delta h$  is reduction per pass. SP35 shows lower specific rolling load and greater maximum reduction than other commercial alloys. Figure 2 shows hardness change of wire products with increasing drawing reduction. SP35 shows lower work hardening than the commercial  $\beta$  alloy Ti-13V-11Cr-3Al. As SP35 has an intermediate alloy composition between  $\alpha + \beta$  alloy such as Ti-6Al-4V and  $\beta$  alloy such as Ti-13V-11Cr-3Al, it shows better cold workability than  $\alpha + \beta$  alloy because of greater amount of  $\beta$  phase and lower deformation resistance than  $\beta$  alloy because of smaller amount of alloying elements.

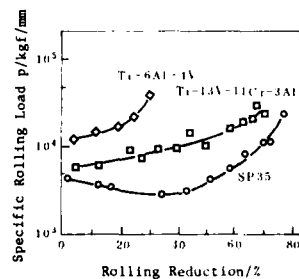


Figure 1 - Comparison of cold rollability

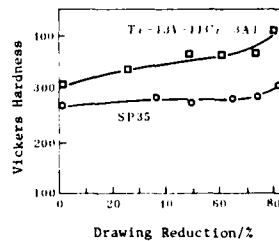


Figure 2 - Comparison of cold drawability

### Superplasticity

High temperature tensile tests were conducted on SP35 alloy bar which has a fine microstructure shown in Figure 3. Figure 4 shows the high temperature tensile properties of SP35 compared with those of Ti-6Al-4V alloy. SP35 is strong from room temperature up to 400°C but softens rapidly beyond 400°C and becomes superplastic at 700°C. Figure 5 shows temperature dependence of flow stress of SP35 at 750°C compared with those of other commercial alloys. SP35 shows lower flow stress at 750°C than Ti-6Al-4V alloy at 800°C, while it shows similar flow stress as Ti-10V-2Fe-3Al at 750°C.

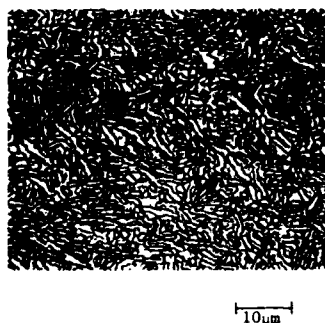


Figure 3 - Microstructure of SP35 alloy bar

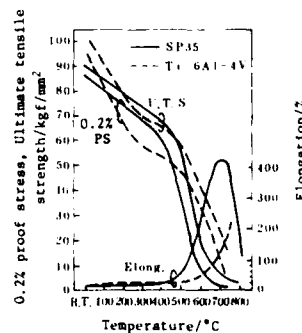


Figure 4 - Comparison of high temperature tensile properties

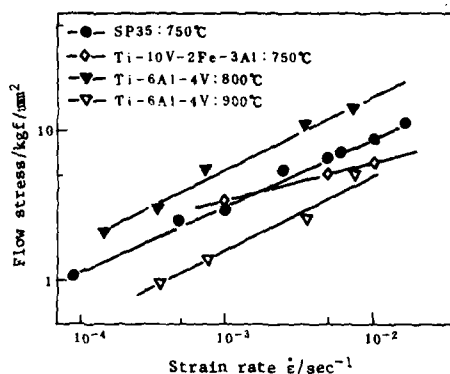


Figure 5 - Comparison of flow stress-strain rate relationship at superplastic condition

#### Superplastic Forging

Superplastic forging was carried out on the preform machined from 85mm diameter bar. The preform was forged at the strain rate of  $5 \times 10^{-4} \text{ s}^{-1}$  and at  $800^\circ\text{C}$ . BN was used as lubricant. Figure 6 shows the preform and forged minimodel disk of 150mm diameter.



Figure 6 - Preform and superplastically forged disk from SP35

#### Thermomechanical Treatment Involving Superplastic Forming

SP35 can be strengthened by solution treatment and aging in the same way as other highly alloyed titanium alloys. Here it was investigated whether solution treatment could be eliminated by rapid cooling in air after superplastic forming. SP35 sheet specimens were superplastically tensile deformed and rapidly cooled in air by removing the furnace. Then they were subjected to aging at  $500^\circ\text{C}$  for 5 hours. Figure 7 shows the relationship between tensile properties and deformation temperature at superplastic forming. By direct aging after superplastic forming at  $750^\circ\text{C}$  tensile strength about  $130 \text{ kgf/mm}^2$  and elongation over 10% are obtained. It is concluded that solution treatment can be eliminated by rapid cooling after superplastic forming.

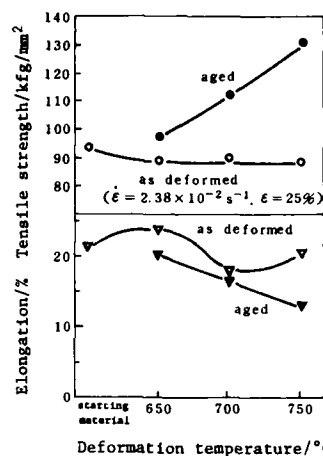


Figure 7 - Tensile properties after direct aging of superplastically deformed SP35 sheet specimen

#### Ductility and Fracture Toughness at Age Hardened Condition

Near  $\beta$  titanium alloy such as Ti-10V-2Fe-3Al is used at age hardened condition and it is desired that it has sufficient ductility and fracture toughness after solution treatment and aging. SP35 and other commercial near  $\beta$  alloys Ti-10V-2Fe-3Al and Ti-17 were heat treated to various strength levels and ductility and fracture toughness were measured. Figure 8 shows the relationship between elongation and 0.2% yield strength of these three alloys. Figure 9 shows the relationship between fracture toughness and 0.2% yield strength as well (2, 3). It is clear that SP35 has superior ductility and fracture toughness to commercial alloys such as Ti-10V-2Fe-3Al and Ti-17.

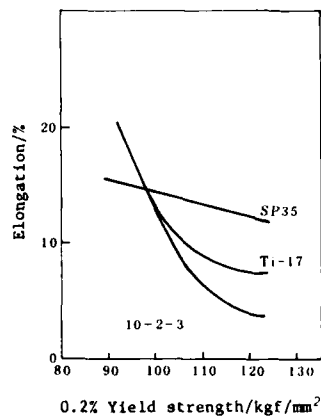


Figure 8 - Comparison of elongation of typical near beta alloys versus 0.2% yield strength

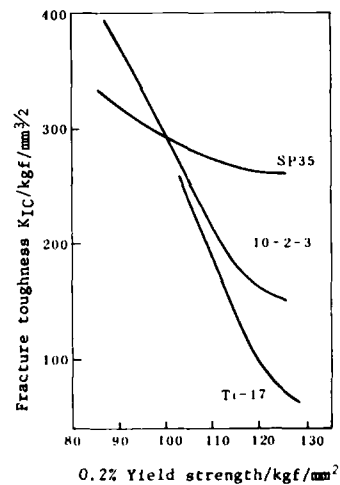


Figure 9 - Comparison of fracture toughness of typical near beta alloys versus 0.2% yield strength

### Conclusions

SP35 was developed as a cold formable and superplastically formable titanium alloy.

1. Thin gauge sheet, wire and foil can be produced from SP35 by cold working
2. SP35 can be superplastically formed or forged at low temperature as well as Ti-10V-2Fe-3Al and strengthened by direct aging after superplastic forming.
3. SP35 is superior in ductility and fracture toughness to other commercial near  $\beta$  alloys at age hardened condition.

### References

1. Y. Mae et al., Proceedings of the 1986 International Conference on Titanium Products and Applications, vol. 1 (Dayton, OH: Titanium Development Association, 1986), 438-445.
2. K. Toyama and T. Maeda, "The Effect of Heat Treatment on the Mechanical Properties of Ti-10V-2Fe-3Al," Journal of the Iron and Steel Institute of Japan, 72(6)(1986), 617-624.
3. T. Matsumoto and T. Nishimura, "Effects of Forging and Heat Treatment Conditions on Mechanical Properties of a High Strength Titanium Alloy, T-17," Journal of the Iron and Steel Institute of Japan, 72(1)(1986), 138-145.

## GRAIN REFINEMENT AND SUPERPLASTICITY

### IN A HARD NICKEL-BASE ALLOY

I. Kuboki\*, Y. Motohashi\*\* and M. Imabayashi\*

\* Department of Metallurgy

\*\* Department of Mechanical Engineering  
Faculty of Engineering, Ibaraki University  
Hitachi, Ibaraki 316, Japan

#### Abstract

The Ni-30Cr-5Al alloy is soft in an as-solid-solution-treated state and can be hardened up to about 600 in vickers hardness at room temperature by an age-hardening in which duplex precipitation of  $\alpha$ -Cr and  $\gamma'$ -Ni<sub>3</sub>Al phases arise. Since, however, an average grain size of the alloy in the solid solution state is usually too large to exhibit superplasticity, being about 300  $\mu\text{m}$ , superplastic formings of the alloy have been impossible up to date.

In the present study, a possibility of superplasticity in the alloy is investigated by refining its crystal grains by means of a thermomechanical treatment consists of a cold rolling and a recrystallization. Since the recrystallization is accompanied with precipitations, a very fine-grained dual phase microstructure composed of a precipitated  $\alpha$  phase and a matrix  $\gamma$ -Ni phase is obtained. The average grain sizes of the recrystallized grains and/or sub-grains of the matrix  $\gamma$  phase are less than 1.5  $\mu\text{m}$ . The precipitated  $\alpha$  phases, the average grain size of which is usually more than 0.6  $\mu\text{m}$ , appear preferentially at grain boundaries. The alloys having such microstructures show total elongations of more than 500% and strain-rate sensitivity index  $m$  of more than 0.4 when deformed at 1225K. The activation energy of the deformation process at temperatures below 1225K is 251 kJ $\cdot$ mol<sup>-1</sup>. The microstructure remains equiaxed during the deformation, though crystal grains grow with the progress of deformation. We conclude from these evidences that the Ni-30Cr-5Al alloy which has been subjected to the thermomechanical treatment stated above shows superplasticity. Moreover, the superplastically deformed alloy can be strengthened to 620 in Vickers hardness by the age-hardening after the solid solution treatment.

Superplasticity and Superplastic Forming  
Edited by C.H. Hamilton and N.E. Paton  
The Minerals, Metals & Materials Society, 1988

## Introduction

The Ni-30Cr-5Al alloy is willingly utilized for an ornamental material such as a watchcase, because the alloy shows a remarkable age-hardening (1) due to duplex precipitation of  $\alpha$ -Cr and  $\gamma'$ -Ni<sub>3</sub>Al phases in addition to the fact that the alloy is soft in an as-solid-solution-treated state. If it is possible to introduce superplasticity in the alloy, then manifold properties, for example, a wide variety of designs given by its superior transcription and diffusion bonding abilities, can be added to the already-known facts.

In the present study, a thermomechanical treatment composed of a cold rolling and a recrystallization and precipitation, i.e., a structure control in which precipitated phases are used not only for strengthening the alloy but also for refining grains and stabilizing structures at high temperatures, is performed to introduce superplasticity in the Ni-30Cr-5Al alloy. And tension test is carried out at different temperatures to see whether the alloy will show superplasticity or not.

## Experimental Procedures

Chemical composition of the alloy is as follows: Cr= 29.97 wt.%, Al= 5.27 wt.%, Ni= balance. The alloy was accepted as a plate of 5.5 mm in thickness which has already undergone a solid solution treatment ( 1373K x 3.6ks  $\rightarrow$  water quenching ). The structure of the alloy is a  $\gamma$ -Ni single phase, with grain size of about 300  $\mu$ m, containing well-developed annealing twins.

The as-received alloy is cold-rolled to 1.1 mm in thickness by 7 to 8 passes. The percentage reduction in thickness is 80 %. A tensile specimen of gauge length 15 mm and width 3 mm with the tensile axis parallel to the rolling direction is cut out from the sheet. Annealings for precipitation and recrystallization of the specimen are then carried out. The annealing conditions are (a) 1125K  $\times$  180ks  $\rightarrow$  O.Q., (b) 1175K  $\times$  18ks  $\rightarrow$  O.Q., and (c) 1225K  $\times$  1.8ks  $\rightarrow$  O.Q., where "O.Q." is oil quenching. Hereinafter the specimens belonging to the conditions (a), (b) and (c) are called Spe.A, Spe.B and Spe.C, respectively.

A tension test is carried out at temperatures from 1125K to 1275K at initial strain-rates from  $3 \times 10^{-4} \text{ s}^{-1}$  to  $2.2 \times 10^{-2} \text{ s}^{-1}$  in a vacuum of 8 to 10 Pa.

## Experimental Results and Discussion

### Grain Refinement

Since a  $\gamma'$ -Ni<sub>3</sub>Al phase is almost dissolved into a matrix  $\gamma$ -Ni phase at temperatures above 1175K, the alloy has a dual phase microstructure composed of the  $\gamma$ -Ni and a precipitated  $\alpha$ -Cr phases between 1175K and 1288K. Since, however, the  $\alpha$  phase is reduced rapidly over 1225K ( $T > 1225\text{K}$ ) even if the temperatures are within its precipitation range, grain growth of the matrix phase predominates. Therefore, the recrystallization of the specimens must be made below 1225K ( $T \leq 1225\text{K}$ ).

Microstructures of Spe.A, Spe.B and Spe.C and a X-ray back reflection pinhole pattern of Spe.C are shown in Fig.1. Round  $\alpha$  phases are precipitating continuously and almost uniformly in each specimen. Whereas, discontinuous precipitation of the  $\alpha$  phase was observed in specimens cold-rolled to less than 70 % reduction. It has been observed in Cu-2Be alloy (2) and so on that, if a severe rolling is added to a specimen showing the

discontinuous precipitation, the continuous precipitation and recovery - recrystallization advance side by side during annealing, and a fine-grained dual phase microstructure is produced. It is most likely that almost the same things are occurring in the present alloy cold-rolled to more than 80 % reduction. Both Debye rings of  $\gamma$ -Ni(331) and  $\gamma$ -Ni(420) are smooth and continuous and  $K_{\alpha}$  double lines are separating perfectly. Almost the same X-ray patterns were observed for Spe.A and Spe.B. From these evidences, we conclude that the recrystallization has been almost finished and fine-grained microstructures have been formed in each specimen. Average grain sizes of the recrystallized  $\alpha$  and  $\gamma$  phases in Spe.C are 0.6 and 1.5  $\mu\text{m}$ , respectively.

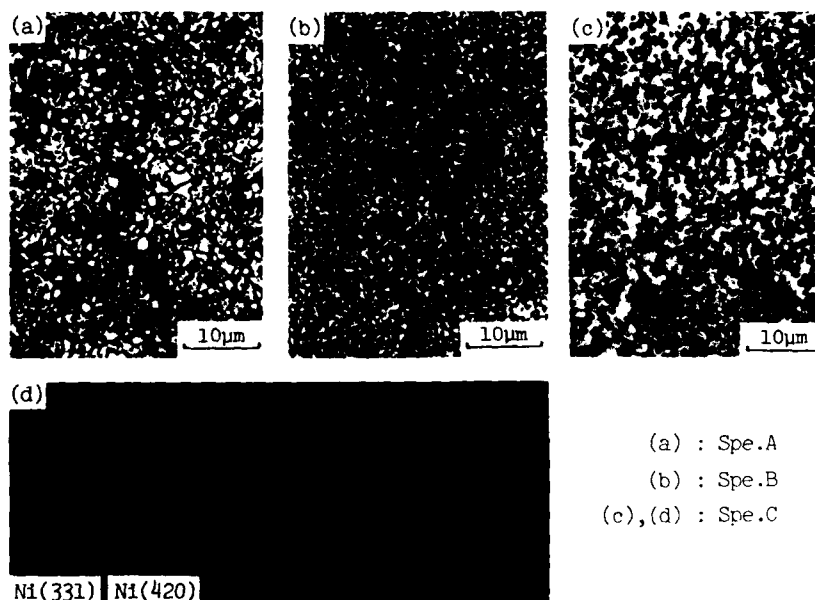


Fig. 1 - (a) to (c): Microstructures of Ni-30Cr-5Al alloys annealed after 80% cold rolling. (d): X-ray pinhole pattern of Spe.C.

We can say that the grains of the matrix phase will be refined fairly well if the specimen is recrystallized at temperatures as low as possible with annealing times as long as possible, because the amount of precipitated  $\gamma'$  or  $\alpha$  phase increases as the annealing temperature is lowered and these precipitated phases can suppress the grain growth of the matrix phase. Therefore, the grain size of Spe.A may be finest of the three and that of Spe.B follows this.

#### Tensile Properties at High Temperatures

It is seen from Fig.2 that a total elongation is largest and a flow stress is lowest at 1225K in each specimen. At each temperature below 1225 K, the elongation of Spe.A is always largest. This result implies that the elongation increases as the structure is refined. The strain-rate at which a maximum elongation occurs shifts to a higher strain-rate side in order of Spe.A, Spe.B and Spe.C, as shown in Fig.3. This result supports that the grain size of Spe.A is finest. On the other hand, the flow stresses of



each specimen are found to be nearly equal with each other at every strain-rate tested. This result implies that the flow stress depends not only on the grain size but also on the amount of precipitates. In this case, strain-rate sensitivity index,  $m$ , is about 0.4. Since, an adequate  $m$ -value for superplastic deformation is believed to be more than 0.3, we can conclude that each of the present specimens can show superplasticity under suitable conditions.

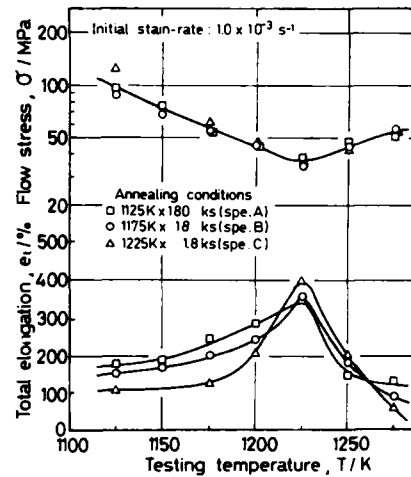


Fig. 2 - Variations of total elongation and flow stress with temperature in each specimen.

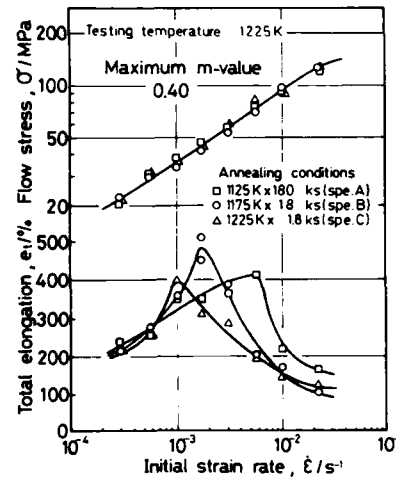


Fig. 3 - Variations of total elongation and flow stress with initial strain-rate in each specimen.

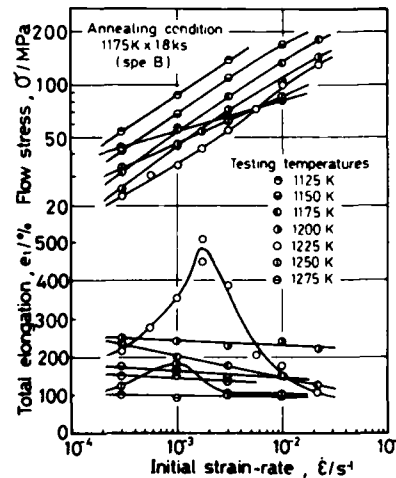


Fig. 4 - Variations of total elongation and flow stress with initial strain-rate on Spe. B.

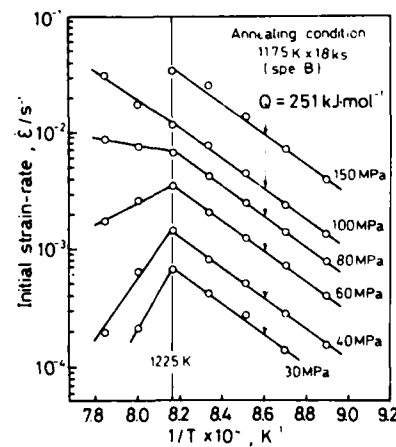


Fig. 5 - The relation between  $\ln \dot{\epsilon}$  and  $T^{-1}$  at a constant stress of Spe. B.

The elongation depends strongly on the strain-rate at 1225K, but the strain-rate dependence is very weak and a maximum elongation is 250% at the most at other temperatures ( see Fig.4 ). The  $m$ -values observed are more than 0.4 below 1225K, but they are 0.25 at the highest above 1250K. The activation energy,  $Q$ , of the deformation process is obtained from the relation between temperature and strain-rate. It is apparent from Fig.5 that the deformation mechanism differentiates at temperatures above or below 1225K. It appears that this phenomenon is originated from a considerable grain growth of the matrix phase over 1225K as will be shown in the next Fig.6. The decrease in the total elongation and the increase in the flow stress over 1225K as already seen in Fig.2 can be comprehended from this, i.e., superplasticity is lost over 1225K by the considerable grain growth. The activation energy was found to be  $251\text{kJ}\cdot\text{mol}^{-1}$  below 1225K. This value is nearly equal to the activation energies of volume diffusions of Ni, Cr and Al in a Ni crystal.

Microstructures at different parts of Spe.B deformed to fracture are shown in Fig.6. Dynamic grain growth of both  $\alpha$  and  $\gamma$  phases is evident at 1225K in a region near to the fracture. Moreover, it should be noted that the microstructures in each temperature remain equiaxed in spite of large deformations.

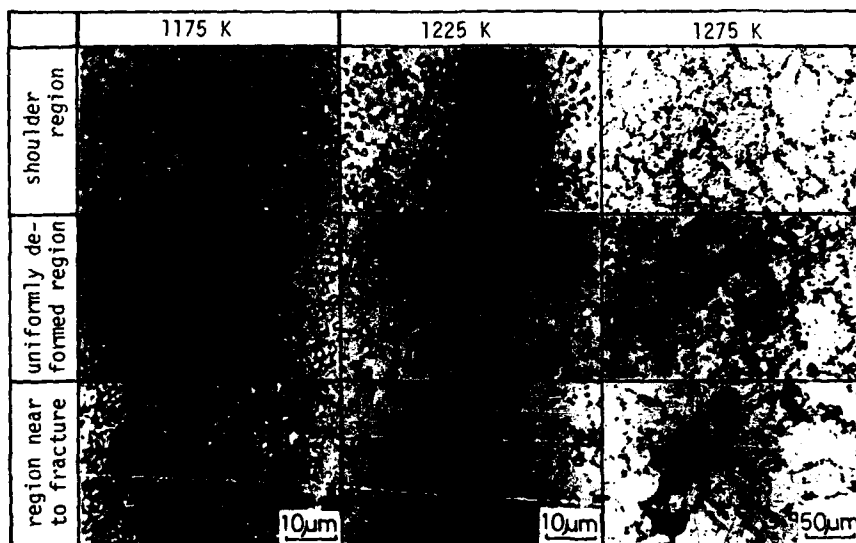


Fig. 6 - Microstructures of Spe.B deformed to fracture at  $\dot{\epsilon} = 1 \times 10^{-3} \text{ s}^{-1}$ .

#### Conclusion

In order to produce a very fine-grained microstructure, cold rollings of more than 80% reduction and recrystallization treatments below 1225K are necessary. The Ni-30Cr-5Al alloy which has been subjected to such a thermo-mechanical treatment shows superplasticity.

#### References

1. K. Suzuki, Sumitomo-Tokushu-Kinzoku Giho, 1984, Jan.
2. H. Kreye, Z. Metallkde., 62 (1971), 556-562.

## SUPERPLASTIC LOW MANGANESE

### ZINC-MANGANESE ALLOYS

N. Dyulgerov, A. Istatkov, N. Mitev, I. Spirov

Institute of Metal Science and Technology  
Bulgarian Academy of Sciences  
Sofia, Bulgaria

#### Abstract

The superplastic properties of Zn-Mn alloys with manganese content: 0,2; 0,4; 1,2; 1,5 and 2,0 vol.% are investigated. It is established that the alloys with ultra-fine grain structure having 0,7; 1,2; 1,5 and 2,0% Mn possess superplastic properties. These properties appear in alloys with manganese content over 0,4%.

It has been studied the dependence of the superplastic flow stress, strain rate sensitivity index and the total elongation on superplastic deformation parameters.

Values for the parameter of relaxation and activation energy of the superplastic flow are obtained.

It has been established that the main mechanism of the superplastic deformation for the elaborated alloys is grain boundary sliding.

It has been proved experimentally that the highest superplastic properties possess Zn-alloys with 0,7 and 1,2% Mn (peritectical and eutectical compositions respectively). It has been established that the superplasticity of the investigated Zn-Mn-alloys is due to the  $\beta$ -phase  $MnZn_{13}$  preventing the process of recrystallization, i.e. providing for the stability of the equi-axed fine-grain structure during deformation.

### Introduction

The aim of the present paper is that the superplastic properties of Zn-Mn alloys of manganese content up to 2% be studied. These alloys, developed in the Institute for Metal Science and Technology, Bulgarian Academy of Sciences and protected by author's certificate, have good mechanical properties and higher recrystallization temperature. These properties provide for their application in the machine engineering practice as construction materials replacing copper and aluminium alloys used in the manufacturing of parts and components in the food, power and other fields of industry.

From theoretical and experimental viewpoints the Zn-Mn system with manganese content up to 2% is also interesting because in the limits of lower than 1% manganese content peritectic and eutectic points in the phase diagram are met. This allows studying and comparing the effect of the type of diagram and presence of characteristic points in it on the superplastic properties of the alloys, without substantial variation of the alloying component.

### Materials and Methods

In the present investigation zinc alloys with 0,2; 0,4; 0,7; 1,2; 1,5 and 2,0 vol.% manganese are used, where the alloy with 1,2% Mn is of eutectic composition and with 0,7% Mn - of peritectic composition. The preparation of the structure includes casting in metal form and plastic deformation with degree of deformation 96% at initial temperature of deformation 573°K and further cooling in air. The billets thus obtained had equi-axed structure with mean grain size of 2 to 4  $\mu$ m.

Specialized installation for investigating the mechanical characteristics of the superplastic flow was used (1) which allowed maintaining a constant strain rate  $\dot{\epsilon}$  as well as its stepless variation in the  $10^{-5}$  to  $10^0$  s $^{-1}$  range. The heating of the experimental specimens was done in salt bath with precise maintenance of the preset temperature  $\pm 3^\circ$ K. The experimental specimens are cylindrical fivefolds with diameter of the working area 5 mm. The experimental installation allows carrying out a hardening under load of the experimental specimen aiming fixation of the structure for making additional metal-physical and metallographic tests. These tests include optic and electron microscopy, internal friction measuring, determination of the activation energy of the superplastic deformation process, Auger spectrometry and X-ray studies.

### Mechanical Tests

Mechanical tests allowed measuring the applied stress of the superplastic flow  $\sigma$ , the total elongation of the experimental specimen  $\delta$  and the strain-rate sensitivity index  $n$ , included in the relationship

$$\sigma = K \dot{\epsilon}^m \epsilon^n \left( \frac{T_r - T}{T_r} \right)^q, \quad (I)$$

taken from data in the literature (2, 3, 4) and specified in relation to the member containing T after the accomplishment of the preliminary investigation by the authors (5, 6). In the relationship I the participant quantities have the following meaning: k - numerical coefficient,  $\dot{\epsilon}$  - strain rate,  $\epsilon$  - degree of deformation,  $T_m$  - melting temperature of the material, T - test temperature, m - strain rate sensitivity index, n - deformation sensitivity index, q - index of temperature effect.

The study of the parameters  $\epsilon$ ,  $\dot{\epsilon}$  and T effects on the  $\sigma$ , and m is executed with varying the temperature in the range of 443 - 643°K and strain rate in the range of  $10^{-4}$  to  $10^{-1}$  s<sup>-1</sup>.

The correlation analysis of the experimentally obtained data showed that, for alloys with manganese content of 0,7; 1,2; 1,5 and 2,0% in the said variation intervals of  $\dot{\epsilon}$  and T, the variation of T and  $\dot{\epsilon}$  while the connection between  $\sigma$  and  $\epsilon$  is weak.

In the carried out regression analysis of the experimental data in the specified temperature-rate range the following regression equations for  $\sigma$  were obtained:

$$\sigma_{0,7} = 25,5 \cdot 10^6 \dot{\epsilon}^{0,35} \left( \frac{T_r - T}{T_r T} \right)^{1,59}, \quad (2)$$

$$\sigma_{1,2} = 54,2 \cdot 10^4 \dot{\epsilon}^{0,28} \left( \frac{T_r - T}{T_r T} \right)^{1,36}, \quad (3)$$

$$\sigma_{1,5} = 36,0 \cdot 10^4 \dot{\epsilon}^{0,21} \left( \frac{T_r - T}{T_r T} \right)^{1,36}, \quad (4)$$

$$\sigma_{2,0} = 61,3 \cdot 10^4 \dot{\epsilon}^{0,27} \left( \frac{T_r - T}{T_r T} \right)^{1,36}. \quad (5)$$

The index  $\sigma$  in the equations (2) to (5) shows the manganese content in vol.%.

The coefficient of multiple correlation for relationships from (2) to (5) is  $R > 0,90$ .

The researches show that an alloy with manganese content of 0,2% does not display superplastic properties and an alloy with Mn content of 0,4% demonstrates initiation of appearance of superplastic properties, however they are insufficiently expressed ( $\delta < 150\%$ ,  $m < 0,20$ ).

Figure 1 shows in diagram form the dependence of the total elongation  $\delta$  on the manganese content (in each diagram are given the values of  $\dot{\epsilon}$  and T, for which maximum values for  $\delta$  are obtained).

Figure 2 shows the dependence of the strain-rate sensitivity index m on the percentage manganese content (the respective values of  $\dot{\epsilon}$  and T are given, for which the maximum values for m are obtained).

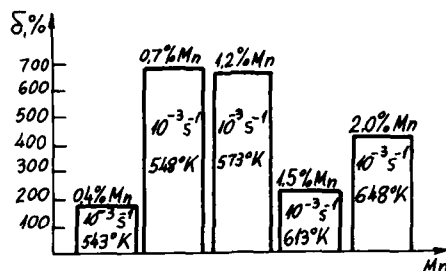


Fig. 1. Dependence of the total elongation on the manganese content

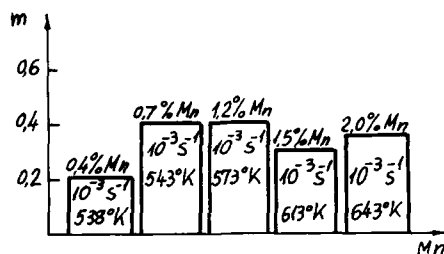


Fig. 2. Dependence of the strain rate sensitivity index m on the manganese content

Figures 1 and 2 show that highest values for  $\delta$  and m are obtained at manganese content of 0.7% and 1.2% (peritectic and eutectic compositions respectively), where for all the examined alloys the optimum strain rate is  $10^{-3} \text{ s}^{-1}$ . It is also seen from the figures that with the increase of the percentage manganese content the maximum values of  $\delta$  and m appeared at higher temperatures. With the increase of the manganese content the recrystallization temperature of alloys also increases - from 473°K for the Zn - 0.5%Mn alloy it increases to 533°K for the Zn - 2.0%Mn alloy.

#### Metal-Physical Investigations

Figure 3 shows the initial structure of specimens with manganese content of 0.7; 1.2 and 2.0% respectively. It is seen that the increase of the percentage manganese content is connected with the enlargement of the intermetallic phase particles. It was established by X-ray test that this was  $\beta$ -phase  $\text{MnZn}_{13}$ .

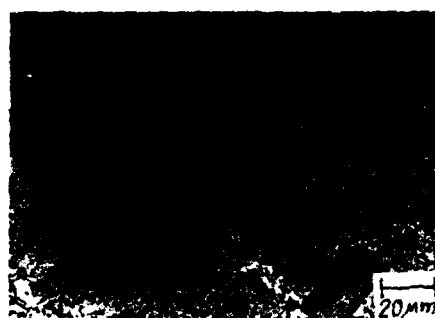
Figures 4, 5 and 6 show electron microscope pictures of alloys with manganese content of 0.2; 0.7 and 1.2%, in each figure different stage of deformation is demonstrated. For Zn - 0.2%Mn alloy it is clearly seen the low quantity of  $\beta$ -phase, as well as formation of dislocation net in the grain volume even at 50% of deformation (Fig. 4). This process leads to fast destruction of the material. Much higher quantity of  $\beta$ -phase is noticed in alloys with manganese content of 0.7% and 1.2% (Figures 5 and 6). In both alloys it is seen the uniform distribution of this phase as well as absence of developed dislocation net in the grain volume during the process of deformation.

Figure 7 shows the variation of activation energy U and the total elongation  $\delta$  on the percentage manganese content. It is clearly seen that the maximum values of  $\delta$  are obtained at manganese content of 0.7 and 1.2% where the activation energy U is of minimum values.



a) Zn - 0,7% Mn, x 500

b) Zn - 1,2% Mn, x 500



c) Zn - 2,0% Mn, x 500

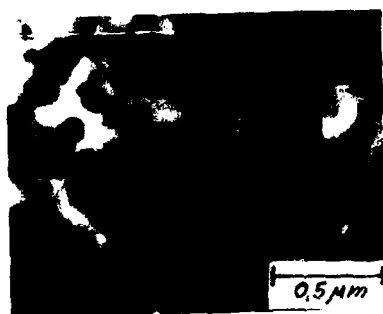
Fig. 3. Initial structure of specimens with different manganese content



a)  $\epsilon = 0$ , x 20000

b)  $\epsilon = 50\%$ , x 40000

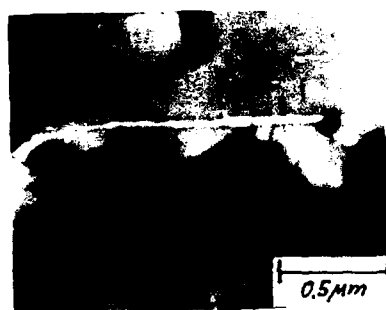
Fig. 4. Electron microscope pictures of Zn - 0,2%Mn alloy at different stages of deformation



a)  $\epsilon = 0$ , x 40000



b)  $\epsilon = 50\%$ , x 20000

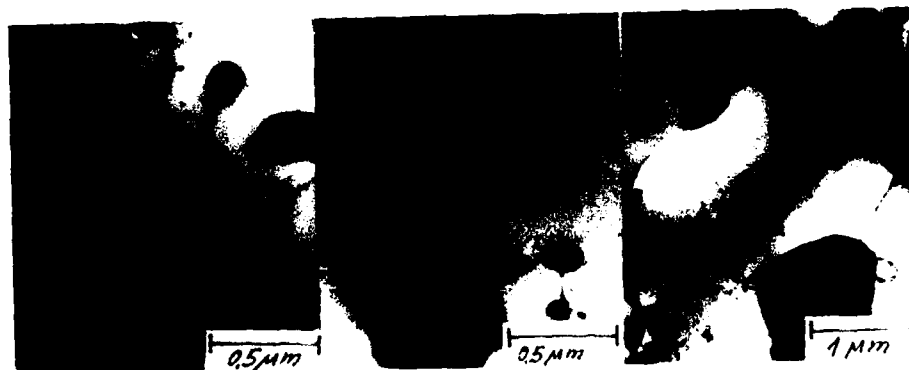


c)  $\epsilon = 100\%$ , x 40000



d) after fracture, x 20000

Fig. 5. Electron microscope pictures of Zn - 0.7%Mn at different stages of deformation



a)  $\epsilon = 50\%$ , x40000



b)  $\epsilon = 100\%$ , x40000



c) after fracture, x 20000

Fig. 6. Electron microscope pictures of Zn - 1.2%Mn at different stages of deformation



The temperature dependence of the internal friction  $Q^{-1}$  for the investigated alloys is shown in Figure 8, and the corresponding numerical values for the activation energy  $U$ , relaxation parameter  $\tau_0$ , as well as for  $m$  and  $\delta$  at test temperature 548°K are shown in Table I.

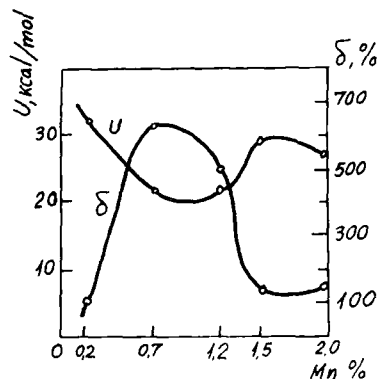


Fig. 7. Variation of the activation energy  $U$  and total elongation  $\delta$  by the manganese content

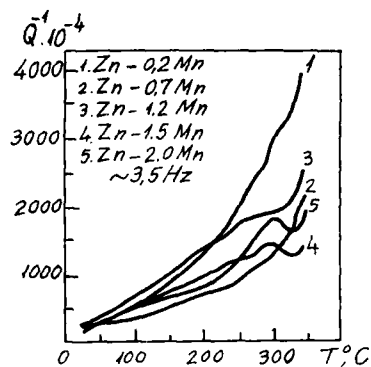


Fig. 8. Temperature dependence of the internal friction  $Q^{-1}$  in Zn-Mn alloys

From the results obtained it is seen that the maxima for internal friction are found in the temperature zone in which alloys display maximum plasticity. The results from the examinations of the internal friction show as well that the kinetic parameters of relaxation  $\tau_0$  and  $U$  strongly depend on the degree of alloying the zinc with manganese. The high values of the internal friction predict increase of the diffusion mobility of atoms, as the calculated values for  $U$  are close to the activation energy for self-diffusion of zinc (close values for  $U$  are obtained in another experimental way by the authors in (7) as well) which also enlightens to a certain extent the question of accommodation processes of grain boundary sliding. This process was clearly proved in connection with the studied alloys by the method of marked grains and observing the changes of marks during deformation.

Table I

No	Alloy	Relaxation $\tau_0$ , sec.	$U$ , kcal/mol	Super-plastic deformation $m$	$T$ , °C	$\delta$ , %
1.	Zn-0,2Mn	$2,43 \cdot 10^{-13}$	32.0	0,17	275	102
2.	Zn-0,7Mn	$1,59 \cdot 10^{-10}$	22.0	0,39	275	620
3.	Zn-1,2Mn	$5,08 \cdot 10^{-10}$	21.8	0,36	275	500
4.	Zn-1,5Mn	$1,45 \cdot 10^{-13}$	29.6	0,27	275	132
5.	Zn-2,0Mn	$7,58 \cdot 10^{-12}$	27.8	0,22	275	150

### Discussion of the Experimental Results

All investigations show that the superplastic properties of the studied Zn-Mn alloys are due to the formed  $\beta$ -phase  $\text{MnZn}_{13}$ . By the Auger-spectrometry it was confirmed that a greater part of it deposits on the grain boundary and prevents the migration at the boundaries at the temperature of performing the superplastic deformation. This on its part contributes to stabilization in time of the equi-axed fine grain structure appearing basic precondition for occurring of the grain boundary sliding process.

The measured values of activation energy which are close to this of the activation energy of the zinc self-diffusion process show that the diffusion processes take part actively as accommodation processes accompanying grain boundary sliding. The absence of developed dislocation net in the grains during superplastic deformation, confirmed by the authors in (8,9) too, shows that the dislocation processes probably run mainly inside the grain boundaries. Noticeable dislocation processes in the grain volume appear at localization of the deformation ending with fracture.

The results from the investigations carried out show that zinc alloys with 0,7% and 1,2% Mn (peritectic and eutectic compositions) have the highest superplastic properties.

#### References:

1. Spirov et al, "Test Equipment for Superplastic Metals and Alloys", HNMS Scientific Session, V. Turnovo, 1981, (Bulg.)
2. Kuibishev O.A., "Superplasticity of Industrial Alloys", Metallurgy, 1984, (Russian).
3. Smirnov O.M., "Pressure Treatment of Superplastic Metals", Mechanical Engineering, 1979, (Russian).
4. Padmanabhan K.A., G.I. Davies, "Superplasticity", Springer-Verlag Berlin Heidelberg New York, 1980.
5. Dyulgerov N. et al., "Examination of the Deformation Level, Specimen Size, Strain Rate and Temperature Effects on the Tension When Testing Zinc Alloy Samples in Structural Superplastic State", HNMS Scientific Session, V. Turnovo, 1982, (Bulgarian).
6. Baikushev A., N. Dyulgerov, T. Trufkin, "Influence of the Thermo-mechanical Conditions of Deformation on the Stress of Superplastic Al Alloy", Material Science and Technology, 1987, No. 15, (Bulgarian).
7. Dyulgerov N. et al., "Activation Energy of Zn Alloy Superplastic Flow", HNMS Scientific Session, V. Turnovo, 1984, (Bulgarian).
8. Dyulgerov N. et al., "X-Ray Study of Superplastic Microalloyed Zn Alloy", Scientific Conference on Plastic Deformation, Varna - Golden Sands, 1987 (Bulgarian).

9. Dyulgerov N. et al., "Investigation of Zn-Mn-Cd Alloy Microstructure at Superplastic Deformation", Scientific Session, Varna, 1987 (Bulgarian).

## PROPERTIES OF A MICRODUPLEX STAINLESS STEEL

### SUPERPLASTICALLY DEFORMED

K. Osada

Technical Research Center,  
Nippon Yakin kogyo Co., Ltd., Kawasaki, Japan

#### Abstract

The new microduplex stainless steel which was highly alloyed with Cr and Mo has been studied with respect to the ambient mechanical properties and the local corrosion resistance after superplastic deformation. Results showed that the deformed steel lost its ductility and also the pitting corrosion resistance. The morphology and the content of sigma precipitates, which varied with strain and strain rate as well as with temperature, was found to be responsible for the deterioration. It was confirmed, however, that a heat treatment recovers the properties.

#### 1. Introduction

A new micro-duplex stainless steel has been introduced. This alloy exhibits superplasticity as well as IN-744 with less voids. Its tensile elongation exceeds 2500%. Even if the steel has elongated, stringer austenites in a banded-ferrite matrix, it showed remarkable superplasticity (1). To understand this outstanding superplastic behavior of the steel, sigma phase precipitation has to be taken into account.

One of most important things among the superplastic material, is post-forming characteristics. There are however, very few reports on the post-forming properties. In this work not only the changes of the mechanical properties, but also that of the corrosion resistance after superplastic deformation was investigated. Additionally the microstructural change that was caused by the deformation, and that which controls the properties, will be discussed.

#### 2. Experimental Procedure

The chemical composition of the alloy is given in Table 1. The alloy was supplied in the form of 50% cold rolled sheet with the thickness of 1.0mm. Samples with the gage length of 10mm and

the width of 28mm, were machined in the perpendicular to the cold rolling direction for subsequent high-temperature uniaxial tensile tests. High temperature tensile tests were carried out in the air at constant cross head speeds at 1223 and 1273K. Samples were held at the test temperature for 300s prior to tension and then pulled to the specified true strain. Deformed specimens were cooled by forced air to room temperature immediately after tensile tests.

The ambient-mechanical properties parallel to the hot-tensile test direction were evaluated at room temperature.

Pitting potential was measured by anodic polarization method in a 3.5% NaCl solution which was de-aerated for 1800s before tests and was being kept at 343K during experiments. Pitting potential was defined as a potential where the anodic current reached to  $10^{-4}$ A.

For optical photomicrographs, specimens were etched in a 5N KOH solution electrolytically followed by electrolytic etching in a 10% oxalic acid.

Table 1 The chemical composition of the alloy (wt %)

C	Si	Mn	Ni	Cr	Mo	N
0.008	0.52	0.66	6.53	25.11	3.20	0.12

### 3. Results and Discussion

#### Changes of Mechanical Properties with Superplastic Strain

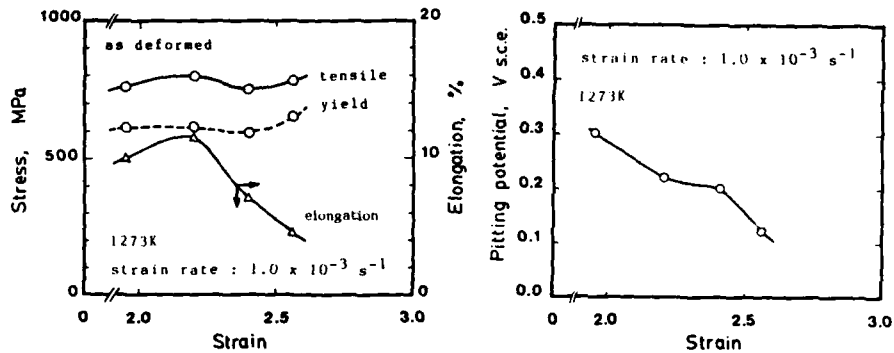
Figure 1 shows the ambient-mechanical properties. Specimens were pulled to various strain levels at the initial strain rate of  $1.0 \times 10^{-3} \text{s}^{-1}$  at 1273K. The tensile strength and the yield stress of deformed specimens slightly increase beyond the strain of 2.50, whereas the elongation decreases with the increase of the strain. The increase of the strength and the decrease of the ductility result as a consequence of the microstructural change during superplastic deformation.

The optical microscopic observations, in photo. 1, indicate that the content of sigma (dark phases) increases with the superplastic strain at 1373K. This temperature is high enough for this alloy to resolve the sigma phase into the surrounding matrix with time. Conclusively the superplastic deformation, therefore, affects the precipitation behavior of sigma compounds, and vice versa.

This alloy is designed to have an excellent corrosion resistance. Chromium and molybdenum are alloyed as much as 25% and 3.2% respectively with 0.1%N for that purpose. As a result, the alloy tends to precipitate sigma compounds fast in the temperature range between 800 and 1250K which roughly corresponds to the range where superplasticity can be expected. The precipitates, if they are relatively hard to deform plastically, may produce voids around them.

Influence of Superplastic Strain on Pitting Potential Pitting potential, which is very sensitive to elemental segregation, clearly decreases with superplastic strain as seen in Fig. 2. The depleted zone of elements like Cr and Mo around the

precipitate is well known to become the critical point for pitting (2). The strain accelerates the elemental segregation and hence produces the depletion.



Degradation of properties by superplastic deformation.

Fig. 1 Ambient-mechanical properties (left),

Fig. 2 Pitting corrosion potential (right).

Influence of strain rate on post-forming mechanical properties and pitting corrosion potential

To examine the effect of strain rate, specimens were pulled to the strain of 2.20 at various strain rates. Figure 3 shows the changes of the post-forming mechanical properties as a function of strain rate. The behavior of yield stress tends to form a maxima at  $1.0 \times 10^{-3} \text{ s}^{-1}$  both at 1223 and 1273K. On the other hand, tensile strength, although it shows the similar behavior to that at 1273K, gradually decreases with strain rate at 1223K. The effect of strain rate as well as strain should be considered because sigma is not a stable compound at 1273K in this alloy composition.

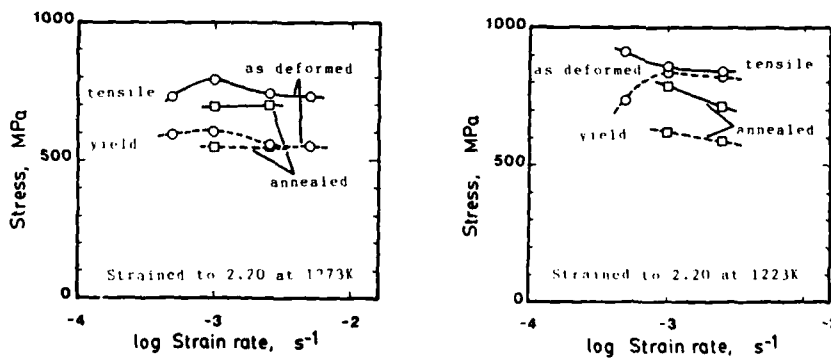
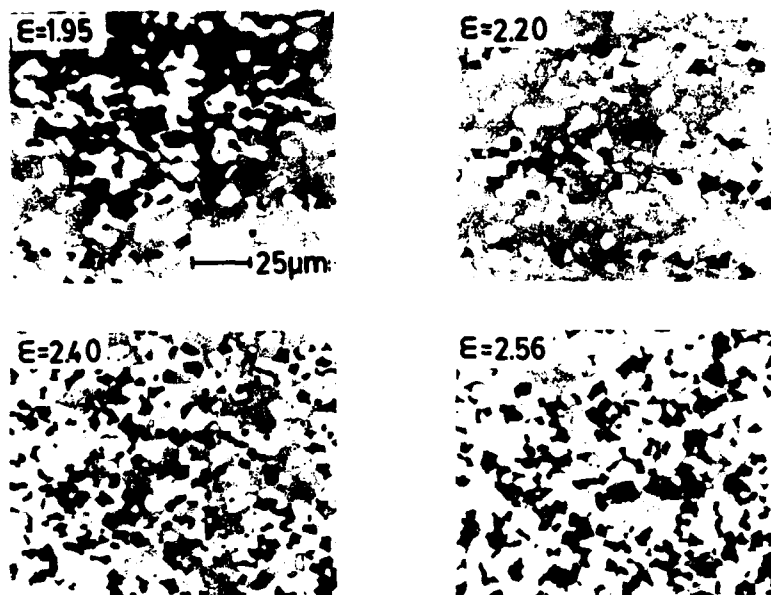
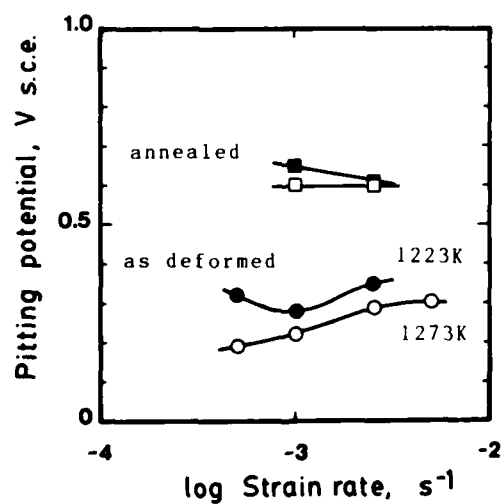


Fig. 3 The effect of strain rates and a heat treatment on the ambient-mechanical properties of as deformed specimens. All specimen was strained to the strain of 2.2.



**Photo. 1** The content of sigma phase increases with the increase of strain at the rate of  $1.0 \times 10^{-3} \text{ s}^{-1}$  at 1273K.



**Fig. 4** The effect of strain rates and a heat treatment on pitting potential. Solid lines with rectangulars show the value annealed at 1323K for 1800S.

Superplastically deformed specimens to the strain of 2.20, were annealed at 1323K for 1800S followed by water quench. The results of ambient-temperature tensile tests of annealed specimens are summarized in Fig. 3 together with that of as deformed ones. The effect of heat treatment is pronounced to reduce the strength and to recover the elongation to the value more than 10%.

Pitting potential of as deformed specimens shows the deterioration of local corrosion resistance as seen in Fig. 4. An addition of molybdenum is well known to be most effective for the improvement of local corrosion resistance in the stainless steel. The precipitation of sigma phase causes a molybdenum depletion zone around them by superplastic deformation. Pitting potential of the specimens deformed at 1223K shows slightly high value compared to that at 1273K, and has the lowest value at strain rate of  $1.0 \times 10^{-3} \text{ s}^{-1}$ . Contrary to that, pitting potential of specimens deformed at 1273K, gradually increases with strain rate. When specimens were deformed at 1273K, their grain size became relatively large and also sigma tended to exist locally.

The pitting potential after the heat treatment indicates the value higher than 0.60 volts s.c.e., but that is 0.1 volts less noble compared to the alloy manufactured by a conventional process.

The acceleration of sigma precipitation by superplastic deformation and insufficient recovery of the properties by the heat treatment at 1273K, indicate that a certain diffusion process which not only extends sigma formation, but also enhances grain boundary sliding, is responsible.

This dynamic effect of superplastic deformation on the metallurgical aspects of the alloy should be studied further.

#### 4. Conclusions

The new superplastic duplex stainless steel was examined in terms of post-deforming properties including mechanical behavior and local corrosion resistance.

- (1) The superplastically deformed microduplex stainless steel increases its yield stress and tensile strength.
- (2) The ductility of deformed specimen drops to the level of less than 10% elongation.
- (3) The superplastic strain shifts the pitting potential less noble.
- (4) The superplastic-deformation process accelerates the sigma precipitation that is responsible for the deterioration.
- (5) The heat treatment which resolves sigma phases recovers the post-forming properties to almost annealed state.

#### 5. References

- (1) K. Osada, S. Uekoh and K. Ebato: "Superplasticity of as Rolled Stainless Steel", Trans. Iron Steel Inst. Jpn., 28(1987), 713.
- (2) K. Osada, R. Nemoto, M. Tsuda and K. Osozawa: "Effect of phase Ratio and Chemical Composition on Hot Workability and Corrosion Resistance of Duplex Stainless Steels", STAINLESS STEEL '84, Inst. Metal., London, (1984), 149.



# THE STUDY OF REDUCING SUPERPLASTIC TEMPERATURE IN TITANIUM ALLOYS

Huang Liping

Shanghai Iron & Steel Research Institute  
Wusong Shanghai, China

## Abstract

This paper describes briefly the relationship between melting temperature, phase transformation temperature and superplastic temperature in ( $\alpha+\beta$ ) phase titanium alloys. It shows that the optimum superplastic temperature range of two phase titanium alloys is within  $40-80^\circ$  below the phase transformation temperature, i.e.

$$T_{\text{supe.}} = T_{\text{transf.}} - (40-80)^\circ\text{C},$$

which is not related to the melting temperature. Adding  $\beta$  phase-stabilizing elements, Mo, Cr, V and etc, can effectively reduce the phase transformation temperature.

This article also introduced that the optimum superplastic temperature can effectively reduced by orthorhombic martensite  $\alpha''$ -phase formed in alloys after appropriate heat treatment, for example, the superplastic temperature can be reduced from  $900^\circ\text{C}$  to  $800^\circ\text{C}$  for TC6 alloy.

Superplasticity and Superplastic Forming  
Edited by C.H. Hamilton and N.E. Paton  
The Minerals, Metals & Materials Society, 1988

### Introduction

The research and utilization of superplasticity of titanium alloy both in materials and technologies have been stressed by many nations. And lots of titanium alloy pieces made by superplastic forming process have been adopted by industries such like aeronautics, aero-spaces, electronics, instruments and chemistries etc, and huge commercial profits are obtained. As for titanium alloys, owing to its high resistance to deformation at room-temperature, the conventional process for them is rather difficult, and the fabricating cost is higher too, all these make the study on superplastic properties and superplastic forming process of titanium alloy an important subject in economical field of the nation. Some western countries have poured millions of money into theoretical research as well as engineering usage of titanium superplasticity. But the superplastic temperature is rather high, and the affinity of titanium with oxygen is rather serious, all of them lead to difficulties and trouble both in research and application. In order to reduce the superplastic temperature, much efforts have been tried out. We devoted our efforts not only to the effects of chemical components, the relationships between superplastic temperature and transformation temperature, but also to the investigation on reducing the superplastic temperature through heat-treatment of alloys to find the ways for reducing the superplastic temperature of two phase titanium alloys. Here is a brief statement about our research work.

### Method of Experiment

The necessary components of Al, Mo were added to the pure titanium to create the alloy. The molten temperature and  $\alpha+\beta\rightleftharpoons\beta$  transformation temperature are measured. The superplastic temperature is measured by high temperature hardness (pressure impression), and elongation is detected through superplastic tensile test. Moreover, based on experimental data of conventional alloys (for example, Ti-6Al-4V, Ti-5Al-4Mo-4Cr-2Sn-2Zr-Nb, TC6, Ti-10V-2Fe-3Al etc.), the mutual relationships among them are found out and compared. Besides, for the same alloy, in order to realized the influence of microstructure on superplastic temperature, special heat-treatments have been carried out.

### Experimental Results and Analysis

The experimental data of Ti-Al-Mo alloy series and some conventional alloys are listed in table I and II, fig.1, fig.2

From data shown in table I and Fig.1, it can be seen that since Al is a phase-stabilizing element, when adding Al into Ti, the melting temperature is reduced; but  $\alpha+\beta\rightleftharpoons\beta$  transformation temperature is heightened. The optimum superplastic temperature is raised. For example, the melting temperature of Ti-5Al-5Mo is nearly 20°C higher than that of Ti-10Al-5Mo, but the phase transformation temperature is 105°C higher on the other side, Mo is a phase-stabilizing element of  $\beta$ -Ti, when adding Mo into Ti-Al alloy, the  $\beta$ -phase region will be enlarged, and the phase-transformation temperature will be reduced. Fortunately, the optimum superplastic temperature is lowered. For example, the melting temperature of Ti-5Al-10Mo is higher than that of Ti-5Al-1.5Mo, but the phase transformation temperature is 68°C lower. In light of this, it can be concluded that the optimum superplastic temperatures of these alloys are about 40-80°C lower than its phase transformation temperature.

Table I Comparison Among Melting Temperature, Phase Transformation Temperature [2] and Optimum Superplastic Temperature of Various Ti-alloys

Chemical components (wt%)			Melting temperature	Phase transformation temperature	Optimum superplastic temperature	Superplastic elongation
Ti	Al	Mo	°C	°C	°C	%
5	/		1660	/	/	/
5	0.5		/	980	910	/
5	1.5		1670	970	870	/
5	2.5		/	920	880	760
5	5		1700	900	850	1100
5	10		1720	880	830	1300
5	20		1780	860	790	/
5	25		/	830	780	/
5	30		1800	820	770	/
5	35		/	720	660	/
5	40		/	/	/	/
10	0.5		1640	1120	1070	/
10	1.5		/	1080	1010	/
10	5		1680	1050	1000	/
10	10		1720	1050	980	/
Ti-6Al-4V [1]			1650	980	930	1100
Ti-5Al-4Mo-4Cr-2Sn-2Zr-Nb			1550	890	820	1300
Ti-10V-2Fe-3Al [1]			/	810	750	760
Zn-22Al			/	330	260	1600

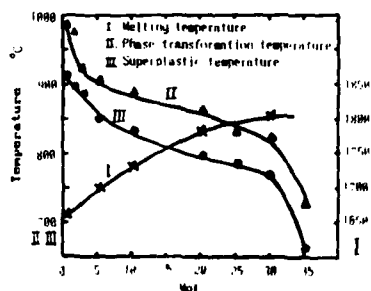


Fig. 1. The influence of Mo on melting temperature, phase transformation temperature and superplastic temperature of Ti-5Al alloys.

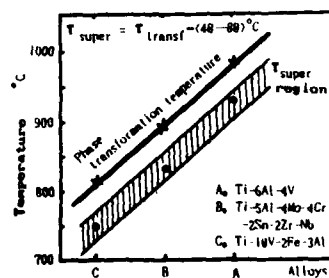


Fig. 2. The relationship between phase transformation temperature & superplastic temperature of various alloys.

$$T_{\text{super.}} = T_{\text{trans.}} - (40-80)^{\circ}\text{C}$$

where,  $T_{\text{super.}}$  -- superplastic temperature optimum.

$T_{\text{transf.}}$  --  $\alpha + \beta \rightleftharpoons \beta$  phase transformation temperature.

In the range 40 to 80°C below transformation temperature, the relative contents of the two phases  $\alpha, \beta$  can mutually restrain each other, preventing the growing of grain size, keeping the superplastic condition being of fine grain, and promote the superplastic forming. On the basis of our experimental results, it can be revealed that there is no direct relation between optimum superplastic temperature and melting temperature. Hence, as the two phases titanium alloys is concerned, the optimum superplastic temperature can be approximately estimated by measuring the  $\alpha + \beta \rightleftharpoons \beta$  transformation temperature. It can be concluded that any element which can reduce the phase transformation temperature of Ti-alloy, can reduce its superplastic temperature too. For example, by adding  $\beta$  phase stabilizing elements Mo, Cr, V etc., into Ti-alloys, both the phase transformation temperature and superplastic temperature can be lowered. The relationship between  $T_{\text{super.}}$  and  $T_{\text{transf.}}$  of several commercial alloys are shown in Fig.2.

Data listed in table II show the microstructure and superplastic elongation data. In  $\alpha + \beta$  two phase Ti-alloys, by means of proper heat treatment, orthorhombic martensite  $\alpha''$ -phase will be formed in its microstructure, the superplastic temperature will be lowered. As referring to TC6 Ti-alloy not containing  $\alpha''$  phase, its superplastic temperature approximately 900°C is obtained by means of ordinary heat-treatment and that containing  $\alpha''$  phase has a superplastic temperature about 800°C. The existence of  $\alpha''$  phase can be detected by X-ray diffraction analysis and was observed by using electronic microscopic with extra high magnification appears to be a needle-like extra fine and phase unstable structure. At high temperature it transforms into  $\alpha + \beta$ . After transformation, lots of vacancies can be observed. The binding force of grain boundary is weakened, the resistance to boundary sliding is lessened, so that the superplastic forming process can be proceeded easily with less flow stress at lower temperature. This is the way to reduce the superplastic temperature of Ti-alloy. To what extent the influence of  $\alpha''$  phase has on the superplasticity of the alloy depends closely on the relative content of  $\alpha''$  phase and its distribution.

Table II. Microscopic structure and Superplastic Tensile Elongat

Microscopic structure	Superplastic tensile elongation at different temperature %				Remarks
	800°C	850°C	900°C	950°C	
$\alpha + \beta$	630	550	880	510	Ti-6Al-1.5Cr -2.5Mo-0.5Fe -0.3S;
$\alpha'' + \alpha + \beta$	1300	970	750	/	

#### Conclusions

On the basis of primary results of our investigations, it can be concluded:

- (1) The optimum superplastic temperature of two phases titanium alloy

has no direct relationship with melting temperature.

(2) The phase transformation temperature of the two phase  $\alpha + \beta$  titanium alloys has close relation with optimum superplastic temperature generally speaking

$$T_{\text{super.}} = T_{\text{transf.}} - (40 \sim 80)^{\circ}\text{C.}$$

Its superplastic temperature can be reduced by adding  $\beta$ -stabilizing elements such as Mo, Cr, V etc into two phase Ti-alloys.

(3) By means of proper heat-treatments, the two phase Ti-alloys will contain certain amount of orthorhombic martensite " which enable to lower the superplastic temperature.

(4) The optimum superplastic temperature of other two phase alloy with have phase transformation can also be estimated by using the formula

$$T_{\text{super.}} = T_{\text{transf.}} - (40 \sim 80)^{\circ}\text{C.}$$

Summary, reducing  $\alpha + \beta \rightleftharpoons \beta$  phase transformation temperature of Ti-alloys or enabling it to contain certain amount of  $\alpha$  phase are the two major ways to reduce superplastic temperature.

#### REFERENCES

1. Aerospace structural Metals Handbook. code 3707 and 3726, Volume 4, 1982
2. Ge Ziming, Research on phase diagram of Ti-Al-Mo-V, 1967

AN APPROACH TO THE SUPERPLASTICITY

OF ALUMINIUM BRASS (HAL 66-3-2)

Su Shenggui, Shen Huanxiang and Song Shengzhe

Northeast Institute of Heavy Machinery  
Qiqihar City, Heilongjiang province, China

Abstract

The paper discusses the superplastic behavior of common industrial material aluminium brass (HAL66-6-3-2) with poor forging property under as-supplied condition. After superplastic stretch, microstructure analysis and surface appearance observations were conducted. A further study about the superplastic deformation mechanism of large grain structure was made.

It is shown through tests that, under as-supplied condition and without any pretreatment, the material exhibits superplasticity which can be attained at higher temperature and strain rate or lower temperature and strain rate respectively, i.e. elongation of 377% can be attained at a temperature of 700°C and strain rate  $2.8 \times 10^{-2} \text{ s}^{-1}$ , and elongation of 258% can be attained at a temperature 575°C and strain rate  $7 \times 10^{-3} \text{ s}^{-1}$ .

It is shown through analysis that the superplastic deformation of the material is chiefly intracrystalline deformation in large grains and it is accompanied with subgrain formation and dynamic recrystallization. The contribution of grain boundary slip is not a major contributory to total deformation. It offers only a rate-controlling effect in the deformation process.

Superplasticity and Superplastic Forming  
Edited by C.H. Hamilton and N.E. Paton  
The Minerals, Metals & Materials Society, 1988

### Introduction

Along with the increased understanding about superplasticity, it is considered more and more that superplasticity is not merely a special phenomenon of certain specific alloy, but one of the intrinsic properties of metallic materials (1). When the internal and external conditions are suitable, superplasticity of metallic materials can be observed.

The aluminium brass HAL66-6-3-2 is featured by high strength high hardness and abrasion resistance. It may be rated the best brass (2). Therefore, it is of great use in industry. Owing to the fact that its aluminium content is high, cleavage occurs easily during forging. Thus, it is significant to study the superplastic behavior of the material under as-supplied condition.

### Experimental Materials

Hot extruded bar supplied on market is adopted as the experimental material. The chemical composition is listed in table 1. The microstructure is shown in Fig.1 the matrix is  $\beta$  phase, the large grain is  $\gamma$  phase, tiny grain is Fe phase and the grain is equiaxed, average diameter of 70 $\mu$ m.

Table 1. Chemical composition of Available Bar Materials

Alloy Elements	Cu	Zn	Al	Fe	Mn	Foreign Matter
Percentage Contents(%)	66.25	21.25	6.58	3.13	2.32	The others

The  $\beta$  phase exhibits disordered state at high temperatures, and ordered state at low temperature. The conversion point between disorder state and ordered state is 570°C.

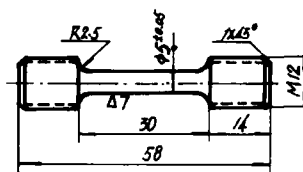


Figure 1-Initial structure 100

Figure 2-Stretching sample

### Experimental Results and Analysis

#### Superplastic Tensile Test

The test sample shown in Figure 2 is stretched at different temperatures and different cross beam moving velocity on a WD-1C type electronic universal testing machine. For different deformation speed (initial strain rate), curves of elongation and temperature are shown in Figure 3. In view

of this, we conclude:

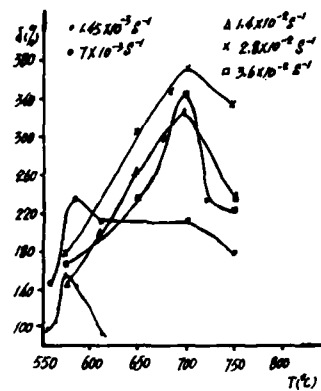


Figure 3-Curves of elongation

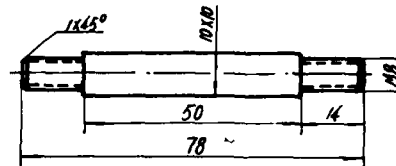


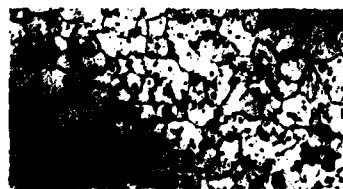
Figure 5-Stretching sample of scratch test

a) When the average diameter of initial grains is  $70\mu\text{m}$ , the material under as-supplied condition and without any pretreatment present superplastic behavior within the range of proper temperature and strain rate.

b) The curve of elongation rate exhibits two peaks at lower temperature and strain rate and higher temperature and strain rate. For the former, an elongation of 258% can be attained at temperature  $575^\circ\text{C}$  and strain rate  $7 \times 10^{-3} \text{ s}^{-1}$ ; for the latter, elongation of 377% can be attained at temperature  $700^\circ\text{C}$  and strain rate  $2.8 \times 10^{-2} \text{ s}^{-1}$ . The maximum value of  $m$  tested by velocity change method is 0.35. During superplastic stretching, the material exhibits a lower rheologic stress value, about  $1.5 \text{ Kg/mm}^2$ .

#### Microstructure Analysis

Test sample A and B are selected from those of optimal superplastic stretch deformed. The elongation of sample A is 369% at deforming temperature  $700^\circ\text{C}$  and strain rate  $2.8 \times 10^{-2} \text{ s}^{-1}$ , the elongation of sample B is 235.8% at deforming temperature  $575^\circ\text{C}$  and strain rate  $7 \times 10^{-3} \text{ s}^{-1}$ . Then, cross sections are cut separately and after etching them in the solution of hydrochloric acid and iron trichloride ( $100\text{ml H}_2\text{O} \cdot 10\text{ml HCL} \cdot 5\text{gFeCl}_3$ ), the microstructural observation can be conducted.



Sample A



Sample B

Figure 4-Microstructure after deformation X100

Figure 4 shows photomicrographs of sample A and B. Analyzing these photos, the f



Figure 4 shows photomicrographs of sample A and B. Analyzing these photos, the following can be seen:

a) The cross sectional grain sizes of sample A and B become smaller after superplastic deformation. It is the result of dynamic recrystallization occurred during deforming process.

b) The grain size of sample A is larger than that of sample B. It is caused by the fact that the deformation temperature of sample A is higher and the deformation amount of sample A is greater. Thus, it is easy for dynamic recrystallization.

There is no essential distinction between the microstructure of sample A and sample B. The mechanism of their superplastic deformation may be the same.

#### Surface Observations

The sample shown in Figure 5 is polished and scratched with corundum powder. Then it is removed for microstructural observation after it is stretched to a certain degree on a Gelleble 1500 thermal/force analog machine. Figure 6 shows the surface shape of the typical photos, where the deformation temperature is 700°C and strain rate is  $2.8 \times 10^{-2} \text{ s}^{-1}$ .

It is shown from the scratch test that the superplastic deformation of the material is chiefly intracrystalline deformation in large grains. The large grain is stretched out at initial stage of deformation, slip and rotation are produced at the grain boundary (Figure 6). When deformation reaches a certain amount, subgrains will be formed within the large grain. Thus, subgrain movements (slip and rotation of subgrain (Figure 6b) become the main factors of mass transfer of deformation. Owing to presence of a large amount of separated substances and the grain boundary becoming wide, the diffusive activity appears to be rapid. The shape of  $\beta$  phase particle remains unchanged (Figure 6c) during deformation process and the shape of  $\beta$  phase is changed, internally helping to bring about the rotation of  $\gamma$  phase partical.

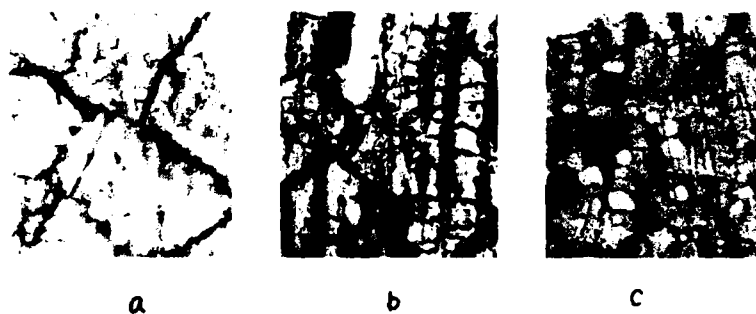


Figure 6-Photos for apperance surface observation  $\times 500$

Through Test, The Reason for Elongations Exhibiting Two Peaks Can Be Considered As:

The peak value presenting at low temperature range (575°C) is related to the phase transformation superplasticity. As the temprature of  $\beta \rightarrow \beta'$  transformation of alloy at 575°C, the phase transformation is a process of thermal activation and diffusion it needs a given time. Thus, only for lower strain rates can the peak value presented at this temperature be obtained. The peak value presented at high temperature range is chiefly caused by dynamic recrystallization. For the sake of keeping the grain of

recrystallization to be tiny, the temperature can not be too high. To assure the dynamic recrystallization, the temperature can not be too low, either. Raising the strain rate is favorable for developing dynamic recrystallization.

#### Conclusion

Under supplying condition and without any pretreatment, aluminium brass (HAL66-6-3-2) is provided with superplastic effect to the application in industrial production.

The superplastic deformation of the material is chiefly intracrystalline deformation in large grains. The subgrain net is formed at the initial stage of deformation and the recrystallized grain is formed immediately afterward. They are the main reason for superplastic deformation. The phase transformation superplasticity offers greater contribution to the superplasticity of low temperature range. The slip of grain boundary can be considered offering the effect of rate-controlling mechanism.

#### References

- (1) JIN KouXY , "Superplasticity Phenomenon", Light Metal, 21(9)(1971), 613-624
- (2) Editorial Group, Manufacturing Handbook of Heavy Non-ferrous Metal, (The Publisher of China Metallurgical Industry, 1976)

# THERMOMECHANICAL PROCESSING AND SUPERPLASTICITY

## IN A COMMERCIAL COPPER-BASE ALLOY

K. Higashi\* and N. Ridley+

\*Department of Metallurgical Engineering, College of Engineering  
University of Osaka Prefecture, Mozu-Umemati, Sakai,  
Osaka 591, Japan.

+Materials Science Center, University of Manchester/UMIST  
Grosvenor Street, Manchester, M1 7HS, England.

### Abstract

Fine stable microstructures can be developed by thermomechanical processing of commercially-based complex aluminium bronzes (Cu-Al-Fe-Ni alloys). The materials have a considerable potential for superplastic behavior during deformation in the  $\alpha + \kappa$  or  $\alpha + \beta + \kappa$  phase fields at temperatures of about 1073K. Tensile elongations of >1300% can be obtained at initial strain rates from  $10^{-4}$ - $10^{-2}\text{s}^{-1}$ , and the materials may be readily bulge formed. The important stages of the processing route required to develop a fine, uniform superplastic microstructure are discussed. Despite the very large uniform strains which can be achieved the materials do show some cavitation at high strains, but this can be controlled by the application of back pressure during forming.

Superplasticity and Superplastic Forming  
Edited by C.H. Hamilton and N.E. Paton  
The Minerals, Metals & Materials Society, 1988

### Introduction

Several copper-base alloys have been thermomechanically processed to develop superplastic microstructures. However, these alloys tend to undergo marked cavitation during superplastic flow, and this leads to fracture at limited strains (1-3). Recent work has shown that stable microstructures can be developed in as-cast commercial aluminium bronzes(4) and these can be used to produce superplastically blow-formed components such as that shown in Figure 1. The present paper deals with the thermomechanical processing of these alloys and with their potential for superplastic behavior.



Figure 1 - Superplastically formed component(750mm length) in aluminium bronze alloys ( Courtesy of KOMATSU Ltd. forming time is less than 10 min ).

### Alloy Compositions and Thermomechanical Processing

The compositions of Cu-Al-Fe-Ni alloys examined in the present work are given in Table I, which also includes typical superplastic properties. At temperatures from 873K to 1173K the alloys have complex microstructures consisting of ( $\alpha + \kappa$ ) or ( $\alpha + \beta + \kappa$ ) phases. The  $\kappa$ -phase, in fact, consists of two aluminides based on  $Fe_3Al$  and  $NiAl$ , respectively.

Table I. Compositions and typical superplastic properties of alloys.

Alloy code	Composition(wt%)				Superplastic performance			
	Al	Fe	Ni	Mn	Temp.(K)	m-value	E(%)	Strain rate(/s)
V	8.2	4.4	5.2	1.5	1073	0.52	>1300	$2 \times 10^{-3}$
W	9.1	5.9	5.1	1.6	1073	0.56	>1300	$8 \times 10^{-3}$
X	8.9	4.1	3.9	0.9	1073	0.48	650	$1 \times 10^{-3}$
Y	10.0	4.5	6.0	1.7	1073	0.57	>1300	$6 \times 10^{-3}$
Z	10.3	5.2	5.0	1.5	1073	0.51	>1300	$4 \times 10^{-2}$

The main steps in the processing schedule used to develop superplastic microstructures are: homogenising treatment, hot rolling, intermediate heat treatment, warm and cold rolling. Important aspects of alloy composition and of the processing procedure are presented below.

### Influence of Composition

The Al, Fe and Ni contents of the alloys affect the volume fractions and types of phases in the microstructure. This can be illustrated by reference to three alloys with different Al, Fe and Ni contents, which after holding at 1073K for 1.8ks, were rapidly cooled to room temperature. In alloy X the microstructure consists of f.c.c.  $\alpha$ -phase grains of mean diameter  $2\mu m$ , with about 15% volume fraction of fine uniformly distributed  $\kappa$  particles,  $<1\mu m$ . Alloy Y consists of equal volume fractions of  $\alpha$  and  $\kappa$  phases each about  $2\mu m$  in size, while alloy Z consists of  $\alpha + \beta + \kappa$  phases having respective volume fractions of 30%, 40% and 30%, and corresponding phase sizes of about  $2\mu m$ ,  $4\mu m$  and  $2\mu m$ .

The changes in flow stress and m value with strain rate at 1073K for the three alloys are shown in Figure 2. The flow stress for alloy Z is

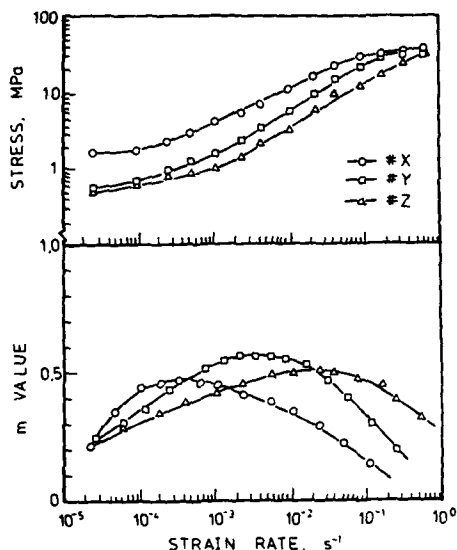


Figure 2 - The changes of flow stress and m-value of alloys X, Y and Z at 1073K with strain rate

fraction of  $\kappa$ -phase on the superplastic elongation of  $\alpha + \kappa$  alloys, the highest elongations are recorded for microstructures with intermediate volume fractions (i.e.  $> 20\%$ ) of each of the two phases.

#### Influence of Intermediate Heat Treatment and Rolling Conditions

Superplasticity in aluminium bronzes is affected by the shape and size of  $\kappa$ -phase particles. In turn, these particles are influenced by alloy composition and by heat treatment after hot rolling. A typical hot rolled microstructure is shown in Figure 3. Much of the  $\kappa$ -phase is of lamellar morphology, resulting from the  $\beta \rightarrow \alpha + \kappa$  eutectoid reaction which occurs during cooling after hot working, while some  $\beta$ -phase is retained and is non-uniformly distributed.



Figure 3 - The typical microstructure of as hot-rolled alloy Y.



Figure 4 - Microstructure of alloy Y after final annealing with intermediate heat treatment at 923K for 24hrs.

The microstructure of sheet material, with an intermediate heat treatment at 923K, which has been annealed at 1073K for 1.8ks after the final rolling treatment is shown in Figure 4. In the alloy without intermediate heat treatment the  $\kappa$ -phase shape and distribution is not unlike

lower and maximum  $m$  is attained at a higher strain rate, than for the other alloys. These observations are due to the presence of  $\beta$ -phase, which is a soft accommodating constituent at high temperatures (1). In the case of alloys showing ( $\alpha + \kappa$ ) microstructures at 1073K, alloy Y has a lower flow stress, and maximum ' $m$ ' at higher strain rates, than for alloy X. This reflects the stabilizing effect of the large volume fraction of  $\kappa$ -phase in alloy Y. The mechanical characteristics of the three alloys are consistent with the superplastic elongations given in Table I.

Although alloys containing  $\beta$ -phase have the greater superplastic deformation potential, it is difficult commercially to develop a uniform microstructure, and also there are problems associated with the post-deformation properties of the material. It is easier to develop and control the  $\alpha + \kappa$  microstructure. Resulting from the effect of volume

that in the hot rolled plate. In material given the intermediate heat treatment at 923K for 24hrs a uniform distribution of  $\kappa$ -phase is achieved, with the lamellar morphology being replaced by rod-shaped particles. The effect of an intermediate heat treatment is to lower the flow stress and to raise the  $m$  value at 1073K for processed sheet. The change in the shape of the  $\kappa$ -phase from lamellar to rod-shaped also reduces cavitation during superplastic flow this observation will be discussed in a later paper.

The rolling conditions in the thermomechanical processing are very important for the development of a uniform microstructure. The effect of various rolling treatments on  $\alpha$ -phase size distributions are shown in Figure 5.

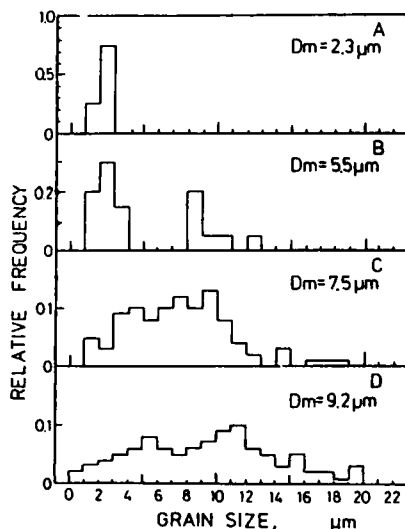


Figure 5 - Initial grain size distributions of  $\alpha$ -phase in alloy Y rolled under the different condition.

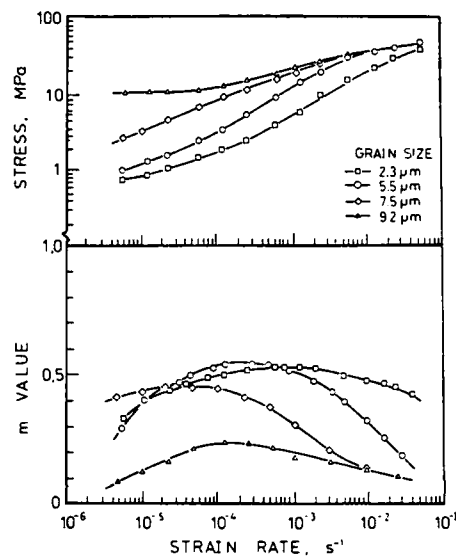


Figure 6 - Variations of flow stress and  $m$ -value with strain rate at 1073K for alloy Y with various grain size distributions (A-D in Figure 5).

Figure 5D shows the distribution in the hot rolled plate annealed at 1073K for 1.8ks. The  $\alpha$  grain size is non-uniformly distributed up to a maximum of 20 $\mu$ m, with a mean value of 9 $\mu$ m. Figure 5C shows  $\alpha$  grain size distributions after cold reduction of 10% before annealing at 1073K for 1.8ks. Most  $\alpha$  grains are <10 $\mu$ m, although the mean size is 7.5 $\mu$ m.

Figure 5B shows  $\alpha$ -phase grain size distribution after a warm rolling reduction of 80% at 923K followed by annealing at 1073K for 1.8ks. the mean grain size is 5.5 $\mu$ m, and the distribution is bimodal with peaks at 2 $\mu$ m and 8 $\mu$ m. Figure 5A shows  $\alpha$ -phase distributions after 80% reduction at 923K and 10% cold rolling reduction followed by annealing at 1073K for 1.8ks. In this case the microstructure is fine and uniform with a very narrow range of  $\alpha$ -grain size with a mean value of 2.3 $\mu$ m.

The effect of these various grain size distribution on flow stress and  $m$  values as a function of strain rate is shown in Figure 6. it can be seen that flow stress decreases and  $m$ -value increases with decreasing mean grain size, with the peak  $m$ -value being moved to high strain rates.

#### Cavitation and the Effect of Hydrostatic Pressure

Cavitation does occur in these materials during superplastic flow but the levels are very low for commercially significant strains. It can be seen in Figure 7 that there is a linear relationship between the volume of cavitation (plotted logarithmically) and true strain. This is consistent with plasticity controlled cavity growth (5).

To reduce cavitation a confining pressure may be applied during the superplastic forming process. Figure 8 shows the effect of increasing hydrostatic pressure on cavitation in an aluminium bronze deformed at  $2 \times 10^{-3} \text{ s}^{-1}$  and 1073K to 2.4 true strain. It can be seen that the volume of cavities is dramatically reduced as the pressure is increased.

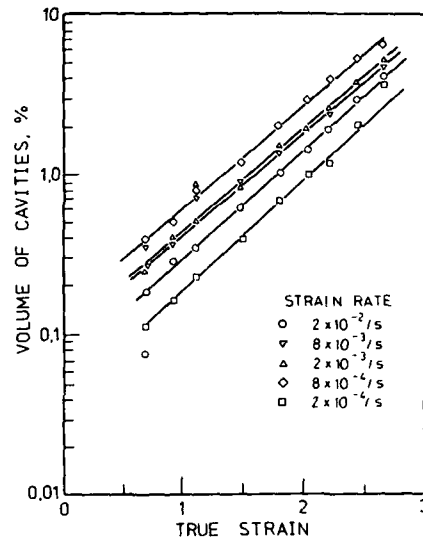


Figure 7 - Cavitation as a function of strain at 1073K in alloy W.

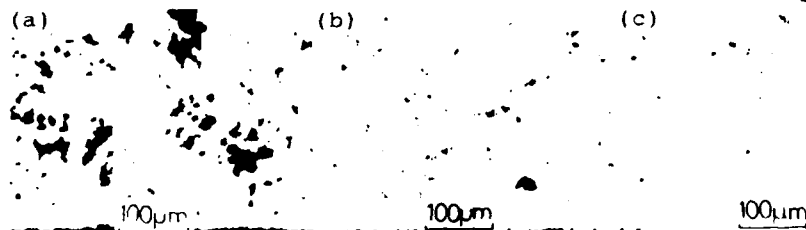


Figure 8 - Typical micrographs showing effect of pressure on the cavity distributions at 2.4 true strain in alloy V deformed at  $2 \times 10^{-3} \text{ s}^{-1}$  and 1073K (a) 0.1MPa, (b) 2.07MPa, (c) 3.45MPa.

#### Conclusions

- 1) As-cast commercial aluminium bronzes based on the Cu-Al-Fe-Ni system may be thermomechanically processed to develop fine uniform stable microstructures.
- 2) After processing the materials show a considerable potential for superplastic deformation in the  $\alpha + \kappa$  and  $\alpha + \beta + \kappa$  phase fields at temperature of about 1073K.
- 3) Tensile elongations of >1300% can be obtained at initial strain rates of  $10^{-4}$ - $10^{-2} \text{ s}^{-1}$ . The materials may be readily bulge formed.
- 4) The materials undergo cavitation during superplastic flow.
- 5) The application of a confining pressure during superplastic forming significantly reduces cavitation levels.

#### References

1. W.J.D. Patterson and N. Ridley, J. Mater. Sci. 16 (1981) 457-466.
2. D.W. Livesey and N. Ridley, Metall. Trans. 9A (1978) 519-526.
3. S.A. Shei and T.G. Langdon, Acta Metall. 26 (1978) 639-646.
4. K. Higashi, T. Ohnishi and Y. Nakatani, Scripta Metall. 19 (1985) 821-823.
5. J. Pilling and N. Ridley, Res. Mechan. 23 (1988) 31-63.

THE EFFECTS OF SUPERPLASTIC DEFORMATION ON THE  
MICROSTRUCTURE AND HARDENING CHARACTERISTICS OF  
HIGH STRENGTH 8091 ALUMINUM-LITHIUM ALLOY

R.D. Tucker and C.H. Hamilton

Department of Mechanical and Materials Engineering  
Washington State University  
Pullman, WA 99163

Abstract

It is well established that the 8091 Al-Li alloy can be heat treated to high strength levels, especially if post-solution heat treatment (SHT) strains are employed. However, for certain applications, a straining step following SHT is impossible. An investigation was therefore conducted to examine the aging characteristics of 8091 Al-Li alloy (Al-2.6 Li-1.90 Cu-0.55 Mg-0.12 Zr) in both the as-rolled and superplastically deformed conditions. A two step strain rate path consisting of  $\dot{\epsilon} = 2 \times 10^{-3} + 2 \times 10^{-4}$  was used to obtain superplastically formed rectangular test pans. The material in each condition was studied during natural aging and isothermal artificial aging. Aging temperatures ranged from 20°C to 225°C, while the associated aging times varied from 15 minutes to 5000 hours. The strengthening kinetics of the alloy were monitored using both Rockwell superficial hardness tests and uniaxial tensile tests. Current results indicate that an SHT of 545°C and aging temperatures of 165°C and 185°C result in peak hardness values and high strength levels in the as-rolled material without the use of post-SHT deformation. Preliminary hardness values show that the strength levels of the superplastically deformed material may be comparable to those of the as-rolled material.

Superplasticity and Superplastic Forming  
Edited by C.H. Hamilton and N.E. Paton  
The Minerals, Metals & Materials Society, 1988



## Introduction

Much of the recent research conducted on Al-Li based alloys has been focused upon the Al-Li-Cu-Mg-Zr system. Through these efforts, the 8091 alloy has been identified as one of the compositions possessing the greatest potential for attaining high strength levels (1). It has also been shown that this alloy exhibits excellent superplasticity (1350% tensile elongation) at 520°C (2). A commercial application combining these two properties could be of significant value.

The strengthening in the 8091 alloy can be attributed to the co-precipitation of the  $\delta'$  ( $Al_3Li$ ) and S ( $Al_2CuMg$ ) phases during aging (3). Zr has been added as a grain refining and recrystallization inhibiting element. The metastable  $\delta'$  phase possesses a very low matrix-to-particle misfit and is known to form homogeneously throughout the matrix during the quenching process (4). Subsequent growth of the  $\delta'$  phase during artificial aging has been found to follow Lifshitz-Wagner kinetics (4). The advantage of the S phase is that it will prevent the severe strain localization, and resulting low ductility, that is inherent in many Al-Li based alloys (5). However, precipitation of the S phase is sluggish and will occur heterogeneously at dislocations and other defect sites (5). A post-SHT stretch has been employed to increase the density of defect sites and thus improve the precipitation of this phase (5). Such a thermo-mechanical treatment, however, would not be feasible in commercial applications where the complex shapes produced by superplastic forming preclude imposition of a pre-strain prior to aging. Unlike other variations within the Al-Li-Cu-Mg-Zr system, the 8091 alloy has been found to display a homogeneous dispersion of the S phase without post-SHT deformation (4). The objective of this work is to examine the aging characteristics of this alloy and identify heat treatment parameters which will maximize the strength.

## Experimental

The 8091 Al-Li alloy (Al-2.6 Li-1.90 Cu-0.55 Mg-0.12 Zr) utilized in this study was provided by British Alcan and Rockwell International Corporation. Specific processing methods, which resulted in a heavily rolled microstructure, were employed to impart superplastic characteristics in the material. An initial sheet gauge of 0.090 inches was used for both the as-rolled and superplastic deformation studies. However, the inherent thinning that accompanies superplastic forming resulted in some thinner gauge sections.

Initially, the strengthening kinetics of the as-rolled material were monitored entirely through Rockwell superficial hardness tests (45T scale) conducted according to ASTM Standard E 18. Hardness test specimens were taken from the sheet stock and SHT for 1.25 hours in air using a cylindrical tube furnace. Temperatures ranging from 515°C to 545°C were chosen in an effort to optimize the SHT temperature and the SHT was followed immediately by a quench into cold water. The rapid and detrimental oxidation behavior of this alloy has been established by previous researchers (6). Therefore, in order to unambiguously determine the bulk hardness of the material, the outer surface of each specimen was removed by grinding. Finally, the prepared hardness samples were aged either at ambient temperature or in a cylindrical tube furnace using the temperature range 20°C to 225°C.

Tensile tests were conducted only on selected tempers of the alloy which were based on hardness results. Heat treat practice identical to that used in the hardness study was employed on the tensile specimens. All tensile specimen dimensions were obtained from ASTM Standard B 557 (subsize specimen, 1.25 inch gage length) and tensile testing was conducted on an Instron Series 2150 servohydraulic testing system. The tensile specimens

were tested in the longitudinal (rolling) direction at a crosshead speed of 0.001 inches per second.

The superplastically formed (SPF) material was obtained from rectangular test pans, approximately 5 inches x 1.5 inches x 0.5 inches in size, which were produced by Rockwell International. A back pressure was employed during SPF to reduce cavitation. A two step strain rate path consisting of  $\dot{\epsilon} = 2 \times 10^{-3} + 2 \times 10^{-4}$  was used to form the pans to an effective strain state of 0.414. Hardness samples were cut from this material and heat treated in a manner similar to that of the as-rolled study. The aging response of the SPF material was examined only under selected parameters derived from the study of the as-rolled material. Metallographic specimens were electrolytically etched using Barker's etch and examined under polarized light.

### Results and Discussion

It was determined that the optimum SHT temperature for this alloy is 545°C which is in good agreement with the results of other researchers (7). The increased hardening response following SHT at 545°C is especially evident during natural aging as shown in Figure 1. Initially, a short incubation period of 8 hours was observed followed by a rapid hardening interval which lasted approximately to times of 300 hours, 500 hours, and 700 hours for the 545°C, 530°C, and 515°C SHT temperatures, respectively. The hardening rate diminished quickly after the initial rapid increase. The higher rate of hardening observed for the 545°C SHT may be the result of increased vacancy supersaturation coupled with increased solutionizing of the intermetallics (4). Several explanations have been proposed to account for the natural aging response in this alloy. A continued precipitation of  $\delta'$  at room temperature has been postulated based on evidence from small angle neutron scattering (SANS) (4). Others have suggested that the natural aging may arise from a precursor to the S phase (8), or perhaps that the reduced solubility of Li in the presence of increased Mg and Cu serves as an enhancement to the  $\delta'$  precipitation (4). Additional explanations include the formation of GP zones from the Al-Cu-Mg system and the formation of dislocation loops and helices from quenched-in vacancies (4).

The results of the artificial aging study, shown in part in Figure 1, revealed that the 165°C aging temperature results in a peak hardness value after 1000 hours of aging time. Highest initial hardening (i.e. within approximately 10 hours) was obtained after aging at 185°C, while 225°C resulted in a low peak hardness and rapid overaging.

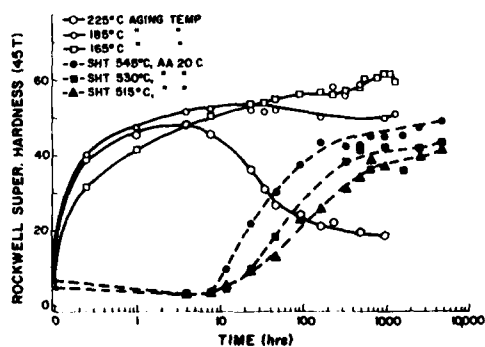


Figure 1. Artificial aging curves after SHT at 545°C, and natural aging curves after SHT at 515°C, 530°C, and 545°C.

The initial rapid hardening found for all three artificial aging temperatures can be related to the homogeneous precipitation of a high volume fraction of the  $\delta'$  phase (4), whereas further hardening is the result of co-precipitation of the  $\delta'$  and S phases. The S phase possesses an orthorhombic structure and is found to form as laths along the  $\langle 100 \rangle$  orientation of the Al matrix (5). Initial nucleation and growth of this phase occurs heterogeneously on low angle grain boundaries (8), and as the aging time and temperature are increased, a widespread homogeneous network of S phase has been observed between the heterogeneous sites (3). It has been proposed that the increased concentration of Cu and Mg found in this alloy results in a greater thermodynamic driving force for S phase precipitation (4), and a reflection of this is a more homogeneous dispersion of the S phase. The aging temperature used on this alloy must be limited to  $190^\circ\text{C}$  to avoid the formation of the equilibrium  $\delta$  phase (AlLi) at the expense of the metastable  $\delta'$  precipitate (8). The hardening characteristics corresponding to the  $225^\circ\text{C}$  aging temperature are an indication of the development of this phase.

The tensile test data corresponding to the hardness results in Figure 1 can be seen in Figure 2. The  $185^\circ\text{C}$  aging temperature resulted in slightly higher initial strength values (i.e. within approximately 2 hours). A transition occurred at 2 hours of aging time where the  $165^\circ\text{C}$  aging temperature resulted in moderately higher strength values. The naturally aged material displayed significantly lower strength values and the shape of these curves appeared to deviate somewhat from the hardness trends. This discrepancy may be explained from the slight seasonal changes in ambient temperature that occurred over the long 5000 hour aging interval. The percent elongation values for all the temperatures appear to decrease with increasing aging time and increasing aging temperature. Clearly, the hardness data indicates that higher strengths are possible by utilizing longer aging times although such times may exceed that which can be considered practical for commercial use. The strength and elongation data in Figure 2 correlates well with previously determined values (1).

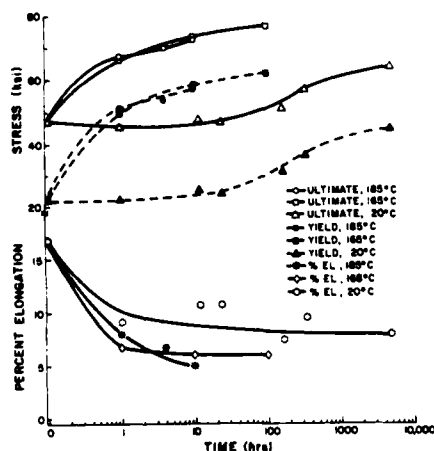


Figure 2. Ultimate strength, yield strength, and percent elongation values after SHT at  $545^\circ\text{C}$  and aging at  $20^\circ\text{C}$ ,  $165^\circ\text{C}$ , and  $185^\circ\text{C}$ .

Some preliminary hardness results for the SPF material aged at  $20^\circ\text{C}$ ,  $165^\circ\text{C}$ , and  $185^\circ\text{C}$  are shown in Figure 3. Apart from the earlier overaging displayed at  $185^\circ\text{C}$ , no

significant differences in aging response could be detected between the 185°C and 165°C aging temperatures. The natural aging behavior of the SPF material was found to be similar to the as-rolled response with the exception of slightly lower hardness values and a plateau at long aging times. In general, the initial hardness values obtained for the SPF material at all aging temperatures are lower than those found from the as-rolled investigation. This difference can be attributed, in part, to the dynamic recrystallization that is known to occur during superplastic deformation (9,10). Figure 4 shows the heavily-worked and partially recrystallized microstructures of the as-rolled and SPF materials, respectively. It is likely that the identity of the precipitating phases has not been altered by the superplastic deformation. However, additional work must be conducted in order to isolate the effects that superplastic deformation may have on the other strengthening mechanisms.

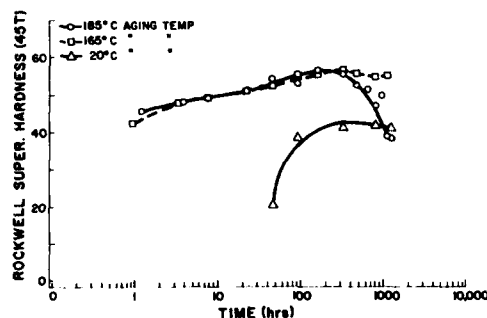


Figure 3. Aging behavior found in SPF 8091 Al-Li alloy at 20°C, 165°C, and 185°C after SHT at 545°C.

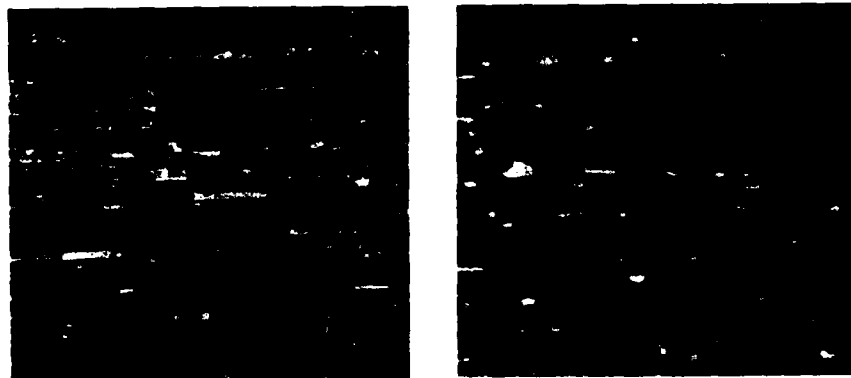


Figure 4. Polarized light optical micrographs of 8091 Al-Li alloy showing a). The as-rolled microstructure and b). The partially recrystallized microstructure found after SPF (longitudinal direction).

### Conclusions

1. The optimum SHT temperature for 8091 Al-Li alloy is 545°C.
2. The 8091 Al-Li alloy is heat treatable to high strength levels without the use of post-SHT strains.
3. Based on preliminary hardness results, superplastically deformed 8091 Al-Li alloy appears to be heat treatable to moderately high strength levels.

### Acknowledgements

Work was conducted through a contract from the Air Force Flight Dynamics Laboratory and Rockwell International Corporation, NAAO, under the direction of Rick Rolfe and Gardner Martin respectively.

### References

1. C.J. Peel, B. Evans, and D. McDarmaid, Aluminum-Lithium Alloys III, p. 26, C. Baker, P.J. Gregson, S.J. Harris and C.J. Peel eds., The Institute of Metals, London, (1986).
2. G. Martin, Rockwell International Corp., NAAO. Private Communication.
2. P.J. Gregson, C.J. Peel, and B. Evans, Aluminum-Lithium Alloys III, p. 516, C. Baker, P.J. Gregson, S.J. Harris and C.J. Peel eds., The Institute of Metals, London, (1986).
4. H.M. Flower, P.J. Gregson, C.N.J. Tite and A. Makhopadhyay, Aluminum Alloys-Their Physical and Mechanical Properties, vol. 3, p. 743, E.A. Starke and T.H. Sanders eds., EMAS, (1986).
5. P.J. Gregson and H.M. Flower, *Acta Metall.*, 33, 527, (1985).
6. J.M. Papasian, G.G. Bott and P. Shaw, *Materials Sci. and Eng.*, 94, 219, (1987).
7. R.F. Ashton, D.S. Thompson, E.A. Starke Jr., and F.S. Lin, Aluminum-Lithium Alloys III, p. 66, C. Baker, P.J. Gregson, S.J. Harris and C.J. Peel eds., The Institute of Metals, London, (1986).
8. W.S. Miller, J. White and D.J. Lloyd, "The Physical Metallurgy of Al-Li-Cu-Mg-Zr Alloys 8090 and 8091" (Paper presented at the 4th International Aluminum-Lithium Conference, Paris, 10-12 June, 1987).
9. R. Grimes and W.S. Miller, Aluminum-Lithium Alloys II, p. 153, T.H. Sanders, Jr., and E.A. Starke, Jr., eds., The Metallurgical Society, Warrendale, PA, (1984).
10. R. Grimes, C. Baker, M.J. Stowell, and B.M. Watts, *Aluminum*, 51, 3, (1975).

# IMPROVEMENT IN THE SUPERPLASTICITY OF Ti-6Al-4V ALLOY BY HYDROGENATION

L. R. Zhao, S. Q. Zhang, and M. G. Yan

Institute of Aeronautical Materials, Beijing, China

## Abstract

This paper reports the analysis of the effects of hydrogen as a transient alloying element on the superplastic flow properties, strain rate sensitivity and flow activation energy of Ti-6Al-4V alloy. The testing temperature was chosen according to the beta-transus temperature which varies with hydrogen concentration to maintain the ratio of  $T_{sp}/T_\beta$  constant. Experimental results show that there is an obvious change in the superplastic flow properties as hydrogen concentration increases from 0.17wt% to 0.29wt%. A maximum strain rate sensitivity appears around the hydrogen concentration of 0.07wt%. Calculation results indicate that there comes a sharp drop in the flow activation energy when hydrogen concentration exceeds 0.2wt%, and the minimum activation energy corresponds to the hydrogen concentration of 0.35wt% at given stresses. The decohesion effect caused by hydrogen atoms is discussed to explain the experimental and calculating results.

Superplasticity and Superplastic Forming  
Edited by C.H. Hamilton and N.E. Paton  
The Minerals, Metals & Materials Society, 1988

### Introduction

In recent years a great interest was focused on the effects of hydrogen on the superplasticity of titanium alloys. Investigations showed that small amounts of hydrogen added in titanium alloys can notably reduce the high temperature flow stress at given deformation velocity(1), or increase the strain rate at applied stresses(2). It has been noticed that the earlier experiments were conducted at given unvaried temperatures. As we know the alpha and beta phase ratio is an important factor influencing the superplasticity of alpha and beta titanium alloys(3), and the phase ratio varies with hydrogen concentration for the beta-transus temperature decreases with the increase in hydrogen concentration(4). In earlier studies the hydrogenation induced improvements in superplasticity have been mainly attributed to the increase in the amount of beta phase at lower temperature. Unfortunately the variation in the phase ratio makes it difficult to understand the direct effects of hydrogen on the superplasticity of titanium alloys.

In our investigation the alpha and beta phase ratio was controlled approximately unvaried by maintaining  $T_{sp}/T_{\beta}$  constant. It is therefore possible to discuss the more direct effects of hydrogen on the superplasticity of titanium alloys. Both experiment and calculation were conducted to examine the improvements in the superplasticity of Ti-6Al-4V alloy induced by hydrogenation.

### Experimental

A rolled Ti-6Al-4V alloy was annealed at 900°C for 4 hours to obtain a stable microstructure. The mean grain sizes of alpha phase and beta phase are 6.84  $\mu$ m and 6.77  $\mu$ m respectively.

All the specimens were hydrogenated in different controlled mixture atmospheres of hydrogen and argon at 650°C, which resulted in saturated hydrogen concentrations from 0.07wt% to 0.53wt%.

The superplastic tests were performed using an Instron-1185 machine. A step-tensile velocity method was employed to obtain the basic phenomenological flow properties of these hydrogenated alloys. The testing temperatures were chosen according to the beta-transus temperature ( $T_{\beta}$ ) which varies with hydrogen concentration to maintain the ratio of  $T_{sp}/T_{\beta}$  constant, as showing in Figure 1. In this way an approximately unvaried phase ratio of  $V_{\alpha}/V_{\beta}$  was obtained. The experimental data are listed in table I.

Table I. Experimental Data

Hydrogen concentration H (wt%)		$T_{\beta}$ (°C)	$T_{sp}$ (°C)	Phase ratio $V_{\alpha}/V_{\beta}$ (%)
Before test	After test			( $T_{sp}/T_{\beta} = 0.89$ )
<0.005	<0.005	990	880	56
0.07	-----	920	820	-----
0.14	-----	875	780	-----
0.17	~ 0.17	860	765	65
0.29	~ 0.29	825	735	-----
0.40	-----	810	720	-----
0.53	-----	805	715	68

## Results and Analyses

### Flow properties

Figure 2 shows the variation in flow stress with strain rate at different hydrogen concentrations (different testing temperatures). All the experimental data were fitted by the exponent function:

$$\log \sigma = 1/[a+b \cdot \exp(-c \cdot \log \dot{\epsilon})] \quad (1)$$

It is clear that there exists an obvious change in the flow behavior as hydrogen concentration increases from 0.17wt% to 0.29wt%.

### Strain Rate Sensitivity

Figure 3 indicates the corresponding relation of strain rate sensitivity ( $m$ ) with strain rate, which comes from the definition:

$$m = \left( \frac{\partial \log \sigma}{\partial \log \dot{\epsilon}} \right)_{T,d} \quad (2)$$

At given flow stresses we obtained the variations of strain rate sensitivity with hydrogen concentration and fitted them by triple-spline function. Figure 4 gives the processing results. It can be noticed that there appears a maximum  $m$  value around the concentration of 0.07wt% at all given stresses even if the corresponding temperature has been lowered from 880 C to 820 C. All the strain rate sensitivities however drop sharp to minimum when hydrogen concentration exceeds 0.07wt% - 0.14wt%.

### Activation Energy

The semiempirical constitutive equation:

$$\dot{\epsilon} = \frac{AGb}{KT} \left( \frac{b}{d} \right)^p \left( \frac{\sigma}{G} \right)^n D_0 \exp\left(-\frac{Q}{RT}\right) \quad (3)$$

was employed to calculate the variation of activation energy ( $Q$ ) with hydrogen concentration (5). Where  $G$ -shear modulus,  $b$ -Burgers vector,  $K$ -Boltzmann constant,  $T$ -Kelvin temperature,  $d$ -grain size,  $\sigma$ -flow stress,  $D_0$ -frequency factor,  $R$ -gas constant,  $A$ -dimensionless constant,  $p$ -grain size index, and  $n$ -flow stress index. Here

$$n = 1/m^* \quad (4)$$

and we can notice that if the variations in the parameters of  $m^*$ ,  $p$ , and  $Q$  with strain rate are neglected:

$$\left( \frac{\partial m^*}{\partial \log \dot{\epsilon}} \right)_{T,d} = 0, \quad \left( \frac{\partial p}{\partial \log \dot{\epsilon}} \right)_{T,d} = 0, \quad \left( \frac{\partial Q}{\partial \log \dot{\epsilon}} \right)_{T,d} = 0 \quad (5)$$

we will have

$$m^* = m = \left( \frac{\partial \log \sigma}{\partial \log \dot{\epsilon}} \right)_{T,d} \quad (6)$$

Experimental results indicate that at constant ratio of  $T_{sp}/T$  as well as at given flow stress and grain size, there exist following relations:

$$T_{sp} = T_{sp}(H), \quad m = m(H), \quad \dot{\epsilon} = \dot{\epsilon}(H), \quad G = G(H) \quad (7)$$

where  $H$  represents hydrogen concentration. These relations are shown in Figure 1 and Figure 4 - Figure 6 respectively. All the experimental data were fitted by exponent function ( $T_{sp} - H$ ), triple-spline function ( $m - H$ ,  $\log G -$



- H), and linear function(log G - H).

According to equation(3), it is easy to induce the partial differential equation:

$$\left(\frac{\partial Q}{\partial H}\right)_{T_{sp}/T_{\beta}, \sigma, d} = \frac{RT_{sp}}{\log e} \left[ \left(\frac{Q}{RT} - 1\right) \left(\frac{\partial \log T_{sp}}{\partial H}\right)_{T_{sp}/T_{\beta}} + \left(1 - \frac{1}{m}\right) \left(\frac{\partial \log G}{\partial H}\right)_{T_{sp}/T_{\beta}} + \frac{\log(G/\sigma)}{m} \left(\frac{\partial m}{\partial H}\right)_{T_{sp}/T_{\beta}, \sigma, d} - \left(\frac{\partial \log \dot{\epsilon}}{\partial H}\right)_{T_{sp}/T_{\beta}, \sigma, d} \right], \quad (8)$$

here we have taken the approximations:

$$m^* = m, \quad \left(\frac{\partial P}{\partial H}\right)_{T_{sp}/T_{\beta}, \sigma, d} = 0. \quad (9)$$

Substituting all the fitted results into equation(8), we can obtain a complex partial differential equation:

$$\left(\frac{\partial Q}{\partial H}\right)_{T_{sp}/T_{\beta}, \sigma, d} = F(H, Q). \quad (10)$$

The Runge-Kutta numerical method was used to solve this differential equation. We have chosen  $Q_0 = 189$  KJ/mol at  $H < 0.005\text{wt}\%$ (6).

Figure 7 and Figure 8 show the calculation results at different flow stress levels. The most notable characteristic is that there is a sharp drop in the activation energy as hydrogen concentration exceeds 0.2wt%, following which there comes a minimum value at the hydrogen concentration of 0.35wt%. Q/T shows the same characteristic in spite of the lowering in temperature.

#### Discussion

It has been noticed that titanium is one of the transition elements. A decohesion effect could be induced by the filling of hydrogen's electron in the 3d electron orbit of titanium atoms(7,8). Such effect would dominate the high temperature superplastic deformation because the elastic distortion caused by the solute atoms of hydrogen is much smaller at high temperature than at ambient temperature.

Experimental results show that small amounts of hydrogen can improve strain rate sensitivity. This improvement could be mainly attributed to the promotion of interface diffusion caused by this decohesion effect, which as a result may induce a more effective interface sliding. As the hydrogen concentration exceeds 0.2wt%, an overall decohesion effect would cause a sharp drop in flow activation energy until to a minimum value at 0.35wt%. Correspondingly, much more lattice dislocations may be activated inside grains dominating the superplastic deformation, which results in an obvious decrease in the strain rate sensitivity as well as a remarkable change in the flow properties. More serious interactions between dislocations and between dislocation and hydrogen atoms would again cause the increase in flow activation energy beyond the hydrogen concentration of 0.35wt%.

The influence of stress levels on the variations in m and Q with hydrogen concentration implies that the effects of hydrogen on the superplasticity of Ti-6Al-4V alloy may be related to the dominating deformation mechanism. Further works are proceeding to investigate the influence of grain size index (p) as well as the crystal defects variations.

#### Conclusions

1. There is an obvious change in the superplastic flow properties of Ti-6Al-4V alloy as hydrogen concentration increases from 0.17wt% to 0.29wt%.

2. A maximum strain rate sensitivity appears around the hydrogen concentration of 0.07wt% at the constant ratio of  $T_{sp}/T_p=0.89$  and at all given flow stresses.
3. There comes a sharp drop in the flow activation energy when hydrogen concentration exceeds 0.2wt%. The minimum activation energy values correspond to the hydrogen concentration of 0.35wt% at given stress levels.

#### Acknowledgement

We would like to acknowledge all the great helps from senior specialist Yanwen Wang and Mrs. Yuelong Huang working in the Beijing Institute of Electric and Mechanical Engineering.

#### References

1. M. Birla and V. Depierre, "A Test Method for Evaluation of Metal Powders" (Report AFML/TR-75-171, Air Force Materials Laboratory, 1975).
2. R. J. Lederich, S. M. L. Sastry, and J. E. O'Neal, Advanced Processing Methods for Titanium (New York, NY: The Metallurgical Society of AIME, 1982), 115.
3. C. H. Hamilton, A. K. Ghosh, and M. M. Mahoney, Advanced Processing Methods for Titanium (New York, NY: The Metallurgical Society of AIME, 1982), 129.
4. W. R. Kerr et al., Titanium'80; Science and Technology, vol.4 (New York, NY: The Metallurgical Society of AIME, 1980), 2477.
5. T. G. Langdon, Superplastic Forming of Structural Alloys (New York, NY: The Metallurgical Society of AIME, 1982), 27.
6. C. H. Hamilton, Superplasticity (15, Quai Anatole France, PA: Centre National de la Recherche Scientifique, 1985), 14.1
7. A. R. Troiano, "The Role of Hydrogen and Other Interstitial in The Mechanical Behavior of Metals, " Trans. A.S.M., 53(1960) 54.
8. R. A. Oriani and P. H. Josephic, "Hydrogen-Enhanced Load Relaxation in a Deformed Medium-Carbon Steel," Acta Metall., 26(1979) 997-1005.

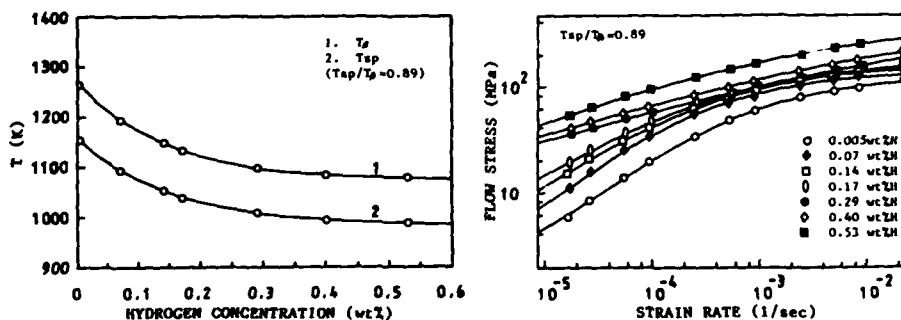


Figure 2 - Relations of flow stress with strain rate at different hydrogen concentrations.

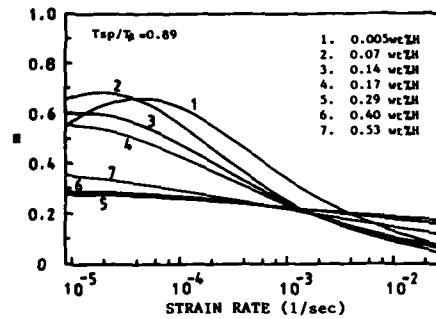


Figure 3 - Relations of strain rate sensitivity with strain rate at different hydrogen concentrations.

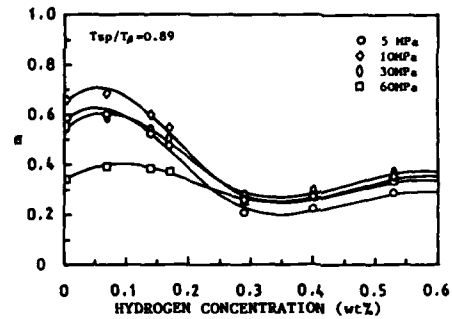


Figure 4 - Variations in strain rate sensitivity with hydrogen concentration at given flow stresses.

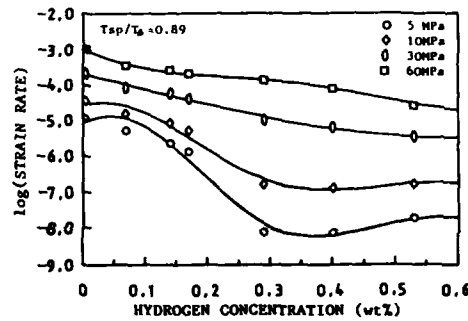


Figure 5 - Variations in strain rate with hydrogen concentration at given flow stresses.

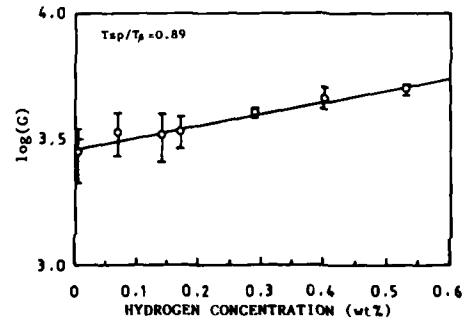


Figure 6 - Relation of shear modulus with hydrogen concentration.

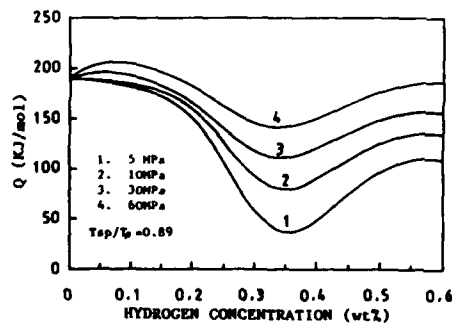


Figure 7 - Variations in activation energy with hydrogen concentration at given flow stresses.

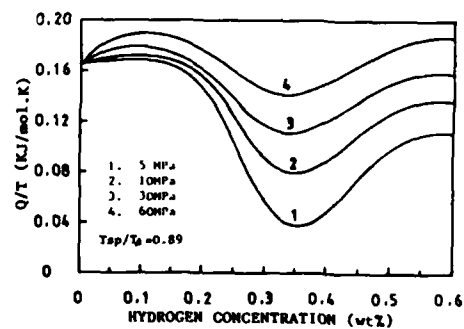


Figure 8 - Variations in (activation energy/testing temperature) with hydrogen concentration at given flow stresses.

A STUDY ON SUPERPLASTICITY OF COMMERCIAL 2024Al ALLOY

† Hailing Huang, ‡ Qingling Wu and † Jin Hua

† Changchun Institute of Optics & Fine Mechanics  
Academia Sinica,  
Changchun, China

‡ Department of Forming Engineering,  
Northeast University of Technology  
Shenyang, China

Abstract

The methods of grain refinement for 2024Al alloy and its superplastic behaviour have been investigated. The grain size of 2024Al alloy can be produced in 5-8  $\mu\text{m}$  by control of recrystallization. The maximum elongation of 485 % and the average about 400 % for the fine-grained 2024Al alloy can be obtained at the temperature 480°C with the strain-rate  $4.17 \times 10^{-4} \text{sec}^{-1}$  and the strain-rate sensitivity index  $m$  is upto 0.4-0.6. The sheets of fine grained 2024Al alloy can be bulged into hemispheres under the low pressure. The study indicates that the fine-grained 2024Al alloy is also a kind of material sensitive to the existence of cavitation, but the refinement of the grain can make superplastic strain well-distributed and cavitation fine, well-distributed. So the refinement of the grains is helpful to restrain the formation of any neck or internal neck during the superplastic deformation, and to improve the superplasticity of the alloy.

### Introduction

Aluminium alloys which have been thermomechanically processed to develop a fine microstructure show considerable superplasticity. The addition of small quantities of alloying elements which serve to prevent grain growth by pinning grain boundaries either with precipitates, has been applied to a range of commercial aluminium alloys, such as Zr additions in the alloys have been utilized to produce a small, stable grain size (1). However, Zr additions in the alloys bring a lot of problems in industrial application. It is notable to develop superplasticity in high strength 7000 aluminium alloys by thermomechanical processing schedule (2), and to expect to develop superplasticity in conventional 2000 aluminium alloys.

2024 aluminium alloy is widely developed commercially because of its interesting mechanical properties. If it is capable to develop superplastic properties, it will be used for forming structural aerospace components and substantial benefits in terms of weight and cost savings have been demonstrated.

The aim of the present work is to show that it is possible to develop superplasticity in a conventional 2024Al alloy (nominal composition Al-4.6 pct Cu-1.6 pct Mg-0.5 pct Mn) using a conventional rolling and heat treatment system that promotes nucleation and limiting grain growth during recrystallization. In the present paper the role of grain size on the nucleation and growth of cavitation in 2024Al alloy will be examined.

### Experimental Details

The work was carried out on the aluminium alloy 2024Al bought from Northeast Light-Alloy Works of China in the form of 14 mm thick plate with composition

Element	Cu	Mg	Mn	Fe	Si	Zn	Ti	Al
Wt pct	4.62	1.61	0.52	0.28	0.20	0.2	0.05	balance

(Wt pct by spectrographic analysis)

Thermomechanical Processing Schedule. In order to obtain a fine grained microstructure the alloy was reduced by hot rolling at 440-400°C to 3-8 mm to produce a convenient thickness for subsequent cold rolling to 1.5 mm.

Tensile specimens were punched longitudinally from the rolled strip to a gage length of 10 mm and width 6 mm from a 1.5 mm thick sheet of 2024Al alloy.

Recrystallization into a fine-grained structure was carried out prior to the superplastic deformation. The thermomechanical processing schedule is shown in Fig. 1.

Uniaxial tensile testing was carried out at constant cross-head velocity at a variety of initial strain-rates in the temperature range 430 to 490°C.

Circular membranes of 2024Al alloy were free-bulged into hemispheres under low gas pressure in the temperature 480°C.

## Results and Discussion

### Fine-Grained Structure

By the controlled recrystallization processing route fine equiaxed grain structure was achieved in 2024Al alloy. The fine grain size of the alloy is about 5-8  $\mu\text{m}$  as shown in Fig.2. It meets the main microstructural requirements for the appearance of superplasticity of materials. One of the microstructural requirements is that the grain size should be less than 10  $\mu\text{m}$ .

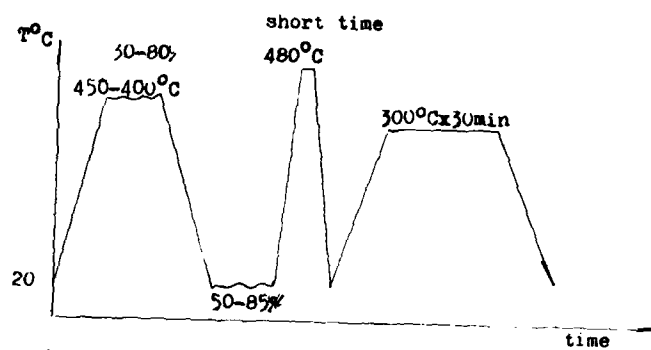


Figure 1 - Thermomechanical processing schedule

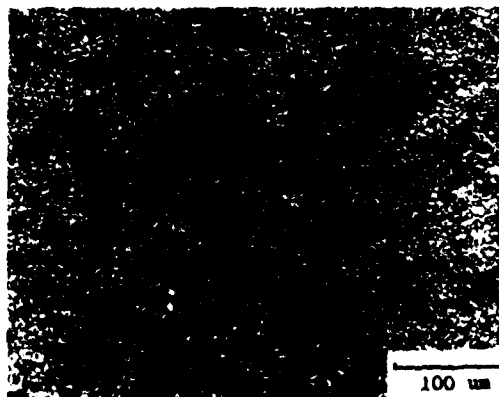


Figure 2 -The fine-grained structure of 2024Al alloy by control of recrystallization  
The size of the grains is about 5-8 $\mu\text{m}$   
( $\times 200$ )

The result proves that it is able to produce fine-grain structure by control of recrystallization process. The alloy was rapidly heated upto high temperature, held a short time then rapidly cooled down. It is the controlled recrystallization processing route by promoting nucleation and limiting grain growth. The alloy held at the temperature 300-350°C for a longer time in order to make fine-grained structure stable.

#### Mechanical Properties

The specimens were first elongated 30 pct at one initial strain rate and then subjected to change rate testing, enabling values of  $m$  to be determined and a  $\ln \sigma$  vs  $\ln \dot{\epsilon}$  ( $\ln$  stress vs  $\ln$  strain-rate) plot to be obtained. The  $\ln \sigma$  vs  $\ln \dot{\epsilon}$  curve of the material at the first 30 pct strain of testing is shown in Fig. 3, and conventional division into Region II and Region III is indicated. Region II is the superplastic regime and displays high strain-rate sensitivity,  $m \approx 0.4-0.6$ . It is shown that 2024Al alloy with fine-grained structure is of high ability of resistant local reduction. (See Fig.4.)

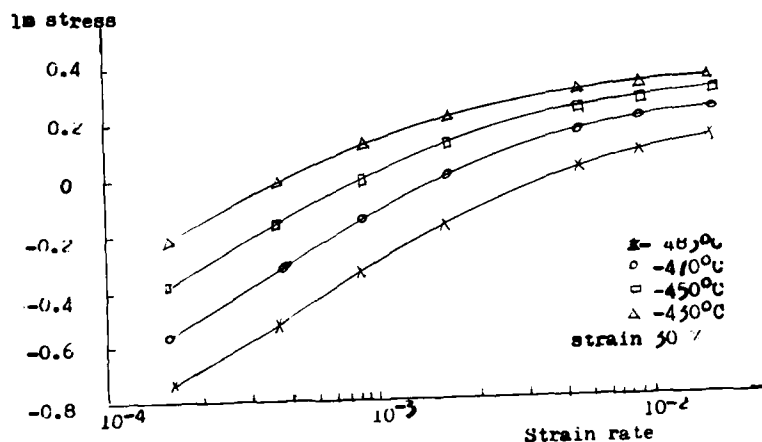


Figure 3 -  $\ln$  stress vs  $\ln$  strain-rate of 2024Al alloy

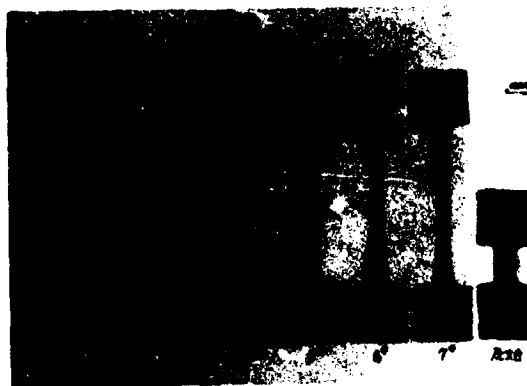


Figure 4 - Tensile test of 2024Al alloy without neck  
Average elongation is more than 400 %

Tensile test shows total elongations more than 300 pct and the maximum elongation of 485 pct was measured in the superplastic condition of 480°C and the strain-rate  $4.17 \times 10^{-4} \text{sec}^{-1}$ . Fig.4 indicates the tensile specimens after superplastic deformation. During the superplastic deformation, the specimens of refine-grained structure differed from that of the received condition in no neck forming. This phenomenon is in agreement with their strain-rate sensitivity  $m$  values, but it is not agreement with their unsatisfied superplastic elongations. There should be much higher superplastic elongations vs the high strain-rate sensitivity  $m$  values.

The reason may be that, when local reduction and neck forming are the main cause of materials damage during the superplastic deformation, the strain-rate sensitivity  $m$  values are in agreement with uniaxial elongations, while cavity role in local flowing,  $m$  values can not be provided quantitative characteristics.

The effect of the refine-grained and original structures on the cavity is shown in Fig.5 and Fig.6. The figures show clearly the beneficial effect of refine-grained structure on cavitation distributed random and fine during the superplastic deformation, while cavitation in original structure sample tended to be confined within the central region of the tensile specimen, in fact, this kind of locally distributed cavitation makes an internal neck in the specimen.

Circular membranes of fine-grained 2024Al alloy were free-bulged into hemispheres under low gas pressure without damage ( see Fig.7 ).



Figure - 4 Superplastic deformation of refine grained 2024Al alloy ( $T = 480^\circ\text{C}$ ,  $\dot{\epsilon}_0 = 8.53 \times 10^{-4} \text{sec}^{-1}$ ) Cavitation in the middle of specimens is fine and well-distribute (strain 385%)





Figure 6 - Superplastic deformation of original 2024Al alloy(  $T = 480^{\circ}\text{C}$ ,  $\dot{\epsilon}_0 = 8.33 \times 10^{-4}\text{sec}$ ) Cavitation in the middle of specimens is tended to form local-distribute like an internal neck in the specimens (strain 150 %)



Figure 7 - Picture of free-bulging under low pressure in several minutes

#### Conclude

1. The grain size of 2024Al alloy can be achieved in 5-8  $\mu\text{m}$  by a conventional rolling and heat-treatment system.

2. It is feasible to develop superplasticity in a standard commercial 2024Al alloy following a simple thermomechanical processing route and yielding elongations more than 300 pct and maximum elongation 485 pct under the condition of superplastic deformation 480°C and initial strain-rate  $4.17 \times 10^{-4} \text{ sec}^{-1}$ .

3. 2024Al alloy after fine-grained treatment is of high strain rate sensitivity exponent  $m$  (higher than 0.4), and a low flow stress at the deformation temperature.

4. The main limitation to the superplasticity of 2024Al alloy and its industrial exploitation is cavity formation during the deformation which leads to premature failure of the alloy during the superplastic deformation.

#### REFERENCES

- (1). B.M. Watts, M. J. Stowell, et al: Metal Sci., 6 (1976) 189.
- (2). C. H. Hamilton, C. C. Hampton and N. E. Paton, Intern. Symp. on Superplastic Forming of Structural Alloys, Met. Soc. AIME, San Diego, CA, (1982) 173-190.

**SPF METHODS  
AND  
DIFFUSION BONDING**

## DIFFUSION BONDING IN SUPERPLASTIC MATERIALS

John Pilling

Department of Metallurgical Engineering  
Michigan Technological University  
Houghton, MI 49931

### Abstract

Diffusion bonding of superplastic titanium alloys is now a well established technology. The extension of diffusion bonding to superplastic aluminium alloys has been limited by the tenacious surface oxide. However, bonding processes which rely of large deformations within the bond zone or a transient liquid phase to displace or fracture the thin alumina film have produced bonds with virtually parent metal strength. The bonds have been shown to be capable of surviving a superplastic forming operation. Nickel base superalloys, which can be rendered superplastic, have been successfully bonded and superplasticity formed. However, for nickel-base materials diffusion bonds are primarily formed between dissimilar materials and the development of Kirkendall porosity in the bond plane during elevated temperature service could be problematic.

Theoretical studies of the micromechanisms of diffusion bonding have, in the case of solid state bonding, reached a sufficient degree of refinement to define a viable process window. However, a corresponding evaluation of the kinetics of transient liquid phase bonding still remains in its infancy.

Superplasticity and Superplastic Forming  
Edited by C.H. Hamilton and N.E. Paton  
The Minerals, Metals & Materials Society, 1988

## Introduction

Diffusion bonding may best be defined as a joining process which involves no macroscopic distortion of the components being joined. Joining is achieved primarily by atomic transport at the mating interfaces which removes the bondline voids. Two types of joining are common, that which takes place entirely within the solid state, and that which relies on the isothermal melting and re-solidification of a thin transient liquid phase. To ensure sufficiently short process times, bonding generally takes place at high homologous temperatures, though the applied pressures must necessarily remain low in order to avoid macroscopic deformation. In the case of superplastic materials, the temperature at which bonding takes place generally corresponds to those where optimum superplasticity is exhibited in order that grain growth during bonding is minimized and the superplastic capabilities of the materials being joined are not lost.

In this paper both the theoretical and practical aspects of diffusion bonding are examined. Particular attention is given to superplastic titanium and aluminium alloys. However, the increasing interest in diffusion bonding dissimilar nickel-base alloys has prompted the inclusion of a section on nickel since many of the alloys being joined are capable of being rendered superplastic, Table 1.

## Bonding Mechanisms and Kinetics

When two surfaces, no matter how smooth, are placed together, contact only occurs at points distributed at random over those surfaces. When a load is subsequently applied the asperities separating the surfaces plastically deform and the contact area increases until it can support the applied load. If it is assumed that a chemical bond forms between the two surfaces when the atoms on those surfaces are within an atomic spacing of each other then the initial area fraction bonded is given by the ratio of the applied stress to the yield strength of the material at the bonding temperature. The bond zone thus consists of 'islands' of bonded material distributed randomly within a 'sea' of voids. During the remainder of the diffusion bonding process the bond zone voids are removed by any or all of several possible mechanisms.

The kinetics of the diffusion bonding process are, if a true chemical bond forms between the two surfaces when the atoms on those surfaces approach, given by the sum of the kinetics of each of the operative independent bonding mechanisms. The mechanisms include diffusion, time dependent plastic collapse and vapor phase transport.

During the initial stages of bonding the islands of contact expand laterally as the asperities collapse by power-law creep (this includes superplastic flow) [1,2]. As the asperities collapse, the free surface approach and thus both the area of interfacial contact and the volume of the interfacial voids is reduced. Derby and Wallach [3,4] have shown that, for all but the most smooth surface finishes, power-law creep (or superplastic flow) is the dominant 'bonding' mechanism. The rate at which the interfacial voids are removed from the bond zone by time dependent plastic flow is dependent on the geometry of the voids but independent of their initial dimensions. The rate of increase in the area fraction of bonded interface,  $f$ , decreases rapidly as  $f$  increases to 0.2 and thereafter remains approximately constant until  $f \approx 0.9$ . The rate of change of the area fraction bonded with time,  $df/dt$ , for an upright cylindrical void closing under isostatic compression is given by

$$\frac{df}{dt} = 2\dot{\epsilon}_r f \quad (1)$$

where  $\dot{\epsilon}_r$  is the radial strain rate in the wall of the cylinder, itself a rather complex function of  $f$  and the applied pressure,  $P$  [5]. The increase in the value of  $f$  in equation (1) during bonding is offset by a reduction in  $\dot{\epsilon}_r$  as the walls of the cylinder thicken and the axial stress compressing the cylinder decreases.

As the voids become smaller, diffusive mass transfer becomes more significant. Void closure can result from the diffusive transfer of material from the bond zone interface to the neck or free surfaces of the void. The flux of atoms is driven by the difference in chemical potential between the nominally stress free void surface and the bond interface which experiences a compressive stress as a result of the applied pressure. Mass transfer can occur via both the interface and the bulk lattice. The bonded area fraction can also increase as a consequence of surface diffusion and vapor phase transport. Again the difference in chemical potential between the low curvature surfaces remote from the bond interface and the high surface curvatures in the neck regions drive both the surface diffusion and vapor phase transport processes. While the transfer of material around the surface of the void cannot change the volume of the void, the cross sectional area of the void in the bond plane decreases as the void spheroidise. The change in the value of  $f$  due to surface diffusion then affects the other mass transfer processes which actually reduce the interfacial void volume. The rate of change of bonded area with time due to diffusive mass transfer under an isostatic pressure,  $P$ , is given by

$$\frac{df}{dt} = \frac{4D_{gb}\delta\Omega P}{\lambda^2 h_o K T} \frac{1}{\sqrt{(1-f)}} \left[ \frac{1}{\ln(1/(1-f))} - f/2 \right] \quad (2)$$

where  $D_{gb}$  is the grain boundary diffusion coefficient,  $\Omega$ , the atomic volume,  $\lambda$ , the wavelength and  $h_o$ , the amplitude of the surface roughness. Since each of the mechanisms operates independently of the others the overall kinetics of the bonding process are given by the sum of the rates of the individual mechanisms. Thus, given the relevant material properties data, the bonding time,  $t$ , can be obtained from

$$t = \int_{P/\sigma_y}^1 \frac{1}{\sum_i (df/dt)_i} df \quad (3)$$

In deriving the rate equations for each process [1-6] it is important to define the geometry of the interfacial voids and the applied stress state in such a way that there is no discontinuity in the rate equations when the voids become isolated from each other. Moreover, it is important to recognize that the surfaces being joined have a complex topography. Often a short wavelength, low amplitude roughness is superimposed on a much longer wavelength, low aspect ratio, waviness and it is normally the latter aspect of the surface geometry that determines the overall bonding time, Figure 1.

Given the uncertainties in the material property data (a factor of 2 to 5 for most values) a truly realistic mode of interfacial asperity collapse is not normally justified. Furthermore, the times for bonding that are predicted by the models should not be regarded as absolute, but rather as a guide to the "process window" in which experimentation should

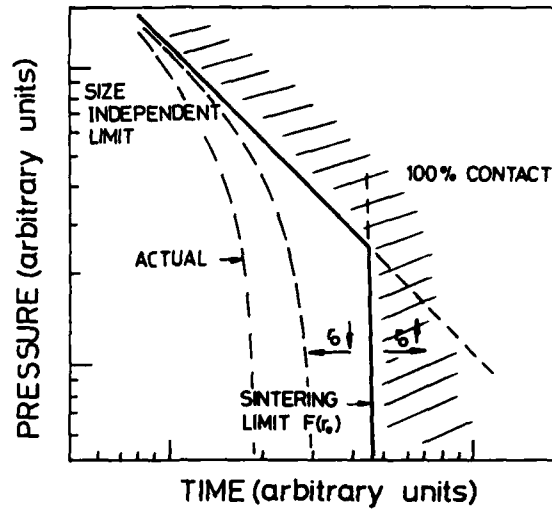


Fig. 1. The variation of bonding time with pressure (schematic) for bonding under isostatic compression. Two limiting cases are apparent: a size independent limit arising from time dependent plastic collapse and a sintering limit, the location of which depends on the magnitude of the surface roughness.

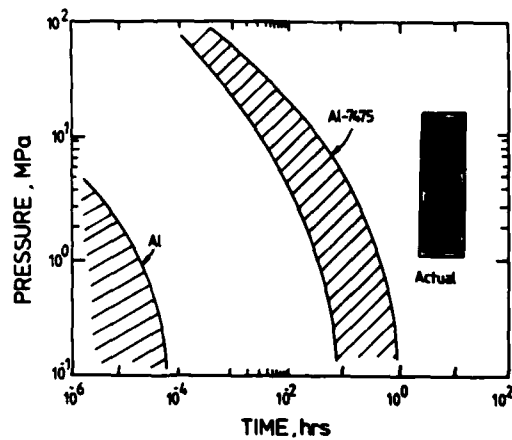


Fig. 2. The calculated variation of bonding time with applied pressure for Al and Al-7475. The bands contain all the solutions for surface finishes in the range 1 to  $20\mu\text{m}$ , applied pressures of 1 to 10 MPa at temperatures within the superplastic regime, 500 to  $520^\circ\text{C}$ . The actual conditions used to develop solid state bonds in Al-7475 are also shown.

be carried out, Figure 2. By isolating the time frame in which bonding would be expected to occur under a given set of bonding conditions (pressure, temperature, surface finish and material) actual experimentation and destructive evaluation of the bond properties can be minimized.

The process of transient liquid phase bonding, while often a practical success, has received little attention in terms of defining the micromechanisms, evaluating their kinetics and hence determining the rate controlling process(es).

#### Testing of Diffusion Bonds

The quality of diffusion bonds can only be reliably assessed by comparing the fracture characteristics of the bond with those of the parent metal after a simulated bonding heat treatment cycle. Nondestructive evaluation of the bond quality is presently incapable of resolving bond line microvoids ( $d < 5\mu\text{m}$ ) since the wavelength of the sound wave ( $\sim 200\mu\text{m}$ ) is much greater than the defect size and, in thin sheets, the transit times are extremely short. More recently, improvements in signal processing have enabled some headway to be made in detecting disbonds in which the two surfaces are often in intimate contact [7]. Once the conditions required to produce a bond of acceptable quality have been determined by destructive testing, strict process control is normally employed to ensure reproducibility of the bond properties. Process control is often supplemented by the proof testing of lugs which have been designed onto the component and which are removed from it after the bonding cycle is complete [8].

A number of mechanical tests have been devised to assess the quality of diffusion bonds. In the case of 'massive' bonds, conventional tensile, rotating bend fatigue and impact test pieces can be readily fabricated and the fracture strength compared with that of the parent material. In practice, parent metal tensile strengths are often achieved in bonds with more than 85% interfacial contact while parent metal fatigue endurance normally requires a complete absence of interfacial microvoids. However, the most discriminating test of bond quality is measured by impact testing, with poor bonds that show complete interfacial contact exhibiting low impact strengths.

Unfortunately, the majority of diffusion bonds are formed between sheet materials and impact testing is inapplicable. In such cases the fracture strength of the joint is measured using a constrained lap shear test piece, though no standard geometry or dimensions exist. Similarly, the attainment of parent metal fracture strength is no guarantee that a high quality bond has been formed, nor that the bond will be capable of resisting peel during superplastic forming. It is this latter capability which might, perhaps, be the most discriminating test for evaluating diffusion bonds between thin sheets.

#### Diffusion Bonds in Superplastic Materials

##### Titanium Alloys

Titanium alloys such as Ti-6Al-4V (IMI 318), Ti-6Al-2Sn-4Zr-2Mo and Ti-4Al-4Mo-2Sn-0.5Si (IMI 550) are readily bonded at temperatures between 880 and 940°C with applied pressures of 0.6 to 2MPa for process times up to 3hrs. The temperatures and pressures used for bonding normally correspond to the conditions under which optimum superplasticity is observed, Table I. In general, as the bonding temperature and time are increased, the integrity of the bonds formed increases. However, excessive temperatures and long process times can lead to grain growth during the bonding cycle



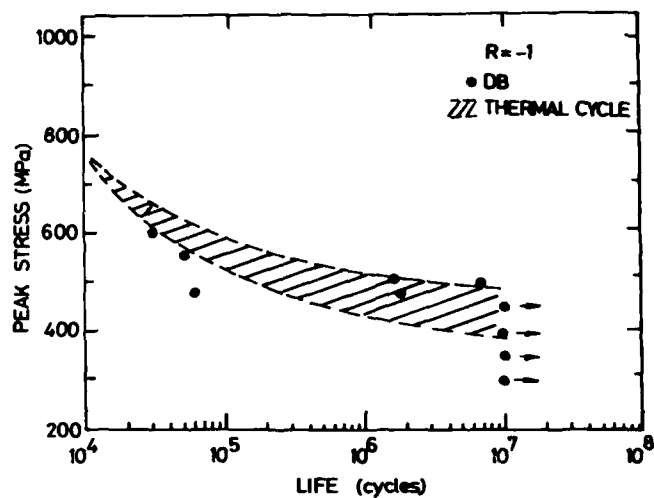


Fig. 3. Fatigue properties of Ti-6Al-4V after bonding for 2 hours at 950°C under an applied pressure of 0.69 MPa [16].

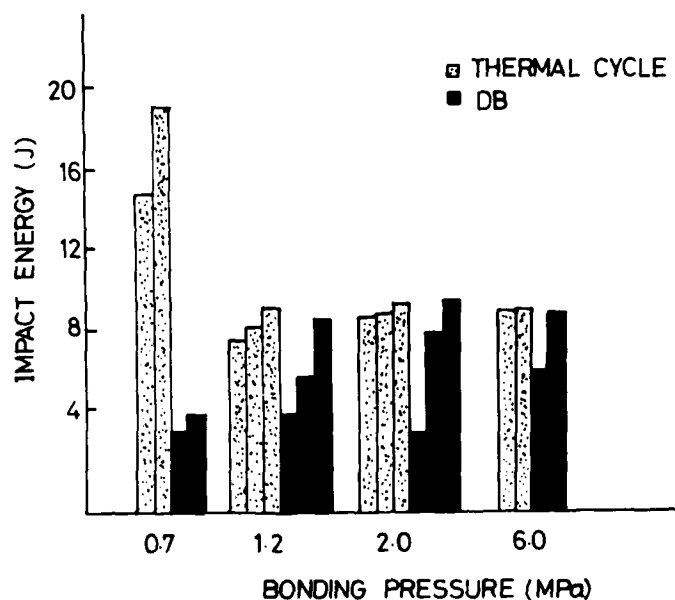


Fig. 4. Impact strength of IMI 550 after bonding for 2 hours at 950°C under various applied pressures [16].

Table 1. Summary of conditions under which superplasticity is developed in commercial titanium, aluminium and nickel based alloys.

Alloy	Temperature °C	Strain Rate %/min	m	Elongation %	Ref.
Ti-6Al-4V (IMI 31P)	790 - 940	0.6 - 6	0.8	700 - 1400	[43-47]
Ti-6Al-2Sn-4Zr-2Mo	900	0.6 - 6	0.6 - 0.7	>500	[35]
Ti-4Al-4Mo-2Sn-0.5Si (IMI 550)	880 - 930	0.6 - 6	0.48 - 0.65	500 - 1200	[36, 37]
Al-6Cu-0.4Zr-0.2Mg (Supral 100)	420 - 480	3 - 24	0.4 - 0.55	800 - 1200	[34]
Al-6Cu-0.4Zr-0.3Mg-0.2Si -0.1Ge (Supral 220)	460	4 - 24	0.65	>1800	[38]
Al-5Mg-0.6Cu-0.7Mn-0.15Cr (Neopral)	480 - 530	6	0.45 - 0.7	700	[39]
Al-5.5Zn-2.5Mg-1.5Cu-0.2Cr (7475)	515	1.2 - 5	0.5 - 0.8	1200	[40]
Al-6.2Zn-2.5Mg-1.7Cu (7010)	520	0.18 - 0.5	0.65	>350	[41]
Al-2.5Li-1.2Cu-0.6Mg-0.1Zr (8090)	500 - 540	0.6 - 6	0.4 - 0.55	500 - 1000	[42]
Ni-10Cr-15Co-5Al-5Ti-3Mo (IN-100)	920 - 1050	2 - 50	0.5 - 0.65	>850	[25, 26]
Ni-16Cr-8Co-3W-3Al-3Ti (IN-738)	900	0.6 - 6	0.4	500	[31]
Ni-8Cr-9Co-9W-5Al-3Ta-1Hf (MAR M-247)	1050	-	0.63	>800	[32]
Ni-15Cr-5Al-4W-2Ti-2Ta-2Mo -1.1 Y <sub>2</sub> O <sub>3</sub> (MAR M-6000)	900 - 1000	60	-	150 - 310	[33]
Ni-19Cr-17Fe-5Nb-3Mo (IN-718)	1000	0.6	0.6	150 - 300	[30]

and a reduction in the subsequent superplastic formability of the alloys. The relative ease with which solid state diffusion bonds can be formed in titanium base alloys is reflected in the growing body of literature and its acceptance as a mainstream manufacturing technology [9-14].

The ease with which titanium can be bonded may be attributed to the ability of titanium to take into solution both its oxide and other surface contaminants, particularly carbon, when subjected to pressure at elevated temperature [15]. It has been found that parent metal fatigue strengths can be attained in titanium diffusion bonds [13], Figure 3, but that impact strengths are often less than those of the parent metal [16], Figure 4. The latter can be improved by heating the bond to the  $\beta$ -transus after bonding is complete allowing grain boundary migration and hence a disruption of the planar bond interface.

#### Aluminium Alloys

After titanium base alloys, the second most important group of superplastic materials are those based on aluminium, in particular Al-7475 and more recently Al-8091. Unfortunately, the tenacious surface oxide has limited the success of diffusion bonding in aluminium alloys (this becomes even worse when lithium is present) and hence the adoption of DR/SPF technology in these materials has been slow. However, studies have shown that 'solid state' diffusion bonds with fracture strengths in excess of those attained using polymeric adhesives can be realized and that two bonding processes have emerged. Firstly, those involving surface modification, notably the deposition of a silver coating on a nominally oxide free aluminium surface and secondly, the use of large scale deformation in the bond zone to fracture the tenacious layer of alumina on the aluminium surface.

Silver coated surfaces have been produced on clad Al-7010 [17,18], Al-2014 and Al-6082 [19], Al-5056, Al-5657 and Al-6351 [20]. In coating the aluminium surface with silver two objectives are thought to be attained; firstly, the protection of the aluminium from the formation of alumina and secondly the generation of an oxide ( $Ag_2O$ ) which is soluble under pressure at elevated temperature. The aluminium surface to be coated was first polished using 1  $\mu$ m diamond paste or finer then sputter cleaned in vacuum using argon ions. The silver coating is applied either by physical vapor deposition or by silver ion plating.

Bonding was generally carried out in vacuum at pressures ranging from 1.5 to 5 MPa at temperatures in the range 450 to 550°C for times up to 1 hour. For the clad Al-7010, bonding was carried out at 200 to 300°C using pressures of 130 to 140 MPa. In all cases, the bond shear fracture strength increased with an increase in the bonding temperature and the extent of deformation in the bond zone. Despite the large number of alloys and conditions investigated, bond shear fracture strengths in the range 50 to 80 MPa were usually obtained, Figure 5. Post-bonding heat treatment, usually to the T6, or equivalent, condition resulted in increased bond fracture strengths of 140 to 180 MPa.

Solid state bonding without the use of a protective coating has been restricted to two alloys, Supral 220 (a fine grain derivative of Al-2004) [21] and Al-7475 [22-24]. In both cases it was imperative that the fine grain size and hence superplastic properties of the parent metal be maintained during bonding. The bonding temperatures and times were therefore limited by the amount of grain growth that could be tolerated during the bonding cycle. Bonds which were fabricated under static compressive loading gave shear fracture strengths in the range 40 to 150

Table 2. Summary of the conditions under which solid state bonds have been achieved in aluminum base materials together with the bond fracture strengths. ( $\tau$ , shear;  $\sigma$ , tensile).

Material	Surface Finish	Coating	Temp °C	Pressure MPa	Time h	Strength MPa	Ref.
clad 7010	polished	Ag ion plated	220-300	130-140	4	74-80 ( $\tau$ )	[17,18]
Al	polished	Ag ion plated	500-550	1.5	<1	53-74 ( $\tau$ )	[19]
5056	polished	Ag vapor dep	450-550	2.5-5.0	<1	50-145 ( $\sigma$ )	[20]
7475	grit blasted	none	515-550	2-20	2-12	40-150 ( $\tau$ )	[24]
7475	ground	none	510	2.76	1	50-150 ( $\tau$ )	[22,23]
2004	grit blasted	none	460-490	1-5	4-6	55-105 ( $\tau$ )	[21]
7475	grit blasted	Zn vapor dep	515	5	5	40-110 ( $\tau$ )	[21]
7475	ground	Al-12Si foil	510	1.38	4	150 ( $\tau$ )	[23]

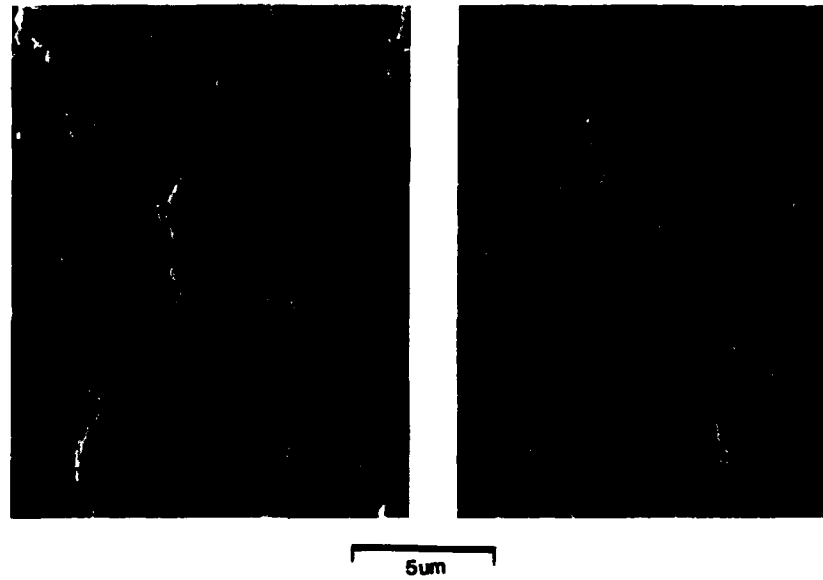


Fig. 5. Fracture surfaces of Al-7475 formed after 5 hours at 515°C under an applied pressure of 5MPa. a) poor bond with a fracture strength  $\tau_f$ ,  $<40 \text{ MPa}$  and b) a medium strength bond,  $70 < \tau_f < 100 \text{ MPa}$ .

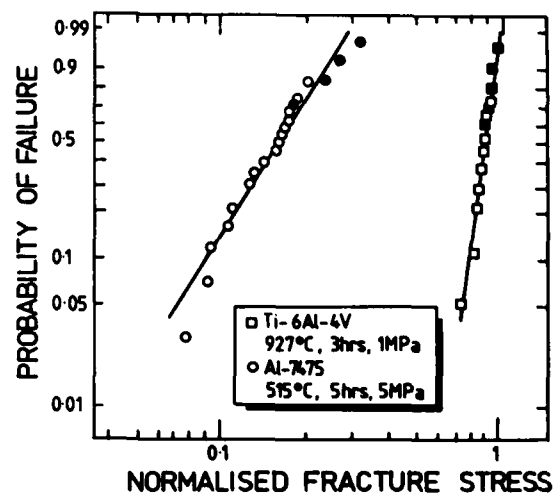


Fig. 6. Probability of fracture, as determined by Weibull Statistics, versus normalized fracture stress ( $\tau_f / \tau_{UTS}$ ) for Al-7475 and Ti-6Al-4V.

MPa. Again, the bond strength could be improved by the application of a post-bonding heat treatment with shear fracture strengths as high as 250 MPa being recorded.

The conditions under which solid state bonds were fabricated in aluminium alloys are summarized in Table 2 together with the reported fracture strengths.

One disquieting feature of solid state bonds formed between two aluminium surfaces, where reported, has been the wide variation in the measured fracture strength of bonds formed under nominally the same conditions. For example, Byun and Yavari [23], who examined 3 to 4 bonds per set of process variables recorded deviations of  $\pm 15\%$  while Pilling and Ridley [24], who examined between 16 and 20 bonds per set of process variables, observed deviations of  $+100\%$  to  $-60\%$  of the mean fracture strength. In the latter study, the variability of the measured bond fracture strength was analyzed using Weibull statistics: Weibull moduli of 4 to 6 were typical of the inherent variability of the bond fracture strength, Figure 6. (By way of comparison, repeated measurements of the yield strength of copper would give a Weibull modulus of  $\sim 40$ , while that of the modulus of rupture of a structural ceramic would be closer to 10).

Although not strictly diffusion bonding, attempts have been made to bond aluminium using a transient liquid phase. By interposing a melting point depressant between the two aluminium surfaces it is possible to form a liquid layer in the bond zone during the bonding cycle. The liquid phase forms directly by melting on heating or by isothermal melting at the bonding temperature as the concentration of the melting point depressant builds up in the surface layer of the parent metal. Application of a moderate pressure after the liquid phase has formed displaces the bulk of the liquid and oxide from the bond zone. During the remainder of the bonding cycle the concentration of the melting point depressant in the bond zone decreases as it diffuses further into the parent metal and the bond zone isothermally solidifies.

Only elements which are compatible with the base alloy are suitable for forming a transient liquid phase. In the case of aluminium the choice is limited to silver, magnesium, silicon and zinc (copper, although compatible, is unsuitable as it causes intergranular embrittlement of the aluminium). The melting point depressants are usually interposed between the aluminium surfaces as elemental coatings [21,23] or as aluminium alloy foils [23].

Fracture strengths similar to those obtained by solid state bonding have been recorded for bonds formed by the transient liquid phase approach, Table 2.

#### Nickel Alloys

After titanium and aluminium, nickel-base alloys are, perhaps, the next most important group of superplastic materials, see Table I. However, their use has been concentrated in massive rather than thin sheet components, applications where their low flow stress at elevated temperature has enabled them to be superplastically forged into complex shapes [25,26]. Diffusion bonding of nickel (super)alloys has recently received considerable attention particularly as a means for joining dissimilar alloys or superplastic, mechanically alloyed, single crystal or directionally solidified materials.

Nickel, like titanium, is capable of taking into solution its surface oxide when under pressure at elevated temperature, though other surface contaminants are not as readily soluble. Nickel base superalloys are normally bonded at temperatures just below the  $\gamma'$  solvus. Depending on the alloy, bonding can be carried out at temperatures between 1100°C and 1250°C with applied pressures in the range 1 to 20 MPa, conditions which corresponds to those where superplasticity can be exhibited. The mechanical strength of bonds formed between dissimilar materials can be degraded by a number of factors which would not normally be apparent when bonds are formed between like alloys, Figure 7. These are [27]:

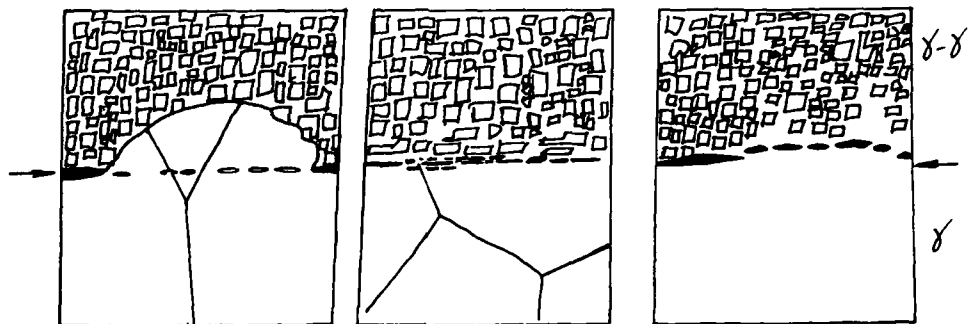


Fig. 7. Schematic illustration of the microstructural changes that accompany diffusion bonding of dissimilar Ni-base alloys.

- (1) Penetration of the single-phase  $\gamma$  microstructure into the two-phase  $\gamma$ - $\gamma'$  microstructure due to diffusion of the  $\gamma'$  forming elements into the single-phase alloy,
- (2) Formation of TiC particles or films at the interface as titanium reacts with adsorbed CO on the mating surfaces, and
- (3) Development of Kirkendall porosity on the aluminium rich side of the joint.

The latter factor would not normally be apparent after fabrication as the isostatic pressure applied to form the bond is often more than sufficient to counteract the necessity to form pores as a result of the flux imbalance between Ni and Al [28]. The diffusion rate of Al in Ni, and hence the flux of Al leaving the Al-rich side of the joint, is greater than that of Ni in Ni, and hence the counter-balancing flux of Ni arriving in the Al-rich side. However, during subsequent service at elevated temperatures porosity will develop rapidly in the absence of a confining pressure [28],

The formation of carbides within the bond zone can be avoided by treating the mating surfaces with  $\text{NH}_4\text{BF}_4$  which decomposes on heating, reacting with TiC to form volatile titanium fluoride and fluoro-carbon [29].

It has been demonstrated that nickel base alloys such as IN-718 can be diffusion bonded and superplastically formed [30]. Bonds were formed at ~1000°C and resulted in fracture strengths of 180 to 690 MPa.

#### Conclusions

Diffusion bonding is now an established joining technology. Its application in the DB-SPF process has enabled low weight - high stiffness cellular structures to be fabricated simply and cheaply using titanium-base alloys. Although it is possible to join superplastic aluminium alloys using both solid state and transient liquid phase techniques, the poor reproducibility of each of those processes has so far limited the introduction of DB-SPF of aluminium alloys. Both superplastic and non-superplastic nickel base alloys can be successfully diffusion bonded. However, where dissimilar materials are to be used at elevated temperatures, careful consideration needs to be given to composition to ensure that Kirkendall porosity does not become evident during service.

#### Acknowledgments

This work was supported, in part, by the National Science Foundation under grant DMR-8508720.

#### References

1. C. H. Hamilton, in "Titanium Science and Technology" (Ed. R. I. Jaffe and H. M. Burte), Plenum Press, NY, 1 (1973) 625.
2. G. Garmon, N. E. Paton and A. S. Argon, Metall. Trans. 6A (1975) 1269.
3. B. Derby and E. R. Wallach, Metal. Sci. 16 (1982) 49.
4. B. Derby and E. R. Wallach, Metal. Sci. 18 (1984) 417.
5. J. Pilling, Materl. Sci. and Eng., 100 (1988) 137.
6. J. Pilling, D. W. Livesey, J. B. Hawkyard and N. Ridley, Metal. Sci. 18 (1984) 117.
7. G. Tober and S. Elze, in "Advanced Joining of Metallic Materials", AGARD CP398 (1986) Ch. 11.
8. R. G. Wing and M. Newnham, in "Diffusion Bonding", (Ed. R. Pearce) Cranfield School of Industrial Science (1987) 159.
9. E. D. Wiesart and G. W. Stacher, in "Superplastic Forming of Structural Alloys", (Ed. C. H. Hamilton and N. E. Paton), TMS, Warrendale, PA (1982) 273.
10. J. R. Williamson, in "Superplastic Forming of Structural Alloys", (Ed. C. H. Hamilton and N. E. Paton), TMS, Warrendale, PA (1982) 291.
11. D. Stephen and S. J. Swadling, in "Advanced Joining of Metallic Materials", AGARD CP398 (1986) Ch. 7.
12. D. Stephen, in "Designing with Titanium", Institute of Metals, London (1986) 108.



13. T. S. Baker and P. G. Partridge, in "Titanium Science and Technology" (Ed. G. Lutjering, U. Zwicker and W. Bunk) DGM, Munich, 2 (1985) 861.
14. V. Alerja, in "Titanium Science and Technology", (Ed. G. Lutjering, U. Zwicker and W. Bunk) DGM, Munich, 2 (1985) 861.
15. Z. A. Munir, Weld. J. Res. Supp. 62 (1983) 333s.
16. T. S. Baker and P. G. Partridge, in "Diffusion Bonding", (Ed. R. Pearce) Cranfield School of Industrial Science (1987) 73.
17. J. Harvey, P. G. Partridge and A. M. Lurshay, Materl. Sci. and Eng. 79 (1986) 191.
18. J. Harvey, P. G. Partridge and C. L. Snooke, J. Materl. Sci. 20 (1985) 1009.
19. R. V. Sharples and I. A. Bucklow, Res. Rep. #307/1986, The Welding Institute, Cambridge, UK (1986).
20. A. E. Dray and E. R. Wallach, in "Diffusion Bonding", (Ed. R. Pearce) Cranfield School of Industrial Science (1987) 125.
21. N. Ridley, J. Pilling, A. Tekin and Z. X. Guo, in "Diffusion Bonding", (Ed. R. Pearce) Cranfield School of Industrial Science (1987) 129.
22. T. D. Byun and R. R. Vastava, "Welding, Bonding and Fastening" (Ed. J. D. Buckley and B. A. Stein) NASA Langley Research Centre, Hampton, VA (1984) 231.
23. T. D. Byun and P. Yavari, in "Superplasticity in Aerospace - Aluminium", (Ed. R. Pearce and L. Kelly) Cranfield, UK (1985) 285.
24. J. Pilling and N. Ridley, Materl. Sci. and Technol. 3 (1987) 353.
25. S. H. Reichman and J. W. Smythe, Int. J. Powder Met. 6 (1970) 65.
26. R. G. Menzies, J. W. Edington and G. J. Davies, Metal. Sci. 15 (1981) 210.
27. Y. Bienvenu, T. Massart, L. Van Wouw, M. Jeandin and A. Morrison, in "Diffusion Bonding" (Ed. R. Pearce) Cranfield School of Industrial Science (1987) 33.
28. H. Yoshizawa and B. J. Pletka, submitted to Scripta Met (1988).
29. T. Massart, Y. Bienvenu and A. Morrison, in "Diffusion Bonding" (Ed. R. Pearce) Cranfield School of Industrial Science (1987) 91.
30. W. T. Chandler, A. K. Ghosh and M. Mahoney, J. Spacecr. Rockets 21 (1984) 61.
31. D. A. Woodford, Metall. Trans. 7A (1976) 1244.
32. Y. G. Nakagawa, H. Yoshizawa and H. Terishima, Materl. Sci. and Technol. 2 (1986) 637.
33. J. K. Gregory, J. C. Gibeling and W. D. Nix, "Superplastic Forming of Structural Alloys" (Ed. C. H. Hamilton and N. E. Paton) TMS, Warrendale (1982) 361.

34. R. Grimes, C. Baker, M. J. Stowell and B. M. Watts, *Aluminium* 51 (1975) 11.
35. M. T. Cope, D. R. Everts and N. Ridley, *J. Materl. Sci.* 21 (1986) 4003.
36. J. Ma, R. Kent and C. Hammond, *J. Materl. Sci.* 21 (1986) 475.
37. D. S. McDermid, *Materl. Sci. and Eng.* 70 (1985) 123.
38. B. Geary, Ph.D. Thesis, University of Manchester (1985).
39. K. Ohori, H. Watanabe, M. Mukaiya and Y. Endo, *Al-aro* 7 (1984) 17.
40. C. C. Bampton, J. A. Wert and M. W. Mahoney, *Metall. Trans.* 13A (1982) 193.
41. P. G. Partridge and A. J. Shakeshaft, Technical Report 82117, Royal Aircraft Establishment, Farnborough (1982).
42. B. Geary, J. Pilling and N. Ridley, Unpublished Research, University of Manchester (1986).
43. D. Lee and W. A. Backofen, *Trans. TMS-AIME*, 239 (1966) 1034.
44. A. Arieli and A. Rosen, *Metall. Trans.* 8a (1977) 1591.
45. A. K. Ghosh and C. H. Hamilton, *Metall. Trans.* 10A (1979) 699.
46. A. K. Ghosh and C. H. Hamilton, *Metall. Trans.* 10A (1979) 241.
47. M. T. Cope and N. Ridley, *Materl. Sci. and Technol* 2 (1986) 140.

DIFFUSION BONDING AND SUPERPLASTIC FORMING,  
TWO COMPLEMENTARY MANUFACTURING TECHNIQUES

P.-J. Winkler

Messerschmitt-Bölkow-Blohm GmbH, Central Laboratories  
Munich, West Germany

Abstract

The importance of Diffusion Bonding (DB) has increased since the early 1970's in conjunction with the development of Superplastic Forming (SPF) as a sheet-manufacturing process. Superplastic Forming without Diffusion Bonding offers a limited spectrum of structural-part applications.

The combined use of Superplastic Forming and Diffusion Bonding (SPF/DB) is highly advantageous for the manufacture of a large number of secondary and primary aerospace parts. The growing demand for high-quality, high-cost materials, such as Ti-alloys and Al-Li-alloys, has increased the necessity of further developing this cost and weight-saving process.

This paper provides a review of the recent progress in Diffusion Bonding as a complementary process to Superplastic Forming.

This overview focusses on the major aerospace materials, i.e. Ti-alloys, Al-alloys and Metal Matrix Composites (MMC) and provides a comparison of the process-development status.

The influence of the main processing parameters such as temperature, pressure, time, atmosphere, and surface roughness on Diffusion Bonding quality will be discussed. Bond-strength values and possible joint defects are considered to be the most important criteria. The status of NDT techniques for detecting joint defects is also evaluated.

Finally, design concepts and exemplary SPF/DB parts are presented and the future prospects of this manufacturing process as well as further research needs are discussed.

Superplasticity and Superplastic Forming  
Edited by C.H. Hamilton and N.E. Paton  
The Minerals, Metals & Materials Society, 1988

### Introduction

Superplastic Forming and Diffusion Bonding are two modern manufacturing methods which are each used individually in the aerospace industry. The high development and application status of Superplastic Forming is impressively demonstrated at this conference.

Diffusion Bonding of Titanium alloys as a manufacturing process in its own right has been used since the sixties for producing integrally stiffened structural parts with better material utilization and lower machining costs. An impressive example of this manufacturing method, which is called "press bonding" is the wing carry-through section of the B1B bomber. [1]

This paper gives an overview of the potential of Diffusion Bonding as a complementary process to Superplastic Forming and provides a review of recent progress (SPF/DB). The growing demand for high-quality, high-cost materials such as Ti-alloys and Al-Li-alloys, has increased the necessity of further developing this cost and weight-saving process.

The term Diffusion Bonding is used in the widest sense and includes all methods for producing complex multi-sheet structural parts, e.g. solid-state diffusion bonding with minimum macroscopic deformation, liquid-phase joining methods and high-deformation/limited-diffusion processes, such as roll bonding.

This overview focusses on the major aerospace materials, i.e. Ti-alloys, Al-alloys and Metal Matrix Composites (MMC).

### Materials

A high fly-to-buy ratio is one of the main economic advantages of SPF/DB in comparison to conventional fabrication methods. Expensive materials like Ti-alloys and recently Ti-Aluminides, high-strength Al-alloys with special emphasis on Al-Li-alloys, exemplary Ni-base alloys for engine applications and MMC materials with an Aluminium and Titanium matrix are therefore especially suitable for manufacturing with this technique.

SPF/DB development of Ti-alloys has proceeded furthest. There are already many parts in production and in application. This is due to the fact that solid-state bonding of Ti-alloys can be realized with mechanical properties similar to the base material. Unfortunately, high-quality diffusion-bonded joints in other alloy systems, for example in Al-alloys, are much more difficult to achieve and require a detailed understanding of the bonding mechanism in the presence of stable oxide layers. Research and development activities worldwide concentrate on the realization of Diffusion Bonding of Al-alloys, because of the high application potential for multisheet Al-alloy structures. SPF/DB processing of MMC materials and of Ti-Aluminides is just at the beginning.

### Combined Benefits of Superplastic Forming and Diffusion Bonding

The benefits of Superplastic Forming concerning technical and economical aspects have been described frequently. The cost savings are mainly based on a high material utilization, reduced part count and resulting low assembly costs. The actual savings achieved are a function of component type, its equivalent conventional method of manufacture, and the material price. [2]

Typical characteristics of diffusion-bonded joints are listed in Fig. 1 [3,4]. They exhibit some distinct advantages in comparison to more conventional joining techniques like riveting, fusion welding and adhesive bonding.

1	Joint strengths approaching or equal to the parent metal.
2	Bonding involves minimum distortion and deformation and close dimensional control is possible.
3	Large area bonds are possible, with improved joint efficiency compared with conventional joining.
4	Thick and thin sections can be joined to each other.
5	Cast, wrought and sintered powder products and dissimilar metals can be joined. May be only choice for metal matrix composites.
6	Process time independent of bond area or numbers of components.
7	Machining costs may be reduced.
8	Corrosion resistance of parent metal or of selected interlayer combination. No fluxes are required.
9	More efficient design and a smaller buy to fly ratio may be possible.
10	May be combined with superplastic forming.

Figure 1 - Some characteristics of diffusion bonded joints [3,4]

The combined application of Superplastic Forming and Diffusion Bonding leads to an almost unlimited design flexibility, the cost savings in comparison to other fabrication methods reach values up to 60 %. These values have been substantiated by a wide range of design-to-cost studies conducted by aerospace companies throughout the Western world. A highly significant factor in respect of these cost savings is an SPF/DB-oriented design instead of reproducing the conventionally devised part.

The design flexibility resulting from the SPF/DB process is demonstrated in Fig. 2, in which one-, two-, three- and four-sheet structural parts are schematically presented [5]. The realization of such structures presumes either bonding before forming or forming before bonding.

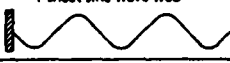
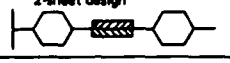

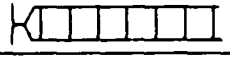
Design	Advantages	Disadvantages
 1-sheet sine wave web	simple tooling	bonding of flanges only on one side possible
 2-sheet design	completely symmetric little spacing	expensive tooling (two dies)
 3-sheet sandwich	nearly symmetric tooling relative simple	formation of grooves if skin is too thin
 4-sheet sandwich	symmetric no formation of grooves	more complicate processing

Figure 2 - Design concepts for SPF and SPF/DB parts [5]

### Multi-Sheet Design Concepts

The concurrent application of SPF/DB can be used either for local reinforcement of single-sheet structures or for production of multi-sheet parts. Subsequently I would like to demonstrate this separately for two-, three- and four-sheet applications.

#### Two-Sheet Structures

Thinning is an inevitable consequence of the SPF process and a limiting factor for the use of those parts. C.H. Hamilton discussed different possibilities in controlling and influencing the thinning process, as can be seen in Fig. 4 [6]. A further possibility to overcome thinning is the local reinforcement of superplastically formed parts as shown exemplarily in Fig. 3, where caps are diffusion-bonded on top of corrugated sheets [7].

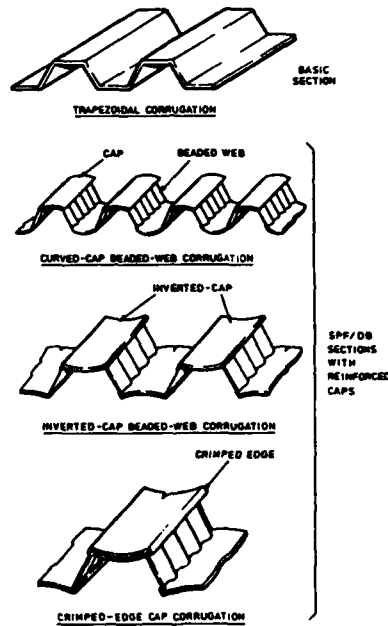


Figure 3 - Corrugated sheet structures made by SPF and SPF/DB [7]

The majority of two-sheet SPF/DB structures is integrally hat-stiffened parts. They usually are fabricated by Diffusion Bonding with subsequent blow forming. Typical examples of this type are door panels [8, 9]. In Fig. 4 a two-sheet SPF/DB version of a door panel is compared with a conventionally produced part made out of 16 single parts and 500 rivets [9]. The published cost savings are in the order of 50 % with weight savings of about 30 %. [8]

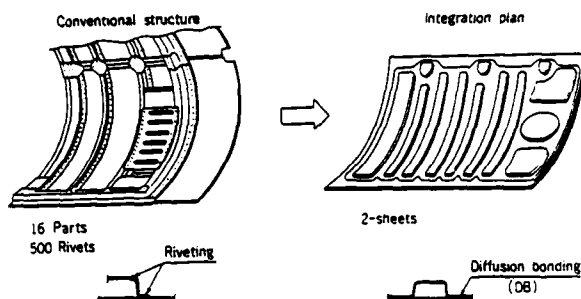


Figure 4 - Conventional structure and integrated plan for door panel using SPF/DB [9]

### Three- and four-sheet structures

Three- and four-sheet SPF/DB techniques permit designing and fabricating stiff and light sandwich structures. While the face sheets of such sandwiches are mostly flat or slightly curved, the core configurations can be varied in many different ways, tailored to the calculated design loads. [10,11]

Design and fabrication of sandwiches with one, two or more core sheets are possible, exemplary core patterns of different two-sheet core versions are shown in Fig. 5 [10]. Spot welding, roll-seam welding or diffusion bonding were used to join the two core sheets. They were then expanded by blow forming to the face sheets and subsequently diffusion bonded to form various types of cells.

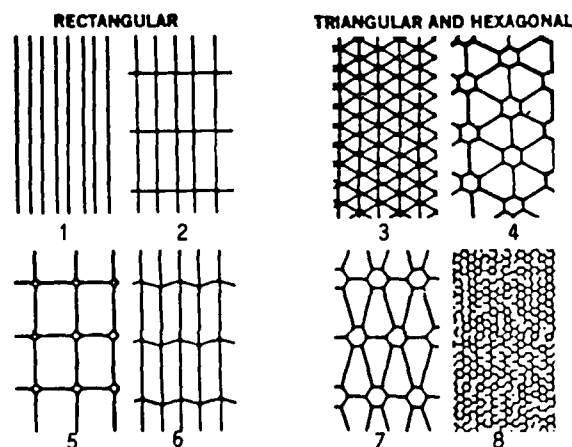


Figure 5 - Exemplary core patterns for producing SPF/DB sandwiches [10]

Core pattern 1 e.g. shows seam welds that form vertical walls with continuous longitudinal webs. This pattern can be used for high axial loading efficiency, when hardly any transverse loading or shear loading is the case. Core pattern 2 is used for typical aircraft structures when some transverse loading and/or shear loading occurs. Core pattern 4 is used if higher axial loadings, pressure loading (bending) and shear loading are the

case. The vertexes of the triangles are spot-welded to form hexagonal shapes. Finally, core pattern 7 was developed to sustain high axial loads with high shear loadings.

Fig. 6 shows four sandwich types for a supersonic wing concept [10]. Design-to-cost analysis indicated that the upper left rectangular core was the best compromise for weight and cost.

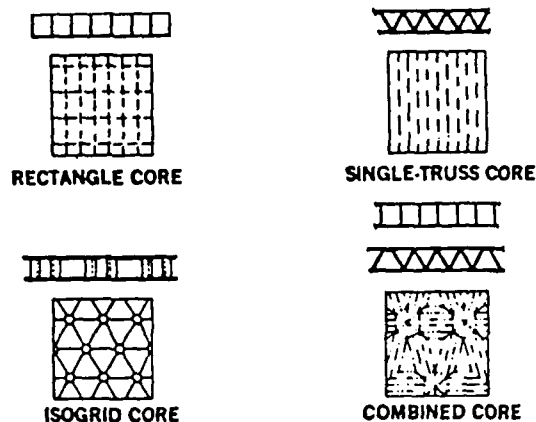


Figure 6 - SPF/DB candidate wing concepts [10]

#### Diffusion Bonding Techniques

There is a big confusion in literature concerning the terminology of Diffusion Bonding and related processes. Some of the terms which have been used synonymously with diffusion welding include diffusion bonding, solid-state bonding, pressure bonding, pressure welding, roll bonding, isostatic bonding, eutectic bonding, hot-press bonding, and so on [12].

The process of Diffusion Bonding is defined in British Standard 499 as "a joining process, wherein all of the faces to be bonded are held together by a pressure insufficient to cause readily detectable plastic flow, at a temperature below the melting point of any of the parts, the resulting solid state diffusion, with and without the formation of a liquid phase, causing bonding to occur. Additional heat may or may not be applied."

In this paper, which aims to illustrate the possibilities of the combined application of Superplastic Forming and Diffusion Bonding, the definition of Diffusion Bonding is extended to high-deformation/limited-diffusion processes according to W.A. Owczarski and D.F. Paulonis [12].

Thereby the methods which can be used to produce multi-sheet parts can be subdivided into:

- solid-state diffusion bonding with minimum macroscopic deformation
- liquid-phase joining methods
- high-deformation/limited-diffusion processes.



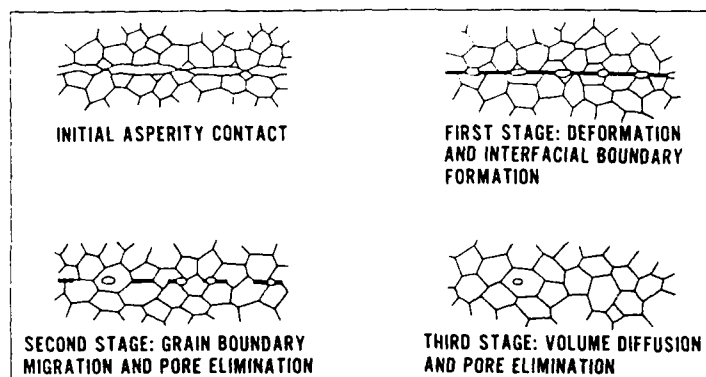


Figure 7 - Solid state bonding stages [12]

Diffusion bonding in the solid state involves the following stages (Fig. 7). The first stage after initial contacting is dominated by yield and creep deformation during which the mating-surface contact area grows to a large fraction of the joint area. During the second and third stages, deformation mechanisms became insignificant and diffusional processes take over as the primary means of grain boundary rearrangement, void elimination and final joint formation. In the second stage, grain boundary diffusion predominates, while in the third stage volume diffusion is most important [12]. Temperature is the most influential parameter since it determines a) the extent of contact area and hence the extent and size of voids to be eliminated during stage 1 and b) the rate of diffusion which governs void elimination during the second and third stages. Pressure is necessary only during the first stage of bonding to produce a large area of contact at the joining temperature.

Surface roughness has a strong influence on bonding quality. In general, rough initial surfaces adversely affect joining by impeding the first stage and by producing large voids. In bonding of materials with a stable oxide layer like Al-alloys, a rough initial surface can be beneficial, because the higher degree of deformation in stage 1 can promote local break up of oxide layers. A protective atmosphere is necessary during the contacting phase to prevent the formation or the growth of oxide layers. The use of non-melting intermediate materials can be of significant practical importance in solid-state bonding of similar and dissimilar materials, e.g. to reduce temperature and/or pressure required for bonding due to better contacting by using soft interlayer materials and/or to prevent the formation of unwanted brittle phases.

Liquid-phase joining processes generally use an interlayer with a melting point lower than that of the base material. The initial bond is made by heating the assembly to a temperature at which the interlayer and perhaps a small amount of the parent metals being joined at least partially melt. The assembly is then held at this or a somewhat lower temperature to raise the remelt temperature of the joint by diffusing critical elements away from the joint region.

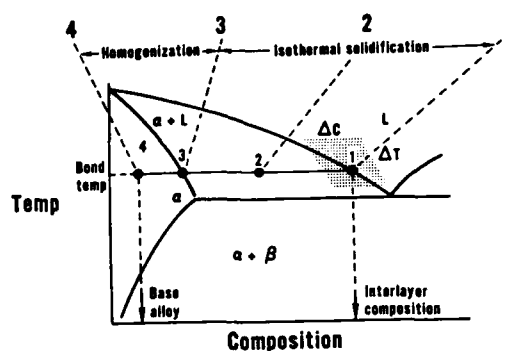


Figure 8 - Schematic illustration of diffusion brazing [13]

Diffusion brazing has been described by Owczarski using Fig. 8 [13]. An interlayer or coating with composition 1 is heated to the bonding temperature and melts. During isothermal annealing, diffusion changes the composition from 1 to 3 and the joint solidifies. Further diffusion results in a large dilution of the interlayer elements with minimal effect on the parent metal.

A variation of this method involves use of interlayers which in themselves will not melt at the bonding temperature but react with the material being joined to form a low melting-point eutectic. Liquid interfaces can also be used in bonding materials with stable oxide layers either to protect deoxidized surfaces from reoxidation or to attack the oxide layer by a chemical reaction.

High deformation/limited diffusion processes, such as, for example, roll bonding and explosive bonding, are mainly used to bond materials with a stable oxide layer or dissimilar materials which form brittle intermetallics during a high-temperature bonding process. High local deformations lead to a break up of the oxide layer and create true metallurgical bonds. The bond quality can be improved by subsequent heat treatment.

Roll bonding has been used as a joining method for many years in the aerospace industry in the cladding of high strength Al-alloys with pure Aluminium for corrosion protection. A high bonding quality all over the sheets is mandatory for this application.

Since about 10 years roll bonding has also been used to prepare multi-sheet structural parts [14]. In this case a selective bonding pattern must be realized. Such a pattern is screened onto the metal strips with an ink that restricts bonding. Almost any type of pattern, such as e.g. dots, lines, arcs, etc. can be applied. When calculating and applying ink pattern, the lengthening of the sheets mainly in longitudinal direction during roll bonding operation must be taken into consideration.

The unbonded areas are blow-formed by two different methods. In one case the pattern ink contains an agent that decomposes to a gas during heat treatment. The gas pressure actually expands or blisters the material, wherever it was inked. The disadvantage of this method is that it may result in an uncontrolled strain rate. Therefore a combination of roll bonding with a neutral ink and a subsequent pressure/time-controlled blow-forming operation is preferred.

Various technical difficulties have to be considered when applying roll bonding to produce multi-sheet structures.

- fine-grained structures should not be destroyed by the hot-rolling process; coarse-grained starting material should recrystallize to a finer grain due to the thermomechanical treatment
- tolerances of the core patterns after the roll bonding process must be calculated and assured with regard to the lengthening of sheets and simultaneously core patterns
- the bonding line should not deviate in the through- thickness direction due to roll bonding

Explosive Bonding results in large distortions when thin sheets are bonded [15]. Therefore the future prospects of this joining technique in connection with Superplastic Forming are rather low.

#### Bonding capabilities of different materials

Fig. 9 summarizes typical strengths of DB joints in Titanium and Aluminium alloys. These are compared for reference with parent material strengths and typical rivetted and adhesively bonded joint strengths [16].

<u>Material</u>		<u>Shear Strength</u> <u>MPa</u>
Titanium 6 AL. 4V	Parent	575
	DB	575
Aluminium	Parent	320
	DB	150 - 170
Riveted Joint (Typical)		10
Adhesive Bond Joint (Typical)		20 - 40

Figure 9 - Mechanical properties of DB joints [16]

Ti6Al4V is especially suitable for solid-state diffusion bonding. Such a joint can reach microstructure and mechanical properties of the base material. At temperatures above 800°C, Titanium and its alloys become highly reactive and will absorb their own limited oxide layer, then producing a self-cleaning action which is compatible with the DB process requirements. The reactivity of Titanium at these temperatures on the other hand does, however, require an inert atmosphere. Because of the self cleaning action associated with Titanium alloys, these materials can be used in the as-received condition with the standard cleaning processes, such as degreasing and pickling.

The bonding parameters for Ti-alloys have been reported in many publications. The creep rate, a determining factor, increases above 850°C and decreases rapidly at the  $\beta$ -transus. Because of the simultaneous application of Diffusion Bonding and Superplastic Forming in manufacturing multi-sheet Ti-parts, the process temperature corresponds to optimum SPF temperature and is in the order of 850°C to 930°C for Ti-alloys.

Liquid-phase joining methods can significantly reduce the pressures and times required to realize a bond. The decrease in bonding strength can be balanced by drastic cost savings. As an example, Royster et alia describe a two-step Superplastic Forming/Weld Brazing process to produce Titanium skin-stiffened compression panels [17-19]. Panel brazing is

accomplished after Superplastic Forming in a vacuum furnace at a pressure of 1.33 MPa and a temperature of 677°C. 3003 aluminium braze alloy was used. Other brazing interlayers for Ti-alloys with interesting properties are AlCuAg-, AgAlMn-, TiCuNi- and TiCuNiBe-alloys.

Al-alloys exhibit a tenacious oxide layer which is insoluble even at DB temperatures and which makes a solid-state diffusion bond as applied to steel and Titanium alloys difficult to achieve. Attempts to overcome this problem have either centered around the removal of oxide followed by the protection of the surface by coating techniques or by the use of interlayers designed to modify or disrupt the natural oxide during bonding. Because solid-state bonding of Al7475 will be presented in detail in the following keynote paper [20], I only want to mention two promising methods in joining high strength Al-alloys. One is a transient liquid-phase bonding using roll-clad Zn alloy interlayers [21]. One of the posters at this conference deals in detail with this method [22]. Another method is the production of oxide-free surfaces on Al-alloys by argon-ion sputter cleaning and subsequent coating with Cu and/or Ag. [23]. Fig. 10 shows microstructures of Al-Li bonded sheets, the left one without any interlayer (plain-bonded), the right one with a roll-clad Zn interlayer.

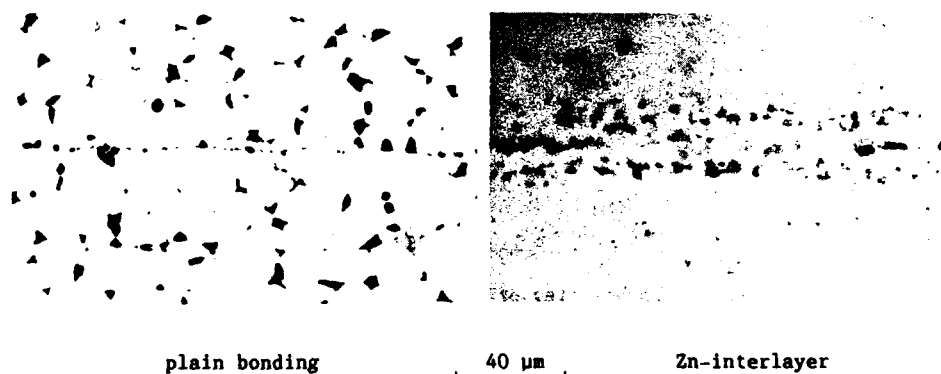


Figure 10 - Exemplary microstructures of Al-Li bonds

The large deformations during roll bonding disrupt the oxide film and assure a good bonding quality. Fig. 11 shows a typical two-sheet roll bonded simplified part, the pattern is visualized by US techniques. The microstructures of roll-bonded joints with different thermomechanical treatments and resulting different grain sizes are shown in Fig. 12.

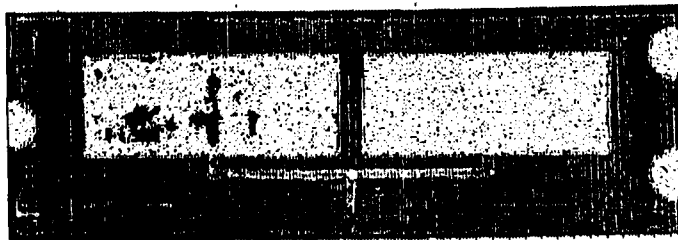


Figure 11 - US-C-scan of roll bonded Al-Li with pattern

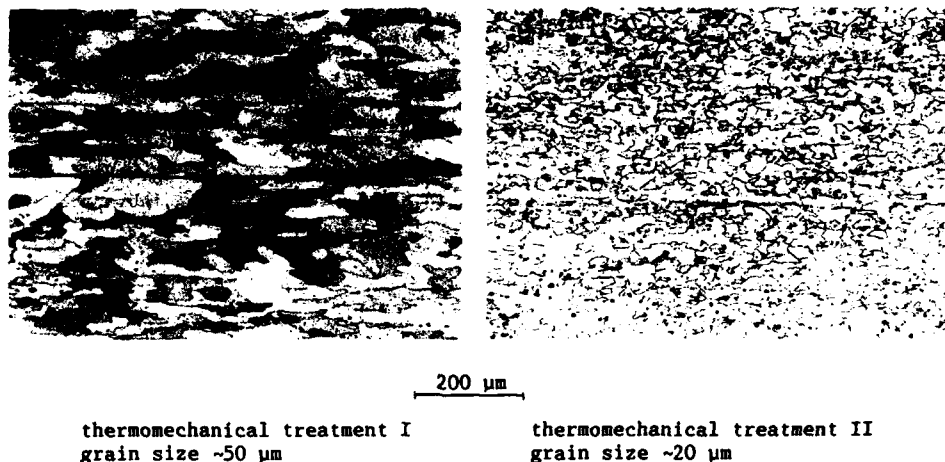


Figure 12 - microstructure of Al 7475, roll bonded with different thermomechanical treatments

New research and development activities aim at the application of SPF/DB processing for MMC materials [24] and Ti-Aluminides [25]. These new materials are becoming of increasing interest for application in hypersonic airplanes and transatmospheric vehicles.

#### Processing

As with SPF processing, hot presses are generally used for SPF/DB processing. They have two main tasks, firstly to heat die and sheet-metal or sheet-metal packages to forming and/or bonding temperature, and secondly to ensure gastightness by pressing together the two halves of the die. The demands in respect of inert atmosphere are much higher for the SPF/DB technique in comparison to simple SPF technology, because bonding quality is mainly influenced by an oxidefree surface.

As far as the production of multi-sheet structures by SPF/DB is concerned, in principle two variations can be distinguished:

- Diffusion Bonding before Superplastic Forming (DB/SPF)
- Superplastic Forming before Diffusion Bonding (SPF/DB).

All the other process variations can be related to these two techniques.

Fig. 13 shows exemplarily the DB/SPF process for fabricating a three-sheet sandwich. The sheets are bonded in a package, the core configuration is determined by the preparation of the single sheet surfaces with a given stop-off pattern [26].

Bonding and subsequent blow forming can be realized in one step within one temperature cycle or in a two-step process. Though the one-step process allows part production without intermediate disassembly of the die, the two-step process has some distinct advantages:

- Diffusion Bonding pressure can be applied either by gas pressure or by mechanical pressing.
- Diffusion Bonding temperature and Superplastic Forming temperature may differ.
- Alternative bonding techniques to solid-state bonding, such as, for example, roll bonding, can be applied.
- Atmosphere quality can be adjusted more easily than e.g. when using steel envelopes.
- Non-destructive testing of DB joints before blow forming is possible.
- Several sheet packages can be bonded in one operation, which increases the economy of the process.

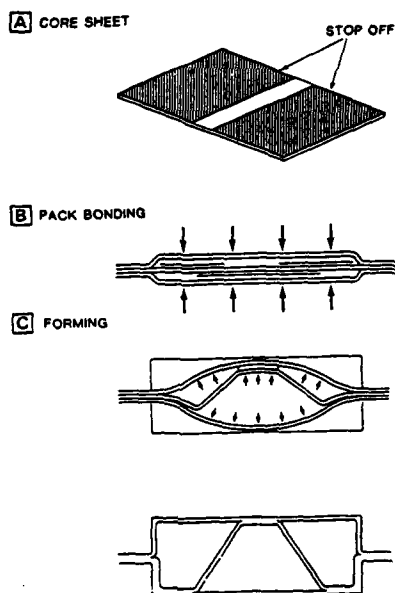


Figure 13 - Schematic illustration of SPF/DB three-sheet fabrication [26]

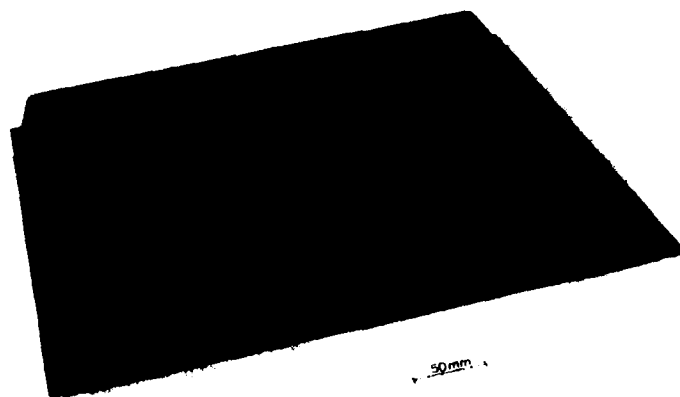


Figure 14 - DB/SPF-Ti6Al4V sandwich structure

Fig. 14 shows a three-sheet sandwich structure processed in the one-step procedure.

The opposite process--Superplastic Forming before Diffusion Bonding--is schematically illustrated in Fig. 15 for producing a four-sheet sandwich with cellular stiffening [26]. The two core sheets are seam-welded in a pattern which determines the final core type. Face sheets and core sheets are diffusion-bonded at the periphery and afterwards blow formed. Diffusion Bonding between the core sheets and between core sheets and face sheets occurs after contacting under high pressure at SPF temperature.

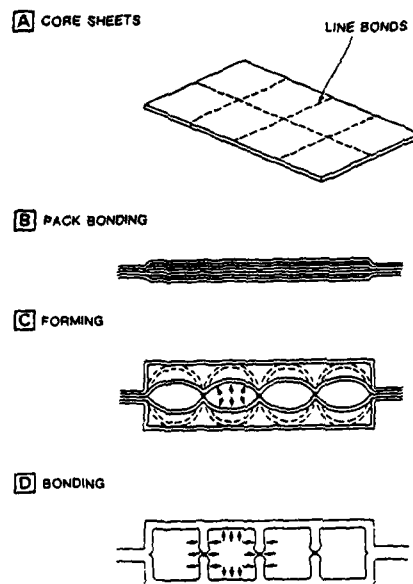


Figure 15 - Schematic illustration of DB/SPF four-sheet fabrication [26]

The secondary diffusion bond is more difficult to realize in comparison to the primary diffusion bond. Diffusion Bonding pressure can only be applied by gas pressure. Contamination of the bonding surfaces due to impurities of argon gas, by the enclosure of the insoluble argon gas, or by residues from stop-offs during the SPF process, may deteriorate bonding quality.

Pressure-time cycles for blow forming have to be optimized for ensuring a constant strain rate in the range of optimum  $m$ -values in critical areas. Activities are increasing which predict pressure-time cycles by FEM methods [27-29].

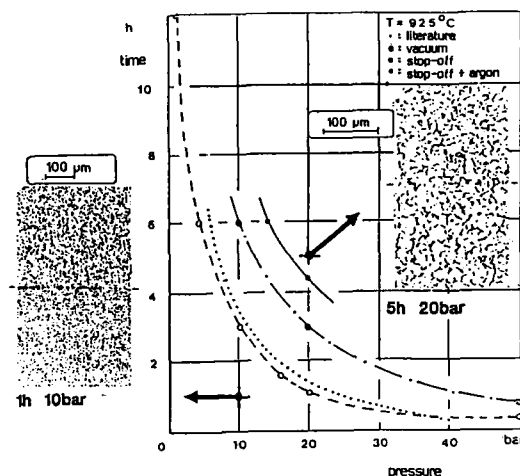


Figure 16 - pressure-time relation for Diffusion Bonding of Ti-alloys [30]

The relation between pressure and time for solid-state Diffusion Bonding of Ti6Al4V is shown in Fig. 16 for the bonding temperature 925°C and different conditions concerning atmosphere and stop-off [30]. Bonding is insufficient below the curves, the presence of argon instead of vacuum and more distinct the presence of stop-offs require higher pressures and/or times to produce a good bond. The two exemplary microstructures illustrate that one hour and 10 bars are insufficient for a good bond, while five hours and 20 bars lead to an excellent bond quality.

#### Quality assurance

The quality and integrity of SPF or SPF/DB components must be ensured and verified. This is the key to converting the manufacturing method from a laboratory technique to a reliable, cost-effective manufacturing process. Quality assurance efforts depend among others on the degree of complexity of the component as well as on stress conditions in operation. In general, dimensional checks, metallographic tests and destructive examination of accompanying process specimens are sufficient for simple SPF parts. This should be preceded by a type sample test on a complete qualification sample applying both destructive and non-destructive investigation. Standard process-control procedures assure consistent component quality.

Naturally, complex SPF/DB multi-sheet structures require a greater quality assurance effort, above all because the quality of the DB joints must be verified through suitable NDT methods. Developing special NDT techniques to check DB joints has concentrated mainly on ultrasonic test methods including conventional US techniques, US spectroscopy and high-frequency US techniques [31, 32]. According to these results, higher-frequency focussing probes proved to be the most suitable ones. A.F. Evans et alia [33] designed a detailed quality assurance evaluation scheme to establish the structural integrity of complex critical load-bearing aircraft engine hardware operating at high temperatures. It involves determining and controlling each of the critical processing steps, and includes dimension measurements, NDT, mechanical tests and metallography.



### Conclusion and Outlook

In recent years, Superplastic Forming has become a recognized manufacturing method. In conjunction with Diffusion Bonding, it enables single- and multi-sheet structures to be made with diverse configurations. The references to application examples published over the last years as well as the lectures and posters at this conference emphasize the spectrum of relevant applications.

SPF/DB development of Ti-alloys has proceeded furthest. There are already many parts in production and application. Future activities should concentrate on increasing the economy of the process. Decreasing production times can be achieved by optimal peripheral-equipment design and, additionally, more time-saving joining techniques in comparison to solid-state bonding, such as liquid-interface bonding.

Al-alloys exhibit a tenacious oxide layer which makes a solid-state diffusion bond difficult to achieve. That is the main reason, to the author's knowledge, why no SPF/DB aluminium parts are in production as of today. Attempts to overcome this problem have centered around the removal of oxides followed by the protection of the surface by coating techniques, by the use of interlayers designed to modify or destroy the oxide, or by extensive deformation processes like roll bonding in order to disrupt the oxide layer. Roll-clad Zn-layers as well as ion etching of the surface followed by ion sputtering of protective Cu and Ag layers seem most promising.

Bond strength values of published Al joints are far from base metal values but already exceed the values of adhesively bonded joints. This allows an optimistic estimation of future prospects. Other bonding techniques, such as roll bonding, also show promising results and should be further pursued.

MMC-materials and Ti-Aluminides are experiencing growing interest due to development activities for hypersonic airplanes and transatmospheric vehicles. Research and development activities in the near future will therefore concentrate more intensively on the realization of SPF/DB structures of these new materials.

### References

- [1] S. Bangs, (Welding Design and Fabrication, Jan. 1976), 43.
- [2] D. Stephen, (AGARD Lecture Series No. 154, 1987), 7-1.
- [3] D. Stephen, (Designing with Titanium; The Institute of Metals, 1986), 108.
- [4] M.M. Schwartz, (Modern Metal Joining Techniques, Wiley (1969). Metals Joining Manual, McGraw-Hill (1979) ).
- [5] R. Holbein and K.-P. Sahm, (Titanium: Science and Technology; Proceedings of the Fifth International Conference on Titanium, Munich, West Germany, 1984. Deutsche Gesellschaft für Metallkunde, 1985), 1237.
- [6] C.H. Hamilton, (AGARD Lecture Series No. 154, 1987), 2-1.
- [7] R.C. Davis, C.T. Mills, P. Prabhakaran and C. Jakson, (NASA Technical Paper 2272, February 1984).
- [8] E.D. Weisert and G.W. Stacher, (Superplastic Forming of Structural Alloys; Proceedings of the Symposium, San Diego, CA, 1982. Warrendale, PA, Metallurgical Society of AIME, 1982), 273.
- [9] M. Ohsumi, (Mitsubishi Heavy Industries Technical Review, Vol. 21, No. 1, 1984), 42.

- [10] J.E. Fischler, (Joining Technologies for the 1990s: Welding, Brazing, Soldering, Mechanical, Explosive, Solid-State, Adhesive; Hampton, Virginia, USA, Oct. 1984), 290.
- [11] B.A. Burroughs, D. Munger, R. Raymond, G. Stacher and L. Israeli, (AFWAL-TR-80-4041, April 1980).
- [12] W.A. Owczarski and D.F. Paulonis, (Welding Journal, February 1981), 22.
- [13] W.A. Owczarski, (Physical Metallurgy of Metal Joining, AIME 1980), 166.
- [14] D.V. Edson, (Design News, June 16, 1986), 67.
- [15] R. Prümmer, (Z. f. Werkstofftechnik, Journal of Materials Technology, 4. Jahrgang 1973, Nr. 5), 236.
- [16] D. Stephen and S.J. Swadling, (AGARD Advanced Joining of Aerospace Metallic Materials, Conc. Proc. No. 398, 1986), 7-1.
- [17] D.M. Royster, T.T. Bales and R.C. Davis, (Welding, Bonding and Fastening, 1984), 253.
- [18] D.M. Royster, T.T. Bales and H.R. Wiant, (27th National SAMPE Symposium, May 4-6, 1982), 569.
- [19] W. Blair, (NASA Contractor Report 165754, Contract NAS1-15646, Aug. 1981).
- [20] J. Pilling, (International Conference on Superplasticity and Superplastic Forming; Blaine, Washington, USA, 1-4 August 1988).
- [21] R. Grimes and J. Ball, (UK Patent No. 2134833).
- [22] R.A. Ricks, J. Ball, H. Stocklossa, P.J. Winkler and R. Grimes, (International Conference on Superplasticity and Superplastic Forming; Blaine, Washington, USA, 1-4 August 1988).
- [23] J. Harvey, P.G. Partridge and A.M. Lurshay, (Mater. Sci. Eng. 79, 1986), 191.
- [24] M.W. Mahoney and A.K. Ghosh, (AFWAL-TR-82-3051, August 1982).
- [25] M.W. Mahoney and D.W. Schulz, (Final Report, Contract No. F33615-78-C-5144, April 1981).
- [26] D. Stephen, (Titanium 1986: Products and Applications; Proceedings of the International Conference, San Francisco, CA, Oct. 19-22, 1986. Volume 2. Dayton, OH, Titanium Development Association, 1987), 603.
- [27] J.H. Agyris and J.St. Doltsinis, (Computer Methods in Applied Mechanics and Engineering, Vol. 46, Sept. 1984), 83.
- [28] M. Bellet and J.L. Chenot, (Titanium 1986: Products and Applications; Proceedings of the International Conference, San Francisco, CA, Oct. 19-22, 1986. Volume 2. Dayton, OH, Titanium Development Association, 1987), 1175.
- [29] C.D. Ingelbrecht, (Journal of Materials Science Letters, Vol. 4, Auf. 1985), 1021.
- [30] W. Beck and P. Knepper, (DVS-Berichte Band 98, Deutscher Verlag für Schweißtechnik (DVS) GmbH, Düsseldorf).
- [31] R. Bilgram, S. Elze, W. Klemmt and G. Tober, (Titanium: Science and Technology; Proceedings of the Fifth International Conference on Titanium, Munich, West Germany, 1984. Deutsche Gesellschaft für Metallkunde, 1985), 955.
- [32] G. Tober and S. Elze, (AGARD Advanced Joining of Aerospace Metallic Materials, Conc. Proc. No. 398, 1986), 11-1.
- [33] A.F. Evans and J.L. Bartos, (Titanium 1986: Products and Application; Proceedings of the International Conference, San Francisco, CA, Oct. 19-22, 1986. Volume 2. Dayton, OH, Titanium Development Association, 1987), 1136.

## Application of Superplastic UHC Steel for Isothermal Forging of Machine Component

J. Wittenauer, P. Schepp, and B. Walser

Sulzer Brothers AG  
Materials Research Division  
Winterthur, Switzerland

### Abstract

In recent years there has been a great deal of interest in the superplastic deformation of engineering alloys. Among these alloys are steels containing more than 1% carbon - the Ultrahigh Carbon (UHC) steels. The UHC steels exhibit superplastic behavior over a wide range of temperature and strain rate. Recently, advanced UHC steels containing up to 10% aluminum have been developed. These new steels further extend the range of superplastic behavior and thus, the UHC steels have become more economically attractive. The aluminum-containing UHC steels are currently being evaluated as candidate materials for the isothermal forming of intricately shaped machine components. Trial castings have been prepared and thermomechanically processed using conventional hammer forging techniques. The forming characteristics of the resulting superplastic material have been investigated. A description of alloy composition and processing history is presented along with mechanical properties data for the alloys under investigation. In particular, experiences with the forming characteristics of UHC steel under conditions of isothermal superplastic die forging are presented.

### Introduction

The superplastic forming of structural components offers several advantages over more traditional methods of metal forming or machining. These advantages include a reduction in energy costs over forging, conservation of material with respect to machining, and ability to form parts of intricate geometry which would be difficult or impossible to fabricate by any other means. It has been demonstrated that alloys based on titanium, aluminum, and iron exhibit useful superplastic behavior. The superplastic forming of titanium-based and aluminum-based alloys have won commercial acceptance. Although there has been a great deal of research activity involving iron-based superplastic materials - particularly the ultrahigh carbon (UHC) steels - there has been no reported use of these materials in an actual fabricated component. The purpose of this report is to provide an example of an industrial application of superplastically formed UHC steel.

The UHC superplastic steels were originally developed in 1975 by Sherby *et al* [1,2]. The material of the original invention contained carbon in excess of 1.0% and a small amount of a carbide stabilizing element such as chromium. By extensively hot and warm working these steels, a microstructure consisting of very fine equiaxed ferrite grains and a dispersion of spheroidized carbides is obtained. Typical ferrite grain size is 1-2  $\mu\text{m}$ . The spheroidized carbides lie along grain boundaries and act to stabilize the fine grain size at intermediate temperatures. Thus fine structure superplasticity is readily obtained for the UHC steels.

The usefulness of a superplastic material can generally be characterized by considering the maximum strain rate and temperature combination at which superplasticity is observed. For the UHC steels, the temperature of optimal superplastic behavior is limited by the ferrite to austenite transition temperature. Above the transformation temperature, a large portion of the carbides dissolve and grain growth occurs. With grain growth comes a reduction in the superplastic capabilities of the material. Thus, for the early UHC steels - the "plain carbon" UHC steels - the

Superplasticity and Superplastic Forming  
Edited by C.H. Hamilton and N.E. Paton  
The Minerals, Metals & Materials Society, 1988

temperature for the maximum superplastic strain rate is in the range of 720°- 730° C. The maximum superplastic strain rate is determined in large part by the ferrite grain size. When grain boundary sliding is the dominant deformation mechanism, smaller grain sizes lead to higher deformation rates. Walser and Sherby have demonstrated that the strain rate for superplastic flow in UHC steels is inversely related to the third power of grain size [3]. One technique for providing and maintaining a smaller grain size is to increase the volume fraction of grain boundary carbides. Thus it has been shown that higher carbon contents in UHC steels lead to an increase in superplastic strain rate [4]. The influence of other alloying additions has been studied as well. For example, chromium [4] and vanadium [5] have been shown to stabilize the cementite and act to prevent graphitization. Nickel promotes graphitization in UHC steels and leads to poor ductility [5].

Recent improvements to UHC steels have resulted from attempts to raise the ferrite to austenite transition temperature through alloy modification. Such alloy modification would lead to higher forming temperatures and, presumably, lower forming stresses. The first successful attempt toward this goal has involved the use of silicon. UHC steels containing from 1% to 4% Si have been shown to raise the ferrite to austenite transition temperature resulting in a stable superplastic microstructure at temperatures as high as 800° C for a 3% Si UHC steel [6] and as high as 850° C for a 4% Si steel [7]. Such large silicon additions, while enhancing the superplastic nature of the UHC steels, tend to promote graphitization and thus, a reduction in tensile ductility is observed.

Most recently, it has been shown that aluminum additions to UHC steel have a marked influence on the ferrite to austenite transition temperature [8]. UHC steels containing 1.6% Al have been shown to exhibit an optimum superplastic response at 780° C while a UHC steel containing 10% Al exhibits an optimum superplastic response at a temperature of 920° C [9]. At these high deformation temperatures, superplasticity is observed at true strain rates approaching  $10^{-2} \text{ sec}^{-1}$  and flow stresses in the range of 10 to 30 MPa. This remarkable advance greatly increases the economic attractiveness of isothermal superplastic forming of UHC steel components.

#### Alloy Selection

In order to exploit the most recent advances in UHC steel alloy chemistry, two aluminum containing UHC steels have been chosen for investigation. The chemical composition of these materials is shown in Table I.

**Table I**  
Composition of UHC Steels in this Investigation (Wt. %)

C	Mn	P	S	Cr	Al
1.32	0.60	0.010	0.012	1.68	1.90
1.11	0.48	0.011	0.002	1.45	9.30

The low aluminum UHC steel was air melted and air cast while the high aluminum steel was vacuum induction melted and vacuum cast: both alloys into 25 kg ingots. Sherby *et al* have determined that the ferrite to austenite transition for the aluminum containing UHC steels occurs over a range of temperatures in which three phases - cementite, austenite, and ferrite - are present [9]. Dilatometric analysis for the alloys of the present investigation indicates that the ferrite to austenite transition occurs over the temperature range of 650° to 810° C for the low aluminum steel and occurs over the temperature range of 690° to 915° C for the high aluminum steel. A knowledge of these transformation temperatures is essential in determining the proper thermomechanical processing procedure which is described below.

#### Processing

In order to produce the desired fine grained superplastic microstructure for UHC steels, a two-stage thermomechanical processing procedure is commonly utilized [10,11]. For the first stage, the as-cast material is heated to a high enough temperature for dissolution of substantial, if not all of the cementite and for chemical homogenization of the coarse cast microstructure. For the low aluminum UHC steel, a temperature of 1120° C was found to be sufficient while for the high aluminum material a temperature of 1220° C was used. The 120 mm diameter castings were held at the elevated temperature for a period of 6 to 8 hours and then hot and warm worked (HWW) while cooling to a temperature below the upper austenite to ferrite transition temperature. This first stage of processing resulted in a billet of 60 mm square cross section having a microstructure of fine pearlite colonies (20 to 30  $\mu\text{m}$  diameter) and a dispersion of proeutectoid cementite.

The second stage of thermomechanical processing was designed to spheroidize the pearlitic microstructure and at the same time produce a semifinished section of geometry suitable for subsequent isothermal forming. A variety of techniques are available for achieving this goal including a Divorced Eutectoid Treatment (DET), a Divorced Eutectoid Treatment with Associated Deformation (DETWAD), and Isothermal Warm Working (IWW) at temperatures below the ferrite to austenite transus [10,11]. In a commercial forging operation, it is common practice to reheat a workpiece intermittently during the forging process. Such intermittent reheating is not compatible with DET and DETWAD processing because these methods are commonly practiced as a single thermal or thermomechanical step. Therefore, IWW by hammer forging and ring rolling was chosen as the most practical method for obtaining the desired fine-grained microstructure. The second stage of processing for the materials of this investigation consisted of heating the 60 mm by 60 mm billet to a temperature below the upper ferrite to austenite transus ( $780^{\circ}\text{C}$  for the low aluminum alloy and  $860^{\circ}\text{C}$  for the high aluminum alloy), upsetting to a disk of 30 mm height and 120 mm diameter, piercing the center of the disk, and final processing on a ring rolling machine to final dimensions of 135 mm inner diameter, 190 mm outer diameter, and a height of 26 mm. The material was reheated periodically whenever the temperature fell to  $50^{\circ}\text{C}$  below the aim processing temperature. The resulting microstructure of the forged ring is shown in Figure 1 for the case of the low aluminum UHC steel. A ferrite grain size of  $1\text{--}2\text{ }\mu\text{m}$  is obtained with a dispersion of spheroidized carbides. This is the desired superplastic microstructure. For the high aluminum UHC steel, a similar microstructure was obtained (Figure 2) except that the grain size was slightly larger -  $3\text{ to }4\text{ }\mu\text{m}$ . It is desirable to have a finer grain size for the high aluminum UHC steel and processing modifications are currently under investigation to produce a grain size in the  $1\text{--}2\text{ }\mu\text{m}$  range for this material.

#### Superplastic Properties

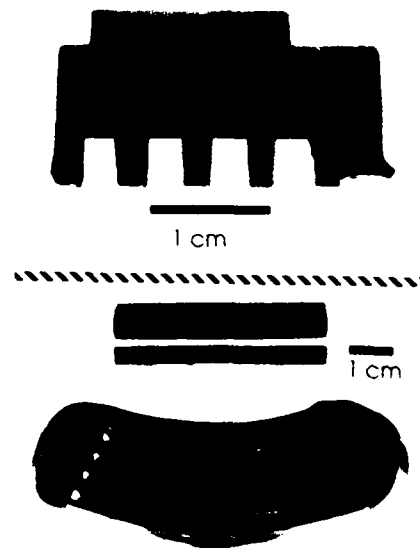
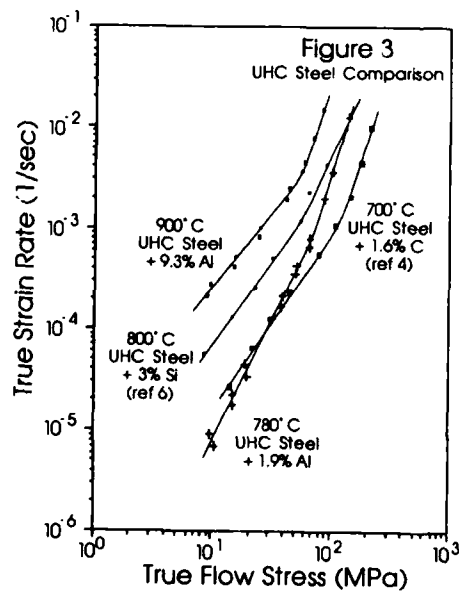
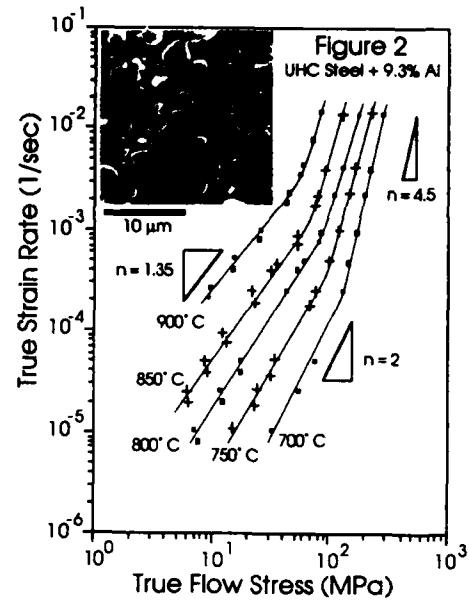
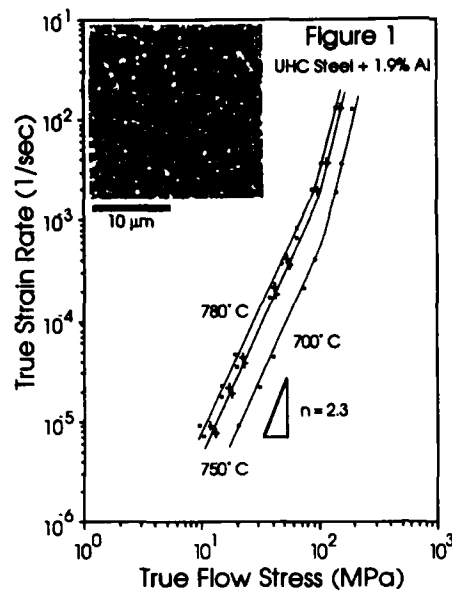
The elevated temperature mechanical behavior of the as-forged steels was determined in tension on cylindrical specimens having a gauge length of 30 mm and a diameter of 4 mm. Elevated temperature strain-rate change tests were performed in air to obtain information on the relationship between flow stress and strain rate. The strain-rate change tests were performed in accordance with previously described procedures [12]. Walser and Sherby have shown that grain growth occurs during the superplastic deformation of UHC steels [3]. Excessive structural change, such as grain growth, during the course of the strain-rate change test could lead to errors in interpretation of the experimental data [13]. In order to determine the influence of grain growth during testing for the UHC steels of the present investigation, some strain rates were applied twice to a specimen during the time of testing. Ideally, for the case of constant microstructure, all data should lie along the same line when true strain rate is plotted as a function of true flow stress. The results of the elevated temperature tests are shown in Figure 1 for the low aluminum UHC steel and in Figure 2 for the high aluminum material. The minimum amount of scatter in the data of Figures 1 and 2 indicates that, while some grain growth did indeed occur during testing, the deviation is small when compared to the magnitude of the quantities being measured.

The low aluminum UHC steel (Figure 1) exhibits a stress exponent of  $n=2.3$ , indicative of superplastic behavior, at true strain rates up to and above  $10^{-3}\text{ sec}^{-1}$ . The optimum strain rate for superplastic flow was obtained at a temperature of  $780^{\circ}\text{C}$ . When tested at temperatures in excess of  $780^{\circ}\text{C}$ , the superplastic behavior of the material degrades somewhat (data not shown). The high aluminum steel (Fig. 2) exhibits an unusually low stress exponent for UHC steels of  $n=1.35$ . The steel exhibits optimum superplastic behavior at  $900^{\circ}\text{C}$  for the temperature range investigated. The results shown in Figure 2 are in close agreement with those reported by Fukuyo for a high aluminum steel of similar composition [7].

To further emphasize the comparative advantage of the aluminum containing UHC steels, a plot comparing the optimum superplastic behavior of a number of UHC steels is presented as Figure 3. Shown are data from a "plain carbon" UHC steel [4], UHC Steel with 3% Si [6], and the aluminum containing steels of the present investigation. It is clear from Figure 3 that the high aluminum-containing UHC steel offers the best combination of low forming stresses and high forming rates observed thus far.

#### Ambient Temperature Mechanical Properties

The room temperature mechanical behavior of the as-forged steels from this investigation are presented in Table II. The steels exhibit high strength but moderate to low ductility. The design requirements for the machine component under consideration call for wear resistance under conditions of light compressive loading. Thus the low tensile ductility of these materials is not



**Figure 4**  
Superplastically Formed  
Machine Component

regarded as a limiting design factor at this time.

**Table II**

Room Temperature Mechanical Properties of UHC Steels Containing Aluminum

Steel	Yield Strength	Ultimate Tensile Strength	Failure Elongation
1.9% Al	788 MPa	896 MPa	14.3%
9.3% Al	786	1050	4.4%

#### Superplastic Forming of Machine Component

In order to determine the engineering feasibility of utilizing isothermal superplastic forming on a production basis, a machine component having a curved geometry with many details was selected for evaluation. An isothermal forging press with a capacity of 8000 kN has been installed at Sulzer. Forming dies have been constructed of a Ni-based superalloy and heat is applied to the dies by means of an induction coil. Initial forming trials have been conducted on a segment of the machine component using the low aluminum UHC steel. The result of one such trial is shown in Figure 4. The part shown was formed in 4 minutes at 760° C requiring a maximum load of 500 Newtons. The complex details of this component (Figure 4) clearly make superplastic forming an attractive alternative to competitive processing technologies such as machining or casting.

Based on this encouraging trial, a die is currently being fabricated for the pilot production of the complete component design. Also, the forming characteristics of the high aluminum UHC steel are being evaluated. The high aluminum material can be superplastically formed at stresses on the order of 10 MPa (Figure 2) and thus offers advantages over the low aluminum material in terms of die wear. Additional work is also being conducted to establish a commercial supplier of UHC steels.

#### Conclusions

Ultrahigh Carbon (UHC) steels have undergone a period of maturation since the material was initially invented in 1975. Recent alloy modifications based upon the addition of aluminum have improved the material to the point where isothermal superplastic forming is now a viable manufacturing alternative. Investigations conducted at Sulzer indicate that it is feasible from an engineering standpoint to cast and forge aluminum-containing UHC steels to an appropriate preform shape having the desired superplastic properties. Further, initial forming trials have been conducted and the results are satisfactory enough to warrant a scaling up of the manufacture of a complex machine component.

#### Acknowledgements

The authors are indebted to the contribution of Prof. Oleg D. Sherby at Stanford University who has provided invaluable assistance to this project over the past years.

#### References

- 1) O.D. Sherby, B. Walser, C.M. Young, and E.M. Cady, *Scripta Met*, 9 (1975), 569.
- 2) O.D. Sherby, C.M. Young, B. Walser, and E.M. Cady, U.S. Patent 3951697, Apr. 1976.
- 3) B. Walser and O.D. Sherby, *Met Trans*, 10A (1979), 1461-1471.
- 4) J. Wadsworth and O.D. Sherby, *J. of Mat. Science*, 13 (1978), 2645-2649.
- 5) J. Wadsworth and O.D. Sherby, *J. of Mech. Work. Tech.*, 2 (1978), 53-66.
- 6) O.D. Sherby, T. Oyama, D.W. Kum, B. Walser, and J. Wadsworth, *J. of Metals*, 37 (1985), 50-56.
- 7) H. Fukuyo, Engineers Thesis, Stanford University, 1987.
- 8) O.D. Sherby, D.W. Kum, T. Oyama, and J. Wadsworth, Int. Patent No. WO87/01735 (1987).
- 9) O.D. Sherby, T. Oyama, and H. Fukuyo, Research in Progress, 1987.
- 10) T. Oyama, O.D. Sherby, J. Wadsworth, B. Walser, *Scripta Metall*, 18 (1984), 799-804.
- 11) T. Oyama, O.D. Sherby, and J. Wadsworth, U.S. Patent 4448613, May, 1984.
- 12) W.A. Backofen, J.R. Turner, and P.H. Avery, *Trans. ASM*, 57 (1964), 980.
- 13) G. Rai and N.J. Grant, *Met Trans*, 6A (1975), 385.

## A dynamic model for diffusion bonding of metals

Huang Yan and Ma Longxiang

Department of Metals forming,  
Northeast University of Technology,  
ShenYang, P.R.C.

### Abstract

Although diffusion bonding of metals has found successful applications in some fields, there is no comprehensive theory which accurately describes the mechanisms and the relative dynamics which operates when the surfaces to be joined are brought together under an applied pressure at an elevated temperature now. In this paper, a dynamic model for diffusion bonding of metals is represented, the aim of which is to give the relationship between the joint strength and the material parameters and the process variables, therefore to be able to choose process variables reasonably. The approach adopted bears some similarity with that used when modelling the recrystallization of deformed metals.

### Introduction

Diffusion bonding of metals is a solid joining process which has been increasingly employed in the past few years in aerospace, nuclear, and other applications. In this technique two surfaces are brought into close contact at elevated temperature in vacuum and with pressure applied normal to the bond line, and allowed to join together. The temperature is usually in the region of  $0.5-0.8T_m$ , where  $T_m$  is the absolute melting point of the metal being joined. The pressure must be sufficiently low so that no large scale deformation of the parts to be joined occurs. If the process is conducted properly, a joint having properties and metallurgical structures indistinguishable from those of the base metal is produced. In this paper, a dynamic model is described to understand how the rate controlling mechanism governing the realization of the metallurgical bond between the two surfaces is affected both by the process variables ( $t, T, p$ ) and by the material parameters of the metal being joined when diffusion bonding similar metals, predict the extent of the bonding at given bonding temperature, pressure, and time.

Dr. C. H. Hamilton (1) represented diffusion bonding as the following four stages: (1) development of intimate physical contact, (2) formation of the metallic bond, (3) interdiffusion, and (4) recrystallization and/or grain growth across the interface. Limitations of the earlier researches (2,3) are, first, only the stages (1) was considered and analyzed, second, the mechanisms proposed were based on the behaviour of individual atom, but that of mass atoms. In the present work, it is the other stages but (1) that are investigated based on the behaviour of the mass atoms in the zone near to



the bonding interface, supposing that the physical contact has been obtained and that the surfaces being joined are clear.

#### Dynamic model

Solids are system formed by atoms bond with intermetallic force. This determines the basic condition of achieving metallurgical joint in diffusion bonding of metals, i.e., formation of metallic bond all over the bonding interface. However this kind of joint can not be found in real crystal metals, because it is neither mechanical equilibrium state nor thermodynamic equilibrium. In fact, the extent of bonding depends on the degree of occupation of the interface by grains across the interface, which is a process same as that of the recrystallization of deformed metals.

The idea to establish the model is like this: micro-plastic deformation of asperities of surfaces being joined produces a number of activation centers which distribute randomly on the interface. The chemical reaction forming metallic bond will occur at the activation center. As the reaction can only release the distortion energy of atoms at surface, the grain boundary formed is unstable. These boundary may migrate under the effect of the chemical potential, and the grains across the bonding interface would be formed. These randomly distributed small joined region are called bond nuclei (abbreviated as bonu). During diffusion bonding, bonu formed grow and new bonu form continuously until the entire bonding interface is occupied by the grains.

Consider the micro-plastic deformed zone near to the interface being joined at a isothermal temperature  $T$  and with a pressure  $p$ . After a time a small joint, i.e. a bonu nucleates at a point of the interface and begins to grow. Frequently, this bonu will increase in size until it impringes upon a neighboring bonu. Suppose the cross section of bonu with the bonding interface is circle with a radius of  $R$ . We may take  $R$  as:

$$R = \int_{\tau}^t G dt \quad (1)$$

at a time  $t$  ( $t > \tau$ ). Where  $G = G(t)$  is the growth rate of the bonu along the bonding interface defined as  $dR/dt$ . Define a nucleation rate:

$$\dot{N} = \frac{\text{number of bonu formed/unit time}}{\text{area not yet bonded}}$$

Between time  $t$  and  $t+dt$ , each bonu grows along the bonding interface by

$$ds = \pi \left( \int_{\tau}^t G(t) dt \right)^2 dt, \text{ where } s \text{ is the bonded area and the bonded area}$$

fraction  $x$  increases by growth into that not yet bonded  $(1-x)$  by:

$$dx = \pi \left( \int_{\tau}^t G(t) dt \right)^2 \dot{N} dt (1-x) \quad (2)$$

$$\text{i.e.} \quad -\ln(1-x) = \pi \left( \int_0^t \left( \int_{\tau}^t G(t) dt \right)^2 \dot{N} dt \right) \quad (3)$$

$$\text{or} \quad x = 1 - \exp \left( -\pi \int_0^t \left( \int_{\tau}^t G(t) dt \right)^2 \dot{N} dt \right) \quad (4)$$

This is the dynamic equation of diffusion bonding of similar metals, when  $G, \dot{N}$  are constant, is neglected,

$$x = 1 - \exp \left( -\frac{\pi}{3} \dot{N} G^2 t^3 \right) \quad (5)$$

Let  $X = \sigma_{db} / \sigma_b$  we have

$$\sigma_{db} = \sigma_b \left( 1 - \exp\left(-\frac{\pi}{3} \dot{N} G^2 t^3\right) \right) \quad (6)$$

where  $\sigma_{db}$ ,  $\sigma_b$  are the bonding strength of joint and the strength of the base metal respectively.

#### Nucleation

It is considered that bonu nucleate by the mechanisms similar to those of the recrystallization. As this occurs under dynamic state, the rate of nucleation  $\dot{N}$ , could be considered constant with time. Dependence of  $\dot{N}$  on the temperature follows the Arrhenius equation

$$\dot{N} = \dot{N}_0 \exp(-Q_n / RT) \quad (7)$$

where  $Q_n$  is nucleation activation energy,  $Q_n = Q_{gb}$ ,  $Q_{gb}$  is the grain boundary self-diffusion activation energy. Thus

$$\dot{N} = \dot{N}_0 \exp(-Q_{gb} / RT) \quad (8)$$

Factor  $N$  associates with the number of activation centers at the bonding interface. What is the activation center in topochemical reaction between metals in solid state? An earlier investigation(4) proved the activation center to be a dislocation with a field of elastic distortions. Let  $\lambda$  be the frequency of emergence of dislocations into the bonding interface. We can determine with the help of kinetics of dislocations as this:

$$\lambda = \frac{2 \dot{\epsilon}}{L b} \quad (9)$$

where  $\dot{\epsilon}$  is the rate of creep of the bonding zone.  $L$  is the distance moved by dislocation and  $b$  is the Burgus vector. For the stage of steady creep, the creep rate can be written as:

$$\dot{\epsilon} = A' p^n \exp(-\Delta H / RT) \quad (10)$$

Thus

$$\lambda = 2 A' p^n \exp(-\Delta H / RT) / L b \quad (11)$$

Where  $A'$  and  $n$  are constant,  $\sigma$  is effective stress of creep,  $p$  is the bonding pressure,  $\Delta H$  is the creep activation energy. If  $\dot{N}_0$  is proportional to  $\lambda$ , we can write:

$$\dot{N}_0 = A p^n \exp(-\Delta H / RT) / L b \quad (12)$$

and so we get:

$$\dot{N} = A p^n \exp(-( \Delta H + Q_{gb} ) / RT) / L b \quad (13)$$

Where  $A$  is a constant associated with materials.

#### Growth of bonu

The growth to be discussed here will be different from that of the classical recrystallization. As the growth of bonu is very complicated, it is impossible to give a detailed physical picture within so small a space. Only some ideas are given below.

The growth of bonu is the process that the junction of the bonu and the bonding interface moves outward to consume the area not yet bonded. This

process may be developed by two mechanisms. First, migration of the grain boundary driven by stored energy, elastic strain, and interface curvature may cause the junction to move. Second, diffusion of atoms in following three ways may cause the junction to move:

- (1) diffusion from volume of bonu to the junction .
- (2) diffusion along grain boundary to the junction.
- (3) diffusion along the bonding interface to the junction.

#### Conclusions

In the model, the dynamic process of the diffusion bonding after attainment of the physical contact is considered to be:

- (1) topochemical reaction forming metallic bond occurs at activation center which is a dislocation with a field of elastic distortions.
- (2) bonu, small local bonded regions, are formed in situ.
- (3) the bonu formed grow and new bonu form continuously until entire bonding interface is occupied by the by the grains across the interface.

It is shown in the model that the strength of the joint depends on the process variables and material parameters in the different degree.

#### Reference

- 1.C.H. Hamilton, Titanium Science and Technology, proceedings of the second International conference, eds. R.I.Jaffee, and N.M.Burte, 1973; vol.1:625, New York, plenum press
- 2.G.Garmong, et al, Metall. Trans.,6A(6), 1975, 1269
- 3.B.Derby and E.R.Wallach, Met. Sci.,16(1), 1982, 49
- 4.Yu.L.Krasulin, Dislocations as active centers is topochemical reactions. Teoretiches-Kaya i eksperimentalnaya Khimiya., vol.III,(7),1967,14

Effects of Transformation Superplasticity on the Early,  
Deformation Process of the Solid State Bonding in Pure Iron

Yasunori Saotome\* and Nobuhiro Iguchi\*\*

\* Department of mechanical Engineering, Faculty of Engineering  
Gunma University, Tenjin-cho, Kiryu, Gunma 376 Japan

\*\* Department of Mechanical Engineering, School of Science and  
Engineering, Waseda University, Ohkubo, Shinjuku-ku  
Tokyo 160 Japan

Abstract

It has been said that the dominant mechanism in the early process of the solid state bonding is deformation in the vicinity of bonding interface. The purpose of this study is to make clear the effects of transformation superplasticity on this process. The specimens of pure iron were bonded to micro-V-grooved tools (30,60,90 deg in V-groove angle and 1 mm in depth) under temperature cycles including A<sub>3</sub> transformation temperature or at a high constant temperature. In the course of the study, the accommodation process at the bonding interface due to semi-macroscopic deformation was simulated with the inflow process of specimen into the micro-V-groove. After bonding, the cross section of the specimen was observed with an optical microscope and the percentage of filled area  $R_f$  was measured. The increase in  $R_f$  is associated with proceeding of transformation superplasticity, depending on the factors of superplasticity (maximum temperature, repeated number of temperature cycles, compressive load) and results in the promotion of the decrease in bonding time. The effective ratio  $\eta = R_f/R_h$  ( $R_h$ : reduction in height of specimen) in the superplastic bonding is larger than that under isothermal condition.

For the semi-macroscopic strain analyses of the deformation in the vicinity of V-groove, grid analyses were carried out at 50  $\mu$ m intervals. As a result, the transformation superplastic deformation mode under compression is found to be incompressible and homogeneous, and is different from that of both creep and plastic deformation at a room temperature. Furthermore, in the vicinity of inflow area of specimen into micro-V-groove, the distribution of direction angle of principal strains (which were measured at 50  $\mu$ m intervals) reveals good agreement with that of principal stresses calculated on the basis of continuum mechanics. These results suggest that transformation superplastic deformation propagates intimately corresponding to the stress gradient at the bonding interfaces and results in the promotion of the accommodation process.

## Introduction

The effect of transformation superplasticity on the initial accommodation at the bonding interface has been reported by Ohashi(1) et. al.. They have pointed out the effect is due to a great ductility of superplasticity. However, the characteristics of semi-macroscopic deformation (in other words; deformation in polycrystalline system) under stress gradient in the vicinity of rough surface has not been studied for transformation superplasticity or creep. Hence, in this study, from this point of view, the semi-macroscopic deformation at the bonding interface is simulated by the deformation of a specimen which flows into the micro-V-grooved tool under compression.

## Experimental Procedures

A schematic diagram of the apparatus is shown in Fig.1.(2) The chemical analysis appears in Table 1. The specimen shown in Fig.2(a,b) and the micro-V-grooved tool(Fig.2(c)) were heated to a given temperature by induction heating and were cooled with a regulated spurt of air or argon gas. During the cycle, the temperature, displacement and compressive load of a specimen were continuously recorded. After the test the reduction in height  $R_h$  were measured and the cross section of the specimen was observed with an optical microscope and the percentage of filled area  $R_f$  of specimen into the V-groove was measured by picture processing as shown in Fig.3. On the other hand, micro-grid analysis in the vicinity of the V-groove was carried out on a specimen shown in Fig.2(b). A typical time-temperature, -compressive strain, and -load curve are shown in Fig.4.

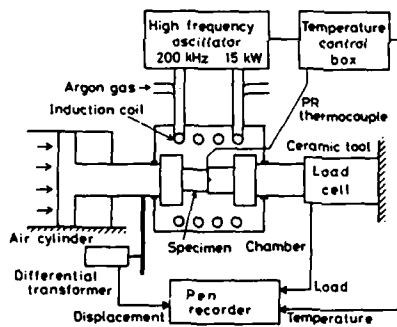


Fig.1 Schematic diagram of test apparatus

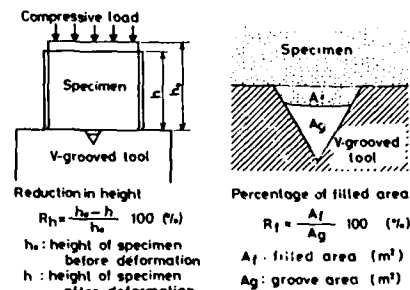


Fig.3 Used nomenclature

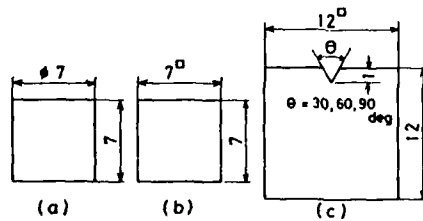


Fig.2 Configurations of (a,b) specimens and (c) V-grooved tool

Table 1 Chemical composition (wt.%)

	C	Si	Mn	P	S
Pure iron	0.012	0.21	0.07	0.009	0.012

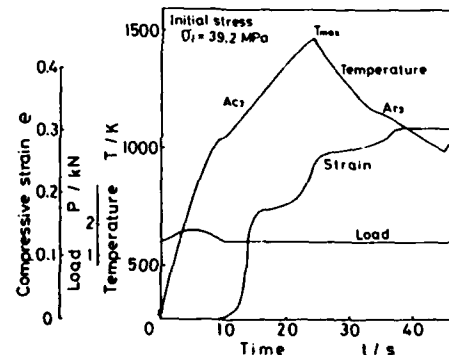


Fig.4 Typical curves of time-temperature, -load, and -strain under compression in pure iron

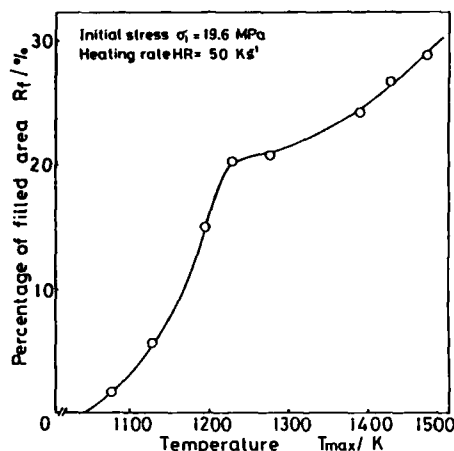


Fig.5 Effect of  $T_{max}$  on  $R_f$  and  $R_h$

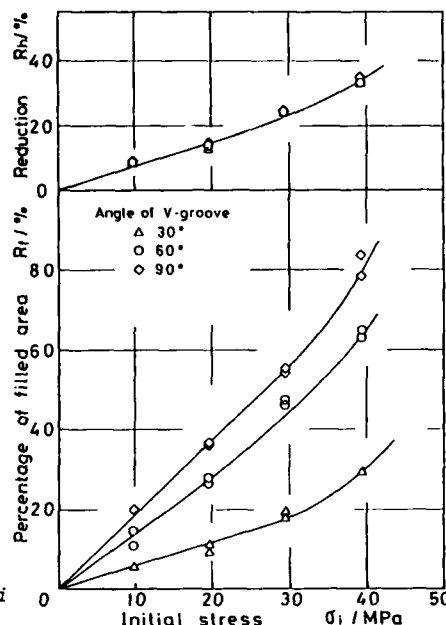


Fig.6 Effect of applied stress  $\sigma_i$  on  $R_f$  and  $R_h$ .

### Results

#### (1) Effect of superplastic factors on $R_f$ and $R_h$ .

The couples of the specimen and the tool were heated up to various maximum temperatures  $T_{max}$  at a heating rate of 50 K/s and were cooled under an initial stress of 19.6 MPa. After the cycle, the reduction in height  $R_h$  and the percentage of filled area  $R_f$  were measured and the results are shown in Fig.5. The inflow of the specimen is found to be caused above about 1100 K and the value of  $R_f$  and  $R_h$  increases considerably at about 1180 K, that is the temperature of  $A_3$  transformation start point ( $Ac_3s$ ). This fact indicates the acceleration of the accommodation due to transformation superplasticity.

The similar experiments were carried out under various initial stresses  $\sigma_i$  up to 40 MPa. Fig.6 shows the effect of  $\sigma_i$  on  $R_h$  and  $R_f$ . In the lower stress range,  $R_f$  increases with an increase of  $\sigma_i$  up to the proportional limit of 20 MPa.

To determine the effect of cycle numbers, specimens were subjected to repeated cycles under a stress of 19.6 MPa. In each cycle, maximum temperature  $T_{max}$  was 1470 K and minimum temperature  $T_{min}$  was 970 K, and the time required was 48 s/cycle. The result is shown in Fig.7. On the other hand, similar tests were carried out at a constant temperature of 1470 K for the equivalent time with that required in the case of the cycles shown above. Fig.7 indicates that the much amount of economy of time for the mechanical accommodation at bonding interfaces can be enabled by transformation superplastic cycles.

#### (2) Effective ratio $\eta = R_f/R_h$ in various deformations

Fig.9 shows  $R_f$  replotted from Fig.8 on the basis of  $R_h$  under transformation superplastic cycle, creep and plastic deformation at a room temperature. The gradient of each line means the effective ratio  $\eta = R_f/R_h$  and indicates the characteristics of semi-macroscopic fluidity against macroscopic ductility and also semi-macroscopic precision formability. The highest value in  $\eta$  is found in the case of transformation superplastic

Fig.7 Inflow area of specimens after superplastic cycles of (a)5 (b)10 and after (c)creep deformation for 480 s at 1470 K, (d) plastic deformation at room temperature under a true stress of 510 MPa.

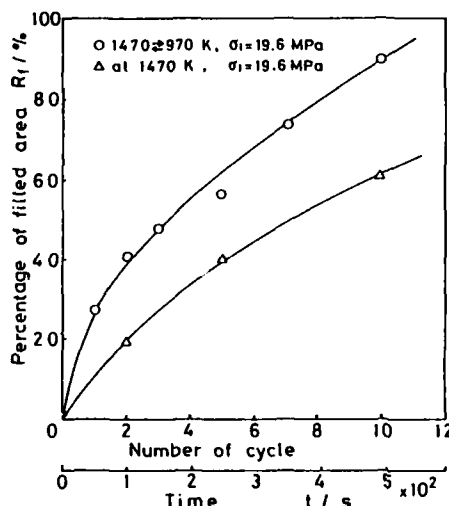


Fig.8 Increases of  $R_f$  by repeated cycles of transformation superplasticity and by holding time of creep deformation at 1470 K

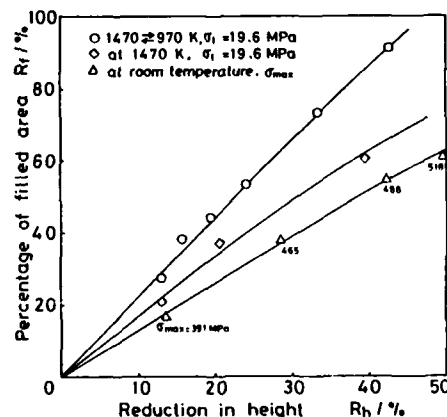


Fig.9 Comparison of  $R_f$  on the basis of  $R_h$  under various conditions of (a)superplastic cycles, (b)creep and (c)plastic deformation

cycle and  $R_f$  will become to be 100 % with the further increase in number of cycles or the macroscopic deformation. On the other hand, in a plastic deformation or creep deformation, further great more amount of time or macroscopic deformation may be required.

### (3) Strain analysis in the vicinity of V-groove under stress gradation

In the previous section, transformation superplastic deformation has been characterized by a good formability in semi-macroscopic scale. Hence, grid analyses(3) were carried out from this point of view under a compressive load. For the first time, an analysis of flow paths of grid points was carried out and the value of 'n' is found to be 2.0 for transformation superplastic deformation in Fig.10. This fact means the deformation is incompressible and homogeneous, and is different from creep or plastic deformation. The semi-macroscopic deformation in the vicinity of micro-V-groove is observed in Fig.11 and the results of the stress and strain analyses are shown in Fig.12. From the figures, the distribution of direction angle of principal strains (which were measured at 50  $\mu$ m intervals) reveals good agreement with that of principal stresses calculated on the basis of continuum mechanics. In a plastic deformation, as shown in Figs.12(b) and 12(d), both direction angles can not always agree in the polycrystalline system by the characteristic factors such as *schmid* factor. These results for transformation superplasticity may be due to the behaviour of transformation interface as a deformation mechanism(3) under stress gradation in polycrystalline system.

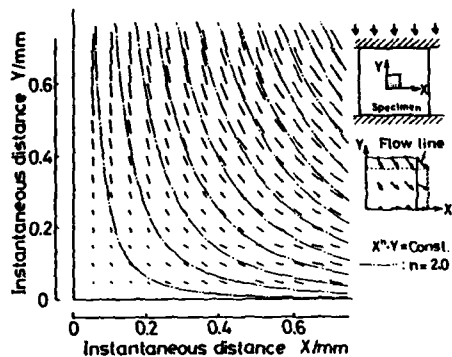


Fig.10 Flow paths of grid points during superplastic deformation under a compressive stress of 19.8 MPa. 'n' is found to be 2.0 in the equation  $X^n \cdot Y = \text{const.}$

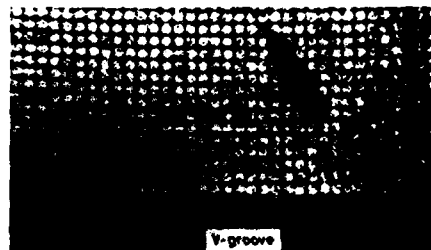


Fig.11 Grid analysis of superplastic deformation in the vicinity of V-groove under the stress  $\sigma_1$  of 19.8 MPa. Grid is 20 lines/mm in density

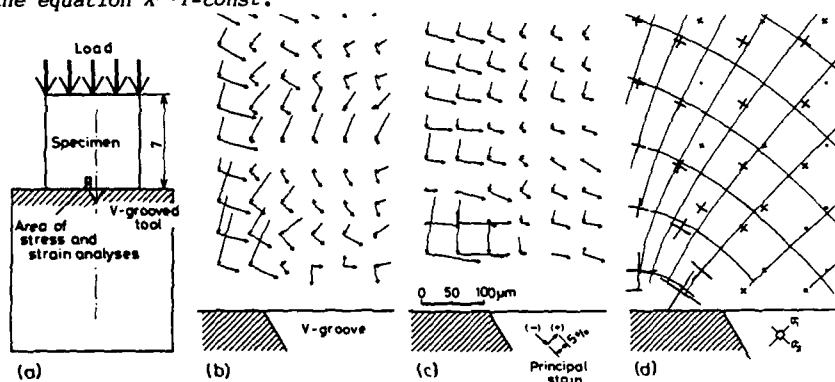


Fig.12 Stress and strain analyses in the vicinity of V-groove. (a)problem definition, location of analysis. Distributions of principal strains in (b)plastic deformation (c)superplastic deformation, and of (d)principal stresses by FEM analysis in the vicinity of V-groove.

#### Conclusion

(1)The inflow into micro-V-groove was caused depending on the factors of transformation superplasticity. The effective ratio  $\eta = R_f/R_h$  for transformation superplasticity is larger than that under isothermal condition and may result in an acceleration of semi-macroscopic deformation at bonding interfaces.

(2)From semi-macroscopic strain analyses, the deformation propagates intimately corresponding to the stress gradation such as that in the vicinity of rough surface and results in a promotion of the accommodation process.

#### References

- 1.O.Ohashi and T.Hashimoto, "Influence of Allotropic Transformation on Diffusion Welding," *Journal of the Japan Welding Society*, 49(1980), 24-29
- 2.Y.Saotome et al., "Dynamic Superplasticity of Steels under Compression," *Proc. 23rd Japan Congress on Materials Research*, (1980), 33-38.
- 3.Y.Saotome and N.Iguchi, "In-situ Microstructural Observations and Micro-grid Analyses of Transformation Superplasticity in Pure Iron," *Trans. Iron and Steel Institute of Japan*, 27(1987), 696-704.



## DIFFUSION BONDING AND SUPERPLASTIC FORMING OF 7475 ALUMINUM ALLOY

J. Kennedy

Corporate Research Center  
Grumman Corporation  
Bethpage, NY

### Abstract

The diffusion bonding (DB) of 7475 aluminum alloy sheet has been evaluated by determining the effect of bonding temperature, pressure, and time on bond mechanical properties and bond interface characteristics. High strength bonds with grain boundary-like interfaces have been produced by bonding 7475 alloy at the superplastic forming temperature (516°C) using very low pressures ( $\leq 100$  psia) without diffusion aids or intermediate materials. The tensile-shear strength and cyclic-shear behavior of 7475-T6 diffusion bonds were comparable to that of 7475 base metal. Also, it has been shown that it is possible to integrate low-pressure diffusion bonding technology with superplastic forming (SPF) for 7475 aluminum. SPF/DB two-sheet, Z-stiffened compression panels were fabricated and had superior buckling resistance compared with riveted built-up panels.

Superplasticity and Superplastic Forming  
Edited by C.H. Hamilton and N.E. Paton  
The Minerals, Metals & Materials Society, 1988

### Introduction

The diffusion bonding of similar material combinations is particularly attractive as a means to fabricate built-up structures of sheet metal or plate materials because machined parts could be joined over large areas with minimal distortion, while reducing machining operations, fastener problems, and material waste. The combined use of superplastic forming and diffusion bonding (SPF/DB) offers the potential to manufacture lighter and cheaper aircraft structures than those made by conventional means. Experience with titanium has shown that diffusion bonding in conjunction with SPF greatly increases manufacturing flexibility, thus allowing consideration of unique integral structures that would not be otherwise possible (1-3).

The use of diffusion bonding in conjunction with superplastic forming to produce integral near-net shapes of aluminum alloys has been severely impeded until now because of aluminum's stable surface oxide, which provides a tenacious barrier against metal-to-metal contact (4-6). Bonding techniques that rely upon high pressure and extensive deformation to fragment surface oxide films are not compatible with the pressure limitations imposed by SPF technology. Therefore, a simple and cost-effective diffusion bonding technique capable of producing high-quality structural joints in a manner compatible with SPF technology could significantly advance the use of aluminum structures.

This paper describes work to evaluate the diffusion bonding of 7475 aluminum alloy sheet. The results of experiments to determine the effects of bonding pressure and time on bond shear strength are presented, and characterization of typical bond interfaces by optical, scanning electron, and transmission electron microscope are discussed. Finally, the results of initial experimentation to integrate low-pressure DB technology with superplastic forming are described.

### Experimental Details

Two sheets of commercially available 7475 aluminum alloy, 1.5 and 2.0 mm thick, were used. They were provided by Alcoa in the WE6 condition after superplastic processing by a proprietary rolling procedure, designated as Schedule E. The composition of the alloy was reported as follows (wt%): 5.7 Zn, 2.3 Mg, 1.6 Cu, 0.12 Fe, 0.22 Cr, 0.1 Si, 0.06 Mn, and 0.06 Ti. Diffusion bonding experiments were conducted with these materials in the as-received condition, i.e., WE6.

Diffusion bonding was accomplished by using a fixture that permitted simultaneous argon gas pressurization at one side of the specimen and air evacuation (pressure  $\approx 1 \times 10^{-3}$  torr) at the other side. The bonded specimens used for shear testing consisted of a pair of 2.0 mm thick 7475 disks, approximately 45 mm in diameter. The disks were prepared for bonding by a proprietary procedure that did not rely upon the use of intermediate materials or diffusion aids. Bonding was conducted in a box furnace at 516°C using various combinations of pressure and time. After heating, the bonding fixture was removed from the furnace and cooled in air to room temperature. Subsequent to diffusion bonding, specimens were heat treated to the T6 condition by solution treating at 482°C for 1 h, water quenching, and then aging at 121°C for 24 h. The shear strength of diffusion bonds were determined by testing lap-shear specimens machined from the bonded disks. The shear specimens were tensile loaded at a crosshead speed of 0.004 mm/s at room temperature. A minimum of five tests to failure were usually conducted for each condition. Bond peel strengths were determined in a similar manner. Fatigue tests were performed on lap-shear specimens in a servohydraulic machine under sine wave loading up to 10 Hz with a load ratio,  $R = 0.1$ . Tests were done on diffusion bonds and base metal in the T6 condition at room temperature in air.

Experiments to integrate low-pressure DB technology with superplastic forming were conducted in a modified DB fixture designed to produce 7475 aluminum alloy SPF/DB two sheet, Z-stiffened compression panels. This was accomplished using baseline bonding parameters by scaling-up the basic DB fixture design. Diffusion bonding of 1.5 and 2.0 mm thick sheet, cut into disks approximately 119 mm in diameter, was done at 516°C and 100 psia for 4 h. During the same heating run, bonding was immediately followed by blow forming, which involved a six-step, pressure-time sequence. Boron nitride was used as a parting agent in selected regions to permit sheet separation during SPF. The SPF/DB Z-stiffened compression panels were fabricated by machining the formed and bonded parts. Subsequently, they were aged to the T6 condition and statically loaded to evaluate

their buckling behavior. Mechanically fastened panels of the same configuration also were tested for comparison.

### Results and Discussion

The effects of pressure and time on bond shear strength are presented in Fig. 1. It is evident that shear strength is time and pressure dependent for these conditions and that the shear strength of the unbonded base metal can be attained. The shear strength of unbonded 7475 base metal was determined using comparably prepared specimens. These results suggest that a minimum pressure-time condition must be satisfied to attain high strength bonds. For example, the data indicate that 4 h is an adequate processing time at the highest pressure but is marginal at lower pressures, which could account for the scatter at those pressures. Low strength and large scatter were mainly attributed to incomplete bonding due to insufficient time or pressure. In contrast, other cases of low strength were observed but have been associated with traceable causes of contamination, such as improper surface preparation or loss of vacuum during bonding. As expected, the size and number of interfacial voids decreases with time at each pressure. After 4 h, the higher pressure bonds appeared to be relatively free of small interfacial voids. Similar effects have been observed in other materials and have led to theoretical models that account for diffusion bonding variables (7-9). Pressure, temperature, and time are intrinsically related to basic bonding mechanisms and subsequent interfacial properties, and thus will continue to be important variable in future work.

The interfaces of high strength bonds can be characterized by their more discontinuous nature, as shown by the optical micrograph in Fig. 2. Although there is evidence of flattened grain boundaries, the trace of the prior straight bond line is interrupted and barely discernible, suggesting interfacial dissolution or migration. In contrast, the interfaces of very low strength bonds were mainly flat and continuous with no apparent grain boundary movement and were characterized by a large number of voids. Fractographic observation of fracture surfaces in 7475 diffusion bonded specimens after shear testing revealed a high degree of metallurgical bonding at the bond interface. The tensile-shear fracture surfaces of high strength bonds had ductile tear ridges. Transmission electron microscopic observations of high strength bonds also revealed that the bond interface looked essentially like a normal grain boundary and did not contain obvious layers or films of oxide. Obviously, the appearance of a grain boundary-like interface is a very positive indication of having attained desirable joint properties. However, microconstituents at the bond interface have not been completely identified nor have the effects of bonding on surface oxides been adequately

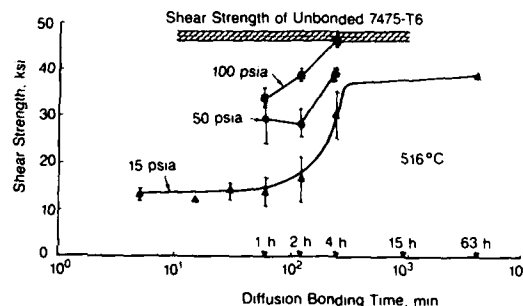


Figure 1 - Effect of DB pressure and time on shear strength.

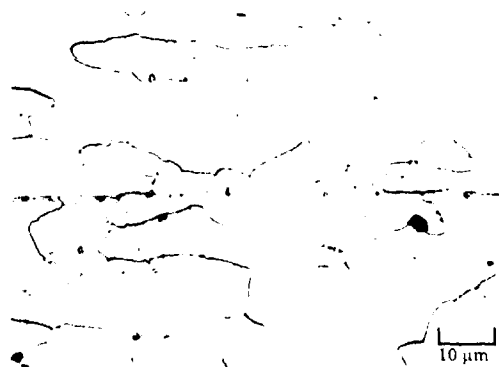


Figure 2 - Microstructure at DB interface of 7475-T6

accounted for. Although an area of great interest, there have been very few definitive studies to identify and characterize oxide fragments (and other debris) at the interface of aluminum alloy diffusion bonds.

A summary of room temperature shear and peel strengths for as-bonded and T6 7475 aluminum alloy diffusion bonds after bonding at 516° C (the superplastic temperature) for 4 h at 100 psia and comparison with unbonded base metal and with general strength ranges common to adhesive bonds are shown in Table 1. In general, the strength of bonds in the as-bonded and heat treated conditions are comparable to those of the base metal and are significantly greater than typical values for adhesive bonded aluminum. These results demonstrate that a low pressure bonding approach for

Material Condition	Shear Strength (ksi)		Peel Strength (lb/in)	
	AS-DB	T6	AS-DB	T6
Diffusion-bonded	23	48	> 400	> 500
Base Metal	23	48	-	-
Adhesive-bonded	1-5	1-5	22-60	22-60

Table 1 - Strength of 7475 aluminum alloy joints.

this alloy can virtually match base metal properties. Fatigue tests on 7475-T6 diffusion bonds also were conducted as part of the evaluation of bond mechanical properties. The results, shown in Fig. 3, indicate that the cyclic shear behavior of 7475-T6 diffusion bonds was comparable to that of 7475 base metal. Similar behavior also was observed for cyclic-shear tests performed on as-bonded material. Overall, these data reinforce the potential for low-pressure bonding and SPF/DB in structural applications.

A diffusion bonded and superplastically formed test article, 4.75 in. in diameter, is shown in Fig. 4. After bonding at 516° C and 100 psia for 4 h, the 0.060 in. thick upper skin was blow formed into a pocket 0.049 in. deep x 1.5 in. wide x 2.8 in. long, to a maximum elongation of approximately 65 %. Subsequently, Z-stiffened compression panels 2.25 in. wide x 2.75 in. long were machined from the bonded and formed parts, as shown in Fig. 5. The results of static loading in the T6 condition to evaluate buckling behavior are shown in Fig. 6. It can be seen that two out of three tests on bonded panels were stopped because their buckling resistance exceeded the loading capability of the test machine. All three tests on riveted panels collapsed at loads below those of the bonded panels. Therefore, compared with riveted built-up panels of the same configuration, the SPF/DB compression test panels offered more buckling resistance and, thus, had increased structural efficiency. The significance of these findings is that improved structural efficiency can be translated directly into weight savings by designing to take advantage of SPF/DB.

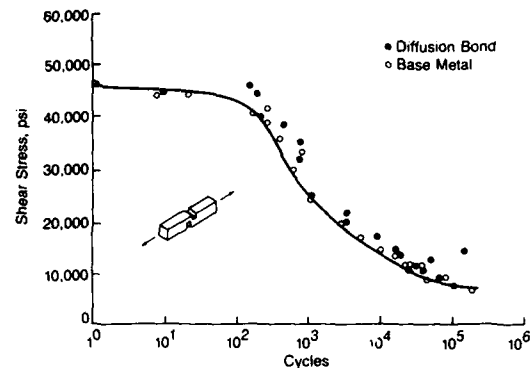


Figure 3 - Cyclic shear behavior of 7475-T6 aluminum alloy.

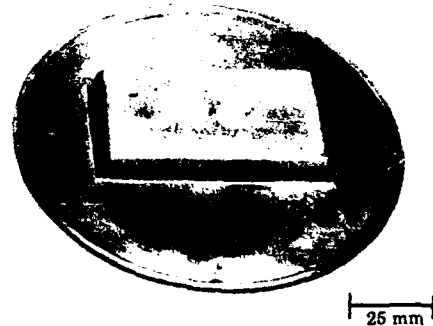


Figure 4 - SPF/DB 7475 aluminum alloy test article

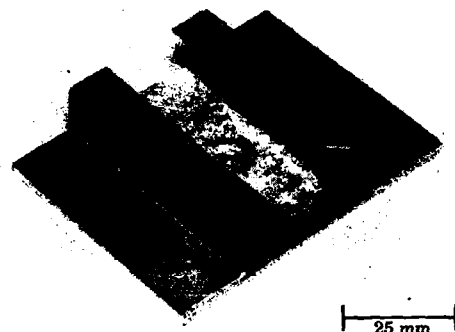


Figure 5 - SPF/DB two-sheet, Z-stiffened 7475 aluminum alloy compression specimen.

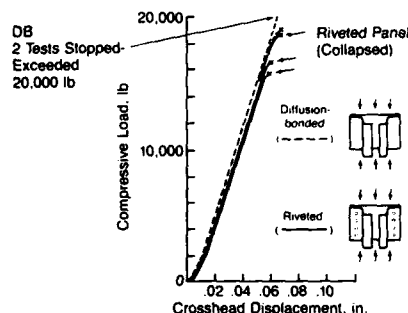


Figure 6 - Buckling behavior of SPF/DB 7475-T6 aluminum alloy stiffened structure

### Summary

It is possible to produce high strength diffusion bonds with grain boundary-like interfaces in 7475 aluminum alloy by bonding at the superplastic forming temperature using very low pressures without the use of diffusion aids or intermediate materials. The tensile-shear strength and cyclic-shear behavior of 7475-T6 diffusion bonds were comparable to that of 7475 base metal. The integration of low-pressure diffusion bonding technology with superplastic forming for 7475 has been demonstrated. SPF/DB two-sheet, Z-stiffened compression panels exhibited superior buckling resistance compared with riveted built-up panels.

### Acknowledgements

It is a pleasure to acknowledge discussions with P.N. Adler, J. Papazian, and E. Ting and the laboratory assistance J. Havranek, H. Baker, and P. Power. This work was performed as part of the Independent Research and Development Program at the Grumman Corporate Research Center.

### References

1. J. Williamson, "Aerospace Applications of SPF and SPF/DB," Superplastic Forming of Structural Alloys, N. Paton and C. Hamilton, eds.; TMS-AIME, Warrendale, PA, 1982, p 291.
2. C.J. Pellerin, "Air Force Perspective on SPF and SPF/DB Titanium Technology," Superplastic Forming, S.P. Agrawal, ed.; ASM, Metals Park, OH, 1985, p 63.
3. E. D. Weisert, "Realization of SPF/DB as a Commercial Fabrication Process," Superplastic Forming, S.P. Agrawal, ed.; ASM, Metals Park, OH, 1985, p 84.
4. R. Tylecote, The Solid Phase Welding of Metals, St. Martin's Press, New York, NY, 1968, p 18.
5. J. Pilling and N. Ridley, Mat Sci and Technology, 3 (1987) p 353-359.
6. D. V. Dunford and P. G. Partridge, "Shear and Peel Strengths of Diffusion Bonded Al-Alloys," Superplasticity in Aerospace-Aluminum, Proceedings, R. Pearce and L. Kelly, eds.; SIS, Cranfield, Bedford, England, 1985, p 257-284.
7. G. Garmon et al., Met Trans, 6A (1975) p 1269-1279.
8. B. Derby and E. Wallach, Met Sci, 18 (1984) p 427-431.

MECHANICAL PROPERTIES OF TITANIUM AND ALUMINIUM

ALLOYS AFTER SUPERPLASTIC DEFORMATION

D. S. McDarmid and P. G. Partridge

Materials and Structures Department  
Royal Aircraft Establishment, Farnborough, UK

Summary

The post-formed mechanical properties of titanium and aluminium alloys may depend upon the thermal cycle, on plastic deformation and on reactions with the environment. The effects of these variables are illustrated with reference to the tensile, creep, fatigue, fracture toughness and impact strength data for SPF and SPF/DB sheet.

*Superplasticity and Superplastic Forming*  
Edited by C.H. Hamilton and N.E. Paton  
The Minerals, Metals & Materials Society, 1988

## Introduction

Superplastic forming (SPF) of thin sheet is now an established process for the manufacture of aerospace structures offering substantial weight and cost reductions compared with alternative processes (1). In recent years the emphasis has moved from the determination of forming parameters towards the measurement of post formed mechanical properties to satisfy design requirements. The post formed properties of current commercial Al- and Ti-alloys and the factors that affect their determination are described in this paper.

## Factors Affecting the Post-Formed Mechanical Properties

Optimum superplasticity requires a small stable grain size and this dictates the sheet processing route for a given alloy system. Commercial superplastic Ti-alloys are readily produced in thin sheet form with a fine-grained equiaxed two phase ( $\alpha + \beta$ ) microstructure. Superplastic Al-alloys however are single phase with either a dispersoid stabilised recrystallised grain microstructure produced by thermomechanical processing (TMT) e.g. 7475E or a cold worked microstructure which dynamically recrystallises during SPF e.g. SUPRAL 100, 150, 200 and Al-Li alloys 8090, 8091 and 2090. With the TMT route sheet thicknesses tend to be limited to <3 mm whereas sheet up to at least 6 mm can be produced by the second route.

The factors affecting post-formed properties can be divided into 3 groups according to their dependence on:-

- 1) The thermal cycles associated with SPF
- 2) Plastic deformation
- 3) Reactions with the environment.

The thermal cycle during forming i.e. heating, holding and cooling from the SPF temperature is responsible for annealing and isothermal grain coarsening in mill annealed Ti-alloy sheet and causes a decrease in strength of up to 12% (2). A similar reduction occurs in SUPRAL alloys due to discontinuous recrystallisation. The effect of cooling rate on mechanical properties depends on whether the alloys are quench sensitive (Al-Cu-Zr, Al-Zn-Mg, Al-Li (8091 and 2090) alloys) or quench insensitive (Al-Li (8090) alloy).

Grain growth is usually greater under SPF conditions than under isothermal conditions as illustrated for Ti-6Al-2Sn-4Zr-2Mo alloy (3) in Figure 1 and for Al-alloys in Figure 2. During SPF of coarse grained  $\beta$ -Ti alloys a reduction in grain and sub-grain sizes occurred but low post-formed elongation values were attributed to severe surface roughening (2).

The alignment of  $\alpha$  and  $\beta$  phases in Ti-6Al-4V alloy lead to both stress and strain anisotropy during SPF (6) (Figure 3). A similar effect can be caused by large grain aspect ratios in Al-alloy sheet. In both cases non-uniform thinning (surface roughening) or local necking may arise and adversely affect mechanical properties. However superplastic strain also has the remarkable effect of causing non-equiaxed grains to become equiaxed and aligned phases to become more homogeneously distributed. This occurs even in fusion welds present in SPF Ti-alloy sheet (7). These changes occur within 50-100% elongation and subsequent deformation is more isotropic.

In Ti-6Al-4V alloy cavitation has been reported at low forming temperatures (<850°C) or in bonded regions deficient in  $\beta$ -phase (8), but it is not considered important in commercial SPF (9). Cavitation can be a

Table I. Effect of SPF at 900°C and post forming heat treatment on tensile properties of IMI 550 sheet [2].

POST - FORMING HEAT TREATMENT	Orien- tation	SP Strain %	0.1PS MPa	0.2PS MPa	0.5PS MPa	TS MPa	E GPa	$\sigma_u$ on 10 mm %	$\sigma_u$ on 12 mm %
Cooled 25°C/min	L	91	899	907	917	984	105	3.9	7.6
		123	931	935	941	1027	104	5.2	8.7
		190	832	841	848	926	98	5.3	7.5
	T	37	961	969	969	1020	112	5.2	8.8
		82	941	947	959	1001	111	3.5	4.8
		120	926	921	922	978	105	4.6	7.8
Cooled 25°C/min 500 °C 24 hrs	L	169	960	965	972	1003	121	2.7	5.9
		172	963	974	983	1019	113	6.0	7.5
	T	172	963	970	979	1059	108	5.5	10.4
		181	907	923	957	1035	96	3.0	10.8
		183	1004	1020	1040	1127	108	5.4	9.5
Cooled 150°C/min 500 °C 24 hrs	L	183	1004	1020	1040	1127	108	5.4	9.5
900°C 24 hrs cooled °C ½ hr, 500 °C 24 hrs	L	191	997	1017	1037	1123	112	3.0	9.0

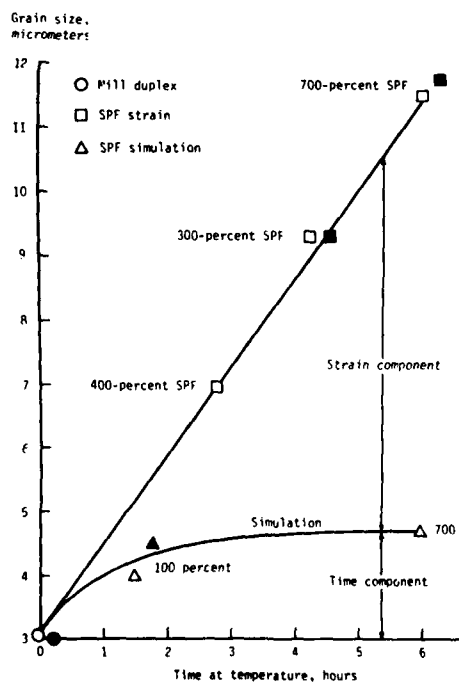


Figure 1 - Effect of SPF at 899°C on grain size of Ti-6242 [3].

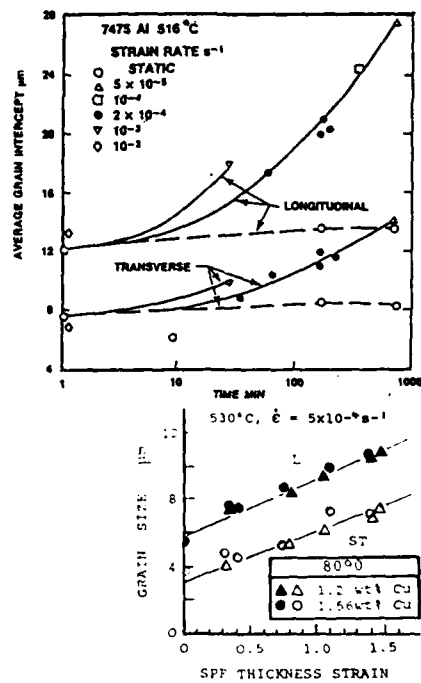


Figure 2 - Effect of forming parameters on grain size a) 7475 [4] b) 8090 [5].



serious problem in Al-alloys since it limits the superplastic elongation and reduces post-formed mechanical properties. The degree of cavitation varies through the thickness and increases with strain. Cavitation can be inhibited or prevented by imposing a net positive pressure of  $\geq 0.6$  of the maximum flow stress (10,11,12) or by the use of a post forming HIP operation (13,14). In the latter it is essential to ensure the cavities are discontinuous and gas free. Vacuum degassing prior to HIPing has been recommended to prevent cavities reforming on re-solution heat treatment.

The literature on the role of texture in superplasticity is very confusing. There are two aspects to be considered, firstly whether the initial texture affects formability and secondly whether the texture changes during SPF affects the post formed properties. The presence of a strong texture has little effect on the formability provided optimum forming conditions are used so that there is no significant contribution from preferred slip modes (15). Superplastic strain tends to weaken and randomise the initial texture, but it may not be eliminated even after strains up to 300% (12,16). However in Ti-alloys the increased randomness can lead to a reduction in the post formed Young's modulus.

Thickness variation is inherent in SPF sheet and depends primarily on the SPF technique used and the  $m$ -value for the material at a given position in the die at a given time. Various techniques can be used to minimise sheet taper but the emphasis in production is on consistency. However tapered sections in test pieces can cause difficulties in determining the post formed mechanical properties and lead to increased scatter in the results and less accurate moduli values.

It may not be appreciated that a significant increase in surface roughness can occur during SPF, particularly on non-die contact surfaces; the effect is greater the larger the grain size and for Ti-alloy sheet with an aligned  $\alpha$  phase microstructure. These factors can contribute to reduced ductility and strength for thin sections. In Ti- and Al-alloys superplastically formed to below 1 mm in thickness elongation values may be reduced from ~8% to ~0.5%. The greater sheet surface area may accentuate surface contamination. Both  $O_2$  and  $H_2$  (from water vapour) can embrittle Ti-alloys. For example the cracks present in  $O_2$ -rich  $\alpha$ -case on Ti-15-3-3 (Figure 5) can reduce the fatigue strength. Surface reaction products can occur on Al-Li alloys formed in air but are less pronounced in argon gas and have not been shown to be detrimental to properties in thick sections.

#### Mechanical Properties of Ti-alloys

The effect of superplastic forming on the tensile strength of Ti-6Al-4V sheet in various thicknesses is shown in Figure 5. Strength reductions of up to 12% were caused by the thermal cycle and smaller reductions (<5%) were caused by superplastic strain. Note the range of strengths achieved in different batches of sheet. Post forming heat treatments can regain some of the strength lost in heat treatable alloys such as IMI 550 (Table 1) but ageing alone could be effective if the cooling rate from the SPF temperature was adequate. Thus components made in "muffle boxes" involving slow cooling would have lower strength than components formed in hot open dies and air cooled (1,7); contamination was more likely in the latter process.

Curves of elevated temperature strength for Ti-6Al-4V sheet after SPF remained lower and approximately parallel to those for the parent sheet up to about 400°C (Figure 6). After SPF an increase in grain size increased the creep resistance of Ti-6Al-2Sn-4Zr-2Mo alloy in the temperature range



Figure 3 - Ti-6Al-4V sheet test piece after machining from bar and SPF at 875°C to 300% elongation [17].



Figure 4 - Cracks in  $\alpha$ -case on Ti-15V-3Cr-3Al-3Sn alloy after 200% elongation in 1.8 h at 910°C in argon.

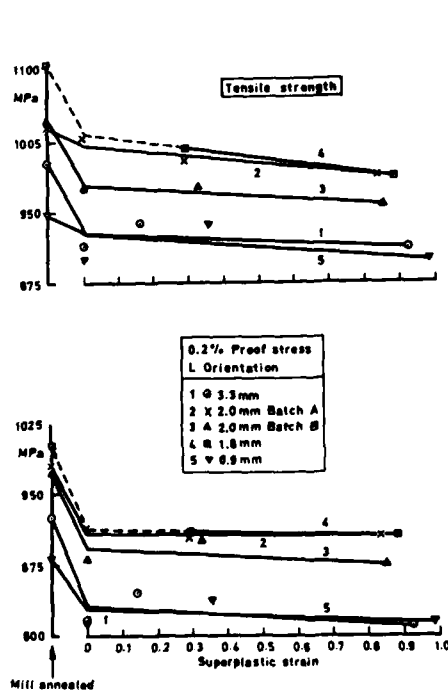


Figure 5 - Effect of SPF at 925°C on strength of Ti-6Al-4V sheet [2].

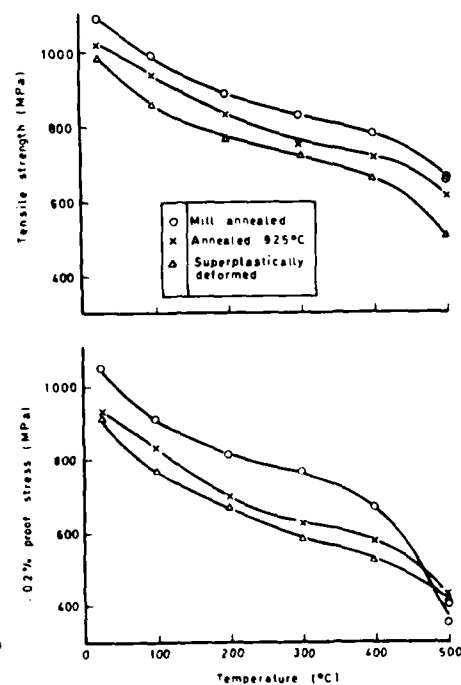


Figure 6 - Effect of SPF at 925°C on elevated temperature strength of Ti-6Al-4V sheet [2].

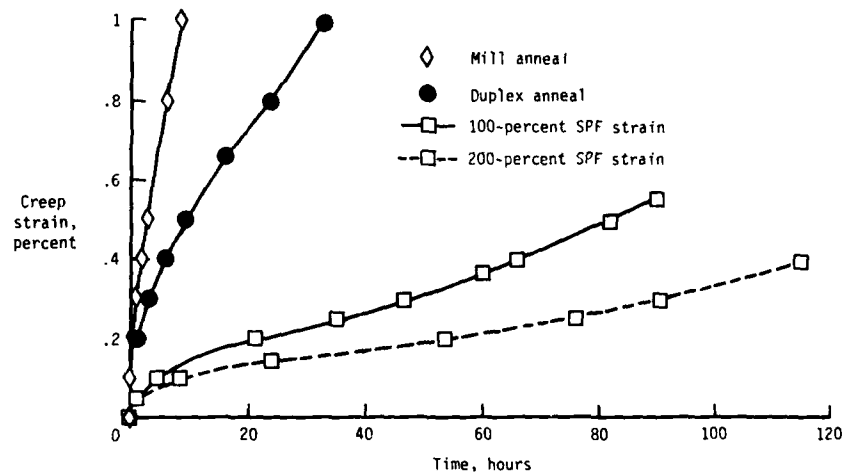


Figure 7 - Effect of superplastic strain on creep rate of Ti-6242 at 538°C and 276 MPa [3].

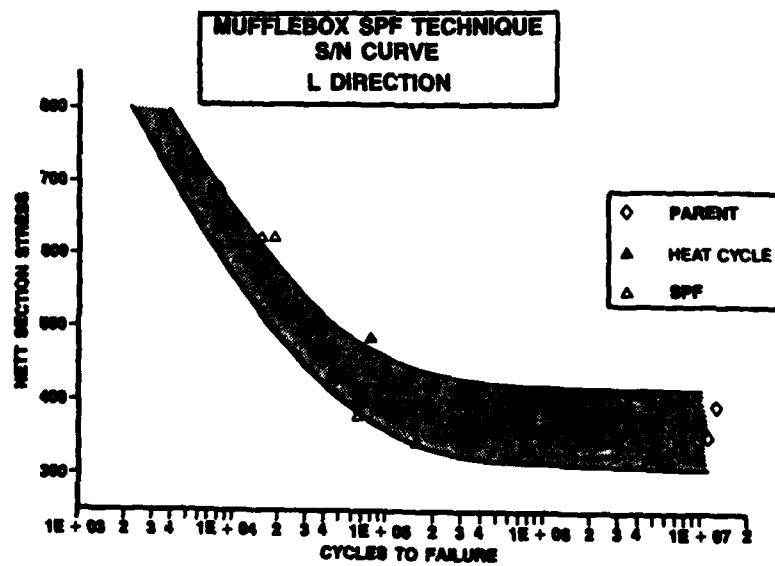


Figure 8 - Notch fatigue curve under constant amplitude loading at stress ratio  $R = 0.05$  and  $K_t = 2.68$  for Ti-6Al-4V after 200% elongation [17].

300-500°C. Creep curves are compared at 537°C and 276 MPa in Figure 7. Attempts to regain the tensile strength by reheat-treatment led to a dramatic decrease in creep strength to that of the original parent sheet (3). Since grain size increased linearly with time (Figure 1) it was concluded that for a given SPF strain a slower superplastic strain rate would result in higher creep strength.

Superplastic forming had negligible effect on notched S/N fatigue strength for  $R = 0.05$  and  $K_T = 2.68$  (Figure 8). Programme loaded fatigue tests (FALSTAFF) for  $K_T = 2.44$  and stress levels of  $\sigma_{32} = 49$  MPa and  $\sigma_{32} = 660$  MPa exhibited considerable scatter (factor 2 in life) with some tendency for longer lives for the hot open die processed sheet. There appeared to be no adverse effects of SPF on crack growth rates or fracture toughness.

Finally some comments on the mechanical properties of diffusion bonded joints are apposite since they may form a critical part of future SPF/DB Ti-alloy structures. Parent metal properties can be obtained for bonded joints between Ti-alloys. Small residual voids reduce the fatigue strength but it may still exceed the notched ( $K_T = 2.4$ ) fatigue strength used in current design. Impact strength appears to be particularly sensitive to residual voids and/or interface contamination. For example 2 Izod fracture surfaces of nominally identical test pieces taken from a gas pressure bonded stack of 1 mm thick sheets are shown in Figure 9. The sheet planes were normal to the test piece axis and no bond defects were detected. However one fracture was rough ( $R_a = 4.4 \mu\text{m}$ ) with coarse ductile cusps and failed at 22.4 J whilst the other fracture was smoother ( $R_a = 0.72 \mu\text{m}$ ) with small ductile cusps and it failed at 12.9 J.

#### Mechanical Properties of Al-alloys

The tensile properties are reduced by superplastic deformation. This degradation was initially correlated with cavitation (Figure 10) and the degradation was greater for clad sheets rather than unclad sheets due to increased cavitation (19). Suppression of cavitation by back pressure does not completely prevent the degradation (Figure 11) which is then attributed to grain growth and in the Al-Li alloy to the loss of sub-grain strengthening due to the gradual replacement of the initial unrecrystallised microstructure by a recrystallised one. The lower strength observed for Supral 220 in lightly strained material is due to the production of large grains up to 200  $\mu\text{m}$  by discontinuous growth compared with fine grains (4-6  $\mu\text{m}$ ) developed by continuous recrystallisation in higher strained material. The Al-Li alloys have the advantage of higher elastic modulus (78 GPa) and lower density. The Al-Li 8090 alloy has the added advantage of being less sensitive to quench rate. This is extremely important since it avoids the risk of distortion in complex shaped SPF components during subsequent solution treatment prior to ageing (Figure 11). However if the copper content in 8090 is increased from 1.2% to 1.6% the alloy becomes quench rate sensitive (5,23) (Figure 12) like 8091, a high copper derivative (5,24). The loss in the as-formed + aged strength is caused by the formation of a copper-rich precipitate containing  $\text{CuMg}(\text{Li})\text{Al}$  during the slow cool (5,23).

Although the Al-Li alloys are recrystallised during SPF the initial crystallographic texture present in the straight rolled sheets is not completely eliminated and results in some anisotropy e.g. the 0.2% PS in the L, 45° and T orientations in 8090 after 250% strain is 320 MPa, 280 MPa and 340 MPa (25), whereas in 2090 after 200% strain the corresponding values are

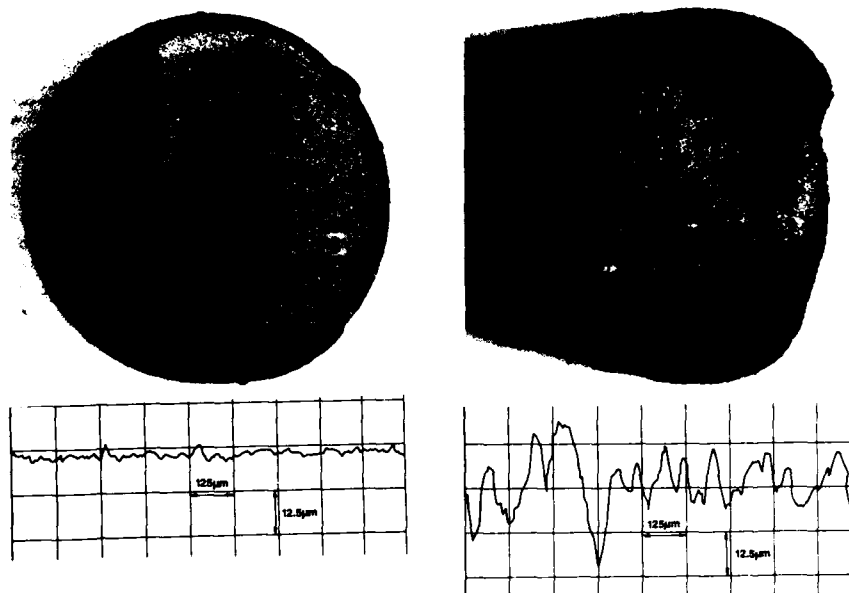


Figure 9 - Impact fracture surfaces of diffusion bonded Ti-6Al-4V sheet stack of a) smooth b) rough fracture.

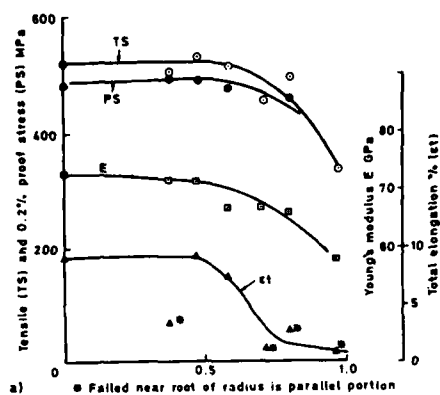
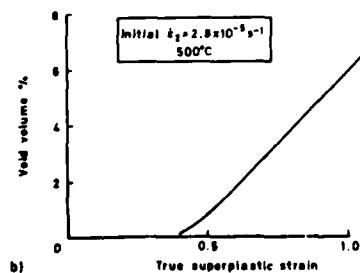


Figure 10 - Effect of uniaxial SPF strain on tensile properties and void volume % in 7010 Al-alloy sheet [18].



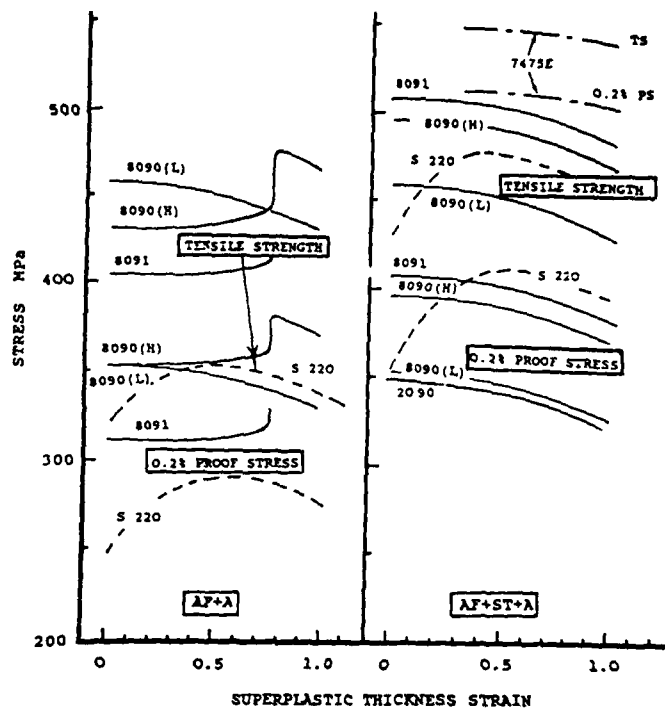


Figure 11 - Effect of post formed heat treatment on strength of biaxially formed Al-alloys under back pressure. 8090 (L) 1.2 wt% Cu, 8090 (H) 1.56 wt% Cu, 8091 [5], SUPRAL 220 [20], 7475E [21], 2090 [22].

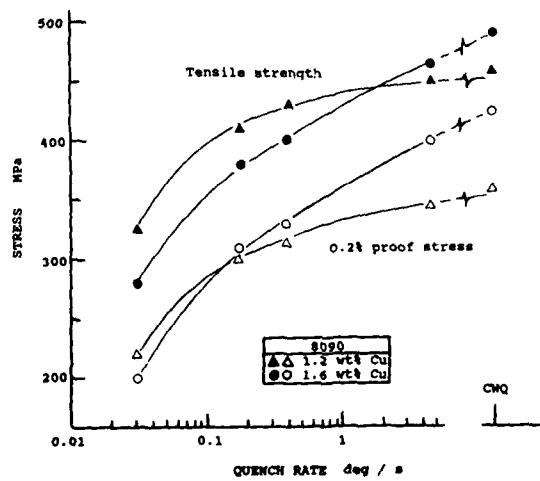


Figure 12 - Effect of quench rate and Cu content on strength of 3 mm thick 8090 sheet [23].

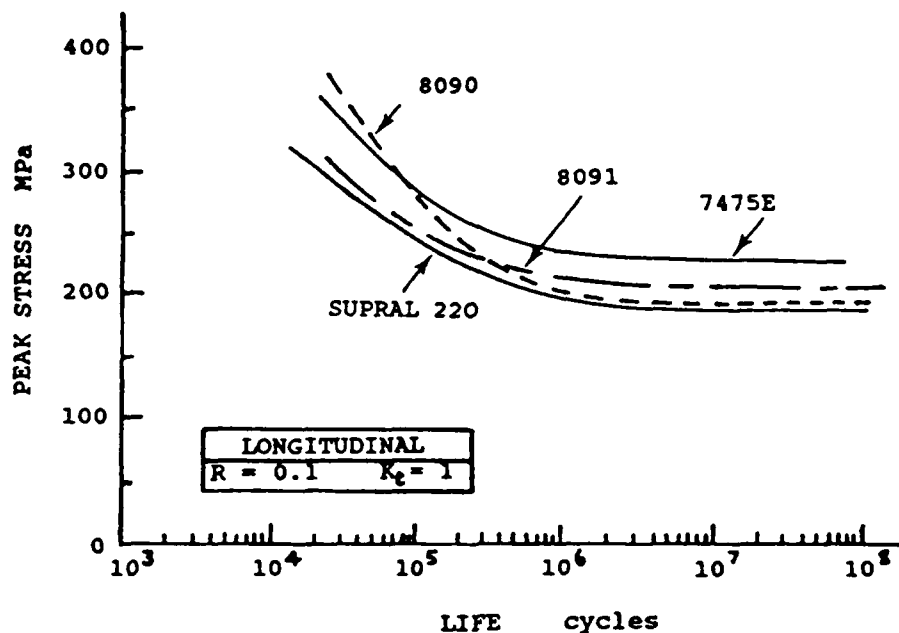


Figure 13 - Comparison of S/N data for biaxially formed Al-alloys after  $\sim 1.2$  superplastic thickness strain. 8090, 8091 [5], SUPRAL 220 [19], 7475E [21].

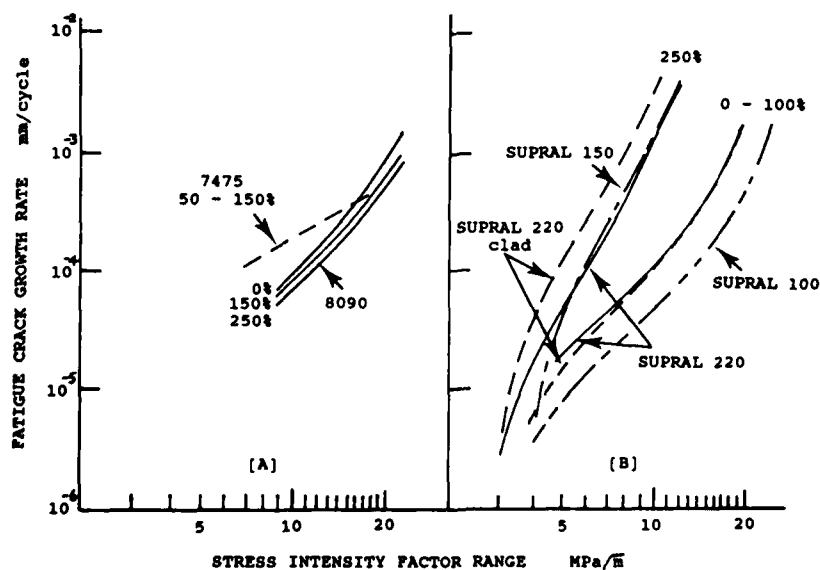


Figure 14 - Effect of biaxial superplastic strain on fatigue crack growth a) with back pressure 7475 [21], 8090 [25] b) without back pressure [19].

320 MPa, 305 MPa and 295 MPa (22). Alcan has now modified the production route for SPF sheet which should reduce the anisotropy.

As in Ti-alloys, fatigue properties (S/N) are less sensitive to superplastic strain than tensile properties and are independent of test piece orientation (5,19,21,26,27,29). The fatigue strength of 8090 (1.2% Cu), unlike the tensile properties, is dependent on the forming temperature; the lower fatigue performance of material formed at 515°C instead of 530°C can however be recovered by a post formed 530°C treatment (5). In the -T6 condition the materials have similar fatigue even though markedly different tensile strengths (Figure 13). This fatigue performance can be obtained in 8090 (1.2% Cu) in the as formed + aged condition by forming at 530°C. Cavitation reduces fatigue strength and increases the scatter (19,28). A clad layer reduces fatigue performance and this reduction is greater after SPF because the more rapid grain coarsening in the cladding favours crack nucleation (19,28). Fatigue crack growth rates (FCGR) appear to be independent of superplastic strain in the absence of cavitation (Figure 14a). In 8090 sheet FCGR in high strained recrystallised material is slightly slower than in initial unrecrystallised material. Without back pressure the FCGR increases with increase in superplastic strain (Figure 14b). FCGR is greater for clad than unclad sheet.

#### Discussion and Conclusions

Although some structures will be strength or fatigue dependent the majority will be stiffness critical and thickness limited. For Al-components Al-Li alloys, particularly 8090 with its lower density and 10% higher modulus, will be superior to Supral and 7475E alloys. In some designs SPF/DB Ti-alloy structures may be competitive with conventional Al-alloy structures in terms of manufacturing costs; although they would have a similar mass there is the additional benefits of good corrosion resistance and elevated temperature capability. Higher stiffness may be obtained with Al and Ti particulate MMC some of which are superplastic (29,30). However their properties will depend on the extent of cavitation and on particle morphology. No post-formed data is available. There will be a need for low quench rate sensitivity in multiple sheet structures to avoid distortion and attainment of the required strengths in the core sheets.

#### References

1. D. Stephen Designing with Titanium, (Inst. Metals, 1986) 108.
2. C. D. Ingelbrecht *ibid* p.252.
3. W. A. Ossu and D. M. Royster NASA Tech. Paper 2674 May 1987.
4. A. K. Ghosh Proc. Conf. "Superplastic forming", (Los Angeles 1984) 23.
5. D. S. McDarmid and A. J. Shakesheff Int. Conf. "Al-Li IV", (Paris 1987) 257.
6. P. G. Partridge, D. S. McDarmid and A. W. Bowen Acta Met 33, (1987) 571.
7. P. G. Partridge and D. Dunford Int. Titanium Conf. Cannes, (1988) In the press.
8. M. T. Cope and N. Ridley Mat. Sci. Tech. 2, (1986) 140.



9. D. Stephen "Superplasticity", (AGARD LS-154) Paper 7 (1987).
10. C. C. Bampton and R. Raj Acta Met 30, (1982) 2043.
11. C. C. Bampton et al Met. trans. 14A, (1983) 1583.
12. A. J. Shakesheff and D. S. McDarmaid Int. Conf. "Superplasticity in Aerospace - Aluminium" (Cranfield, 1985) 180.
13. P. J. Mesch, P. S. Pao and R. J. Lederich Scripta Met 18, (1984) 83.
14. H. Ahmed Ph.D. Thesis, (Cranfield 1986).
15. D. S. McDarmaid and P. G. Partridge J. Mat. Sci. 21, (1986) 1525.
16. P. G. Partridge, A. W. Bowen, C. D. Ingelbrecht and D. S. McDarmaid, Int. Conf. "Superplasticity" (Grenoble 1985) 10.
17. P. G. Partridge, D. S. McDarmaid, I. Bottomley and D. Common as Ref 9 Paper 6.
18. P. G. Partridge and A. J. Shakesheff RAE Tech. Report TR 84020 (1984).
19. A. J. Shakesheff as Ref 12 p.36.
20. D. S. McDarmaid, A. J. Shakesheff and B. Ginty RAE Tech. Report TR 85091 (1985).
21. S. P. Agrawal and J. M. Truss as Ref 12 p.296.
22. C. W. Cho, B. A. Cheney, D. J. Lege and J. I. Petit as Ref 5 p.277.
23. S Kyle-Henney and A. J. Shakesheff Unpublished MOD work.
24. R. Grimes, W. S. Miller and R. G. Butler as Ref 5 p.239.
25. D. S. McDarmaid Unpublished MOD work.
26. C. C. Bampton and J. Edington J. Eng. Mat. Tech. 105, (1985) 55.
27. C. C. Bampton, F. McQuilkin and G. Stacher as Ref 4 p.76.
28. H. C. Lipsius, J. Stock and A. Shames AFWAL-TR- 85-3050 Pt. 1 1985. Wright-Patterson AF Base, Ohio 45433.
29. R J. Lederich, P. J. Meschter, and S. M. L. Sastry ASTM STP 890 p.319.
30. Mahoney and A. K. Ghosh Met. Trans. A 18, (1987) 653.

THE APPLICATION OF SUPERPLASTIC FORMING FOR  
MAKING PLASTIC INJECTION MOULD

---CAVITY DESIGN AND SUPERPLASTIC PRESSING

Zhang Dixiang

Radio Manufacture Factory, Beijing, China

Abstract

A kind of mould cavity with complicated shape, which is used for injecting plastic radio cabinet(118x70x15), is formed through superplastic technique. The experience in forming as well as the characteristic in design are introduced.

The cavity of mould was made from the superplastic alloy Zn-4%Al-1%Cu. Considering the lower strength and hardness of this alloy in design, the surrounding of the cavity mould was covered with some steel jacket. So the guide for side loose cores was borne mainly by the steel jacket, so as to decrease the wear of the mould parts.

There are 340 sound holes with diameter of 1.2 mm on the main surface of the capinet of radio MX108. A newly designned structure was adopted, in which the sound holes were fixed by the core of cavity of rest die and were formed through rendezvous with the grid in moving die.

Semi-closed superplastic pressing was taken at low speed. The terrace die and formed parts were at the same temperature of 350°C throughout the process. Much higher accuracy, better geometric shape and clearer arris line are got with superplasticlly formed cavity than that made by traditional process.

In production, fully according to the process requirment of conventional condition, after 35000 times of injection, through examing, the cavity is still undamaged.

Superplasticity and Superplastic Forming  
Edited by C.H. Hamilton and N.E. Paton  
The Minerals, Metals & Materials Society, 1988

### Introduction

Die plays an important part in modern industry. But die making is of precision and difficulty, special-purpose equipments and high-level technicians are frequently needed. High cost and long period of production are resulted. This situation can be improved by the use of new materials, new techniques and new processes. Some medium experiments have been made on a kind of superplastic zinc alloy and superplastic forming of it for die making. The complex cavity mould of Zn-alloy which is used for injecting plastic cabinet of radio has been formed through SPF. Some basic aspects as well as the characteristics in design are introduced as following.

#### The Possibility of Making Plastic Injection Mould with Zn-Alloy

The physical and mechanical properties of Zn-4Al-1Cu alloy are shown in table 1. Comparing with general die materials, it possesses lower melt temperature, lower strength and hardness. Is it possible to make plastic injection mould with it? This is the question that many people have raised.

Table 1. Some Physical and Mechanical Properties of Zn-4Al-1Cu

Melting Point	Yield Stress (kg/mm <sup>2</sup> )	Hardness HB
660-661K	27-29	110

Fig.1 shows the hardness as the function of temperature. It can be seen that the hardness of Zn-4Al-1Cu lowers sharply with the rise in temperature. The hardness at 423K is only about HB50. Normally, plastication temperature is 433-453K. But according to the demand of forming process, the temperature of die is in the range of 303K to 353K. The hardness under the condition is above HB90. Based on the properties of the alloy, thermal deformation does not take place at that temperature.

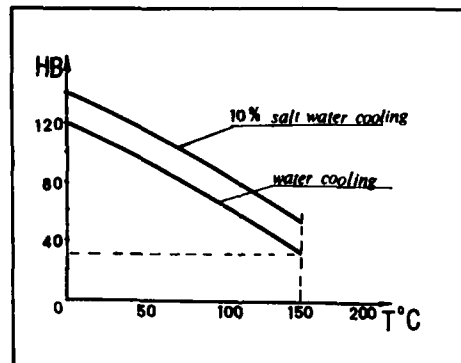


Fig.1. Hardness change with temperature

Adopting certain die structure, in which the Zn-alloy is only responsible for plastic forming, not for load-bearing, the affect of low strength of the alloy can be avoided.

Design of Plastic Injection Mould of MX-108 Radio Cabinet

The size, shape and structure of plastic part as well as forming characteristics of Zn-alloy should be considered in die design.

There are three 1X0.5mm grooves on the facade of the cabinet, which can add effect of exterior view (Fig.2). Forming static mould cavity through superplastic pressing with Zn-alloy is suitable for above characteristics.



Fig.2, Exterior view of the cabinet of MX-108

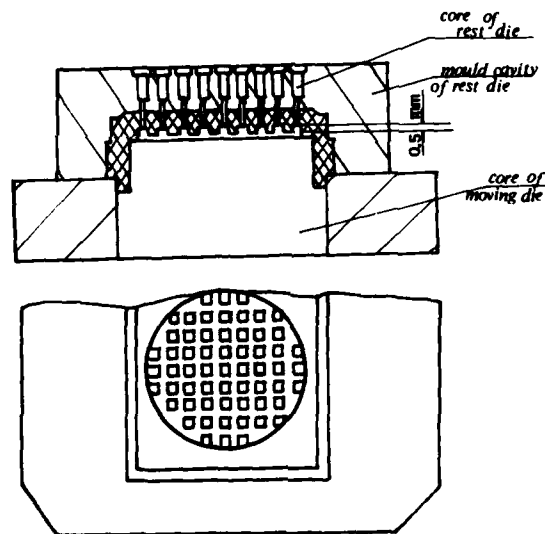


Fig.3, The schematic diagram of the loose-core structure in the die

There are 340 sound holes with diameter of 1.2mm on the main surface of the cabinet. The spring loose cores are used for the conventional structure. But the reliability of this structure is poor. While some breakdown takes place such as spring fatigue failure, 340 loose cores can not be taken out, plastic part can fall into static cavity mould. At that

situation the workers can only take out the cabinet with pry bar. Even prying steel mould with copper bar, the mould cavity are often damaged. So a new structure is adopted, in which the sound holes are formed through butting of the cavity cores in rest die and the grids in moving die.

From Fig.3, it is easy to be seen that the plastic part definitely falls onto the moving die due to contracting with cold while opening the die after forming.

There are a 22X4mm rectangle hole and a 7 mm diameter round hole on the side of the plastic part. Side loose cores are used, the guided way of which relies on steel cover.

#### Results and Conclutions

Up to now more than 30,000 plastic parts have been made using Zn-alloy mould which was formed through superplastic pressing. The plastic cabinet are more regular than that made by steel mould. Their lines and edges are more artistic. The mould was measured after 25,000 plastic parts had been injected. No size change was found. Its smoothness was raised to some extent.

It has been proved that superplastic Zn-alloy and superplastic pressing process are feasible in die making in some cases.

## COMBINED EXTRUSION OF SUPERPLASTIC Al-Zn SYSTEM ALLOYS

M. HIROHASHI and H. ASANUMA

Department of Mechanical Engineering,  
Faculty of Engineering, Chiba University  
Chiba, Japan

### Abstract

A new method named "Combined Extrusion" similar to backward extrusion has been developed. The characteristic of this method is the reactional movement of the die or the back-up punch against the movement of the upper punch. In this study, formability of the superplastic Al-78Zn alloy was investigated using the developed controlling system. As a result of experiment, the alloy could be easily formed into thin-walled cylindrical vessel with complicated outside shape in one working process. As for the control of forming, constant load extrusion was easier than constant speed extrusion. Non-superplastic alloys such as cast Al-78Zn alloy and Al-Zn system alloys with less Zn content were also tried to be applied to this equipment. Formability of these alloys were not so good as that of superplastic alloy. It decreased with decreasing Zn content. But such alloys also could be formed by suitable forming conditions, that is, higher forming load, slower extrusion speed and higher forming temperature by this method.

Superplasticity and Superplastic Forming  
Edited by C.H. Hamilton and N.E. Paton  
The Minerals, Metals & Materials Society, 1988

## Introduction

In order to apply the good flowability of Al-78Zn alloy to plastic forming, the authors have developed an equipment which can form a block of the alloy into a thin-walled product which has non-uniform cross section and complicated outside shape in one working process. Furthermore, Al-78Zn superplastic alloy powder could be made into a composite with SiC whisker by compacting and forming in this equipment (1). There are a few similar methods (2)(3), but there cannot be seen such a method as the combined extrusion method which can extrude and jut material in the direction perpendicular to that of extrusion at the same time. In this study, as the first step to industrial use, oil pressure circuit of combined extrusion equipment was designed to control the forming load and speed and factors which affect formability were examined. In addition to Al-78Zn superplastic alloy, this method was tried to be applied to non-superplastic alloys of the same system.

## Materials and Experimental Methods

Commercially extruded bar of Al-78Zn eutectoid alloy (named BE) which was composed of fine and equiaxed crystal grains and exerted superplasticity was mainly used. The factors affecting formability were made clear providing this alloy at the superplastic temperature of it 250°C. This forming process was also applied to metal-mold casted Al-78Zn alloy (named AC) and Al-(78-30)Zn alloys. These were non-superplastic alloys and the specific strength was improved by reducing Zn content. Three ways of movement of the die and the punches are schematically shown in Figure 1 (a)-(c). Combined extrusion corresponds to (b) or (c). In this paper, so the die installed with heater was fixed, oil pressure circuit to control upper punch and lower back-up punch in the manner of Figure 2 was designed and then factors which affect formability were clarified. Constant load or constant speed in forming was obtained by using valve ① and ② or ① and ③, respectively. Forming temperature was varied between 150 and 400°C.

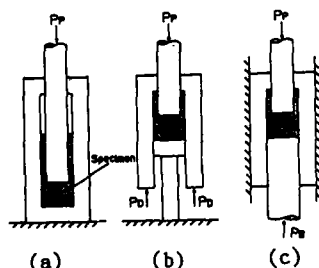


Figure 1 - Schematic diagrams for extrusion,  
(a) closed packaged  
(b) combined extrusion (lower punch fixed)  
(c) combined extrusion (fixed die).

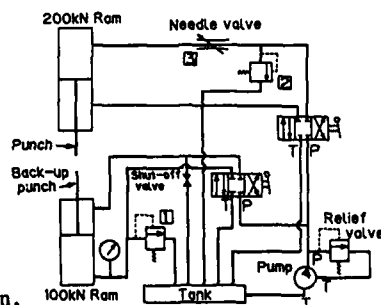


Figure 2 - Oil pressure circuit  
for combined extrusion.

## Results and Discussions

### Forming Process

In Figure 3, forming processes with screw type and fin type dies are explained by showing the cross sections of die and specimens. The specimen is set at stage (a) and is under forming at (b) and (c). Characteristics of this method is described as follows. The specimen compressed by both punches is juttred into screw or fin pattern of the die and fitted there.

So, only the part under forming is moving downward. According to this forming process, friction force generated between sample and die is neglected and forming load is reduced as compared to conventional backward extrusion. Examples of products obtained with various dies are summarized in Figure 4.

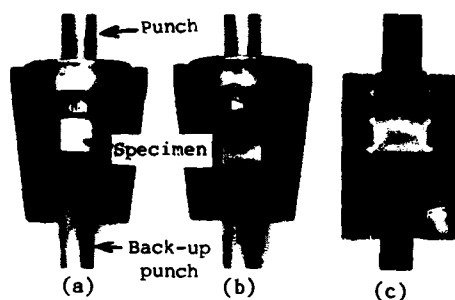


Figure 3 - Cross sectional photographs during forming process, (a) before forming (b) screw die (c) fin die.

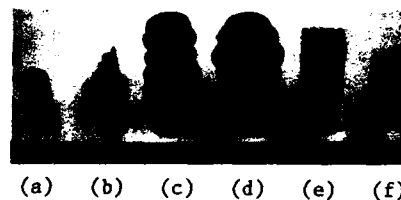


Figure 4 - Forming samples, (a) specimen (b) flat plate with fins (c) fin type A (d) fin type B (e) spline type (f) screw type.

#### Formability under Constant Punch Loads

Forming under control of constant punch loads as shown in Figure 5 was examined. The load difference  $dP$  between punch load  $P_p$  and back-up punch load  $P_b$  is given by equation  $dP = P_p - P_b$ .  $P_b$  corresponds to net compressive force on specimen, but  $P_p$  includes frictional forces generated among die punch and material. Therefore,  $P_b$  was kept constant ( $=10\text{kN}$ ) and  $dP$  was varied. As shown in Figure 6, forming speed varied depending on  $dP$ . Forming speed was about constant when  $dP=10\text{kN}$ , accelerated when  $dP>10\text{kN}$ , and when  $dP<10\text{kN}$ , it reduced because the contribution of friction increased. Forming speed also depends on  $P_b$ . If  $P_b$  was reduced under constant  $dP$ , forming speed increased. But, when it was excessively reduced, the sample broke because material flow became insufficient. Contrary to this occasion, that is, when  $P_b$  was excessively applied, material penetrated into the thin gap of split dies. States of products formed under various conditions are summarized in Figure 7, where  $V_{B20}$  stands for the speed of back-up punch when its stroke is 20mm. As shown in this figure, perfect forming region exists widely between the broken region or the imperfect forming region and the over load region.

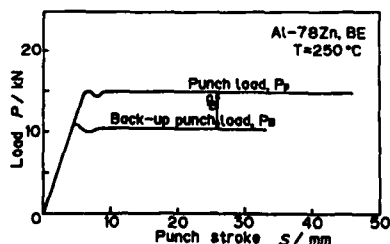


Figure 5 - Combined extrusion load—stroke diagrams under constant forming load.

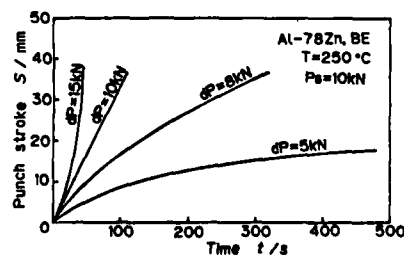


Figure 6 - Effect of forming load on forming speed.



### Formability under Constant Punch Speed

The punch load  $P_p$  depending on punch stroke under constant punch speed and back-up punch load is shown in Figure 8.  $P_p$  attains to a maximum value which seems to correspond with the maximum load that appears uniaxial compression test. In Figure 9, dependence of  $dP_{max}$  on punch speed  $V_p$  at various extrusion temperatures is shown. At every temperature,  $dP_{max}$  proportionally increases with increasing temperature. This tendency corresponds to the results of closed-die forging reported by Takei et al. (4). Though Al-78Zn superplastic alloy was used here, forming load simply decreased with increasing temperature regardless of its superplastic temperature.

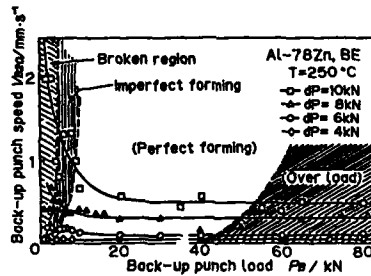


Figure 7 - Forming limit diagram for combined extrusion.

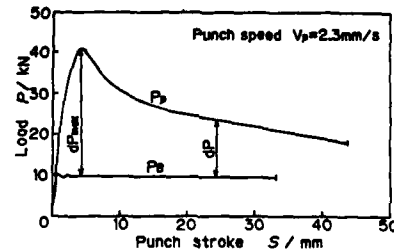


Figure 8 - Forming load—stroke curves under constant punch speed.

### Formability of Hypo-eutectoid Al-Zn Alloys

The combined extrusion equipment was applied to the forming of non-superplastic cast hypo-eutectoid Al-Zn alloys. In Figure 10, dependence of  $dP_{max}$  on punch speed  $V_p$  for the Al-(50-78)Zn alloys is shown. At the same punch speed,  $dP_{max}$  for the superplastic Al-78Zn alloy (BE) is the smallest. But non-superplastic alloys are also formable by higher load and temperature. Forming limit of such cast alloys at 250°C is shown in Figure 11, where symbol "O" indicates a product without breakage and "X" indicates a broken product. According to this figure, speed limit for forming becomes higher with increasing Zn content. Though Al-30Zn alloy is not formable at this temperature, it becomes formable if temperature is increased up to 320°C as shown in this figure or  $P_B$  is increased.

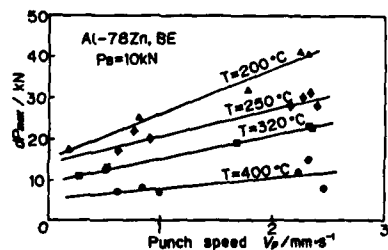


Figure 9 - Dependence of punch speed on the maximum punch load at various extrusion temperature.

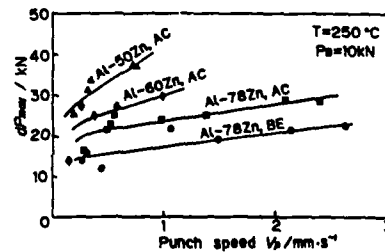


Figure 10 - Formability of the Al-(50-78)Zn alloys at 250°C under constant back-up load.

### Strength of Products

The forming condition should be decided also by taking the strength of product into account. In Figure 12, effect of forming temperature on

Vickers-hardness of the products is shown for different alloys and cooling rates from forming temperature, that is, water quenching and air cooling. The hardness of products of the eutectoid alloys does not depend on the micro-structures before forming, that is, AC or BE, but depends on the temperature and cooling rate. Over the eutectoid temperature (275°C), cooling rate clearly had an effect on the hardness. In this temperature range, air cooled product was hardened depending on the increase of temperature because volume fraction of peralite structure increased with increased temperature. As for Al-60Zn alloys, the hardness almost corresponded with air cooled eutectoid alloy even when it was water quenched. This means that specific strength and fabrication cycle can be improved by reducing Zn content from 78% to 60%.

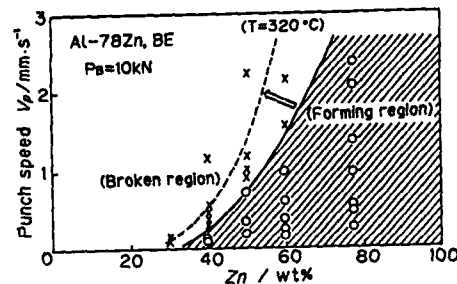


Figure 11 - Forming limit of the cast alloy with Zn concentration at 250 °C.

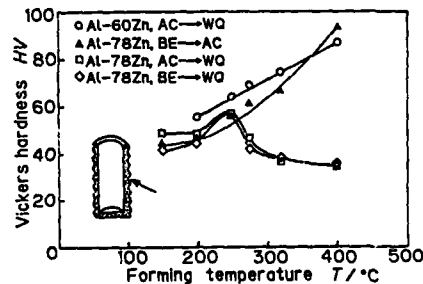


Figure 12 - Effect of forming temperature on the hardness of the products in various alloys.

### Conclusion

- (1) By using combined extrusion equipment, forming of superplastic Al-78Zn alloy into complicated shape products in one working process became possible under constant load or constant speed. Comparing these two forming conditions, the former was rather easier.
- (2) There existed formable limitations to this method. When back-up punch load was set between 20kN and 40kN, comparatively wide perfect forming region and high forming speed were obtainable.
- (3) This method could be also applied to non-superplastic Al-Zn system alloys such as hypo-eutectoid alloys or metal-mold casted alloy. Though formability of these was inferior to that of superplastic alloy, it could be improved by increasing temperature or back-up punch load.
- (4) In case of Al-78Zn alloy, the strength of formed products strongly depended on forming temperature and cooling rate from it rather than the micro-structure before forming. As for water-quenched Al-60Zn alloy, the hardness almost corresponded with air-cooled eutectoid alloy.

### References

1. H. Asanuma, M. Hirohashi and E. Kawai, "Combined Extrusion of SiC Whisker/Al-Zn Air-Atomized Powder Composites", *Advanced Technology of Plasticity*, I(1987), 487-492.
2. M. Kunogi, "Plastic Flow in Piercing Process", *Journal of JSME*, 22(118) (1956), 429-437.
3. B. Avitzur, *Handbook of Metal-Forming Processes*, (Wiley-Interscience, 1983), 167.
4. H. Takei, T. Oshita and T. Hatayama, "Closed Die Forging of Superplastic Zn-22Al Alloy", *Journal of the JIM*, 48(7)(1984), 742-747.

# SUPERPLASTIC BEHAVIOUR OF DIE STEEL 4Cr3Mo3W2V AND APPLICATION

Yang Yongchun

Beijing Research Institute of Mechanical and Electrical Technology  
Beijing, China

## Abstract

Hot die steel 4Cr3Mo3W2V is normally used to make hot forging die. Through pretreating specially, the structure of the steel can be fully fined, and the average grain size is 2 to 4  $\mu\text{m}$ . This paper studies the relationship between plasticity of pretreated steel and deformation temperature/strain rate by tensile tests. The results show that the steel can display superplasticity in the proper range of deformation temperature and strain rate. In the state of superplasticity, flow stress is under 60 MPa, maximum elongation is up to 307%, and strain rate sensitivity ( $m$ ) is about 0.38.

On the basis of above-mentioned results, two kinds of finish forging dies made of 4Cr3Mo3W2V steel have been manufactured by superplastic hobbing and used in production. The dies have good accuracy and finish. After forming, further machining for the cavities is no need before they are put into service. In addition, as a result of superplastic forming, the structure is improved, the grain is refined, and the longer service life of dies is obtained. Comparing with the normal manufacture methods, superplastic forming of dies has less invest in equipment and puts into production easily. The cost for making dies can be reduced above 30%.

Superplasticity and Superplastic Forming  
Edited by C.H. Hamilton and N.E. Paton  
The Minerals, Metals & Materials Society, 1988

### Introduction

In the last few years, researches on superplastic forming technology of dies manufacture have been more and more. The involved die materials include Zn-alloys, low melting alloys, Al-alloys, Cu-alloys and steels. Recently, superplastic forming technology of steel die has been developed fast. In China, more than 20 sorts of steels have been studied in this field, which are mainly for industrial uses. By superplastic forming, various dies have been produced and applied, e.g., hot forging die, cold extrusion die, die casting die, trimming die and plastic extrusion die.

Tab.I shows some results of our laboratory(1). The materials studied are die steels widely used in production, which show superplasticity under definite conditions. Many kinds of dies made of these steels can be formed superplastically.

Tab.I Superplasticity Data and Application of Steels

Material	Elongation $\delta$ (%)	Flow Stress $\sigma$ (MPa)	m	Application
GCr15	543	27		
Cr12MoV	258	61	0.4	cold extrusion die
5CrMnMo	530	49	0.58	hot forging die
3Cr2W8V	307	57	0.35	die casting die
4Cr3Mo3W2V	307	59	0.38	hot forging die

The research on 4Cr3Mo3W2V steel introduced in this paper is one of the last achievements, and has been applied in industry.

### Tensile Testing Material and Method

4Cr3Mo3W2V steel contains more carbide forming elements, and has good wear resistance and high temperature strength. Its room temperature strength is above 1600MPa, and the elongation is below 8%. The chemical composition is shown as Tab.II (2).

Tab.II Chemical Composition of 4Cr3Mo3W2V Steel (%)

C	Si	Mn	Cr	Mo	W	V
0.32-0.42	0.60-0.90	<0.65	2.80-3.30	2.50-3.00	1.20-1.80	0.60-1.20

The specimen is machined from 15 mm diameter bar which is reformed. In order to show the material superplasticity, the ultra-refining pre-treatment of material must be carried out.

At various temperatures and tensile rates, the pretreated specimens are stretched at isothermal condition. The relationships between flow stress ( $\sigma$ )/elongation ( $\delta$ ) and temperature/strain rate ( $\dot{\epsilon}$ ) can be obtained, from which the optimum range of deformation temperature and strain rate can be defined. The strain rate sensitivity ( $m$ ) is determined by the step strain rate test.

### Isothermal Tensile Testing of Material (3)

Before isothermal tensile testing, the specimens must be taken place ultra-refining pretreatment. Through the treatment, grain is fully refined, substructure is developed, the quantity, shape, size and distribution of the second phase are reformed, interface is increased greatly, so that the mechanism of superplasticity related to interface movement is fully carried out. The reformation of material structure can prevent the formation and development of cavity and help to raise plasticity. There are different ways of pretreatment. It is simple to use heat treatment to refine structure. Quenching and tempering can make the grain size of 4Cr3Mo3W2V steel refine to 2-4  $\mu\text{m}$ . It ensures the structure condition to realize superplasticity.

The temperature is the one of important parameters during superplastic deformation. At various temperatures, the flow stress, maximum elongation and strain rate sensitivity are all different. Beyond a deformation temperature range, material can not show superplasticity. As for many metal materials, the superplasticity is closely related to phase transformation. Superplastic deformation temperatures of many steels are placed near  $A_c$ , above or below  $A_c$ , 20-300°C. The optimum deformation temperature can be determined by tests.

The 4Cr3Mo3W2V steel tensile specimens pretreated are tested isothermally at a same strain rate but various temperatures. The results (Tab.III) show that the maximum elongation is obtained at 880°C, when the speed of crosshead of tension machine is 0.25 mm/min.

Tab.III Isothermal Tensile Testing at Various Temperatures

Temperature $T(^{\circ}\text{C})$	Speed of Crosshead $S(\text{mm/min})$	Flow Stress $\sigma(\text{MPa})$	Elongation $\delta(\%)$
870	0.25	70.4	220
880	0.25	57.5	307
890	0.25	56.5	190
900	0.25	66.9	240

Another important parameter of superplastic deformation is strain rate. At the same temperature, the flow stress, the maximum elongation and  $n$  value of material change with strain rate. If strain rate is too high or low, material does not show superplasticity because it can not be suited to intrinsic speed of related superplasticity mechanisms. Under definite microstructure condition and deformation temperature, there is an optimum range of strain rate, in which the best superplasticity can be obtained.

Tensile testing is done at 880°C and various strain rates. The results (Tab.IV) show that the optimum tensile speed is about 0.25 mm/min, and there is a quite wide range of strain rate, in which the material has high plasticity. By means of the step strain rate testing, strain rate sensitivity is measured, and the maximum  $n$  value is 0.38.

### Superplastic Hotbing of Finish Forging Dies

At superplasticity state, the plasticity of materials is much higher than normal, and resistance to deformation becomes very low. This property of material can be used for die manufacture, so a new way of making die,

superplastic forming technology, appears.

In our research, two finish forging dies, connecting rod die and transmission fork die, for motor bicycle parts are selected. Both of them are used on friction press. Now, they are made by superplastic hobbing, instead of common machining or electrosparking. The procedure of the new die manufacture method is as following. At first, the blank with protective agent and lubricant is heated to superplastic deformation temperature. Then at this temperature, a smooth punch with high accuracy is extruded into the blank at definite velocity. After putting out the punch, a cavity is formed in the blank, and its surface finish and accuracy are as high as those of punch. After machining contour and heat treatment, the die can be used.

Tab.IV Isothermal Tensile Testing at Various Strain Rates

Temperature T(°C)	Speed of Crosshead S(mm/min)	Flow Stress $\sigma$ (MPa)	Elongation $\delta$ (%)
880	0.1	43.4	193
880	0.2	52.0	212
880	0.25	57.5	307
880	0.3	61.4	224
880	0.35	64.9	217

The pretreatment procedure, deformation temperature and hobbing velocity for superplastic hobbing of dies can be designed on the basis of the results of tensile testing.



Fig.1 Motor Bicycle Connecting Rod Die Made by Superplastic Hobbing



Fig.2 Motor Bicycle Transmission Fork Die Made by Superplastic Hobbing

Fig.1 and 2 show the 4Cr3Mo3W2V steel connecting rod die and transmission fork die made by superplastic hobbing. They have been applied in production.

The dies made by superplastic hobbing have high accuracy, finish and shape repeatability of cavity. This new technology is suitable for mass production. Sometimes, it is very easy to form superplastically the cavity dies which are made difficultly by machining and electrosparking. The

material streamline in the surface layer of die made by superplastic hobbing is not cut off, and very uniform, fine structure is obtained after hobbing. The comprehensive mechanical properties are enhanced, so the service life of die is improved in varying degree.

Because material is in superplasticity state, the formability of blank is better during superplastic hobbing than hot or cold extrusion, and extrusion force is smaller (200 to 300 MPa). The cavity with a more complex shape and considerably great deepness can be formed, and power to be needed for hobbing can be reduced.

By superplastic forming, the expense in manufacture of die is lower, and the service life of die is longer, so the total cost of dies is obviously reduced. Normally, the cost can be saved more than 30%.

#### Conclusions

1. 4Cr3Mo3W2V steel is a commercial hot die steel contained more carbide formers. Pefined properly, it can show superplasticity under the condition of definite deformation temperature and strain rate. The maximum elongation is 307%, and the flow stress of material is below 60 MPa. It can meet the needs of superplastic hobbing technology of die.
2. Finish forging die can be made by superplastic hobbing. The shape repeatability, accuracy, surface finish of die are very good. The service life of die is improved. Normally, the cost of die can be saved more than 30 % (4).

#### Acknowledgements

This paper is cooperative achievement of the author and Engineer Qin Xiaoyu, Engineer He Jinxue, Assistant Engineer Jiang Li, Assistant Engineer Fu Jie and graduate student Li He.

Especially, thank Shanghai Die Forging Factory for helpful cooperation in inspection dies.

#### References

- (1) Cion-Japan Joint Symposium on Superplasticity 1985 p.66-67
- (2) Handbook of Alloy Steels (3), Metallurgical Industry Public House 1983 p.166-167
- (3) Yang Yongchun, "Study on Superplasticity of Hot Die Steel 4Cr3Mo3W2V" (paper, Beijing Research Institute of Mechanical and Electrical Technology) 1987
- (4) Qin Xiaoyu. "The Analysis of Benefit about Superplastic Forming Technology of Finish forging Die" (paper, Beijing Research Institute of Mechanical and Electrical Technology) 1987

BONDING OF ALUMINIUM-LITHIUM BASE ALLOYS USING  
ROLL CLAD ZINC INTERLAYERS

R A Ricks\*, J Ball\*, H Stoklossa+, P J Winkler+ and R Grimes\*

\* Alcan International Limited, Southam Road, Banbury, Oxon  
OX16 7SP ENGLAND

+ M.B.B. Central Laboratories, D 800 Muenchen, FEDERAL REPUBLIC OF  
GERMANY

• British Alcan Aluminium, c/o Alcan International Limited,  
Southam Road, Banbury, Oxon OX16 7SP ENGLAND

Abstract

Structural aluminium alloys are now commercially available in a form specifically processed for superplastic forming. In order to allow the successful incorporation of such alloys into lightweight expanded structures, a method of bonding is required which will withstand the superplastic forming operation. This problem is exacerbated in aluminium alloys by the tenacious oxide film which effectively prevents the successful deployment of solid state bonding as applied to steels and titanium alloys. Attempts to overcome these effects have either centred around the removal of oxide followed by the protection of the surface by coating techniques, which may also promote bonding by liquation, or by the use of interlayers designed to modify or disrupt the native oxide during bonding.

This paper reports some results obtained through a collaborative research programme between Alcan International Limited (Banbury) and M.B.B. Central Laboratories (Ottobrunn). A wide variety of surface treatments are under investigation and in this paper the use of a protective coating of a Zn base alloy, applied by roll cladding techniques, is described. It is shown that successful transient liquid phase bonds (T.L.P.) may be obtained using this process provided the correct combination of process parameters is employed.

Superplasticity and Superplastic Forming  
Edited by C.H. Hamilton and N.E. Paton  
The Minerals, Metals & Materials Society, 1988



### Introduction

The concept of using roll-clad protective surface coatings to promote the bonding of aluminium base alloys, by either solid or transient liquid phase means, has attractive potential owing to the initial dispersion of the tenuous aluminium oxide film during the cladding operation. The choice of surface coating is rather restrictive in the case of aluminium, owing to the relatively low melting point of the metal. The requirement to maintain some degree of microstructural integrity after bonding, either for subsequent superplastic forming operations or simply to achieve adequate post-bond property levels, favours the use of transient liquid phase bonding, since solid state bonding with the associated long bonding times would tend to cause microstructural degradation. This latter point is especially valid when the bonding temperatures of the surface layers need to be chosen so as to avoid liquation or degradation of the substrate.

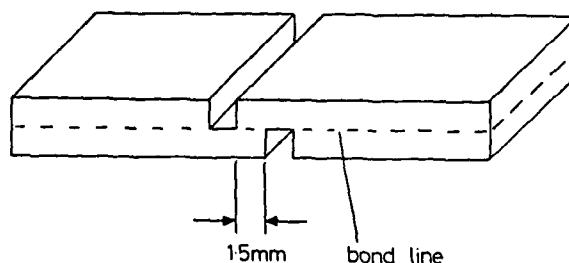
The selection of surface coatings available which would successfully lead to an ability to liquate and bond at the appropriate temperatures is further reduced when the requirement to prevent undue surface oxidation prior to liquation is taken into consideration. Of the pure metals which meet these requirements, zinc is possibly the most attractive, especially when consideration is also given to the physical properties match needed to actually allow roll-cladding to be successfully achieved.

This paper describes some results which have been produced as part of a joint research programme between Alcan International Limited and M.B.B. Central Laboratories, concerned with the development of bonding methods which are compatible with superplastic forming conditions in Al-Li alloys. A wide range of bonding techniques are under evaluation, although in this paper only the use of roll-clad Zn interlayer materials will be reported<sup>(1)</sup>. Consideration is given to the type of interlayer alloy chosen, the thickness of interlayer required and the bonding conditions necessary to achieve true transient liquid phase bonding during the bonding cycle.

### Experimental

For this study, the substrate material used was the Al-Li alloy 8090 (Al-2.4% Li-1.2% Cu-0.6% Mg-0.12% Zr nominal composition). Various clad layer materials were employed, including a) pure Zn, b) Zn-Cu alloys, c) commercial purity Zn, and each was roll-clad to the 8090 substrate to give a range of cladding thicknesses ranging from approximately 1% to 2.5% of the total final sheet thickness. Considerable care was taken with the roll-cladding operation to ensure minimal oxidation took place at the Zn-8090 interface before any metallurgical bond was developed in the rolling operation.

Specimens for bonding trials were cut to a 50 x 50 mm square shape and bonding was carried out in a specially constructed diffusion bonding apparatus designed to allow either vacuum or inert atmosphere conditions to prevail during bonding. Pressure was applied hydraulically and temperature control was achieved by the use of closed loop, feedback controlled R.F. induction heating of the platens and specimen, allowing bonding temperatures to be reached after ~ 20-30 mins. For this study a bonding time of 60 mins and



**Figure 1** Lap-shear test specimen geometry

pressure of 5 MPa were chosen with an argon atmosphere, since these would be typical of conditions achievable in a gas-forming press used for superplastic forming operations. In addition, these conditions were known to achieve adequate bonding pressures without undue specimen deformation.

Bond strengths were assessed using simple shear-lap specimen geometries, as shown in Figure 1. Although not providing fundamental data necessary to understand the likely behaviour of the bonds during any subsequent superplastic forming operation, this method of testing proved very useful in determining the comparative strengths of bonds made using varying process conditions.

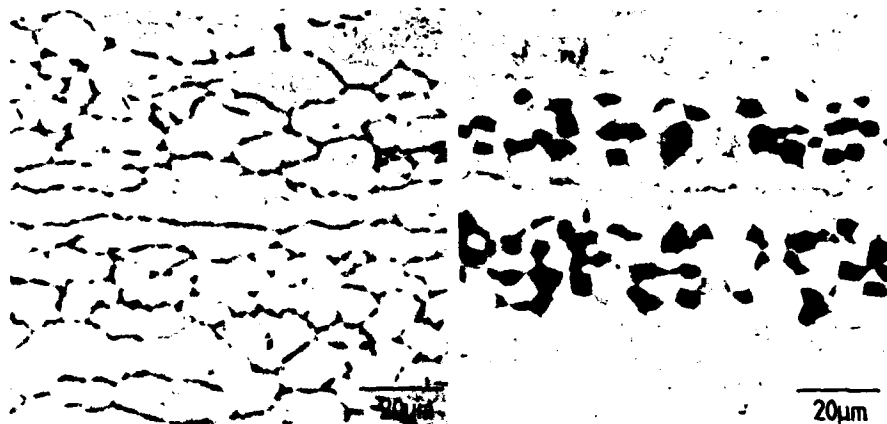
Bond microstructures were determined from the specimen halves after shear testing, enabling correlation between bond strength and microstructure to be carried out. This technique enabled any strength variations to be quickly assessed in terms of quality of bond microstructure. Both optical and scanning electron microscopy were used for this examination.

#### Results

Initial work in this investigation was concerned with optimisation of the cleaning procedures of the Zn cladding necessary to achieve consistent bond strengths. Details of these processes must remain confidential at this time, but it may be stated that specimen surface geometry and topography must be consistent with the demands for optimum cleanliness and oxidation prevention prior to liquation.

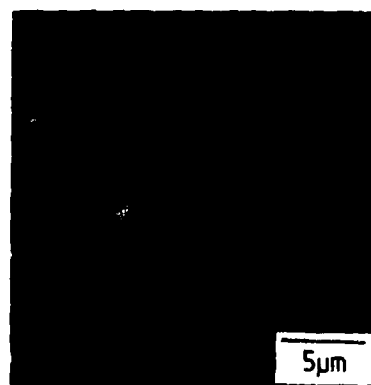
**Table 1**

<u>Interlayer Materials</u>	<u>Typical Bond Strength Range (MPa)</u>
Pure Zn	90-140
Zn-Cu Alloy	93-150
Commercial Zn Sheet	60- 85

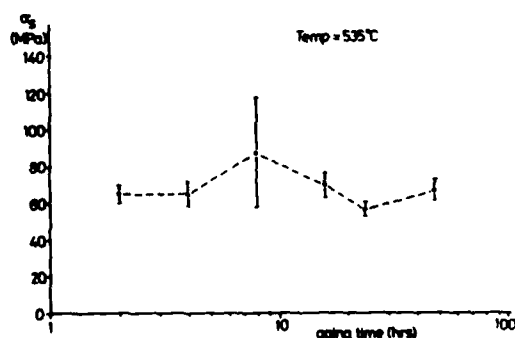


**Figure 2** As-bonded microstructures for Zn-Cu alloy interlayer (a) and commercial purity Zn interlayer (b)

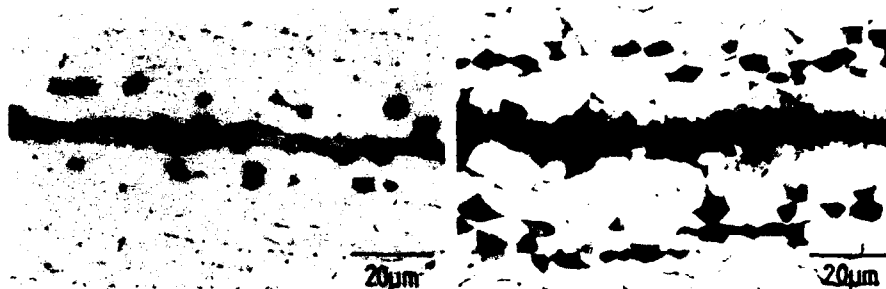
For the given set of bonding conditions used in this study no significant difference in final bond strength could be detected between the use of pure Zn and Zn-Cu alloy interlayers. A large reduction was detected if commercial purity Zn sheet was used, these data are given in Table 1. Examination of the microstructures of these bonds showed, for a constant thickness of cladding, that the bond microstructures obtained were different for these two cases (Figure 2). In the case of pure Zn and pure Zn-Cu alloys, diffusional processes had effectively removed the interlayers during the bonding cycle and bonding had taken place (Figure 2a) leaving grain boundary precipitates rich in Zn and Cu (Figure 3). If commercial purity Zn sheet was used, the bond microstructure was seen to consist of wide bands of Zn-rich intermetallics (Figure 2b) positioned either side of the bond line. Post-bond heat treatments could be employed to cause dissolution of these precipitates but no improvement in bond strength was observed (Figure 4). Close



**Figure 3** Back scattered S.E.M. image and Zn - X-ray map of Zn-Cu bond area



**Figure 4** Effect of post-bond ageing on bond strength for commercial purity Zn interlayer



**Figure 5** Intermetallic formation at the bond line after ageing commercial purity Zn interlayer

**Figure 6** Solidification cracking observed with thick interlayers of commercial purity Zn

examination of bonds made with commercial purity Zn interlayers after complete dissolution of Zn-rich precipitates revealed the existence of further intermetallic formation at the bond line (Figure 5), caused by the impurities present in the Zn sheet, which effectively reduced the strength of the bond.

Thickness of roll-clad interlayer was found to be crucial in determining the degree of bonding achieved during the heating cycle. If the cladding thickness was too great, incomplete solidification took place during the bonding cycle, resulting in either complete separation upon completion of heating or solidification cracks during cooling (Figure 6). Conversely problems could also arise if the cladding layer became too thin during processing, since diffusional processes were found to alter the chemistry of the interlayer material leading to poor bond properties. This problem is obviously exacerbated when the substrate material contains rapidly diffusing species such as Li.

#### Discussion and Conclusions

The results of this study have demonstrated that roll-clad Zn alloy interlayers can be used to develop useful shear strengths by a process of transient liquid phase bonding. To achieve these bond strengths care must be taken during all stages of the material production, surface cleaning and bonding cycle and that the correct interlayer alloy must be chosen. Further work is now in progress to exploit these bond strengths in a combined diffusion bonding - superplastic forming operation. Previous studies in this field have already indicated that simple shapes may be fabricated by this means<sup>(2)</sup>, future work will be targeted at the development of a wider understanding of the process requirements.

#### References

1. R Grimes and J Ball. UK Patent No. 2134833
2. A J Barnes. "Commercial Superplastic Aluminium Alloys - Opportunities and Challenges". Proc Int Conference "Superplasticity in Aerospace - Aluminium", 12-16 July 1985, Cranfield, England, eds R Pearce and L Kelly. P424.

# TRANSFORMATION SUPERPLASTICITY SOLID-STATE BONDING IN STEELS

Wang Yanwen      Feng Zezhou      Sun Shangchen

Beijing Research Institute of Mechanical  
and Electrical Technology of SCMI  
Beijing, China

## Abstract

The multi-cycle heating the metal through solid state transformation point under a small stress produces superplasticity. If a small pressure is applied, then it is the result that two pieces of metal, which has been pressed closely with the surface, could be bonded.

The transformation superplasticity bonding in the carbon steels was so observed. It was shown that the bonding strength was related to the maximum heating temperature, the value of pressure, the cooling speed and the roughness of the machined surface of the specimen.

The bonded specimen was observed microscopically. It was shown that the deformation, the migration of materials and the recrystallization took place during cyclic phase-transformation.

Some complex metal parts were manufactured by this solid-state bonding method and applied in the factories.

Superplasticity and Superplastic Forming  
Edited by C.H. Hamilton and N.E. Paton  
The Minerals, Metals & Materials Society, 1988

### Introduction

The transformation superplasticity in metal can be obtained by multi-cycle heating through the solid state transformation point under a small stress. The metal solid-state bonding based on the transformation superplasticity effect occurs under pressure condition. So the following two tests to observe the transformation superplasticity behavior under pressure condition were designed. The material of specimen was carbon steel with 0.2%C. The extra pressure acting on the specimen was loaded smoothly by a double-lever mechanism. The specimen was heated by single-circle inductor. The data of the experiment were recorded by electronic potentiometer type XWX-2040 (1).

#### 1. The transformation superplasticity effect in 0.2%C steel under pressure condition

A thermo-cycling transformation test and a constant heating test were carried out respectively. The dimension of specimen, the time length of the test and the value of pressure were identical for each test. The results were presented in Fig.1 and table 1. It was shown that, the total deformation obtained from the cycling transformation test was about 5.3 times as large as the total deformation from the constant heating test, though the heating temperature in the later case was the highest temperature (1173K) in the transformation case. The value of creep in transformation superplasticity was less than 1/5 of the total deformation. So it can be said, the superplasticity effect was obvious in the transformation case.

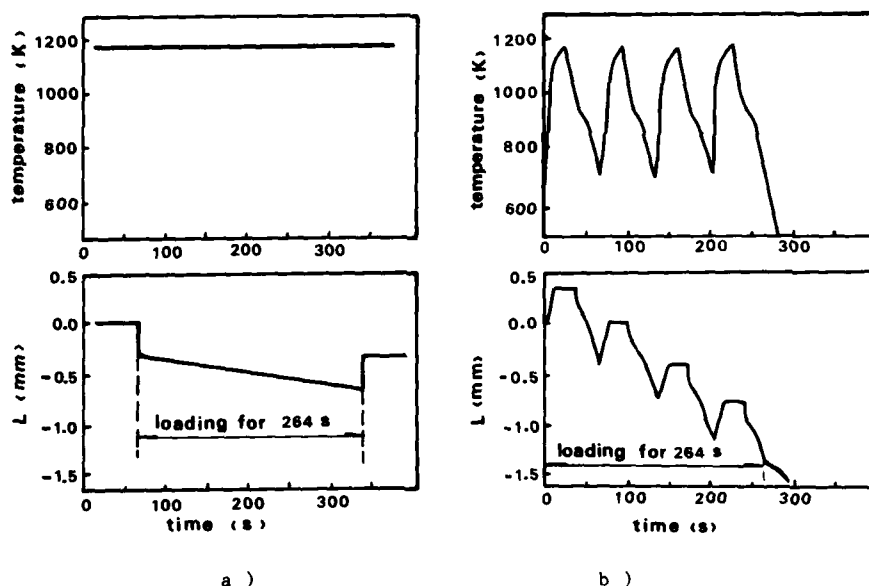


Figure 1 - Deformation of 0.2%C steel, a) constant heating test b) cycling heating test.

#### 2. A comparison method to estimate the relationship $\sigma-\epsilon$ and $\sigma-\dot{\epsilon}$ in the case transformation superplasticity under the pressure condition.

In order to eliminate the cycling heating influence on the measurement of the deformation during test, the superplastic deformation was measured

by means of a comparison method, i.e. to compare the variation in length of

Table 1. Deformation of 0.2%C Steel under Pressure

Thermo-schedule	Stress ( $\text{kg/mm}^2$ )	Temperature (K)	Time (s)	Original length (mm)	Length after diformation (mm)	Total deformation (mm)
Constant heating	3.26	1173	264	29.62	29.32	0.3
Cycling heating	3.26	1173 $\pm$ 773 4 cycles	264	30.00	28.40	1.6

the specimen under the pressure condition with the variation of the specimen in the free state. The process of the test was shown in Fig. 2. Where, the displacement ( $L_B - L_A$ ) represents the variation in length of specimen in the free state during heating for one cycle; ( $L_D - L_C$ )--in the pressure loading case during heating; ( $L_C - L_B$ )--in the free state during cooling; ( $L_E - L_D$ )--in the pressure loading state during cooling. Then, the displacements due to the superplasticity effect in the pressure condition during heating and cooling for one cycle will be  $\Delta L_h = (L_D - L_C) - (L_B - L_A)$  and  $\Delta L_c = (L_E - L_D) - (L_C - L_B)$  respectively, and the total displacement ( $\Delta L = \Delta L_h + \Delta L_c = L_E - L_C$ ) represents the total deformation for one cycle in the pressure condition.

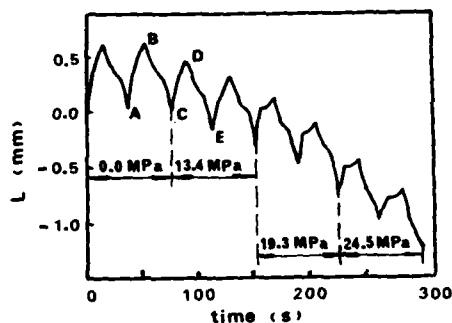


Figure 2 - Relationship between stress and deformation of 0.2%C steel.

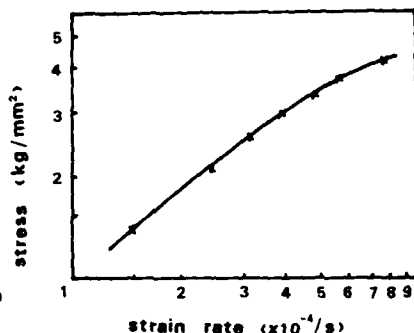


Figure 3 -  $\ln \sigma - \ln \dot{\epsilon}$  curve.

Further, to convert  $\Delta L$ ,  $\Delta L_h$  and  $\Delta L_c$  into  $\epsilon$ ,  $\epsilon_h$  and  $\epsilon_c$ , and based on this, the Fig. 4 was plotted, the curve slope as shown in Fig. 3 is the value  $m$ ; when  $\sigma < 3 \text{ kg/mm}$ ,  $m = 0.85$ , when  $\sigma > 3 \text{ kg/mm}$ , the value  $m$  decreases, when  $\sigma = 5 \text{ kg/mm}$ , the value  $m$  decreased to 0.5.

#### Transformation Superplasticity Bonding in 0.2%C Steel

The bonding was performed on two pieces of steel of  $\phi 13 \times 30 \text{ mm}$ . After bonding, the specimen was manufactured as the tensile specimen with parallel length of  $\phi 6 \times 30 \text{ mm}$ , and then the tensile test was carried out. The result of the test showed that the bonding strength of specimen had a connection with various factors such as the thermo-process and the value of pressure. The experimental results were shown in table 2 and 3.

Table 2. The Bonding Results under Different Pressures

Bonding pressure (kg/mm <sup>2</sup> )	Percentage expanded ( $\alpha$ , %)	Tensile strength (kg/mm <sup>2</sup> )	Fracture site
1.36	1.0	44.4	Bonding seam
2.12	1.2	46.2	Bonding seam
2.88	1.92	55.6	Bonding seam
3.64	2.5	56.6	Bonding seam
4.35	3.3	59.5	Bonding seam
5.10	4.1	57.2	Matrix

$$\alpha = \frac{\text{Original diameter} - \text{Diameter after bonding}}{\text{Original diameter}} \times 100\%$$

Table 3 The Bonding Results in Different Maximum Temperatures and Different Cooling Speeds

Maximum temperature (K)	1073				1173			
Cooling speed (K/S)	5	26	45	270	5	26	45	270
Bonding Strength (kg/mm <sup>2</sup> )	42.8	46.2	49	--	54.1	54.9	57.7	67.7

#### The Relationship Between Deformation and Bonding Strength

It was observed from the test mentioned above that the bonding strength was related to the percentage of expanding ( $\alpha$ ). Further micro-analysis showed that the bonding strength was in the direct ratio of the no reflection percentage ( $\eta$ ) on the bonding surface of the specimen, which has been parted in tensile test after bonding. The Fig.4 gave the microphotographs of the bonded surface of the specimen with different bonding strength. The black part of the photo was the bonded area, and the white part was no bonded. The percentage of the black part was measured by means of a quantitative metallographic microscope (OPTON MV-2) and was the percentage of the bonded area ( $\eta$ ) in fact. These micro-photos showed vividly that the bonding strength was the additive strength from a lot of micro bonded area. The more the micro bonded area was, the higher the bonding strength would be. The relationship among the bonding strength, the percentage of expanding ( $\alpha$ ) and the fraction of the bonded area ( $\eta$ ) was shown in Fig.5. It was concluded that there must be a certain relationship between the micro bonded area and the plastic deformation formed during cycle phase transformation. The micrograph of the vertical section close to the bonding seam of the specimen was shown in Fig. 6. In the photo, it was visible, that there was no definite line at the place well bonded, and that the unbonded place showed many voids.



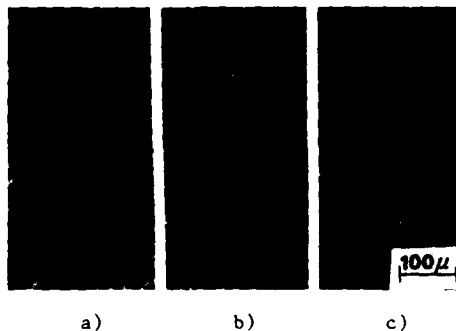


Figure 4 - Bonded surfaces, which have been parted in tensile test after bonding. a)  $\sigma_b = 44.4 \text{ kg/mm}^2$ ,  $\eta = 0.71$ ;  
b)  $\sigma_b = 55.6 \text{ kg/mm}^2$ ,  $\eta = 0.90$ ;  
c)  $\sigma_b = 59.5 \text{ kg/mm}^2$ ,  $\eta = 0.96$ .

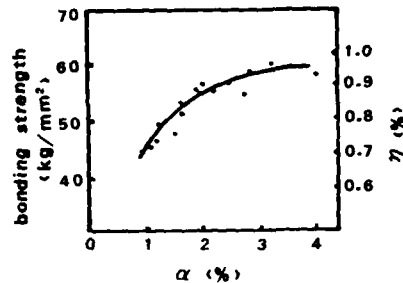


Figure 5 - Relationship among bonding strength, expanding percentage and bonded area percentage.

#### The Application of the Transformation Superplasticity Bonding

The bonding between the materials of same sort and also the materials of different sort can be done by the utilization of the effect of transformation superplasticity. We have made tools and dies of bimetal based on this way. Fig.7 showed the extrusion die (1), the cold forging die for nut (2), the head part of the extrusion die for aluminium cover for tooth-paste (3), the punch for nut (4), the small punch for silicon steel plate (5), and the cold extrusion die for steel shuttle of seamer (6).



Figure 6 - Vertical section close to bonding seam.

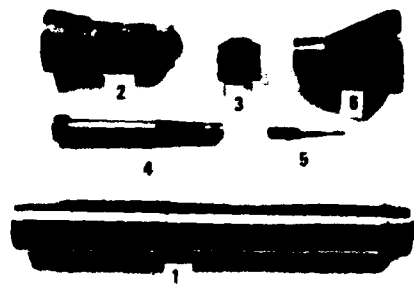


Figure 7 - Complex dies and tools by bonding.

#### Reference

1. Wang Yanwen and Feng Zezhou, "Transformation Superplasticity under Pressure in Steels and Bonding", Proceeding of Japan-China Joint Symposium on Superplasticity, 1986, Yokohama, 145-148.

**DESIGN CONCEPTS  
AND  
FUTURE DIRECTIONS**

## DEVELOPMENT OF SUPERPLASTIC FORMING TECHNOLOGY IN CHINA

Hai Jintao, Dai Jilin, Chen Sanshan

Beijing Research Institute of Mechanical  
and Electrical Technology

Z.R.Wang, Zhang Kaifeng  
Harbin Institute of Technology

### Abstract

The superplastic research in China began in early 1970's. Chinese researchers repeated the work of foreigners to study Zn-Al alloy in this period. Since 1980's, we have caught up with advanced countries step by step. We have emphasised the application of superplasticity and given priority to study on the superplasticity of existing-alloys other than that of new alloys. We have organized the researchers who study in different fields such as material, mechanics, mechanism and plastic material machining together and extended superplastic research into more new fields.

This paper introduces the development, strategy and practical application of superplastic technology in china. The superplasticity of several tons of alloys have been systematically investigated

such as Ti-alloys, Al-alloys, Cu-alloys and steels, and several hundreds of practical applications in different domains have been obtained, among which the application of Ti-alloys and Al-alloys achieved especially good results. We have also made obviously progress in the transformation superplasticity, diffusive bonding, powder superplasticity and other fields.

Now there are near one hundred organizations and enterprises all over the country participating in the research and application of superplasticity. Superplastic technology is entering a steady stage of industrial application.

Superplasticity and Superplastic Forming  
Edited by C.H. Hamilton and N.E. Paton  
The Minerals, Metals & Materials Society, 1988

### The General Situation of the Study on Superplasticity in China

The study on superplasticity in China began in early 1970's with the cooperation between industry and scientific research institutes. The cooperation is carried out up to now and become a noticeable feature, that means pay attention to the industrial application of superplasticity. Now the application of superplasticity has extended to about 400 kinds of products including the fields of aerospace, instrument, electronics, machinery and light industry.

With the progressing of study and the extending of its applications, researchers and technicians from many fields join in the study of superplasticity and form the feature of wide distribution of the researchers. In China today, there are more than 300 professors, scientists and engineers from about 100 units engaging in the study of superplasticity. The Dr. and MA students both in university and scientific research institute play an important role in the study, more than 30 students have got their Master's Degree and a few people got a PhD.

At the same time of paying attention to the forming technology, Chinese scientists study material deeply. The combination of material and forming technology gives another noticeable feature in the development of superplasticity in China. More than 50 kinds of superplastic alloy have been investigated and applied. (see Table 1.) While developing new alloys, Chinese scientists pay much attention to the increasing ductile properties of existing commercial alloys in order to put them into practical use as soon as possible. It has been shown the measures mentioned above shorten the time from laboratory investigation to industrial application.

Up to now, four sessions of symposium on superplasticity have been held in China with about 300 academic papers having been published. Many projects on superplasticity are superplasticity are supported by the Chinese government. In 1980, the National Superplasticity Academic Council was established.

### The Superplastic Hobbing of mould and die cavity

In the die cavity superplastic hobbing, the materials used at the beginning of research were Zn-alloys (ZnAl22, ZnAl4, ZnAl5, ZnAl27, ZnAl22, Cu0.5). The advantages of Zn-alloys are the

No	Alloys and Contents (weight %)	Superplas- tic tem- perature	Strain rate $S^{-1}$	$n$ Value	max elonga- tion (%)
1	Al-6Cu-0.5Zr	430	$1.3 \cdot 10^{-3}$	0.42	1600
5	Al-10Zn-1Mg-0.4Zr	550	$10^{-3}-10^{-2}$	0.64	1950
6	Al-8Zn-1Mg-0.4Zr	525	$10^{-3}-10^{-2}$	0.6	1650
7	Al-6Zn-2.2Mg-1.39Cu -0.25Mn-0.14Cr(LC4)	516	$8.33 \times 10^{-4}$	0.85	1550
8	LC9	500	$8.33 \times 10^{-4}$		1300
2	Al-5.5Ca	550	$3.3 \times 10^{-3}$	0.40	715
3	Al-5Ca-4.8Zn	550	$8.33 \times 10^{-3}$	0.38	930
4	Al-6Cu-0.35Mg-0.4Zr	440	$1.67 \times 10^{-3}$	0.47	1320
9	Al-4.5Cu-1.5Mg-0.6M (Ly12)	440	$1.67 \times 10^{-4}$	0.36	330
10	Al-6Mg-0.6Mn-Re	520	$8.33 \times 10^{-4}$		1000
11	Al-13Si	520	$8.33 \times 10^{-4}$	0.5	248
12	62Cu-38Zn(162)	750	$3.3 \times 10^{-4}$	0.65	1174
13	59Cu-40Zn-1pb(Hpb-1)	620	$2 \times 10^{-4}$	0.45	615
14	66Cu-6Al-3Mn-2Fe (4AL:In66-6-3-2)	720	$2.8 \times 10^{-2}$	0.32	400
15	95Cu-2.8Al-1.8Si-0.4	600	$6 \times 10^{-3}$		750
16	Ti-6Al-4V(TC4)	900-925	$-10^{-3}-10^{-5}$	0.6	1500
17	Ti-5Al-4Mo-4Cr-2Sn- 2Zr	800-840	$10^{-4}-10^{-5}$	0.6	2000
18	TC6	900			2000
19	Ti-4Al-7Mo-10V-2Fe	450-550	$10^{-4}-10^{-5}$	0.4	300-500

lower deformation resistance force and forming temperature, they are easy to flow in the deformation. So, they are suitable for the making of plastic bulging and injection moulds. Fig.1 shows the plastic parts using superplastic forming dies. This mold-making technology can reduce the production period and cut down the manufacture expense. The surface finish of mould is good. Among those die cavity moulds, the maximum depth is 131mm, the ratio of height to diameter is 11, the maximum extrusion area is 460 cm<sup>2</sup>, The forming force required is less than 1000 KN.

The successful application of superplastic die forming of Zn-alloys encourages the Chinese researchers to investigate the superplastic forming of steel moulds in order to get over the limits of the lower working temperature and lower strength of Zn-alloy moulds. For the die cavity area of 460 mm<sup>2</sup> mentioned above, more than 100, 000 KN forming force is needed when the die is extruded for mild steel. In superplastic forming the load can be reduced to 1/5 to 1/3 of the original value.

In the developing of superplasticity of ferrous metal, the Chinese researchers pay much attention to those used currently in industry, such as 5CrMnMo, 5CrNiMo, 3Cr2W8V, 9SiCr, CrWMn, Cr12MoV, GCr15. The elongation is between 260-560%, the yield stress is 2/3-4/5 lower than the non-superplastic materials. The superplasticity of steel has been successfully used in the making of moulds of connecting rod in the car, cold extrusion moulds and others. Fig.2 is a photo of a steel mould made by the aid of superplasticity.

#### The Superplastic Forming of Alloys Which are Difficult to Machine

The difficult machined alloys which are widely used in China are Ti-alloys and Ni-alloys. They are difficult both for plastic forming and cutting process. The reform of machining process of difficult machined alloys is becoming the key in many technical fields, such as aerospace engineering.

It is fortunate that the superplastic properties of Ti-alloys are so good that some Ti-alloys can be superplastic formed in commercial supply state. Almost all of the forming techniques of metals are employed by the superplastic forming of Ti-alloys in China, such as superplastic extrusion, superplastic forging, sheet metal bulging, bulging with empty centre and the compound process of bulging and diffusion.

The superplastic forming of Ti-alloy products brings about great technical and economical interests. The successful forming of a kind of turbine disks with dense rows of axial blades made of Ti-alloy (the distance between vanes is 1.8mm, the thinnest thickness is 0.3mm) reduces the manufacture cost from 300 yuan per piece to 30 yuan per piece, therefore 2,700,000 yuan can be saved for every 10,000 pieces. On the other hand, the total ex-

pense of research and technical reform is within 10% of the figure above.

The high pressure spherical vessels made of Ti-alloy play an important role in space equipment. Because of the difficulty of machining of Ti-alloy, they have been made by the aid of two-piece welding structure before. The technical processes are:

workpiece+first forging+twice die forging on a120,000KN hydraulic press+mechanical working of surface+heat treatment+welding+X-ray test+hydraulic test

The superplastic forming of gas bulging can produce one-piece high pressure spherical vessels with nonwelding seam, the technical process is as following:

tube billet+cutting+necking by spinning +superplastic forming by bulging+mechanical working of tube mouth+hydraulic test

It is known from the comparison between these two technical processes that the superplastic bulging of whole sphere exceeds the high capacity equipments and welding process, the gas bottle with nonwelding seam eliminate the unsafe effects, the stability is improved greatly and the manufacturing cost is also reduced largely.

The superplastic formed turbine disks and gas bottles made of Ti-alloy are shown in Fig.3.

Another widely concerned problem in the field of superplastic forming research in China is the solving of the lower forming capacity of Ni base super alloys. The superplastic forming of Ni base super alloys can be achieved by hot extrusion of the power of Ni base alloys, from which material with fine grains will be obtained. The optimal temperature is investigated by experimental results show that great force is needed when the working temperature is low. On the contrary, if the extrusion temperature is high no superplastic deformation will occur. The Ni base super alloy after the extrusion under the proper temperature will obtain rather high elongation. Experiments show this process is of practical significance to the making of turbine disks and other workpieces made of Ni base super alloys.

It is known that the cutting property of Ni base high temperature alloys is terrible. In cutting, the tools are worn rapidly, the cutting force and cutting heat increase greatly and the surface condition is also poor. The Chinese scientists

have obtained the ultra-thin specimen which is less than 10  $\mu\text{m}$  (see Fig.4) on each point within the small cutting region by the aid of a specimen making method called "m.t", and find that  $\gamma'$  hardening phase disappears when the temperature is between 930-1080  $^{\circ}\text{C}$ . From this point, a new concept called "superplastic cutting" is introduced, this means under a certain temperature the material within the small cutting region is of superplastic state and high efficiently machining can be achieved. It has been proved by experiments that the cutting force can be reduced by 30%, the tool wear reduce by 40% and the cutting efficiency of material increase by 100% with the superplastic cutting method. This method set up a new approach for the cutting of those difficult machined material.

#### The Superplastic Forming of Arts Craft Articles

In plastic forming, the minimum radius of product on the corners is restricted by the flowing ability of material. Therefore, with the normal extrusion and hydraulic bulging methods it is restricted and difficult to produce a product with fine detail surface and complex appearance which is just what arts and craft articles need.

Since the opening of China to the rest of the world, the tourist enterprise and international commerce have provided a wide market for arts and craft articles. In such circumstance, superplastic forming prompts the combination between metal forming technology and arts and craft articles. At superplastic state metal flow easily and form a sharp corner, which meet the need of the copying of the fine and complex appearance of arts and craft articles. The extruded memorial coins and air bulging craft articles with Chinese national feature gains wide popularity among Chinese and foreign people (see Fig.5).

Besides what are mentioned above, a series results have been made on the phase transformation superplastic welding of steel on compressive state and the applications of both Ni-alloys and Al-alloys.

#### The Study and the Development of the Deformation Mechanism and Mechanics of Superplasticity

Apart from the application research, the Chinese researchers



of superplasticity have made a series of theoretical researches on the deformation mechanics and the analysis of stress and strain from the points of metal physics, metal science and engineering plasticity correspondingly

The superplastic deformation mechanism of the fine and coarse grain and the effect of adding trace elements

The study of superplastic deformation are focussed on three aspects:

A. The superplastic deformation of fine grain

On this aspect the conclusions we obtained accord with what other references mentioned.

B. The effects of trace elements on the fine grain superplastic deformation mechanism, especially the reform of superplasticity of rare-earth elements.

It has been verified by experiments that some rare-earth element Ce collects on the crystal boundaries apart from uniformly dispersed base, which fined grains, in other words, the proper adding of rare-earth can refine cast structure.

C. Deformation mechanism of coarse grain superplastic materials

It is found in experiments that some materials with grain size over 200um still show very good superplasticity properties. This kind of material is considered to have high value of applications. Grain refining treatment is not necessary for this kind of material and it is superplastic in commercial state of coarse grains. The chemical components of an industrial copper alloy are shown in Table 2.

Table 2. The content of copper alloy

CONTENT	Cu	Zn	Al	Mn	Pb	Fe
PERCENTAGE	52.06	40.39	2.56	4.37	0.50	0.01

The initial grain size is about 200um with each grain having subgrains, but the density is different in each grain. The large grains extends in the direction of tension after tension and the number of subgrains decrease. This shows that the superplastic deformation of coarse grained alloys is mainly within grains, in the form of turning and twisting of subgrains. Intergrain

slip does not take leading place. The superplasticity temperature is 400°C and elongation can be reached 300%.

#### Mechanical analysis of superplastic deformation

The research on superplastic mechanics in China initiated almost at the same time with the development of superplastic materials. And progress is being rapidly made in this field. This includes the following aspects:

A. Yielding path and constitutive equations of superplastic materials.

It is to be verified by experiment whether the yield path and constitution equations are applicable to superplastic materials. The Zn-Al alloy and Sn-Pb alloys thin tubes were used under the combination of tension-torsion. The yield path, as shown in Fig. 6, could be obtained based on the experimental results of shear stress  $\tau$  and normal stress  $\sigma$ . This path lies in between the Tresca and Mises paths. Experimental investigations also shows that the yield path extends uniformly expands as the strain rate increases.

Some new constitutive equations have been proposed for better explanation of this phenomenon of superplasticity

B. Test of strain rate sensitive exponent  $m$

The exponent  $m$  in Backofen equation  $\sigma = k \dot{\epsilon}^m$  is an important parameter to represent superplasticity characteristics. Much emphasis has been put on the test of  $m$  from investigators of many countries including China. A lot of test methods have been proposed, most of which are simple in test means and sufficient in accuracy and easy to use, etc.

First, the method of changing cross sections. When a specimen of changing cross section is stretched because of the strain rate sensitivity of stress. Rather, deformation spreads from the part of small section to that of large one. A formula is given to calculate  $m$  in changing section tension test:

$$m = \ln(A_2/A_1) / \ln(\epsilon_2/\epsilon_1) \quad (1)$$

where,  $A$  is area of cross section,  $\epsilon$  is strain, foot numbers 1 and 2 shows parts of different sections.

Second, the method of load-specimen length. The calculating

formula is

$$m = -d \log^P / d \log l - 1 \quad (2)$$

where, P is load and l the length.

In addition, there are methods of changing loads, hardness and so on. A series of new ideas are presented of the physical sense of m, the relation ship between m and elongtion  $\delta$  and the unification of the testing methods of m.

C. Some methods of classical plasticity applied to superplasticity deformation analysis

At present, the primary conditions for analysing superplastic deformation are: 1. Accept that superplastic deformation observes Mises yield criterion 2. Constitution equation is  $\sigma = k \dot{\epsilon}^m$ , or Backofen equation. In essence, it is the introduction of strain rate sensitivity, characterized by Backofen equation, into classical plasticity methods. Of course, this brings about some difficulties for analysis. Up till now, many methods of engineering plasticity have been used to solve problems of superplasticity.

The key to analyze superplasticity deformation using the slab-method lies in the introduction of Backofen's equation into the equilibrium equations. For a thick-walled tube under uniform inner pressure, the radial stress  $\sigma_r$  is

$$\sigma_r = \left( \frac{R}{r} \right)^{2m-1} \frac{r_0^{2m} p}{r_0^{2m} - R^{2m}} \quad (3)$$

where, m is strain rate sensitivity exponent.

For most problems, a formula like (3) can be obtained. Take the superplastic compression of circular ring, numerical integral of the equations are needed to obtain the standard curve for testing friction coefficient of superplastic deformation (see Fig.7).

The slab methods has also been used in air bulging of sheet metals. Bulging of circular sheet and V-slot has been analysed.

Other methods such as variational method and visual plasticity are said to be noticed.

As a new branch of science, superplasticity is still unknown in many respects. Its application will be extremely wide. We

Chinese researchers will co-operate with colleagues in other countries in this new branch of science.

In this paper, only an outline is given of the progress of superplasticity technology in China in recent years. Other new achievements will be presented else where in the same collection of this conference.

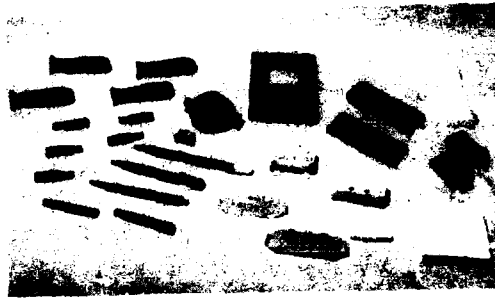


Fig.1 The plastic products made from the superplastic formed moulds

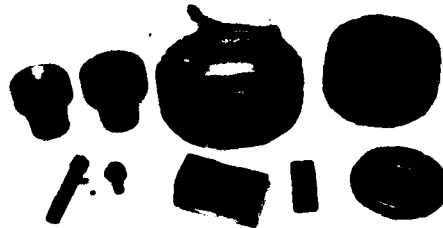


Fig.2 The photo of a steel mould  
from superplastic forming

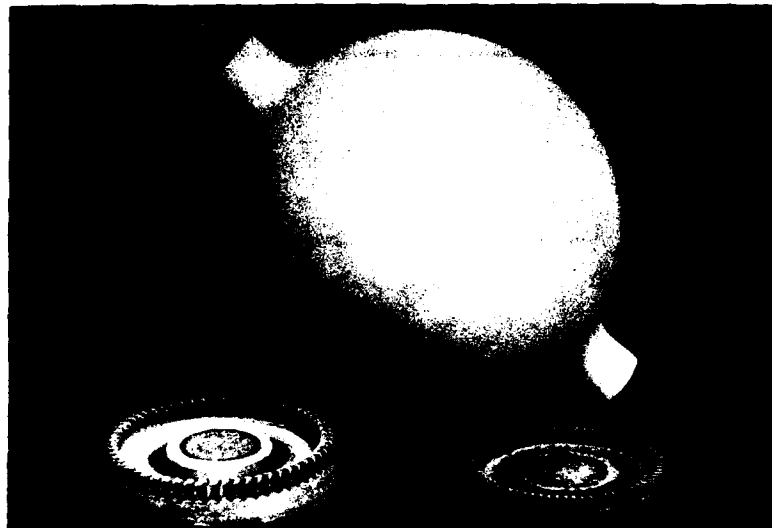


Fig.3 The superplastic formed turbine disks and gas bottles made of Ti-alloy

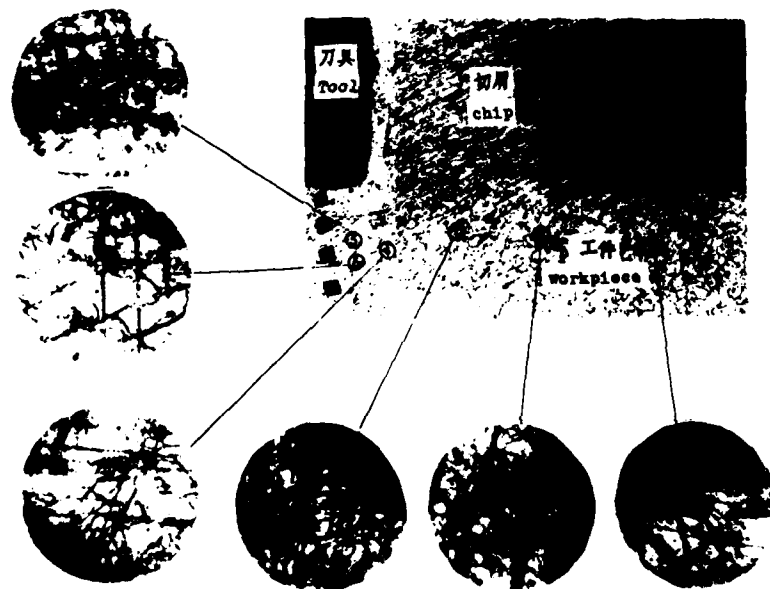


Fig.4 The phenomenon of cutting region of Ni base super alloy



Fig.5 Superplastic formed craft articles

(The Great Wall)

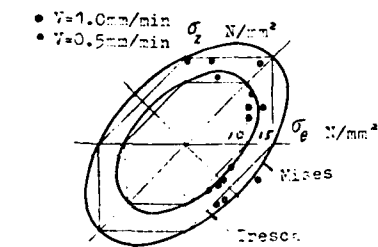


Fig.6 Yield locus of  
superplastic deformation

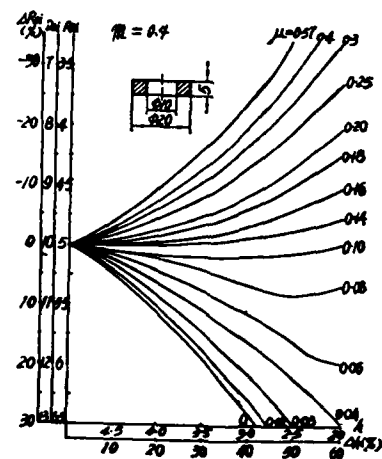


Fig.7 Calibration curves of  
friction factor considered  
strain rate hardening effect.

## MECHANISMS OF SUPERPLASTIC DEFORMATION IN CERAMICS

Rishi Raj

Department of Materials Science and Engineering  
Bard Hall, Cornell University  
Ithaca, NY 14853-1501

### ABSTRACT

Three types of atomistic mechanisms are proposed for superplastic deformation in ceramic materials. They are distinguished by the structure of grain interfaces since matter transport between interfaces is invariably the key feature of superplasticity in crystalline materials. In Type I, boundary structure is such that the exchange of atoms at the interface is much faster than grain boundary diffusion. In this type boundaries generally have a high angle structure. In Type II, boundaries contain a small amount of fluid which leads to enhanced diffusion at the interface provided that the crystal phase is at least somewhat soluble in the liquid. In Type III the interfaces are predominantly low angle boundaries. Interestingly, the last type produces the fastest rates of superplastic deformation and, therefore, is technologically most significant, but also is the least understood. We speculate that grain boundary dislocations shuttle between interfaces to produce Type III superplasticity.

Superplasticity and Superplastic Forming  
Edited by C.H. Hamilton and N.E. Paton  
The Minerals, Metals & Materials Society, 1988

## INTRODUCTION

Superplastic flow is the ability of polycrystalline solids to deform at temperatures considerably below the melting point in a way that is phenomenologically similar to the flow of glass. Elongations of several thousand percent can be obtained without flow localization and fracture that characterizes ordinary deformation of crystalline solids. The technological significance of superplastic flow is highlighted by the fact that materials which are very hard such as ceramics can deform in superplastic flow with ease. Often, superplastic deformation is the only mechanism that can be employed in net-shape forming of hard materials.

A detailed understanding of superplastic flow develops when the phenomenon is approached from several standpoints that include the mechanics of flow localization in large deformations, modelling of superplastic flow using a materials science approach, and the knowledge of the atomic structure of grain boundaries. Each is discussed below:

### (a) Mechanics of Flow Localization

From a continuum standpoint, large deformations in a strain rate sensitive material are possible only if the strain rate sensitivity index,  $m$ , in the flow equation is close to unity. The ability of a material to resist flow localization is explicitly related to the strain rate sensitivity index (1). The index is defined by the relationship between the deviatoric (or shear) stress,  $\sigma_e$ , and the deviatoric strain rate,  $\dot{\epsilon}_e$ , as given below:

$$\sigma_e = B \dot{\epsilon}_e^m \quad (1)$$

The parameter  $B$  in Eq. (1) includes the effects of temperature and microstructure. The equation assumes that the microstructure remains constant during deformation.

The formability of a material is tied to the value of  $m$  in Eq. (1). In the ideal case,  $m=1$ , the material behaves like a Newtonian viscous fluid, and is indefinitely deformable. In reality, even smaller values of  $m$  lead to ductility that is large enough for most forming operations (2). Generally, in polycrystals, the flow is assumed to be potentially superplastic if  $m$  lies in the range  $0.4 < m < 1.0$ .

### (b) Micromechanistic Modelling of Superplastic Flow

The success of superplastic flow emanates from the fact that two classical mechanisms of diffusional creep known as Nabarro-Herring creep (3) and Coble creep (4), lead to an equation of the type given by Eq. (1) where  $m=1$ . The mechanism involves transport of atoms from one interface to another either by lattice diffusion (N-H creep), or by boundary diffusion (Coble creep). In fact both transport paths are additive, leading to the following general equation for diffusional creep (5,6):

$$\sigma_e = \dot{\epsilon} \frac{d^3}{14\Omega(\delta D_b + \pi d D_v)} \quad (2)$$

where  $\Omega$  is the atomic volume,  $d$  is the grain size and  $D_b$  and  $D_v$  are the boundary and lattice diffusion coefficients.  $\delta$  is the diffusional width of the grain boundary. The derivation of Eq. (2) assumes that grain interfaces are ideal sources and sinks of atoms, that is, the interface reac-



tion is much faster than the time required for the atoms to diffuse over a distance of about one grain size.

Equation (2) assumes that the entire polycrystal deforms by diffusional creep. If this were so then the ideal value of  $m=1$  will be obtained. Indeed, that has been found to be the case for hard materials such as ceramics (7,8,9). But in metals, other deformation mechanisms intervene which have a smaller value of  $m$ ; this often creates mixed mode deformation involving both diffusional creep for which  $m=1$ , and dislocation creep for which  $m \approx 0.25$ .

### (c) Grain Boundary Structure

The derivation of Eq. (2) assumes the grain boundary to have very simple properties. It assumes (a) that the boundary provides a path for fast diffusional transport (10), and (b) that the atoms can be absorbed and emitted at the boundary with ease. The fact that the second assumption appears to hold in many materials is remarkable; it implies that the growth of a crystal that meets another crystal at a grain boundary can be at least as fast as the growth of free crystal surface from the vapor phase.

The structure of interfaces can influence superplastic flow in various ways. The transport properties of the interface are likely to be structure dependent. The rate at which atoms can exchange with the crystals may become limited by the structure of the interface. In ceramics, in particular, the interface can trap a very thin film of a fluid phase that can enhance diffusion. Another consequence of structure is that the growth and dissolution of crystals can lead to enhanced mobility of the interface; this results in grain growth that is entirely strain induced. The phenomenon of strain induced grain growth is not only interesting fundamentally, it is also technologically important since the flow stress increases as the third power of the grain size (see Eq. 2); a large increase in the flow stress can abort a superplastic forming process.

The ideas given above reflect unusual experimental aspects of superplastic behavior that cannot be explained in terms of Eq. (2). They reflect the importance of the structure of the grain boundary. In order to give form to these ideas we classify the relationship between superplastic flow and the structure of grain boundaries into three types:

Type I. Here the boundaries are assumed to be high angle boundaries. Typically these will be found in single phase materials when the grain size is greater than a few micrometers.

Type II. Fine grained polycrystals that contain a few volume percent of a fluid phase in grain interface regions form an important class of ceramic materials. The presence of even a very small amount of the fluid, less than 1 percent, for example, can have a dramatic effect on the superplastic characteristics of the polycrystals.

Type III. This type is the least understood and potentially of greatest technological importance because it appears to produce very fast rates of deformation. We assume that in this case boundaries are assumed to be predominantly of low angle. Their structure is described as arrays of lattice dislocations. Recent work shows that the population of low angle boundaries in polycrystals increases as the grain size gets smaller; thus Type III may be relevant to ultra fine grained ceramics, for example zirconia.

In the following sections features of each of the three types are discussed with the intention of showing the different ways in which grain boundary structure can lead to distinctly different superplastic behavior.

A schematic description of the three types of grain boundaries is given in Fig. 1.

TYPE I: Superplastic Flow by Nabarro-Herring/Coble Creep

In his classical derivation of diffusional creep Herring (3) assumed that grain boundaries are perfect sources and sink of vacancies. The mechanism is illustrated schematically in Fig. 2 by means of a single grain that changes its shape by diffusion of atoms along the surface. The interesting point about this mechanism is that the rate of deformation can be related explicitly to the kinetics of atom transport and to the kinetics of crystal growth and dissolution at grain boundaries. Just as crystal

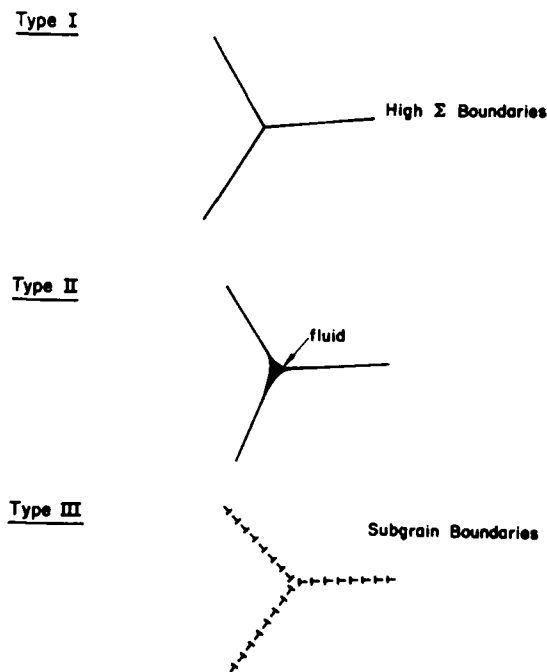


Fig. 1. The three types of superplastic flow are based upon differences in grain boundary structure. In Type I boundaries are normal, high  $\Sigma$  boundaries. They occur most commonly in single phase polycrystals having a grain size of a few  $\mu\text{m}$ . In Type II boundaries contain a thin film of a fluid phase; this is often the case in ceramic materials. In Type III the boundaries are predominantly low angle or subgrain boundaries.

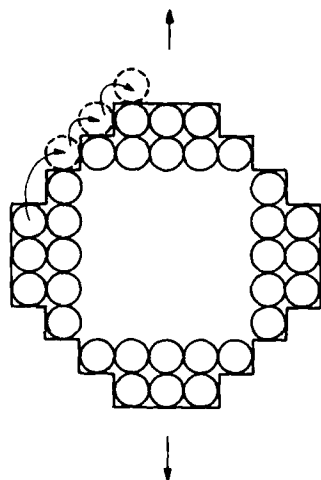


Fig. 2. A schematic showing how a crystal grain can change its shape by the diffusion of atoms along its surface. A similar process can occur in polycrystals except that atoms move along interfaces.

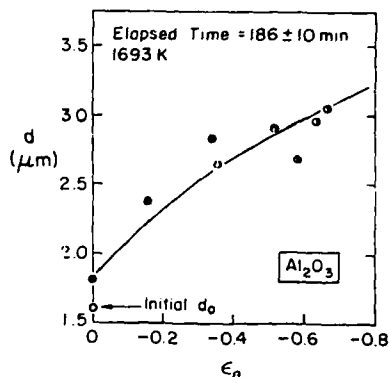


Fig. 3. Strain induced grain growth in alumina during superplastic deformation. The open point is the virgin grain size. The full points have the same time and temperature history but represent varying amounts of applied strain; the  $\epsilon = 0$  specimen was annealed without deformation while the other specimens were deformed at increasing strain rates.

growth and solid state transformation kinetics can be interface limited or diffusion limited (11), diffusional creep can also be limited either by the rate at which atoms are removed from or attached to the crystals at the grain boundaries, or by the rate at which the atoms are transported over a distance of about one grain size.

The assumption inherent in Eq. (2), that creep is diffusion rather than interface reaction limited, can be experimentally confirmed by studying the grain size dependence in the equation. Interface limited creep would give a linear grain size dependence (12) instead of the square or the cubic dependence obtained for the diffusion limited case. Nearly all experimental data, obtained on a variety of materials, shows a cubic grain size dependence (fast strain rates of deformation require a grain size of a few micrometers or smaller; at these grain sizes the boundary diffusion term in Eq. (2) is dominant which prescribes a cubic grain size dependence of flow stress). Clear evidence of linear grain size dependence has not yet been obtained, leading to the inference that grain boundaries do not create a barrier to the growth and dissolution of crystals. In one sense this is not a surprising result. Since boundaries have structure, the diffusion of atoms along the interface probably involves jumps between ledge sites, which is also mechanism that underlies the growth and dissolution of the crystal;

diffusion over the distance of several atom spacings, therefore, would be necessarily slower than the interface reaction.

The fact that interfaces have definite structure is believed to lead to the unusual phenomenon of strain induced grain growth in superplastic deformation of single phase materials. The results for alumina (7) are shown in Fig. 3; the open circle shows the initial grain size and the full circles show the grain size as a function of the applied strain. The full circles represent specimens which had experienced the same time and temperature history but different strain (and strain rate) history; for example, the point at zero strain was simply annealed without deformation, and the other points were deformed for the same time and at the same temperature but to different strains (by varying the rate of deformation).

In summary, Type I superplasticity is limited by the transport properties of grain interfaces. Single phase polycrystals that contain mostly high angle boundaries follow this behavior. The unusual effect of interface structure is that it leads to strain induced grain growth; this phenomenon is most probably tied to the atomistic mechanism involved in superplastic deformation where atoms are transported in order to change the shape of the grains by a crystal-growth-and-dissolution-like process. The structure in the boundary can produce asymmetric growth in the crystals that meet at an interface; as a result some crystals can grow at the expense of their neighbors leading to strain induced grain growth. A definitive study of this mechanism has not yet been carried out.

#### TYPE II: Superplastic Flow Enhanced by a Fluid Phase

Impurity segregation in grain boundaries can create a liquid phase if the segregants form a low temperature eutectic with the crystalline phase. In ceramics, the presence of silica at interfaces is a common cause of a liquid eutectic phase. The residual silica can arise from additives that are used to promote sintering (example: silicon nitride), or from incomplete crystallization of the glass in glass ceramic materials (example: 8-spodumene), or from unintentional absorption of silica during powder processing and sintering since silica is a common impurity in the environment and, especially, in the insulation materials used in high temperature furnaces. The presence of a thin fluid layer of a silicon-oxy-nitride glass in silicon nitride has a dramatic effect on the creep rate (13). The data in Fig. 4 show that silicon-nitride that is processed with a glass additive deforms much faster than the reaction bonded material which is free from silica. In another study (14) a comparison between the creep of aggregates of potassium chloride that were saturated in one case with water, and in another case with alcohol, demonstrated that creep enhancement is not possible unless the crystal has some solubility in the fluid (15).

A mechanistic understanding of how the liquid phase enhances creep is not entirely understood, principally because the atomistic details of the structure are not clear. High resolution microscopy of interfaces in silicon-nitride show that the glass resides at the triple junctions while a thin layer, approximately 1 to 2 nm thick, is trapped at the two grain junctions (16); this result agrees with thermodynamic analysis that is based upon interface free energy arguments (17). A simple view of liquid phase enhanced creep is that the fluid enhances the rate of diffusional transport through the interface; since the thickness of this layer is believed to be independent of the total volume fraction of the glass we infer that only a small amount of the liquid is needed to promote creep enhancement; although definitive studies of this point have not been done, in general the data support this prediction.

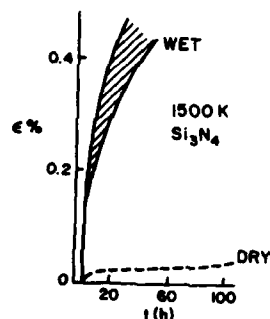


Fig. 4. The influence of approximately 1 to 5% liquid phase on the creep rate of silicon-nitride (13).

The details of the interface structure become important when one considers the thermodynamic driving force for matter transport (the normal traction gradient at interfaces), and the kinetics of matter transport (interface diffusion). The dichotomy arises because on the one hand we require the interface to support a gradient in normal traction, while on the other we ask for the presence of a continuous fluid film that can enhance diffusional transport; the conceptual difficulty arises because a continuous fluid film cannot support a gradient in normal traction. In one proposal (18) the interface is assumed to have an island structure where solid-to-solid contacts support traction gradients and the interpenetrating fluid provides a path for fast diffusion (see Fig. 5). The matter remains unresolved. An important phenomenological difference between Type I and Type II behavior is that strain induced grain growth that occurs in Type I is not seen in Type II superplasticity (9); the explanation should lie in the difference in the structure of the interface. The other difference between the two cases is that interface limited creep (with linear grain size dependence of the flow stress) definitely occurs in Type II (9,18) but has yet to be unambiguously reported in Type I superplasticity.

The flow equation for Type II superplasticity has been derived in Refs. 15 and 18 by invoking the mechanical work argument that equates the external work done to the energy dissipated in diffusional transport. Here we give the result for the diffusion limited case (15):

$$\sigma_e = \dot{\epsilon} \frac{\eta d^3}{2.3 \bar{c} \sigma \Omega} \quad (3)$$

where  $\bar{c}$  is the molar solubility of the crystal in the fluid,  $\eta$  is the viscosity of the grain boundary phase,  $\Omega$  is the atomic volume,  $d$  is the grain size, and  $\alpha$  is a factor that depends on the structure of the grain boundaries. Note that the equation does not depend on the volume fraction of the liquid phase but it does depend on its viscosity. The linear relation between stress and strain rate, and the cubic dependence on grain size have been unambiguously established experimentally (9) in a model glass ceramic

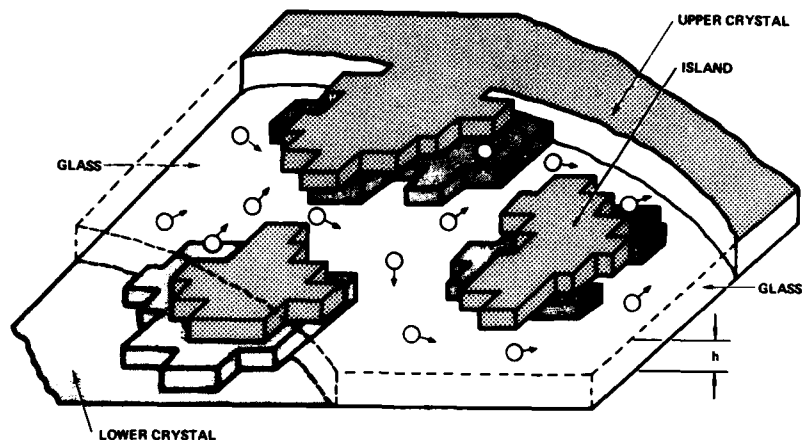


Fig. 5. A proposed island structure of the interface in polycrystals where the fluid phase leads to enhanced rates of deformation. The solid-solid contacts can support the traction gradients while the topologically interconnected fluid layer provides a path for enhanced diffusion (18).

material. A picture showing superplastic deformation in a specimen is reproduced in Fig. 6.

Interestingly, Eq. (3) predicts that the viscosity of a ceramic polycrystal is directly proportional to the viscosity of the glass phase even when the glass is present in small amounts. Presence of dopants can change the viscosity of the glass by several orders of magnitudes, and is, therefore, an important processing variable. The results in Fig. 7 show the wide range of strain rates that are obtained in  $\beta$ -spodumene glass ceramics simply by changing the chemistry of the intergranular glass. The graph shows the grain size normalized strain rate plotted against the flow stress. The linear slope for each data set shows adherence to Eq. (3), but the change in the strain-rate intercept is the result of the change in the viscosity of the intergranular glass. As the glass becomes increasingly pure silica, its viscosity decreases; the change spans several orders of magnitude.

In summary, Type II superplasticity is produced by the presence of a very thin layer of a fluid phase at grain interfaces. The film enhances diffusion but in contrast to Type I superplasticity, strain induced grain growth is not observed. Also, Type II superplasticity shows evidence of interface reaction controlled deformation which has not yet been seen unambiguously in Type I superplasticity. These differences reflect the difference in the atomic structure of interfaces with and without a fluid phase, but are not well understood at this time.



Fig. 6. Superplastic deformation of a ceramic material containing less than 5% residual glass (9).

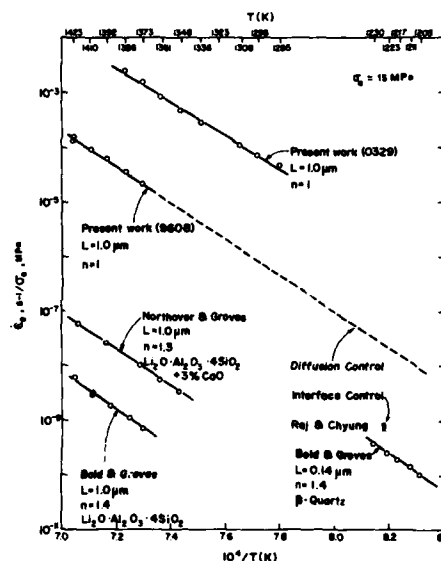


Fig. 7. Effect of the composition of the segregated glass phase on the strain-rate of polycrystals of the same crystalline material. The linear slope between grain-size compensated strain rate and the flow stress is in agreement with Eq. (3), (9).

### TYPE III: Sub-Grain Superplasticity

The diffusional mechanisms of superplasticity described as Type I and Type II lead to a strain rate sensitivity,  $m$ , equal to unity. In sub-grain superplasticity  $m$  is approximately equal to 0.5. This case of superplasticity has been much less studied than the previous two. The mechanism is not well understood and features of this mechanism described here are likely to be controversial. In-depth studies are particularly needed because this type of superplasticity leads to the highest rates of deformation and, therefore, is technologically significant. The special features of Type III superplasticity are now discussed.

Measurement of the strain rate sensitivity and the grain size dependence of the flow stress can distinguish between the diffusional and the dislocation mechanisms of deformation. As discussed earlier the diffusional mechanism requires a grain size dependence such that the flow stress increases rapidly with increasing grain size. In the dislocation mechanism the flow stress is either independent of the grain size or decreases with

increasing grain size. The  $n$  value is not an unambiguous indicator of a distinction between the dislocation and diffusional mechanisms. While  $n=1$  necessarily implies diffusional creep,  $n<1$  can be a result of either diffusional or dislocation creep, or a combination of both.

In at least two ceramic materials evidence of subgrain superplasticity has been obtained. In magnesium aluminate spinel,  $n=0.5$  was measured and the flow stress was found to drop with increasing grain size (19). In zirconia,  $n=0.5$  (20) was measured and dominant mechanism was ascertained to be dislocation creep (21). The behavior of these two ceramics resembles the very high strain rate superplasticity that has been reported in specially processed aluminum alloys (22); here, two very interesting observations were made with regard to the grain structure: first, the grain size depended on the deformation parameters (strain rate and temperature) rather than on the initial grain size of the polycrystal, and second, the grain boundaries were generally low angle boundaries with a misorientation of between one and five degrees. In aluminum alloys the subgrain size was approximately  $1\text{ }\mu\text{m}$ , in the spinel the subgrain size varied from 10 to  $15\text{ }\mu\text{m}$ , while in zirconia it is not yet confirmed whether or not the interfaces were low angle boundaries.

Assuming that the subgrain boundaries in Type III superplasticity consist of arrays of lattice dislocations, a model has been proposed (22) where deformation accrues by the transfer of dislocations from one boundary to another via the crystal lattice, as shown schematically in Fig. 8. In the steady state, the emission rate of the dislocations, will be equal to the arrival rate of dislocations at the adjacent interface; both will be equal to the ratio of the dislocation velocity through the lattice divided by the subgrain size, which we call  $d'$ . If it is assumed that the dislocation velocity is related to the applied shear stress by a linear coefficient of friction  $\mu$ , then it can be shown (22) that:

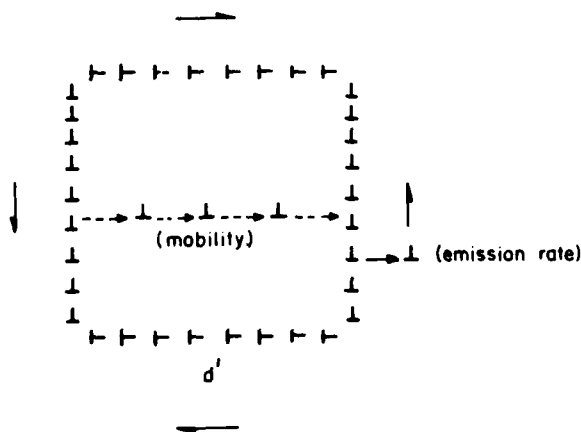


Fig. 8. A schematic explaining the mechanism of Type III superplasticity. The grain boundaries are assumed to be low angle boundaries and deformation occurs by emission and absorption of dislocations between the boundaries. The dislocations travel through the crystal lattice.



$$\sigma_e = \frac{\dot{\epsilon}_e d'}{\Delta\theta} \cdot \frac{kT}{2\mu\Omega} \quad (4)$$

where  $\Delta\theta$  is the misorientation at the boundaries and  $\Omega$  is the atomic volume. At a fixed value of the subgrain size,  $d'$ , the equation predicts a linear relation between stress and strain rate. Actually, experience shows that the subgrain size decreases with increasing strain rate, which means that the flow stress will increase less rapidly with strain rate than suggested by the linear relationship, leading to a strain rate sensitivity of less than one. Eq. (4) is a first step in understanding this type of superplastic flow, where the macroscopic deformation behavior is linked to the structure of interfaces.

In summary, Type III superplasticity is believed to be a result of a polycrystal that contains predominantly small angle grain boundaries. It is the least understood of the three types discussed in the paper but is technologically most significant because it produces very high strain rates. Further work should emphasize this case of superplastic deformation.

#### ACKNOWLEDGMENTS

The work presented here is derived predominantly from Cornell doctoral dissertations by J. G. Wang, K. R. Venkatachari, and P. C. Panda. Their research was funded by the Department of Energy under Grant No. DE-AC02-77ER4386 with partial support from the National Science Foundation through the Materials Science Center at Cornell University.

#### REFERENCES

1. E.W. Hart, *Acta Metall.* 15, 351 (1967).
2. A.K. Ghosh and R.A. Ayers, *Metall. Trans.* 7A [10] 1589-91 (1976).
3. C. Herring, *J. Appl. Phys.*, 82, 87-93 (1951).
4. R.L. Coble, *J. Appl. Phys.*, 34 [6] 1679-84 (1963).
5. M.F. Ashby and R.A. Verrall, *Acta Metall.*, 21 149 (1973).
6. R. Raj and M.F. Ashby, *Metall. Trans.* 2A 1113 (1971).
7. K.R. Venkatachari and R. Raj, *J. Am. Ceram. Soc.* 69 [2] 135-138 (1986).
8. C. Carry and A. Mocellin, *ibid.* Ref. 16, pp. 16.1-16.19.
9. J.-G. Wang and R. Raj, *J. Am. Ceram. Soc.* 67 [6] 399-409 (1984).
10. R.E. Hoffman and D. Turnbull, *J. Appl. Phys.* 22 634 (1951).
11. J.W. Christian, in *The Theory of Transformations in Metals and Alloys*, 1st ed., 1965, Pergamon Press, Chaps. X, XI.
12. M.F. Ashby, *Scripta Metall.* 3 837 (1969).
13. R. Osborne, *Proc. British Ceram. Soc.*, vol. 25 (1975).
14. G.M. Pharr and M.F. Ashby, *Acta Metall.*, 31, 129-138 (1983).
15. R. Raj, *J. Geophys. Res.*, vol. 87, No. B6, 4731-4739 (1982).

16. D.R. Clarke and G. Thomas, J. Am. Ceram. Soc. 60 [11-12] 491-95 (1977).
17. R. Raj, J. Am. Ceram. Soc. 64 [5] 245-248 (1981).
18. R. Raj and C.K. Chyung, Acta Metall. 29, 159-166 (1981).
19. P.C. Panda and R. Raj, J. Am. Ceram. Soc. 68 [10] 522-29 (1985).
20. F. Wakai, this volume.
21. P.C. Panda, J. Wang and R. Raj, "Sinter Forging Characteristics of Fine Grained Zirconia," to appear in J. Am. Ceram. Soc. (1988).
22. R. Raj, A.K. Ghosh and C. Gandhi, "Subgrain Superplasticity," unpublished work (1985).

FORMING NON-SUPERPLASTIC MATERIALS WITH SUPERPLASTIC MEMBRANES

D.M.Ward

Incoform Limited,  
Wiggin Street,  
Birmingham. England.

Abstract

Knowledge of superplasticity has led to the development of a related technology that uses a superplastic sheet to form non-spf alloys. The process developed by Incoform for aerospace components is called 'membrane' forming and uses a throwaway or reusable standard spf (membrane) sheet to form the non-spf (component) sheet.

The purpose behind this development was to apply the benefits of superplastic forming i.e. one die, accuracy of form, repeatability, no spring back to non-spf alloys for the additional cost of a membrane.

The results of membrane forming show that while the spf sheet (membrane) is being blow formed in the standard spf process it draws the non-spf sheet along with it into the form of the die. Because the non-spf sheet is free to move it forms with much less thinning and structural damage than if it had been stretched to shape. Nickel, titanium and aluminium non-spf alloys are formed to complex curvatures by membrane forming without structural damage and with little or no thinning. Aluminium and titanium spf alloys formed by the same membrane technique also show the same benefits of reduced thinning and minimal structural damage.

Potentially, the new technique can be used on numerous alloys. Inevitably, there are limits on the complexity of shape that can be formed by this technique and it is likely to be limited to the aerospace industry because of the added cost of the membrane.

### Introduction

The benefits that accrue from superplastic forming are many and are documented in the technical publications on this subject. For aerospace applications these benefits often outweigh the added process cost which comes from relatively small batch production which is needed to minimise degradation of surface finish from build up of lubricant and from airborne dust which sticks to the die and imprints the superplastically formed components. Also the forming rates of  $10^{-3}/10^{-4}$  per second used to minimise sheet thinning, and the high forming temperatures, at least  $0.5 T_m$ , i.e.  $500^{\circ}\text{C}$  for aluminium alloys,  $900^{\circ}\text{C}$  for titanium alloys and  $1000^{\circ}\text{C}$  for stainless steels both add to the process cost. Outweighing these high process costs are important benefits of close conformance to shape, which reduces assembly costs, repeatability of shape without spring back, which therefore reduces rectification work needed for the superplastically formed parts, and the requirement for only one female (or male) die, instead of the matching die set needed with creep forming, which gives additional cost benefits to superplastic forming.

Superplasticity has found its niche in sheet forming technology and research and development is trying to extend its range of applicability. This has been directed towards a wider range of alloys viz aluminium alloys, 7475 and 8090 for aerospace applications, and stainless steels Avesta 2205 and Sandvik 3RE60 for non aerospace applications. Developments have improved process economics by reducing forming temperature viz titanium alloy development, and by applying superplastic forming techniques to non-superplastic materials viz membrane forming. Incoform has developed a hybrid superplastic forming process called membrane forming which uses a sheet of superplastic material - the membrane - to form a smaller sheet of non-superplastic material - the component - into a die (Figure 1). The component material may be but need not be superplastic. In practice the superplastic membrane presses, and then flattens the component against the die at its forming pressure. Because only the membrane and not the component is trapped by the pressure seal on the flange, the component is free to slide down the die and is drawn into shape by the membrane until it conforms exactly to the die. The drawing rather than stretching action in the component causes far less thinning than is caused by the completely stretching action in the membrane, (Figure 2).

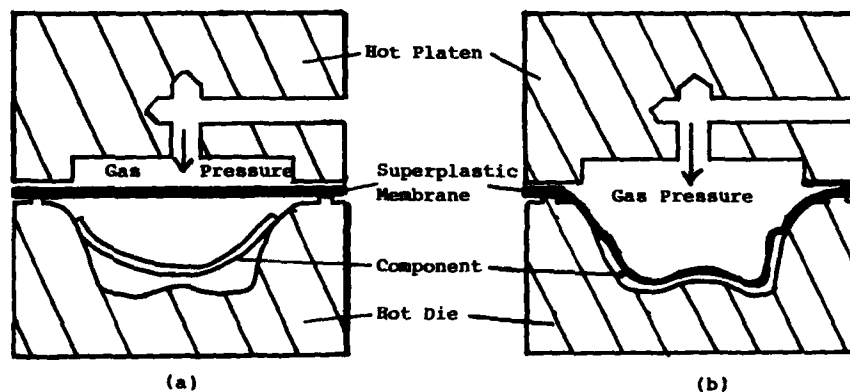


Figure 1 Membrane and component (a) before forming (b) after forming



Thickness A - A <sup>1</sup> strain	B - B <sup>1</sup>
Component 0,.10,0	0,0,0
Membrane .18,.43,.54	.68,.46,.13

Figure 2 Trimmer made in  
Nimonic alloy 263

The requirements for membranes are that they are superplastic at the forming temperature of the component, that they have sufficient ductility so they do not fracture or puncture during forming and release the pressure prematurely and that the membrane is able to transmit the gas pressure applied to it through to the component. This means that the membrane has to have a flow stress low enough that it forms into all the die cavities and does not restrict the forming radii of the component. Beyond these requirements, the membrane should add a little or no process cost to the operation by being of low initial cost itself, or by being designed to be used a second or multiplicity of times in forming components. In its favour, provided the membrane does not burst, there is no need for a low forming rate, indeed higher strain rates leading to thinner material at some points will actually aid forming by reducing the forming pressure needed. The component is not stretching significantly say 0.10/.20 strain and for this strain rate is unimportant. The membrane therefore should have a wide range of ductility with strain rate like Formall 700 (Figure 3) which has adequate ductility over a wide strain rate range. (Shown by kind permission of Alusuisse ).

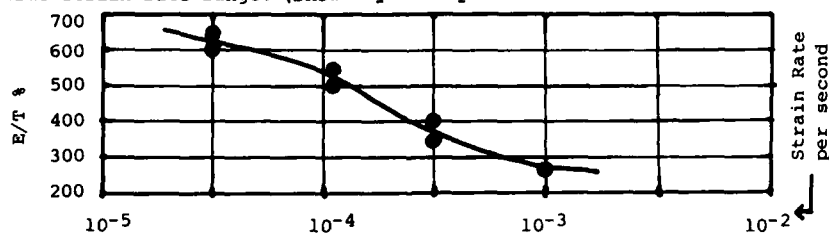


Figure 3 Total elongation versus strain rate Formall 700 (7475)

#### Membrane Forming Stainless Steels and Nickel Base Alloys

Hot forming of stainless steels and nickel base alloys by gas pressure requires forming temperatures as high as 950° to 1050°C or 1100°C. Beyond about 0.30 strain, cavitation occurs in many alloys causing marked structural damage (Figure 4a). However in membrane forming the strain levels are low (Figure 2) and no cavitation occurs (Figure 4b) furthermore mechanical properties are unimpaired by the process (Table I).

Other complex forms have been used to demonstrate the application of membrane forming to forming of a range of nickel base alloys and stainless steels. Results show about 0.16 max strain on mixer lobes made in 304 stainless steel (Figure 5a). Results for Hastelloy X, Nimonic alloy PE11, and 86 are given in Table II.

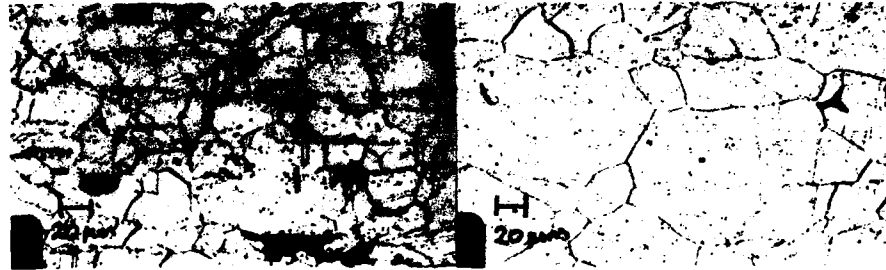


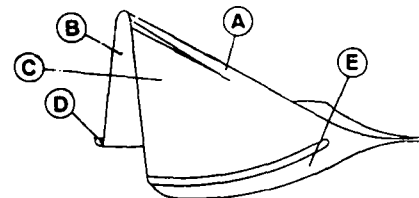
Figure 4(a) Blown with cavitation (b) Membrane formed, no cavitation

Table I Properties of Nimonic<sup>®</sup> alloy 263 membrane formed

Condition	RT Hardness	780°C UTS	El
Membrane formed and aged 8h 800°C	316 Hv <sub>30</sub>	640 N/mm <sup>2</sup>	24%
Specification	280 min.Hv <sub>30</sub>	540 min.N/mm <sup>2</sup>	9%min.

#### Membrane Forming of Titanium Alloys

Hot forming/superplastic forming of titanium alloys is well known and practised extensively. Creep forming has some drawbacks because of the cost of the matching die set and the propensity for scratching and scoring of the component by the dies. With superplastic forming there is a reduction of sheet thickness consistent with the depth/width aspect ratio and bend radii of the part being formed. By using long forming times (low strain rates), lubrication, and judicious prethinning of the sheet by chemi-milling prior to forming, some control over thinning can be achieved. However, in membrane forming where the component is free to move, much better thickness distributions are achieved.



(a) AISI 304S/S

.03	0	.05
.16	0	.16
0	0	.02
0	0	0
D	A	E

(b) Ti 6Al 4V

.01	0	.01
.12	0	.12
.03	0	.03
.01	.04	0
D	A	E

B .06 .09 C .09.05 B .03.07 C .06 .01

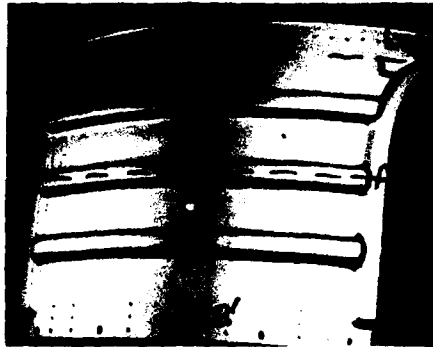
Figure 5 Thickness strain 12-lobe mixer

Table II Maximum Strain on Mixer

Alloy	D	B	A	C	E
Hastelloy X	.06	.05	.06	.06	.05
Nim. PE11	.10	.08	.02	.12	.08
Nim. PK33	.06	.07	.11	.09	.08
Nim.86	.04	.05	.08	.06	.07
Ti 2Cu	.14	.07	.03	.12	.19

<sup>®</sup> is an Inco Trademark.

Examples are shown in Figure 5b for Ti 6Al4V alloy and in Table II for Ti 2Cu alloy, membrane formed onto the mixer die which have only 0.2 strain even for this complex shaped component.



Section	Component	Membrane
A - A <sup>1</sup>	.02 .08 .02	.29 .26 .25
B - B <sup>1</sup>	.04 .08 .02	.27 .34 .22
C - C <sup>1</sup>	.24 .03 .23	.60 .51 .74

Figure 6 Duct floor thickness strains

A duct floor of an engine with a ribbed reinforcing panel shows strains of 0.2 in Ti 6Al4V alloy 2mm thick when produced by membrane forming. Comparison of the thickness strain distribution between membrane and component shows the benefit of very much improved thickness distribution in the component than in the superplastically formed membrane (Figure 6) which had marked thinning up to 0.7.

#### Membrane Forming of Aluminium Alloys

With superplastic forming of aluminium alloys there are added cost penalties to overcome viz quench sensitivity, and cavitation. The quench sensitivity in 7475 requires water quenching from solution temperature to develop full T6 properties on ageing. Without jiggling this causes distortion in the sheet components. With the problem of cavitation there was little choice, until now, but to apply significant back pressure during forming to minimise the structural damage. Equipment for this is complex and expensive to operate. With membrane forming there is a real alternative for many components to be produced without cavitation. In early trials on Formall 700 at Incoform, properties of membrane formed components with 520 N/mm<sup>2</sup> for 0.2% PS, 575 N/mm<sup>2</sup> for UTS and 10% El. are comparable with properties on superplastically formed products using high back pressures.

#### Concluding Remarks

Membrane forming may be used to apply the benefits of superplasticity to non-superplastic material viz only die, accuracy of form, and repeatability with no spring back. There is an additional cost involved that of the membrane but there are additional benefits to be gained viz greater uniformity of thickness, and in nickel and aluminium alloys less structural damage. With the forming of stainless steels and nickel base alloys the thickness range has been limited so far to 2mm for stainless steels and 1.2mm for Hastelloy X and Nimonic 263. For titanium alloys thicknesses of over 3mm have been formed successfully by this technique. Because membrane forming produces much less structural damage than superplastic forming, it could be of great value in forming alloys that are prone to cavitate. Die design and part configuration are important variables that need to be defined for this process to be exploited fully for the forming of aluminium alloys.

## S.P.F-D.B. APPLICATIONS FOR MILITARY AIRCRAFT

AVIONS MARCEL DASSAULT - BREGUET AVIATION

Bruno ROLLAND

### 1/ INTRODUCTION

My company, AVIONS MARCEL DASSAULT, has been involved with SPF-DB for nearly 10 years. All the research and development facilities are located in Paris, in the plant where we are manufacturing military prototypes. In this paper, you will not find the research aspects of SPF-DB, but only SPF-DB applications through some of our aircraft parts. The following points will be approached :

- Process to fabricate four sheets sandwich
- Manufacturing of leading edge slat
- Manufacturing of the MIRAGE 2000 strake
- SPF-DB tools
- Quality assurance
- Poitiers production plant.

### 2/ PROCESS TO FABRICATE FOUR SHEETS SANDWICH

It's well known that titanium is a famous material for aerospace application. But because of the raw material and fabrication cost, other material was substituted for it. In 1970, the use of SPF and SPF-DB titanium structure became cost effective. Among titanium alloys, 6-4 has long been the aerospace worldwide material, used mainly because of its properties. The 6-4 also is well suited for superplastic forming and diffusion bonding.

Amid the fundamental types of structure that can be fabricated by SPF-DB, the four sheets sandwich structure was employed. This structure, in many respects, seemed well adapted to the parts that we intended to manufacture. The fabrication of such a structure involves three main steps (see figure 1). As soon as 900°C temperature is reached, gas pressure is introduced between sheets 1 and 2 on the one hand, and the same gas pressure between sheets 3 and 4 on the other hand. Using this pressure the external sheets 1 and 4 are formed until they come in contact with the tool. At the same time the core sheets are diffusion bonded on selected areas. This step needs about two hours and the main difficulty is to maintain the core sheets in the middle of the part.



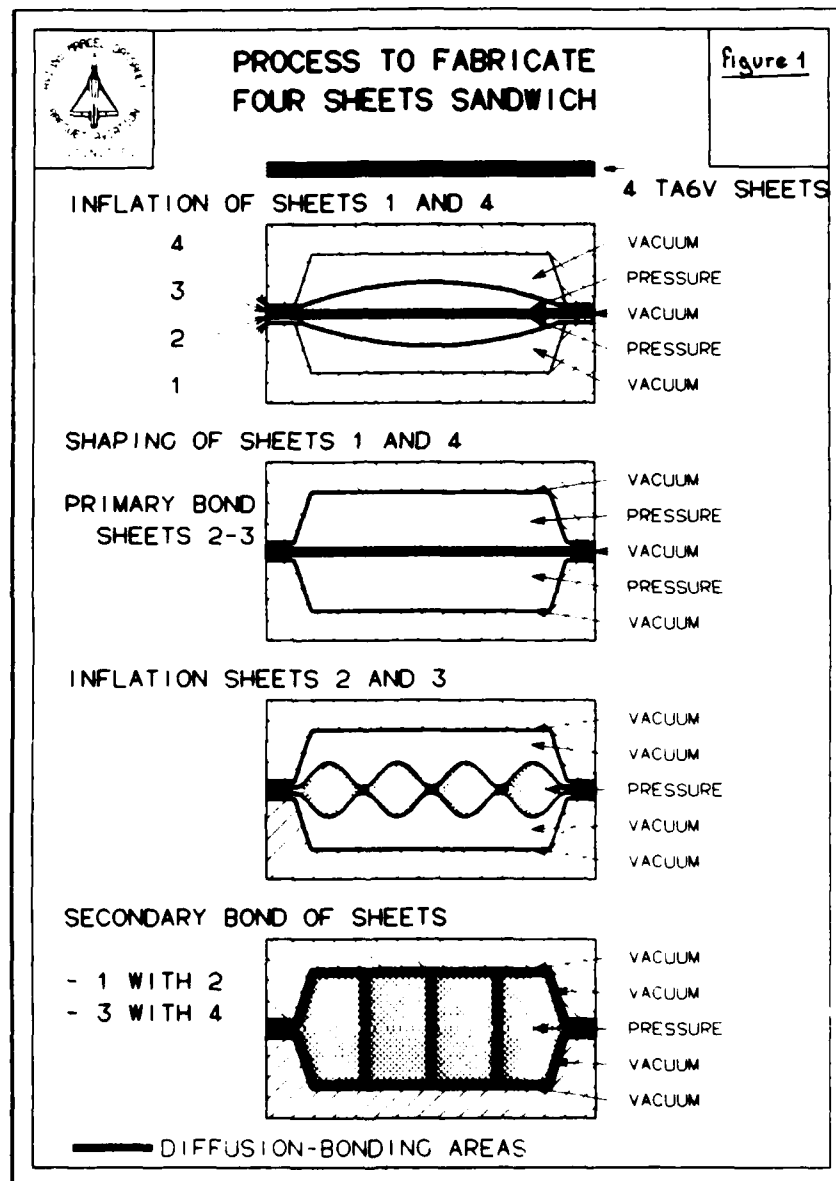


Figure 1

The second step consists in forming the two core sheets until they contact the external sheets and face sheets. During the third step the pressure is maintained for two hours to allow diffusion bonding of all the mating surfaces. The pressure is about 16 bars. A monolithic structure is thus obtained.

Among the problems we met when applying this technology, one is concerning the thickness.

As a matter of fact, the thickness of this structure decreases between the side wall and the corner and then increases (see figure 2). This is due to the fact that when the sheet contacts the mold or the other sheet, further thinning is inhibited and subsequent deformation is confined to the free region of the sheet. The minimum thickness is in the cell corners where rupture can occur during superplastic forming. Because of that we ought to select thick sheet, but this would make the component heavier.

The technique we use to improve on the thickness distribution in order to avoid rupture and save weight was chemical milling. Figure 3 presents such a sheet after chemical milling. The thicker area is located in the deeper and stiffening portion of the component.

The different thicknesses result in more homogenous thickness distribution after forming and of course allow weight saving.

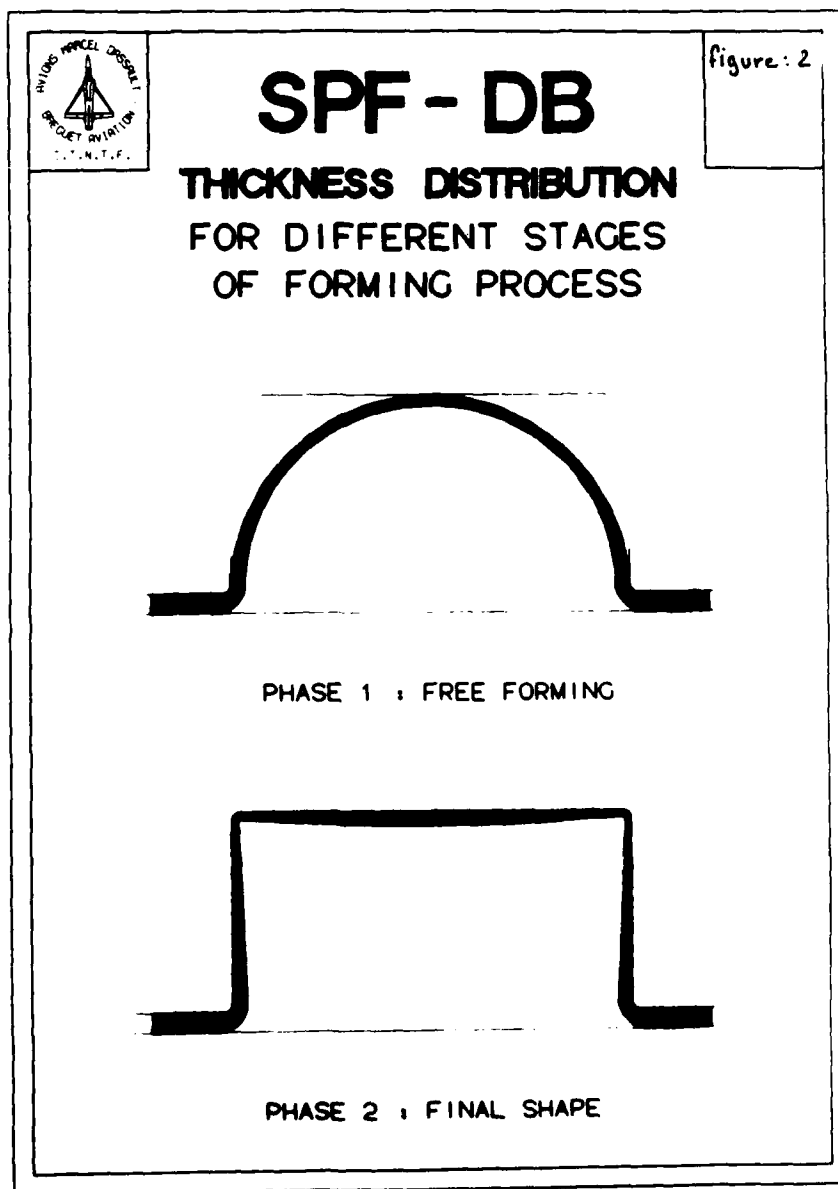
### 3/ MANUFACTURING OF LEADING EDGE SLAT

This part is four sheets sandwich structure made with 6-4 sheets (figure 4). These are manufactured by RMI. After chemical milling, their thickness is between 0.8 mm and 2 mm. This part is composed of a small spar from end to end and ribs. Spars and ribs come from the two core sheets.

These parts are from 64 inches to 100 inches long and from 12 inches to 24 inches width. After SPF-DB, these parts are cleaned by mechanical and chemical etching processes to remove surface contamination.

Subsequent treatment includes trimming and finishing. Due to the high quality of the forming surface tool, the skins of these parts are very smooth.

The dimensional check gave generally good accuracy. In fact, dimensional accuracy depends on the quality of the tool and the handling when the parts are removed from the dies. The structure validation also gave very good results. We conducted static and fatigue tests. Static tests check the stiffness of the components. With the fatigue test we widely cover the in-flight life limit of such parts. These parts have been tested in flight on RAFALE experimental fighting aircraft since July 1986 and also on MIRAGE 2000. As far as the weight is concerned, we save up to 40 % compared to the aluminum part. The price is cheaper than the aluminum part. These parts are on production on MIRAGE 2000. About 100 parts have been produced. Figure 1.



**Figure 2**

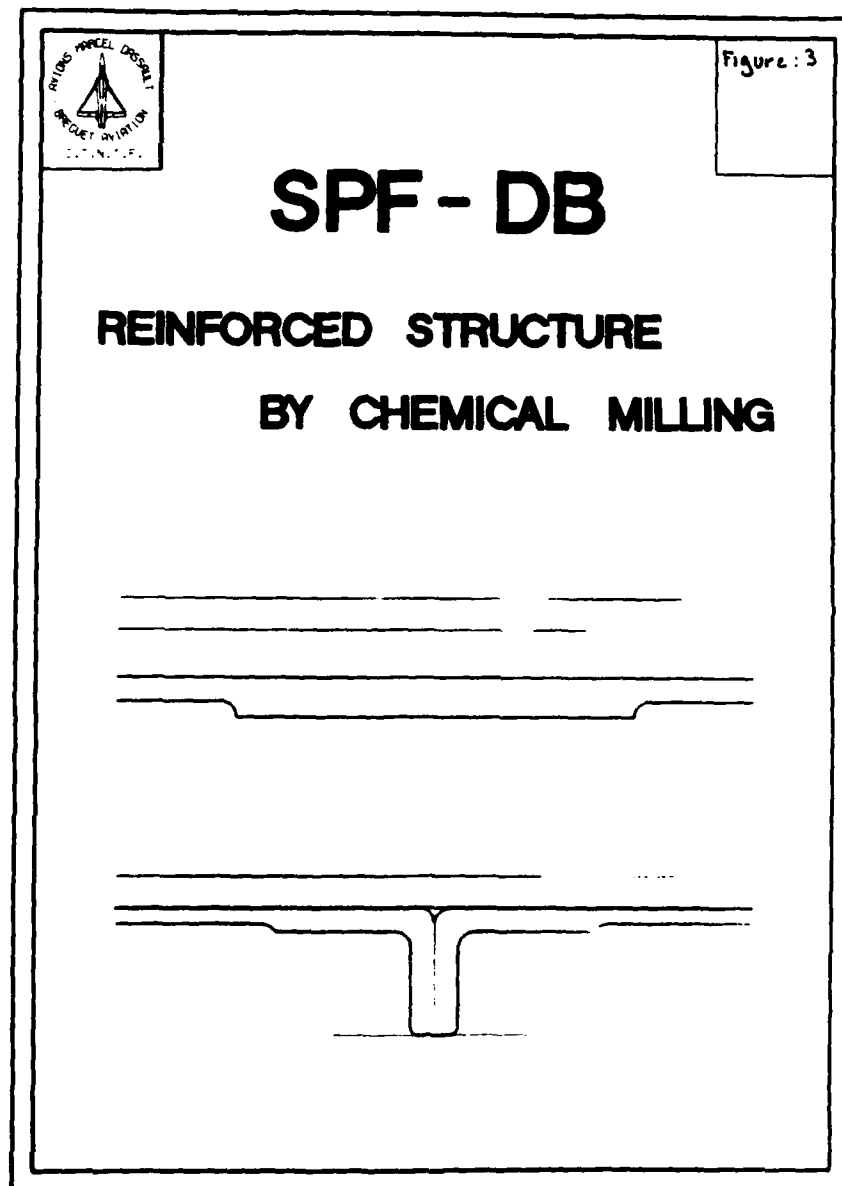


Figure 3

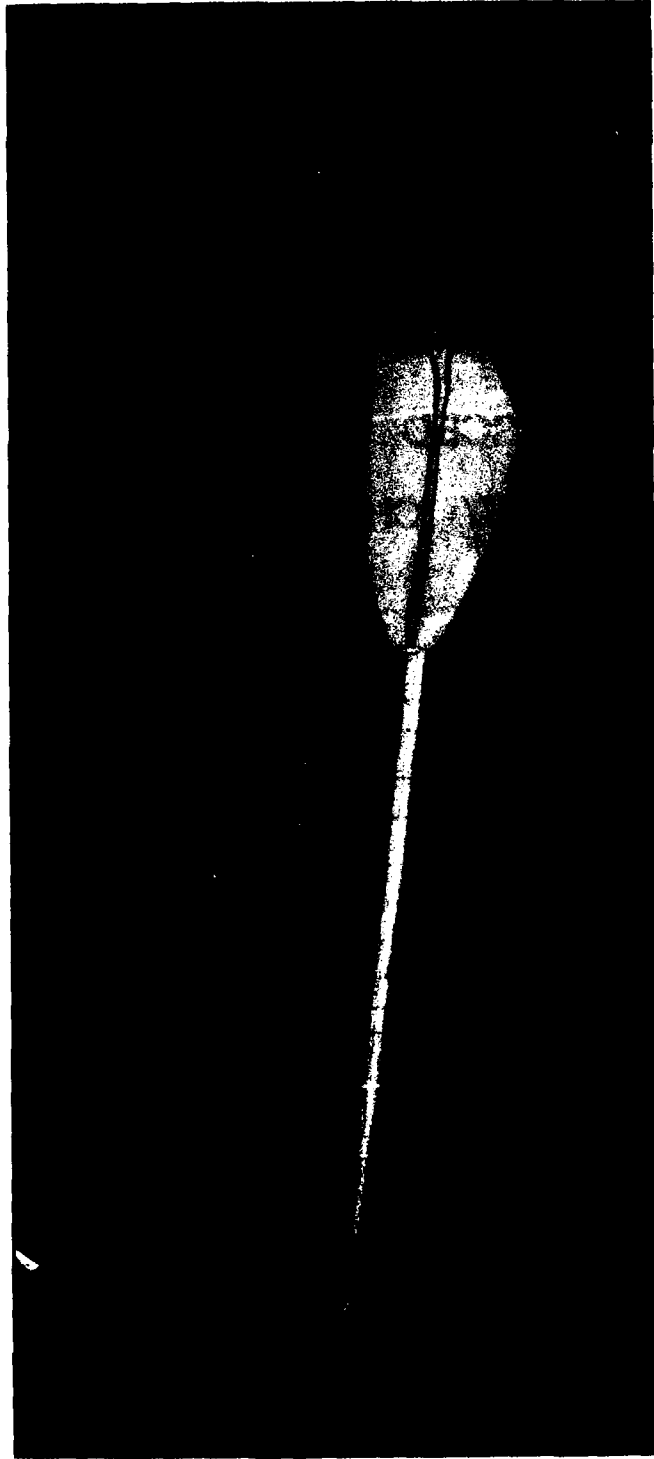


Figure 4

#### 4/ MANUFACTURING OF THE MIRAGE 2000 STRAKE

This part is a four sheet sandwich structure made with 6-4 sheets. The sheets have undergone chemical milling. The structure consists of an end rib and perpendicular to it few other ribs (figure 5). One of the requirements of this part is the integration of blocks during the process. These blocks are required to fasten the strake on the fuselage. This part was tested through static and fatigue cycle. All the results were very satisfactory. Since April 1986, a MIRAGE 2000 has been flying with these parts. Figure 6 presents a comparison of the conventional aluminum alloy solution and the SPF-DB one.

We save some weight ; we save a lot of primary parts which are machined or cast ; we also eliminate a significant number of fasteners as well as the drilling of their holes and their installation. The SPF-DB structure includes four sheets, six blocks and just a few fasteners.

#### 5/ SPF-DB TOOLS

All dies were machined from cast 49M stainless steel. They were cast by ESCO (PORTLAND). Each die has a weight of about 1 ton.

This alloy is a useful material for superplastic forming tool. It has suitable high temperature strength and it resists to oxidation. The material is weldable. Many gas tubes are welded around the die.

#### 6/ QUALITY ASSURANCE

Quality Inspection mainly consists of :

- Check of process parameters
- Radiography
- Inspection of diffusion bonding area
- Measurement of thickness

##### Check of process parameters

We consider that quality assurance depends heavily on process control.

During the SPF-DB process, we record all the parameters (temperature, time, pressure, vacuum). The quality assurance consists in comparing the records of the charts, which guarantee the quality of the parts. The numerous SPF-DB parts so far manufactured show us the perfect reproducibility of the process when all the parameters are well controlled.

##### Radiography

Radiography provides an excellent method for observing the core structure and mainly the existence of the cell walls. We can accurately check the location of the primary bond which has an effect on the final thickness of the core sheet after elongation.

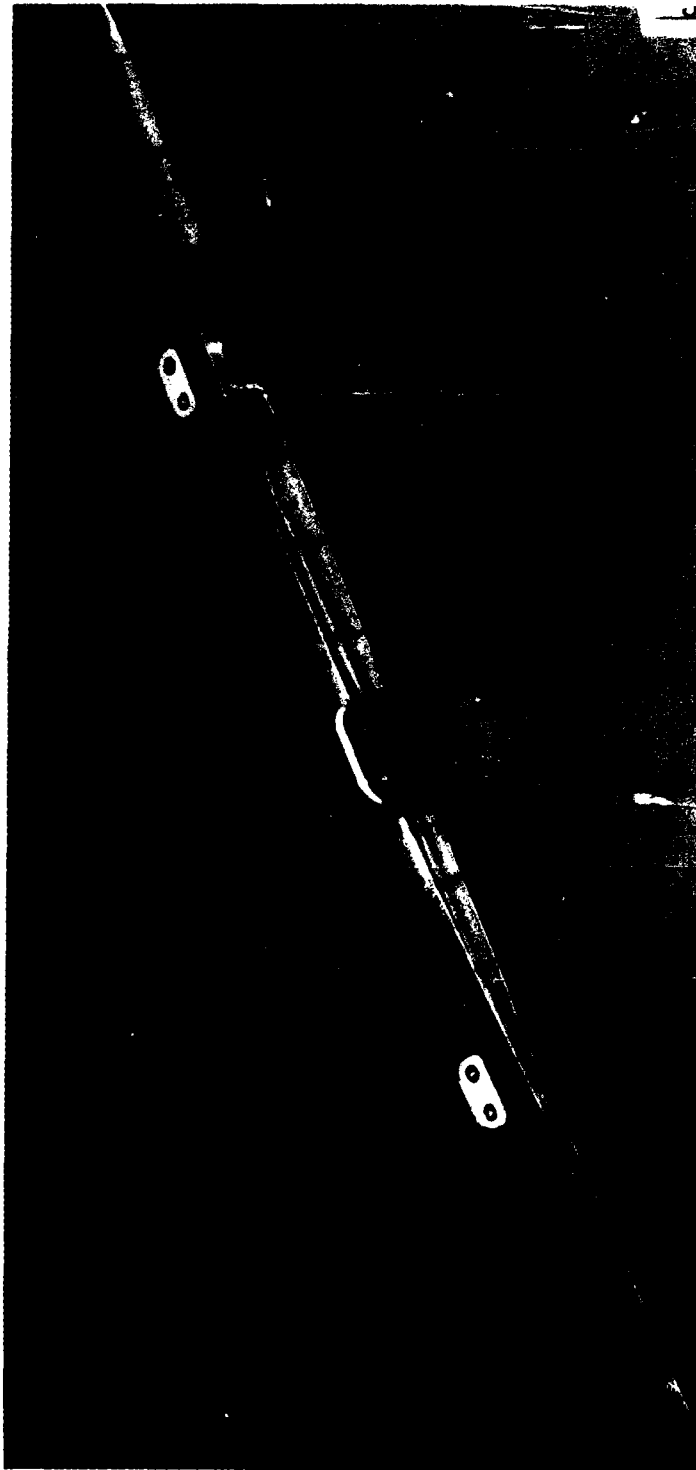


Figure 5

# NOUVELLE TECHNOLOGIE DE FABRICATION NEW MANUFACTURING TECHNOLOGY

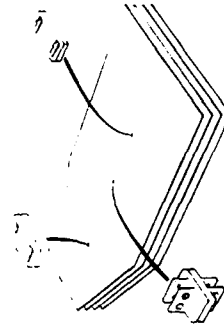
FORMAGE SUPERPLASTIQUE ET SOUDAGE PAR DIFFUSION DE L'ALLIAGE DE TITANE TA6V  
SUPERPLASTIC FORMING DIFFUSION BONDING Ti6-4 TITANIUM ALLOY

SPF / DB



Fabrication conventionnelle  
(alliage d'aluminium)  
Conventional built up construction  
(aluminium alloy)

CONVENTIONNELLE CONVENTIONAL	SPF / DB
3.2 kg	2.8 kg
10	4
155	6
	FIXATIONS FASTENERS



SPF / DB  
TA6V

Figure 6



In other respects this control gives information about the quality of the primary bond which is practically guaranteed if the cell wall is formed. Since this bond is subject to tensile stress during the forming, from our experience, it is the appropriate method to evaluate core quality.

#### Inspection of bonding area

Four sheets sandwich structure presents two kinds of bond (figure 1) :

- The primary bond
- The secondary bond.

An ultrasonic inspection of the first one is practically impossible to apply as its accessibility is not easy. For this reason we don't try to detect bond flaws. We only use as we said the information given by the radiography. Our experience from numerous observations indicates that it's a reliable method.

As far as the secondary bond is concerned, ultrasonic inspection is applied to the skin area. This control is capable of detecting about 0,02 inches flaws. For the cell wall bond, we consider from our experience that this area is very similar to the skin area and consequently we use the result of the previous control. In addition all the parts cut off have their bonds examined by micrography.

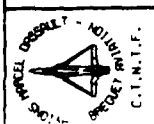
#### Measurement of thickness

The thickness of the skins is measured by ultrasonic method and compared to the drawing requirements. As far as the cell walls are concerned, their thicknesses are checked by considering the position of the primary bond and the skin thickness.

### 7/ POITIERS PRODUCTION PLANT

The production of SPF-DB parts takes place in Poitiers plant. There, we decided to put all the facilities to manufacture the fully part. The main workshops consist of :

- Laser cutting for titanium sheet and chemical milling mask
- Chemical etching
- Chemical milling
- stopoff screen printing
- 1000 T hot platen press for SPF-DB (1600°F). Figure 7 :
  - . with automatic loader
  - . computer controlled for ramps, heating and SPF-DB cycle
- Mask spray equipment
- Sand blasting equipment
- Inspection facilities :
  - . X ray system
  - . Ultrasonic system.



1000 TONS MARCEL DASSAULT PRESS

TITANIUM SUPERPLASTIC FORMING AND DIFFUSION BONDING

# SPECIFICATIONS

- WORK AREA :  
141,7" x 51,2"
- MAXIMUM SIZE FOR PARTS :  
127" x 37,4" x 16" (HEIGHT)
- PLATENS :
  - HEATED WITH CARTRIDGE (300 KW)
  - OPERATING TEMPERATURE : 1670 F°
- AUTOMATIC LOADER
- COMPUTER CONTROLLED FOR HEATING AND SPF-DE CYCLE

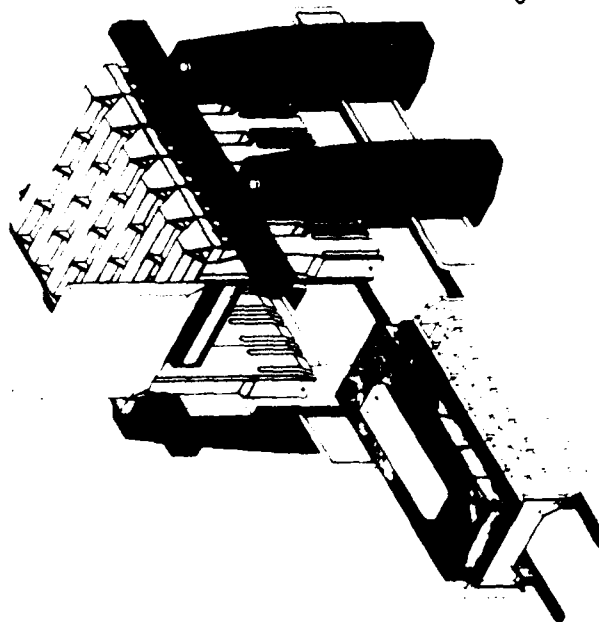


Figure 7

Figure 7

8/ CONCLUSION

As other companies, AVIONS MARCEL DASSAULT has demonstrated that SPF-DB is an optimum way to produce parts with many advantages for aircraft manufacture. The use of titanium offers excellent properties and the means to save money and weight.

Because SPF-DB is a relatively new technology, these advantages will be gained on the condition that we think SPF-DB when we design parts. That is to say, people must adapt parts to SPF-DB and not the contrary.

SPF-DB is really a new way for manufacturing and I am convinced that its possibilities are limitless.

## FABRICATION OF FIBER REINFORCED METAL USING SUPERPLASTIC METAL

### POWDER AS MATRIX

H. Nishimura, S. Wakayama, H. Yamamoto and S. Yamagishi

Department of Mechanical Engineering, Faculty of Technology,  
Tokyo Metropolitan University,  
Tokyo, Japan

#### Abstract

As an application of superplasticity, the powder metallurgical technique of fabricating 'ductile' FRM (Fiber Reinforced Metal) was developed. Superplastic zinc (SPZ) alloy was used for matrix metal and SiC fibers were used for the reinforcements. Since the FRM was fabricated at relatively low temperature under low pressure which was contributed by superplasticity of matrix metal, the damage of fibers and the nucleation of chemical reaction layers at fiber/matrix interfaces can be prevented. At first, the most suitable fabricating condition was examined by tensile tests at 250 °C. It should be noticed that compacting temperature is below 500 °C, the compacting duration is less than 30 min. and the compacting pressure is less than 150 MPa. To control the ductility at fiber/matrix interfaces for after-forming processes, initial (360 °C x 1h., WQ) and secondary (250 °C x 30 min., AC) heat treatment techniques were adopted. Following results were obtained. (1) The most suitable condition was determined as 410 °C, 5 min. and 70 MPa. (2) For the FRM fabricated under the most suitable condition, the ratio of the tensile strength,  $\sigma_c$ , to the value calculated using the rule of mixture,  $\sigma_{ROM}$ , exceeded 80 % and the ratio of Young's modulus,  $E_c/E_{ROM}$ , exceeded 100 %. (3) From the fractographs, the penetration of matrix metal between fibers was sufficient. Furthermore, the damage of fibers and the nucleation of chemical reaction layer at the interfaces were prevented during the fabrication. (4) The ductility at the interfaces was controlled successfully. The ductility was increased at the forming process by initial heat treatment and the strength was recovered after the forming by secondary heat treatment. (5) 70° V bending was carried out successfully at 250 °C.

### Introduction

Recently, fiber reinforced metal (FRM) composites have been expected as one of the near-future materials because of its high specific rigidity, high specific strength and high thermal resistance. On the other hand, it has some problems to be conquered such as low reliability and brittleness caused by the poorly controlled compatibility at fiber/matrix interfaces. Furthermore, the formability of FRM is one of the most important problems.

In this study, the ductile FRM was fabricated using powder metallurgical technique. Reinforcement is continuous SiC fiber and matrix is superplastic zinc alloy (SPZ; 22Al-Zn) with four types of initial particle sizes. At first, suitable fabricating conditions, i.e. temperature, duration and pressure of hot-pressing, were examined. The V-bending tests were also carried out in order to establish the technique of forming of FRM. Consequently, FRM plates were bent successfully until 70° at 250 °C.

### Experimental Procedure

#### Fabrication of FRM

SPZ powder used for matrix metals has four types of initial diameter, i.e. A: 44 μm, B: 44-74 μm, C: 74-149 μm and D: 149-296 μm. SiC fibers used for reinforcements have diameter of 15 μm, tensile strength of 2.45 GPa, Young's modulus of 180 GPa and density of 2.55 g/cm<sup>3</sup>. At first, SiC fibers were cut and laminated into die with SPZ powder alternatively. 1 layer contains 50000 fibers and 38 g SPZ powder.

FRM plates were fabricated at the conditions tabulated in Table 1. Fabricated FRM have the average thickness of about 2 mm and the fiber volume fraction,  $V_f$ , of 5.8 %.

Table I Fabricating conditions of FRM.

Temperature / °C	250	300	350	410
Pressure / MPa	120	120	120	70
Duration / min.	10	10	10	5

#### Testing Procedure

Tensile tests of fabricated FRM were carried out at 250 °C under the constant crosshead speed of 3 mm/min. Fractured surfaces were observed using scanning electron microscope in order to examine the bonding of fiber/matrix interfaces. For the discussion of formability of FRM, V-bending tests were also carried out at 250 °C, under the constant punch speed of 1 mm/min and with punch radius of 3 mm.

### Results and Discussion

#### Examination of Fabricating Condition

Figure 1 shows the effect of compacting temperature on (a) high temperature tensile strength and (b) the ratio of the strength obtained by tensile test at 250 °C,  $\sigma_c$ , to the value simply calculated from the rule

of mixture,  $\sigma_{ROM}$ . The FRM was fabricated under the conditions of Table 1 from the four types of initial powders. For the fabricating temperature below 350 °C, the FRM from the smallest size (A) powder only have sufficient strength.

Fractographies of the FRM from the largest (D) powder are shown in Fig. 2 (a) fabricating temperature = 410 °C, pressure = 70 MPa, duration = 5 min. and (b) 350 °C, 120 MPa, 5 min. From the fractographies, it can be observed that metal matrix well penetrate between fibers and the bondings at interfaces are developed in the case of (a) 410 °C in comparison with (b) 350 °C. Consequently, the fabricating condition was decided that temperature is 410 °C, pressure is 70 MPa and duration is 5 min.

The relationship between Young's modulus at room temperature and initial powder diameter is shown in Fig. 3. The figure shows that FRM

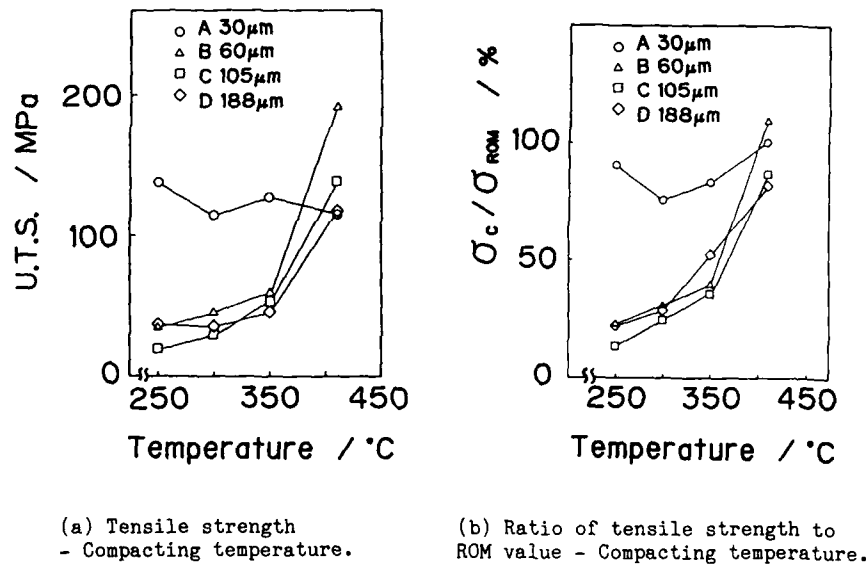


Fig. 1 Effect of compacting temperature on tensile strength at 250 °C.

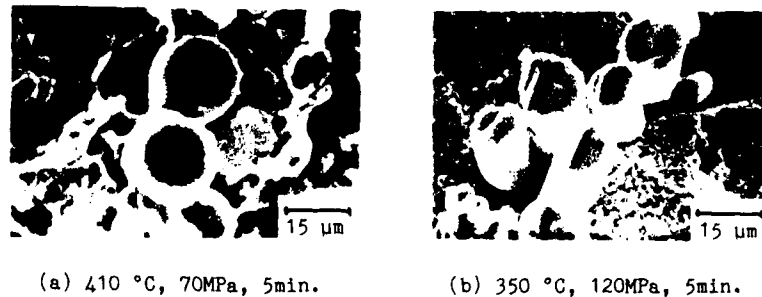


Fig. 2 Fractographies of FRM tested at 250 °C.

fabricated under the decided condition have the sufficient Young's modulus, which are beyond the ROM value and independent from initial powder size.

#### Heat Treatment of FRM

From the view point of after-forming processes, the ductility of FRM should be considered. In order to enhance the ductility, initial heat treatment ( $360^{\circ}\text{C} \times 1 \text{ h.}$ , WQ) was attempted. Figure 4 shows the load-displacement curve of the FRM with (solid line) and without (broken line) initial heat treatment. As can be seen from the figures, first heat treatment increase the ductility. But the heat treatment, to increase the ductility for the purpose of after-forming, in the same time decrease the high temperature strength (Fig. 5), that is one of the advantages of FRM, because of the poor shear strength of matrix metal.

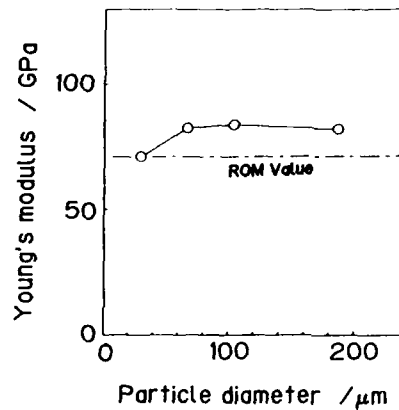


Fig. 3 Relationship between Young's modulus and initial powder diameter.

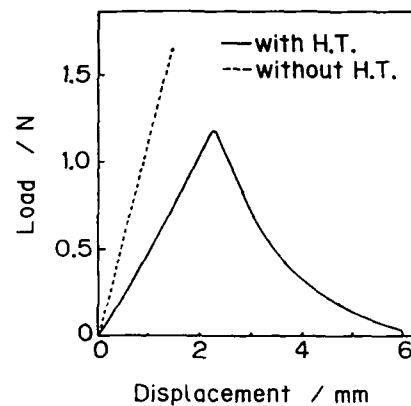


Fig. 4 Load - Displacement curve of FRM with and without heat treatment.

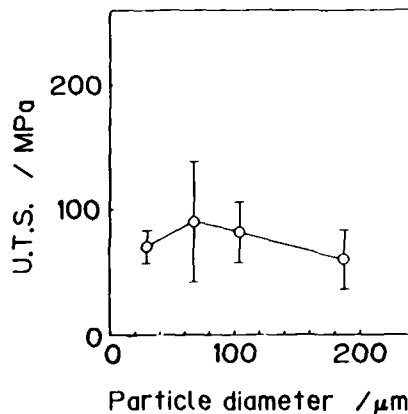


Fig. 5 Tensile strength of FRM with initial heat treatment.

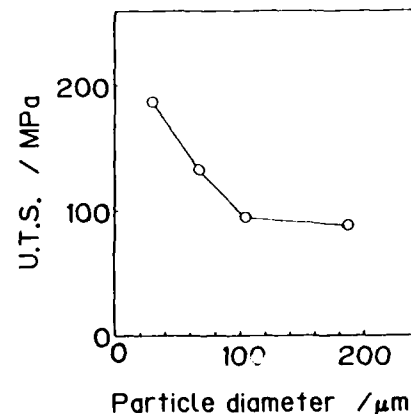


Fig. 6 Tensile strength of FRM with initial and secondary heat treatment.

Therefore, an additional attempt, that is the secondary heat treatment was carried out. Figure 6 shows the high temperature strength of FRM with second heat treatment (250 °C x 30 min., AC) following first heat treatment. From Fig. 1 (a) and Fig. 6, it can be concluded that strength, which has decreased by initial heat treatment, is recovered by secondary heat treatment.

#### Three Point Bending

In order to examine the after-formability of fabricated ductile FRM, three point bending tests were carried out. Figure 7 show the results of three point bending of FRM fabricated from four types of initial powder. When the ductility of matrix and the bonding of fiber/matrix interface are sufficient, successful bending is established until bending angle of 70° without failure.

#### Concluding Remarks

(1) SiC/SPZ composites with the high temperature strength of 200 MPa were fabricated by powder metallurgical technique as an application of superplasticity. Previously, the most suitable fabricating condition was decided, i.e. temperature is 410 °C, pressure is 70 MPa and duration is 5 min.

(2) Heat treatment techniques for controlling the mechanical properties of FRM were established. Initial heat treatment (360 °C x 1 h., WQ) increase the ductility, which enables after-forming processes, and secondary heat treatment (250 °C x 30 min., AC) recover the high temperature strength which has been decreased by initial heat treatment.

(3) The result of three point bending at 250 °C suggested the possibility of after-forming processes of FRM.

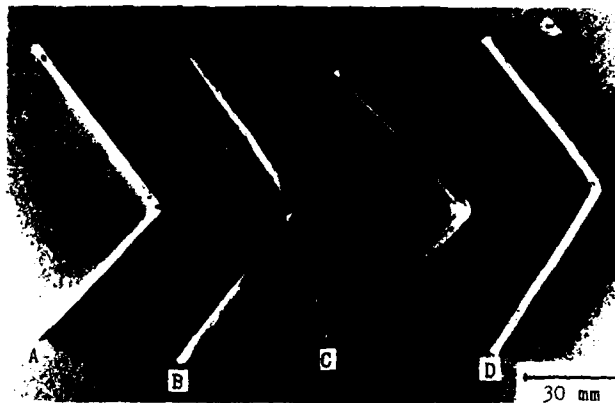


Fig. 7 Results of V-bending tests.  
A, B, C and D indicate the initial powder type of each FRM.



## SUPERPLASTICITY OF $ZrO_2$ TOUGHENED CERAMICS

Fumihiro Wakai

Ceramic Science Department  
Government Industrial Research Institute, Nagoya  
Nagoya, Japan

### Abstract

Zirconia-toughened ceramics (ZTC) can be regarded as model materials for studying superplasticity in ceramics. The superplasticity in quasi-single phase system (Yttria-stabilized tetragonal  $ZrO_2$  polycrystals, Y-TZP) and the superplasticity in two-phase system ( $ZrO_2/Al_2O_3$  composites) are reviewed in this paper.

#### 1) Superplasticity in Quasi-Single Phase System

The Y-TZP material was elongated more than 200 % at a constant flow stress when it had the grain size of less than 1  $\mu m$ . The flow behavior (stress exponent of 2) and the microstructural observation indicated the dominant role of grain boundary sliding during superplastic flow. The ductility was greatly reduced with coarsening the grain size by heat treatments. The Nabarro-Herring creep was observed in the deformation of coarse grained  $ZrO_2$ . The transition in deformation mechanism was interpreted by assuming that interface-reaction controlled process and lattice diffusion controlled one are sequential processes for accommodation.

#### 2) Superplasticity in Two-Phase System

Grain growth is retarded by the presence of the second phase grains in various  $ZrO_2$ -toughened ceramics which are two-phase composites. As a result, the micrograin superplasticity is expected to occur if the initial grain size of the composites are small enough. In  $ZrO_2-Al_2O_3$  system two composites, one is a  $ZrO_2$ -based material containing  $Al_2O_3$  grains and another is a  $Al_2O_3$ -based material containing  $ZrO_2$  grains showed superplastic elongation. The flow behavior of the composites containing the second phase grains could be described by a rheological model as a non-Newtonian flow modified by the second phase grains.

Superplasticity and Superplastic Forming  
Edited by C.H. Hamilton and N.E. Paton  
The Minerals, Metals & Materials Society, 1988

### Introduction

Superplasticity refers to the ability of polycrystalline materials to exhibit extraordinary large elongations in tension tests (1). The phenomenon has been known in metallurgy for more than half a century. However it was the mid-1980's when the micrograin superplasticity of ceramics was demonstrated definitely without any doubt for the first time. (2,3,4).

Now it is found that there are at least two types of mechanism for superplasticity in ceramics; (a) superplastic flow enhanced by a liquid phase, where deformation is characterized by stress exponent of one. (b) superplasticity of polycrystalline materials, where the deformation is characterized by a non-Newtonian flow.

The  $\beta$ -spodumene glass ceramics (2) is an example of materials showing superplasticity of type (a). The material contains a fairly large amount of glassy phase at grain boundaries. It is believed that the diffusional creep enhanced by solution-precipitation process in the liquid phase is the mechanism for this type of superplasticity. The strain rate is proportional to the stress (Newtonian flow).

The materials which exhibit the superplasticity of type (b) do not contain a liquid phase, or contains a negligibly small amount of amorphous phase, if any. Most of the superplastic alloys and metals belong to this type. The strain rate of typical superplastic alloys is proportional to the square of stress (Non-Newtonian flow)(5).

The superplasticity of  $Y_2O_3$ -stabilized tetragonal  $ZrO_2$  polycrystals (Y-TZP) was found recently (4). It was revealed that Y-TZP behaved like a material which showed superplasticity of type (b). The fundamental atomic bonding, the crystal structure, and the structure of grain boundaries are different between ceramics and metals. Thus the investigation to clarify the difference and the similarities between the superplasticity of ceramics and that of metals will provide an opportunity to understand the superplasticity of polycrystalline materials from a general point of view. Furthermore, the discovery of superplasticity in Y-TZP bring about a prospect for superplastic forming of advanced ceramics.

One of the attractive features of Y-TZP is that this material has an ideal microstructure for studying superplasticity. Over the last decade, a large variety of zirconia-toughened ceramics have been developed (6). The results obtained on Y-TZP can be generalized by investigating these ceramics with different microstructures systematically.

### Superplasticity of Quasi-Single Phase System

TZP is the material containing a minimum amount of amorphous phase at grain boundaries. Though some TZPs contains both tetragonal phase and cubic phase, the mechanical and chemical properties of both phases can be regarded as approximately the same. Thus, Y-TZP can be conveniently called "Quasi-single phase materials".

The most important prerequisite for micrograin superplasticity is that the grain size should be fine. The Y-TZP material was deformed infinitely at a constant flow stress when it had the grain size of less than  $1 \mu m$ . The ductility was greatly reduced with coarsening the grain size by heat treatments, see Fig. 1 (7).

The microstructural observation after the deformation is as follows.

- a) The density of intragranular dislocation did not increase distinctly.
- b) The equiaxed grain shape was maintained. The contribution of intragranular strain to the total strain was much smaller than strain due to the grain boundary sliding.

It was concluded that the dominant mechanism of micrograin superplasticity was the grain boundary sliding. Ashby and Verral obtained an expression for the grain boundary sliding accommodated by diffusion (8).

Case 1: Interface reaction-controlled creep

$$\dot{\epsilon}_i = A_i \frac{\sigma^2}{d} \quad (1)$$

Case 2: Diffusion creep of lattice diffusion of cation

$$\dot{\epsilon}_d = A_d \frac{\sigma}{d^2} \quad (2)$$

When the case 1 and the case 2 are sequential processes, strain rate is expressed by the following equation.

$$\frac{1}{\dot{\epsilon}} = \frac{1}{\dot{\epsilon}_d} + \frac{1}{\dot{\epsilon}_i} \quad (3)$$

The broken line in Fig. 2 is the result of curve fitting using Eqs. (1), (2), (3). According to this model, superplasticity of Y-TZP is related to an interface-controlled diffusion creep (9, 10).

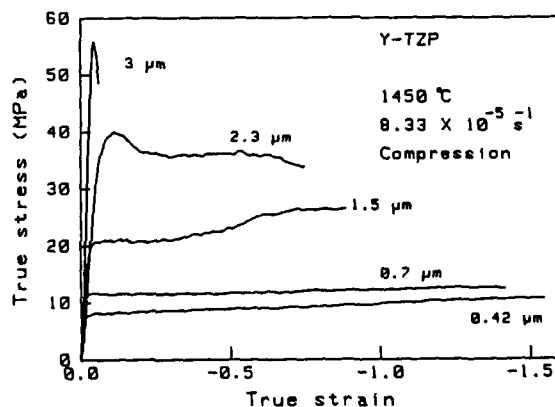


Fig. 1 Effect of grain size on stress-strain curve for 3 mol%  $Y_2O_3$ -TZP.

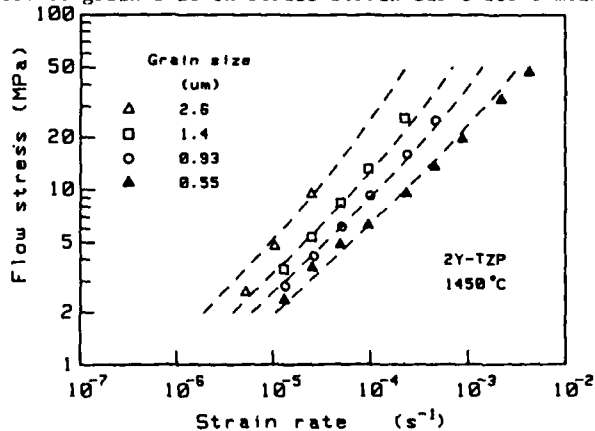


Fig. 2 Relationship between stress and strain rate for 2 mol%  $Y_2O_3$ -TZP.

### Superplasticity of Two-Phase System

The essential characteristic for micrograin superplasticity is the microstructural stability during deformation, namely the stability of grain size and shape, and the suppression of cavity nucleation and growth. Two phase structure is preferable for keeping the grain size small enough.

The superplasticity of the TZP-based composite in which the second phase  $\text{Al}_2\text{O}_3$  grains were dispersed uniformly among the matrix  $\text{ZrO}_2$  grains essentially corresponded to the superplasticity of quasi-single phase TZP (Fig. 3) (11). The superplasticity of composites in which the matrix phase and the second phase exchanged their roles was studied, that is, the superplasticity of  $\text{ZrO}_2$ -toughened  $\text{Al}_2\text{O}_3$  in which  $\text{ZrO}_2$  grains were dispersed among  $\text{Al}_2\text{O}_3$  matrix (12).

The deformation of the composites in which the second phase grains were uniformly distributed among the matrix grains was explained by a rheological model. The non-Newtonian flow of the matrix may be expressed by Norton's equation as,

$$\dot{\epsilon} = A \cdot \sigma^n \quad (4)$$

Chen's (13) rheological considerations predicted that the constitutive equation of the composite containing spherical inclusion of volume fraction ( $\rho$ ) should become,

$$\dot{\epsilon} = (1 - \rho)^q A \cdot \sigma^n \quad (5)$$

The exponent  $q$  is positive when the second phase is "harder" than the matrix, and negative when the second phase is "softer" than that.

The interface-controlled diffusion creep (Eq. 1) is the major deformation mechanism for fine grained  $\text{Al}_2\text{O}_3$  (14). From a rheological point of view, the line of  $\text{Al}_2\text{O}_3$ -based composite (3Y80A) and that of  $\text{ZrO}_2$ -based composite should be parallel to the lines of matrix phases in Fig. 4 (12). The flow behavior of composites was expressed by  $n = 2$  as expected.

### Superplastic Forming and Joining

Superplastic properties can be utilized to the forming of  $\text{ZrO}_2$ -toughened ceramics. Superplastic forming, bulge forming, and superplastic joining were successfully performed (15). Cavity formation occurred in superplastically elongated TZP/ $\text{Al}_2\text{O}_3$  composite. However the

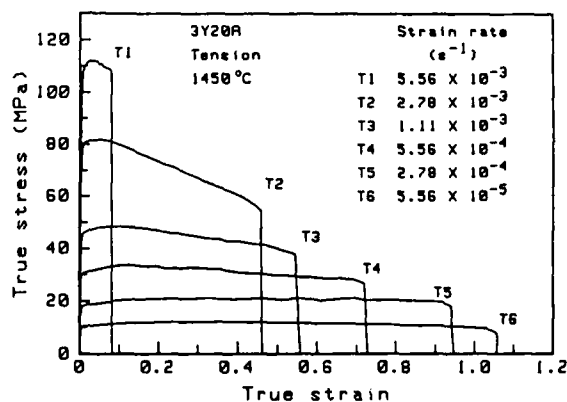


Fig. 3 Stress-strain curve for TZP/ $\text{Al}_2\text{O}_3$  (20 wt%) composite.

cavitation damage could be reduced by keeping the strain rate low enough that a specimen elongated 100 % at elevated temperature maintained a strength of 1800 MPa at room temperature (11).

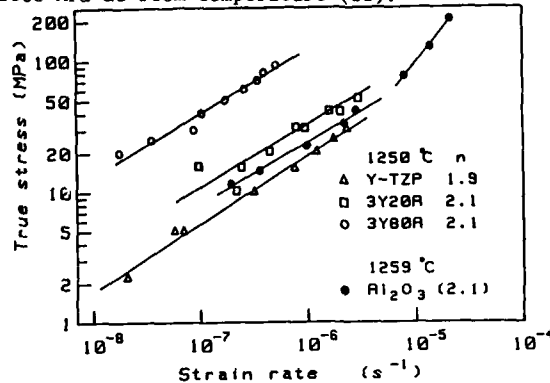


Fig. 4 Flow behavior of composites (containing 0, 20, 80, 100 wt%  $\text{Al}_2\text{O}_3$ ).

#### References

1. J. W. Edington, K. N. Melton, and C. P. Cutler, "Superplasticity," *Prog. Mater. Sci.*, 21 (1976) 61-170.
2. J.-G. Wang and R. Raj, "Mechanism of Superplastic Flow in a Fine-Grained Ceramic Containing Some Liquid Phase," *J. Am. Ceram. Soc.*, 67 (1984) 399-409.
3. B. Baudalet and M. Suery, ed., *Superplasticity* (Edition du CNRS, 1985), 16. C. Carry and A. Mocellin
4. F. Wakai, S. Sakaguchi and N. Murayama, "Superplasticity of Yttria-Stabilized Tetragonal  $\text{ZrO}_2$  Polycrystals," *Advanced Ceramic Materials*, 1 (1986) 259-263.
5. J. J. Burke, R. Mehrabian and V. Weiss, ed., *Advances in Metal Processing* (Plenum Press, 1981), 1, O. D. Sherby et al.
6. N. Claussen, M. Rühle and A. H. Heuer, ed., *Advances in Ceramics, Vol. 12, Science and Technology of Zirconia II* (The American Ceramic Society, 1984), 325, N. Claussen.
7. F. Wakai, S. Sakaguchi, and H. Kato, "Compressive Deformation Properties and Microstructures in the Superplastic Y-TZP," *J. Ceram. Soc. Japan (Yogyo-Kyokai-Shi)*, 94(8)(1986), 721-725.
8. M. F. Ashby, and Verral, "Diffusion-Accommodated Flow and Superplasticity," *Acta Metall.*, 21 (1973) 149-163.
9. F. Wakai, and T. Nagano, "Role of Interface-Reaction Controlled Creep on Superplasticity of  $\text{Y}_2\text{O}_3$ -Stabilized Tetragonal  $\text{ZrO}_2$  Polycrystals," *J. Mater. Sci. Letter.*, in press.
10. F. Wakai, "Non-Newtonian Flow and Micrograin Superplasticity of Ceramics" (Paper presented at the MRS International Meeting on Advanced Materials, Tokyo, 1 June 1988).
11. F. Wakai, and H. Kato, "Superplasticity of TZP/ $\text{Al}_2\text{O}_3$  Composite," *Advanced Ceramic Materials*, 3(1)(1988) 71-76.
12. J. D. Mackenzie and D. R. Ulrich, ed., *Ultrastructure Processing of Advanced Ceramics* (John Wiley & Sons, 1988), 50, F. Wakai and H. Kato.
13. B. Baudalet and M. Suery, ed., *Superplasticity* (Edition du CNRS, 1985), 5. I-Wei Chen.
14. R. M. Cannon, W. H. Rhodes, and A. H. Heuer, "Plastic Deformation of Fine Grained Alumina: I, Interface Controlled Diffusional Creep", *J. Am. Ceram. Soc.*, 63(1-2)(1980) 46-53.
15. W. Bunk, and H. Hausner ed., *Ceramic Materials and Components for Engines* (Deutsche Keramische Gesellschaft, 1986), 315 F. Wakai et al.

### Extrusion of tet-ZrO<sub>2</sub> at Elevated Temperatures

B. Kellett, P. Carry, and A. Mocellin

Laboratoire de Céramique  
Ecole Polytechnique de Lausanne  
CH-1007, Switzerland

#### **Abstract**

The workability of Y<sub>2</sub>O<sub>3</sub> doped tetragonal-ZrO<sub>2</sub> polycrystals (Y-TZP), recently discovered to be highly deformable in tension and compression, is here gauged by extruding powder compacts. Stresses needed to achieve extrusion are sufficient for complete densification under most circumstances, and pieces extruded can be strong and have smooth surfaces. The ability to extrude from a diameter of 30 to 10 mm (equivalent to a true strain of 2.20) while retaining submicron grain size suggests the viability of more practical forming operations.

A slab analysis has been employed to describe extrusion of power law material. We find:

$\frac{v}{d_p} = k \sigma_p^n K_{\text{geom.}}$ , where  $K_{\text{geom.}}$  describes the effect of die geometry and depends on the friction behaviour, and stress exponent  $n$ . The stress exponent found in extrusion is consistent with that found in uni-axial compression and tension.

## 1. Introduction

In the late-60's and early 70's a few isolated attempts at forming ceramic materials at elevated temperatures were undertaken. [1] Although it was recognized that fine grain size was desirable, technology then available was only able to produce materials with grain sizes above a micron (in particular MgO doped  $Al_2O_3$ ). To achieve sufficient ductility temperatures in excess of 1700°C were found necessary. Uncontrolled grain growth, and subsequent loss of plasticity was recognized as a serious deficiency and consequently, work on deformation forming was abandoned. [2]

Renewed interest in high temperature forming is in large part due to recent advances in powder technology which have resulted in a number of fine grain materials, in particular Y-TZP. [3,4,5] Deformed Y-TZP specimens show submicron grain size and limited grain shape anisotropy, insufficient to account for the recorded deformation, suggestive of a superplastic grain boundary sliding mechanism. Fine, siliceous grain boundary films do exist on a minority of grain boundaries and three grain junctions (not an uncommon observation in ceramic materials) which most probably contribute to superplastic behavior by promoting solution-reprecipitation reactions and grain boundary sliding. [6]

## 2 Experimental Procedures

To gauge Y-TZP workability a series of extrusion tests were conducted at 1500°C in vacuum with unsupported graphite dies. Dies were machined as shown in figure 1 with a cone angle  $\phi=26.6^\circ$ , a piston diameter ( $d_p$ ) of 30mm, and a final diameter ( $d_f$ ) of either 10mm or 20mm. Extrusion diameter ratio's ( $D=d_p/d_f$ ) of 3 and 1.5 are equivalent to true strains of 2.20 and 0.41. Experiments were performed with tetragonal (3 mole% -  $Y_2O_3$ )  $ZrO_2$  powder. The manufacturer (Toyo Soda LTD) provided the following information: crystal size of 26 nm, concentrations in weight percent:  $Y_2O_3$ -5.19,  $Al_2O_3$ -0.005,  $SiO_2$ -0.006,  $Fe_2O_3$ -0.010,  $Na_2O$ -0.008, and ignition losses of 0.6 wt. %.

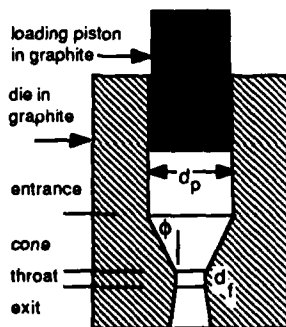


fig. 1 Die geometry, not to scale, divided into four distinct regions: entrance, cone, throat, and exit.

As-received powder was directly poured into the 'corked' die and cold pressed at 10 MPa to approximate 25% of theoretical density (6.1g/cc). Graphite paper was both used as a lubricant and to separate powder from die wall. Temperature was measured from outside the die using a type R thermocouple. Specimens were heated at 20°C/min to 1000°C and thereafter 10°C/min to the extrusion temperature (1500°C). Loading ram displacements were measured from outside the furnace with an LVDT. Dilatation of the graphite was subtracted.

## 3. Results

### 3a. General extrusion behaviour

Shown in figure 2 are piston velocities, under various piston loads, resulting from the densification and extrusion of a 100 gram powder compact. With initial heating and small piston loads high piston velocities are achieved, presumably from the densification of the powder compact. Interrupting the experiment at 100 minutes revealed that this was indeed the case, since the specimen had not extruded and was at full theoretical

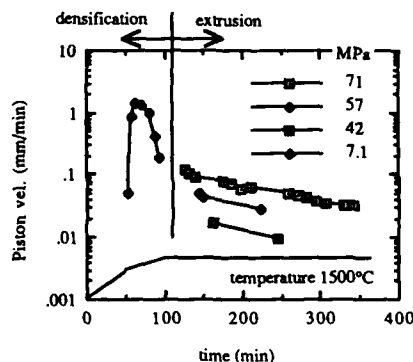


Fig 2. Piston velocities for the densification and extrusion of Y-TZP through a conical die ( $d_p/d_f=3$ ,  $26.6^\circ$ , 100grams powder).

density. The slug, which densified into the shape of the die, was then refitted into the die to continue the experiment. In the extrusion regime piston velocities are noticeably slower, even at larger stresses, than those previously achieved during densification. Also, piston velocities diminish somewhat with time.

Factors affecting piston velocity include; temperature, die configuration (shape, die angle, diameter change, etc.) piston load and friction. In this paper we will discuss the effects of applied load and lubrication on piston velocity and surface finish.

### 3b. Effects of Lubrication

Lubrication was achieved by covering the various die surfaces with graphite paper. Specifically, two schemes were tried, involving either one or two

sheets of graphite. The two experiments shown in figure 3 illustrate that piston velocities increase 50% when a single sheet of graphite paper covers the converging nozzle of the die.

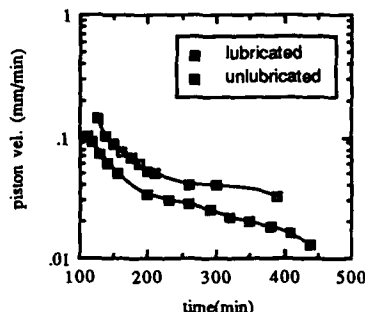


fig. 3 Piston velocities in the extrusion regime illustrating the benefit of lubricating the conical surface of the die with a single sheet of graphite paper ( $d_p/d_f=3$ ).

Even more dramatic though is the change in surface finish with lubrication, while the surface of the unlubricated specimen is torn, with tears about 0.5 mm deep, the lubricated specimen is smooth (figure 4).

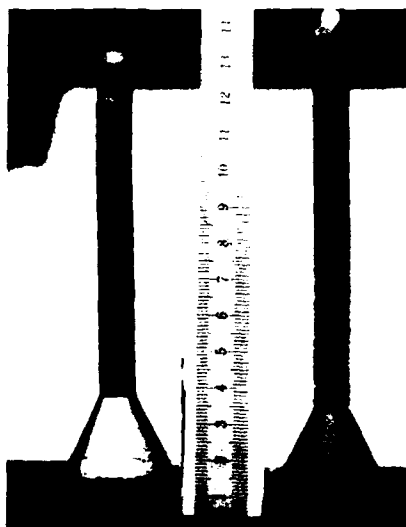


Fig. 4 Lubricated (left) and unlubricated (right) illustrating the drastic improvement in surface finish when graphite paper is used as a lubricant.

Since these extrusions began from a 'filled' die, the deformation needed to exit the die is non-uniform. This may explain the decreased tearing one can observe near the tip of the unlubricated specimen. Also, the tip of the unlubricated specimen is cracked.

This occurred some months after the experiment, and may suggest a combination of residual stresses and environmental attack. Graphite also reduces  $ZrO_2$  causing blackening. Microstructural aspects of Y-TZP will be presented elsewhere.[7]

Friction can be further reduced by utilizing two sheets of graphite paper, so as to allow one sheet to slide over the other, in effect allowing co-extrusion of the ceramic within a sheath of graphite paper. Figure 5 demonstrates that for dies with an extrusion ratio ( $D$ ) of 1.5 piston velocities can be increased by over an order of magnitude. In these cases the inner graphite sheet strongly adheres, and reacts with the zirconia producing a high gloss 'metallic like' surface. We note here that lubrication is difficult to control. For example, for dies of  $D=1.5$  even the single sheet of graphite paper tended to brake, and co-extrude with the ceramic.

Friction in the die entrance region (see figure 1) also has an effect on piston velocity. Experiments using a larger batch of powder have a larger 'head' and tend to have somewhat lower velocities. Extrusion causes this 'head' to diminish, suggesting that at constant stress velocities should increase. Both these trends are observed in figure 5.

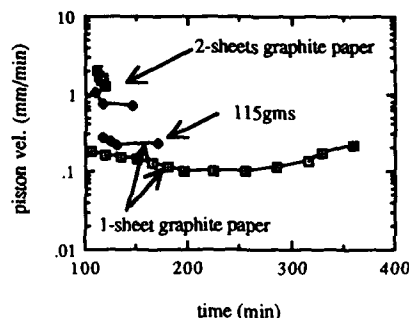


fig. 5 Comparison of piston velocities when two sheets of graphite paper are used, allowing one to slide over the other. ( $D=1.5$ ,  $1500^\circ C$ ,  $35.4 MPa$ . Mass of the powder batch is 200gms except where indicated.)

### 3c. Piston load-velocity relation

Rapid stress changes were used to both gauge piston load-velocity relationships and determine the effect of extrusion velocity on surface finish. Figure 6 shows that piston velocity correlates well to the stress cubed, for a diameter ratio ( $D$ ) of 3 and graphite paper lubrication. Data is taken from figure 2. No discernable differences in surface finish were found with extrusion velocity.



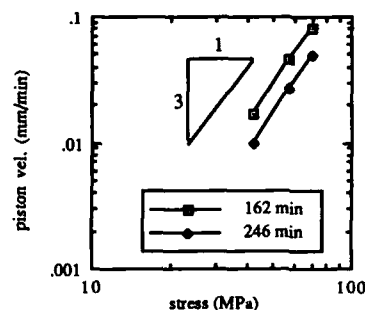


fig. 6 Piston velocity stress curves illustrating that the stress exponent is 3 for  $D=3$ . Graphite paper was folded over the conical surface of the die. Time at  $1500^{\circ}\text{C}$  is found by subtracting 100 min from that shown.

#### 4. Analysis

To correlate piston velocity ( $v_p$ ) to the applied stress a typical slab analysis will be employed. [8]

From force balances in the axial and radial directions:

$$\Sigma F_z = 0 = d(\sigma_z \pi \frac{d^2}{4}) + (\tau \cos \phi + P \sin \phi) dA \quad (1)$$

$$\Sigma F_r = 0 = -\sigma_r dz + (\tau \sin \phi - P \cos \phi) dl \quad (2)$$

where  $dA = 2\pi \frac{dr}{\sin \phi}$ ,  $dl = \frac{dz}{\cos \phi}$ , and  $d$  is the diameter of the slab pictured in figure 7, one can derive an equation which describes the change in axial stress ( $\sigma_z$ ) with  $z$ :

$$\frac{d\sigma_z}{dz} = -\frac{4 \tan \phi}{d} [\tau (\tan \phi + \cot \phi) + \sigma_z - \sigma_r] \quad (3)$$

Equation 3 illustrates that during extrusion the radial stress is more compressive than the axial (compressive stresses are negative). Relationships for the frictional ( $\tau$ ), axial ( $\sigma_z$ ) and radial stresses ( $\sigma_r$ ) are now postulated: frictional behavior is assumed to be simple, i.e. either frictionless or newtonian ( $\tau = \mu P$ , where  $P$  is the stress normal to the die wall), and the difference  $\sigma_z - \sigma_r$  is equated to an equivalent strain rate ( $\dot{\epsilon}_e$ ) by a power law equation:

$$\dot{\epsilon}_e = k \sigma_e^n \quad (4a)$$

where

$$\dot{\epsilon}_e^2 = \frac{2}{3} \frac{(\dot{\epsilon}_z - \dot{\epsilon}_r)^2 + (\dot{\epsilon}_r - \dot{\epsilon}_\theta)^2 + (\dot{\epsilon}_\theta - \dot{\epsilon}_z)^2}{3} \quad (4b)$$

and

$$\sigma_e^2 = \frac{(\sigma_z - \sigma_r)^2 + (\sigma_r - \sigma_\theta)^2 + (\sigma_\theta - \sigma_z)^2}{2} \quad (4c)$$

The equivalent strain rate and stress, while proportional to the deviatoric components of their respective tensors, are defined so that they reduce to

their uniaxial values under uniaxial conditions. In our definition of the effective stress and strain rate we have neglected the shear terms which in effect assumes that the radial and axial directions are principle directions. It can be shown that these terms are negligible for the die angles considered here. [9]

With a power law relationship we depart from a typical 'metallurgical' analysis, which would have equated  $\sigma_z - \sigma_r$  to a rate insensitive yield point. At elevated temperatures ( $T > T_{\text{fusion}}/2$ ) materials deforming by diffusional mechanisms are rate sensitive.

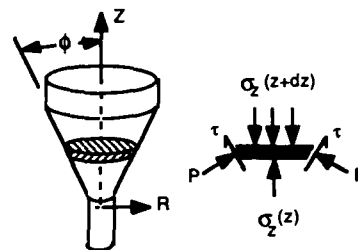


fig. 7 Slab extrusion model, illustrating stresses considered: axial stress ( $\sigma_z$ ), wall pressure ( $P$ ), and friction ( $\tau$ ).

The applied piston load is nearly always sufficient to achieve full density prior to extrusion in Y-TZP and cavitation does not appear to be a problem, given the large compressive stresses involved. [7] We therefore set  $\dot{\epsilon}_z + \dot{\epsilon}_r + \dot{\epsilon}_\theta = 0$ , and given the axial symmetry of this problem set  $\sigma_\theta = \sigma_r$  and  $\dot{\epsilon}_\theta = \dot{\epsilon}_r$ .

The equivalent strain rate is calculated from the geometry of the die and the velocity of the piston. Each slab, pictured in figure 7, will contract in the radial direction and elongate in the axial direction during its journey through the die. The equivalent strain rate of a given slab is a function of its diameter ( $d$ ), die angle ( $\phi$ ), piston diameter ( $d_p$ ), and velocity ( $v_p$ ):

$$\dot{\epsilon}_e = 4 \frac{v_p}{d_p} \tan \phi \left( \frac{d_p}{d} \right)^3 \quad (5)$$

Equating the equivalent strain rate to the equivalent stress:  $\sigma_e = \sigma_r - \sigma_z$ , we substitute into equation 3:

$$\frac{d\sigma_z}{dz} = \frac{4 \tan \phi}{d} \left( \tau (\tan \phi + \cot \phi) + \left( \frac{\dot{\epsilon}_e}{k} \right)^{1/n} \right) \quad (6)$$

For frictionless conical dies equation 6 is integrated with boundary conditions  $\sigma_z = 0$  at the die throat and  $\sigma_z = \sigma_p$  (stress applied by the piston) at the die entrance. We find:

$$\frac{v_p}{d_p} = k \sigma_p^n K_{ideal} \quad (7)$$

where

$$K_{ideal} = \frac{1}{4 \tan \phi} \left( \frac{3}{2n(D^{3/n} - 1)} \right)^n \quad (8)$$

and  $D$  is the diameter ratio  $d_p/d_f$ . The  $v_p/d_p$  calculated here is a convenient strain rate term for extrusion.

For dies displaying newtonian friction equation 4 is integrated numerically. As will be shown in the next section, solutions have functional behaviour similar to equation 5 allowing us to write:

$$\frac{v_p}{d_p} = k \sigma_p^n \exp\left(\frac{-2\mu y}{d_p}\right) K_{geom.} \quad (9)$$

with the geometrical factor  $K_{geom.}$  found through numerical integration. The exponential term in equation 7 derives from friction in the die entrance region ( $y$  is the distance between piston and cone in figure 1).

## 5. Discussion

Piston velocity was shown in equation 9 to be proportional to both the microstructure factor  $k$  and the applied stress to exponent  $n$  as could be found from a tensile or compression test. The stress exponent determined in extrusion is approximately 3 (see figure 6) which correlates well with the values found for fine grain materials.[10]

The microstructural parameter  $k$  has grain size dependency, usually expressed by exponent  $m$  ( $k = k^*/d^m$ ). The decrease in extrusion velocity, shown in figure 2 and 3, are reasonably explained in the context of grain growth: increases of 50%, from 0.4 to 0.6  $\mu m$ , were observed at 1500°C with dies of diameter ratio 3. However, other factors, for example strain hardening, can not be ruled out. We defer microscopic aspects to a forthcoming paper. [7]

Friction, in the entrance and cone regions, has a large effect on piston velocity as shown in figure 3 and 5. To determine  $K_{geom.}$  for newtonian conditions ( $\tau = \mu p$ ) we make the following substitutions in equation 4:

$$\tau = \mu p = -\sigma_r \frac{\mu}{1 - \mu \tan \phi} \quad (10)$$

$$\sigma_r = \sigma_z \cdot \left( \frac{\dot{\epsilon}_z}{k} \right)^{1/n} \quad (11)$$

and

$$\sigma_z = -\beta \left( \frac{1}{k} \frac{v_p}{d_p} \right)^{1/n} \quad (12)$$

Equation 4 can now be expressed in terms of  $\beta$  where

$$K_{geom.} = \frac{1}{\beta^n} \quad (13)$$

Assuming no friction in the die entrance region (i.e.  $y=0$  in equation 9) we numerically integrate up from the die exit where  $\beta=0$  (since  $\sigma_z=0$ , see equation 12) and find that  $K_{geom.}$  is a strong function of the friction coefficient  $\mu$  (figure 8) for both an extrusion diameter ratio of 3 and 1.5.

In principle friction coefficients could be determined, without knowledge of the microstructure factor  $k$ , since differences in extrusion velocities are equivalent to differences in  $K_{geom.}$  when  $k$ 's are equal. The friction coefficients could then be found by lining up these  $\Delta K_{geom.}$  so that the friction coefficients are equal for the same lubricant. However, as mentioned previously, it is difficult to ensure equivalent lubrication. Never the less velocity differences in figure 3 and 5 suggest reasonable differences in the friction coefficients.

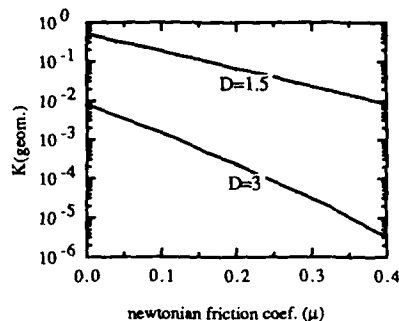


fig. 8. Numerically calculated  $K_{geom.}$  for conical dies  $D=1.5, 3$  and  $n=3$ .

However figure 8 also indicates that for the same lubricants greater piston velocity differences should be found for dies of larger diameter ratios ( $D$ ), in contradiction with the results shown in figures 3 and 5. Newtonian friction may not be a good approximation for high temperature forming operations. In a following paper we consider a more reasonable interfacial mechanism, where it is reasoned that drag results from the uneven flow of material over a rough die surface.[9]

## 6. Conclusions

With the development of extremely fine-grain microstructures ceramic materials have begun to achieve ductilities sufficient to justify high temperature forming operations, like close die forming. Extrusion experiments are convenient in gauging workability and the effectiveness of lubricants on macro and microstructure. Experiments indicate that large deformation strains can be achieved. Conveniently, powders can be extruded to full density, reducing the work involved in preparing billets and enabling the achievement of finer-grain microstructures.

## Acknowledgements

This work was funded by the Swiss Federal Office of Education and Science (OFES).

## 7. References

1. Rice, R.W., "Hot-working of oxides," in High Temperature Oxides, Part III, A.M. Alper (Ed.), Academic Press, 235-280 (1970).
2. A.H. Heuer, D.J. Sellers, and W.H. Rhodes, "Hot-Working of Aluminum Oxide: I, Primary Recrystallization and Texture," *J. Am. Ceram. Soc.*, **52** [9] 468-74 (1969).
3. Carry, C. and Mocellin, A., "Examples of Superplastic Forming Fine-Grained  $\text{Al}_2\text{O}_3$  and  $\text{ZrO}_2$  Ceramics," in High Tech Ceramics, P. Vincenzini. (Ed.), Elsevier Science Publishers, 1043-1052 (1987).
4. Kellett, B.J. and Lange, F.F., "Hot Forging Characteristics of Fine-Grained  $\text{ZrO}_2$  and  $\text{Al}_2\text{O}_3/\text{ZrO}_2$  Ceramics," *J. Am. Ceram. Soc.* **69** [8] C-172 (1986).
5. Wakai, F., Sakaguchi, S. and Kato, H., "Compressive Deformation Properties and Microstructures in the Superplastic Y-TZP," *J. Ceram. Soc. of Jap.* **94**, 721 (1986).
6. Rühle, M. and Claussen, N., "Microstructural Studies of  $\text{Y}_2\text{O}_3$ -Containing Tetragonal  $\text{ZrO}_2$  Polycrystals (Y-TZP)," in Science and Technology of Zirconia II, (Vol. 12 Advances in Ceramics), N. Claussen, M. Rühle, and A. Heuer (Eds.), published by the Am. Ceram. Soc., 352-370 (1984).
7. B. Kellett, and P. Carry, "High Temperature Extrusion Behaviour of T-ZYP," to be published.
8. Thomsen, E. G., Yang, C. T. and Kobayashi, S., Mechanics of Plastic Deformation in Metal Processing, The Macmillan Company, New York, chapter 15 (1965).
9. B. Kellett, and A. Mocellin, "Upper Bound Analysis of Power Law Extrusion," to be published.
10. C. Carry, "High Ductilities, Superplastic Behaviors and Associated Mechanisms in Fine Grained Ceramics," to be published in the Proceedings of the Symposium on Superplasticity of the International Meeting on Advanced Materials (Material Research Society, 5/30-6/3 1988, Tokyo Japan).

## SUPERPLASTIC DEFORMATION OF Y-TZP ZIRCONIA

T. Hermansson, K.P.D. Lagerlöf \* and G.L. Dunlop  
Department of Physics, Chalmers University of Technology  
S-41296 Göteborg, SWEDEN

\* Now at Case Western Reserve University, Cleveland, Ohio 44106 USA

### ABSTRACT

Y-TZP  $\text{ZrO}_2$  was superplastically deformed in bending and tension in the temperature range 1180 - 1450°C and in the strain-rate range  $10^{-6}$  -  $10^{-3} \text{ s}^{-1}$ . The  $\log \dot{\epsilon} / \log \sigma$  relationship was highly linear with  $n \sim 2$ . A maximum tensile elongation of 246% was obtained. The activation energy for deformation was 580 kJ/mol. Microstructural examination showed that some strain enhanced grain growth occurred during deformation together with limited intergranular cavitation. Some grain strain took place during deformation but no significant increase in dislocation content was noted. Measurements of grain strain and loss of density due to pore growth and cavitation indicated that ~0.83 of the total strain was due to grain boundary sliding during superplastic tensile deformation at 1450°C and an initial strain-rate of  $4.8 \cdot 10^{-5} \text{ s}^{-1}$ .

Superplasticity and Superplastic Forming  
Edited by C.H. Hamilton and N.E. Paton  
The Minerals, Metals & Materials Society, 1988

## INTRODUCTION

This paper is concerned with a microstructural study of the superplastic deformation of yttria partially stabilized tetragonal  $\text{ZrO}_2$  (Y-TZP). Work in recent years has shown that superplastic flow is possible in a number of fine-grained ceramic materials (1-4) and, in particular, Wakai et al. (4) have demonstrated that tensile ductilities well in excess of 100% can be achieved with Y-TZP.

It is at present unclear just how closely the phenomenon of superplasticity in ceramics is related to superplasticity in metals but it is apparent there are significant similarities between the two. As is the case for metals, ceramics need to have very fine grain sizes and have to be deformed at high temperatures ( $T > 0.5T_m$ ) within a certain range of strain-rates in order to exhibit maximum superplasticity. The tensile ductilities, which have been obtained so far for superplastic ceramics (160%), are however considerably less than those which can be obtained for some metals (4-5000%) and the typical three region sigmoidal stress/strain-rate flow behaviour for metals does not seem to be repeated by the superplastic ceramics. Just as in the case of metals, these general observations point to the likely importance of grain boundary sliding as a major strain-providing flow mechanism in the superplastic deformation of ceramic materials but it is clear that there are likely to be some differences in the details of the micromechanisms of flow in the two types of material.

## EXPERIMENTAL

Specimens were first formed by cold isostatic pressing Y-TZP powder \*. They were subsequently sintered in air to 96-98% theoretical density by heating in the sequence: 1100°C 1h; 1250°C 1h; 1400°C 1h. The sintered material had an average grain size of 0.3 $\mu\text{m}$ . Specimens for bend tests were in the form of rectangular cross-section bars 45-6.4mm and the shape of tensile specimens is shown in Fig.1. The latter had a gauge length of 15mm and cross section of 4.4mm.

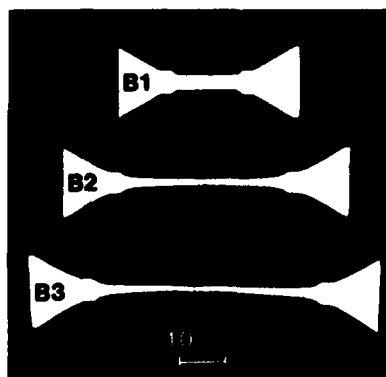


Fig. 1. Superplastic tensile deformation of Y-TZP  $\text{ZrO}_2$ . B1: As-sintered specimen prior to testing. B2: Strained 164% at  $\dot{\epsilon}=4.8 \cdot 10^{-5} \text{s}^{-1}$  and 1450°C. B3: Strained to fracture (246%) under the same conditions.

Both four-point and three-point bend tests were carried out in the temperature range 1180-1400°C with a range of different constant load point deflection rates. Higher total strains were achieved in the three-point tests. Tensile tests to even greater strains were carried out at 1450°C at constant cross head speeds which gave initial strain rates in the range  $10^{-5}$ - $10^{-4} \text{s}^{-1}$ .

\* TZ-3Y powder from Toyo Soda Inc.

## FLOW BEHAVIOUR

It is convenient to discuss the superplastic flow behaviour in terms of the creep equation:

$$\dot{\epsilon} = A\sigma^n \exp(Q/RT) \quad (1)$$

where  $\dot{\epsilon}$  is the strain rate,  $A$  is a material constant partly dependent upon grain size,  $\sigma$  is the flow stress,  $n$  the stress exponent,  $Q$  is the creep activation energy,  $R$  is the gas constant and  $T$  is the absolute temperature.

Stresses and strain-rates which were developed during four-point bending were calculated using the theory of Hollenberg et al. (5) for four-point bending creep tests. Stresses and strain-rates, which were developed at the lower face of the test bars (i.e. the plane of maximum tensile strain and stress), are plotted in Fig.2 together with similar data obtained from the tensile tests carried out at 1450°C. It can be noted from Fig.2 that the stress/strain-rate relationships for all temperatures were highly linear with a stress exponent  $n$  in the range 1.9-2.3. Although bending tests and tensile tests were not conducted at the same temperatures the data shown in Fig.2 indicate that the results obtained from these two types of tests were approximately consistent with each other.

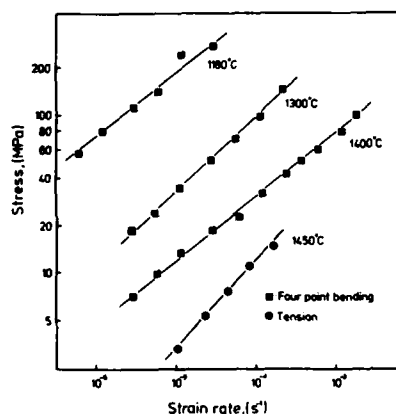


Fig. 2. Stress/strain-rate relationships for both four-point bending and tensile tests.

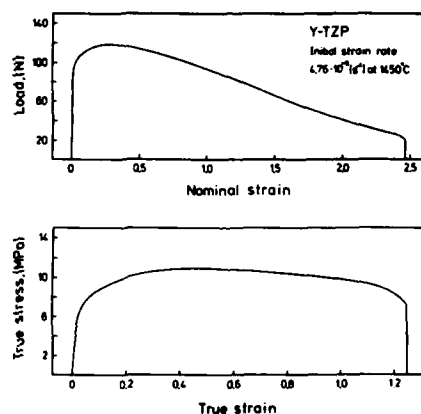


Fig. 3. Tensile curves for  $\dot{\epsilon} = 4.8 \cdot 10^{-5} \text{ s}^{-1}$  at 1450°C. Top: load vs. elongation. Bottom: true stress vs. true strain.

The maximum strain achieved in the tensile tests was 246% at an initial strain-rate of  $4.8 \cdot 10^{-5} \text{ s}^{-1}$  and 1450°C. The load/elongation curve for this test is shown in Fig.3 together with the corresponding derived true stress/true strain relationship. From this latter curve it can be seen that some deformation hardening (possibly due to grain growth) occurred for the first 100% of nominal strain. The creep activation energy,  $Q$ , was determined by varying the temperature during four-point bending. A value of  $Q = 580 \text{ kJ/mol}$  was obtained which is in good agreement with the earlier work of Wakai (4).

## MICROSTRUCTURAL OBSERVATIONS

X-ray diffractometry showed that the as-sintered material was mainly tetragonal  $\text{ZrO}_2$  but it also contained ~10% cubic  $\text{ZrO}_2$ . The amount of cubic phase increased slightly from ~10% to ~17% during deformation to a nominal strain of 164% at 1450°C. The larger amount of cubic phase agrees well with the equilibrium content predicted by Scott's  $\text{ZrO}_2\text{-Y}_2\text{O}_3$  phase diagram (6).

Grain sizes were measured prior to and after tensile testing. The mean diameter was estimated as  $d=A^{0.5}$  where A is the average cross-sectional area of the grains on a polished section. The as-sintered material had a grain size of 0.3  $\mu\text{m}$  and this increased to 0.37  $\mu\text{m}$  in the grip section of a test specimen after 10h at 1450°C. In the gauge length of the specimen, which had been strained 164%, the grain size had further increased to 0.48  $\mu\text{m}$ . This effect of strain induced grain growth appears to be a general feature of the superplastic deformation of metals and has also been previously observed for some oxide ceramics (2).

Measurements of the mean linear intercept grain sizes after 164% tensile strain, made on micrographs such as Fig. 4, showed that  $d_{\parallel}=1.37d_{\perp}$  where  $d_{\parallel}$  is the intercept grain size parallel to the tensile axis and  $d_{\perp}$  is perpendicular to the tensile axis. Use of the expression for grain strain,  $\epsilon_g$  (7):

$$\epsilon_g = 2/3 \ln(d_{\parallel}/d_{\perp}) \quad (2)$$

gave the contribution to the total strain from grain elongation as  $\epsilon_g \sim 20\%$ .

Density measurements on the tensile specimen deformed to 164% strain showed that this specimen had suffered a density loss of ~8%. Microstructural examination showed that this was due mainly to the growth of existing pores in the material and also, to a lesser degree, to the formation of intergranular cavities. More intergranular cavitation occurred for ~30% strain in three-point bending at the faster strain-rate of  $\sim 2 \cdot 10^{-4} \text{ s}^{-1}$  and lower temperature of 1400°C (see Fig. 5). Compared with the as-sintered material, superplastic deformation did not seem to cause any significant increase in dislocation content.

SEM examination of the surfaces of strained bars indicated that considerable grain boundary sliding (GBS) had occurred during superplastic deformation (Fig. 6). Measurements of grain elongation ( $\epsilon_g \sim 20\%$ ) and porosity increase (~8%), which were made on the specimen that had been deformed 164% suggests that the strain due to GBS was  $\epsilon_{\text{GBS}} \sim 136\%$ , i.e. ~0.83 of the total strain was due to GBS.

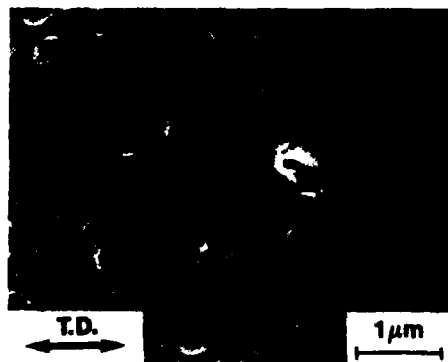


Fig. 4. Polished section of tensile specimen after 164% strain (thermally etched, SEM). Note the slight grain elongation in the tensile direction (arrowed).



Fig. 5. Intergranular cavitation (arrowed) at triple grain junctions in the three-point bend specimen deformed 30% at 1400°C (TEM).



Fig. 6. Surface of three-point bend specimen strained 20% at  $10^{-3} \text{ s}^{-1}$  and  $1250^\circ\text{C}$  showing grain offsets due to GBS (arrowed). The tensile direction is also indicated (SEM).

### CONCLUDING REMARKS

It is clear from Fig.2 that Y-TZP  $\text{ZrO}_2$  exhibits a highly linear  $\log \dot{\epsilon}/\log \sigma$  relation over at least three decades of strain-rate rather than the sigmoidal behaviour common to superplastic metals. Thus, using previous terminology (8), region II is very extensive for Y-TZP and no indication of its limits were found. The absence of region III, for the strain rates investigated here, is no doubt due to the difficulty of dislocation creep in ceramic materials. The measured value of  $n \sim 2$  is consistent with values normally obtained for superplastic metals (8) and is also consistent with arguments that GBS is rate controlling during superplastic flow (9).

Financial support from STU's Technical Research Council is gratefully acknowledged.

### REFERENCES

1. K.R. Venkatachari, and R. Raj, "Superplastic Flow in Fine-Grained Alumina," *J. Amer. Ceram. Soc.*, 69 (2) (1986), 135-38.
2. C. Carry, and A. Mocellin, "High ductilities in fine grained ceramics," Proc. Conf. on Superplasticity Grenoble (Paris, C.N.R.S. 1985), 16.1.
3. P.C. Panda et al., "Superplastic Deformation in Fine-Grained  $\text{MgO-2Al}_2\text{O}_3$  Spinel," *J. Amer. Ceram. Soc.*, 68 (10) (1985), 522-29.
4. F. Wakai, S. Sakaguchi, and Y. Matsuno, "Superplasticity of Yttria-Stabilized Tetragonal  $\text{ZrO}_2$  Polycrystals," *Advanced Ceramic Materials*, 1 (3) (1986), 259-63.
5. G.W. Hollenberg, G.R. Terwilliger, and R.S. Gordon, "Calculation of Stresses and Strains in Four-Point Bending Creep Tests," *J. Amer. Ceram. Soc.*, 54 (4) (1971), 196-99.
6. G.G. Scott, "Phase Relationship in the Zirconia-yttria system," *J. Mater. Sci.*, 10 (1975), 1527.
7. F. Wakai, H. Kato, S. Sakaguchi, and N. Murayama, "Compressive Deformation of  $\text{Y}_2\text{O}_3$ -Stabilized  $\text{ZrO}_2/\text{Al}_2\text{O}_3$  Composite," *J. Ceram. Soc. Japan*, 94 (9) (1986), 1017-19.
8. D.M.R. Taplin, G.L. Dunlop, and T.G. Langdon, "Flow and Failure of Superplastic Materials," *Ann. Rev. Mater. Sci.*, 9 (1979), 151-89.
9. L.K.L. Falk et al., "The Role of Matrix Dislocations in the Superplastic Deformation of a Copper Alloy," *Acta Metall.*, 34 (7) (1986), 1203-14.



## POST-SPF FATIGUE PROPERTIES IN Ti-6Al-4V ALLOY

Y. Mutoh\*, M. Kobayashi\*, Y. Mae\*\* and K. Toyofuku\*

\*Department of Mechanical Engineering, Technological  
University of Nagaoka, Nagaoka 940-21 JAPAN

\*\*Central Research Institute, Mitsubishi Metal Corp.,  
Omiya 330 JAPAN

### Abstract

Post-SPF fatigue properties in Ti-6Al-4V alloy were investigated. Regardless of SPF conditions, fatigue strengths of the SPF materials were almost identical and lower than that of the mill annealed material. The change in crack initiation mechanism resulted in the lower fatigue strengths in the SPF materials: The deformation was localized in the grain boundary  $\beta$  phase in the SPF materials, while slip line formation and subsequent cracking in the  $\alpha$  phase was observed in the mill annealed material.

## Introduction

Recent investigations have shown that changes in microstructure due to various thermal treatments result in significant changes in mechanical and fatigue properties for titanium alloys (1-5). In the superplastic forming, superplastic deformation as well as thermal cycle may influence on mechanical and fatigue properties. In spite of the academic interest in and commercial development of superplastically formed titanium alloys only little information is available on their post-SPF properties (6,7). This paper presents the post-SPF fatigue properties of Ti-6Al-4V alloy.

## Experimental procedure

The material used was a Ti-6Al-4V sheet with thickness of 3.0mm. Specimens for superplastic forming, as shown in Fig.1(a), were cut from the sheet, the tensile axis of which coincided with the rolling direction. After superplastic forming a specimen shown in Fig.1(b) for fatigue tests was machined from the center region of the superplastically formed specimen. Eight kinds of specimens were prepared, as listed in Table I: The material A is an as-received (mill annealed) one. The materials B, C and D are superplastically formed ones at 1173K upto superplastic strain of 100% under various strain rates to investigate the effect of strain rate on post-SPF fatigue properties. The materials E and F are

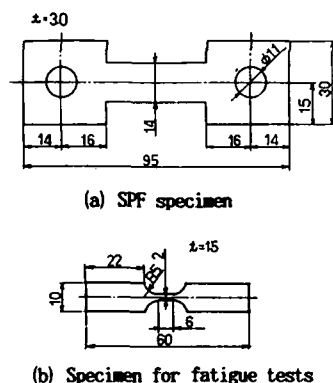


Fig.1 Specimens.

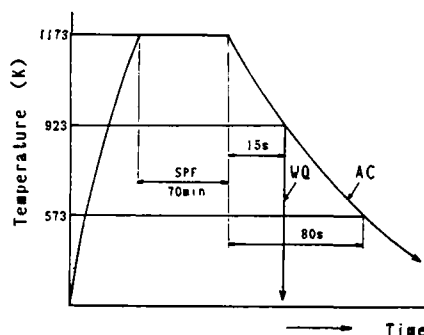


Fig.2 Schematic thermal cycle in SPF.

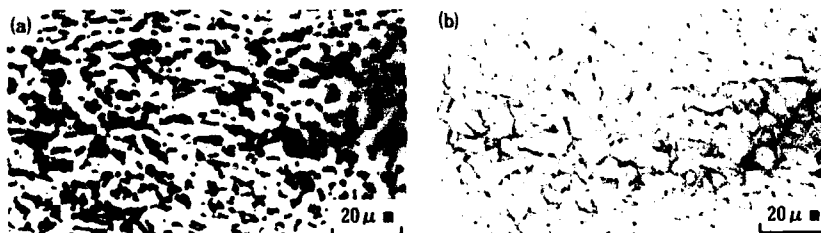


Fig.3 Microstructures. (a) As-received material (b) Material D

Table I The conditions for SPF, relevant mechanical properties and fatigue limits.

Material	Conditions for SPF				Mechanical properties					Fatigue limit (MPa)
	Temp. (K)	Strain rate (s <sup>-1</sup> )	SP-strain	Cooling	$\sigma_{0.2}$ (MPa)	$\sigma_b$ (MPa)	E (GPa)	Elong. (%)	H <sub>v</sub> (GPa)	
A	as-received (mill annealed)				1034	1085	104.3	24.9	3.26	325
B	1173	$2.77 \times 10^{-3}$	100%	WQ	-	1010	99.6	-	2.99	-
C	1173	$2.77 \times 10^{-3}$	100%	WQ	-	1045	98.7	-	3.05	-
D	1173	$2.77 \times 10^{-4}$	100%	WQ	907	1095	116.3	27.1	2.95	140
E	1173	70 min	-	WQ	896	1113	89.0	18.6	3.08	140
F	1173	70 min	-	AC	924	1084	104.8	17.2	3.17	210
G	1173	$2.77 \times 10^{-4}$	100%	AC	858	1016	102.7	20.2	3.08	190
H	1073	$2.77 \times 10^{-4}$	100%	AC	869	982	95.5	25.0	2.96	140

thermally cycled to the superplastic forming temperature ie 70min at 1173K to investigate the effect of superplastic deformation. The material G is the superplastically formed one with the same SPF conditions as the material D except the cooling condition. The material H is the superplastically formed one with the same SPF conditions as the material G except the SPF temperature. The typical thermal cycle for SPF and thermal cycling with no superplastic deformation is schematically illustrated in Fig.2.

From the observations of microstructures for the materials used, no significant difference in microstructure was found among the materials from B to H. Typical micrographs for the as-received and D materials are shown in Fig.3. The microstructure of the as-received material has a matrix of primary  $\alpha$  with particles of  $\beta$ . The microstructure of the SPF and thermal cycling materials has a matrix of recrystallized  $\alpha$  with grain boundary  $\beta$  particles. The globular shape of  $\alpha$  phase was maintained even after large superplastic deformation. From these observations and the measurements of density, the formation of cavity was hardly found in the range of the present SPF conditions.

Fatigue tests were carried out in air at 297K and 55% relative humidity using a servohydraulic testing machine under a load-controlled condition of R=0.05 at a frequency ranged from 5 to 40 Hz.

#### Results and discussion

The relationship between stress amplitude  $\sigma_a$  and number of cycles to failure N, is shown in Fig.4. Since the present fatigue test was carried out under R=0.05, the maximum stress  $\sigma_{max}$  is given as

$$\sigma_{max} = 2 \sigma_a / (1-R) = 2.1 \sigma_a$$

Fatigue limits obtained from Fig.3 are listed in Table I. From the figure, the fatigue lives of the SPF and thermal cycling materials were almost identical and shorter than that of the mill annealed material. Busch et al (6) also reported that fatigue lives under the annealed and the

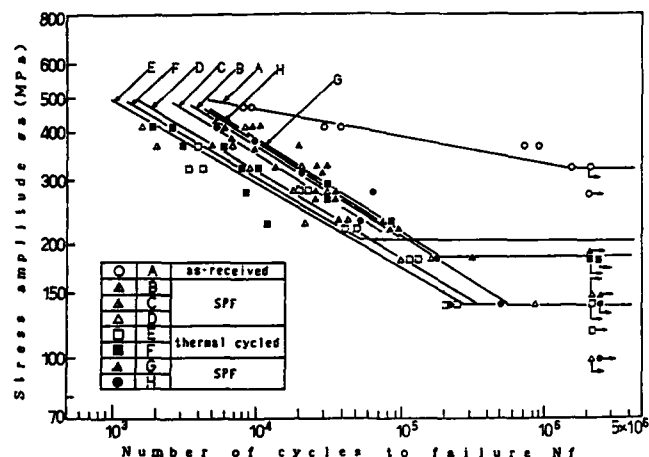


Fig. 4 S-N diagram.

superplastically formed conditions were almost identical and both of them were shorter than that under the as-received one. Therefore, superplastic deformation will not play an important role in the fatigue properties at least in the case of SPF without void formation. As can be seen from Table I, the SPF and thermal cycling produced a significant reduction of 35-57% in fatigue limit.

The crack initiation mechanisms vary from slip line formation and subsequent cracking in the  $\alpha$  phase,  $\alpha/\beta$  interface cracking or slipless cracking of the  $\alpha$  phase (8). Slip line formation and subsequent cracking in the  $\alpha$  phase was reported to be the main initiation mechanism in the  $\alpha/\beta$  structure (1). In the present as-received material, since the facets fractured along slip lines were observed, as shown in Fig. 5(a), slip line formation and subsequent cracking in the  $\alpha$  phase seems to be the main initiation mechanism. It was reported (4) that, in the recrystallized anneal material, microstructure of which was almost identical with those the SPF and thermal cycling materials used, the deformation was localized in the grain boundary  $\beta$  phase and the recrystallized  $\alpha$  phase was nearly dislocation free but the  $\beta$  phase had numerous defects. In the SPF and thermal cycling materials, since the transgranular and cleavage facets were observed as shown in Fig. 6(a), localized deformation in the grain boundary  $\beta$  phase and subsequent cracking seems to be the main initiation mechanism.

Irving and Beevers (2) showed that the fatigue crack growth rates of the heat treated materials (as-received + 1203K 30min or 1073K 30min + air cool) agreed well with that of the as-received (mill annealed) material except in the near threshold region. In the fracture surface far from the initiation point, the striation was observed in all materials used. No significant difference in morphology of the striation was found among the materials used, as shown in Fig. 5(b) and 6(b). Therefore, the change in crack initiation mechanism will be a main reason for the lower fatigue strengths in the SPF and thermal cycling materials.

The material E, which was thermally cycled to the

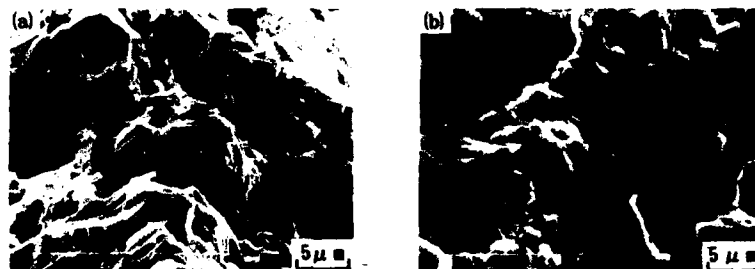


Fig.5 Fractographs for the as-received material. (a) Initiation region (b) Striation

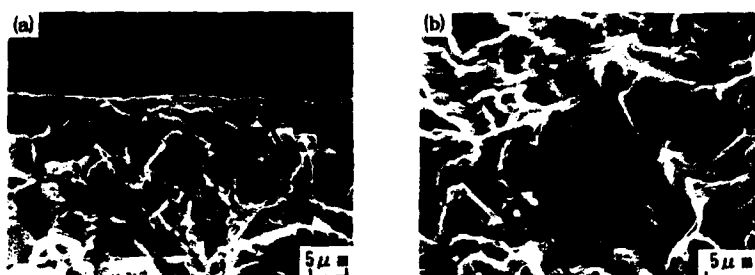


Fig.6 Fractographs for the material D. (a) Initiation region (b) Striation

superplastic forming temperature but not superplastically deformed, was heat-treated under the conditions of 1223K, 1h, WQ. This heat treatment increased fatigue life by a factor of 1.45. Further investigations are needed for improving the post-SPF fatigue properties.

#### References

1. Stubbington C.A. and Bowen A.W., "Improvements in the Fatigue Strength of Ti-6Al-4V Through Microstructure Control," J.Mat. Sci., 9(1974)941-947.
2. Irving P.E. and Beevers C.J., "Microstructural Influences on Fatigue Crack Growth in Ti-6Al-4V," Mater.Sci.& Eng., 14(1974) 229-238.
3. Thompson A.W. et al., Titanium and Titanium Alloys, (Plenum Press, NY, 1976) Vol.1, 691-704.
4. Gilmore C.M. and Iman M.A., Titanium and Titanium Alloys, (Plenum Press, NY, 1976) Vol.1, 637-648.
5. Nishimura T. et al., Titanium and Titanium Alloys, (Plenum Press, NY, 1976) Vol.3, 1977-1988.
6. Busch W.B. and Kunze H.D., Titanium, Science and Technology, (Deutsche Gesellschaft Fur Metallkunde E.V., 1984) Vol.2, 725-732.
7. Ingelbrecht C.D. et al., Titanium, Science and Technology, (Deutsche Gesellschaft Fur Metallkunde E.V., 1984) Vol.2, 761-767.
8. Steele P.E. and McEvily A.J., "The High-Cycle Fatigue Behavior of Ti-6Al-4V Alloy," Eng.Fract.Mech., 8(1976)31-37.

THE MANUFACTURE OF SPF MILITARY AIRCRAFT DOORS IN

ALUMINIUM ALLOY

Dr G W Hughes

Mr S H Johnston & Mr B Ginty

British Aerospace Public Limited Company  
Aircraft Group - Warton Division

**Abstract**

SPF/DB titanium is a proven production technology at BAe. Until recently SPF of aluminium alloys has been confined to secondary and tertiary aircraft structures due to the lack of a suitable structural alloy. Project studies have indicated that useful cost and weight savings can be achieved by the application of SPF aluminium to various military aircraft primary structure components. The development of high strength 7475E and 8090 SPF aluminium alloys offers the potential of manufacturing such structures.

The objectives of achieving manufacturing cost savings and weight benefits have been verified through design and manufacture of the L/H module door for Tornado. The subsequent scale-up manufacture of a large complex S shaped SPF 8090 EAP main undercarriage door has also been demonstrated.

This paper discusses the manufacture of the Tornado door.

Superplasticity and Superplastic Forming  
Edited by C.H. Hamilton and N.E. Paton  
The Minerals, Metals & Materials Society, 1988

### Introduction

During the early 1970's British Aerospace (formerly British Aircraft Corporation) and North American Rockwell established the manufacturing methods for SPF/DB titanium structures (1) - (4). This has matured to a fully proven production technology with several thousand production components having now been manufactured at the Military Aircraft Division, Warton Unit. About this time development of SPF aluminium materials and processes also commenced, but production maturity was delayed due to the lack of a high strength material.

Early work was mainly concerned with the zinc alloy ZAM, followed later by the Supral 100/150 alloys and the Al-Ca alloy 08050. Considerable manufacturing data with respect to tooling, processing techniques and associated manufacturing costs was gained from this work. However, these materials were of relatively low strength and unsuitable for most primary structural applications with the Supral materials generally being confined to secondary and tertiary aircraft structures (5).

The emergence of the high strength 7475 and more recently Al-Li alloys (6) has led to a re-assessment of SPF aluminium structural applications and the subsequent development of the manufacturing technology at BAe to a state of production readiness.

This paper outlines the manufacture of a SPF aluminium Tornado L/H module door and also refers to the subsequent scale up manufacture of a large complex S shaped SPF 8090 main undercarriage door for the EAP (Experimental Aircraft Programme).

### Applications

An assessment of the potential SPF aluminium applications for future military aircraft has been carried out by BAe and substantial usage identified. Similar conclusions have been derived by other aerospace companies (7). As a result of these studies one of the areas of technology application which showed potential cost and weight pay-offs was the manufacture of aircraft doors.

To validate the applications studies and to create a design and manufacturing database an extensive technology development programme has been carried out at BAe.

#### Manufacture of Tornado SPF L/H Module Door

As part of the technology development programme a Tornado module door was re-designed for SPF manufacture.

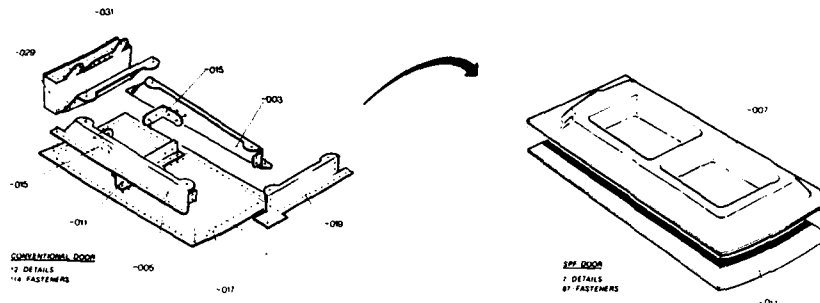
The objectives of the module door demonstrator programme were:-

- To validate the design.
- To prove the tooling concepts.
- To prove the manufacturing process produced components of an acceptable accuracy and quality.
- To verify cost savings.

#### Component Design

The conventional door is a fabricated aluminium assembly consisting basically of Z-member stiffeners rivetted to a stretch formed skin. The SPF version is basically a two sheet structure consisting of a superplastically formed inner skin, in this case rivetted to the conventionally formed outer skin. For skins of more complex shape it is more likely that the outer skin would also be SPF'd.

A reduction in parts count from 12 to 7 and in fasteners from 114 to 87 is achieved by the change of design to SPF as shown in the exploded views of the two doors, figure 1.



**Figure 1** Exploded views of doors

For the purpose of this exercise the shoot bolt locations, hinges and associated packers are common to both versions of the door. These have been included in the total parts count although they are not shown in figure 1.

#### Comparison of Manufacturing Routes

For the conventional door the manufacturing route consists of manufacturing individual details by hand forming, rubber press forming and stretch forming which are subsequently assembled by rivetting. A table showing the number of tools required for the manufacture of all details is shown in figure 2 (18 tools in total). Both manufacturing techniques require one assembly jig. This method of production although tried and tested is labour intensive and it is the reduction in manufacturing hours that is primary in driving the SPF technology. The comparison between manufacturing costs of the conventional and SPF door will be discussed in more detail later. However, as previously indicated, the parts count for the SPF door is reduced resulting in a modular approach to build, with a reduction in the number of tools required to 5.

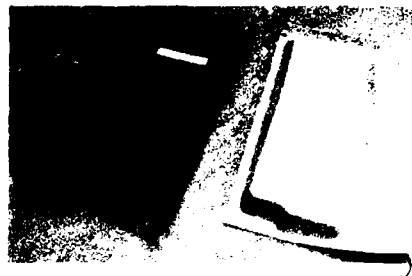
CONVENTIONAL			SPF		
Detail	Form Tool	Template	Detail	Form Tool	Template
-003	1	1	-007	1	2
-005	1	1	-017	1	1
-011	1	1			
-015	2				
-017	1	1			
-019	1	2			
-029	1	1			
-031	2	1			
TOTAL	10	8	TOTAL	2	3

**Figure 2** Comparison of Tooling Requirements

The differences in construction are further highlighted in the photographs of the two assembled doors figure 3. Although for the purpose of this exercise the SPF door was assembled by rivetting, the design of the SPF



structure, unlike conventional structure is particularly suited to advanced assembly techniques such as adhesive bonding, diffusion bonding (8) and weld bonding (9). These techniques are currently under development with a view to further reducing cost and mass.



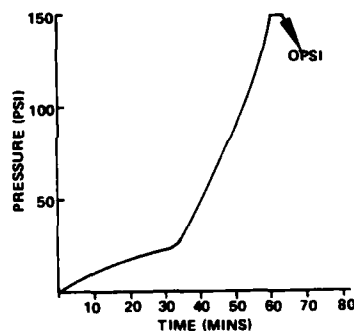
**Figure 3** Comparison of Assembled Doors

#### SPF Manufacture

The SPF form tool was designed to enable both the manufacture of the waffle pressing and outer CPL skin. The form tool is shown in figure 4. The waffle was manufactured by loading the flat blank into the heated form tool at  $515 \pm 10^\circ\text{C}$ . The initial curvature of the door was formed by closing the tool. The pressure time cycle was then initiated (figure 5) and the pressing formed (figure 6). Cavitation was suppressed during the manufacture of the waffle. Post form heat treatment operations were carried out.



**Figure 4** Form Tool



**Figure 5** Typical Pressure Time Profile

#### Cost Analysis

Having successfully demonstrated the manufacture of a superplastically formed door a comprehensive exercise to identify the cost benefits of the technology was carried out. The cost of tooling, material and detail manufacture and component assembly for both versions of the door were considered in determining the final manufacturing costs. Savings in indirect engineering costs are not included. In determining the material costs all the fittings are regarded as common, and therefore only the skin and waffle are considered. Although the cost of the 8090 alloy is about 10 times the cost of conventional aluminium in terms of the overall component cost, the material cost increase is insignificant in this case.

The results of this exercise are presented in Table 1. It is of interest to note that although the number of tools required for manufacture of the SPF assembly is reduced from 19 to 6 the overall tooling bill is increased by approximately 14%. This is not as surprising as it first appears given the complexity of the SPF tool.

	CONVENTIONAL ASSEMBLY	SUPERPLASTIC ASSEMBLY
TOOLING	19 tools	6 tools
	1575 manhours	1774 manhours
DETAILS &	12 details	7 details
ASSEMBLY	21 hrs 33 min	6 hrs 40 min

Table 1 Cost Comparisons

The cost benefits of the process are obviously associated with the lower number of details and the simplified assembly. In this respect a cost saving of 66% is recorded for the superplastic assembly.

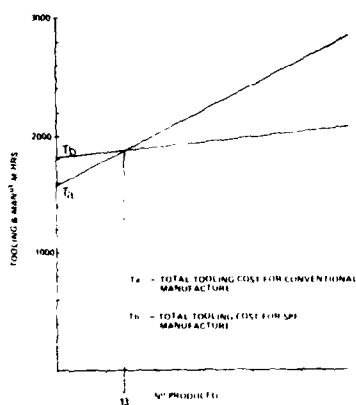


Figure 6 SPF Cost New Project

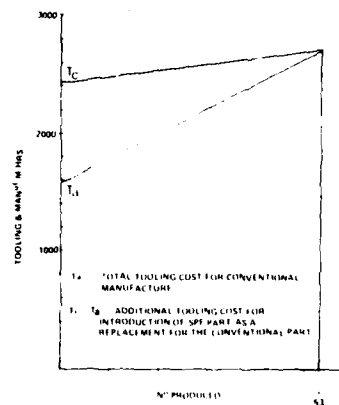


Figure 7 SPF Cost Existing Project

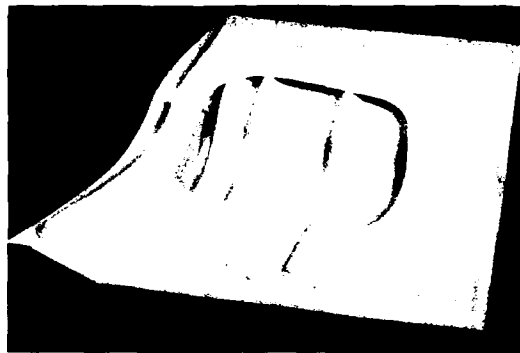
The economic advantages of introducing the SPF technology into production are easily illustrated by plotting the cumulative manufacturing costs, with the non-recurring tooling costs for both versions of the door. This has been done in figure 6. Analysis of this graph shows that although the introduction costs are higher, the process becomes cost competitive after the production of only 13 assemblies. In many instances however on established projects the cost of existing tooling needs to be written off before the benefits of the new technology can be realised. This is shown clearly in figure 7, where it can be seen that the break even is achieved after the manufacture of 53 assemblies.

#### EAP SPF 8090 Undercarriage Door

One of the aims of the Experimental Aircraft Programme is to demonstrate advanced manufacturing technologies such as CFC, PEEK, SPF/DB titanium and SPF aluminium. As part of this programme the EAP undercarriage door was selected to demonstrate the SPF aluminium technology. Confidence for selection of this item was gained from the manufacture of the Tornado door. Although similar in concept this door is far more complex due to its size, geometry and performance requirements and therefore the manufacture of this door would extend the technology significantly.

The conventional door is approximately 1m x 0.75m plan size of S-shape cross section having both inner and outer skins separated by numerous small stiffeners. Generally the internal structure comprises fabricated channels and Z sections with machined inserts at the hinges and jack attachment brackets. Cleats are required at all the stiffener junctions and all attachments are by mechanical fasteners.

The SPF structure comprises of a inner and outer skin separated by a single sheet waffle pressing with local cut outs and chemi-etch pockets for weight reduction, which replaces all the detail stiffeners. A reduction in parts from 96 to 11 and in fasteners from 1466 to 540 is achieved by the change in design to SPF.



**Figure 8** EAP Door

The SPF door with a local skin cut-away to expose the waffle is shown in figure 8. The predicted cost saving was 60% and a mass saving of 18% was achieved compared with the fabricated door.

#### Conclusions

Components of an acceptable quality and accuracy to the required design have been produced by using SPF technology with high strength aluminium alloys. The predicted cost benefits have been proven. In addition mass savings have been demonstrated.

#### References

1. British Patent No. 1,398,929.
2. British Patent No. 1,429,054
3. U.S. Patent No. 3,927,817.
4. British Patent No. 1,480,168.
5. R. Sawle - Proceeding of AIME Conference San Diego 1982 Superplastic forming of Structure Alloys (p. 307).
6. P. G. Partridge, D. S. McDermid - AGARD lecture Series 154  
D. Common, I. Bottomley Superplasticity (P6 - 1).
7. C. Bampton, F. McQuilkin - Proceedings of ASM Symposium on Superplastic Forming - Los Angeles March 22 1984 (P 76).
8. British Patent No. 216,732,9A.
9. H. Lipsius, J. Stock, A. Shomes - Int. Conference Superplasticity in Aerospace Aluminium - Cranfield 1985. Secondary Fabrication techniques for superplastically formed aluminium.

## SPF/DB ON THE WAY TO THE PRODUCTION STAGE FOR TI AND AL

### APPLICATIONS WITHIN MILITARY AND CIVIL PROJECTS

Dr. H. E. Friedrich, R. Furlan und M. Kullick

Messerschmitt Bölkow Blohm GmbH

#### Abstract

The development of new production methods in the aerospace industry is basically geared towards achieving cost and weight advantages. Whilst a reduction in manufacturing costs is one of the factors determining the final price of the aircraft, reductions in weight permit more favourable specific fuel consumption or higher payload. Owing to the highly structured and complex component geometries of both today's and future aircraft programs, the production methods of superplastic forming (SPF) and diffusion bonding (DB) and in particular, a combination of both methods (SPF/DB) have secured themselves an important position amongst other innovative technologies.

The SPF and SPF/DB processes in particular can be used to form parts with a reduction in material consumption or metal cutting and achieve a shape similar to the final contour (i.e. largely corresponding to the final dimensions) and to join them in one operation. The development and production work conducted to date by MBB has achieved weight reductions of up to 35% for SPF and for SPF/DB titanium parts. Overall, the activities relate to titanium alloys and high-strength aluminium alloys.

Ti Al6 V4 largely complies with the SPF Process requirements <sup>\*)</sup> such as fine-grained structure, high structure stability in respect of grain growth (in this case, as high an *m*-value as possible should be reached and retained during the forming process <sup>1)</sup> and high purity of the structure (reduced percentage of inclusions in order to guarantee a low sensitivity to pore formation). Purity of the contact surface and appropriate surface roughness are important in respect of joining materials when subject to pressure and temperature in the DB process.

Aluminium alloys are altogether more critical with regard to their processing parameters.

Although it is possible to achieve an adequately fine-grained structure in alloy type Al Zn Mg Cu (AA 7475) by carrying out a special thermomechanical treatment during sheet manufacture, aluminium alloys still tend to suffer from the fact that they develop porosity during the forming process.

<sup>\*)</sup> largely covered by the material specified by "MIL-T-9046F, Type III, Comp. C annealed".

Superplasticity and Superplastic Forming  
Edited by C.H. Hamilton and N.E. Paton  
The Minerals, Metals & Materials Society, 1988

The formation of pores can be attributed to the diffusion related agglomeration of vacancies and/or a plasticity-related shearing effect at the grain boundaries, or more likely, at a second phase or inhomogeneity in the structure. Special measures are necessary to achieve adequate mechanical properties in alloys having undergone a large degree of plastic deformation.

Forming with a superimposed hydrostatic back-pressure has proved its practicality in this case. Unlike Titanium alloys, the oxide layer on aluminium alloys has proved to be the barrier to the diffusion process necessary for the successful combination of SPF and DB. Methods of reducing or removing this oxide layer are still in the development stage.

The following examples of SPF and SPF/DB components ready for series production result from combat aircraft development, technology spin-offs from civilian aircraft programs (Airbus) and applications in the automobile and engineering industries.

#### **Superplastic Forming of Titanium**

The Augsburg plant of the helicopters and aircraft division is currently engaged in series productions of a family of sheet-metal system fairleads for the pressure bulkhead of the Airbus A320 (Fig. 1) and a maintenance panel which is used as a modification in the Airbus A300/A310.

Originally, deep drawing of steel was one of the competing material/process combinations for the manufacture of the 4 sheet-metal fairleads. In the end, the superplastic forming of titanium was chosen because of

- o the weight advantage: this method reduces the weight per pressure bulkhead by approx. 1,0 kg and
- o design reasons. The difference in stiffness between the pressure bulkhead and the sheet-metal "fairleads" should be as small as possible.

When series production was commenced, no suitable hot press was yet available to the production department in Augsburg so that development and manufacture were conducted in parallel using furnace technology and jointly with the MBB central laboratory using hot press techniques. Furnace techniques require

- o friction-locked bolted dies, made of high-temperature-resistant, non-scaling materials (Fig. 2)
- o cooling of the die to approx. 100 °C, in order to release the bolted connection when changing batches; resulting in long cycle times,
- o 2-sheet technique for creating a pressure-tight chamber

These facts make it clear that the furnace technique was suitable only as a transition method while awaiting the installation of the more attractive hot-press in the plant.

Since the component is formed at 925 °C, the shape (male or female tool) and material of the forming tool must be carefully chosen to prevent the component shrinking on to the tool. A steel tool (insert made from austenitic stainless steel in a cast frame made of 22-4-91 (similar to 1.4875)) was manufactured to enable male forming in either a furnace or a hot-press. The male forming process was chosen because of the better final thickness distribution in the component.

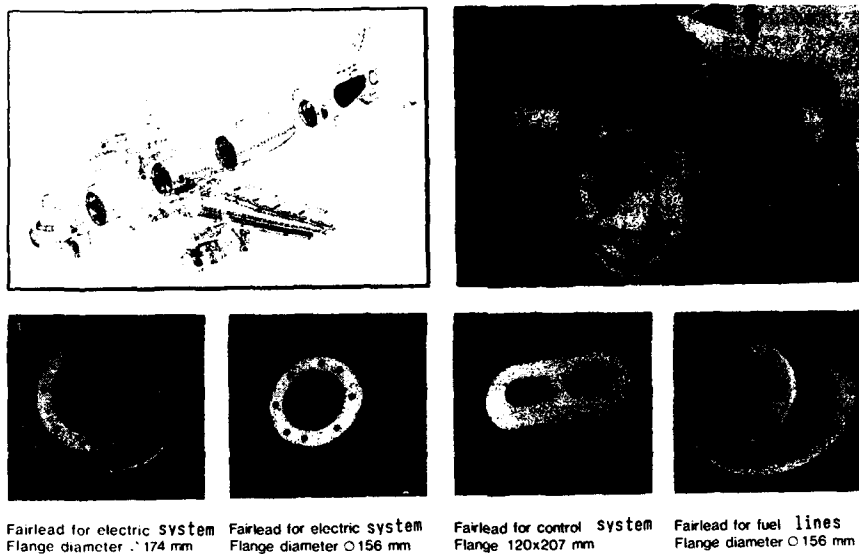


Fig. 1: Titanium system fairleads for the Airbus A 320

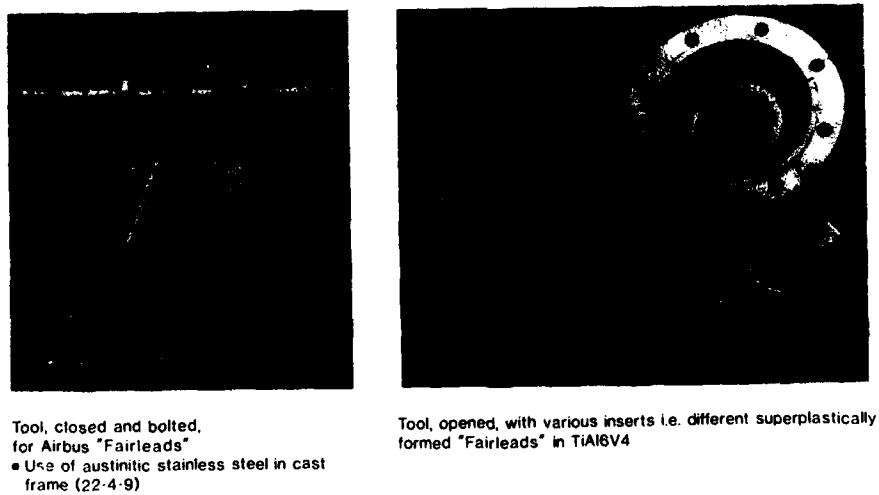


Fig. 2: Die for system fairleads

The pressure as a function of time is programmed on a mobile pressure control system. A maximum of 50 individual steps permit pneumatically actuated needle valves to be controlled in such a way as to ensure reproducible process parameters.

Apart from the occasional modification, it was possible to stipulate the series parameters for all parts after a very short development period. Only the so-called "oval" sheet-metal "fairlead" suffered initially from an inadmissibly high degree of thinning at exposed points and this could only be rectified by careful optimisation of the pressure/time curve and with a larger aperture in the plate of the series tool.

Freedom from flaws was verified by penetrant crack testing. Alpha-case layers with a thickness of between 50 and 100  $\mu\text{m}$  were removed by chemical milling.

When manufacturing the A300/A310 maintenance panel (Fig. 3), the weight advantage of titanium as compared with steel was very important. The weight of the titanium component is 37% less. Deep-drawing in stainless steel, in particular removal of the hinge-pocket areas from the mould, was categorized as difficult. In addition, a titanium component afforded the advantage of more favourable corrosion behaviour, this being a dominant factor in the affected area of the aircraft. (Fig. 4)

The female forming process was therefore selected, especially since this enabled maximum wall thickness to be obtained in the flange. For reasons of component shrinkage, a ceramic tool was selected for the furnace technique.

For the hot-press process where the component is removed (hot-die technique) without cooling the press, (hot removal enabling more efficient processing and resulting in higher component strength) a steel die made of heat-resistant, stainless material (1.4859) was used. Plasma-sprayed  $\text{Y}_2\text{O}_3$  coatings were used as diffusion-inhibiting barrier layers for the steel die and boron nitride spray coatings were used for the ceramic die.

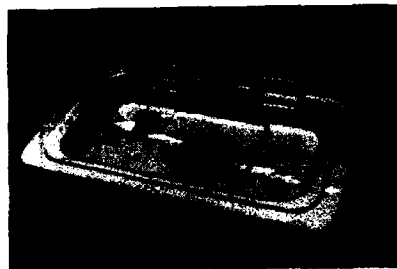
Production of the series components for the Airbus is monitored by regular type sample tests. The strength values determined indicate only a slight drop after SPF, as compared with the initial value, and always lie above the set target values (Table 1).

The Augsburg plant has also successfully diversified the uses of its innovative technologies, moving into other branches that are commercially viable. One example of this is the SPF titanium wheel hub designed as an optional extra for high-performance passenger cars. This part, made for a renowned supplier of the automotive industry, enabled both a reduction in un-sprung weight and an incorporation of contemporary design to be achieved. In this case, the component was designed specially for the SPF process (Fig. 5) before entering the development phase.

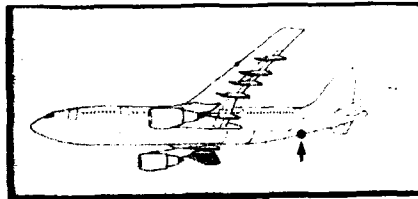
Since this component was destined from the start for the hot-press, it was possible to experiment with steel dies made using the ceramic shell moulding technique. The availability of this tool technology enables rapid turn-around and means cost efficient hot press and SPF moulds.

#### **Diffusion Bonding of Titanium in Combination with SPF**

The fact that SPF forming represents a favourably priced production method also and particularly in combination with an intelligent joining technique (DB) is substantiated by one example from the engineering field: Rotation shells made of Ti Al6 V4 for a high pressure centrifuge (Fig. 6).



▲ Superplastically-formed service panel in TiAl6V4 for Airbus A300/A310



Service panel finished and mounted ►

Fig. 3: Maintenance panel made of Ti Al6 V4 for the Airbus A 300 / 310

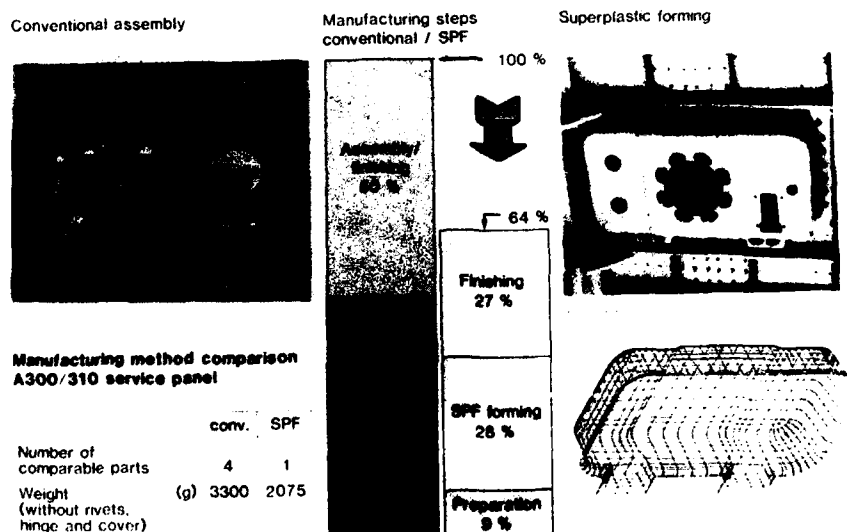


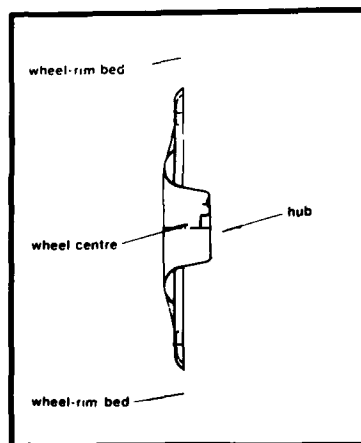
Fig. 4: Manufacturing steps conventional assembly / Superplastic forming of maintenance panel



		$R_{p0.2}$	$R_m$	$A$	$R_{p0.2}$	$R_m$	$A$
		N/mm <sup>2</sup>	N/mm <sup>2</sup>	L=50 mm %	N/mm <sup>2</sup>	N/mm <sup>2</sup>	L=50 mm %
1st	L + LT						
2nd	L + LT						
WL 3.7164.1				Test sheet "Fairlead"			

Mechanical properties of TiAl6V4,  
in each case before SPF (1.8 mm sheet thickness) and of a sample after SPF.  
Comparison with specified values according to material specification sheet and/or MBB test sheet  
for component "Fairlead".

Table 1: Strength values of Ti Al6 V4



Principle of wheel-rim assembly



Wheel centre (TiAl6V4)  
after SPF (above) and after trimming (below)

Fig. 5: Wheel hub made of Ti Al6 V4

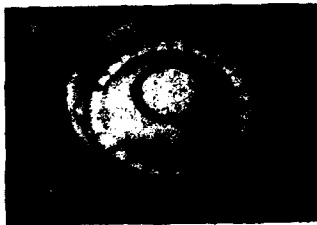


Centrifuge in TiAl6V4  
3 step process: DB/SPF/DB  
Outside diameter approx. 360 mm

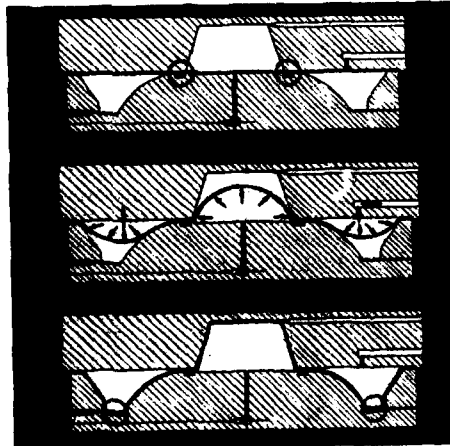


Components for a production operation  
1) Upper dish made from 6 mm sheet  
(after DB with ring).  
plate 480 mm  
2) Ring 5 mm x 160 mm  
3) 24 stiffeners, 1.3 mm thick

Fig. 6: Centrifuge in a 3-stage process DB/SPF/DB



Upper and lower tool-halves for  
DB/SPF/DB component "Centrifuge"  
Material: 1.4541



Manufacturing steps for production process  
i) DB: ring with plate before forming  
ii) SPF: disk  
iii) DB: stiffeners with formed plate

Fig. 7: Die halves and work steps for centrifuge

The important operating requirements of the centrifuge are as follows:

- o high strength and toughness
- o resistance to chemical substances (lyes and cleaning agents)
- o perfect rotation alignment

User tests with one Al cast variant did not produce satisfactory service lives. A steel version (deep drawing) could not be used owing to reasons of cost. Redesigning to achieve a contour suitable for SPF/DB produced a favourably priced Ti Al6 V4 version. Optimum utilisation of material with a forming as close as possible to the final contour produces weight reductions of 43% as compared with a steel version.

The important components of a shell manufactured in one production process are as follows.

- o shell structure made of 6.00 mm plate (circular blank), (1)
- o ring (2)
- o 24 reinforcing plates (3)

2 shells were used in each case for one centrifuge and the "hat" must be removed from the lower half.

A die made of 1.4541 was manufactured (Fig. 7) for DB/SPF/DB production. The lower section of the mould is provided with recesses for the ring and the small reinforcing plates.

The following work steps are included in one production process of the hot press: (Fig. 7)

- o DB of ring and non-formed circular blank (i) by applying the press pressure at forming temperature.
- o SPF of the circular blank (ii) simultaneously in 2 directions
- o DB of the small reinforcing plates and circular blank (iii) using pressure from the deforming plate during the last work step.

Finishing of the formed and bonded components is restricted to trimming the material inlet and reworking the ring (h 7 fit).

Using the DB/SPF/DB component as an example let us briefly discuss the suitability of the material and the component investigation. Metallographic investigations on the 6.0 mm starting gauge material are obligatory. The structure which is always fine-grained shows a partially "laminar" structure but this does not appreciably influence the suitability for SPF. To supplement this, the m-value was determined in a 12-stage speed controlled test run at 920°C under inert gas. At a forming speed of  $6 \times 10^{-4} \text{ s}^{-1}$ , max. m-values of 6.0 are achieved, thus identifying good material properties (Fig. 8)

The component investigations are based upon the numerous findings from the basic programs which have been conducted in the MBB central laboratory.

Random samples on the component permit the following statements to be made:

- o Grain coarsening resulting from the process occurs only to a slight extent
- o The drop in strength after SPF is negligible and sufficient for component function
- o The DB zone is free of flaws (Fig. 9)
- o The surface contamination is adequately eliminated by chemical milling.

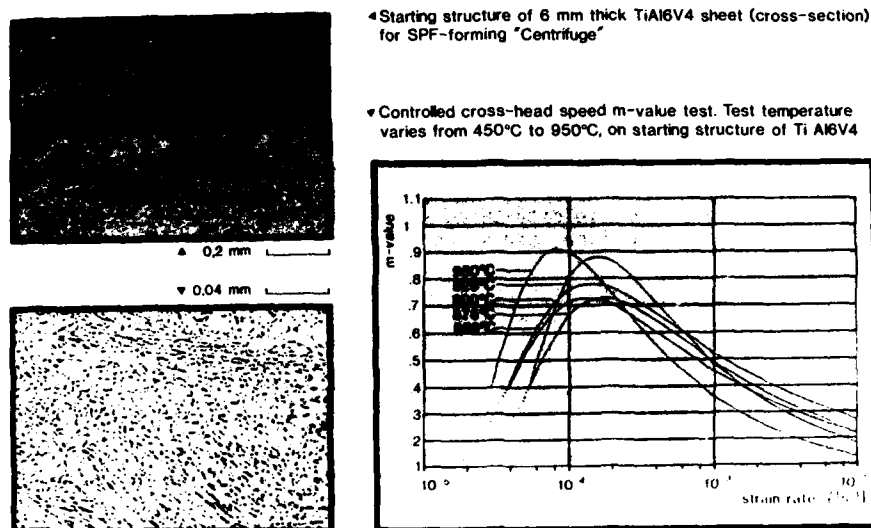


Fig. 8: Ti Al6 V4 - initial structure and m-value test

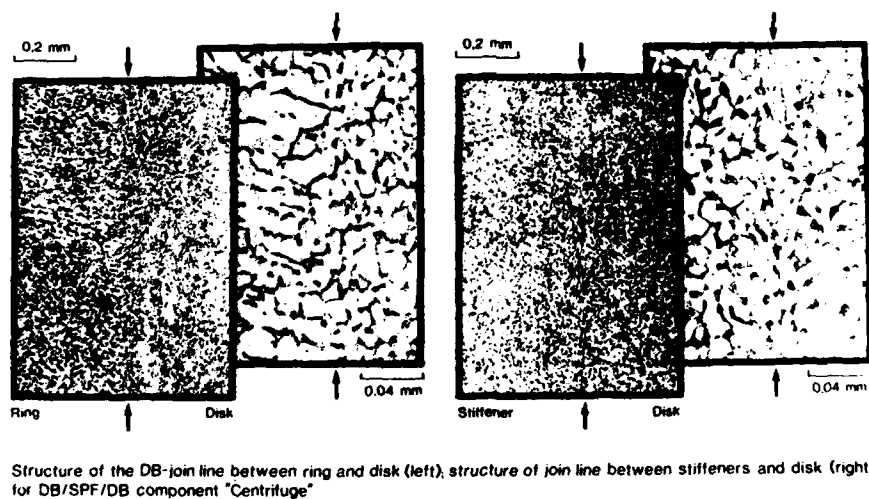


Fig. 9: Resultant structure of DB or SPF/SB on Ti Al6 V4

### Superplastic Forming on High-Strength Aluminium Alloys

The continual demand for greater performance and reduced weight forces those who develop combat aircraft to produce complex, integral designs made of Al and Al-Li alloys. The aim is to achieve cost and weight advantages over conventional design. SPF forming of high-strength aluminium alloys has been the subject of intensive research at MBB for approximately 5 years now. We shall show the work involved in refinement for series production, using the example of a shear wall, a typical combat aircraft component (Fig. 10), which must possess high rigidity owing to the stresses to which it is subjected and, at the same time, serves as a partition wall between tank compartments.

The high-strength alloy AA 7475 (Al Zn Mg Cu) and the medium-strength AA 8090 alloy (Al Li Cu Mg) were selected for SPF manufacture of the shear wall. The AA 8090 alloy was only able to be purchased in standard quality owing to availability, but had adequate SPF properties in this condition for the component (work conducted by the manufacturers into a specific quality Al-Li had not yet been completed during the period under review) to be made.

Development work commenced with hemispheres and components (400 x 400 mm). The fundamentals of the procedure elaborated in the laboratory were accompanied by parallel production trials on the hot press of the production department and transferred to production (Fig. 11) ready for the full scale component (900 x 700 mm). The dies were made of heat-treated steel (1.1191) for reasons of economy/availability.

In order to obtain a structure which is largely free of pores after forming, a backpressure system was developed and constructed to permit a quasi-hydrostatic pressure to be applied to the sheet metal panel and a superimposed pressure to enable forming. This mobile system (Fig. 12) does, of course, permit suitable backpressure/forming/time sequences to be programmed.

Comparing the process control curves used for the full-scale component in 7475 and the 8090 available up to now permits us to state that Al-Li can basically be formed at higher initial forming pressure but with the same time sequences. Although 8090 was not capable of such a large elongation as the 7475, in this case, it can be assumed that, since this 8090 sheet was not optimised for the SPF process, 8090 in general exhibits less tendency to form pores. Extensive material investigations were conducted in order to determine forming parameters and to qualify the procedure. The emphasis was on determining the mechanical properties of the SPF-formed Al material. The following parameters were determined on specifically defined test specimens:

- o static characteristics
- o dynamic characteristics with
  - various strains caused by deformation (deformation  $\epsilon = 50\%$ ,  $\epsilon = 100\%$ )
  - different initial sheet thickness and
  - different surface treatments after forming, in each case.

The influence of strain (up to 100%) on the fatigue behaviour could not be tested during our investigations, but surface treatment using a high-powered spray containing small abrasive particles brought a marked improvement (Fig. 13).

The structure of 7475, formed without backpressure is characterized by a regular distribution of angular pores which tend to be stretched in the forming direction, over the entire cross-section of the sample. These are formed at the existing grain boundaries or grain boundary intersections. Optimizing the pressure/time characteristic permits the maximum pore volume

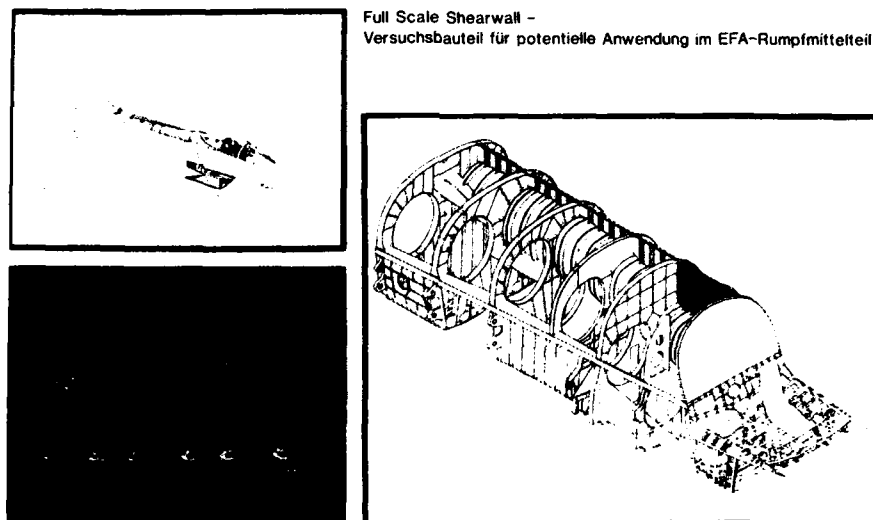


Fig. 10: Al shear walls for combat aircraft

Development program/trial components for SPF in high-strength Al and Al-Li alloys

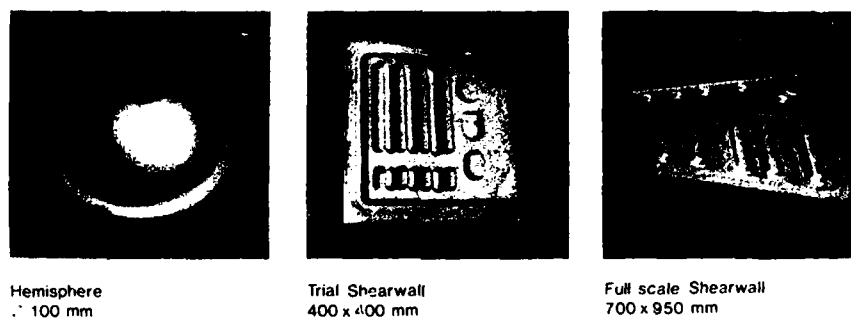


Fig. 11: Development program/test specimens for SPF components on Al and Al-Li alloys

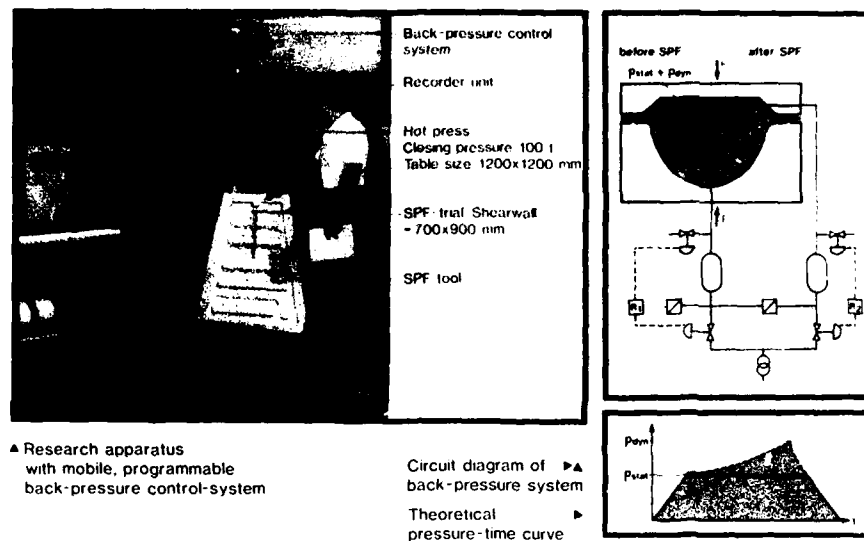
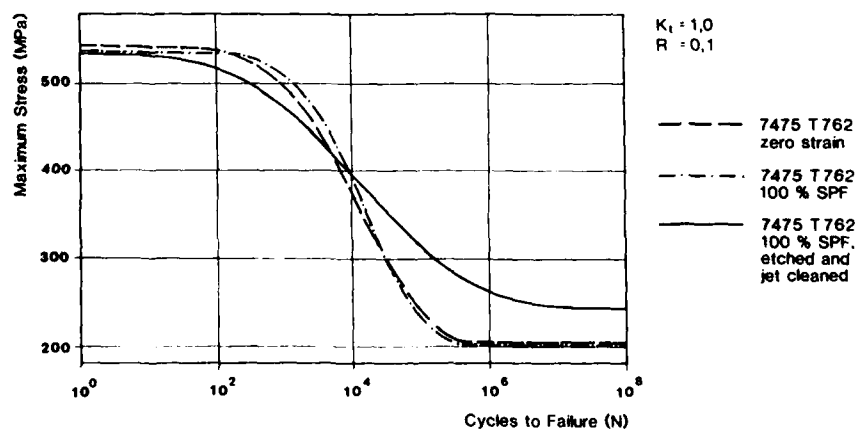


Fig. 12: Experimental set-up with backpressure system



Fatigue behaviour of 7475. Comparison of non-SPF formed material, 100 % SPF deformation and 100 % SPF deformation with subsequent jet cleaning.

Fig. 13: Fatigue behaviour of SPF 7475

percentage to be restricted to 0,4% in the case of hemispheres with a strain in the thickness direction of  $\epsilon_z$  for instance. One further appreciable reduction can be achieved by forming with back-pressure, whereby a figure of 0,005%-Vol.% was detected (Fig. 14) with 40 MPa. In the case of Al-Li 8090 we can assume a smaller tendency to form pores, as a comparison of samples made of 7475 and 8090 formed with 15 bar backpressure and a deformation strain of  $\epsilon = 100\%$ , shows (Fig. 15).

The investigations were not pursued since the available Al-Li 8090 was not in optimum SPF condition. However, one fact which must be noted is a typical formation of a pore-rich band close to the component surface, occurring regardless of the deformation strain and which can be explained by the diffusion of lithium (and magnesium) or the formation of brittle precipitation phases due to changed chemical composition (cf.5)

Micro-structure investigations were carried out on various components and it can be stated that a percentage porosity which, for instance, corresponds to or is less than the impurity content scheduled in the aerospace Standard specification sheet can be achieved with a typical back-pressure of 15 MPa and optimum pressure/time sequences up to a strain  $\epsilon = 100\%$ . Investigations of the dependence of the service life on pore content established no appreciable impairment up to a maximum pore percentage of 2% but the individual values are, nevertheless, subject to great scatter. Investigations into intercrystalline corrosion, stress corrosion cracking and lamellar corrosion were conducted in order to establish the corrosion behaviour and the behaviour in saline fog was also tested. At this point, it must be mentioned that fine-grained Al 7475 is susceptible to intercrystalline corrosion, but in comparison with 7075, is not characterized by an increase in SCC (stress corrosion cracking) in heat-treatment condition T76. There is only a slight tendency to exhibit exfoliation or lamellar corrosion.

#### Diffusion Bonding on Al and Al-Li Alloys

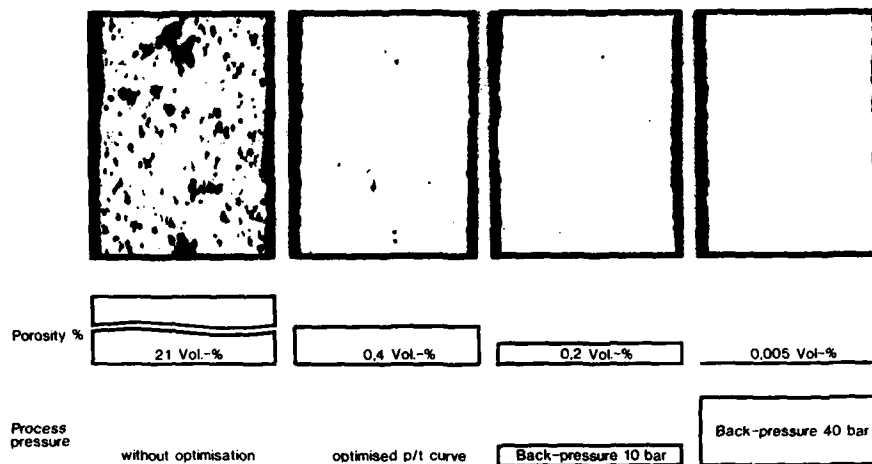
To achieve further design advantages with conventional alloys as well as Al-Li, the SPF process requires an intelligent joining technique to complement it. A study into alternative designs of an air inlet duct for combat aircraft has established that an SPF-DB design produces important weight savings and primarily, cost reductions of 57% as compared with a conventional design. This advantage is attributable to the lower material consumption and the more favourable production structure.

MBB is currently involved in research into this task with various possible solutions, this task, naturally, being made more difficult by the resistant Al oxide layer. One promising approach would seem to be the vacuum route (ion etching). This cost-competitive technology combines a good metallurgical base for the diffusion of material with the resulting high reproducibility of the obtained shear strengths.

Figure 16 shows an Al 7475 sample after DB, the mechanical properties of which (shear tension) correspond to approx. 180 N/mm<sup>2</sup>. Non-destructive testing of such joints generally consists of ultrasonic pulse echo testing, in an immersion tank, with a test frequency of 50 MHz. In this case results are shown in C-scan with colour graduation. An artificial flaw size of 0,5 mm can be reliably detected.

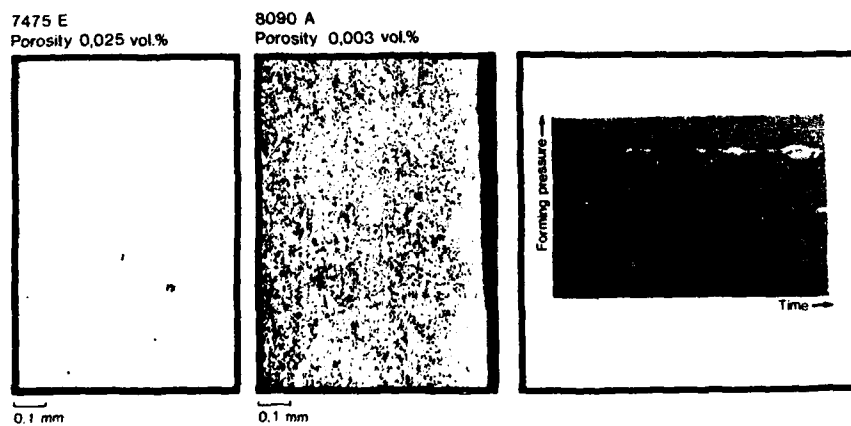
The helicopter and aircraft division at the Augsburg plant has two identical hot presses with table sizes of 1250 x 1250 mm and closing pressures of 100 tonnes for development and series production. An 800 tonne press operating on the shuttle principle which is currently being procured will also permit manufacture of larger components: the planned table area is 1600 x 1800 mm.





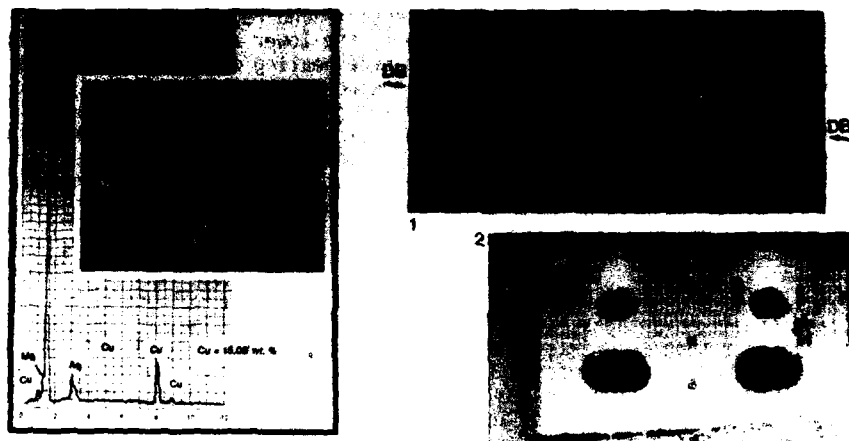
Comparison of the microstructures of SPF-Hemispheres in AA7475 as a function of the Time/Pressure curve and variable applied back-pressure, Equivalent strain  $\Psi_e = 0.67$ ; Maximum forming pressure ca. 1.5 bar, Forming time 60 to 90 minutes.

Fig. 14: Percentage porosity in SPF 7475 as a funktion of the pressure/time characteristic and backpressure



Microstructures after SPF of 2 mm sheet in 7475 E and 8090 A. Each has 50 % equivalent strain and optimised Pressure/Time curve. Back-pressure 15 bar. Comparison of theoretical Pressure/Time curves for 7475 E and 8090 A.

Fig. 15: Comparison of 7475 and Al-Li 8090 A



Energy-dispersive micro-analysis of the DB zone in Ag-coated (2x1800 A) Al-Li (2091)

1) Structure after DB of Cu-coated AlZnMgCu (7475)  
2) C-scan analysis using US-method: 50 MHz.  
Immersion technology using a sample with artificial faults

Fig. 16: DB on Al: Energy-dispersive analysis of the DB zone, structure and C-scan evaluation after ultrasonic testing.

#### References:

- /1/ Winkler, P.-J.: Eigenschaften und Anwendungen superplastischer Werkstoffe für die Luft- und Raumfahrt, Aluminium 60 (1984) H.4, S.261-266
- /2/ Paton, N. E., Hamilton, C. H.: US-Patent 4.092, 181 (1978)
- /3/ Pilling, J., Ridney, N.: Effect of Hydrostatic pressure on cavitation in Superplastic Aluminium Alloys Acta Met., Vol.34, (1986) pp 669-679
- /4/ Ilschner, B.: Hochtemperaturplastizität, Springer, Berlin (1973)
- /5/ Smith, A.F.: Aluminium-Lithium Alloys IV, Paris (1987)
- /6/ Koch, U.: The Influence of SPF on the Micro-structure of High Strength 7475 Al-Alloys. Vortrag anlässlich TMS Annual Meeting, Phoenix, Arizona (1987)

In order to guarantee adequate process stability and regulation of temperature for aluminium alloys as well as others, the lower and upper hot plates are each subdivided into 12 segments. The side heating surfaces have to be divided in 2 planes, one above the other, owing to the opening height (max. 600 mm). The hot press will be completely integrated into the information flow and logistics systems of non-cutting operations. The main precondition for this is the existence of a specific periphery, specially designed for the SPF/DB production unit and containing the areas Sheet and Tool preparation, Preheating oven, Hot-press with shuttle and Cooling (Fig. 17).

#### Summary:

To date it has been possible to achieve average weight-reductions of up to 35%. Additional advantages, such as the possibility of using high grade corrosion resistant materials, the reduction in individual parts and the resultant reduction in manufacturing operations and assembly costs, are considerable and will increase in importance.

In an aircraft assembly such as an integral fuselage fuel tank, the use of SPF/DB integral constructions could drastically reduce the number of sealing operations in critical areas. SPF/DB provides a fast and cost-competitive manufacturing solution for a whole family of covers and doors as sandwich panel constructions. Results from tests on diffusion-bonded aluminium panels in 7475 and Al-Li allow the assumption that this joining method has a future with these materials as well as with Titanium.

Studies into future applications describe reductions in component weight of up to 50%. The described production facilities, in particular the 800 tonne hot press which will be integrated completely in the information/logistic concept of the non-cutting production sector, will provide the MBB helicopters and aircraft division with the capability of providing a cost-effective manufacturing process for large complex structures for the requirements of the 21st Century.

## PRODUCTION OF Ti6Al4V-COMPONENTS FOR A NEW TURBO-FAN-ENGINE

R. Furlan\*, P.-J. Winkler\*, D. Hagg\*\*, L. Reisinger\*\*

\* MBB, Central Laboratories, Munich/FRG

\*\*MTU, Development Manufacturing, Munich/FRG

### Abstract

The new turbo-fan engines such as the V2500, are far more economical regarding fuel consumption. By consequently reducing the engine weight using titanium instead of steel, the engine components can be reduced in weight up to 50%.

The use of the high-strength Ti6Al4V alloy requires a weight and cost-effective fabrication technique such as superplastic forming, for instance.

This paper presents the production development of an air-cooling system for a turbo-fan engine; six different parts are produced by superplastic forming.

A development program thoroughly investigated the aspects relevant to cost-optimized production.

The development included: Redesign and tooling for SPF application, "stop-off" materials and hot die technique. During component qualification, changes in microstructure and the influence of SPF on static and dynamic strength were investigated.

The titanium parts are currently being qualified by test runs and will be used for the entire V2500 series.

### Introduction

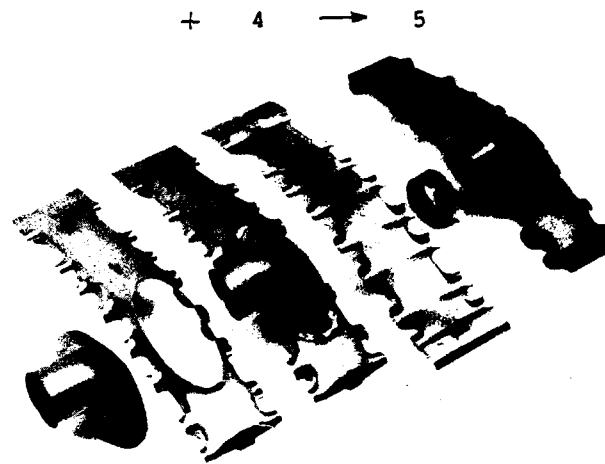
The SPF materials behavior has been developed for Ti6-4 to a cost-effective finishing technique. Based on numerous fundamental investigations on superplasticity, the transfer to production leads to new tasks within processing.

A rational production sequence was the basis for cost-effective application of SPF technology. Further cost reductions could be achieved by minimizing the test effort and simplifying the materials incoming inspections.

In order to reduce the clearance losses, cooling systems are used in engine design. The SPF production of a Ti6-4 cooling system for the V2500 turbine casing is described in this article.

Cooling is achieved by forcing air around the casing with a pressure of 0.4 to 0.5 MPa with temperatures less than 200°C.

The unit consists of an inlet pipe made from TiCu2, an SPF-formed distributor casing and subsequently a tubing assembly. The air is projected onto the surface through defined boring within the casing and the tubing assembly. The SPF-formed single components together with the entire unit ready for assembly are shown in Fig. 1.



- 1 + 2 → 3 +
- 1 Elbow, upper + lower halves
  - 2 Casing, upper part
  - 3 Elbow + casing upper part
  - 4 Casing, lower part
  - 5 Completed casing + elbow

Figure 1 - Cooling case assembly

The components are elbow and casing upper and lower halves. The die insert to produce the third part, a branching tube, is shown in Fig. 2.

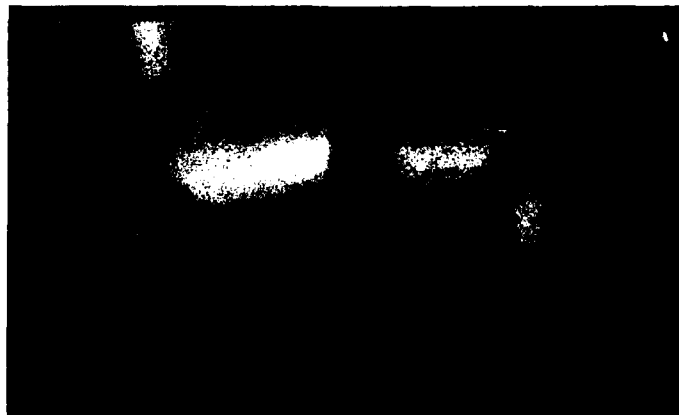


Figure 2 - Die insert branching tube

For the first step the elbow upper and lower halves are welded together using the WIG process. The casing underpart is then joined by welding onto the elbow unit and in a further step the part is completed by mounting the adapting ring.

By a further step the cold formed Ti6-4 tubes are added (see Fig. 3).

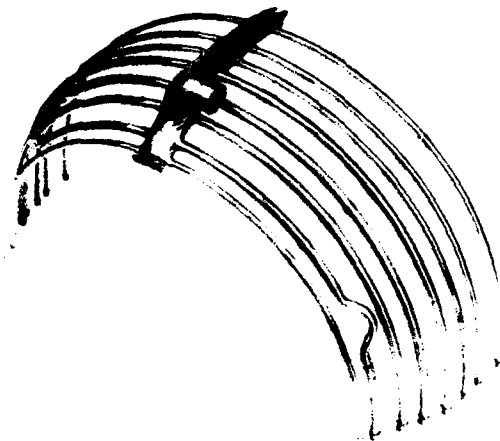


Figure 3 - Cooling component

The assembled unit is shown in Fig. 4.



Figure 4 - Assembled condition

### Equipment and tooling

For the forming processes, specially adapted hot presses are used to achieve a forming temperature of 920°C. The main functions of the press are applying a pressure to the tool and tool heating.

In addition, the part can be removed at forming temperature due to a mobile press underpart (shuttle technique). By inserting a new sheet the process can be continued after a short reheating period. A specially designed gas-management system ensures a computer-controlled forming sequence for SPF of aluminum and titanium parts. The process can be observed and controlled by using gas-flow meters.

### Tooling: Material choice

Due to the relatively low number of parts, the tool costs play a big role in the calculation of production costs. The elevated SPF temperatures demand the use of oxidation and temperature-resistant materials. Three material groups (steels, ceramics, carbon fibre reinforced composites) were investigated for tool construction. Important criteria for the characterization are creep strength, machining, repairing possibilities and material availability together with costs.

[1]

For producing a great number of parts, steel is the best choice of material. Tools made of an inferior steel quality were used for preliminary testing. Even with this low quality, steel parts for 30 engines were produced. For production the use of steel castings (ESCO 49M) has been planned because of its relatively low costs and long life. It has been shown that a suitably constructed steel tool can be used without reworking for the overall production.

### Tooling: Design requirements

One of the most important factors for successful application of SPF is the optimization of tool construction. The attained result is influenced mainly by the tool geometry and process parameters. The thickness trends can be influenced by using either male or female die inserts. The result of forming is also influenced by the extent of sloping and radii on the tool edges. The number of inserts and their location within the tool are also influential. Small radii, sharp



contours and acute angles must be avoided in design. The production costs are reduced and the material efficiency is increased by using multiple die inserts. For example four casing underparts can be produced in one SPF cycle (see Fig. 5).



Figure 5 - Die inserts - casing underparts

"Stop-offs" are used to avoid reactions between steel die and titanium sheet at high pressures and temperatures. In order to attain a resistant separating layer the tool surface was coated with a ceramic plasma coating of good surface quality. By using a nickel bond coat the bond strength of the 10 to 50 micron ceramic layer is increased. The most successful ceramic coating was found to be aluminum oxide. A resistant coating with a high-surface-quality has been produced (see Fig. 6).



Figure 6 - Aluminum-oxide-coated die inserts

A boron nitride suspension is applied to the die inserts in addition to the coating before the first cycle. For production, the sheets for forming are coated with a thin boron nitride layer.

#### Material qualification

The 1.27 mm and 1.0 mm sheets used for forming undergo preliminary inspection complying with the MBB and MTU SPP specification for sheet material. These specifications have been developed within a material qualification program.

#### Preliminary material testing

As a result of discussions with material suppliers and our own experience it was found that for the assurance of SPP formability of sheet material microstructure testing is sufficient. After heating at 920°C for one hour the material should show a homogenous microstructure with a grain size smaller than 12 microns. Inhomogeneities such as  $\alpha$ -banding, blocky  $\alpha$ ,  $\beta$ -flocks and widmannstätten  $\alpha$  are unacceptable. In addition, the regular testing methods for titanium sheets are carried out.

In addition to the relatively simple microstructure analysis the  $m$ -value testing shows good possibilities for the determination of SPF properties. The  $m$ -value test allows the determination of the optimum forming rate for a fixed temperature. The test results showed consistently high  $m$ -values between 0.8 and 0.9. The  $m$ -value test is only used to clarify the material quality if forming problems occur. Although the material used for development work showed some  $\alpha$ -banding, the results after forming were acceptable. The material ordered for production will only be accepted with a microstructure agreeing with the specified microstructure for SPF quality. [2]

#### Quality control

The production tests for the first 30 engines showed for all parts strength values above the specified limits of yield strength =  $870 \text{ N/mm}^2$  and ultimate strength =  $920 \text{ N/mm}^2$ . To ensure that no diffusion zones remain after chemical milling a cold bending test has been found simple and successful. Thanks to chemical milling of 70 microns on both sides, a surface free of embrittlement was achieved (see Fig. 7 and 8). After the process was stabilized the amount of testing was significantly reduced.

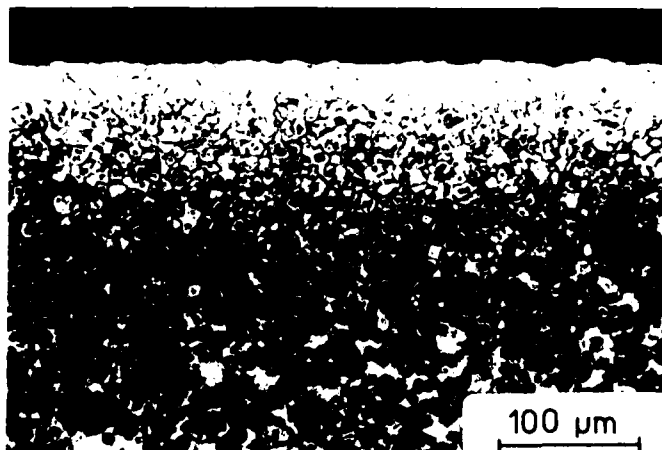


Figure 7 - Microstructure after SPF  
 $\alpha$ -case = 70 microns

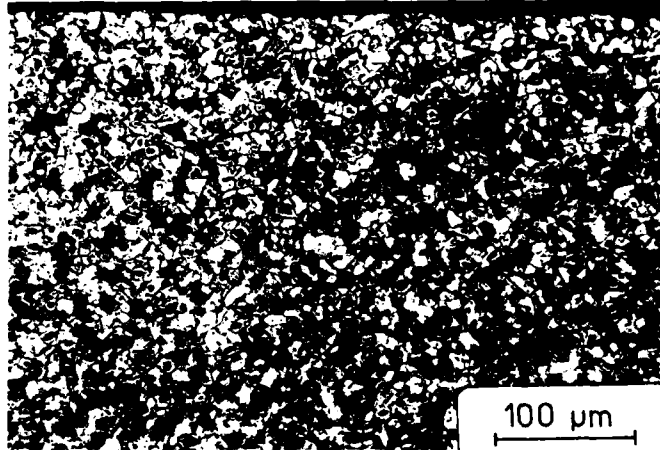


Figure 8 - Microstructure after chem. milling  
without  $\alpha$ -case

The chemically milled part surfaces must be free of diffusion zones because the remaining  $\alpha$ -case leads to a reduction in ductility. Fig. 8 clearly shows the influence on the dynamic properties with an increase of fatigue strength after 40-, 70- and 110- micron milling. [3]

#### Process Parameters

The parts were formed within a temperature range of  $920^{\circ}\text{C} \pm 10^{\circ}\text{C}$ . The location of the thermocouples are important because of temperature gradients over the tool.

The reproducibility of the process is achieved by controlling temperature and forming pressure and is documented for each forming cycle.

By tolerating temperature differences as mentioned above and limiting pressure differences to less than 0.01 MPa. The forming results are consistent.

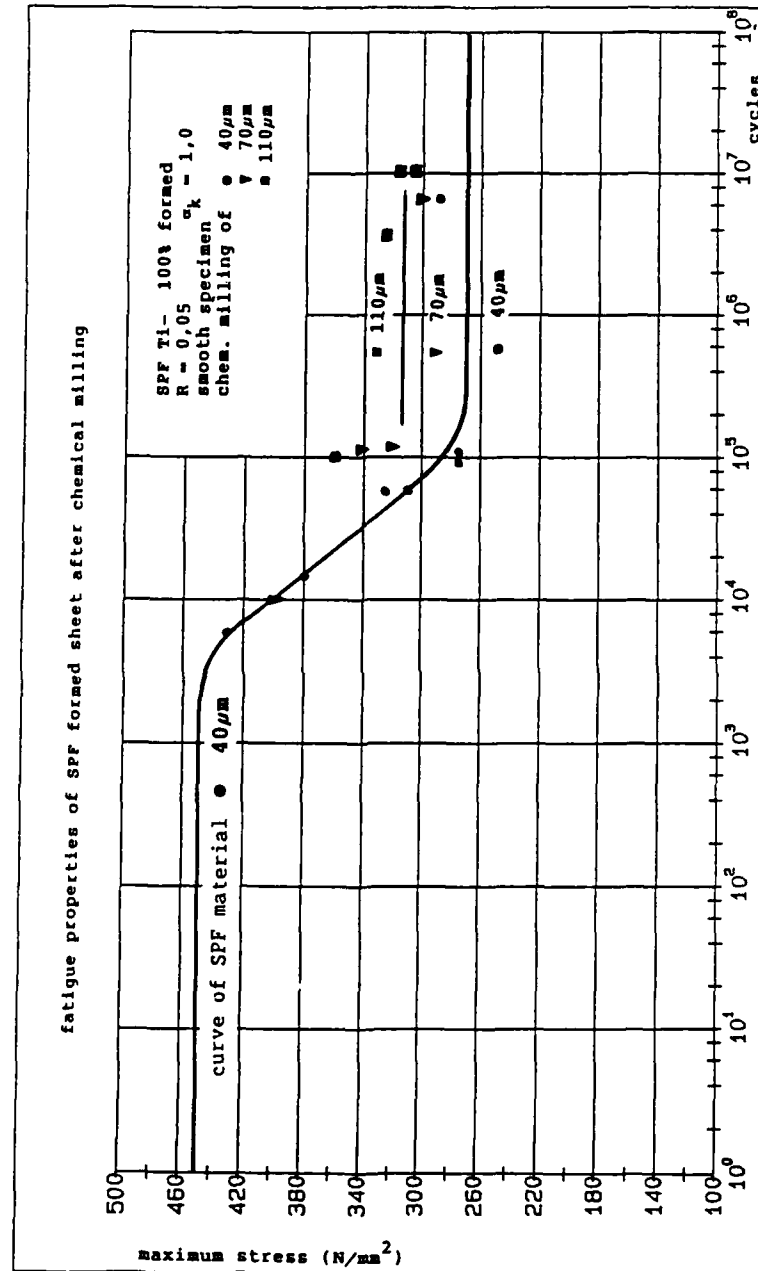


Figure 9 - Fatigue strength of superplastically formed sheet after milling of • 40 $\mu\text{m}$  ▽ 70 $\mu\text{m}$  ■ 110 $\mu\text{m}$

#### "Stop-off" influences

Different agents can be used for the "stop-off" process. The most frequently used agents are "KALGARD" (graphite basis), boron nitride and yttria oxide [4]. The requirements of these agents are: good anti-bonding properties, the least possible reaction with titanium and good adhesion. The extent of adsorption as regards reaction and diffusion is investigated both on heat-treated and SPF-formed specimens. The "stop-off"-influenced zone is investigated by auger-electron spectroscopy. Fig. 10 shows the activity of a graphite based "stop-off" on a cross section of a specimen surface. The specimen surface reveals a graphite layer of 0.4 microns followed by a reaction zone of titanium carbide with a thickness of 2.5 microns. As can be seen from Fig. 10, the "stop-off" remnants are within a range of maximally 5 microns. Therefore they are removed by chemical milling as is normal for SPF parts. All "stop-off" agents have been proved as non-critical with regard to surface contamination. The easy application of boron nitride and the good anti-bonding properties make it the best choice of "stop-off".

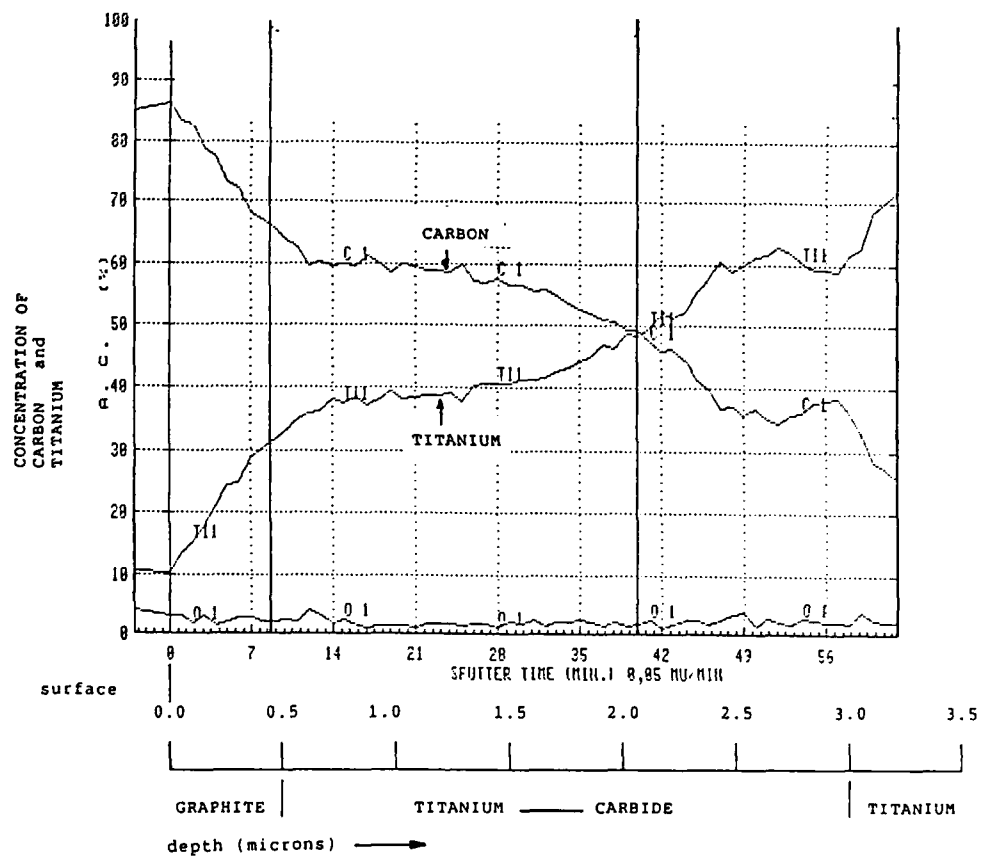


Figure 10 - Auger-electron spectroscopy of KALGARD "stop-off" on as formed SPF-material

### Conclusion

The process development for the production of SPF-formed engine parts has been completed. It was shown that SPF technology can be applied to the series production of engine components.

The development program showed that the static properties complied with the requirements in the material data sheet (WL 3.7164.1).

Due to the good results, the amount of testing has been significantly reduced, thus saving costs.

Cost effective parts were made after optimizing production sequences and using multiple dies.

The use of ceramic "stop-off" material permits a large number of production cycles.

Merely spot checks have been made concerning the effects hot die forming has on the dynamic properties. Initial test results show structural instability due to rapid cooling, which influences fatigue properties.

### References

- [1] Groß, Werkstoffauswahl für SPF/DB-Werkzeuge (MBB-Report TN-TE334-212/86, Bremen, 1986).
- [2] RMI - Material Specification: RMI-MS-005 Rev. A 1986.
- [3] R. Bilgram, A. Olbricht, P.-J. Winkler, Werkstoffuntersuchungen an superplastisch umgeformten, diffusionsgeschweißten TiAl6V4-Legierungen (MBB Report Z-68/86, MBB Ottobrunn, 1986).
- [4] F. Nitschke, AES-Untersuchung der Wechselwirkung Trennmittel/Werkstoff beim superplastischen Umformen von TiAl6V4 (MBB Report TN-BT21-3/84, MBB Ottobrunn, 1984).



STUDY ON SPF AND SPF/DB  
OF THE BULK-HEAD STRUCTURE WITH NON-SYMMETRIC SHAPE

Li You-qin and zhang shi-ling

Beijing Aeronautical Manufacturing Technology  
Research Institute  
Beijing, China

ABSTRACT

Generally, the metal sheet parts by SPF and SPF/DB are symmetric in shape, such as spheres and hemi-spheres, cylinder-type parts, box-type parts, corrugated plates and panels, etc.. The complicated parts with non-symmetric shape are studied by the authors. This paper describes the research result of Ti-6Al-4V bulk-head structure with non-symmetric shape and the notches accessed by stringers by SPF and SPF/DB. The paper includes the selection of SPF method; the forming method and process; the thickness distribution of parts and their homogeneity; SPF/DB method and coordination problems, and finally, states the feasibility of producing the complicated structures with non-symmetric shape by SPF and SPF/DB.

The research result has been applied in aviation industry.

Superplasticity and Superplastic Forming  
Edited by C.H. Hamilton and N.E. Paton  
The Minerals, Metals & Materials Society, 1988

## Introduction

Generally, the titanium alloys sheet parts by SPF and SPF/DB are symmetric in shape, such as spheres and hemi-spheres, cylinder-type parts, box-type parts, corrugated plates and panels, etc.. In fact, the authors have also researched the manufacture technology about Ti-6AL-4V bulk-head structure with non-symmetric shape. This paper describes the research result of the bulk-head structure with non-symmetric shape and the notches accessed by stringers by SPF and SPF/DB.

## The Selection of SPF Schemes

The structure part with full sizes has five notches accessed by the stringers and a narrow-long strengthen flat, which is non-symmetric in shape. The strengthen flat is connected with inside flange by DB. The notches accessed by the stringers and other parts are formed by SPF. The configuration sizes are about 660 X 56 X 19 mm, as shown in figure 1(a). The deformation of all the bulk-head part has three types, i.e. bidirectional stretch, single directional stretch and single bending. The difficult point by SPF is that "triangle" area at the notches accessed by the stringers has complicated shape and is bidirectional stretch with a great deformation extent. The rate of the area change  $\psi$  is up to 343%.

For this reason, we have to solve the SPF problems first.

To start with the test parts that are shown in figure 1(b), in order to form the notches accessed by the stringers, three SPF schemes are considered (Fig.2): a). the female die forming; b). the male die forming; c). the die with "incline type" mould cavity forming. For the first scheme, the outside surface sizes of the formed parts have high precision, its configuration is accurate, save on material, and because the parts have thinner web, which results in weight reduction. Therefore this scheme is suitable for the aeroplane structures that require the accurate configuration and light in weight. But to produce the dies is somewhat difficult and the round angle area of the part bottom is thinner. By second scheme, to produce the dies is

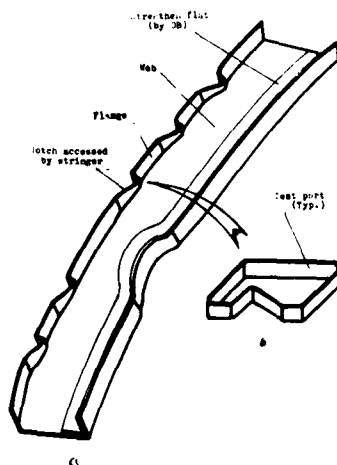


Figure 1-The bulk-head structure with non-symmetric shape.

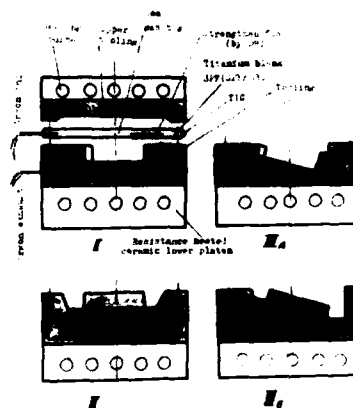


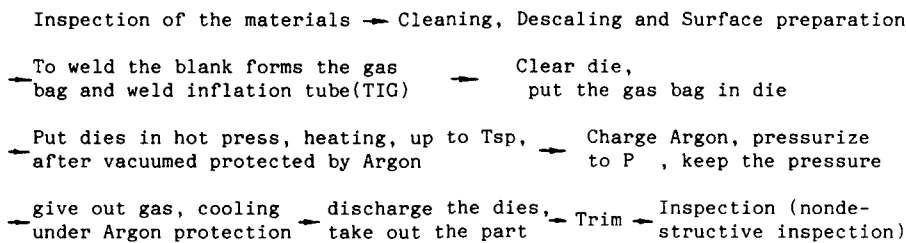
Figure 2-The three SPF(SPF/DB) schemes.

easier. But waste on the blank, the web of the part is rather thick, thus the part weight is increased. The third scheme may be formed supply sufficient materials when the "triangle" area is formed. But it is rather difficult to work the dies and the widthwise thickness of the part is not uniform. After comprehensive consideration, the third scheme is discarded, we have selected the first and the second schemes, of which is tested first.

#### The Forming Method and Technological Process

The specific forming method is gas pressure forming by dies at superplastic forming temperature and protective gas against contamination.

The technological process flow diagram is shown as following:



The forming parameters are mainly superplastic temperature, strain rate, forming pressure and dwell time.

Optimum SPF temperature is 925°C. SPF is highly sensitive to the strain rate  $\dot{\epsilon}$ , the  $\dot{\epsilon}$  is readjusted by control the pressure increasing velocity,  $V = 0.01-0.04 \text{ MPa/m}^3 \cdot \text{s}$  is selected, the relevant strain rate  $\dot{\epsilon} = (1.3-4.2) \times 10^{-4} \text{ s}^{-1}$ . SPF pressure  $P = 1.4 \text{ MPa}$ ,  $P_{\text{max}} = 1.8 \text{ MPa}$ . The dwell time is in the range of 30-40 min.

#### Thickness Distribution and Uniformity

The parts discussed in this paper are non-symmetric in shape, the configurations are complicated and with sudden change ("triangle" area), thus the deformation at different location is greatly different, resulting in non-uniform thickness distribution. It is certain that the stretch deformation in longitudinal direction and transverse direction will cause the compression deformation in thick direction. After the 'non-triangle' area of the blank expands to attach the tooling wall, thin out of the part will be stopped immediately. The continuous expansion will be concentrated on 'triangle' area where the blank does not attach to the tooling wall. A large number of tests indicate, that for the blank with different thickness, the non-uniformity has somewhat the same trend. The thickness distribution of the test part is shown in Fig.3, the blank thickness is 1.0 mm, which has provided the valuable and available reference data for reasonably selecting the structure sizes and the material thickness.

#### SPF/DB Process and Coordination Problems

The test parts and the full-size bulk-head parts all done by the SPF/DB process that is DB first and SPF following. For the inside flange of full-size parts, the strengthen flat is connected to the SPF basic body by DB. For DB, the difficult point in making this structure is that the narrow-long strengthen flat with 50:1 of length/width will be connected as one complete

set on the non-symmetric single-side according to the technical requirements of DB.

The technological process of SPF/DB is shown as following (see also the above-mentioned SPF technological process flow diagram): (After blanking and cleaning)—

- the strengthen flat and the basic blank
- is positioned by point welding, non DB → to seal bag by welding
- part is coated with the stopoff. → to weld gas tube(TIG)
- to clear the tooling, position
- the sealed bag(blank) on the → put the die in hot press, heated to
- tooling, intall the tooling Tsp(DB) after vacuumed protected Argon
- give the mould cavity let the A out the (following the same
- the gas(A), DB. → mould cavity, give Ar → process as SPF
- in the sealed bag,SPF

The DB technology parameters are mainly the temperature, pressure and dwell time.

$T_{DB}$  is similar to  $T_{SPF}$ , the optimum  $T_{DB}$  is also  $925^{\circ}\text{C}$

$P_{DB}=1\text{ Mpa}$ ,  $P_{DB_{max}}=1.2\text{ MPa}$ ;

The dwell time is within 1 hour.

Consideration of the coordination problems of DB is very important. The coordination method is shown in Fig.4. By this method can the desired results be achieved.

On the fully test base for of the test parts and full-size test parts, and to consult with the design department, the structure configuration, the structure sizes, the material (blank) thickness etc. are modified suitably, and adopt the male method to manufacture full-size installed parts. The

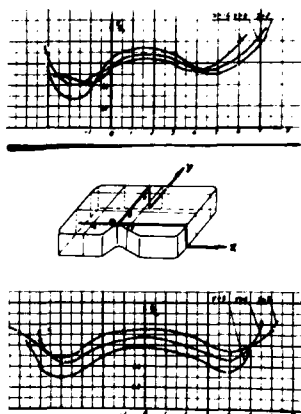


Figure 3-The variations of relative thickness of the test part.

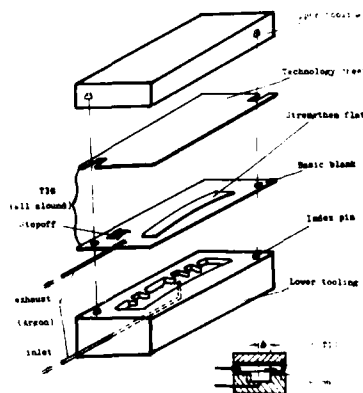


Figure 4-Coordination mthod among basic blank-strengthen flat-tooling (SPF/DB).

results show that the part quality is superior and satisfies design requirements, which have been put in production applications.

It must be emphasized that due to the narrow and long full-size structure with the notches accessed by the stringers distributed non-uniformly (see Fig.1 (a) ), and to the tooling material being different from the blank material, the influence caused by high temperature must be taken into consideration. Thus, it is necessary to make the shrink scale templet (contour templet) according to the shrink scale coefficient, again to make the tooling according to the shrink scale templet. So the tooling employed by SPF/DB is the shrink scale tooling.

#### Conclusions

a). This study indicates that even the non-symmetric airplane bulk-head with the notches accessed by the stringers and the narrow-long strengthen flat can be also manufactured by SPF and SPF/DB. But we must point out that the above-mentioned non-symmetric shape structure are not the typical structure which must be done by SPF and SPF/DB. It has provided the valuable experiences to expand the application of SPF and SPF/DB;

b). In order to manufacture the qualified products, it is necessary to solve a series of problems, such as technology parameters, tooling materials and tooling design (including the shrink scale calculation), argon inlet and exhaust prevention the paths blocking, environment protection, stop-off, the part separating from the tooling etc., so it is necessary to conduct a large number of tests for the test parts;

c). The parts after SPF and SPF/DB all satisfy the design and application requirements in the metallgraphic structure, the oxygen and hydrogen contents, the mechanical properties etc.;

d). As compared with the original technology, the full-size structure by SPF/DB reduces the part number (by about 12%), decreases the weight (by about 8.8%), reduces the tooling quantity (by about 50%) etc., which are all obvious advantages;

e). In order to expand the application of the new technology, it is important to keep close contact with the design department, the research manufacturing technology institute and application department.

DB/SPF COOLER OUTLET DUCT FOR

AIRCRAFT APPLICATION

W. Beck

Materials and Processes Development Department  
MBB-UT, Bremen, F.R. G.

Abstract

Different SPF/DB methods have been analysed to fabricate a cooler outlet duct. The development is successfully finished. Component and DB/SPF process are certified. Series production has started. Cost and weight savings have been realized as predicted.

Superplasticity and Superplastic Forming  
Edited by C.H. Hamilton and N.E. Paton  
The Minerals, Metals & Materials Society, 1988

## 1. Introduction

Titanium as a structural material is used in areas where other materials show disadvantages. The favourable combination of good thermal strength, high specific strength and outstanding corrosion resistance gives titanium an advantage despite its costly processing with conventional techniques.

Titanium today makes up for about 2 % to 7 % of structural weight in running civil subsonic projects. Future civil subsonic transports will have a slight increase in titanium to about 9 %. Titanium in military aircraft, e.g. in a European fighter, today has a share of about 19 %.

This paper will show possibilities of introducing SPF/DB components of titanium alloy Ti6Al4V as a replacement for conventionally formed titanium components. The SPF/DB technology offers a potential for cost and weight decrease.

## 2. Component Analysis

Considering the fuselage and the equipment of military fighter aircraft, there are a lot of structural components in the engine area and some components of the "bleed air system" already made of titanium sheets. Fire protection hazards and thermal loads automatically led to titanium materials. Mainly commercially pure titanium (CpTi) occurs. This article focusses on components of the bleed air system only. When looking for components suitable to be redesigned for SPF and/or DB with the aim of cost improvement, the relation of material prices of CpTi to Ti6Al4V led to the understanding that only components assembled from several parts with a lot of assembly work are worth to be analysed.

The bleed air system consists of different tubing, branches and items with specific functions. It is mainly built out of CpTi. For assembly reasons, the system is divided into several segments. Tubes have diameters of 2.5" to about 7". There are also different branches and some complex components with inner stiffeners. The small forming capability of CpTi necessitates "short" and "simple" portions. Conventional forming consists of manufacturing half shells by deep drawing or drop hammer forming followed by a stress relieving operation. Shells are trimmed to shape and welded together by TIG. Production is costly due to the amount of steps. A lot of jigs and tools are necessary.

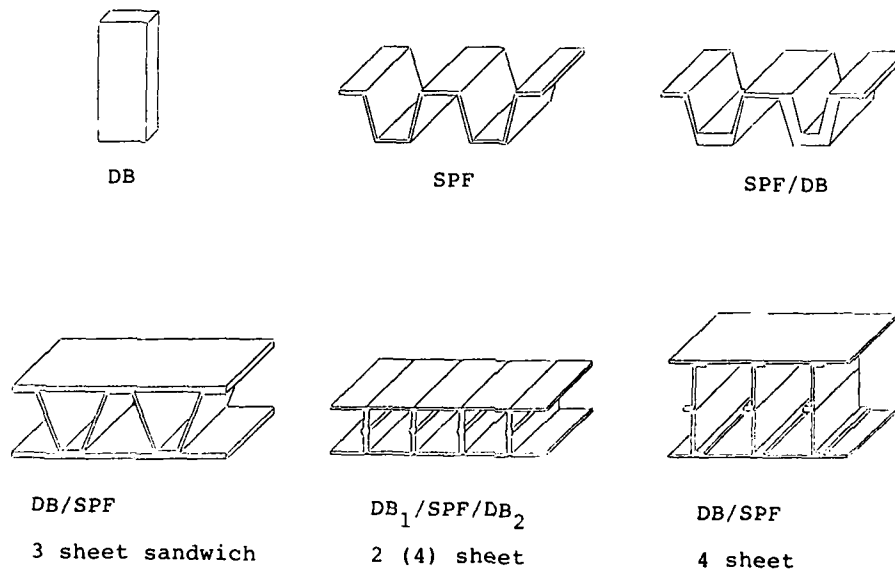


Figure 1: SPF and DB components (cross section)

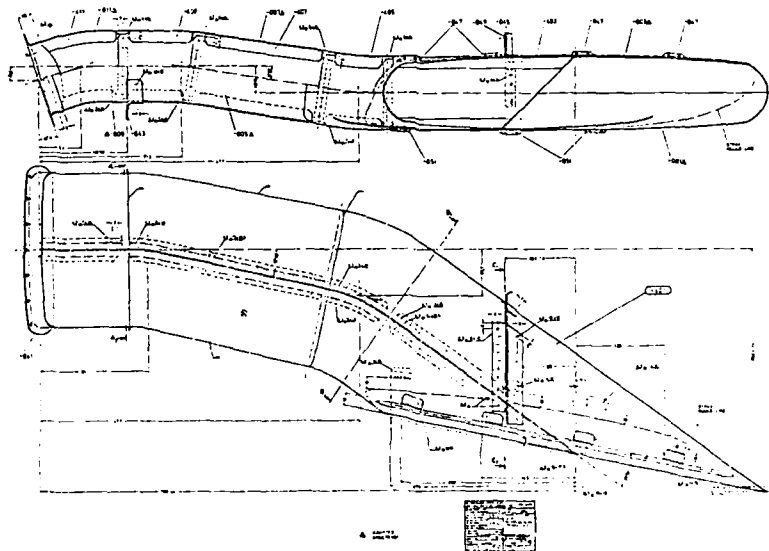


Figure 2: Conventional cooler outlet duct



Integration of as many parts as possible into one complex structure offers cost and weight advantages.

To demonstrate this capability of SPF and DB processes, the cooler outlet was chosen. Within the analysed spectrum of components, it had the best potential to show the advantages of manufacturing an integral component with SPF/DB.

### 3. Existing design

The cooler outlet is used as an exhaust duct to transfer hot and compressed air from the heat exchanger of the air conditioning unit to the outer skin. Picture 2 shows the conventional design. Design features are suitable for the SPF and DB process. An inner web is necessary to prevent buckling due to inside pressure. Outer dimensions are 1000 x 250 x 120 mm. The initial sheet thickness for the conventional layout is 1.0 mm.

### 4. SPF and DB design

The test component had to meet the following requirements:

- Full interchangeability
- Identical design due to matching areas and parts
- Weight decrease
- Cost advantage.

To meet these targets the SPF/DB designs known from (2) had to be modified. Picture 1 shows typical sections of SPF/DB components.

For cooler outlet development two different SPF/DB approaches have been made. A "formed duct" is produced with both alternatives. With flanges, fittings and carriages welded on, the part is completed to be the cooler outlet component.

Process parameters for SPF and DB have already been presented (3) and are mostly quite similar to other components (1 + 2).

#### 4.1 Two-sheet technology, $DB_1$ -SPF- $DB_2$

This two sheet technology is depicted in picture 3. Bonded together in the flange area and the centreline at first, the part is superplastically formed onto the tool shape and afterwards diffusion bonded for the second time to obtain an integral web.

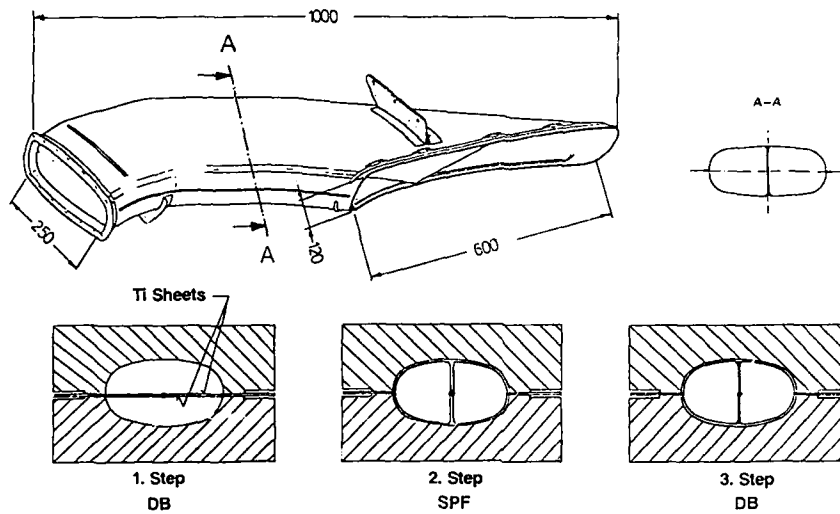


Figure 3: DB<sub>1</sub>/SPF/DB<sub>2</sub> design

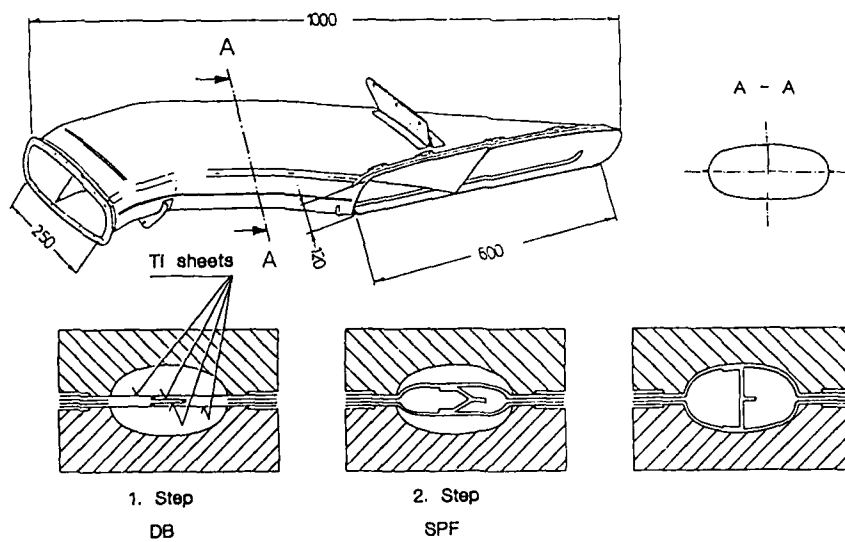


Figure 4: DB-SPF design

#### 4.2 Four-sheet technology, DB-SPF

The sketch in picture 4 shows the fabrication method used. A pack of four sheets is diffusion bonded in the flange area, between the inner sheets in a narrow zone and the inner sheets to the outer ones at the centre-line. During superplastic forming of the outer sheets, the web is formed automatically with a "bending" movement.

#### 5. Manufacture of SPF and DB components

With a hot working hydraulic press of 200 to ram force the components are manufactured in a "hot die" technique. See picture 5. Tools are heated up in a pre-heating oven. The tool material is a highly heat resistant, scalefree cast steel. The inner contour of the die describes the formed duct geometry.

Commercially available titanium sheet additionally specified concerning microstructure is cleaned and the stop-off applied. DB and SPF run automatically. Temperatures and pressures are documented continuously. When taken out, the components cool down in air. Mild chem-milling must be carried out due to  $\alpha$ -case layers on the surfaces.

Pictures 6 and 7 show formed ducts, the one fabricated with  $DB_1$ -SPF- $DB_2$  and the other with DB-SPF.

During a preproduction run a number of components of both alternatives were produced to test the processes and fit of the ducts with matching structure and to show cost and weight situation.

#### 6. Testing of SPF and DB components

Since early results showed advantages of 4-sheet-DB/SPF concerning cost and weight situation, most of the testing was performed on these components. During production, quality assurance was gained as follows: Accidental errors are checked by inspection operations in sensitive steps. Systematical errors are checked by examining samples that have accompanied the component. Such samples are easy to obtain from excess material.

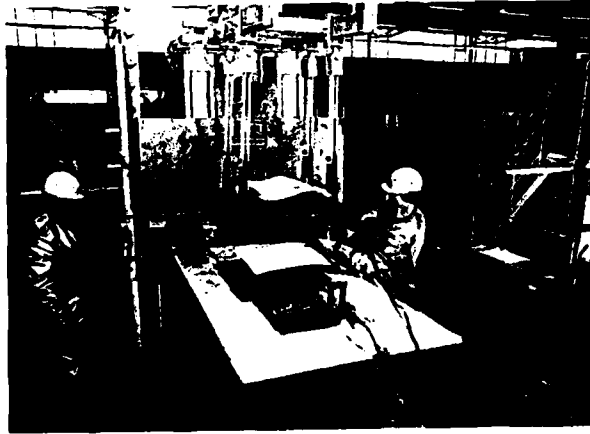


Figure 5: SPF-DB Press 200 tons

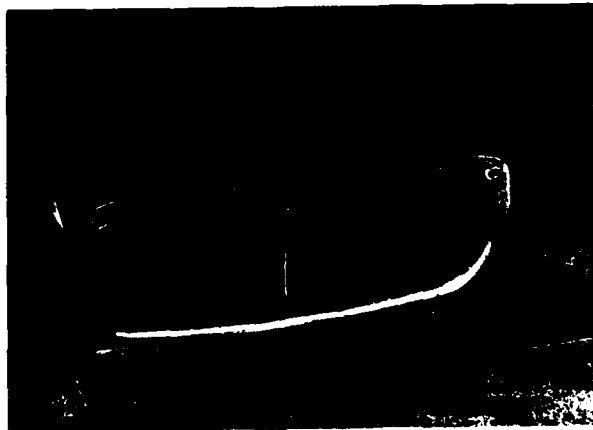


Figure 6: Two sheet component



Figure 7: Four sheet component

### 6.1 Tolerance accuracy

The cooler outlet has the smallest allowances on the exhaust side due to aerodynamic tolerances of the fuselage skin. With the help of a digital measuring machine and by installation of components in different aircraft, it has been demonstrated that cooler outlets fabricated with SPF-DB fit well. Reproducibility is better than with conventional ducts. Indeed, the allowable variation of surrounding components requires minor corrective work on the duct. Even the Ti6Al4V-components have sufficient plasticity for these operations.

### 6.2 Static and dynamic strength

The cooler outlet is subjected to temperature and pressure loads. There are "no" dynamic loads to take into account. The calculated minimum thickness is well exceeded. Tensile samples, taken from the ducts both out of DB and SPF areas, and photomicrographs show that the material properties are well beyond the specified values.

An additional pressurisation test of a duct section showed that the safety factor is much higher than required.

### 6.3 DB-quality

DB-quality depends on cleanness and care during preparation and on the correct process parameters. No problems have occurred with DB-SPF 4-sheet components. Picture 8 shows a typical photomicrograph of the bonding zones, taken from a cross-section.

Fabrication of the two-sheet DB<sub>1</sub>-SPF-DB<sub>2</sub> is not as easy since contamination of bonding surfaces, induced roughness from forming and grain growth trouble the second diffusion bonding process. (3). As a result, bonding time has to be extended considerably to obtain a satisfactory bonding quality. Picture 9 shows the photomicrograph of a typical cross-section.

Satisfactory bonding quality is so far assured by testing some accompanying samples, by photomicrographs and by tensile specimens taken from the ends of the formed ducts and by inspection of selected preparation steps before bonding. The duct itself is inspected additionally by penetrant testing.

Some newly developed ultrasonic inspection techniques (4) allow detection of microfaults down to a size of 15  $\mu\text{m}$  in diameter and a width of less than 1  $\mu\text{m}$ . These techniques are in the testing stage and may be introduced on future, higher loaded components.

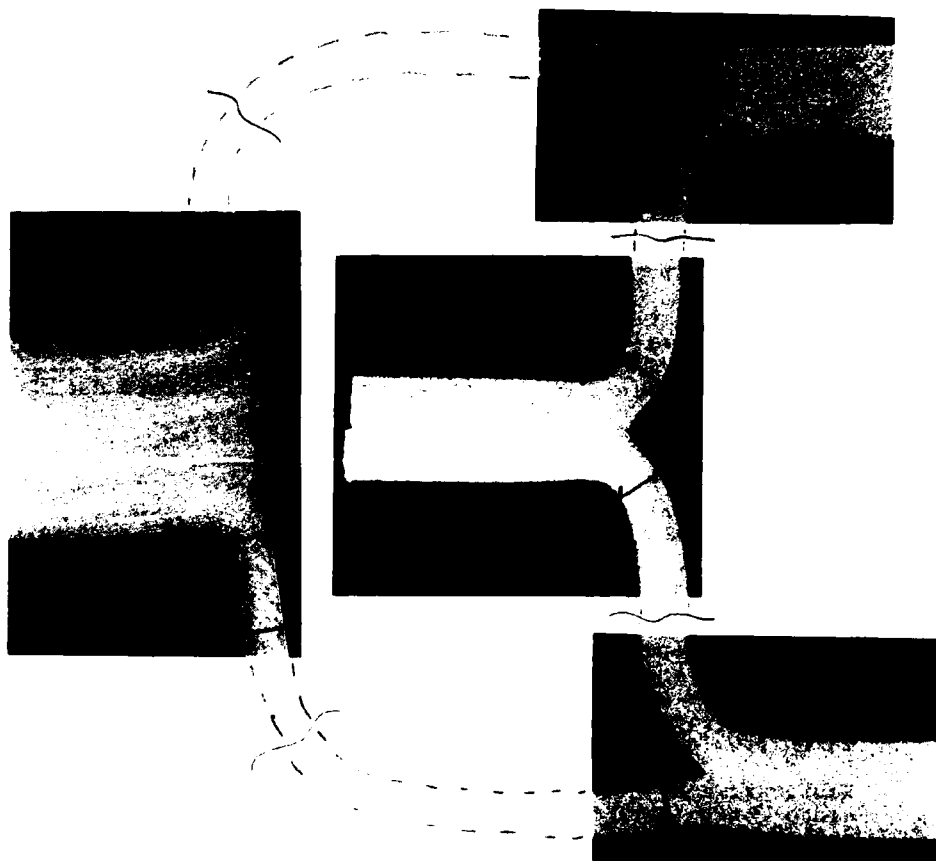


Figure 8: Photo micrograph DB-SPF, 4-sheet

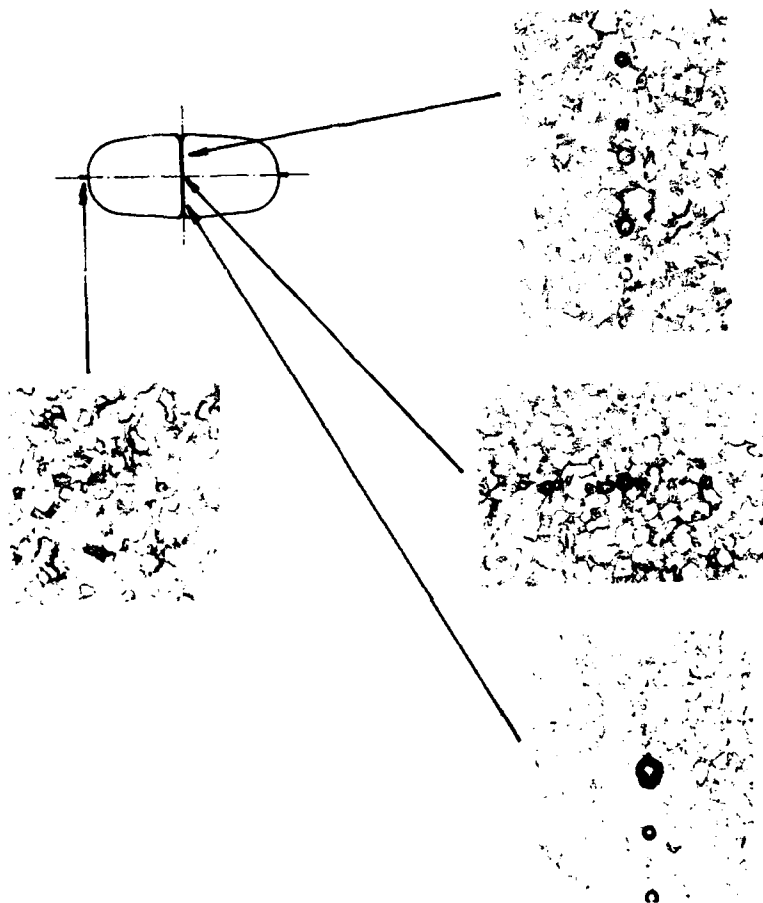


Figure 9: Photomicrograph,  $DB_1$  / SPF /  $DB_2$   
2 - sheet



7. Results

Both SPF/DB fabrication alternatives DB<sub>1</sub>/SPF/DB<sub>2</sub> and DB/SPF have been realized. The components fit well, their properties are reproducible and meet all requirements.

Cost and weight data indicate that preference should be given to the four sheet DB/SPF. Cost reductions of about 18 % and weight decreases of about 24 % are achievable in comparison with the conventional component.

8. Conclusions

Components of the bleed air system, especially the presented ducts, can be manufactured by SPF and DB with significant cost and weight advantages.

Not every SPF/DB technique is equally suitable. For future application preference may be changing from part to part. Some questions are still being worked on, e.g. NDT techniques to test bonding quality and strength, influences of tool alloy on titanium material and optimisation of SPF process parameters concerning strain rate and forming temperature.

Development of DB/SPF cooler outlet duct has been successfully finished with certification of process and component.

The experiences with the cooler outlet component showed that further development work is necessary to establish more detailed data about SPF and DB processes. Application on other complex components are being considered and will show superior capabilities of the SPF/DB process.

### References

- 1 Swadling, S.J.  
Fabrication of Titanium at High Temperatures  
AGARD, Florence, Italy, Sep. 24-29, 1978
- 2 Stacher, G.W., und E.D. Weisert  
Concurrent Superplastic Forming/Diffusion Bonding of B-1 Components  
AGARD, Florence, Italy, Sep. 24-29, 1978
- 3 Beck, W. und P. Knepper  
Superplastisches Umformen und Diffusionsschweißen einer Zellenkomponente aus TiAl6V4  
DVS-Berichte, Band 98
- 4 Tober, G. und S. Elze  
Ultrasonic Testing Techniques For Diffusion-Bonded Titanium Components  
AGARD, Conference Proceedings No. 398
- 5 Winkler, P.-J. und W. Keineth  
Superplastische Umformung, ein werkstoffsparendes und kostengünstiges Fertigungsverfahren für die Luft- und Raumfahrt  
Metall, 6 (1980) 34, S. 519 ff

## Subject Index

- Acoustic emission, 111, 112
- Activation energy, 461
  - Ti alloy, 267
  - Zn-Mn alloys, 425
- Aging of Al-Li alloy
  - after superplastic deformation, 457
- Aircraft parts
  - SPF/DB, 602, 603
- Alloy design
  - computer-aided, 355
  - titanium alloy, 358-361
- Alpha grain boundary
  - in titanium alloy, 459-463
- Aluminum alloys, 367
  - 6Mg-2Zn-1Mn-1Cr-5Zr, 384
  - 7075, 309-313
  - 7475, 251-255, 276, 303-308, 367, 597, 643, 643, 653, 654
  - 7475-0.7Zr, 395-399
  - 8090, 643, 646, 647, 653
  - Al-2.2Cu-2.0Li-1.6Mg-0.08Zr, 222-225
  - Al-2.32Li-1.3Cu-0.8Mg-0.13Zr, 174
  - Al-2.4Li-1.2Cu-6Mg-12Zr, 558-561
  - Al-2.4Li-1.2Cu-0.6Mg-0.1Zr, 121-125
  - Al-2.4Li-1.2Cu-0.7Mg-0.1Zr, 216
  - Al-2.4Li-2.6Cu-0.2Zr, 239-243
  - Al-2.6Li-1.9Cu-0.55Mg-0.12Zr, 453-457
  - Al-4%Ti, 28
  - Al-4Zn-2Mg-0.5(Mn+Cr+Ti), 246-249
  - Al-4.7Si-8.2Mg, 257-261
  - Al-6Cu-0.5Zr, 109-113
  - Al-6Zn-2.3Mg-1.7Cu-0.11Zr, 216
  - Al-10Mg-0.1Zr, 389-393
  - Al-13Si, 257-260
  - Al-Li, 58
  - Al-Mg, 58-59
  - Al-Zn-Mg-Cu, 27
  - diffusion bonding, 654
  - IN90211, 161-164
  - LC4, 40
  - LC4, LC5 (7075, 7475), 97-101
  - LY-12, LC4, 329
  - mechanically alloyed, 59
  - membrane forming, 599
  - post-formed properties, 530, 531
  - SPF, 651
  - surface roughness, 215-218
- Amorphous alloy ribbon, 279
- Anelasticity, 33-37
- Anisotropy
  - in titanium, 209
- Annealing
  - time between roll passes, 389-393
- Applications
  - SPF
  - SPF/DB, 686
- Art craft articles
  - superplastic, 576
- Artificial aging
  - Al-Li alloy, 453-457
- Bend test
  - superplastic ceramics, 632
- Bending
  - metal-matrix composite, 617
- Beta surface equation
  - titanium alloy, 359
- Bi-axial deformation, 251-255
- Bonding
  - mechanisms, 476
  - nucleation and growth, 514-516
  - of Al-Li alloys, 377-381
  - shear strength, 377-381
  - Zn interlayers, 377-381
- Bulge forming, 303-308
  - aluminum alloy, 303-308
  - experimental, 304
  - modeling, 304, 305
- Bulging, 253-255
  - constant strain rate, 309
- Cavitation, 142-145, 152-158, 173-178, 203-207, 253-255, 367
  - at particles, 259
  - ceramics, 622, 623
  - copper alloy, 448-451
  - cracking, 195
  - growth, 192-193, 197, 198, 201
  - in superplastic alloys, 155, 156
  - in Al alloy, 279
  - in Al-Li alloys, 223-225
  - in ceramics, 634
  - nucleation, 152, 194
  - and growth, 235-237
  - reduction, 156
  - sintering, 34, 36
- Cavity interlinkage, 197, 198, 201, 202
- Ceramics, 3, 4, 11, 14

- fine grain size, 59
- flow properties, 622, 623
- superplastic, 372, 373, 631-635
  - extrusion, 625-630
  - mechanisms, 583-594
- superplasticity, 583-594
- $Y_2O_3$ - $ZrO_3$ , 625-630
- Yttria stabilized  $ZrO_2$ , 59, 619-623
  - 631-635
- $ZrO_2$  toughened, 620, 621
- $ZrO_2/Al_2O_3$ , 619-623
- Coble creep, 34
- Combined extrusion, 545, 546, 548, 549
- Commercial applications, 507-511
- Composites
  - laminated, 58-60
  - SiC/Al, 59
- Compression forming, 328-331
  - of superplastic materials, 180-183
- Computer simulation
  - SPF process, 291
- Constant strain rate bulging, 309
- Constitutive equations, 578, 579
- Continuous recrystallization
  - Al-Li alloy, 377-381
- Copper alloys, 174, 369
  - aluminum
    - brass (HAL 66-3-2), 441-445
    - bronze, 447-451
  - brasses, 406
  - Cu-1.9Be-0.2Ni, 63
  - Cu-40Zn-2.5Al-4.3Mn-0.5Pb, 577
  - H62 brass, 233-237
  - manganese brass, 233-237
- Core-mantle model, 21-22, 24
- Costs
  - SPF, 645, 646
- Crack initiation
  - Ti-6Al-4V, 640
- Cracking
  - cavity growth, 173, 174, 176-178
- Creep
  - diffusion, 40, 42, 43
  - dislocation, 43
- CSL boundary distribution
  - Al alloy, 389-393
- Damage
  - cavitation, 142-145
  - deformation defect, 138, 139
  - geometrical defect, 137, 138
  - grain growth, 141, 142
  - thickness distribution, 146, 147
- Deep drawing
  - limiting draw ratio, 167, 168, 171
- Deformation
  - mechanisms, 36, 37, 64-66, 247
  - uniaxial, 252, 253
- Design
  - concepts, 493
  - SPF, 643, 644
- Die
  - inserts, 668, 671, 672
  - steel, 551-555, 563-567
- Diffusion, 48
  - bonding, 475-489, 491-492
  - 7475 aluminum, 523-537
  - Al alloys, 377-381, 483-485, 558-561, 664
- Al
  - roll cladding, 558-561
  - transient liquid phase, 558-561
  - zinc interlayers, 558-561
- cyclic shear strength, 7475 Al, 526
- deformation related to, 517-521
- kinetics, 475
- liquid phase joining, 497
- mechanisms, 475
- microstructure, 7475 Al, 525
- models, 513-516
- quality, 687
- shear strength, 7475 Al, 525
- techniques, 480, 496
- titanium alloy, 651
- Ti-alloys, 475-489
- transformation
  - plasticity, 517-521
  - superplasticity, 563-567
- bonds
  - aluminum alloys, 482, 500, 501
  - characteristics, 493
  - mechanical properties, 499
  - nickel alloys, 485
  - titanium alloys, 479, 532
- in Al-Li alloy, 225
- in Inconel 718, 75
- Dimensional tolerance, 37
- Dislocation
  - activity in superplasticity, 205, 206
  - glide
    - solute drag, 164
  - structure
    - after superplastic deformation, 64-66
- Dislocations, 46, 47, 48
  - grain boundary, 132
  - lattice, 111, 112
- Domes, 303-308
  - geometry, 303, 306, 308
  - height, 303, 305, 308
- Ductility, 110-112

- Duplex stainless steels
  - mechanical properties, 430, 431
  - pitting potential, 430, 432, 433
- Dynamic
  - recrystallization, 5, 11, 14, 123-125, 368, 370, 372, 398
    - aluminum brass, 441-445
    - grain refinement by, 97-101
    - in Al-Li alloy, 242
    - in superplasticity, 91, 92, 95
  - strain rate hardening, 309, 310, 313
- Elongation, 228-232
  - aluminum alloy, 277
  - in Inconel 718, 74, 75
  - mechanisms, 73-77
  - superplastic, 397
  - alloys, 573
- Equiaxed fine grain structure, 398
- Extrusion, 545-549
  - analysis, 346-348
  - ceramics, 623-628
  - experiments, 348, 349
- Fatigue
  - post-SPF, 637-641
  - thermal, 37
- Fine grain
  - microstructure, 3, 4, 9, 13
  - sizes, 58-59
- Fine stable microstructure
  - copper alloy, 448-451
- Finite element method
  - SPF modeling, 291, 292, 293, 295
- Floating grains, 25
- Flow
  - behavior
    - superplastic ceramics, 631
  - hardening, 116-119
  - localization, 151
  - stress
    - effect of temperature, 265
    - minimization Al-Li alloy, 377-381
    - nickel-base alloy, 357
    - strain rate sensitivity, 17, 20
- Formability, 546, 548
- Forming
  - ceramics, 626-630
  - hot, 596-599
  - membrane, 596-599
  - methods
    - selection, 680
- Fractography
  - post-SPF fatigue, 641
- Fracture
  - elongation, 187-189
  - necking, 136-148
  - strain, 136-148
- Friction
  - in superplastic forming, 297-302
- Gas atomization, 396
- Grain
  - boundaries, 6, 10, 12, 14, 46, 47, 49
  - boundary
    - dislocations, 40, 42, 43
    - migration, 34
    - misorientation Al alloy, 389-393
    - sliding, 6, 8, 12, 14, 40, 42, 43, 163, 164
    - contribution to total strain, 17, 20
    - diffusion controlled, 619
    - in ceramics, 635
    - interface reaction controlled, 621
  - structure, 129-132
    - in ceramics, 583
  - emergence
    - between grains, 53, 55
    - in a fissure, 53-55
  - growth
    - deformation induced, 115-119
    - during deformation, 243
    - effect on necking, 141, 142
    - in Al-Li alloy, 243
    - mechanisms, strain-enhanced, 86-89
    - strain induced, 585
    - strain-enhanced, 84-88
    - under strain reversal, 85, 86
    - neighbor switching, 34-35, 37
    - refinement, 53, 55, 280, 414
    - aluminum alloy, 97-101
    - size, 415
    - ceramics, 619
    - critical, for superplasticity, 249
- Hardness, 549
- Hemispheres
  - by superplastic forming, 315-319, 321-326
- High strain rate, 59
  - superplasticity, 161-162
- Hobbing, 572
  - superplastic steel, 551-555
- Hydrogen
  - effect on titanium superplasticity, 460-463
- Hydrostatic pressure
  - aluminum bronze, 450, 451
- Inconel 718, 74, 75-77
- Indentation
  - study of Sn-38Pb, 21-29

Injection molding dies, 545-549  
 Intermetallics, 3, 4, 8, 11, 14  
 Internal friction, 425  
 Iron alloys, 369  
     30CrMnSiAl, 329  
     Fe-0.2C, 563, 567  
 Isothermal forging, 409  
  
 Joining  
     ceramics, 622  
  
 Lithium loss  
     in Al-Li alloy, 224  
  
 m value, 557-561  
     superplastic alloys, 573  
     Ti alloys, 652, 673  
 Magnesium alloys  
     Mg-4.3Al-0.4Mn-1.0Zn, 70  
     Mg-5.3Zn-0.5Zr, 68-71  
     Mg-6Zn-6Zr, 91-95  
 Manufacture  
     SPF, 644, 645  
 Material qualification  
     alpha case, in Ti alloys, 673, 674  
 Mechanical properties  
     Al, 653, 654  
     formed parts, 598, 599  
     high temperature, 27-31  
     post-formed, 529  
     static and dynamic strength, 673-675  
     Ti-6Al-4V, 639  
     UHC steel, 511  
 Mechanically alloying  
     aluminum, IN 90211, 161-164  
 Mechanisms  
     of superplasticity in ceramics, 583-594  
     superplastic deformation, 68-70  
 Melt spinning, 396  
 Membrane  
     element model  
     for SPF, 283-289  
     forming  
         aluminum alloys, 599  
         nickel alloys, 597  
         stainless steels, 597  
         titanium alloys, 598  
         superplastic, 597  
 Metal-matrix composite  
     fabricating, 614, 615  
     superplastic matrix, 614-617  
 Micro-grid analysis, 521  
 Microcomputer control, 309, 311  
 Microduplex microstructure, 106  
  
 Microhardness  
     high temperature, 258  
 Microstructural  
     evolution, 557, 561  
     Al-Li alloys, 377-381  
     instability, 81-89  
 Microstructure  
     after cryogenic working, 280  
     after direct strip casting, 280  
     amorphous alloy ribbon, 279  
     control for superplasticity, 401-405  
     -property correlation, 27-31  
     yttria stabilized ZrO<sub>2</sub>, 631, 632, 634, 635  
 Modeling  
     extrusion of ceramics, 628  
     superplastic flow in ceramics, 584  
  
 Nanoindenter, 21-23  
 Natural aging  
     Al-Li alloy, 454-457  
 Necking, 197, 200, 202, 227-232  
 Nickel alloys, 354-363  
     Hastelloy X, 598  
     Inconel 718, 73-77  
     membrane forming, 597  
     Ni-8Cr-3Ta-9Co-5Mo-9W-5Al-1Hf, 272  
     Ni-30Cr-5Al, 413-415, 417  
     nimonic alloys, 596  
     thermomechanical processing, 413-417  
 Non-symmetric shape forming, 678  
 Non-uniform deformation, 227-232  
 Notch geometry, 227-232  
  
 Partitioning ratio  
     titanium alloy, 359  
 Phase ratio  
     in titanium alloy, 460  
 Physical metallurgy, 27-29  
 Pitting potential  
     duplex stainless steels, 430, 432, 433  
 Plastic instability  
     biaxial stress state, 144-147  
     uniaxial stress state, 136-144  
 Post-formed properties  
     Al-Li alloy, 456  
 Post-SPF fatigue  
     properties, 637-641  
 Powder  
     aluminum alloys, 27, 28, 31  
     superplastic Zn-22Al, 614  
 Pressure profile  
     for forming, 287  
     for superplastic forming, 301

Processing  
   superplastic alloys, 366  
 Property control, 47  
  
 Quality  
   assurance, 603  
   control  
     penetrant crack test, 651  
     ultrasonic test, DB Al, 654  
  
 Recrystallization  
   aluminum alloy, 280  
   continuous, 377-381, 557-561  
   dynamic, 368, 370, 372  
   in Al-Li alloys, 222, 457  
   in Al-Li-Cu-Zr alloy, 121-125  
   Inconel 718, 74-77  
   static, 368  
 Rheological criteria  
   for superplastic deformation,  
   179-183  
 Rheology  
   model, 622  
 Roll bonding, 498  
  
 Sandwich structure, 601  
 Seamless tubes  
   by superplastic forming, 318  
 Sheet forming, 596-599  
 SiC fiber  
   in superplastic matrix, 614-617  
 SPF  
   applications, 653  
   shear wall SPF, 653  
   Ti alloy engine components, 667-669  
   Ti and Al alloys, 649-664  
   titanium alloys, 650  
   /DB, 475-489, 491, 601-605, 679-683, 687  
   aluminum, 7475, 523-527  
   test article, 523-527  
 Spherical vessel  
   superplastic formed, 315-319  
 Stainless steel  
   duplex, 429  
   In-744 alloy, 429-433  
   membrane forming, 595  
 Steel  
   4Cr3Mo3W2V, 551-555  
   dies, 551-555  
   UHC superplastic, 508-511  
 Stop-off  
   SPF of titanium alloys, 671, 672,  
   672-675  
 Strain  
   hardening, 136-139, 313, 368  
   during superplastic deformation, 241  
  
 rate  
   hardening, 339-343  
   path, 169  
   sensitivity, 110-112, 136-148, 161-162,  
   188, 189, 265  
   aluminum alloys, 278  
   effect of strain, 241, 244  
   Inconel 718, 74, 75  
   index, m, 233-237  
   nickel-base alloys, 273  
   softening, 313  
 Strength  
   Al-Li at room temperature, 456, 458  
 Stress-strain behavior  
   oscillatory, 54, 55  
   room temperature, 52-54  
 Subgrain  
   formation, 441  
   structure, 398  
 Submicron structures, 49  
 Superalloys, 279  
 Superplastic  
   alloys, 573  
   deformation, 5, 12  
   room temperature, 52  
   tests, 340  
   elongation  
     nickel-base alloy, 357  
   extrusion, 345-349  
   flow, 3, 5, 8, 9, 13, 14  
   by Nabarro-Herring creep, 586-588  
   enhanced by liquid phase, 588  
   yttria stabilized ZrO<sub>2</sub>, 631-635  
   forging  
     titanium alloy, 409  
   forming, 304, 328-331, 511  
   Al-Li alloys, 377-381  
   ceramics, 622  
   evaluation criteria, 333-337  
   friction, 297-302  
   modeling, 283-289, 291-295, 297-302  
   technology, 571-624  
   UHC steel, 511  
   mechanisms, 577  
   magnesium alloys, 67-71  
   parts  
     titanium alloy, 580  
   temperature  
     effect of phase transformation, 436,  
     437  
   testing, 509  
 Superplasticity  
   ceramics, 619-623  
   criterion, 17, 20  
   mechanisms, 27-31

- physical model, 46, 47, 49
- sub-grain, 591
- Surface
  - observations
    - aluminum brass, 444
    - roughness, 215-219
- Tensile
  - stability, 82
  - test
    - ductility, 167-170
    - high strain rate, 161-163
    - high temperature, 161-163
    - large ductility, 161-163
    - properties, 415
    - strain rate, 167-170
- Tension-torsion tests, 340
- Tests
  - activation energy, 425
  - index, m, 421-422
  - internal friction, 425
  - manganese content, 421-423
  - superplastic properties, 419-420
  - total elongation, 421-422
- Texture
  - Al alloy, 386
  - effect of superplasticity, 64
- Thermomechanical processing, 413, 414, 417
  - aluminum, 276
  - Al alloy, 384, 390-393
  - cold rolling, 413, 414
  - copper alloy, 447-451
  - precipitation, 413, 414
  - recrystallization, 413, 414, 417
  - titanium alloy, 404
- Thickness
  - distribution, 254, 681, 682
  - non-uniformity, 303-308
  - profiles, 294, 596-599
  - dome, 287
  - rate, 305
  - strain, 305-308
    - in hemisphere, 325
- Thin sheet, 291, 292, 293, 295
- Thinning profiles, 298
  - in hemispheres, 325
- Threshold stress
  - Orowan stress, 163
- Tin alloys
  - Sn-38Pb, 340
- Tin-lead alloys
  - Sn-38Pb, 21-25
- Titanium alloys, 358-363, 370
  - 6Al-4V, 329
  - applications, SPF, SPF/DB, 650-652
  - bar and extrusion, 209-211
  - diffusion bond, 532
  - membrane forming, 598
  - post formed properties, 530-532
  - TC9 alloy, 233-237
  - Ti-2.5Mo-9.5V-3Al, 407-411
  - Ti-5Al-1V-3Mo, 404, 405
  - Ti-5.4Al-2.8Sn, 103-107
  - Ti-6Al-4V, 129-132, 209-213, 216, 315-319, 459-463, 597-599, 601-603, 637-641, 665-677, 679-683, 686
  - Ti10V-2Fe-3Al, 263-267
  - Ti-13V-3Cr-3Al-3Sn, 216
  - Ti-Al-Mo alloys, 435-439
  - surface roughness, 215-218
- Tool design, 670-672
- Tooling
  - SPF, 645, 647
  - of titanium alloys, 668-672
  - stop-off coating, 671, 672
- Tools
  - for SPF-DB, 603
- Torsion
  - for grain refinement, 97-105
  - study of Sn-38Pb, 21-24
- Transformation
  - laminar microstructure, 103, 104, 106
  - superplasticity, 517-521
  - steel alloy, 563-567
- Transition regions
  - strain rate, 245, 247
- Threshold stress
  - temperature dependence, 163
- UHC steel, 508-511
  - alloy effects, 508
- Ultra-fine grain structure, 401-405
- Uniformity of deformation, 188, 189
- Yield
  - criterion
    - for superplastic deformation, 339-343
    - superplastic flow, 580
  - function, 339-343
  - surface, 339-343
- Zinc alloys
  - Al-(50-78)Zn, 478
  - Zn-1.1Al, 109-113
  - Zn-4Al, 348
  - Zn-4Al-1Cu, 542
  - Zn-5Al-0.03Mg, 310-313
  - Zn-5Mg-0.6Mn, 115-119
  - Zn-22Al, 107, 198, 199, 202, 227-232, 348, 401-405, 466, 545-549, 614-617
  - Zn-Al, 33, 35
  - Zn-Mn alloys, 419-427
- Zirconia, 625-628, 629



## Author Index

- Asanuma, H., 545  
 Ash, B., 239  
  
 Bai Bingzhe, 97  
 Ball, J., 557  
 Baudelet, B., 135  
 Beck, W., 685  
 Bieler, T.R., 161  
 Blandin, J.J., 191, 221, 251  
 Bonet, J., 291  
  
 Carry, P., 625  
 Chandra, N., 283  
 Chao Shuzhi, 333  
 Chen Bingkin, 315  
 Chen Hechun, 233  
 Chen Puquan, 63, 67  
 Chen Sanshan, 571  
 Chin Liu, 39  
 Chokshi, A.H., 149  
 Crooks, R., 73, 389  
  
 Dai Jilin, 571  
 Defen, T., 383  
 Dunford, D.V., 209, 215  
 Dunlop, G.L., 631  
 Dyulgerov, N., 419  
  
 Eiichi Sato, 115  
  
 Feng Zezhou, 563  
 Friedrich, H.E., 649  
 Fumihiko Wakai, 619  
 Furlan, R., 649, 665  
  
 Ginty, B., 643  
 Grimes, R., 557  
 Guo Dianjian, 339  
 Guo Xusheng, 97  
 Guo, Z.X., 303  
  
 Hagg, D., 665  
 Hai Jintao, 315, 571  
 Hailing Huang, 465  
 Hales, S.J., 389  
 Hamilton, C.H., 121, 239, 453  
 Hammond, C., 365  
 Hazzledine, P.M., 33  
 Hermansson, T., 631  
  
 Hideo Takei, 185  
 Higashi, K., 447  
 Hirohashi, M., 545  
 Huang Liping, 435  
 Huang Yan, 513  
 Hughes, G.W., 643  
  
 Imabayashi, M., 413  
 Istatkov, A., 419  
  
 Jianzhong Ciu, 245  
 Jin Hua, 465  
 Jin Quanlin, 97  
 Jin Tao, 63  
 Johnston, S.H., 643  
  
 Kaibyshev, O.A., 3  
 Kaibyshev, R.O., 91  
 Kakuhiko Kuribayashi, 115  
 Kellett, B., 625  
 Kennedy, J., 523  
 Koczak, M.J., 27  
 Kuboki, I., 413  
 Kullick, M., 649  
  
 Lacroix, J.Y., 221  
 Lagerlöf, K.P.D., 631  
 Lai Weihua, 97  
 Langdon, T.G., 173, 197, 227  
 Li Xiu-Qing, 203  
 Li You-qin, 679  
 Lian Shu-jun, 345  
 Liqin Wang, 39  
 Liu Weimin, 263  
 Longxiang, M., 309, 513  
 Lukac, P., 109  
 Luo Ying-She, 327  
 Lutfullin, R.Y., 103  
  
 Ma Longxiang, 369, 513  
 Mae, Y., 407, 637  
 Mahoney, M.W., 73  
 Masaru Kobayashi, 271  
 Matsuki, K., 395  
 Mayo, M.J., 21  
 McDarmaid, D.S., 529  
 McNelley, T.R., 389  
 Michio Yamazaki, 353  
 Mitev, N., 419

Mocellin, A., 625  
Motohashi, Y., 413  
Mukherjee, A.K., 149, 161  
Murty, G.S., 27  
Mutoh, Y., 637

Negrete, J., 51  
Nieh, T.G., 57, 161  
Nishimura, H., 613  
Nix, W.D., 21  
Nobuhiro Iguchi, 517  
Norio Furushiro, 17, 197  
Novikov, I.I., 401

Ohsawa, H., 167  
Oka, T., 407  
Osada, K., 429

Padmanabhan, K.A., 321  
Pan Xa qin, 263  
Partridge, P.G., 209, 215, 529  
Peng Xu, 257  
Pilling, J., 303, 475  
Portnoy, V.K., 401

Qinglin Wu, 465  
Qinling, Wu, 245  
Qu Li, 333

Raj, R., 583  
Reisinger, L., 665  
Ren, B., 121  
Ricks, R.A., 377, 557  
Ridley, N., 303, 365, 447  
Rolland, B., 601  
Roy, B., 283  
Ryo Horiuchi, 115

Salishchev, G.A., 103  
Schepp, P., 507  
Shanyou Zhou, 39  
Shariat, P., 227  
Shen Huanxiang, 441  
Sherby, O.D., 57  
Shigenori Hori, 17  
Sing Hailong, 333  
Smirnov, O.M., 179  
Song Shengzhe, 441  
Song Yu-quan, 345  
Song Zuo Zhou, 263  
Spirov, I., 419  
Staniek, G., 395  
Stoklossa, H., 557  
Story, J.M., 297  
Su Shenggui, 441  
Suéry, M., 135, 191, 221, 251  
Sun Shangchen, 563

Takuji Okabe, 185  
Tao Shuxue, 369  
Todd, R.I., 33  
Tokizawa, M., 395  
Tomei Hatayama, 185  
Toyofuku, K., 635  
Tucker, R.D., 453

Valiev, R.Z., 45  
Varloteaux, A., 251  
Venkataswamy, S., 321  
Villaseñor, G.T., 51  
Viswanathan, D., 321

Wadsworth, J., 57, 161  
Wakayama, S., 613  
Walser, B., 507  
Wang Cheng, 327  
Wang Chunrong, 333  
Wang, H., 257  
Wang Yanwen, 563  
Wang, Z.R., 339, 571  
Ward, D.M., 595  
Wilkinson, D.S., 81  
Winkler, P.-J., 377, 491, 557, 665  
Wittenauer, J., 507  
Wood, R.D., 291

Xu Yanwu, 339

Yamagishi, S., 613  
Yamamoto, H., 613  
Yamazaki, S., 407  
Yan, H., 513  
Yan, M.G., 129, 459  
Yan Ma, 173  
Yang, J.F., 257  
Yang Yongchun, 551  
Yang Zhenheng, 233  
Yasunori Saotome, 517  
Yin Changkui, 339

Zaripov, N.G., 91  
Zhang Dixiang, 541  
Zhang Hong, 97  
Zhang Kaifeng, 571  
Zhang, S.Q., 129, 459  
Zhang Si-ling, 679  
Zhang Yanhui, 383  
Zhang Zhen-jun, 345  
Zhang Zhimin, 383  
Zhao, L.R., 129, 459  
Zhao Min, 63, 67  
Zhao You-Chang, 203  
Zhou Tiecheng, 383  
Zienkiewicz, O.C., 291